UNIVERSITAT DE BARCELONA

Exploring heterocyclic scaffolds in the development of multi-target anti-Alzheimer and multi-trypanosomatid compounds

Ornella Di Pietro

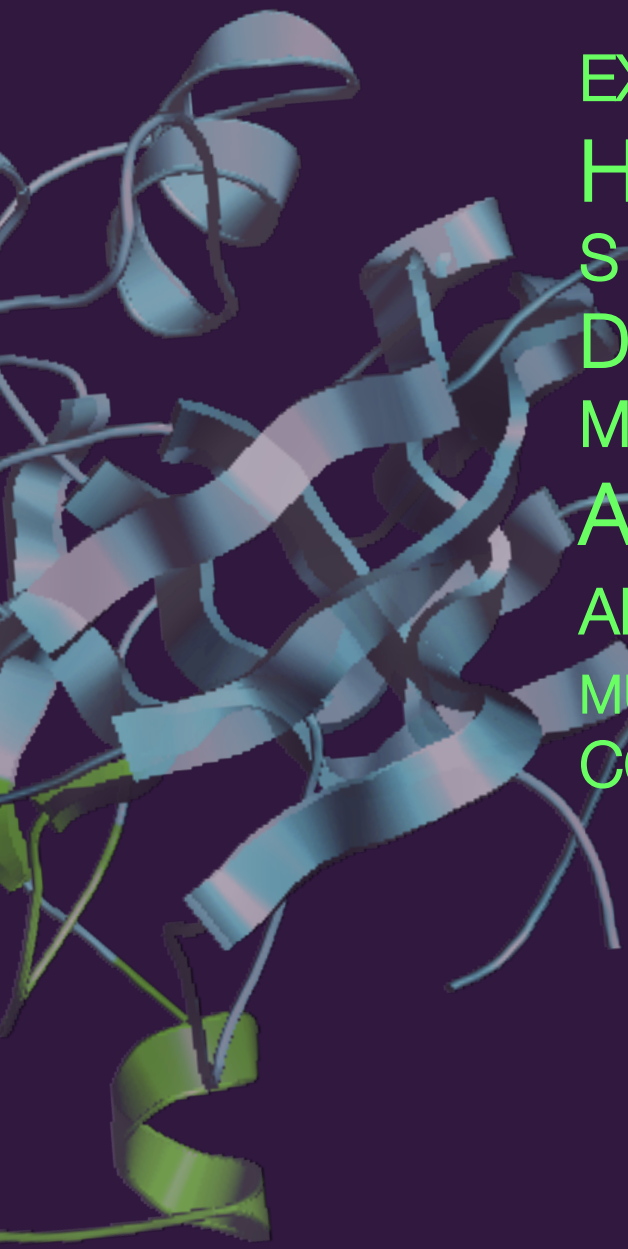

EXPLORING HETEROCYCLIC SCAFFOLDS IN THE DEVELOPMENT OF MULTI-TARGET ANTI–ALZHEIMER AND MULTI-TRYPANOSOMATID COMPOUNDS

Ornella Di Pietro

2015

UNIVERSITAT DE BARCELONA

FACULTAT DE FARMÀCIA

LABORATORI DE QUÍMICA FARMACÈUTICA
DEPARTAMENT DE FARMACOLOGIA I QUÍMICA TERAPÈUTICA

EXPLORING HETEROCYCLIC SCAFFOLDS IN THE DEVELOPMENT OF MULTI-TARGET ANTI-ALZHEIMER AND MULTI-TRYPANOSOMATID COMPOUNDS

Ornella Di Pietro
2015

UNIVERSITAT DE BARCELONA

FACULTAT DE FARMÀCIA

Programa de doctorat:
Química Orgànica Experimental i Industrial

EXPLORING HETEROCYCLIC SCAFFOLDS IN THE DEVELOPMENT OF MULTI-TARGET ANTI-ALZHEIMER AND MULTI-TRYPANOSOMATID COMPOUNDS

Memòria presentada per Ornella Di Pietro
per optar al títol de Doctor per la Universitat de Barcelona

Dirigida per:

Dr. Diego Muñoz-Torrero López-Ibarra

Dr. F. Javier Luque Garriga

Tutor: Dr. Diego Muñoz-Torrero López-Ibarra

Ornella Di Pietro
Barcelona, 2015

El trabajo experimental reflejado en esta memoria ha sido realizado en el Laboratorio de Química Farmaceutica de la Facultad de Farmacia de la Universidad de Barcelona bajo la dirección del doctor Diego Muñoz-Torrero. La parte relacionada con los estudios de modelización molecular ha sido realizada en el Laboratorio de Biología Computacional y Diseño de Fármacos del Departamento de Fisicoquímica de la Facultad de Farmacia de la Universidad de Barcelona bajo la dirección del doctor F. Javier Luque.

La presente Tesis Doctoral ha sido posible gracias a la concesión de una Beca d'Ajut de personal investigador en Formació (APIF-2011) por parte de la Universidad de Barcelona y de una Beca per a la Formació de Personal Investigador (FI-2012) concedida por la Agència de Gestió d'Ajuts Universitaris i de Recerca de la Generalitat de Catalunya.

El presente trabajo ha sido financiado por el Ministerio de Ciencia e Innovación (CTQ2011-22433), el Ministerio de Economía y Competitividad (SAF2014-57094-R) y la Generalitat de Catalunya (2009SGR1396 y 2014SGR52).

Los recursos computacionales han sido proporcionados por el *Barcelona Supercomputing Center* (BSC), el *Consorci de Serveis Universitaris de Catalunya* (CSUC) y el *UK National Supercomputing Service* (ARCHER).

Prologue

The present PhD thesis has been drawn up as a compendium of publications and draft manuscripts. According to the legislation in force it has been divided into 9 chapters including an *Introduction* to each of the two main research lines followed, namely Alzheimer's disease (*Chapter 1*) and Neglected Tropical Diseases (*Chapter 2*), the *Objectives* (*Chapter 3*), a *Discussion* about the work carried out and the main outcomes for each of the 5 research projects developed (*Chapters 4-8*), and finally the overall *Conclusions* (*Chapter 9*).

It is worth noting that *Chapter 4* contains the publication entitled "1,2,3,4-Tetrahydrobenzo[*h*][1,6]naphthyridines as a new family of potent peripheral-to-midgorge-site inhibitors of acetylcholinesterase: synthesis, pharmacological evaluation and mechanistic studies" (Di Pietro O. *et al.*, *Eur. J. Med. Chem.* **2014**, *73*, 141) preceded by a preliminary discussion about the synthetic approach adopted for the preparation of the target compounds, the molecular modelling studies and the overall results.

Chapter 5 includes an initial discussion regarding the multidisciplinary contribution, including both synthetic and computational works, given to the development of a picomolar dual binding site acetylcholinesterase inhibitor as a potential anti-Alzheimer *lead* candidate, followed by the derived publication entitled "Tetrahydrobenzo[*h*][1,6]naphthyridine–6-chlorotacrine hybrids as a new family of anti-Alzheimer agents targeting β-amyloid, tau, and cholinesterase pathologies" (Di Pietro O. *et al.*, *Eur. J. Med. Chem.* **2014**, *84*, 107).

Chapter 6 contains a brief dissertation about the selective MAO-B inhibition as an attractive therapeutic approach to Alzheimer's disease, the rational design of a novel series of 1,4-disubstituted triazole-based propargylamines and the synthetic strategy adopted, envisaging a click-chemistry approach as the key step. It follows the draft manuscript entitled "Design, synthesis and biological evaluation of *N*-methyl-*N*-[(1,2,3-triazol-4-yl)alkyl]propargylamines as novel monoamine oxidase B inhibitors", which gathers the synthetic, the computational and the biological aspects of the multidisciplinary work carried out.

Principal Component Analysis (PCA) method allowed an exhaustive study of the intrinsic high flexibility of the loops defining the walls of the novel secondary pocket and found to affect the orientation of a crucial residue for the ligand binding (Arg307), as also attested by the available X-ray structures (draft manuscript). In light of the results obtained, a virtual screening of a library of 500,000 commercially available fragments has been carried out and three suitable candidates have been selected for further hybridization with huprine Y.

Finally, given the trypanocidal activity displayed by a benzonaphthyridine derivative previously developed in our research group as a *peripheral anionic site*-binding AChEI, a small library of quinolines and tricyclic heterofused quinolines has been synthesized *via* a Povarov MCR approach and subjected to a phenotypic *whole-cell* screening against *Trypanosoma brucei*, *T. cruzi*, and *Leishmania infantum*. Several low micromolar multi-trypanosomatid agents have emerged as suitable *hit* candidates for a future *lead* optimization (Di Pietro O. *et al. Eur. J. Med. Chem.* **2015**, accepted with minor revision).

Summary

The aim of this PhD thesis consists of the synergistic combination of both highly efficient synthetic approaches and molecular modelling tools for the structure-based drug design and synthesis of novel bioactive heterocyclic compounds. The work carried out has followed two main research lines, namely the development of novel disease-modifying anti-Alzheimer agents and still unexplored chemical entities for the treatment of Neglected Tropical Diseases (NTDs).

In the context of the anti-Alzheimer therapeutic strategies, the innovative so-called Multi-Target Directed Ligands (MTDLs) approach has inspired, on the one hand, the structure-based design and synthesis of a novel dual binding site picomolar acetylcholinesterase inhibitor (AChEI) as one of the most potent non-covalent AChEIs ever described in the literature. The rational design of this hybrid compound, based on a 6-chlorotacrine unit conveniently combined with a propidium-related fragment easily accessed through a Povarov multicomponent reaction (MCR) approach, has been carried out in two consecutive steps, reflected in two publications (Di Pietro O. *et al. Eur. J. Med. Chem.*, **2014**, *73*, 141; Di Pietro O. *et al. Eur. J. Med. Chem.*, **2014**, *84*, 107). The first one consisted of the preliminary *hit-to-lead* optimization of a practically inactive propidium-related compound that successfully led, through a double O → N bioisosteric replacement, to a nanomolar lead candidate, which was finally combined with a 6-chlorotacrine unit following a molecular dynamics (MD)-driven optimization of the length of the linker.

On the other hand, other protein targets, recently emerged as attractive "*druggable alternatives*" for the development of innovative anti-Alzheimer therapeutic strategies, have been explored, namely MAO-B and BACE-1.

Thus, the high versatility of the click-chemistry synthetic approach in its *Cu*-catalyzed azide-alkyne cycloaddition version, in combination with suitable computational chemistry tools, has given easy access to a novel series of *N*-methyl-*N*-[(1,2,3-triazol-4-yl)alkyl]propargylamines as novel irreversible MAO-B inhibitors (draft manuscript) with the perspective to be linked to a second pharmacophoric moiety to derive novel MTDLs as potential anti-Alzheimer drug candidates.

Moreover, in the framework of a direct anti-amyloid approach for the treatment of Alzheimer's disease, strong experimental evidences together with previous computational studies prompted us to postulate the existence of a secondary transient druggable pocket in

the enzyme BACE-1 never described so far. Then, an extensive computation of the BACE-1 *apo* conformational ensemble through the synergic combination of the MD technique with the Principal Component Analysis (PCA) method allowed an exhaustive study of the intrinsic high flexibility of the loops defining the walls of the novel secondary pocket and found to affect the orientation of a crucial residue for the ligand binding (Arg307), as also attested by the available X-ray structures (draft manuscript). In light of the results obtained, a virtual screening of a library of 500,000 commercially available fragments has been carried out and three suitable candidates have been selected for further hybridization with huprine Y.

Finally, given the trypanocidal activity displayed by a benzonaphthyridine derivative previously developed in our research group as a *peripheral anionic site*-binding AChEI, a small library of quinolines and tricyclic heterofused quinolines has been synthesized *via* a Povarov MCR approach and subjected to a phenotypic *whole-cell* screening against *Trypanosoma brucei*, *T. cruzi*, and *Leishmania infantum*. Several low micromolar multi-trypanosomatid agents have emerged as suitable *hit* candidates for a future *lead* optimization (Di Pietro O. *et al. Eur. J. Med. Chem.* **2015**, accepted with minor revision).

Abbreviations

ACh	Acetylcholine
AChE	Acetylcholinesterase
AChEI	Acetylcholinesterase inhibitor
AD	Alzheimer's disease
apoE	Apolipoprotein E
APP	β-Amyloid precursor protein
aq.	aqueous
Aβ	β-Amyloid peptide
$A\beta_{40}$	40 amino acid β-amyloid peptide
$A\beta_{42}$	42 amino acid β-amyloid peptide
BACE-1	β-Secretase
*b*AChE	Bovine acetylcholinesterase
BBB	Blood-brain barrier
BChE	Butyrylcholinesterase
BChEI	Butyrylcholinesterase inhibitor
$(Boc)_2O$	di-tert-butyl-di-carbonate
CAS	Catalytic Anionic Site
CDA	Carbo−Diels Alder
Cdk5	Cyclin-dependent kinase 5
CNS	Central Nervous System
CuAAC	Copper-catalyzed azide-alkyne cycloaddition
DA	Diels-Alder
DALYs	Disability adjusted life-years
DDQ	Dichlorodicyanobenzoquinone
DEAD	Diethyl azodicarboxylate
DEPT	Distortionless enhancement by polarization transfer
DMF	*N,N*-dimethylformamide
DMPK	Drug Metabolism and Pharmacokinetic
EDC	1-Ethyl-3-(3-dimethylaminopropyl)carbodiimide
*ee*AChE	Electrophorus electricus acetylcholinesterase
FAD	Familial Alzheimer's Disease
FAD	Flavin Adenine Dinucleotide
FDA	Food and Drug Administration
GSK-3β	Glycogen Synthase Kinase 3β
*h*AChE	Human Acetylcholinesterase
HAT	Human African Trypanosomiasis
HBA	Hydrogen Bond Acceptor
*h*BChE	Human Butyrylcholinesterase
HBD	Hydrogen Bond Donor
HDA	Hetero−Diels-Alder

HOBt	*N*-hydroxybenzotriazole
HTS	High-throughput screening
IC_{50}	Concentration that inhibits 50% of the enzymatic activity
K_i	Inhibition constant
*m*AChE	Mouse acetylcholinesterase
MAO	Monoamine Oxidase
MCR	Multicomponent Reaction
MD	Molecular Dynamic
MS	Mass Spectrometry
Ms	Mesilate
MTDLs	Multi-Target Directed Ligands
NAC	Non β-Amyloid Component
NECT	Nifurtimox/Eflornitine Combination Therapy
NMDA	*N*-Methyl-di-Aspartate
NMEs	New Molecule Entities
NTDs	Neglected Tropical Diseases
NTFs	Neurofibrillary Tangles
p-TsCl	*p*-Toluenesulfonyl Chloride
PAS	Peripheral Anionic Site
PC	Principal Component
PCA	Principal Component Analysis
PDB	Protein Data Bank
PDPs	Product Development Partnerships
PHF	Paired Helical Filaments
PTRE	Post-Treatment Reactive Encephalopathy
QM	Quantum-Mechanical
r. t.	room temperature
RMSD	Root-Mean-Square Deviation
ROS	Reactive Oxygen Species
sAPPα	Secreted Amyloid Precursor Protein-α
SAR	Structure-Activity Relationships
sat.	saturated
SBDD	Structure-Based Drug Design
SI	Selectivity Index
SIE	Solvation Interaction Energy
sol.	solution
T.b.	*Trypanosoma brucei*
TBSCl	Tert-Butyldimethylsilyl Chloride
TcAChE	*Torpedo californica* Acetylcholinesterase
THF	Tetrahydrofuran
TLC	Thin Layer Chromatography
TryR	Trypanothione Reductase
WHO	World Health Organization

Table of contents

1 Introduction to Alzheimer's disease

Chapter

1.1 Alzheimer's disease

Alzheimer's disease (AD) is the most common type of dementia and the third cause of death in elderly people in developed countries, approaching epidemic proportions and affecting 36 millions of people worldwide.[1,2] Its prevalence raises steadily with age, so that after 65 the likelihood of developing AD doubles every 5 years. The prevalence of AD is expected to increase, affecting 66 million people in 2030 and 115 million people in 2050, along with the increase of average life expectancy and the aging of the population, becoming a major social and sanitary concern in developed countries.[3,4]

Although the cost of coping with AD is already substantial in terms of either loss of life quality and productivity and despite the huge economic efforts that are being made to take care of AD patients and decipher how to treat AD, near-term predictions indicate that the expense will soon be unaffordable for our society. The total worldwide estimated cost associated with AD currently accounts for approximately 1% of the world's gross domestic product. The lack of effective therapies, a large aging population, and increasing life expectancy are rapidly converging into an impending crisis for health care providers.[5]

It is believed that the pathological events of AD begin decades before measurable symptoms appear. It is clinically characterized by deterioration of cognitive function, dementia, memory loss and altered behaviour. The earliest symptoms are usually subtle, intermittent deficits in the remembrance of minor events of everyday life, referred to as loss of episodic memory. After many months of gradually progressive memory loss, other cognitive symptoms appear and slowly advance. Over a further period of years, profound dementia develops and affects multiple cognitive and behavioural spheres. Death usually comes by way of minor respiratory complications, such as aspiration or pneumonia.[6,7]

AD is mainly related to age, while genetic predisposition to suffering the disease only accounts for 3% of all cases.[8] Three main mutations on genes encoding for transmembrane

[1] *Alzheimer's Disease International. World Alzheimer Report: The global prevalence of dementia* **2009**.
[2] Muñoz-Torrero, D. *Curr. Med. Chem.* **2008**, *15*, 2433.
[3] *Alzheimer's Disease International. World Alzheimer Report*: *The benefits of early diagnosis and intervention* **2011**.
[4] Walsh, D.M.; Selkoe, D.J. *Neuron* **2004**, *44*, 181.
[5] Gray, L. *Cell* **2012**, *18*, 6.
[6] Cummings, J.L.; Askin-Edgar, S. *CNS Drugs* **2000**, *13*, 385.
[7] Leonard, B.E. *Hum. Psycopharmacol.* **1998**, *13*, 83.
[8] Lahiri, D.K.; Farlow, M.R.; Sambamurti, K.; Greig, N.H.; Giacobini, E.; Schneider, L.S. *Curr. Drug. Targets* **2003**, *4*, 97.

proteins capable of driving an early appearance of the disease have been described, namely the gene coding for the β-amyloid precursor protein (APP) on chromosome 21, preseniline-1 on chromosome 14, and preseniline-2 on chromosome 1.[9,10] Nevertheless, most of the patients suffering AD do not have familiar precedents or show any of the previously described genetic mutations.[11]

1.2 Pathogenesis of Alzheimer's disease

The etiology of AD is still incompletely understood. However, two characteristic neuropathological key events are now clearly defined, namely senile plaques and neurofibrillary tangles (NFTs), which are mainly composed of β-amyloid peptide (Aβ) and hyperphosphorylated tau protein, respectively. These two proteins seem to be at the root of the pathogenesis of the disease. Some debate exists about which of them occurs first and which one is the consequence or even if they are both consequences of the disease.[12,13,14] However, so far, the most prevailing hypothesis on the cause of AD is the so-called "*amyloid cascade hypothesis*", which points to the aggregation of Aβ into oligomers or fibrils as the key process associated with the progression of AD. This hypothesis establishes that increased production, aggregation and accumulation of Aβ in the brain triggers a cascade of neurotoxic events, which eventually leads to a widespread neuronal degeneration and to the clinical symptomatology of the dementia.[15,16,17,18]

Aβ is a 39-43 amino acid peptide generated by proteolytic cleavage from the transmembrane glycoprotein APP through the sequential action of β-secretase (BACE-1) and γ-secretase. In healthy people, APP is processed by α- and γ-secretase to give non-amyloid products that in fact show neurotrophic and neuroprotective effects, but in people suffering

[9]Goate, A.; Chartier-Harling, N.C.; Mullan, M.; Brown, J.; Crawford, F.; Fidani, L.; Giuffra, L.; Haynes, A.; Irving, N.; James, L.; Mant, R.; Newton, P.; Rooke, K.; Roques, P.; Talbot, C.; Pericak-Vance, M.; Roses, A.; Williamson, R.; Rossor, M.; Owen, M.; Hardy, J. *Nature* **1991**, *349*, 704.
[10]Sherringtone, R.; Rogaev, E.I.; Liang, Y.; Rogaeva, E.A.; Levesque, G.; Ikeda, M.; Chi, H.; Lin, C.; Li, G.; Holman, K.; Tsuda, T.; Mar, L.; Foncin, J.-F.; Bruni, A.C.; Montesi, M.P.; Sorbi, S.; Rainero, I.; Pinessi, L.; Nee, L.; Chumakov, I.; Pollen, D.; Brookes, A.; Sanseau, P.; Polinsky, R.J.; Wasco, W.; Da Silva, H.A.R.; Haines, J.L.; Perikac-Vance, M.A.; Tanzi, R.E.; Roses, A.D.; Fraser, P.E.; Rommens, J.M.; St. George-Hyslop, P.H. *Nature* **1995**, *375*, 754.
[11]Levy-Lehad, E.; Wijsman, E.M.; Nemens, E.; Anderson, A.L.; Goddard, K.A.B.; Wiltfang, J. *Brain* **2006**, *129*, 743.
[12]Klafki, H.-W.; Staufenbiel, M.; Kornhuber, J.; Wiltfang, J. *Brain* **2006**, *129*, 2840.
[13]Schönheit, B.; Zarski, R.; Ohm, T.G. *Neurobiol. Aging* **2004**, *25*, 743.
[14]Castellani, R.J.; Zhu, X.; Lee, H.-G.; Moreira, P.I.; Perry, G.; Smith, M.A. *Expert Rev. Neurother.* **2007**, *7*, 473.
[15]Hamley, I.W. *Chem. Rev.* **2012**, *112*, 5147.
[16]Goedert, M.; Spillantini, M.G. *Science* **2006**, *314*, 777.
[17]Hardy, J.; Allsop, D. *Trends Pharm. Sci.* **1991**, *12*, 383.
[18]Hardy, J. *Curr. Alzheimer Res.* **2006**, *3*, 71.

AD Aβ synthesis is increased, especially the one leading to the most insoluble form, called $Aβ_{42}$, which is also the one that shows the strongest tendency to aggregate (**Figure 1.1**).[19]

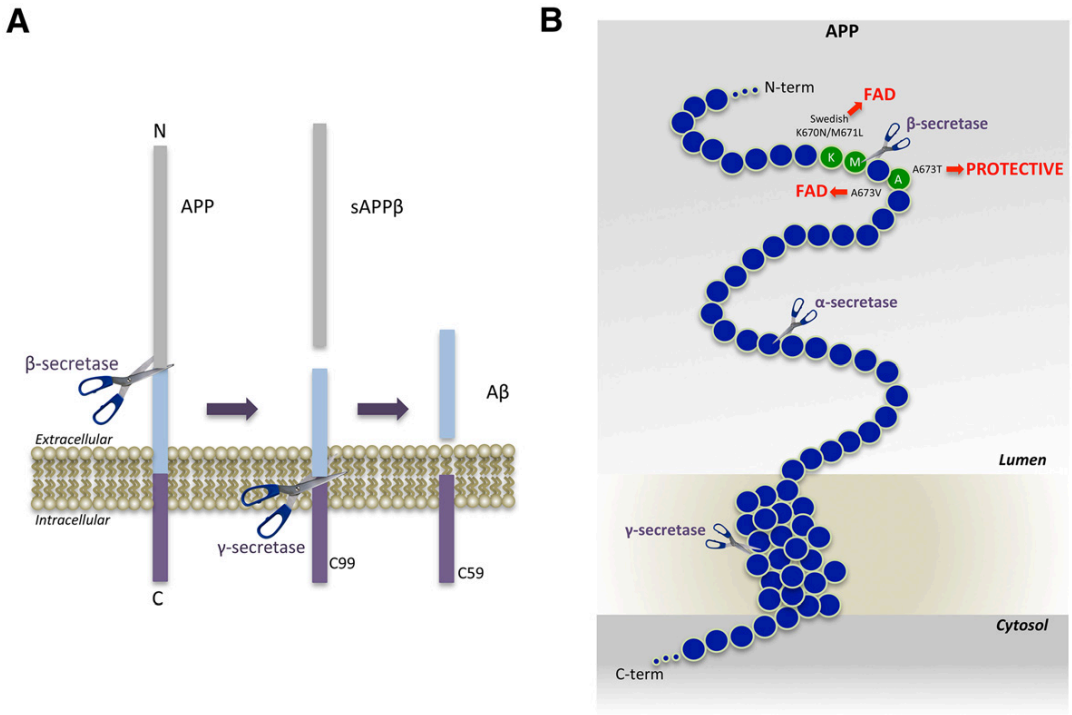

Figure 1.1 A: The β-secretase enzyme cuts APP to create the *N*-terminus of Aβ. Two APP fragments are produced: membrane-bound C99 and secreted sAPPβ ectodomain. Subsequently, C99 is cleaved by the γ-secretase enzyme to generate the *C*-terminus of Aβ. Aβ is then released into the lumen of the endosome and secreted into the extracellular medium. An intracellular domain, C59, is also produced. **B**: The amino acids in and around the Aβ domain of APP are represented as blue circles. Amino acids that affect β-secretase processing of APP in humans are green circles. The Swedish and the A673V mutations cause familial AD (FAD) by increasing β-secretase cleavage and Aβ production, while the A673T mutation protects against AD by doing the opposite. All the three mutations occur at or within one amino acid of the β-secretase cleavage site. (Image source: Vassar, R. *Alzheimers Res. Ther*. **2014**, *6*, 89).

$Aβ_{42}$, the variant preferentially implicated in AD, nucleates more rapidly, is more fibrillogenic and shows higher toxicity than $Aβ_{40}$. Early and selective deposition of $Aβ_{42}$ as well as a reduction of its clearance is observed in AD patients.[15] Fibrillar aggregated Aβ is deposited in amyloid plaques (senile plaques) in the brain of AD patients, constituting a prominent hallmark of the disease (**Figure 1.2**). Plaque-derived Aβ fibrils enhance oxidative stress and inflammation, leading to kinases and phosphatases alteration and neuronal toxicity.[20,21] Particularly, cholinergic and glutamatergic neurones are the most commonly affected by Aβ peptide neurotoxicity.

[19]Coughlan, C.M.; Breen, K.C. *Pharmacol. Ther.* **2000**, *86*, 111.
[15]Hamley, I.W. *Chem. Rev.* **2012**, *112*, 5147.
[20]Bartolini, M.; Andrisano, V. *ChemBioChem* **2010**, *11*, 1018.
[21]Citron, M. *Nat. Rev. Drug Discovery* **2010**, *9*, 387.

Senile plaques are extracellular deposits of amyloid in the grey matter of the brain. They are variable in shape and size, on the average 50 μm. In AD they are primarily composed of Aβ, however, non β-amyloid component (NAC) is also co-deposited along with Aβ in plaques.[22] NAC comprises different proteins or peptidic fragments that may act as chaperones, which in some cases may facilitate aggregation, deposition and neurotoxicity of Aβ.[19] Typical extracellular matrix proteins are also observed, such as type V collagen, entactin and laminin. Furthermore, in the central part of the plaque other proteins, such as α_1-antichymotrypsin, ubiquitin, lysosomal proteins, acetylcholinesterase (AChE), apolipoprotein E (apoE) and residues 61-95 of α-synuclein can be found.[23]

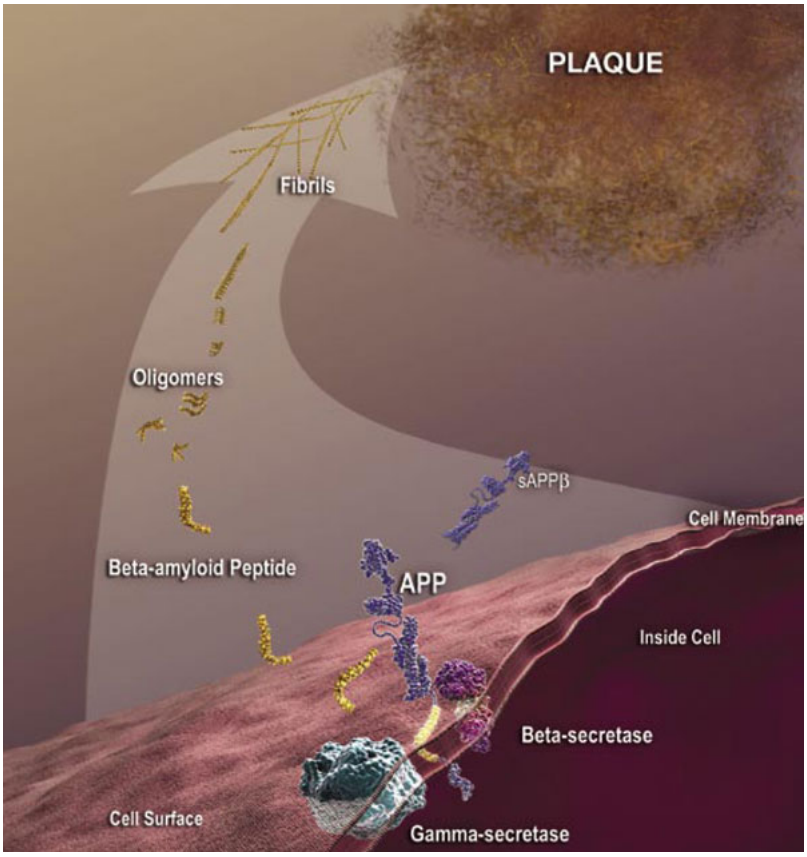

Figure 1.2 Schematic representation of *sAPPβ* aggregation into oligomers, fibrils and, finally, senile plaques. (Image source: National Institute on Aging website: https://www.nia.nih.gov/).

NFTs are aggregates of hyperphosphorylated tau protein commonly known as a primary marker of AD. They are produced inside the cell by hyperphosporylation of a microtubule-associated protein known as tau, by different kinases such as Cdk5 and GSK-3β, causing it to

[22]Bodles, A.M.; Gurthrie, D.J.S.; Greer, B.; Irvine, G.B. *J. Neurochem.* **2001**, *78*, 384.
[19]Coughlan, C.M.; Breen, K.C. *Pharmacol. Ther.* **2000**, *86*, 111.
[23]Inestrosa, N.C. *Las incomunicaciones del Alzheimer, Atenea Impresores Ltda.* **2007**.

aggregate, first as oligomers, namely paired helical filaments (PHF), and later on in an insoluble form, namely the neurofibrillary tangles.[24] Although the protein tau has been considered to have an important role in AD progression, recent discoveries point out that its processing occurs downstream of Aβ accumulation.[15]

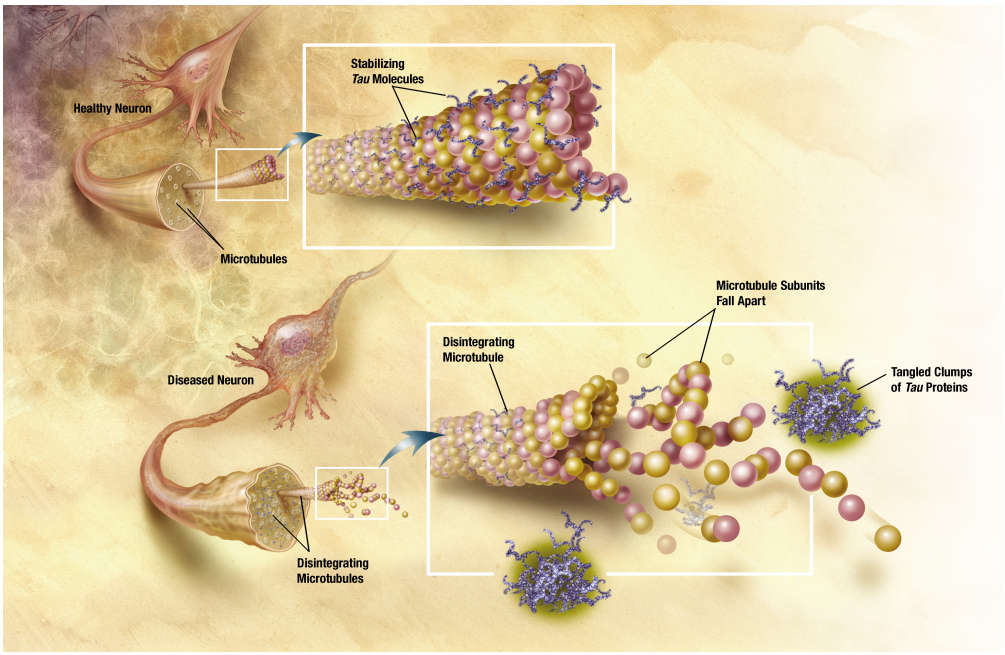

Figure 1.3 Schematic representation of how microtubules disintegrate with AD, as consequence of tau hyperphosphorylation. (Image source: National Institute on Aging: https://www.nia.nih.gov/).

1.3 Currently commercialized anti-Alzheimer drugs

The current therapeutic arsenal for AD is dominated by a group of drugs which were conceptually developed to treat the very late symptoms of dementia, mainly arising from the deficit in central nervous system (CNS) of different neurotransmitters, particularly acetylcholine (ACh). This strategy is based upon the so-called "*cholinergic hypothesis*" that connects cognitive and functional decline in AD to a lack of ACh in the CNS caused by the degeneration of the cholinergic neurons of basal nuclei, projecting their axons towards the hippocampus. Consequently, the use of cholinomimetic agents, able to compensate for this deficit, should allow the alleviation of the symptomatology of the disease.[25]

[24]Goedert, M. *Trends Neurosci.* **1993**, *16*, 460.
[15]Hamley, I.W. *Chem. Rev.* **2012**, *112*, 5147.
[25]Camps, P.; Muñoz-Torrero, D. *Mini-Rev. Med. Chem.* **2002**, *2*, 11.

Human AChE (*h*AChE) is a 583 amino acid residues protein, additionally provided with a 31 residues signal peptide, and responsible for the hydrolysis of ACh neurotransmitter (**Figure 1.4**). The reaction takes place inside the catalytic site of the enzyme (*catalytic anionic site*, CAS), localized at the bottom of a 20 Å long gorge. The CAS is constituted by a catalytic triad, consisting of residues Ser203-His447-Glu334 (Ser200-His440-Glu327 in *Torpedo californica Tc*AChE) that is responsible for the hydrolysis of the neurotransmitter, and a neighbouring anionic hydrophobic site (Trp86-Glu202-Tyr337-Tyr341-Phe338), which stabilizes the positive charge of the quaternary ammonium group of ACh and allows to position its ester group in an orientation that enables it to face the CAS. Moreover, at the mouth of this narrow gorge a secondary interaction region, namely the *peripheral anionic site* (PAS), is located, which early binds the substrate and directs it towards the CAS (**Figure 1.5**).[26]

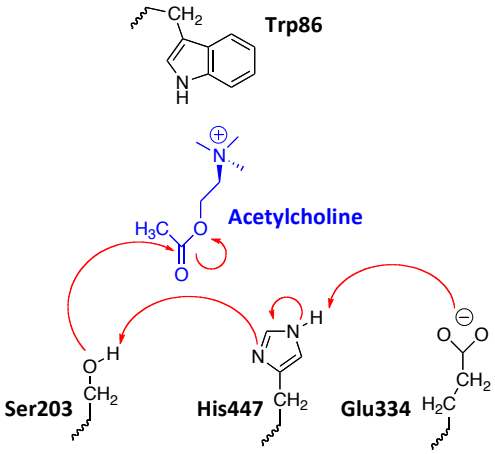

Figure 1.4 Schematic representation of the hydrolytic degradation of ACh in the CAS of AChE

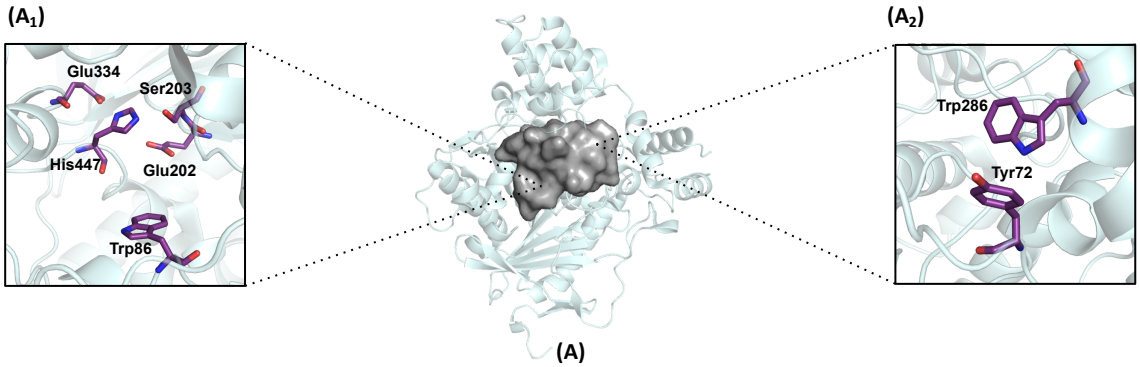

Figure 1.5 X-ray structure of the human recombinant AChE (PDB ID: 3LII) with the details of the CAS (**A_1**) and the PAS (**A_2**).

[26]Sussman, J.L.; Harel, M.; Frolow, F.; Oefner, C.; Goldman, A.; Toker, L.; Silman, I. *Science* **1991**, *253*, 872.

In healthy brains AChE hydrolyses the majority of ACh while the second cholinesterase present in human blood, namely butyrylcholinesterase (BChE), plays a secondary role. However, it is worth noting that as AD progresses, the activity of AChE decreases, while increased levels of BChE are observed in the hyppocampus and temporal cortex.[27,28] Thus, in recent years both selective and non-selective BChE inhibitors (BChEIs) have received increasing attention, since recent clinical trials have shown that patients treated with inhibitors of both AChE and BChE show minor cortical atrophic changes and attenuated loss of brain volumes.[29,30,31,32,33] These findings are consistent with the hypothesis that inhibitors of both enzymes may have neuroprotective and disease-modifying effects.[34]

1.3.1 Acetylcholinesterase inhibitors (AChEIs)

With the sole exception of the glutamate NMDA receptor antagonist memantine, **1** (marketed as Auxura® in 2002, **Figure 1.6**),[35] the other four commercialized anti-Alzheimer drugs, namely tacrine, **2** (marketed by Parke-Davis as Cognex® in 1993, **Figure 1.6**),[36,37] donepezil, **3** (marketed by Pfizer as Aricept® in 1996, **Figure 1.6**),[38,39] rivastigmine, **4** (marketed by Novartis as Exelon® in 2000, **Figure 1.6**),[40] and galantamine, **5** (marketed as Reminyl® in 2001, **Figure 1.6**),[41] are cholinomimetic agents with the pharmacological profile of AChEIs, which increase the levels of ACh at the synapse. Tacrine, donepezil and galantamine are reversible AChEIs, while rivastigmine is considered a pseudoirreversible AChEI, since it contains a carbamate group that reacts with Ser203, carbamoylating the enzyme, whose activity is slowly recovered after hydrolysis of the serine carbamate group.

[27]Fernández-Bachiller, M.I.; Pérez, C.; Monjas, L.; Rademann, J.; Rodríguez-Franco, M.I. *J. Med. Chem.* **2012**, *55*, 1303.
[28]Perry, R.H.; Blessed, G.; Tomlinson, B.E. *Neuropathol. Appl. Neurobiol.* **1978**, *4*, 273.
[29]Lane, R.M.; Potkin, S.G.; Enz, A. *Int. J. Neuropsychopharmacol.* **2006**, *9*, 101.
[30]Greig, N.; Utsuki, T.; Ingram, D.; Wang, Y.; Pepeu, G.; Scali, C.; Yu, Q.; Mamczarz, J.; Holloway, H.; Giordano, T.; Chen, D.; Furukawa, K.; Sambamurti, K.; Brossi, A.; Lahiri, D. *Proc. Natl. Acad. Sci. U.S.A.* **2005**, *102*, 17213.
[31]Venneri, A.; McGeown, W.J.; Shanks, M.F. *Neuroreport* **2005**, *16*, 107.
[32]Venneri, A.; Shanks, M.F.; Staff, R.T.; Pestell, S.J.; Forbes, K.E.; Gemmell, H.G.; Murray, A.D. *Neuroreport* **2002**, *13*, 83.
[33]Venneri, A.; Lane, R. *Neuroreport* **2009**, *20*, 285.
[34]Shanks, M.; Kivipelto, M.; Bullok, R.; Lane, R. *Curr. Med. Res. Opin.* **2009**, *25*, 2439.
[35]Lipton, S.A. *Nature* **2004**, *428*, 473.
[36]Gualtieri, F.; Due, S.; Manetti, D.; Romanelli, M.N. *Farmaco* **1995**, *50*, 489.
[37]Davis, K.L.; Thal, L.J.; Gamzu, E.R.; Davis, C.S.; Woolson, R.F.; Gracon, S.I.; Drachman, D.A.; Schneider, L.S.; Whitehouse, P.J.; Hoover, T.M. *New Engl. J. Med.* **1992**, *327*, 1253.
[38]Marx, J. *Science* **1996**, *273*, 50.
[39]Sugimoto, H.; Iimura, Y.; Yamanishi, Y.; Yamatsu, K. *J. Med. Chem.* **1995**, *38*, 4821.
[40]Polinsky, R.J. *Clin. Therap.* **1998**, *20*, 634.
[41]Sramek, J.J.; Frackiewicz, E.J.; Ctler, N.R. *Expert Opin. Invest. Drugs* **2000**, *9*, 2393.

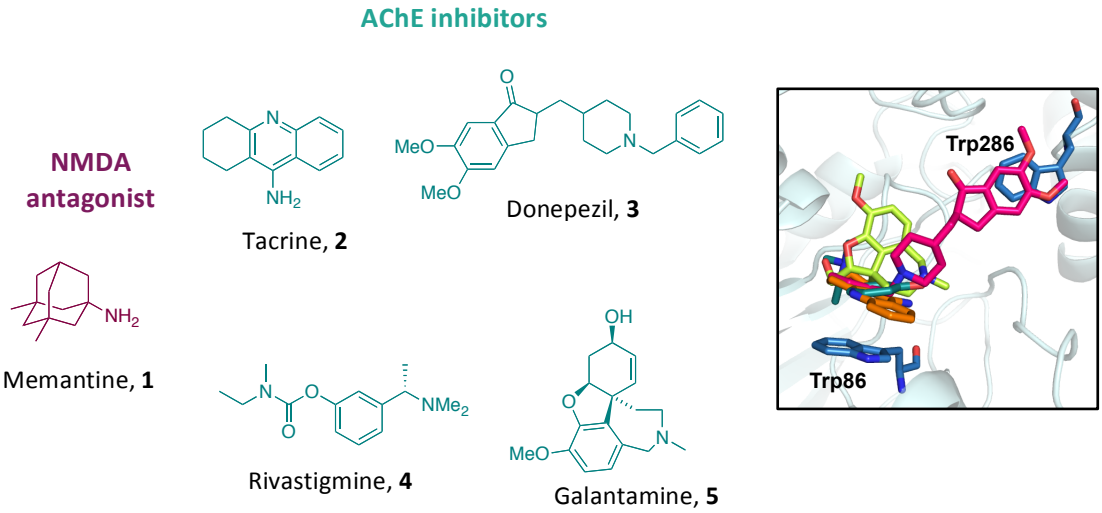

Figure 1.6 Left: Structure of the five marketed anti-Alzheimer drugs. Right: Binding mode of the four AChEIs in the gorge of AChE: tacrine, **2** (orange structure, PDB ID: 1ACJ); donepezil, **3** (magenta structure, PDB ID: 1EVE); rivastigmine, **4** (green structure, PDB ID: 1GQR); galantamine, **5** (yellow structure, PDB ID: 4EY6).

The analysis of the X-ray structures of the four commercialized AChEIs in complex with AChE pointed out that while tacrine, **2**, rivastigmine, **4**, and galantamine, **5**, do clearly interact within the active site of the enzyme, conversely donepezil, **3**, is the sole marketed AChEI exhibiting a dual-site binding mode of interaction.[42] In fact, it spans the whole length of the gorge, simultaneously interacting with both Trp86, a characteristic residue of the CAS, and Trp286 in the PAS (**Figure 1.6**).

1.3.2 Neuroprotective effects of AChEIs

AChEIs currently represent the most effective treatment to achieve a short-term (6 to 12 months) cognitive and functional improvement. They are considered as a merely symptomatic treatment, showing modest overall results and being effective in only a third part of the patients.[42] Nevertheless, over the past few years numerous preclinical, radiologic and clinical studies have evidenced a plethora of neuroprotective effects associated to the administration of AChEIs, which challenge the prevailing view of these compounds just as palliative drugs, and suggest their potential efficacy in the frame of a disease-modifying therapeutic

[42]Giacobini, E. *Neurochem. Res.* **2000**, *25*, 1185.

approach.[43,44,45,46] In particular, the blockade of the glutamate-induced excitotoxicity through antagonism of NMDA receptors,[47] the overexpression of the antiapoptotic protein bcl-2 following stimulation of $\alpha_4\beta_2$ nicotinic receptors,[48,49] and the mobilization of calcium pools from the intracellular reticulum following activation of σ_1 receptors[50,51] have been proposed among the putative mechanisms proposed to explain the neuroprotective effects of AChEIs.

1.4 Connection between cholinergic and amyloid hypotheses

Most of the above mentioned neuroprotection mechanisms involve biological targets other than AChE, thus making it difficult any structural rationalization to assist the design of novel drugs hitting these specific targets.[2] A distinct scenario is found when considering an additional neuroprotection mechanism connected with the effect of AChEIs on Aβ aggregation. As reported by Prof. N. Inestrosa (*Pontificia Universidad Católica de Chile*), AChE, which colocalizes with Aβ in the senile plaques, can bind the Aβ peptide, accelerating its aggregation and increasing its neurotoxic potential. Thus, AChE would act as a "pathological chaperone" inducing a conformational change from a non-amyloidogenic form of Aβ towards a β-sheet rich conformer provided with an increased tendency to form aggregates (**Figure 1.7**).[52,53] The macromolecular complex formed upon binding of AChE to Aβ has been found to be even more neurotoxic than Aβ fibrils alone both *in vitro* (PC12 cells and primary retina cells)[54] and *in vivo* (rat hippocampus).[55]

[43]Francis, P.T.; Nordberg, A.; Arnold, S.E. *Trends Pharmacol. Sci.* **2005**, *26*, 104.
[44]Riepe, M.W. *Eur. J. Neurol.* **2005**, *12*, 3.
[45]Geerts, H. *Brain Res. Bull.* **2005**, *64*, 519.
[46]Muñoz-Torrero, D. *Neuroprotección en la enfermedad de Alzheimer*, Edicomplet **2007**, Madrid.
[47]Wang, X.-D.; Chen, X.-Q.; Yang, H.-H.; Hu, G.;-Y. *Neurosci. Lett.* **1999**, *272*, 21.
[48]Takada-Takatori, Y.; Kume, T.; Sugimoto, M.; Katsui, H.; Sugimoto, H.; Akaike, A. *Neuropharmacology* **2006**, *51*, 474.
[49]Kihara, T.; Sawada, H.; Nakamizo, T.; Kanki, R.; Yamashita, H.; Maelicke, A.; Shimoama, S. *Biochem. Biophys. Res. Commun.* **2004**, *325*, 976.
[50]Meunier, J.; Ieni, J.; Maurice, T. *Br. J. Pharmacol.* **2006**, *149*, 998.
[51]Meunier, J.; Ieni, J.; Maurice, T. *J. Pharmacol. Exp. Ther.* **2006**, *306*, 53.
[2]Muñoz-Torrero, D. *Curr. Med. Chem.* **2008**, *15*, 2433.
[52]Inestrosa, N.C.; Alvarez, A.; Pérez, C.A.; Moreno, R.D.; Vicente, M.; Linker, C.; Casanueva, O.I.; Soto, C.; Garrido, C. *Neuron* **1996**, *16*, 81.
[53]Alvarez, A.; Alarcón, R.; Opazo, C.; Campos, E.O.; Muñoz, F.J.; Calderón, F.H.; Dajas, F.; Gentry, M.K.; Doctor, B.P.; De Mello, F.G.; Inestrosa, N.C. *J. Neurosci.* **1998**, *18*, 3213.
[54]Muñoz, F.; Inestrosa, N.C. *FEBS Lett.* **1999**, *450*, 205.
[55]Reyes, A.E.; Chacón, M.A.; Dinamarca, M.C.; Cepa, W.; Morgan, C.; Inestrosa, N.C. *Am. J. Pathol.* **2004**, *164*, 2163.

Figure 1.7 Left: Aβ aggregation in presence of bovine AChE (*b*AChE), human AChE (*h*AChE) or mouse AChE (*m*AChE), quantified according to the increase of fluorescence due to Thioflavin T, a compound that binds the β-sheets of Aβ when it is forming aggregates (Aβ 240 μM, AChE 2.4-9.6 μM, r. t., 48 h). Right: Electronic micrographies of Aβ fibrils alone or in the presence of *Tc*AChE.

The results obtained by Prof. Inestrosa were further confirmed by independent *in vivo* studies carried out by Prof. S. Brimijoin (Mayo Clinic, USA) with doubly transgenic mice expressing human APP and *h*AChE in brain, which pointed out that the simultaneous expression of human APP (and therefore Aβ) and *h*AChE resulted in clear earlier onset of amyloid plaque formation in cerebral cortex compared to singly transgenic animals expressing only human APP (30-50% sooner).[56] These evidences led to reconsider the role played by AChE in the pathogenesis of AD and to place it upstream in the neurotoxic cascade.[57] More interestingly, Inestrosa pointed out that Aβ binds a hydrophobic environment located close to the PAS of AChE. Indeed, propidium, **6**, a specific PAS-binding inhibitor, is known to inhibit (at 50 μM) by 75% the AChE-induced Aβ aggregation, while the CAS-binding inhibitor edrophonium, **7**, has no effect on Aβ aggregation at 100 μM (**Figure 1.8**).[58] Overall, these findings paved the way to the exploitation of AChE-induced Aβ aggregation inhibitors as a promising disease-modifying strategy for the treatment of AD. However, despite the outstanding Aβ antiaggregating profile displayed by propidium, **6**, *in vitro*, its cationic character precludes the entrance into the CNS, and, hence, its effectiveness as an anti-Alzheimer drug.

Taking into account the structure of AChE, where active and peripheral sites are close enough as to be simultaneously spanned by donepezil, **3**, the development of dual binding site AChEIs has strongly emerged in the last decades as a much more promising alternative to the design of selective CAS- or PAS-binding AChEIs. Accordingly, this strategy offers the advantage

[56]Rees, T.; Hammond, P.I.; Soreq, H.; Younkin, S.; Brimijoin, S. *Neurobiol. Aging* **2003**, *24*, 777.
[57]Rees, T.M.; Brimijoin, S. *Drugs Today* **2005**, *39*, 75.
[58]De Ferrari, G.V.; Canales, M.A.; Shin, I.; Inestrosa, N.C. *Biochemistry* **2001**, *40*, 10447.

of providing compounds with enhanced AChE affinity and AChE-induced Aβ antiaggregating properties, thereby being effective at the early stages of the neurodegenerative cascade.[59]

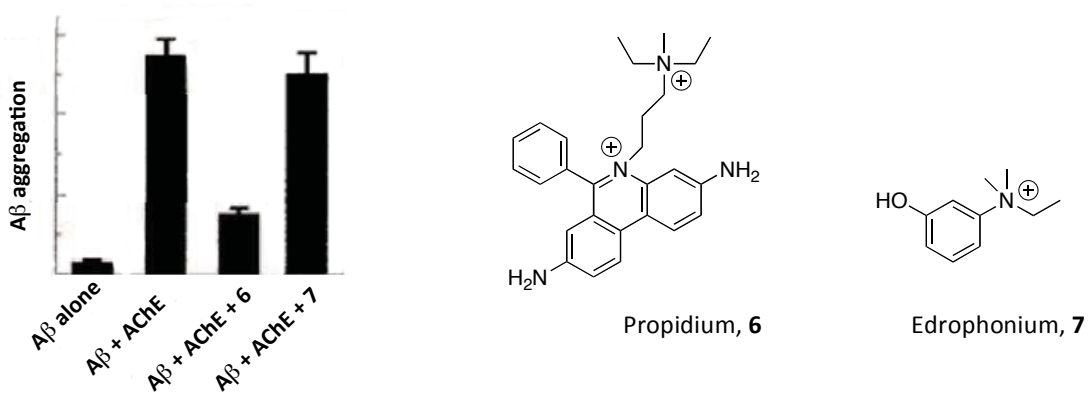

Figure 1.8 Left: Aβ aggregation alone and in the presence of AChE, propidium and edrophonium quantified according to the increase of fluorescence due to thioflavin T (Aβ 240 μM, AChE 2.4-9.6 μM, r. t., 48 h). Right: Structure of propidium, **6**, and edrophonium, **7**.

1.5 Dual binding site AChEIs

A large number of dual binding site AChEIs with a well-documented Aβ antiaggregating activity has been reported in literature so far. Among them, it is worth mentioning *bis*(7)-tacrine, **8** (*h*AChE IC_{50}: 0.40 nM; AChE-induced Aβ antiaggregating activity: 68% at 100 μM),[60,61,62] the donepezil-coumarine derivative AP2238, **9** (*h*AChE IC_{50}: 45 nM; AChE-induced Aβ antiaggregating activity: 35% at 100 μM),[63] the tacrine-indole hybrid **10** (*h*AChE IC_{50}: 20 pM; AChE-induced Aβ antiaggregating activity: 96% at 100 μM),[64] and memoquine, **11** (*h*AChE IC_{50}: 1.55 nM; AChE-induced Aβ antiaggregating activity: 87% at 100 μM) (**Figure 1.9**).[65]

[59]Castro, A.; Martínez, A. *Curr. Pharm. Design* **2006**, *12*, 4377.
[60]Pang, Y.-P.; Quiram, P.; Jelacic, T.; Hong, F.; Brimijoin, S. *J. Biol. Chem.* **1996**, *271*, 23646.
[61]Carlier, P.R.; Han, Y.F.; Chow, E.S.-H.; Li, C.P.-L.; Wang, H.; Lieu, T.X.; Wong, H.S.; Pang, Y.-P. *Bioorg. Med. Chem.* **1999**, *7*, 351.
[62]Bolognesi, M.L.; Cavalli, A.; Valgimigli, L.; Bartolini, M.; Rosini, M.; Andrisano, V.; Recanatini, M.; Melchiorre, C. *J. Med. Chem.* **2007**, *50*, 6446.
[63]Piazzi, L.; Rampa, A.; Bisi, A.; Gobbi, S.; Belluti, F.; Cavalli, A.; Bartolini, M.; Andrisano, V.; Valenti, P.; Recanatini, M. *J. Med. Chem.* **2003**, *46*, 2279.
[64]Muñoz-Ruiz, P.; Rubio, L.; García-Palomero, E.; Dorronsoro, I.; del Monte-Millán, M.; Valenzuela, R.; Usán, P.; de Austria, C.; Bartolini, M.; Andrisano, V.; Bidon-Chanal, A.; Orozco, M.; Luque, F.J.; Medina, M.; Martínez, A. *J. Med. Chem.* **2005**, *48*, 7223.
[65]Cavalli, A.; Bolognesi, M.L.; Capsoni, S.; Andrisano, V.; Bartolini, M.; Margotti, E.; Cattaneo, A.; Recanatini, M.; Melchiorre, C. *Angew. Chem. Int. Ed.* **2007**, *46*, 3689.

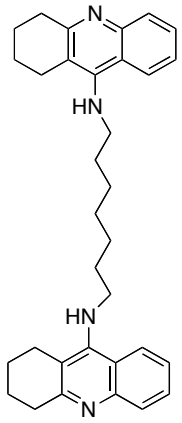

Bis(7)-tacrine, **8**

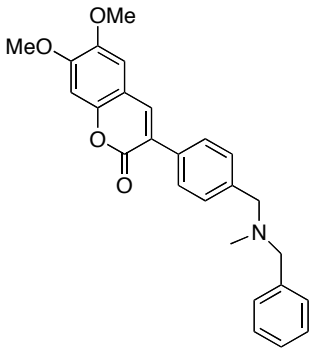

AP2238, **9**

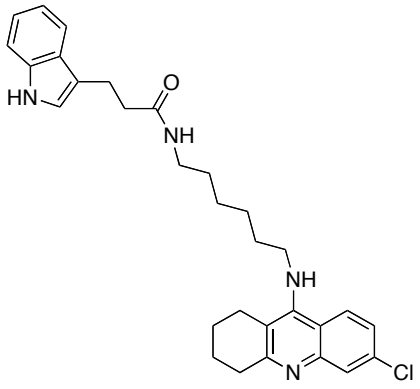

10

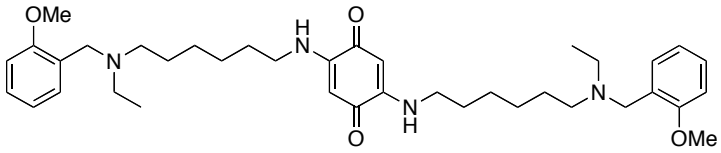

Memoquine, **11**

Figure 1.9 Structure of some dual binding site AChEIs.

1.5.1 Dual binding site AChEIs developed in our research group

About 15 years ago Profs. P. Camps and D. Muñoz-Torrero (*Universitat de Barcelona*, Spain) reported a novel class of potent CAS-binding AChEIs referred to as huprines.[66] Since then, several families of huprine- and tacrine-based dual binding site AChEIs displaying Aβ antiaggregating effect have been developed in our research group. Among the most recent efforts, it is worth noting the development of two series of 6-chlorotacrine-based compounds hybridized with a pyrano[3,2-*c*]-quinoline scaffold, reminiscent of the PAS-binding inhibitor propidium, **6** (**Figure 1.10**). Particularly, compound **13** retained the AChE inhibitory activity of the parent 6-chorotacrine, **12**, (IC_{50} 7.03 nM), while exhibiting *in vitro* inhibitory activity towards the AChE-induced (28.6% inhibition at 100 μM) and self-induced Aβ aggregation (21.5% inhibition at 50 μM), and towards BACE-1 (18.5% inhibition at 2.5 μM concentration of inhibitor), thus making it a suitable lead amenable to further optimizations.[67]

[66]Camps, P.; El Achab, R.; Görbig, D.M.; Morral, J.; Muñoz-Torrero, D.; Badia, A.; Baños, J.E.; Vivas, N.M.; Barril, X.; Orozco, M.; Luque, F.J. *J. Med. Chem.* **1999**, *42*, 3227.
[67]Camps, P., Formosa, X.; Galdeano, C.; Gómez, T.; Muñoz-Torrero, D.; Ramírez, L.; Gómez, E.; Isambert, N.; Lavilla, R.; Badia, A.; Clos, M.V.; Bartolini, M.; Mancini, F.; Andrisano, V.; Arce, M.P.; Rodríguez-Franco, M.I.; Huertas, O.; Dafni, T.; Luque, F.J. *J. Med. Chem.* **2009**, *52*, 5365.

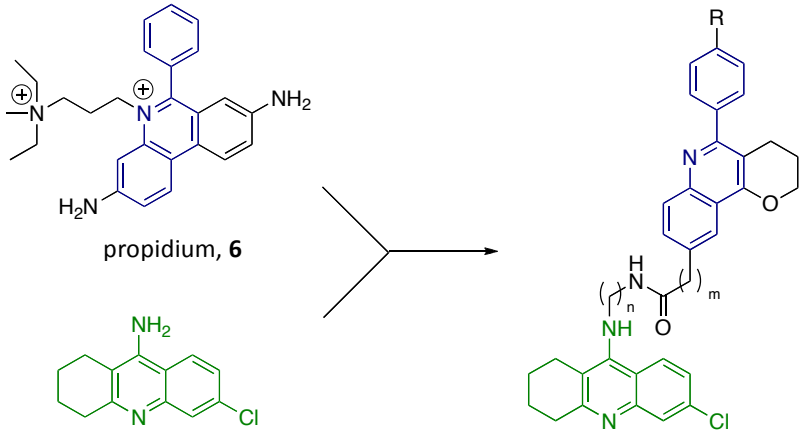

Figure 1.10 Structure of propidium, **6**, and general structure of the pyrano [3,2-*c*]quinoline-6-chlorotacrine hybrids **I** developed in our research group.

1.6 New hopes for treatment of Alzheimer's disease

1.6.1 Aβ-directed strategies

In the last years, important efforts have been made to develop anti-Alzheimer drugs capable of modifying the progression of the disease through inhibition of the formation and aggregation of Aβ.[68,69] However, clinical trials carried out with different Aβ-directed agents have been quite disappointing. As exemplifying cases, clinical trials carried out with vaccine AN1792 and tramiprostat, an Aβ aggregation inhibitor, were discontinued due to safety and efficacy issues. In spite of these failures, other drug candidates are pursued, such as the second generation Aβ-directed vaccines with a better safety profile compared to AN1792, namely CAD-106 (Novartis) (phase II clinical trials) and V-950 (Merk) (phase II clinical trials completed in Jan. 2012), anti-Aβ monoclonal antibodies such as LY2062430 (Eli Lilly) (phase III clinical trials),[70] BACE-1 inhibitors, such as CTS-21166 (CoMentis) (phase I clinical trials).[71]

Among the Aβ-directed strategies, BACE-1 constitutes a prime therapeutic target, as it is involved in the initial and rate-limiting step of the proteolytic cleavage of APP to Aβ.[72] BACE-1

[68]Melnikova, I. *Nat. Rev. Drug Discovery* **2007**, *6*, 341.
[69]Skovronsky, D.M.; Lee, V.M.-Y.; Trojanowski, J.Q. *Annu. Rev. Pathol. Mech. Dis.* **2006**, *1*, 151.
[70]Chiang, K.; Koo, E.H. *Annu. Rev. Pharmacol. Toxicol.* **2014**, *54*, 381.
[71]Vassar, R. *Alzheimers Res. Ther.* **2014**, *6*, 89.
[72]De Strooper, B.; Vassar, R.; Golde, T. *Nat. Rev. Neurol.* **2010**, *6*, 99.

is a membrane-associated, pepsin-like aspartic protease whose active site is a hydrophilic 20 Å long cavity of nearly 1000 Å^3. Two characteristic aspartic acid residues, namely Asp32 and Asp228, are responsible for the hydrolytic cleavage of the substrate inside the binding cleft, which results partially covered by a highly flexible antiparallel hairpin-loop, referred to as the "*flap*" (**Figure 1.11**).[73]

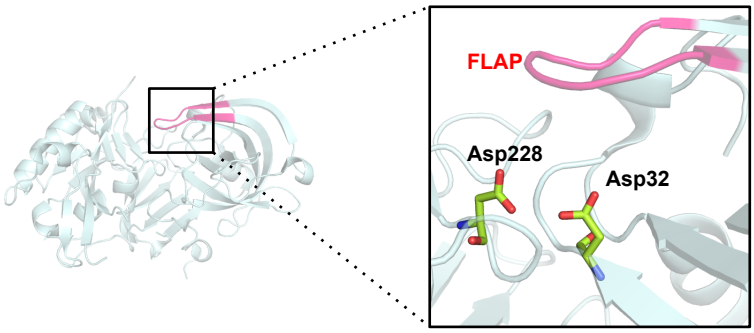

Figure 1.11 X-ray structure of BACE-1 (PDB ID: 1SGZ) with the details of the catalytic anionic dyad.

A series of issues have limited so far the successful development of effective BACE-1 inhibitors. In first instance, BACE-1 has several substrates other than APP, thereby its complete inhibition might lead to serious side effects. Particularly, some subtle effects on both peripheral and central myelin formation have been associated to administration of BACE-1 inhibitors.[74] However, the partial inhibition of BACE-1 has been proposed to overcome the side effects arising from a complete enzymatic inhibition. In fact, heterozygous BACE-1 knockout APP transgenic mice with only 15% reduction of brain Aβ show a dramatic decrease in brain amyloid burden at old age.[75] Secondly, although highly active *in vitro* peptide inhibitors, such as the transition state analogue OM99-2 (K_i 1.6 nM), have been reported, their poor pharmacokinetics limits the effectiveness as drug candidates.[76] On the other hand, the situation does not improve when the chemical space spanned by small molecules is considered. Thus, among the few BACE-1 inhibitors currently in clinical trials, only AZD3293

[73]Kacker, P.; Bottegoni, G, Cavalli, A. *Curr. Med. Chem.* **2012**, *19*, 6095.
[74]Willem, M., Garratt, A.N.; Novak, B.; Citron, M., Kaufmann, S.; Rittger, A.; De Strooper, B.; Saftig, P.; Birchmeier, C.; Haass, C. *Science* **2006**, *314*, 664.
[75]McConlogue, L.; Buttini, M.; Anderson, J.P.; Brigham, E.F.; Chen, K.S.; Freedman, S.B.; Games, D. Johnson-Wood, K.; Lee, M.; Zeller, M.; Liu, W.; Motter, R.; Sinha, S. *J. Biol. Chem.* **2007**, *282*, 26326.
[76]Hong, L.; Koelsch, G.; Lin, X.; Wu, S.; Terzyan, S.; Ghosh, A.K.; Zhang, X.C.; Tang, J. *Science* **2000**, *290*, 150.

and MK-8931 have reached the phase II/III.[71] Therefore, novel small molecule BACE-1 inhibitors able to cross the blood-brain barrier (BBB) are urgently needed.

1.6.2 Neurofibrillary tangles-directed strategies

Although hyperphosphorylated tau is a primary component of NFTs, the amyloid cascade hypothesis relegated it to a secondary role in AD pathogenesis. However, interest in developing tau therapeutics is now rising partly because of the unsuccessful trials of compounds targeting Aβ.[70] Hence, therapeutic strategies relying on downstream effectors of Aβ might be critical for halting disease progression once Aβ or Aβ-initiated abnormalities are already apparent, assuming that the effectors are responsible for a significant portion of the neurodegenerative phenotype and that ongoing deterioration is dependent on their continued presence. Among the major tau kinases, glycogen synthase kinase 3 (GSK-3) has been implicated in Aβ production, suggesting that GSK-3 inhibition may affect neurodegeneration on multiple fronts.[77] However, the sheer number of both phosphorylated tau residues and tau kinases have made it difficult to ascertain those that are pathologically relevant, and the off-target challenges stemming from kinase promiscuity justify the small amount of kinase inhibitors which moved beyond the preclinical stage.

1.6.3 Monoamine oxidase-directed strategies

Although the cholinergic deficit underlies the loss of cognitive functions in AD patients, other neurotransmission pathways, such as the serotoninergic and noradrenergic ones, are thought to be involved in the symptomatology of the disease.[78,79] In particular, the modulation of the monoamine oxidase (MAO) activity contributes to restore the physiological monoaminergic transmission.

MAO is a mitochondrial flavoenzyme that catalyzes the oxidative deamination of biogenic amines. The binding site consists of a gorge connecting the protein surface with the Flavin Adenin Dinucleotide (FAD) cofactor. At the mouth of the gorge a hydrophobic region of 290 $Å^3$

[71]Vassar, R. *Alzheimers Res. Ther.* **2014**, *6*, 89.
[70]Chiang, K.; Koo, E.H. *Annu. Rev. Pharmacol. Toxicol.* **2014**, *54*, 381.
[77]Martínez, A.; Castro, A.; Dorronsoro, I.; Alonso, M. *Med. Res. Rev.* **2002**, *22*, 373.
[78]Dringenberg, H.C. *Behav. Brain Res.* **2000**, *115*, 235.
[79]Garcia-Alloza, M.; Gil-Bea, F.J.; Diez-Ariza, M.; Chen, C.P.L.H.; Francis, P.T.; Lasheras, B.; Ramirez, M.J. *Neuropsychologia* **2005**, *43*, 442.

is located, whose entrance is partially obstructed by the loop between residues 99-112.[80] The catalytic site is located in a deeper region of the gorge and consists of a highly hydrophobic cavity of about 400 Å^3. Between the mouth region and the catalytic site, several crucial *bottleneck* residues have been individuated, playing a key role in the substrate selectivity towards the two isoforms of the enzyme, a fact that has to be carefully taken into account in the development of MAO inhibitors in order to avoid the serious "cheese" side effects deriving from the unspecific MAO-A inhibition (**Figure 1.12**).[81]

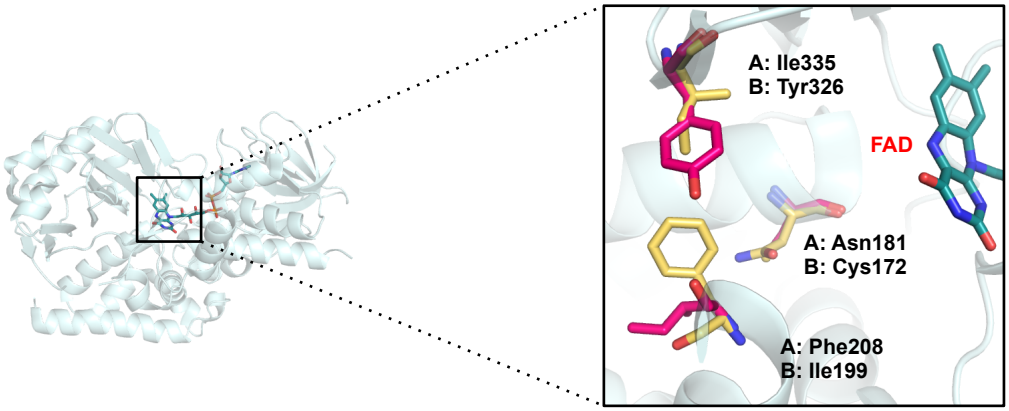

Figure 1.12 X-ray structure of MAO with the details of the main differences between the binding sites of MAO-A and MAO-B (PDB IDs: 2BYB and 2BXR).

It has been reported that MAO-B activity increases with age and high concentrations of this protein have been observed at the senile plaques.[82] Moreover, MAO-B produces hydrogen peroxide when carrying out the oxidative deamination of endogenous amines, suggesting its possible implication in the production of reactive oxygen species (ROS) and the oxidative stress associated to AD.[83] In this frame, selective MAO-B inhibitors, such as selegiline, **13**, and rasagiline, **14**, have been reported as potential anti-Alzheimer candidates (**Figure 1.13**).[84]

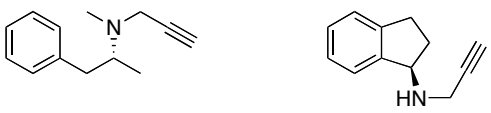

Selegiline, **13** Rasagiline, **14**

Figure 1.13 Structure of some selective MAO-B inhibitors.

[80]Binda, C.; Newton-Vinson, P.; Hubálek, F.; Edmondson, D.E.; Mattevi, A. *Nat. Struct. Biol.* **2002**, *9*, 22.
[81]Youdim, M.B.H.; Weinstock, M. *Neurotoxicology* **2004**, *25*, 243.
[82]Carreiras, M.C.; Marco, J.L. *Curr. Pharm. Des.* **2004**, *10*, 3167.
[83]Good, P.F.; Werner, P.; Hsu, A.; Olanow, C.W.; Perl, D.P. *Am. J. Pathol.* **1996**, *149*, 21.
[84]Ebadi, M.; Sharma, S.; Shavadi, S. El Refakey, K. *J. Neurosci. Res.* **2002**, *67*, 285.

1.7 Multitarget-directed ligands (MTDLs) strategy

The complexity of AD remarks the limitations of the classical approach in drug design, consisting of optimizing the interaction between a drug and a single biological target. Hence, the multifactorial nature of AD has led to the concept that an effective drug should be able to exert effect on multiple targets. Thus, in opposition to the traditional "one target-one disease" paradigm, in the last years drug discovery has been oriented towards the development of therapeutic interventions able to hit different biological targets (polypharmacology).[85,86,87,88,89] The most traditional strategy consists of resorting to cocktails of drugs, whose benefits, unfortunately, may not match with an acceptable patient compliance. Recently, there has been a move towards multicomponent drugs or fixed-dose combinations where two or more agents are co-formulated in a single pill to improve patient compliance. Nevertheless, a complex host of risks is connected with multicomponent drugs, spreading from high likelihood of drug-drug interactions to differences in the relative rates of metabolism between patients, which can produce highly complex pharmacokinetic/pharmacodynamics relationships, as well as possible formulation issues.[90] As an alternative, a novel strategy consists of developing a single chemical entity capable of modulating multiple targets simultaneously. Compared to multicomponent drugs, the multitarget drug approach has a positive risk-benefit profile as it is devoid of drug-drug interaction issues. However, the main challenge associated to this strategy is achieving properly balanced activities at different targets and stages of the disease.[89,90]

In the context of anti-Alzheimer drug discovery, research efforts have gradually shifted towards this latter approach, aimed at simultaneously hitting those biological targets involved in the mechanisms that drive the progression of the disease. Some eminent examples of successful application of the MTDLs strategy are depicted below (**Figure 1.14**).[91,92,93,65]

[85]Hopkins, A.L. *Nat. Chem. Biol.* **2008**, *4*, 682.
[86]Hopkins, A.L. *Nat. Biotechnol.* **2007**, *25*, 1110.
[87]Janga, S.C.; Tzakos, A. *Mol. BioSyst.* **2009**, *5*, 1536.
[88]Bianchi, M.T. *Medical Hypotheses* **2010**, *74*, 297.
[89]Viayna, E.; Sola, I., Di Pietro, O. Muñoz-Torrero, D. *Curr. Med. Chem.* **2013**, *20*, 1623.
[90]Morphy, R.; Rankovic, Z. *J. Med. Chem.* **2005**, *48*, 6523.
[91]Viayna, E.; Sola, I.; Bartolini, M.; De Simone, A., Tapia-Rojas, C.; Serrano, F.; Sabaté, R.; Juárez-Jiménez, J.; Pérez, B.; Luque, F.J.; Andrisano, V.; Clos, M.V.; Inestrosa, N.C.; Muñoz-Torrero, D. *J. Med. Chem.* **2014**, *57*, 2549.
[92]Sterlig, J.; Herzig, Y.; Goren, T.; Finkelstein, N.; Lerner, D.; Goldenberg, W.; Miskolczi, I.; Molnar, S.; Rantal, F.; Tamas, T.; Toth, G.; Zagyva, A.; Zekany, A.; Finberg, J.; Lavian, G.; Gross, A.; Friedman, R.; Razin, M.; Huang, W.; Krais, B.; Chorev, M.; Youdim, M.B.; Weinstock, M. *J. Med. Chem.* **2002**, *45*, 5260.
[93]Farina, R.; Pisani, L.; Catto, M.; Nicolotti, O.; Gadaleta, D.; Denora, N.; Soto-Otero, R.; Mendez-Alvarez, E.; Passos, C.S.; Muncipinto, G.; Altomare, C.D.; Nurisso, A.; Carrupt, P.-A.; Carotti, A. *J. Med. Chem.* **2015**, *58*, 5561.
[65]Cavalli, A.; Bolognesi, M.L.; Capsoni, S.; Andrisano, V.; Bartolini, M.; Margotti, E.; Cattaneo, A.; Recanatini, M.; Melchiorre, C. *Angew. Chem. Int. Ed.* **2007**, *46*, 3689.

Multipotent inhibitors
AChE/BACE-1

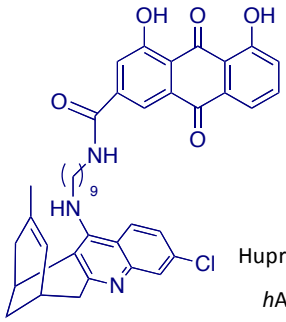

Huprine-rhein hybrid, **15**

*h*AChE IC_{50} 2.39 nM
BACE-1 IC_{50} 80 nM

Multipotent inhibitor
AChE/MAO-B

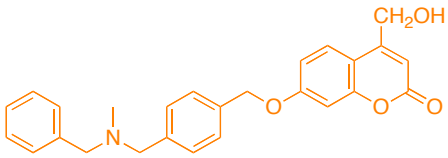

2*H*-Chromen-2-one derivative, **16**

*h*AChE IC_{50} 120 nM
MAO-B IC_{50} 10 nM

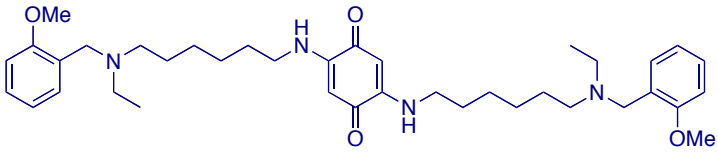

Memoquine, **11**

*h*AChE IC_{50} 1.55 nM
BACE-1 IC_{50} 108 nM

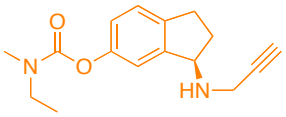

Ladostigil, **17**

*in vitro h*AChE IC_{50} 52.4 µM
25-40% ChE inhibition after oral administration of 35-100 µmol/kg
in vitro MAO-B IC_{50} 37.1 µM
80% MAO-A and -B inhibition after daily oral administration of 75 µmol/kg for 2 weeks

Figure 1.14 Structure of some multitarget anti-Alzheimer agents.

2 Introduction to Neglected Tropical Diseases

Chapter

2.1 Neglected Tropical Diseases (NTDs)

Neglected tropical diseases (NTDs) are an heterogeneous group of infectious diseases caused by parasites, viruses and bacteria, affecting over one billion people worldwide (**Figure 2.1**) and estimated to cause 534,000 death annually.[94]

The World Health Organization (WHO) has currently identified 17 core NTDs: dengue, rabies, tracoma, buruli ulcer, endemic treponematoses, leprosy, Chagas disease, human African trypanosomiasis (HAT), leishmaniasis, taeniasis/cisticercosis, dracunculiasis, echinococcosis, food-borne trematodiases, lymphatic filariasis, onchocerciasis, schistosomiasis, and soil-transmitted helminthiases.[95]

NTDs represent a leading cause of morbidity and mortality in developing countries, where poor sanitary and enviromental conditions, inadequate nutrition, educational deficiences and undeveloped public health care systems lead to high risks of contracting infections. Further exacerbating the impact of NTDs on human and economic development activity is the huge host of NTD-associated disabilities,[96,97,98] spreading from impaired physical and cognitive development to paralysis. Thus, it is extimated that 57 million disability adjusted life-years (DALYs) are lost every year due to these diseases.[99] These factors all together contribute to catch infected individuals and their communities in a health-related "poverty trap", which has been often associated with societal disruptions, political instability and destabilization of local communities.[100]

Despite the huge impact in the society and the serious socio-economic cost put into play, historically NTDs have collectively attracted much lower research investment that "first world diseases". Between 1975 and 1999 only 1% of the new drugs introduced were specifically for NTDs, while central nervous system (CNS) and cardiovascular diseases accounted for 15% and 12%, respectively, of the new drugs introduced in this period.[101] However, a significant improvement in drug discovery efforts has been recently registered in

[94]Centre for Disease Control and Prevention, Neglected Tropical Diseases, http://www.cdc.gov/globalhealth/ntd/, accessed 4th April 2015.
[95]World Health Organization, Neglected Tropical Diseases, http://www.who.int/neglected_diseases/diseases/en/, accessed 4th April 2015.
[96]McMichael, A.J. *Philos. Trans. R. Soc. Lond. B Biol. Sci.* **2004**, *359*, 1049.
[97]De Silva, N.R.; Brooker, S.; Hotez, P.J.; Montresor, A.; Engels, D.; Savioli, L. *Trends Parasitol.* **2003**, *19*, 547.
[98]Mackey, T.K.; Liang, B.A.; Cuomo, R.; Hafen, R.; Brouwer, K.C.; Lee, D.E. *Clinic. Microb. Rev.* **2014**, *27*, 949.
[99]WHO. **2013**. Sustaining the drive to overcome the global impact of neglected tropical diseases. World Health Organization, Geneva, Switzerland, http://www.who.int/en/.
[100]Hotez, P.J., Pecoul, B. 2010. *PLoS Negl. Trop. Dis.* **2010**, *4*, 718.
[101]Trouiller, P.; Olliaro, P.; Torreele, E.; Orbinski, J.; Laing, R.; Ford, N. *Lancet* **2002**, *359*, 2188.

this field, since 4% of new drugs in the last 10 years has been developed for NTDs, a number which is projected to be duplicated in the next 10 years.[102,103]

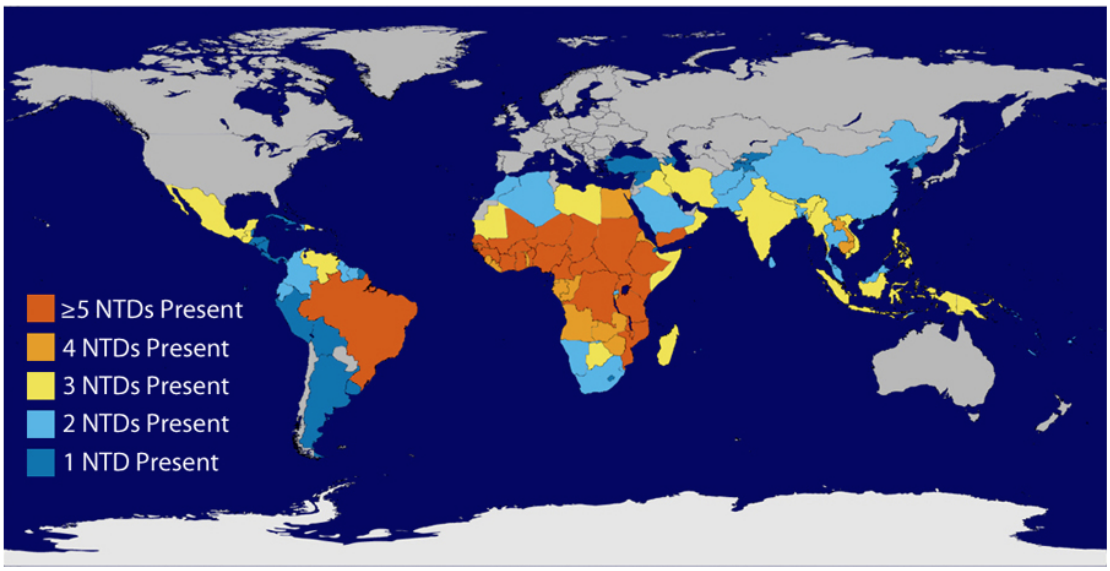

Figure 2.1 Map illustrating geographical prevalence of NTDs: guinea worm, lymphatic filariasis, onchocerciasis, schistosomiasis, soil-transmitted helminthes, and tracoma. [Source: Centers for Disease Control and Prevention (www.cdc.gov)].

2.2 Parasitic protozoan NTDs

2.2.1 Human African trypanosomiasis (HAT)

HAT, also known as "*sleeping sickness*", is a protozoan disease currently endemic in 36 countries throughout sub-Saharan Africa, and estimated to afflict near to 30,000 human beings per year.[104, 105]

HAT is caused by infection with the protozoan parasites *Trypanosoma brucei gambiense*, located in West and Central Africa, and *T.b. rhodesiense*, found in East and Southern Africa.[106] When an infected tsetse fly takes a blood meal, trypanosomes are inoculated into the host (**Figure 2.2**). Over the following few weeks, during the so called first or hemolymphatic stage, the parasites multiply within the lymphatic and vascular system producing nonspecific clinical

[102]Pedrique, B.; Sturb-Wourgaft, N.; Some, C.; Olliaro, P.; Trouiller, P.; Ford, Pécoul, B.; Bradol, J.-H. *Lancet Global Health* **2013**, *1*, 371.
[103]Njoroge, M.; Njuguna, N.M.; Mutai, P.; Ongarora, D.S.B.; Smith, P.W.; Chibale, K. *Chem. Rev.* **2014**, *114*, 11138.
[104]Simarro, P.P.; Diarra, A.; Ruiz Postigo, J.A.; Franco, J.R.; Jannin, J.G. *PLoS Negl. Trop. Dis.* **2011**, *5*, 1007.
[105]Jones, A.J.; Avery, V.M. *Expert Opin. Drug Discov.* **2013**, *8*, 495.
[106]Pepi, J.; Meda, H.A. *Adv. Parasitol.* **2001**, *49*, 71.

symptoms in the patient such as headache, fever, nausea, and lymphedema.[107,108] If not treated adequately, the parasites invade the CNS. Then, the infection evolves to the second or CNS stage characterized by a host of symptoms including hand tremors, mental disturbances, anxiety, hallucinations and manic episodes.[109,110] However, the most indicative feature of CNS HAT is represented by the periods of daytime somnolence alternated to night-time insomnia.[111,112] Depending on the infecting subspecies, substantial differences in the time frame between the first and the second stage of the disease are reported. Indeed, *T.b. rhodesiense* is responsable for an acute infection which can progress from the first to the second stage of the disease in a matter of weeks. Conversely, *T.b. gambiense* produces a chronic infection, thus many months to years can pass before developing the CNS disease.

Due to the limited therapeutic arsenal currently available, associated with prolonged administration schedules and severe side effects, the prognosis is almost always lethal.

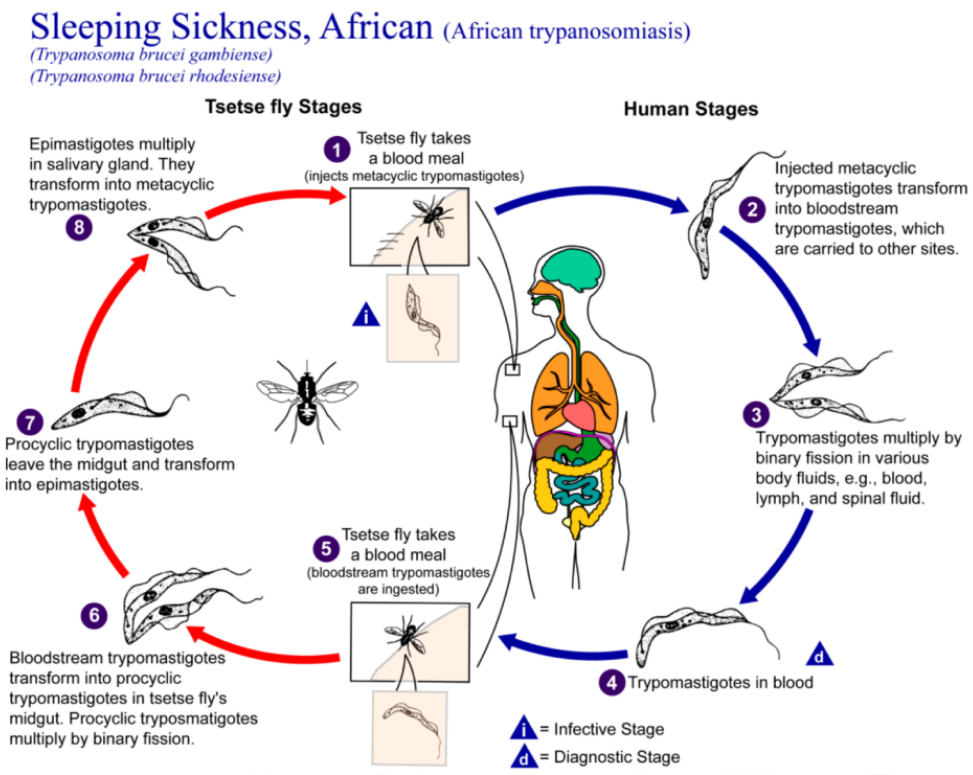

Figure 2.2 Infection cycle of human African trypanosomiasis (Source: Public Health Image Library, provided by CDC-DPDx, Alexander J. Da Silva and Melanie Moser).

[107] Vickerman, K. *Br. Med. Bull.* **1985**, *41*, 105.
[108] Apted, F.I.C.; Mulligan, H.W. George Allen and Unwin LTD, London, **1970**, 661.
[109] Atouguia, J.L.M.; Kennedy, P.G.E.; Davis, L.E. Butterworth-Heinemann, Oxford, **2000**, 321.
[110] Gelfan, M. *Trans. R. Soc. Trop. Med. Hyg.* **1947**, *41*, 255.
[111] Lundkvist, G.B.; Kristensson, K.; Bentivoglio, M. *Physiology* **2004**, *19*, 198.
[112] Bentovoglio, M.; Grassi-Zucconi, G.; Olsson, T.; Kristensson, K. *Trends Neurosci*. **1994**, *17*, 325.

2.2.1.1 Current treatment of HAT

Hemolymphatic *T.b. gambiense* and *T.b. rhodesiense* infections are treated by parental administration of pentamidine, **18**, and suramin, **19**, respectively. Both drugs are generally well tolerated; only minor adverse reactions, including mild proteinurea, nausea, vomiting, fever, exfoliative dermatitis, leucopenia and hypoglycemia have been reported.[113, 114, 115] Nevertheless, none of them is capable of crossing the blood-brain barrier (BBB), thus precluding any possible indication for CNS-stage HAT infection.

The available therapeutic arsenal for treatment of CNS-stage infection is formed by three main drugs: melarsoprol, **20**, eflornithine, **21**, and nifurtimox, **22** (**Figure 2.3**). Administration of the trivalent arsenical melarsoprol is associated with many adverse reactions, with the most serious one being a post-treatment reactive encephalopathy (PTRE) that results fatal in 5% of the cases.[116] A much better tolerated and safer drug, originally developed as an antineoplastic agent, eflornithine, was discovered in the late 1980s.[117] In order to reduce its complicated administration schedule, not feasible in the majority of hospitals in which HAT patients are treated, eflornithine monotherapy was then substituted by the equally effective nifurtimox/eflornithine combination therapy (NECT).[118, 119] Unfortunately, since this combination has not been evaluated against *T.b. rhodesiense*, melarsoprol still remains the only treatment option for patients infected by this subspecies.

Hence, new, effective, nontoxic, and ideally orally available treatment options are desperately needed to turn into reality the challenge of eliminating HAT, as a public health problem, by 2020.

[113] Apted, F.I.C.; Mullerhorvath, R. George Allen and Unwin Ltd, London, **1970**, 684.
[114] Burri, C.; Stich, A.; Brun, R. CABI Publishing, Trowbridge, **2004**, 403.
[115] WHO. Control and surveillance of African trypanosomisis. World Health Organization, Geneve, **1998**.
[116] Pepin, J.; Milord, F. *Adv. Parasitol.* **1994**, *33*, 1.
[117] Bacchi, C.J.; Nathan, H.C.; Hutner, S.H. *Science* **1980**, *210*, 332.
[118] Priotto,G.; Kasparian, S.; Ngouama, D. *et al. Lancet* **2009**, *374*, 56.
[119] Priotto, G.; Kasparian, S.; Ngouama, D. *et al. Clin. Infect. Dis.* **2007**, *45*, 1435.

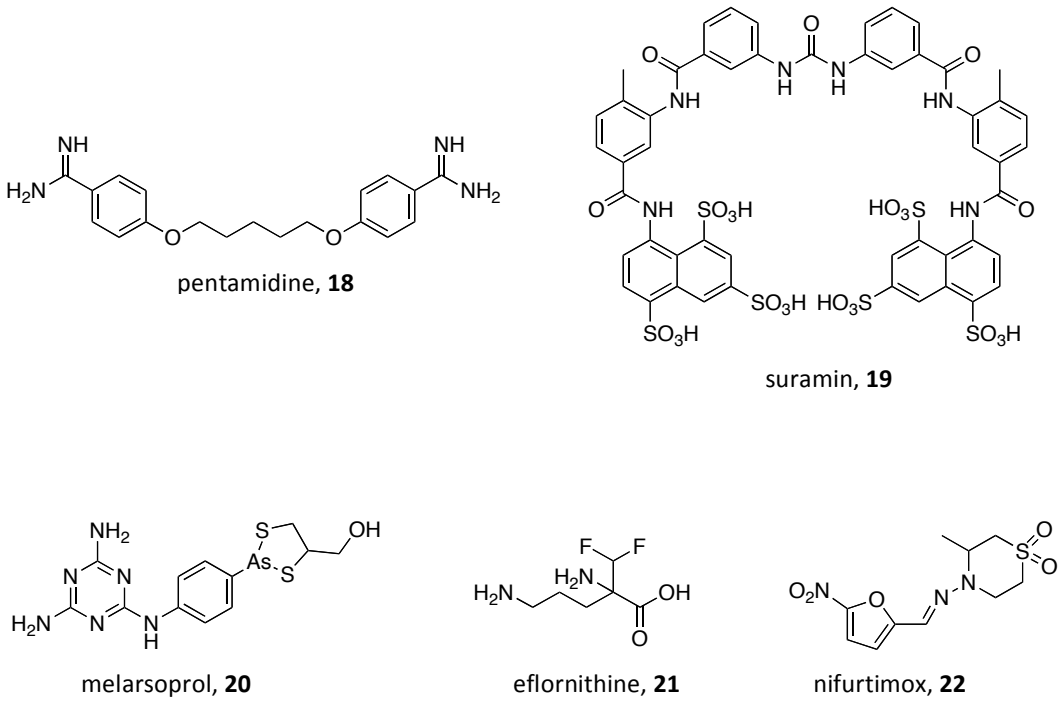

Figure 2.3 Drugs currently used in the treatment of HAT.

2.2.2 Chagas disease

Chagas disease, also known as American trypanosomiasis, is a chronic, systemic infection caused by the protozoan parasite *Trypanosoma cruzi*. The disease, impacting 8 million people worldwide, is endemic in the poor areas of Latin America where is responsable for significant economic losses due to early-age mortality and disability.[120, 121, 122] The life cycle of *T. cruzi* is characterized by a succession of four biochemically and morphologically distinct development forms, resulting from the adaptation process to the different vertebrate and invertebrate hosts. In the insect vector the *epimastigote* replicates in the midgut before differentiating into the non-replicative metacyclic *trypomastigote* in the hidgut. Once introduced into the bloodstream of the mammalian host, the metacyclic *trypomastigote* invades cells and differenciates into the *amastigote*, which finally multiplies and differenciates into bloodstream *trypomastigote*, ready to either initiate another round of infection or, alternatively, complete the life cycle by being taken up by the insect vector.[123]

[120]Rossi, A.; Marin-Neto, J.A. *Lancet* **2010**, *375*, 1388.
[121]Nunes, M.C.P.; Dones, W.; Morillo, C.A.; Encina, J.J.; Ribeiro, A.L. *J. Am. College Cardiol.* **2013**, *62*, 767.
[122]Conteh, L.; Engels, T.; Molyneux, D.H. *Lancet* **2010**, *375*, 239.
[123]Manning-Cela, R.; Jaishankar, S.; Swindle, J. *Arch. Med. Res.* **2006**, *37*, 593.

The parasite can infect a variety of both wildlife and domestic animal species reservoirs and is spread to humans through contact with *T. cruzi*-containing fecal matter deposited by the insect vector, or alternatively, can also be transmitted by blood through congenital exposure, transfusion, organ transplantation, and reactivation due to immunosuppression and orally transmitted after ingesting contaminated food or liquids.[124,125] Chronic infection can result in severe organ damage often evolving into digestive megasyndromes and cardiomyopathy.

The main efforts to combat the disease are focused on large-scale vector control programs, blood donor screenings and surveillance.[126] Chemotherapeutic treatment for Chagas disease envisages long-term subministration with the antiparasitic drugs benznidazole, **23**, (**Figure 2.4**) or nifurtimox, **22** (**Figure 2.3**). However, the development of a vaccine or safer antiprotozoan drugs represents a crucial issue for a more effective and systematic management of the disease.[127]

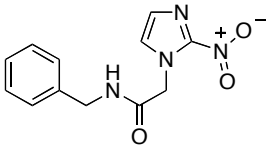

benznidazole, **23**

Figure 2.4

2.2.3 Leishmaniasis

Leishmaniasis, currently affecting around 350 million people worldwide, is caused by different species of the protozoan *Leishmania* parasite and transmitted to humans through the bite of certain species of sandfly.[128,129] In a general overview, the infection can arise in visceral, cutaneous, mucocutaneous and dermal forms;[130] particularly, infection by *L. donovani* and *L.*

[124]Bern, C.; Kjos, S.; Yabsley, M.J.; Mongtomery, S.P. *Clin. Microbiol. Rev.* **2011**, *24*, 655.
[125]Lattes, R.; Lasala, M.B. *Clin. Microbiol. Infect.* **2014**, *20*, 300.
[126]Hashimoto, K.; Yioshoka, K. *Adv. Parasitol.* **2012**, *79*, 375.
[127]Hotez, P.J.; Molyneux, D.H.; Fenwick, A.; Kumaresan, J.; Sachs, S.E.; Sachs, J.D.; Savioli, L. *N. Engl. J. Med.* **2007**, *357*, 1018.
[128]World Health Organization, Global Health Observatory Map Gallery, http://gamapserver.who.int/mapLibrary/, accessed 23th April 2015.
[129]World Health Organization, Leishmaniasis, The disease and its epidemiology, http://www.who.int/leishmaniasis/disease_epidemiology/en/index.html, accessed 25th April 2015.
[130]Burrows, J.N.; Elliot, R.L.; Kaneko, T.; Mowbray, C.E.; Waterson, D. *Med. Chem. Commun.* **2014**, *5*, 688.

infantum species may result in a chronic disseminating disease in the liver and spleen, i.e visceral leishmaniasis, often fatal unless treated by chemotherapy.[131]

The dimorphic life cycle of *Leishmania* consists of an extracellular flagellated stage (*promastigote*) within the midgut of a sandfly vector, and an intracelular *amastigote* stage within macrophages of a mammalian host.

Effectiveness of anti-leishmanial drugs strictly depends on their capability to cross multiple membranes and their chemical behaviour through a pH gradient, due to the fact that the parasite is found inside acidic phagolysosomes (pH ≈ 5) within patient macrophages (pH ≈ 7.4). Current drugs for leishmaniasis, some of them containing undesirable functional groups or elements like antimony, are characterized by high molecular weight and very low lipophilicity, thus resulting administrable only by slow, painful intravenous infusion or intramuscular injection. Furthermore, serious toxic reactions ranging from nephrotoxicity and cardiotoxicity to pancreatitis and teratogenicity have been reported.[37]

2.3 Recent approaches to chemical discovery and development against NTDs

The therapeutic arsenal currently available for treatment of NTDs has resulted to be an extremely insufficient weapon in the fight against these diseases. Indeed, most of the current drugs belong to a chemical space characterized by high molecular weight, very low lipophilicity, presence of undesired functional groups, which lead to unacceptable and even lethal side effects, and generally require painful, long-term administration treatments, obviously not feasible within the context of undeveloped public health systems.

The primary reason of the deficit registered in this drug discovery field can be ascribed to the intrinsic and unique challenges thrown down by NTDs. Patient populations may be very large, often situated in remote areas without access to adequate healthcare systems. Moreover, there is a lack of knowledge regarding validated drug targets. Additionally, the complex nature of the pathogens themselves poses serious challenges, including drug-resistance mechanisms, latent and persistent forms, intracellular location and multiple life forms for those transmitted by vectors. Nevertheless, the most constraining factor obstructing the path towards the development of new and effective chemical entities is the historical lack of investment by the majority of research-based pharmaceutical companies, due to the prospect of inadequate commercial return on drugs for developing countries.

[131]Leifso, K.; Cohen-Freue, G.; Dogra, N.; Murray, A.; McMaster, W.R. *Mol. Biochem. Parasitol.* **2007**, *152*, 35.

In the last decade an intense research effort has been made and strong drug development pipelines for NTDs have been established, primarily as a result of the emergence of public-private product development partnerships (PDPs). On the occasion of the London Declaration on NTDs in January 2012, politicians, pharmaceutical companies, and global health organizations committed to reduce the burden of NTDs by 2020, throughout increasing research and development (R&D) to find new-generation treatments, providing funding and resources, and enhancing both national and international collaborative networks.[132,133] In this light, a set of novel drug discovery strategies, such as target-based screening, virtual docking studies and genomic-based approaches, have been used to identify new drug candidates for NTDs. Recently, whole-cell high-throughput screening (HTS), often in combination with drug repositioning strategies, has beaten target-based screening and *de novo* drug discovery, thus constituting a promising option for identification of new *hit* candidates against NTDs.[134]

2.3.1 Phenotypic whole-cell high-throughput screening (HTS)

The advances in genomics and combinatorial chemistry have fostered the recourse to HTS as preferential method for fast biological assays of a huge amount of compounds (typically ≥100,000/day). HTS facilitates screening at different biological levels, from individual protein targets to uni- and multicellular organisms.[135] A recent analysis showed that the contribution of cell-based phenotypic screening to drug discovery between 1999 and 2008 exceeded that of target-based methods. Phenotypic screening offers a broad set of advantages with respect to target-based approaches, principally related to the fact that it takes into account the real biological context in which compounds interact with targets, thus yielding *hits* that already possess drug-like properties such as good cell-penetration. This avoids, then, the recourse to purified recombinant enzymes and enables more effective pharmacokinetic optimizations to give potential *lead* compounds.[136] Furthermore, this strategy is very advantageous when the biology of the disease is poorly understood, as in the case of NTDs.[137,138]

[132]Wellcome Trust, Neglected tropical diseases, the London declaration, http://wellcometrust.wordpress.com/2012/01/31/neglected-tropical-diseases-the-london-declaration/, accessed 4th April 2015.
[133]London Declaration on Neglected Tropical Diseases, http://www.unitingtocombatntds.org/downloads/press/london_declaration_on_ntds.pdf, accesses 22th March 2015.
[134]Swinney, D.C.; Anthony, J. *Nat. Rev. Drug Discovery* **2011**, *10*, 507.
[135]Denny, P.W.; Steel, P.G. *J. Biomol. Screening* **2015**, *20*, 56.
[136]Butera, J.A. *J. Med. Chem.* **2013**, *56*, 7715.
[137]Kotz, J. *Sci. Exch.* **2012**, *5*, 1.
[138]Wells, T.N.C. *Science* **2010**, *329*, 1153.

Recently, a broad spectrum of chemical scaffolds displaying promising *in vitro* and, in some cases, also *in vivo* activity against *T. brucei* has been reported from phenotypic whole-cell HTS studies. In 2012, Syked *et al.* described the use of an Alamar blue fluorescence-based whole-cell HTS of a library of more that 87,000 compounds for antiproliferative activity against *T. brucei*.[139] The preliminary screening gave rise to five distinct chemical structures (**24**-**28**) with moderate potency (in the low micromolar range) and good selectivity against parasitic cells with respect to mammalian ones (**Figure 2.5**).

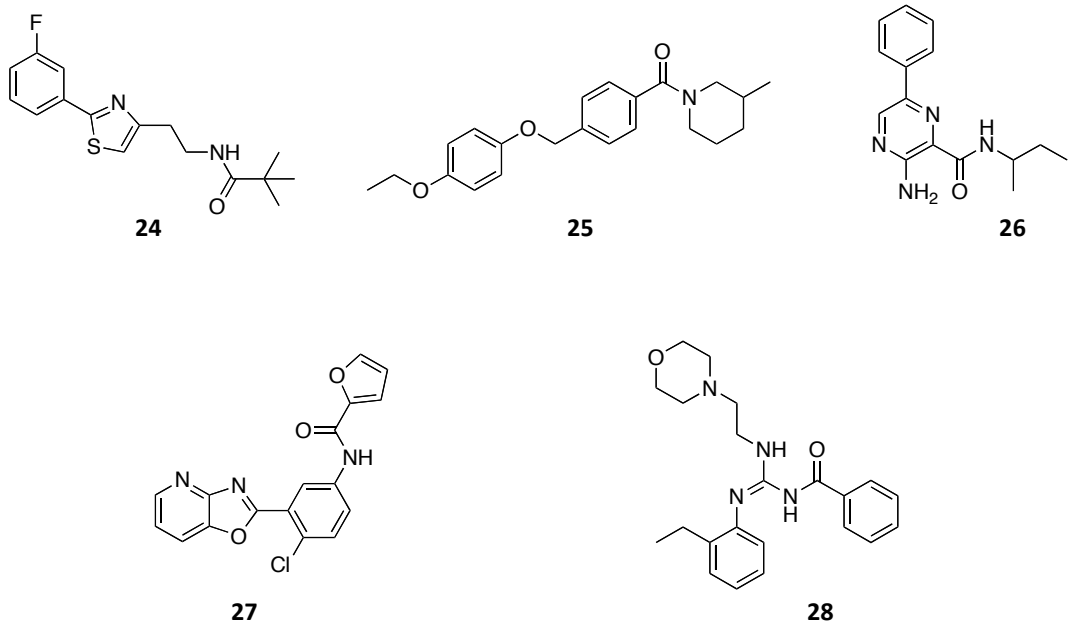

24 **25** **26**

27 **28**

Figure 2.5 Representative antitrypanosomal compounds from scaffolds identified by Syked *et al*.

Particularly, oxazolopyridine **27** displayed the best profile against different pathogenic kinetoplastid species with IC_{50} values of 0.22 and 0.59 μM against *T.b. brucei* and *T.b. rhodesiense*, respectively, and 0.23 and 1.8 μM against *T. cruzi* and *L. donovani*, respectively. The replacement of the 2-furan ring to the 3-furan analogue (**29**) led to the most significant improvement in potency with respect to the *hit* series (**Figure 2.6**). *Lead* **29** resulted to be much more potent against *T.b. rhodesiense* than the parent compound *in vitro* (IC_{50} value of 0.091 μM), while remaining almost equipotent against *T.b. brucei* and *T. cruzi*. Additionally, in comparison with its *T.b. rhodesiense* activity, much lower cytotoxicity against L6 (rat skeletal myoblast) mammalian cell line, with a selectivity index of approximately 700, was reported for

[139]Sykes, M.L.; Baell, J.B.; Kaiser, M.; Chatelain, E.; Moawad, S.R.; Ganame, D.; Ioset, J.-R., Avery, V.M. *PLoS Neglected Trop. Dis.* **2012**, *6*, 1896.

29. This compound also resulted to be more potent than the control drug miltefosine, **30**, *in vitro* against *L. donovani* amastigotes (IC_{50} 0.34 μM) (**Figure 2.6**).[140]

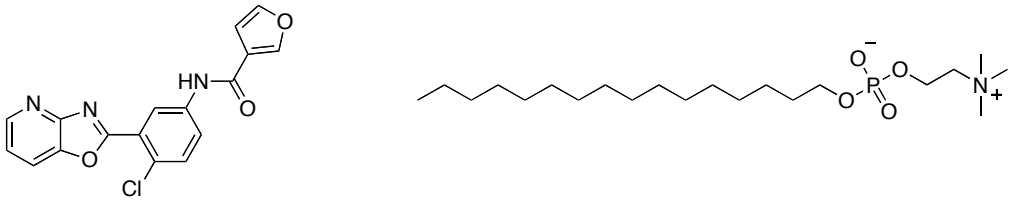

29 miltefosine, **30**

Figure 1.6. Chemical structures of *lead* compound **29** and control drug miltefosine, **30**.

With respect to the development of novel drugs for treatment of CNS-stage HAT infection, the most promising discovery has been the series of oxaborole-6-carboxamide compounds first reported in 2010.[141] The activity of these new chemical scaffolds was initially uncovered by HTS of a focused library of anti-infective oxaboroles, none of which was previously considered to possess antitrypanosomal activity.[142] Compound **31** resulted potent in *in vitro* assays on all three *T. brucei* strains tested (**Figure 2.7**). *In vivo*, **31** cured all mice by intraperitoneal administration of 2 x 50 mg/kg for 14 days in a stage II model of the disease. Conversely, oral administration reduced its efficacy at the same dose for 7 days, probably due to its reduced brain exposure. *C-3* substitutions of the benzoxaborole scaffold resulted in improved brain penetration and exposure. Particularly, the *C-3* dimethyl analogue **32** was completely effective when administered intraperitoneally at a single dose of 25 mg/kg in a stage I model of the disease (**Figure 2.7**). Remarkably, **32** was also curative in a stage II model at an oral dose of 25 mg/kg administrated once daily for 7 days. This compound progressed into phase I clinical trials in March 2012.[143]

[140]Ferrins, L.; Rahmani, R.; Sykes, M.L.; Jones, A.J.; Avery, V.M.; Teston, E.; Almohaywi, B.; Yin, J.; Smith, J.; Hyland, C.; White, K.L.; Ryan, E.; Campbell, M.; Charman, S.A.; Kaiser, M.; Baell, J.B. *Eur. J. Med. Chem.* **2013**, *66*, 450.
[141]Nare, B.; Wring, S.; Bacchi, C.; Beaudet, B.; Bowling, T.; Brun, R.; Chen, D.; Ding, C.; Freund, Y.; Gaukel, E.; Hussain, A.; Jarnagin, K.; Jenks, M.; Kaiser, M.; Mercer, L.; Mejia, E.; Noe, A.; Orr, M.; Parham, R.; Plattner, J.; Randolph, R.; Rattendi, D.; Rewerts, C.; Sligar, J.; Yarlett, N.; Don, R.; Jacobs, R. *Antimicrob. Agents Chemoter.* **2010**, *54*, 4379.
[142]Ding, D.; Zhao, Y.; Meng, Q.; Xie, D.; Nare, B.; Chen, D.; Bacchi, C.J.; Yarlett, N.; Zhang, Y.-K.; Hernandez, V.; Xia, Y.; Freund, Y.; Abdulla, M.; Ang, K.-H.; Rstman, J.; McKerrow, J.H.; Jacobs, R.T.; Zhou, H.; Plattner, J.J. *ACS Med. Chem. Lett.* **2010**, *1*, 165.
[143]Jacobs, R.T.; Nare, B.; Wring, S.A.; Orr, M.D.; Chen, D.; Sligar, J.M.; Jenks, M.X.; Noe, R.A.; Bowling, T.S.; Mercer, L.T.; Rewerts, C.; Gaukel, E.; Owens, J.; Parham, R.; Randolph, R.; Beaudet, B.; Bacchi, C.J.; Yarlett, N.; Plattner, J.J.; Freund, Y.; Ding, C.; Akama, T.; Zhang, Y.-K.; Brun, R.; Kaiser, M.; Scandale, I.; Don, R.; *PLoS Neglected Trop. Dis.* **2011**, *5*, 1151.

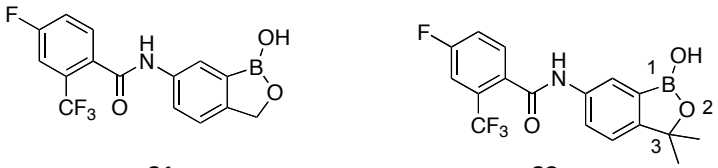

31 **32**

Figure 2.7 Oxaborole hit and optimized clinical candidate.

2.4 The concept of privileged structures in rational drug design

It is broadly acknowledged that modern drug discovery has been suffering from a widespread "productivity crisis", mainly reflected in the unbalance between the excessively long and costly R&D programs and the final outcome of R&D productivity.[144] Only 19 new molecule entities (NMEs) were registered by the FDA in 2007, the least productive year of the past two decades. This number increased only to 21 in 2008. Conversely, the costs associated with the development of a novel drug have increased from $500 million to $1.8 billion.[145]

Introduction of HTS methodologies in the early 1990 was expected to boost the number of robust drugs released to the market. Nevertheless, despite some successful cases, a third of drug candidates failed or were later removed from the market, generally due to lack of efficacy, toxicity and unfavorable drug metabolism and pharmacokinetic (DMPK) properties.[52]

To overcome the problem of attrition in the post-HTS era, many efforts have been focused on designing more chemically diverse and drug-like compound libraries.[146,147] In this light, the concept of "privileged structures", introduced for the first time by Evans *et al.* in 1988, has been proposed as an affordable strategy to carry out a more reliable drug discovery process.[148,149]

[144]Munos, B. *Nat. Rev. Drug Discov.* **2009**, *8*, 959.
[145]Paul, S.M.; Mytelka, D.S.; Dunwiddie, C.T.; Persinger, C.C.; Munos, B.H.; Lindborg, S.R.; Schacht, A.L. *Nat. Rev. Drug Discov.* **2010**, *9*, 203.
[146]Bleicher, K.H.; Böhm H.J.; Müller, K.; Alanine, A.L. *Nat. Rev. Drug Discov.* **2003**, *2*, 369.
[147]Fattori, D. *Drug Discov. Today* **2004**, *9*, 229.
[148]Evans, B.E.; Rittle, K.E.; Bock, M.G.; Di Pardo, R.M.; Freidinger, R.M.; Whitter, W.L.; Lundell, G.F.; Veber, D.F.; Anderson, P.S.; Chang, R.S. *J. Med. Chem.* **1988**, *31*, 2235.
[149]Bongarzone, S.; Bolognesi, M.L. *Expert Opin. Drug Discov.* **2011**, *6*, 251.

2.5 Quinolines as privileged motifs

Quinolines are heterocyclic aromatic moieties that encompass a broad spectrum of biologically active compounds. This trait can be related to their ability to form a range of stacking interactions with nucleic acid bases, aromatic amino acids and porphyrines. As a paradigm of privileged structures, they have been broadly exploited in a variety of medicinal chemistry programs.[150] Indeed, apart from being currently employed as antimalarial,[151] antifungal[152] and antiprotozoan agents,[153] quinolines have been also investigated as potential anti-obesity,[154] anti-diabetes[155] and anti-cancer drugs,[156] and included for treatment of neurodegenerative disorders (**Figure 2.8**).

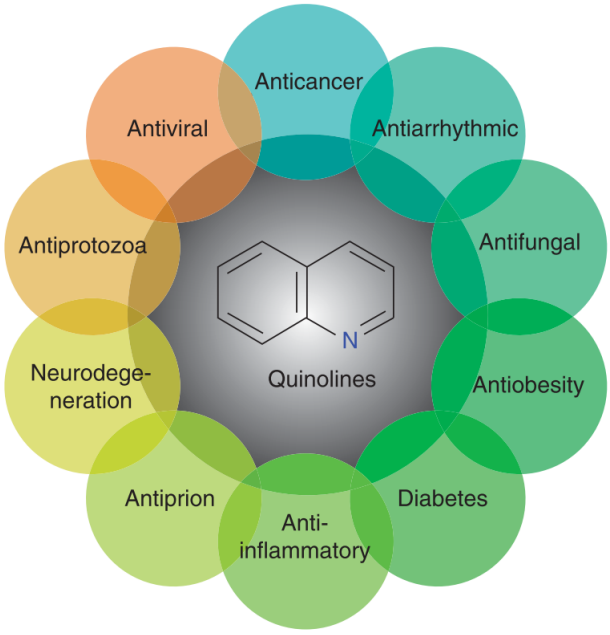

Figure 2.8 Schematic representation of the spectrum of biological activities displayed by quinolines [Source: Bongarzone, S.; Bolognesi, M.L. *Expert Opin. Drug Discov.* **2011***, 6, 251*].

[150]Welsch, M.E.; Snyder, S.A.; Stockwell, B.R. *Curr. Opin. Chem. Biol.* **2010**, *14*, 347.
[151]O'Neil, P.M.; Ward, S.A.; Berry, N.G.; Jeyadevan, J.P.; Biagini, G.A.; Asadollaly, E.; Park, B.K.; Bray, P.G. *Curr. Top. Med. Chem.* **2006**, *6*, 479.
[152]Musiol, R.; Serda, M.; Hensel-Bielowka, S.; Polanski, J. *Curr. Med. Chem.* **2010**, *17*, 1960.
[153]Tekwani, B.L.; Walker, L.A. *Curr. Opin. Infect. Dis.* **2006**, *19*, 623.
[154]Warshakoon, N.C.; Sheville, J.; Bhatt, R.T.; Ji, W.; Mendez-Andino, J.L.; Meyers, K.M.; Kim, N.; Wos, J.A.; Mitchel, C.; Paris, J.L.; Pinney, B.B.; Reizes, O.; Hu, X.E. *Bioorg. Med. Chem. Lett.* **2006**, *16*, 5207.
[155]DeRuiter, J.; Brubaker, A.N.; Whitmer, W.L.; Stein, J.L. Jr. *J. Med. Chem.* **1986**, *29*, 2024.
[156]Knight, S.D.; Adams, N.D.; Burgess, J.L.; Chaudhari, A.M.; Darcy, M.G.; Donatelli, C.A.; Luengo, J.I.; Newlander, K.A.; Parrish, C.A.; Ridgers, L.H.; Sarpong, M.A.; Schimdt, S.J.; Van Aller, G.S.; Carson, J.D.; Diamond, M.A.; Elkins, P.A.; Gardiner, C.M.; Garver, E., Gilbert, S.A.; Gontarek, R.R.; Jackson, J.R.; Kershner, K.L.; Luo, L.; Raha, K.; Sherk, C.S.; Sung, C.-M.; Sutton, D.; Tummino, P.J.; Wegrzyn, R.J.; Auger, K.R.; Dhanak, D. *ACS Med. Chem. Lett.* **2010**, *1*, 39.

2.5.1 Quinolines and protozoan diseases

The extreme versatility displayed by the quinoline motif makes this "promiscuous" heterocyclic ring an attractive scaffold in the search for new, effective antiprotozoan drug candidates. In fact, the possibility to act on multiple metabolic pathways in parasitic cells constitutes a preferentially pursued requisite in NTDs drug discovery, mainly because of the enormous economic advantage that the dosage of a drug for more than a single parasitic infection would imply for both pharmaceutical companies and public sanitary systems in undeveloped countries.

The prototype of quinoline as antiprotozoan agent is the antimalaric chloroquine, **33**, later followed by other various 8-substituted quinolines, namely primaquine, **34**, and pamaquine, **35**, and 4-substituted quinolines, such as mefloquine, **36**, and amodiaquine, **37** (**Figure 2.9**).[157] Nevertheless, emergence of resistance and severe side effects limit seriously the use of these drugs.[158]

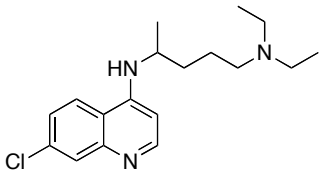

chloroquine, **33**

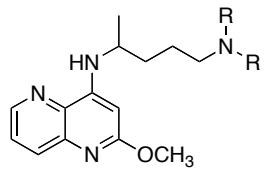

primaquine, **34** R= H
pamaquine, **35** R= Et

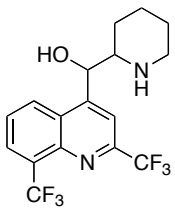

mefloquine, **36**

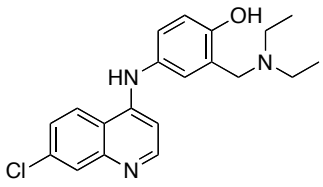

amodiaquine, **37**

Figure 2.9 8-Aminoquinoline, 4-aminoquinoline, and other quinoline derivatives for protozoan diseases.

[157]Dorn, A.; Vippagunta, S.R.; Matilde, H.; Jaquet, C.; Vennerstrom, J.L.; Ridley, R.G. *Biochem. Pharmacol.* **1998**, *55*, 727.
[158]Kaur, K.; Jain, M.; Reddy, R.P.; Jain, R. *Eur. J. Med. Chem.* **2010**, *45*, 3245.

A recently investigated strategy to avoid emergence of resistance consists of inhibiting multiple targets within the same parasite through the design of "dual inhibitors".[159,160] Combination of two or more 4-aminoquinoline moieties with linkers of different lenghts and chemical nature led to several chloroquine-analogue "double drugs". As an example, piperaquine, **38**, a bis-quinoline derivative, is an antimalarial drug extensively used in China and Indochina for prophylaxis and treatment,[161] while compound **39** showed additional potency against *L. donovani*.[162]

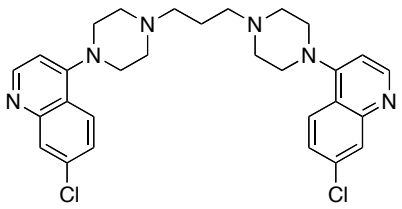

piperaquine, **38**

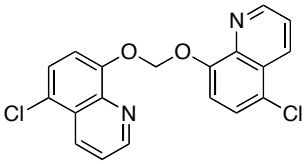

39

Figure 2.10 Bis-quinoline derivatives.

2.5.2 4-Aminoquinoline dimerization strategy: Screening of an in-house huprine Y-based library of heterodimeric compounds against T. brucei and P. falciparum

Huprines, a structural class of compounds bearing a 4-aminoquinoline moiety, were developed a decade ago in our research group as brain permeable inhibitors of acetylcholinesterase (AChE). Recently, huprines have been also described as moderately potent and selective trypanocidal and, in few cases, also antiplasmodial agents, with the so-called huprine Y, **40** (**Figure 2.11**), displaying the most potent activity against *T. brucei* (IC_{50} = 0.61 μM; IC_{90} = 2.94 μM) and one of the best selectivity indices over rat myoblast L6 cells (SI = 13).[163]

[159]Kouznetsov, V.V.; Gomez-Barrio, A. *Eur. J. Med. Chem.* **2009**, *44*, 3091.
[160]Muregi, F.W.; Ishih, A. *Drug Dev. Res.* **2010**, *71*, 20.
[161]Davis, T.M.; Hung, T.Y.; Sim, I.K.; Hung, T.Y. *Drugs* **2005**, *65*, 75.
[162]Palit, P.; Paira, P.; Hazra, A., Banerjee, S.; Das Gupta, A.; Dastidar, S.G.; Mondal, N.B. *Eur. J. Med. Chem.* **2009**, *44*, 845.
[163]Defaux, J.; Sala, M.; Formosa, X.; Galdeano, C.; Taylor, M.C.; Alobaid, W.A.A.; Kelly, J.M.; Wright, C.W.; Camps, P.; Muñoz-Torrero, D. *Bioorg. Med. Chem.* **2011**, *19*, 1702.

In the PhD thesis of Irene Sola, molecular dimerization was further explored as a promising strategy to address multiple resistances developed by protozoan parasites against currently available monomeric aminoquinoline drugs, such as chloroquine.

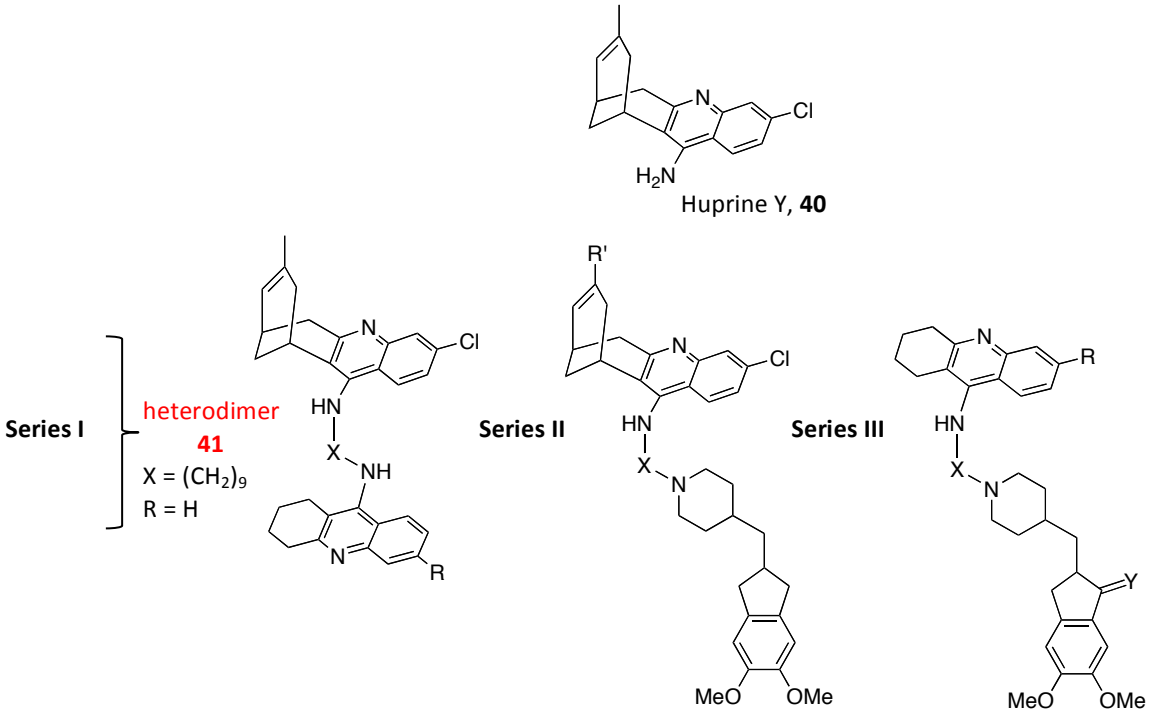

Figure 2.11. Structures of huprine Y, and 4-aminoquinoline-based scaffolds of series **I**-**III**.

Phenotypic screening of a small library of 27 4-aminoquinoline-based heterodimeric compounds allowed the identification of several dual submicromolar trypanocidal-antiplasmodial compounds (**Figure 2.11**). Among them, heterodimer **41** emerged as an interesting *hit* featuring balanced dual trypanocidal (IC_{50} = 0.21 µM) and antiplasmodial (IC_{50} = 0.35 µM) activity and selectivity indices of 34 and 20 over rat L6 cell citotoxicity. Mechanistic studies suggested that the high trypanocidal potency of these heterodimers can be partially ascribed to inhibition of the enzyme trypanothione reductase (TryR), whereas their antiplasmodial activity can be likely ascribed to the inhibition of the haem detoxification process, similarly to the antimalarial drug chloroquine.[164]

[164]Sola, I.; Castellà, S.; Viayna, E.; Galdeano, C.; Taylor, M.C.; Gbedema, S.Y.; Pérez, B.; Clos, M.V.; Jones, D.C.; Fairlamb, A.H.; Wright, C.W.; Kelly, J.M.; Muñoz-Torrero, D. *Bioorg. Med. Chem.* **2015**, *23*, 5156.

2.6 *Multicomponent reactions (MCRs): A successful approach for the synthesis of structurally varied quinoline scaffolds*

Reactions combining three or more different components in one reaction vessel, leading to the formation of a single product, are denoted under the term *multicomponent reactions* (MCRs).[165,166,167] This group of transformations is labelled as operationally simple, atom economic, and bond-forming efficient.[168,169]

MCRs provide an impressively powerful option of generating the high molecular diversity required by combinatorial approaches for the preparation of bioactive compounds. Although 68% of drugs in late development or on market are heterocycles, where *N*-heterocyclic molecules are highly preponderant, their incorporation has frequently posed special problems, among them multistep sequences, lack of generality and preparation from acyclic precursors. Hence, the list of successful synthetic strategies for the construction of heterocyclic scaffolds is strictly limited.[170,171] In this context, the *Povarov* reaction, a particular kind of imino (aza)–Diels-Alder reaction, holds an impressive potential for speeding up the generation of large libraries of related *N*-heterocyclic compounds.[77]

2.6.1 Povarov MCR. A three-component imino Diels-Alder (DA) reaction

"*Diene synthesis*" represents a standard method frequently employed for the formation of six-membered rings under high regio-, diastereo-, and enantio-selective controls.[172,173] The DA methodology contains two basic variants, classified as carbo-DA reaction (CDA) and hetero-DA reaction (HDA), which can be further subdivided as oxa-DA reaction (HDA of carbonyl compounds) and imino (aza)-DA reaction (HDA of imines) (**Figure 2.12**).

[165]Ugi, I.; Dömling, A.; Hörl, W. *Endeavour* **1994**, *18*, 115.
[166]Zhu, J.; Bienaymé, H. Wiley-VCH, Weinheim, **2005**.
[167]Dömling, A. *Chem. Rev.* **2006**, *106*, 17.
[168]Bienaymé, H.; Hulme, C.; Oddon, G.; Schmitt, P. *Chem-Eur. J.* **2000**, *6*, 3321.
[169]Brauch, S.; van Berkel, S.S.; Westermann, B. *Chem. Soc. Rev.* **2013**, *42*, 4948.
[170]Kouznetsov, V.V. *Tetrahedron* **2009**, *65*, 2721.
[171]Lavilla, R.; Bernabeu, M.C.; Carranco, I.; Díaz, J.L. *Org. Lett.* **2003**, *5*, 717.
[172]Kumar, A. *Chem. Rev.* **2001**, *101*, 1.
[173]Nicolaou, K.C.; Snyder, S.A.; Montagnon, T.; Vassilikogiannakis, G. *Angew. Chem. Int. Ed.* **2002**, *41*, 1669.

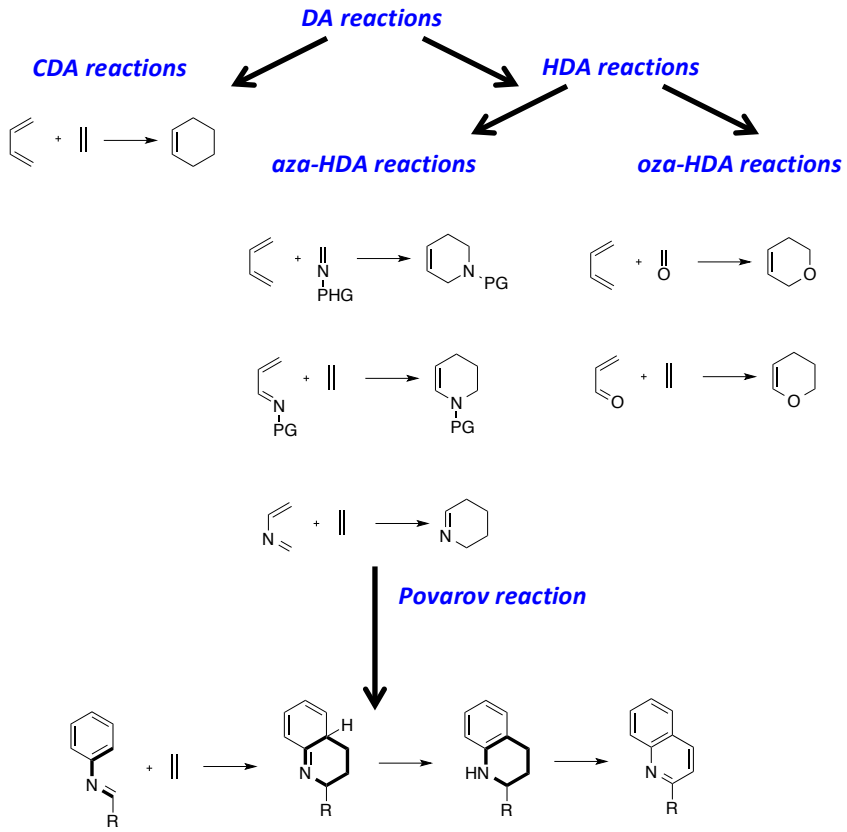

Figure 2.12 Schematic representation of DA reactions.

In the group of the imino (aza)-DA, the acid-mediated [4+2] cycloaddition reaction of *N*-aryl imines (Schiff's bases) with nucleophilic olefins, namely the *Povarov* reaction, has become in contemporary organic chemistry an established route to various tetrahydroquinolines, obtained as mixture of four diastereomers (**Figure 2.13**).[174]

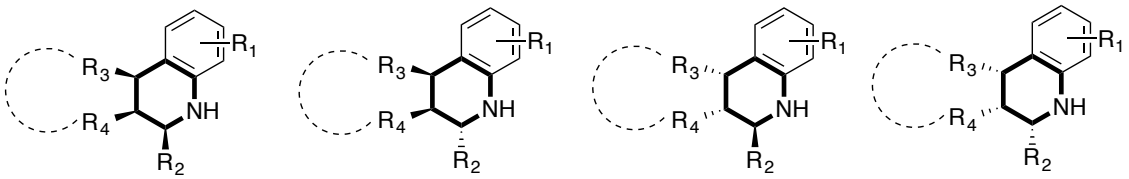

Figure 2.13 Diastereomeric mixture resulting from the *Povarov* reaction.

[174]Povarov, L.S. *Russ. Chem. Rev.* **1967**, *36*, 656.

In this acid-promoted variant, the poorly reactive Schiff's bases, normally generated *in situ* by reaction between an aniline and an aldehyde, are activated by a wide set of Lewis acids, mainly $BF_3{\cdot}OEt_2$, $Sc(OTf)_3$, TMSCl, and $InCl_3$. Among the electron-rich dienophiles, vinyl enol ethers, vinyl enamides, vinyl sulfide, cyclopentadiene, indene, alkynes and enamines have been largely used.[175,176]

The *Povarov* reaction can also take place intramolecularly when a molecule contains both diene and dienophile moieties, wich are connected by a chain at position *C-1* of the diene (*type 1* intramolecular DA reaction) or at position *C-2* of the diene (*type 2* intramolecular acyl imino DA reaction); as a result, fused bicyclic adducts and bridged bicyclic compounds are obtained (**Figure 2.14**).[177, 178]

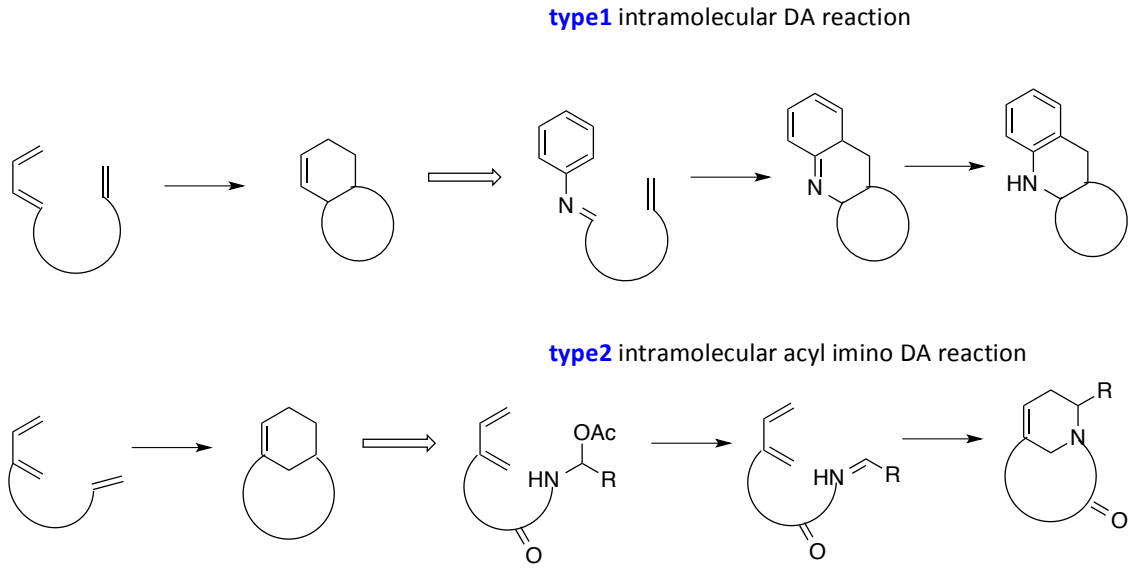

Figure 2.14 Schematic representation of intramolecular *Povarov* reactions.

[175]Zhu, J.; Bilnaymé, H.; Eds.; Wiley-VCH: Weinheim, **2005**.
[176]Orru, R.V.A.; de Greef, M. *Synthesis* **2003**, 1471.
[177]Taber, D.F. Springer: Berlin, **1984**.
[178]Bear, B.R.; Sparks, S.M.; Shea, K.J. *Angew. Chem. Int. Ed.* **2001**, *40*, 820.

The reaction mechanism has been a matter constant debate. The previous proposed concerted [4+2] asynchronous mechanism seems to have been recently replaced by a stepwise ionic mechanism, involving the electron-rich olefin addition upon the *in situ*-formed imine and the subsequent cyclization of the aromatic amine upon the carbocation intermediate thus generated (**Figure 2.15**).[179,180,181]

In this PhD thesis, the $Sc(OTf)_3$-catalyzed version of the reaction has been successfully performed with various combinations of activated alkenes, different substituted anilines and aromatic aldehydes, as the key step in the synthesis of either several structure-based designed peripheral-site AChE inhibitors for the treatment of Alzheimer's disease, [182] and a small library of ligand-based designed antiprotozoan *hit* compounds.[183]

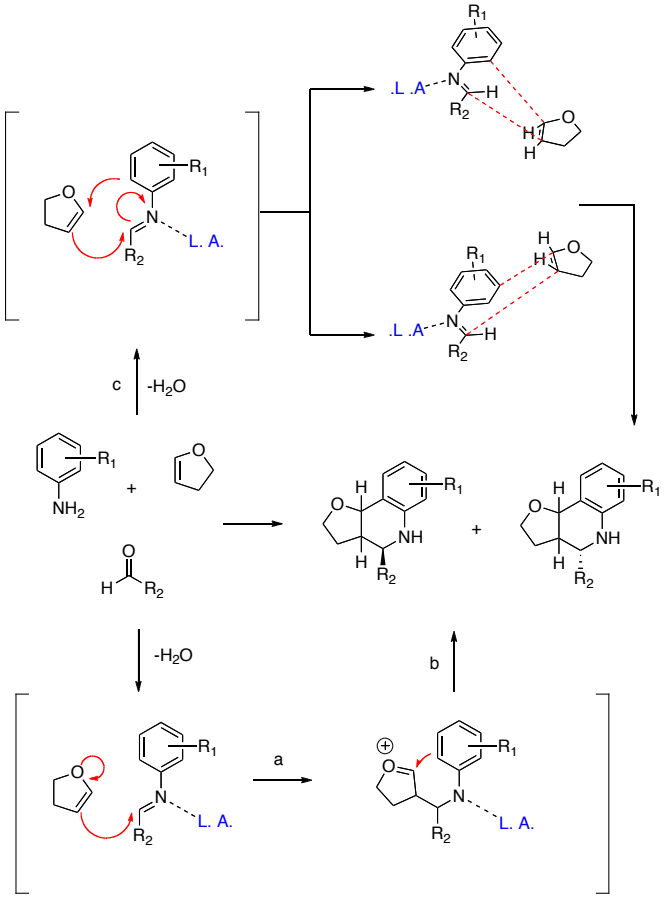

Figure 2.15 Two alternative *Povarov* reaction mechanisms.

[179]Kobayashi, S.; Ishitani, H.; Nagayama, S. *Synthesis* **1995**, 1195.
[180]Buonora, P.; Olsen, J.-C.; Oh, T. *Tetrahedron* **2001**, *57*, 6099.
[181]Alves, M.J.; Azoia, N.G.; Fortes, A.G. *Tetrahedron* **2007**, *63*, 727.
[182]Di Pietro, O.; Viayna, E.; Vicente-García, E.; Bartolini, M.; Ramón, R.; Juárez-Jiménez, J.; Clos, M.V.; Pérez, B.; Andrisano, V.; Luque, F.J.; Lavilla, R.; Muñoz-Torrero, D. *Eur. J. Med. Chem.* **2014**, *73*, 141.
[183]Di Pietro, O.; Vicente-García, E.; Taylor, M.C.; Berenguer, D., Viayna, E.; Lanzoni, A.; Sola, I.; Sayago, H.; Riera, C.; Fisa, R.; Clos, M.V.; Pérez, B.; Kelly, J.M.; Lavilla, R.; Muñoz-Torrero, D. *Eur. J. Med. Chem.* **2015** (accepted with minor revision).

3 Objectives

Chapter

3.1 Hit-to-lead optimization of the tetrahydrobenzo[h][3,2-c]naphthyridine scaffold as a peripheral site AChEI (*Eur. J. Med. Chem.* **2014**, *73*, 141)

Taking into account the promising pharmacological results of the first generation of tetrahydrobenzo[*h*][3,2-*c*]naphthyridines (general structure **II**, **Figure 3.1**), a novel family of propidium-related peripheral site AChEIs previously synthesized in our research group in collaboration with Dr. Rodolfo Lavilla (*Universitat de Barcelona*), the first project to be developed in this PhD thesis envisioned the design, synthesis and mechanistic studies of an optimized second generation of benzonaphthyridine derivatives (general structure **III**, **Figure 3.1**).

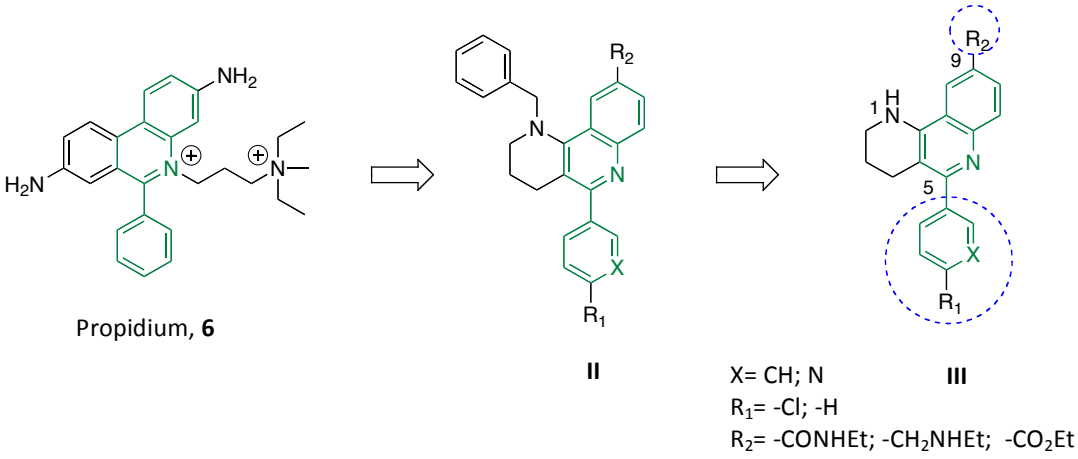

Figure 3.1 Structure of propidium, **6**, and general structure of the first and the optimized second generation of tetrahydrobenzo[*h*][3,2-*c*]naphthyridines, **II** and **III**.

For the preparation of this novel series, the *Povarov*-type multicomponent reaction (MCR) and subsequent oxidation of the resulting diastereomeric mixture of octahydrobenzo[*h*][3,2-*c*]naphthyridines were envisioned. Thus, an appropriate activated alkene, an aniline and two alternative aromatic aldehydes were selected, whereas further derivatization of the ethyl esther group at position 9 was envisioned through a number of standard organic synthesis transformations, with the overall perspective of exploring the effect of different substitution patterns at positions 5 and 9 of the benzonaphthyridine scaffold on AChE inhibitory activity.

Furthermore, molecular modelling studies, consisting of both preliminary docking calculations, molecular dynamics (MD) simulations and binding free energy estimations, were planned with the aim of establishing the binding mode of this novel propidium-related fragment in the PAS of AChE.

3.2 Structure-based design, synthesis and molecular modelling studies of tetrahydrobenzo[h][1,6]naphthyridine-6-chlorotacrine hybrids, as dual binding site AChEIs

(*Eur. J. Med. Chem.* **2014**, *84*, 107)

With the aim of improving the poor pharmacological profile displayed by the pyrano[3,2-*c*]quinoline **45**, previously synthesized in the PhD thesis of Dr. Carles Galdeano,[67,184] and keeping in mind the results of the *hit-to-lead* optimization of the PAS-binding unit (section ***3.1***),[182] a double O → NH bioisosteric replacement was envisioned, in combination with the molecular hybridization with a 6-chlorotacrine fragment and the molecular dynamics-driven optimization of the tether length, leading to the design of a trimethylene-linked tetrahydrobenzo[*h*][1,6]naphthyridine-6-chlorotacrine hybrid and its tetra-, penta-, and octamethylene-linked homologues (general structure **IV**, **Figure 3.2**), as novel dual binding site AChEIs. The synthesis of these hybrids was envisaged through a route consisting of the initial preparation of the aminoalkyl-6-chlorotacrine intermediates, through aromatic nucleophilic substitution of the 6,9-dichloroacridine intermediate with the appropriate commercially available α,ω-alkanediamines, and further amidation-coupling reaction with the tetrahydrobenzo[*h*][1,6]naphthyridine **66**·HCl, using EDC as electrophilic activating agent, and HOBt as nucleophilic auxiliary.

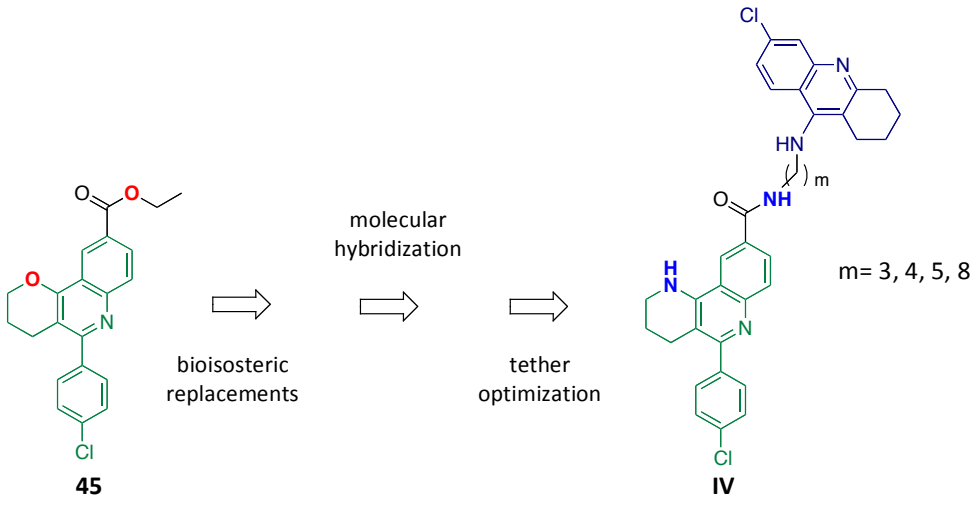

Figure 3.2 Structure of pyrano[3,2-*c*]quinoline **45** and general structure of the novel tetrahydrobenzo[*h*][3,2-*c*]naphthyridine-6-chlorotacrine hybrids **IV**.

[67]Camps, P.; Formosa, X.; Galdeano, C.; Muñoz-Torrero, D.; Ramírez, L.; Gómez, E.; Isambert, N.; Lavilla, R.; Badia, A.; Clos, M.V.; Bartolini, M.; Mancini, F.; Andrisano, V.; Arce, M.P.; Rodríguez-Franco, M.I.; Huertas, O.; Dafni, T.; Luque, F.J. *J. Med. Chem.* **2009**, *52*, 5365.

[184]Galdeano, C. PhD thesis. *Unitat de Química Farmacèutica, Departament de Farmacologia i Química Terapèutica, Universitat de Barcelona*, **2012**.

[182]Di Pietro, O.; Viayna, E.; Vicente-García, E.; Bartolini, M.; Ramón, R.; Juárez-Jiménez, J.; Clos, M.V.; Pérez, B.; Andrisano, V.; Luque, F.J.; Lavilla, R.; Muñoz-Torrero, D. *Eur. J. Med. Chem.* **2014**, *73*, 141.

3.3 Synthesis of 1,2,3-triazole-based propargylamine compounds, as irreversible MAO-B inhibitors

Because of the increasing interest in MAO-B inhibitors in the treatment of AD, the molecular modelling-guided design of a novel 1,2,3-triazole-based propargyl amine scaffold has been recently undertaken in our research group. The weak activity displayed by the first set of triazole derivatives, synthesized in the PhD thesis of Dr. Elisabet Viayna,[185] was mainly ascribed to the high hydrophilicity of the triazole scaffold. Hence, the design and synthesis of a series of nine compounds provided with more balanced physicochemical properties was planned in this PhD thesis (general structure **V**, **Figure 3.3**). Different chemical substitutions at positions 1, 4 and 5 of the triazole nucleus were envisioned to improve both the lipophilicity of the scaffold and MAO-B over MAO-A selectivity.

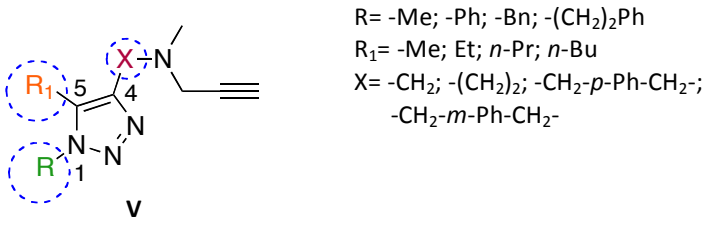

Figure 3.3 General structure of the novel triazole derivatives **V**.

The preparation of the desired triazoles was envisaged through *Cu*-catalyzed 1,3-dipolar cycloaddition of a battery of azides to various alkynes, followed by a sequence of standard organic synthesis transformations. When the required alkynes were not commercially available, an alternative methodology was applied, envisioning, prior to the click-chemistry key step, the preliminary preparation of the desired alkyne building block through *Negishi* reaction of the halide precursor with trimethylsilylacetylene.

[185]Viayna, E. PhD thesis. *Unitat de Química Farmacèutica, Departament de Farmacologia i Química Terapèutica, Universitat de Barcelona*, **2013**.

3.4 Conformational analysis and searching for novel transient druggable pockets in BACE-1. Definition of new pharmacophores

A novel rhein-huprine hybrid with a multitarget pharmacological profile has been recently developed in our research group as disease-modifying anti-Alzheimer agent (**15**, general structure **VI**, **Figure 3.4**). Among its multiple biological effects, it displayed high inhibitory potency against BACE-1 (IC_{50} 80 nM),[91] even though this trait was not specifically pursued when these compounds were designed. Interestingly, none of its two fragment precursors showed a significant BACE-1 inhibitory activity. Previous computational studies on the much less potent homologue **143** (IC_{50} 2020 nM), and a significant example in the literature of other structurally related low micromolar tacrine-chromene BACE-1 inhibitors (general structure **VII**, **figure 3.4**),[186] provided strong support to the hypothesis that the rhein moiety of **15** could reasonably fill a floppy secondary pocket never described so far.

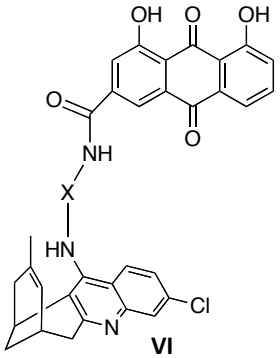

VI

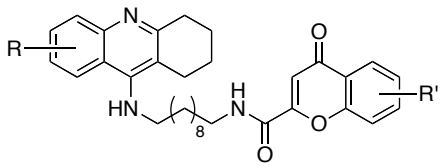

VII

15, X= $-(CH_2)_9-$
143, X= $-CH_2$-*p*-phenylene-CH_2-

Figure 3.4 Structures of the BACE-1 inhibitors **15** and **143**, and general structure of the tacrine-chromene hybrids **VI** developed by Rodríguez-Franco *et al*.

In this context, an extensive computation of the BACE-1 *apo* conformational ensemble combined with the application of the Principal Component Analysis (PCA) method was envisaged. Part of this work was developed during an internship at the Centre for Biomolecular Sciences (CBS) of the University of Nottingham, under the supervision of Prof. Charles Laughton. As the final scope of the work, the identification of the rhein binding site and the definition of a new pharmacophore would allow the virtual screening of a library of commercially available fragments for further drug discovery purposes.

[91]Viayna, E.; Sola, I.; Bartolini, M.; De Simone, A., Tapia-Rojas, C.; Serrano, F.; Sabaté, R.; Juárez-Jiménez, J.; Pérez, B.; Luque, F.J.; Andrisano, V.; Clos, M.V.; Inestrosa, N.C.; Muñoz-Torrero, D. *J. Med. Chem.* **2014**, *57*, 2549.
[186]Fernández-Bachiller, M.I.; Pérez, C.; Monjas, L.; Rademann, J.; Rodríguez-Franco, M.I. *J. Med. Chem.* **2012**, *55*, 1303.

3.5 Preparation of a small library of quinoline-based antiprotozoan compounds

Given the surprising trypanocidal activity (*T. brucei* IC_{50} 3.33 µM) displayed by the anticholinesterasic PAS binding compound **57**, the last project of this PhD thesis envisaged the synthesis of a small library of quinoline-based derivatives (general structure **VIII**, **Figure 3.5**) for whole-cell phenotypic screening, with the final purpose to individuate promising antiprotozoan *hit* compounds.[183]

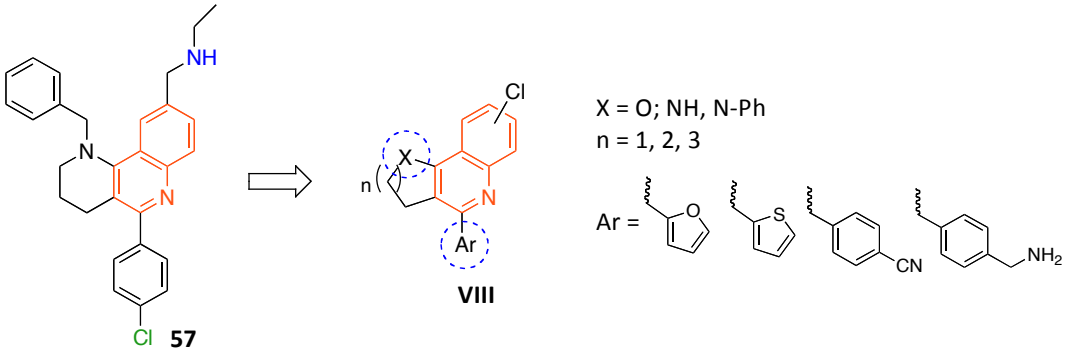

Figure 3.5 Structure of the anticholinesterasic compound **57** and general structure of the novel quinoline-based antiprotozoan compounds **VIII**.

With this scope in mind, the recourse to the *Povarov* MCR was used as powerful strategy for the synthesis of differently substituted heterofused quinolines. Interestingly, in a more advanced phase of the project, the pyran ring-opening side reaction provided an additional substrate (general structure **IX**, **figure 3.6**), which inspired further derivatizations of the terminal alcohol group at the side chain.

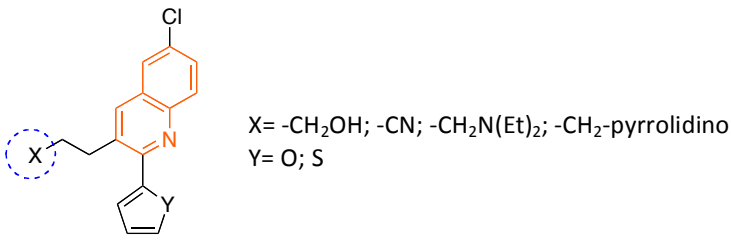

IX

Figure 3.6 General structure of the novel quinoline-based antiprotozoan compounds **IX**.

[183]Di Pietro, O.; Vicente-García, E.; Taylor, M.C.; Berenguer, D., Viayna, E.; Lanzoni, A.; Sola, I.; Sayago, H.; Riera, C.; Fisa, R.; Clos, M.V.; Pérez, B.; Kelly, J.M.; Lavilla, R.; Muñoz-Torrero, D. *Eur. J. Med. Chem.* **2015** (accepted with minor revision).

4 PAS-binding AChE inhibitors

Chapter

(*Eur. J. Med. Chem.* **2014**, *73*, 141)

4.1 Preparation of a propidium-related PAS AChEI in our research group

Noncatalytic actions displayed by different classes of enzymes are currently attracting an increasing interest in medicinal chemistry. AChE is a representative case due to the multiplicity of nonclassical roles that seems to complement the hydrolytic reaction.[187] In particular, the pivotal finding that the PAS of AChE can bind Aβ, thereby promoting Aβ aggregation in an early stage of the neurodegenerative cascade,[52,53] has boosted the design of dual binding site AChEIs, as promising disease-modifying anti-Alzheimer drug candidates.[2]

These multipotent compounds consist of an active site interacting unit, deriving from a well validated CAS AChEI, linked by means of a tether of suitable length to a PAS interacting unit capable to stack against Trp286 *via* π-π and/or cation-π interactions.

Propidium, **6**, as prototype of PAS binding AChEI, has represented a paradigm for the design of novel PAS binding fragments. According to the information retrieved from the available crystallographic structure (PDB ID 1N5R) and the computational studies carried out by Cavalli *et al.*,[189] it is broadly acknowledged that propidium can bind the PAS with two main orientations resulting from a flip of 180° around the phenanthridinium pseudosymmetry axis, and establish a π-π stacking, reinforced by additional cation-π interaction, with Trp286, and a supplementary hydrogen bond between one of its aromatic amine groups and His287 (**figure 4.1**).[188]

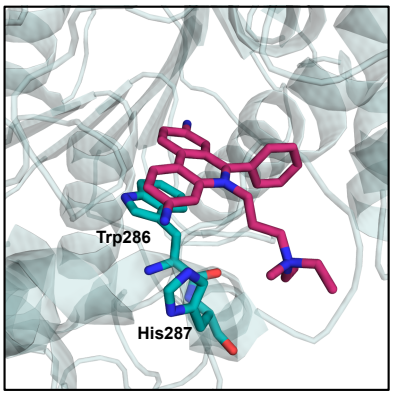

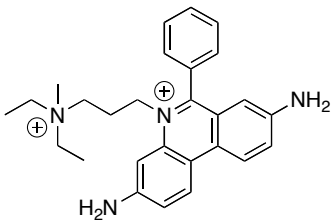

Propidium, **6**

Figure 4.1 Binding mode of propidium to the PAS of AChE and structure of propidium, **6**.

[187]Soreq, H.; Seidman, S. *Nat. Rev. Neurosci.* **2001**, *2*, 294.
[52]Inestrosa, N.C.; Alvarez, A.; Pérez, C.A.; Moreno, R.D.; Vicente, M.; Linker, C.; Casanueva, O.I.; Soto, C.; Garrido, C. *Neuron* **1996**, *16*, 81.
[53]Alvarez, A.; Alarcón, R.; Opazo, C.; Campos, E.O.; Muñoz, F.J.; Calderón, F.H., Dajas, F.; Gentry, M.K.; Doctor, B.P.; De Mello, F.G.; Inestrosa, N.C. *J. Neurosci.* **1998**, *18*, 3213.
[2]Muñoz-Torrero, D. *Curr. Med. Chem.* **2008**, *15*, 2433.
[188]Cavalli, A.; Bottegoni, G., Raco, C.; De Vivo, M.; Recanatini, M.A. *J. Med. Chem.* **2004**, *47*, 3991.

On the basis of these premises, in the PhD Thesis of Dr. Carles Galdeano, the pyrano[3,2-*c*]quinoline 4**5** was designed and synthesized envisaging, as the key step, a *Povarov* MCR reaction between 3,4-dihydro-2*H*-pyran, **42**, aniline **44** and benzaldehyde **43** (**Scheme 4.1**).[184,67,174]

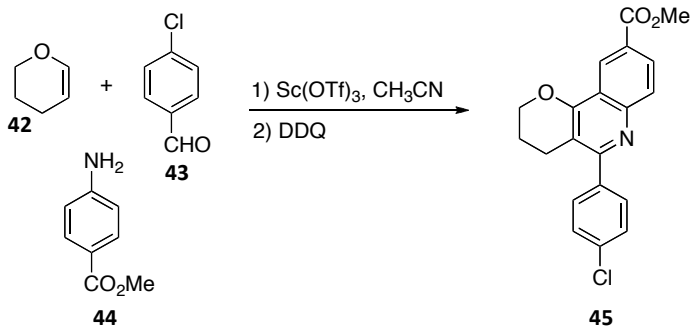

Scheme 4.1

Although computational studies confirmed the ability of the pyranoquinoline **45**, not protonated at physiological pH, to interact with PAS by means of a π-π stacking with the side chain of Trp286, a moderate AChE inhibitory activity was found for **45** (*h*AChE IC_{50} >10 μM).

4.2 Hit-to-lead optimization of a PAS-binding AChEI

4.2.1 Design of the first generation of tetrahydrobenzo[h][1,6]naphthyridines (49-61)

The low affinity displayed by compound **45** towards the PAS suggested that the formation of a cation-π interaction reinforcing the π-π stacking with Trp286 would be necessary for enhancing the inhibitory potency. Since the quinoline nitrogen atom of **45** was non protonated at physiological pH, an increased basicity was assumed to enhance the affinity towards the PAS. Thus, in the frame of the PhD Thesis of Drs. Elisabet Viayna and Esther Vicente, and my Leonardo Project, carried out previously to this PhD Thesis, the bioisosteric replacement of the pyran oxygen atom by nitrogen drove the subsequent *hit-to-lead* optimization of structure **45**. To this end, the *Povarov* MCR strategy allowed to combine with high versatility commercially

[184]Galdeano, C. PhD thesis. *Unitat de Química Farmacèutica, Departament de Farmacologia i Química Terapèutica, Universitat de Barcelona*, **2012**.
[67]Camps, P.; Formosa, X.; Galdeano, C.; Muñoz-Torrero, D.; Ramírez, L.; Gómez, E.; Isambert, N.; Lavilla, R.; Badia, A.; Clos, M.V.; Bartolini, M.; Mancini, F.; Andrisano, V.; Arce, M.P.; Rodríguez-Franco, M.I.; Huertas, O.; Dafni, T.; Luque, F.J. *J. Med. Chem.* **2009**, *52*, 5365.
[174]Povarov, L.S. *Russ. Chem. Rev.* **1967**, *36*, 656.

available or easy to prepare building blocks, affording a novel family of tetrahydrobenzo[*h*][1,6]naphthyridines (structures **49**-**61**, **Schemes 4.3**-**4.6**).[186,189,182]

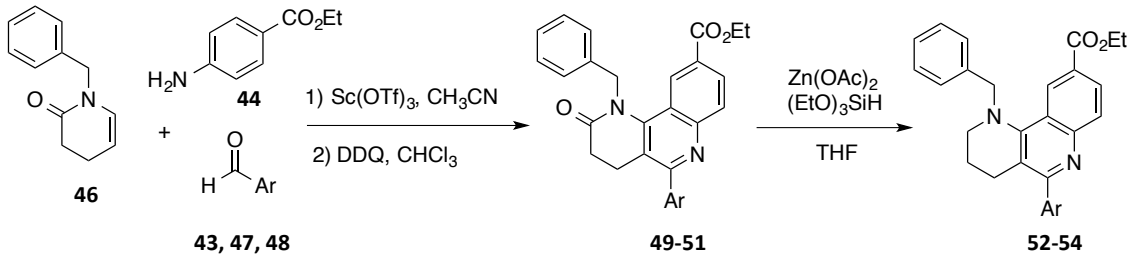

43, **49**, **52**, Ar = *p*-chlorophenyl
47, **50**, **53**, Ar = *p*-CO_2MePh
48, **51**, **54**, Ar = 3-pyridyl

Scheme 4.3

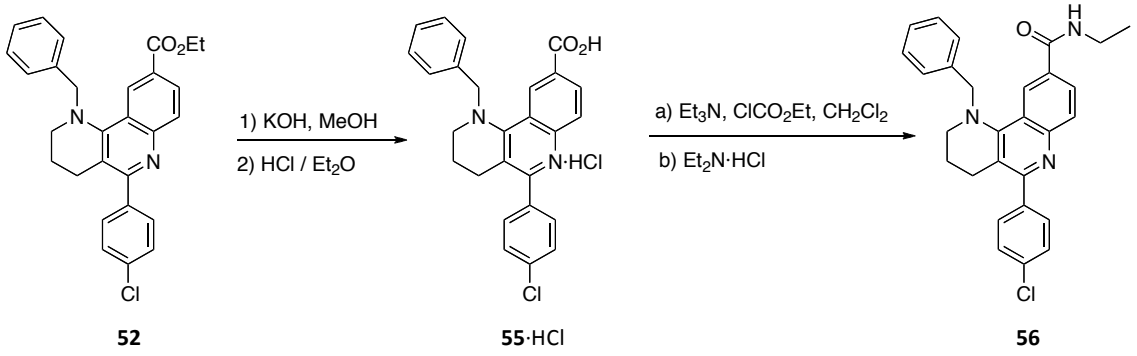

Scheme 4.4

[186]Viayna, M.E. PhD thesis. *Unitat de Química Farmacèutica, Departament de Farmacologia i Química Terapèutica, Universitat de Barcelona*, **2013**.
[189]Vicente-García, E. PhD thesis. *Unitat de Química Farmacèutica, Departament de Farmacologia i Química Terapèutica, Universitat de Barcelona*, **2013**.
[182]Di Pietro, O.; Viayna, E.; Vicente-Gracía, E.; Bartolini, M.; Ramón, R.; Juárez-Jiménez, J.; Clos, M.V.; Pérez, B.; Andrisano, V.; Luque, F.J.; Lavilla, R.; Muñoz-Torrero, D. *Eur. J. Med. Chem.* **2014**, *73*, 141.

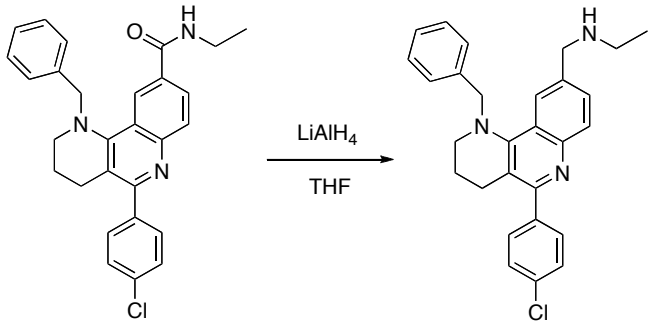

56 **57**

Scheme 4.5

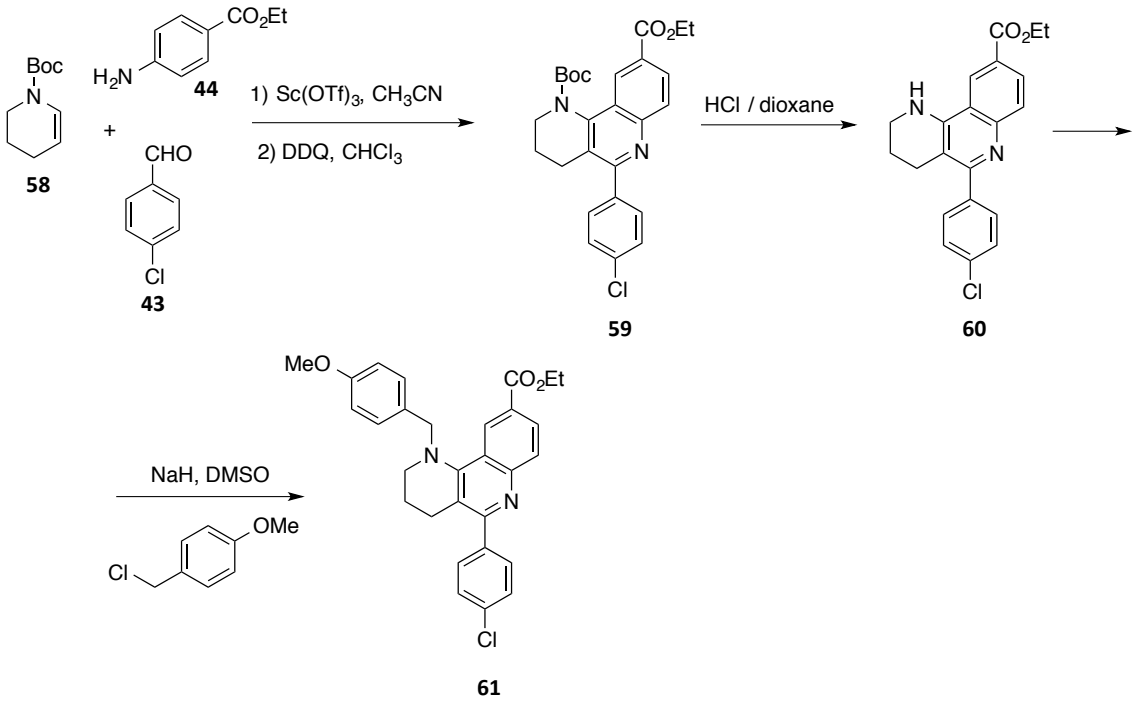

Scheme 4.6

After a preliminary evaluation against *ee*AChE, the inhibitory potency of benzonaphthyridines **49**-**61** against human recombinant AChE (*h*AChE) was determined with the method of Ellman *et al.*[190] Interestingly, despite IC_{50} values in the same range as that of propidium (*h*AChE IC_{50} 32.3 μM)[191] were expected, these novel class of PAS-binding ligands resulted to be low micromolar or, in some cases, even nanomolar inhibitors of *h*AChE.

[190]Ellman, G.L.; Courtney, K.D.; Andres, B. Jr.; Featherstone, R.M.; *Biochem. Pharmacol*. **1961**, *7*, 88.
[191]Bolognesi, M.L.; Andrisano, V.; Bartolini, M.; Banzi, R.; Melchiorre, C. *J. Med. Chem.* **2005**, *48*, 24.

Table 4.1 *ee*AChE, *h*AChE and *h*BChE inhibitory activities of the first generation benzonaphthyridine derivatives **49-61**.[a]

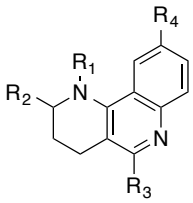

	R_1	R_2	R_3	R_4	IC_{50} (μM) *ee*AChE[a]	IC_{50} (μM) *h*AChE[a]	% inhibition at 30 μM *h*BChE
49	Bn	O	*p*-chlorophenyl	CO_2Et	5.21 ± 0.33	4.15 ± 0.16	8.41%
50	Bn	O	*p*-CO_2MePh	CO_2Et	13.61 ± 1.85	> 25	5.54%
51	Bn	O	3-pyridyl	CO_2Et	> 30	13.0 ± 0.8	4.42%
52	Bn	H, H	*p*-chlorophenyl	CO_2Et	6.33 ±1.85	> 25	8.68%
53	Bn	H, H	*p*-CO_2MePh	CO_2Et	6.62 ± 0.62	> 25	6.61%
54	Bn	H, H	3-pyridyl	CO_2Et	1.97 ± 0.17	1.06 ± 0.09	*nd*
56	Bn	H, H	*p*-chlorophenyl	C(O)NHEt	5.48 ± 0.512	0.801 ± 0.069	25.3%
57	Bn	H, H	*p*-chlorophenyl	CH_2NHEt	0.147 ± 0.01	0.942 ± 0.038	*nd*
60	H	H, H	*p*-chlorophenyl	CO_2Et	0.281 ± 0.03	> 25	20.3%
61	PMB	H, H	*p*-chlorophenyl	CO_2Et	> 30	> 25	12.4%

[a]Values are expressed as the mean ± SEM of at least four experiments; IC_{50}: inhibitory concentration (μM) of *Electrophorus electricus* AChE or human AChE. *nd* means not determined.

The structure-activity relationships (SAR) extracted from the data in **Table 4.1** disclosed some trends with respect to the AChE inhibitory potency of this first generation of tetrahydrobenzo[*h*][1,6]naphthyridines. As expected, reduction of the amidoquinoline moiety to the corresponding aminoquinoline, generally resulted in an enhanced inhibitory potency, with **53** and **54** being 2-fold and 12- fold more potent against *ee*AChE and *h*AChE, respectively, than their amidoquinoline analogues **50** and **51**. This can be attributed to the increased basicity of the quinoline nitrogen atom in the aminoquinoline system with respect to its oxidized analogue, a property that would allow the formation of an additional cation-π interaction with Trp286, as hypothesized in the initial design. Moreover, the debenzylation of the piperidine nitrogen atom produced, at least in *ee*AChE, an increase in the binding affinity, since **60** was almost 23-fold more potent than its benzylated analogue **52**. Finally, a considerable increase in potency was also found when a second protonatable nitrogen atom was introduced. Thus, the 3-pyridyl derivative **54** and compound **57**, bearing a *N*-ethylaminomethyl substituent at position 9, are 3- and 43-fold, respectively, more potent in *ee*AChE compared with its *p*-chlorophenyl analogue **52**. Conversely, the effect of introducing

an ethylamide group on the biological activity is less clear. Indeed, while reduction of ethylamide group to the corresponding amine does not produce any significant effect on *h*AChE inhibition (note that both **56** and **57** IC_{50} values are in the same range), in *ee*AChE this chemical modification resulted, instead, in a 37-fold increased potency for **57**. On the other hand, replacement of the ethyl ester group at position 9 of **52** with the corresponding amide function increased the potency against *h*AChE by more than 31-fold for **56**, a trend not maintained in *ee*AChE, where **52** and **56** resulted to be practically equipotent.

4.2.2 Design of the second generation of tetrahydrobenzo[h][1,6]naphthyridines

In light of these SAR trends, the first project carried out within this PhD thesis, in collaboration with Dr. Esther Vicente, was the design and synthesis of an optimized second generation of tetrahydrobenzo[*h*][1,6]naphthyridines. As shown in **Figure 4.2**, the best substitution patterns found for the first generation compounds were separately introduced in the novel structures with the aim of identifying a *lead* PAS-binding fragment suitable for further hybridization with an appropriate *N*-aminoalkyl−6-chlorotacrine unit.

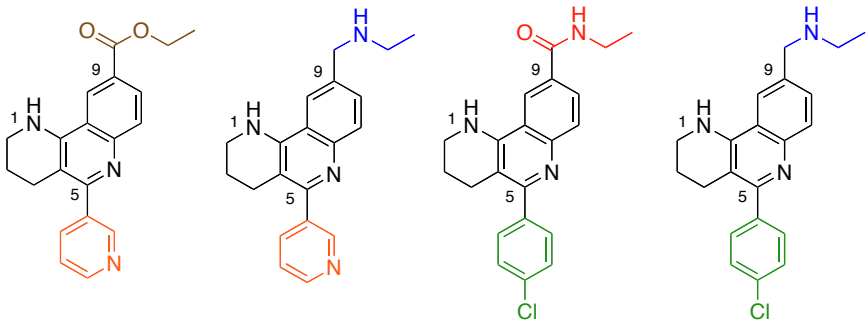

62 **63** **68** **69**

Figure 4.2

Analogously to the first generation compounds, also the optimized benzonaphthyridines **62**, **63**, **68** and **69** were evaluated *in vitro* against both *ee*AChE and *h*AChE, and their capability to cross the BBB was attested through the well-established PAMPA-BBB assay. According to the pharmacological results, the optimization process successfully led to the *lead* compound **68** (IC_{50} 65nM), displaying more than 154-fold enhanced potency against *h*AChE with respect to the *hit* compound **45**. Further kinetic studies attested that a "mixed-type" mode of inhibition is at the base of the anticholinesterase activity displayed by this novel class of

benzonaphthyridine derivatives, and the propidium-displacement assay strongly confirmed their ability to tightly bind the PAS.

4.3 Synthesis of the tetrahydrobenzo[h][1,6]naphthyridines 68 and 69

Benzonaphthyridines **68** and **69** were prepared *via* a synthetic route consisting, in its first step, of a *Povarov* MCR of *p*-chlorobenzaldehyde, **43**, with aniline **44** and the *N*-Boc protected enamine **58** in anhydrous acetonitrile, stirring for 3 days at r. t., under $Sc(OTf)_3$ catalysis. This reaction afforded a diastereomeric mixture of octahydrobenzo[*h*][1,6]naphthyridines **64** in 63% yield, after silica gel column chromatography purification (**Scheme 4.7**).

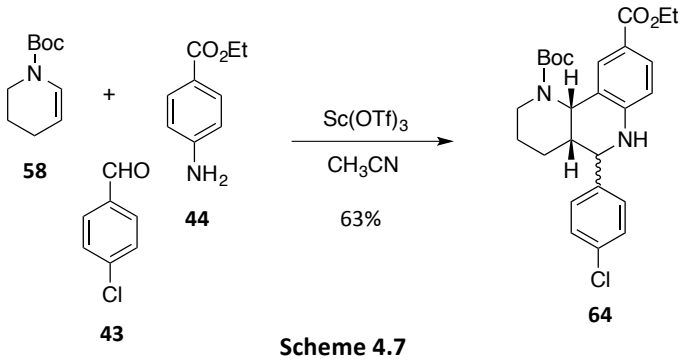

Scheme 4.7

The diastereomeric mixture **64** was then dissolved in anhydrous chloroform, treated with 2 equivalents of DDQ and stirred at r. t. overnight, thus providing the corresponding oxidized derivative **65** in 89% yield, after column chromatography purification (**Scheme 4.8**).

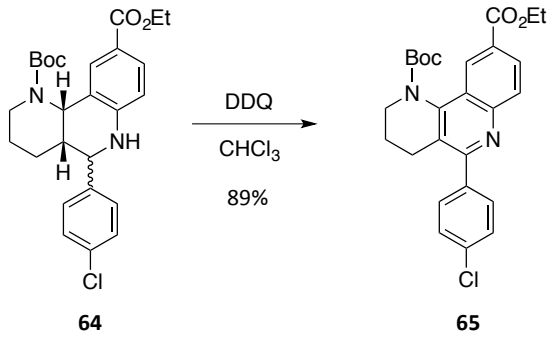

Scheme 4.8

Next, the hydrolysis of the ethyl ester group at position 9 to the corresponding carboxylate was performed by overnight treatment with an excess of KOH at the reflux temperature of

MeOH. After concentration under reduced pressure of the reaction mixture, the resulting solid residue was acidified with an excess of a 0.5 N solution of HCl in Et_2O. The suspension was concentrated again under reduced pressure to afford the hydrochloride salt of the desired carboxylic acid **66**. Then, **66**·HCl was dissolved in anhydrous CH_2Cl_2, treated at 0 °C with freshly distilled Et_3N and $ClCO_2Et$. The resulting mixture was stirred at 0 °C for 30 min to be subsequently treated with $EtNH_2$·HCl and stirred at r. t. for 3 days, finally affording the desired *N*-Boc protected amide derivative **67** in 50% yield, after column chromatography purification (**Scheme 4.9**).

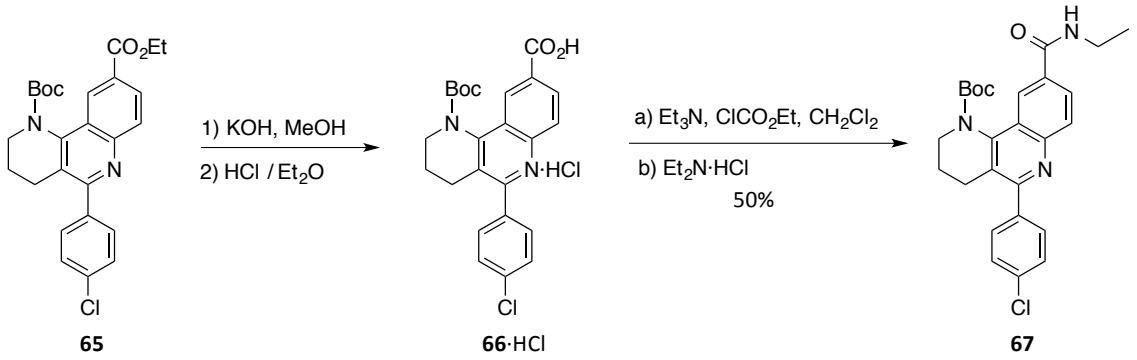

65 **66**·HCl **67**

Scheme 4.9

Unexpectedly, the $LiAlH_4$ reduction reaction of **67** directly provided the desired deprotected amine **69** in 35% yield after column chromatography purification, together with a lower amount of the deprotected amide **68** (14% yield, **Scheme 4.10**).

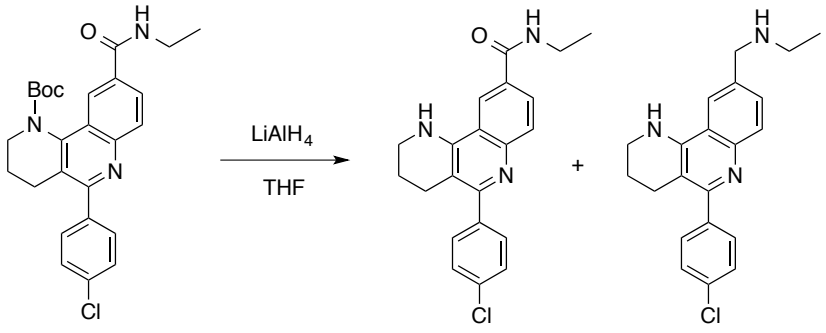

67 **68** 14% **69** 35%

Scheme 4.10

It is worth noting that an alternative synthetic route, which was successful for the preparation of the antiprotozoan quinoline derivative **167** (see *Chapter 8*), was also performed.

The above mentioned synthetic route envisaged the preliminary preparation of aniline **72**, *via* reductive amination reaction of acetaldehyde with amine **70** using $NaBH(AcO)_3$ as reductor, or, alternatively, *via* alkylation of **71** with EtBr. While this latter approach did not afford the desired product **72** (**Scheme 4.11**), the reductive amination reaction, after treatment of the resulting crude with $(Boc)_2O$ in anhydrous THF and subsequent column chromatography purification, provided the *N*-Boc protected amine **72** in 19% overall yield (**Scheme 4.12**).

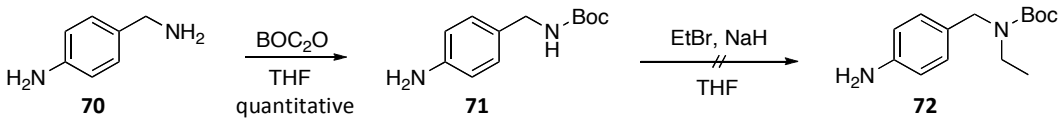

Scheme 4.11

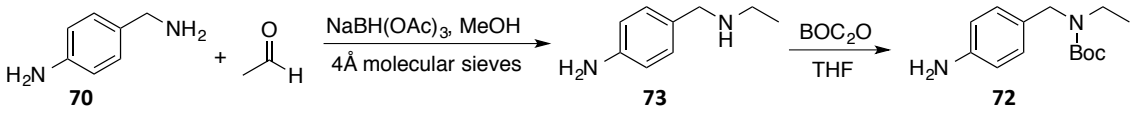

Scheme 4.12

Unfortunately, when the *Povarov* MCR of **72** with benzaldehyde **43** and enamine **58** was attempted, a complex mixture, not containing the desired benzonaphthyridine **74**, was obtained. Therefore, the possibility to resort to the longer synthetic route previously described (**Schemes 4.7**-**4.10**) was reconsidered, thus leading to the desired benzonaphthyridines **68** and **69**.

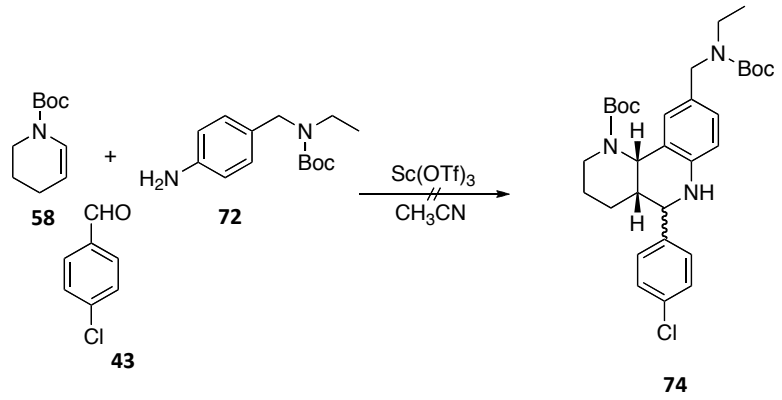

Scheme 4.13

4.4 Molecular modelling studies on benzonaphthiridines 68 and 69

Since the debenzylated amide and amine derivatives, **68** and **69**, turned out to be the most potent *h*AChEIs of the series, displaying an IC_{50} value of 0.065 μM and 0.556 μM, respectively, both compounds were selected for further computational studies aimed at shedding light on the molecular determinants of their high inhibitory potency. Thus, preliminary docking calculations were carried out with rDock, after validation of the program's effectiveness in predicting the binding mode of a number of AChE inhibitors to the enzyme. The X-ray structure of the human recombinant AChE (PDB ID: 3LII) was used and three different orientations of Trp286, as emerged from inspection of the available crystallographic structures, were considered.

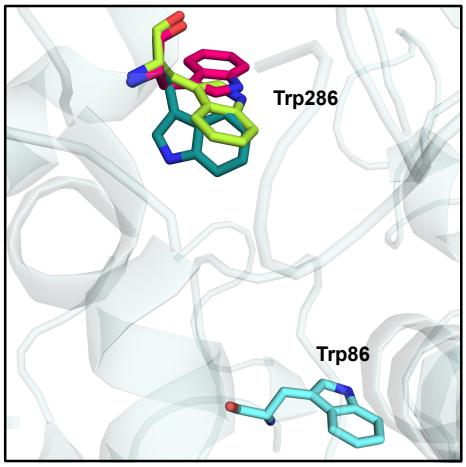

Figure 4.3 Representation of the three major conformations adopted by Trp286 upon inspection of the available X-ray structures [PDB ID: 1N5R (cyan structure), 1Q83 (magenta structure), 2CKM (yellow structure)].

According to the docking results, **68** and **69** displayed a preferential binding to the AChE model in which Trp286 adopts the same orientation as in the AChE-propidium complex (PDB ID: 1N5R). This finding reflects the structural similarity of these compounds to propidium. Thus, the binding mode predicted by the docking calculations was further refined throughout a 100 ns MD simulation. The RMSD analysis pointed out that, apart from an initial rearrangement of the ligand, which did not alter either the orientation of the neighboring residues or the shape of the binding site, the simulations provided structurally and energetically stable trajectories (**Figure 4.4**).

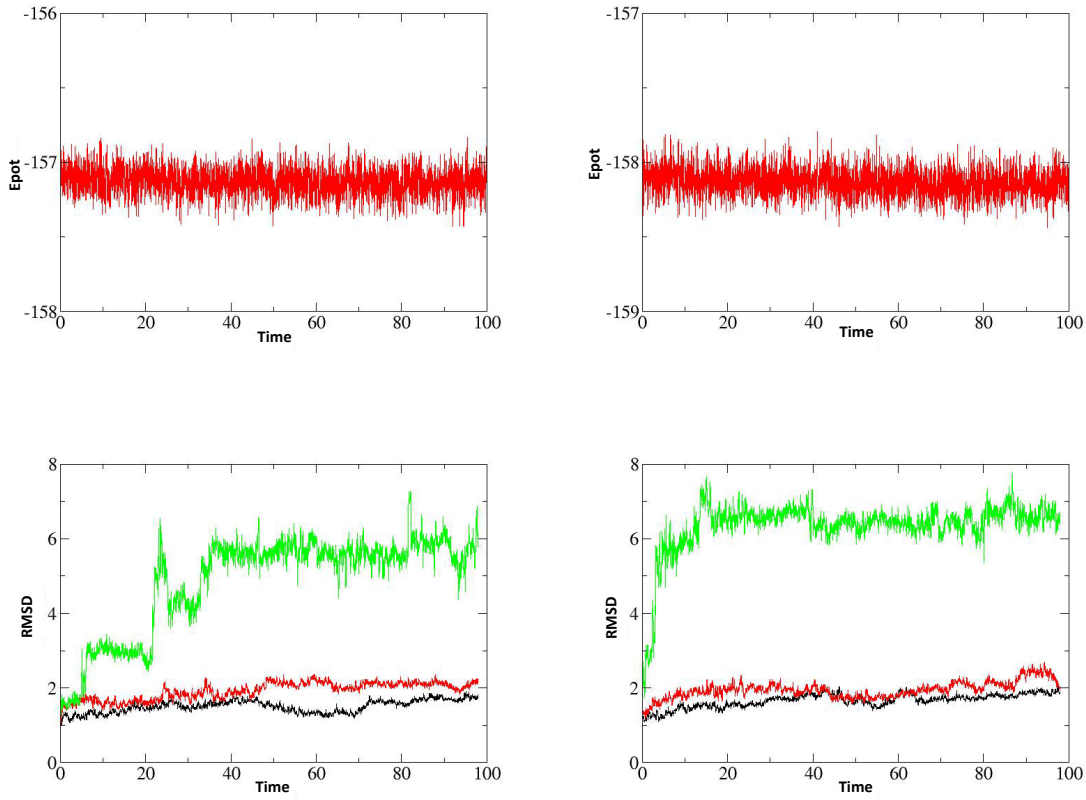

Figure 4.4 (Top) Time evolution of the potential energy (× 10^3; kcal/mol) determined for the simulations of the AChE complexes with compounds **68** (right) and **69** (left). (Bottom) Time evolution of the RMSD (Å) determined for the backbone (black), the heavy atoms of the residues that define the binding site (red) and the ligand (green) for the simulations of the AChE complexes with compounds **68** (right) and **69** (left).

In a general overview, a similar binding mode was predicted for **68** and **69**, which formed a network of interactions with different residues at the PAS and midgorge sites. The results confirmed the formation of a cation-π interaction between the protonated quinoline nitrogen atom of the ligands and Trp286 in the PAS, as pursued in the initial design of this novel family of benzonaphthyridine compounds. Moreover, such binding mode was further stabilized by the formation of hydrogen bonds between the quinoline nitrogen atom and the hydroxyl

group of Tyr72 and between the amide NH group and the hydroxyl group of Tyr124. The protonated amine of the side chain at position 9 was involved in the formation of a water-mediated bridge with Asp74, a cation-π interaction with Tyr341, and water-mediated hydrogen bonds with the carbonyl groups of Ser293 and Phe338 through the NH group at position 1 (**Figure 4.5**).

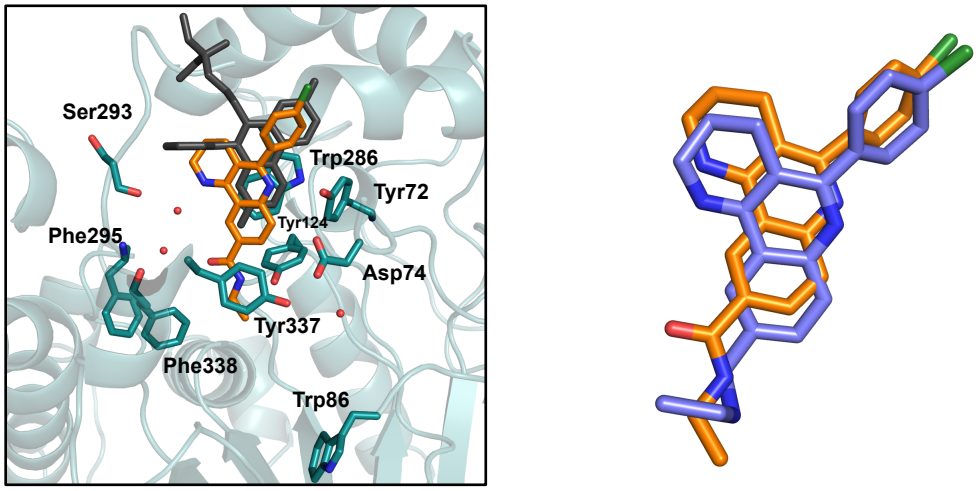

Figure 4.5 (Left) Representation of the binding mode of compound **68** (in orange) obtained at the end of the 100 ns MD trajectory. The side chains or backbone units of the residues involved in interactions are shown as cyan-colored sticks. Water molecules that mediate interactions of the ligand are shown as red spheres. Propidium is shown as grey sticks. (Right) Superposition of the compounds **68** (orange) and **69** (purple) as found at the end of the MD trajectories.

The predicted binding mode for the debenzylated compounds **68** and **69** also provided a rationale of the weaker potency displayed by the benzylated derivatives **56** and **57**, a result mainly ascribed to the steric perturbation of the network of stabilizing interactions upon attachment of the *N*-benzyl group at position 1.

Furthermore, to gain more insight into the molecular determinants of the higher inhibitory activity of **68** compared to **69**, their binding affinities were determined using the Solvation Interaction Energy (SIE) calculations. According to the results extracted from **Table 4.2**, the SIE method predicted similar binding affinities for both **68** (–8.5 ± 0.4 kcal/mol) and **69** (–8.8 ± 0.6 kcal/mol), which strongly compare, within the intrinsic uncertainty of the method itself, with the experimental value determined from the inhibition constant for **68** (–9.7 kcal/mol). Thereby, since both compounds exhibit a similar binding mode, it is reasonable to conclude that the large desolvation penalty of the protonated amine at position 9 of **69** is counterbalanced by its enhanced coulombic stabilization, the overall effect leading to the prediction of similar binding affinities through the SIE method.

Table 4.2

Free energy components determined from Solvent Interaction Energy (SIE) computations for the binding of compounds **68** and **69**.[a]

Component	68	69
van der Waals (ΔE_{vW})	–44.1 ± 2.8	–42.2 ± 2.8
Coulombic (ΔE_{Coul})	–93.6 ± 5.7	–198.8 ± 6.1
Reaction Field (ΔG_{RF})	92.6 ± 5.0	192.2 ± 4.9
Cavity (γ ΔSA)	–8.1 ± 0.5	–7.7 ± 0.5
Total (ΔG) [a]	–8.5 ± 0.4	–8.8 ± 0.6

[a] Evaluated from the expression $\Delta G = \alpha\left[\Delta E_{vW} + \Delta E_{Coul} + \Delta G_{RF} + \gamma \Delta SA\right] + C$, where the parameters α (0.1048) and C (–2.89 kcal/mol) were fitted to the absolute binding free energies of 99 protein–ligand complexes.

European Journal of Medicinal Chemistry 73 (2014) 141–152

Contents lists available at ScienceDirect

European Journal of Medicinal Chemistry

journal homepage: http://www.elsevier.com/locate/ejmech

Original article

1,2,3,4-Tetrahydrobenzo[*h*][1,6]naphthyridines as a new family of potent peripheral-to-midgorge-site inhibitors of acetylcholinesterase: Synthesis, pharmacological evaluation and mechanistic studies

Ornella Di Pietro [a], Elisabet Viayna [a], Esther Vicente-García [b], Manuela Bartolini [c], Rosario Ramón [b], Jordi Juárez-Jiménez [d], M. Victòria Clos [e], Belén Pérez [e], Vincenza Andrisano [f], F. Javier Luque [d], Rodolfo Lavilla [b,g,*], Diego Muñoz-Torrero [a,**]

[a] *Laboratori de Química Farmacèutica (Unitat Associada al CSIC), Facultat de Farmàcia, and Institut de Biomedicina (IBUB), Universitat de Barcelona, Av. Joan XXIII 27-31, E-08028 Barcelona, Spain*
[b] *Barcelona Science Park, Baldiri Reixac 10-12, E-08028 Barcelona, Spain*
[c] *Department of Pharmacy and Biotechnology, Alma Mater Studiorum, University of Bologna, Via Belmeloro 6, I-40126 Bologna, Italy*
[d] *Departament de Fisicoquímica, Facultat de Farmàcia, and IBUB, Universitat de Barcelona, Prat de la Riba 171, E-08921 Santa Coloma de Gramenet, Spain*
[e] *Departament de Farmacologia, de Terapèutica i de Toxicologia, Institut de Neurociències, Universitat Autònoma de Barcelona, E-08193 Bellaterra, Barcelona, Spain*
[f] *Department for Life Quality Studies, University of Bologna, Corso d'Augusto 237, I-47921 Rimini, Italy*
[g] *Laboratori de Química Orgànica, Facultat de Farmàcia, Universitat de Barcelona, Av. Joan XXIII 27-31, E-08028 Barcelona, Spain*

ARTICLE INFO

Article history:
Received 14 October 2013
Received in revised form
5 December 2013
Accepted 6 December 2013
Available online 18 December 2013

Keywords:
Benzo[*h*][1,6]naphthyridines
Povarov reaction
Dual inhibitors
AChE PAS binding
AChE midgorge binding

ABSTRACT

A series of 1,2,3,4-tetrahydrobenzo[*h*][1,6]naphthyridines differently substituted at positions 1, 5, and 9 have been designed from the pyrano[3,2-*c*]quinoline derivative **1**, a weak inhibitor of acetylcholinesterase (AChE) with predicted ability to bind to the AChE peripheral anionic site (PAS), at the entrance of the catalytic gorge. Fourteen novel benzonaphthyridines have been synthesized through synthetic sequences involving as the key step a multicomponent Povarov reaction between an aldehyde, an aniline and an enamine or an enamide as the activated alkene. The novel compounds have been tested against *Electrophorus electricus* AChE (EeAChE), human recombinant AChE (hAChE), and human serum butyrylcholinesterase (hBChE), and their brain penetration has been assessed using the PAMPA-BBB assay. Also, the mechanism of AChE inhibition of the most potent compounds has been thoroughly studied by kinetic studies, a propidium displacement assay, and molecular modelling. We have found that a seemingly small structural change such as a double O → NH bioisosteric replacement from the hit **1** to **16a** results in a dramatic increase of EeAChE and hAChE inhibitory activities (>217- and >154-fold, respectively), and in a notable increase in hBChE inhibitory activity (>11-fold), as well. An optimized binding at the PAS besides additional interactions with AChE midgorge residues seem to account for the high hAChE inhibitory potency of **16a** (IC_{50} = 65 nM), which emerges as an interesting anti-Alzheimer lead compound with potent dual AChE and BChE inhibitory activities.

1. Introduction

Alzheimer's disease (AD) is a progressive and ultimately fatal neurodegenerative disorder that is currently threatening every health system worldwide. The number of people with AD increases rapidly, and in line with this, both prevalence and costs are also increasing [1]. Currently, it is estimated that dementia, of which AD is the most common type, is affecting 36 million people, with a total cost amounting to as much as 1% of global gross domestic product [1]. AD is among the top ten causes of death, but, worryingly, the only one that cannot be prevented, cured or slowed down [2], thereby making it imperative the development of efficacious drugs.

Current therapeutic options, i.e. the acetylcholinesterase (AChE) inhibitors donepezil, galantamine and rivastigmine and the glutamate NMDA receptor antagonist memantine, are regarded as merely symptomatic, and very promising β-amyloid (Aβ)-directed

* Corresponding author. Barcelona Science Park, Baldiri Reixac 10-12, E-08028 Barcelona, Spain. Tel.: +34 934037106; fax: +34 934024539.
** Corresponding author. Laboratori de Química Farmacèutica (Unitat Associada al CSIC), Facultat de Farmàcia, and IBUB, Universitat de Barcelona, Av. Joan XXIII, 27-31, E-08028 Barcelona, Spain. Tel.: +34 934024533; fax: +34 934035941.
E-mail addresses: rlavilla@pcb.ub.es (R. Lavilla), dmunoztorrero@ub.edu (D. Muñoz-Torrero).

0223-5234/$ – see front matter © 2013 Elsevier Masson SAS. All rights reserved.
http://dx.doi.org/10.1016/j.ejmech.2013.12.008

drug candidates designed to confront the underlying mechanisms of AD are inexorably failing in late stage clinical trials due to lack of efficacy or safety. The increasingly accepted notion that Aβ is not *the* cause but *one of the* causes of AD [3] is spurring the development of multi-target drugs that simultaneously hit Aβ formation and aggregation as well as other important targets such as tau hyperphosphorylation and aggregation, oxidative stress and cholinesterases, among others, as a more realistic option to effectively treat AD [4].

In every case, any single-target or multi-target drug candidate purported to modify AD progression would need to be administered in the early presymptomatic or preclinical stage of AD, before neurodegeneration is too widespread. Indeed, preclinical AD has been proposed as the initial stage of AD in the new criteria and guidelines for diagnosing AD [2]. Accurate and reliable biomarkers, indicative of the earliest signs of the disease, are necessary both to identify individuals in the presymptomatic stage of AD, amenable to early interventions with disease-modifying drugs and to monitor their effects. Many research endeavours are being made to select the best diagnostic biomarkers or combinations thereof [5] but much more work is still needed before preclinical AD can be diagnosed [2]. Meanwhile, diagnosis of AD will remain based on symptoms, i.e. on the occurrence of cognitive decline, for whose alleviation AChE inhibitors (AChEIs) are the best therapeutic option [6], thereby warranting the search for novel AChEIs.

Most known AChEIs have been designed to interact with the catalytic site of the enzyme, which is placed at the bottom of a 20 Å deep narrow gorge. The entrance of the gorge contains the so-called peripheral anionic site (PAS) [7], which can be also targeted either separately or simultaneously by potential inhibitors [8]. Recently, we have developed a new family of AChEIs that consisted of a pyrano[3,2-*c*]quinoline moiety connected through linkers of different lengths to a unit of the potent active site AChEI 6-chlorotacrine [9]. Among those hybrids, the most potent human AChE (hAChE) inhibitors bore a 5-(4-chlorophenyl)pyrano[3,2-*c*]quinoline moiety, which is present in their synthetic ester precursor **1** (Fig. 1) and is reminiscent to the phenyl-substituted tricyclic system of the AChE PAS inhibitor propidium (**2**, Fig. 1). Not unexpectedly, molecular dynamics simulations suggested that the 5-(4-chlorophenyl)pyrano[3,2-*c*]quinoline moiety of the hybrids interacts at the PAS of AChE, namely by establishing π–π stacking interactions with residues Trp286 and Tyr72 (hAChE numbering), whereas the 6-chlorotacrine unit interacts with the active site residues Trp86 and Tyr337. Strikingly, despite the predicted ability of the 5-(4-chlorophenyl)pyrano[3,2-*c*]quinoline moiety to interact with the AChE PAS, compound **1** was found to be essentially inactive as inhibitor of hAChE ($IC_{50} > 10$ μM).

In the light of these results, we inferred that substitution of the oxygen atom at position 1 of the pyrano[3,2-*c*]quinoline system of **1** by a nitrogen atom would result in increased basicity of the quinoline nitrogen atom, which would become protonatable at physiological pH. This would enable the resulting benzo[*h*][1,6]naphthyridine system to establish cation–π interactions additionally to the π–π stacking, thereby potentially increasing its affinity for the PAS of AChE and the AChE inhibitory activity. These interactions would be similar to those established by the phenanthridinium system of propidium, but unlike propidium, the non-permanent character of the positive charge at the quinoline nitrogen atom of the benzo[*h*][1,6]naphthyridine system would not preclude their penetration into the central nervous system (CNS).

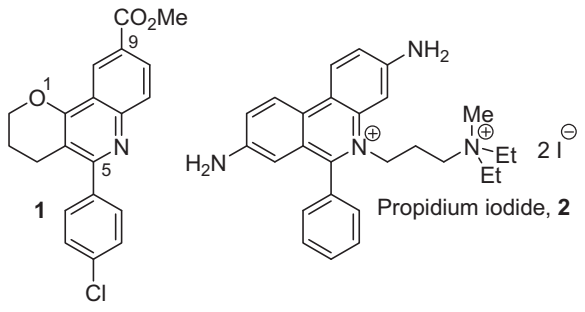

Fig. 1. Structure of the pyrano[3,2-*c*]quinoline derivative **1** and the peripheral site AChE inhibitor propidium iodide.

Herein, we describe the synthesis, cholinesterase inhibitory activity evaluation and a comprehensive assessment of the binding mode to AChE by kinetic, propidium displacement and molecular modelling studies of a series of 1,2,3,4-tetrahydrobenzo[*h*][1,6]naphthyridines differently substituted at positions 1, 5, and 9. Moreover, the brain penetration of these compounds has been assessed using the parallel artificial membrane permeation assay (PAMPA-BBB).

2. Results and discussion

2.1. Synthesis of the target compounds

To assess the effect on cholinesterase inhibitory activity of substitution at position 1, we initially planned the synthesis of 1,2,3,4-benzo[*h*][1,6]naphthyridines bearing an ethyl ester group at position 9 and a 4-chlorophenyl substituent at position 5, like in the pyrano[3,2-*c*]quinoline analogue **1**, and either a benzyl group (**10a**), hydrogen atom (**12a**) or a 4-methoxybenzyl group (**13a**) on the nitrogen atom at position 1 (Scheme 1). Also, to ascertain the effect of the substituent at position 5, we planned the synthesis of the 1-benzylated ethyl ester analogues bearing a 3-pyridyl (**10b**) or 4-methoxycarbonylphenyl (**10c**) substituent at position 5. Finally, to shed light on the role of the substituent at position 9, we studied the substitution of the ethyl carboxylic ester group of **10a** by an *N*-ethyl carboxamide (**14a**) and an ethylaminomethyl (**17a**) group. Following the evaluation of the AChE inhibitory activity of this first generation of 1,2,3,4-benzo[*h*][1,6]naphthyridine derivatives and the establishment of structure–activity relationships, we additionally envisioned the synthesis of compounds **12b**, **16a**, **18a**, and **18b** (Scheme 1) as second generation optimized analogues (see below).

The synthesis of compounds **10a**–**c** was envisaged through a three-step sequence involving an initial Povarov multicomponent reaction [10] between the known cyclic enamide **3** [11], as the activated alkene, ethyl 4-aminobenzoate, **5**, and the aromatic aldehydes **4a**–**c**, under $Sc(OTf)_3$ catalysis in acetonitrile (Scheme 1). These reactions afforded in moderate to good yields and 1:1 to 1.7:1 diastereomeric ratio the diastereomeric mixtures of *cis*-fused octahydronaphthyridines **6a**–**c**, which were subjected to DDQ oxidation [12] to yield the lactams **9a**–**c** in 73%, 5%, and 36% yield, respectively, after silica gel column chromatography purification. In an attempt to improve the yield of **9b**, the oxidation of the mixture **6b** with MnO_2 [13] instead of DDQ only afforded unreacted material and open-ring byproducts. Chemoselective reduction of lactams **9a**–**c** with $(EtO)_3SiH$ under $Zn(OAc)_2$ catalysis [14] provided the desired benzonaphthyridines **10a**–**c** in low to moderate (15–52%) yields.

Analogously, the Povarov reaction of aniline **5**, aldehydes **4a**,**b** and the commercially available *N*-Boc-protected cyclic enamine **7**, followed by DDQ or MnO_2 oxidation of the resulting diastereomeric mixtures **8a**,**b** afforded the *N*-Boc-protected derivatives **11a** and **11b** in 57% and 24% overall yields (Scheme 1). Acidic deprotection of **11a** quantitatively yielded the target benzonaphthyridine **12a**, which was also used as starting material for the synthesis of the 1-(4-methoxybenzyl)-substituted benzonaphthyridine **13a** (40% yield) by deprotonation with NaH and alkylation with 1-

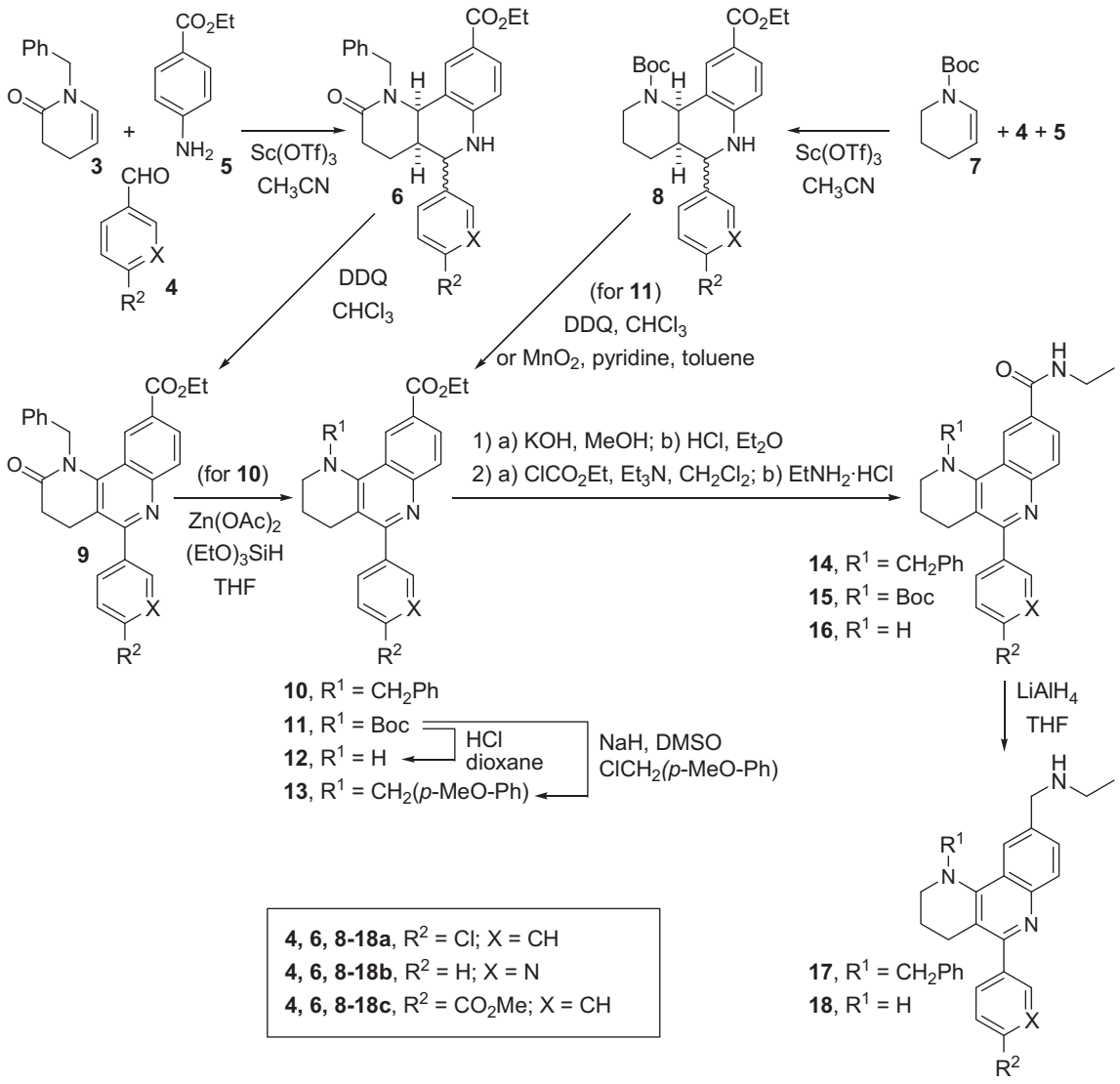

Scheme 1. Synthesis of the target 1,2,3,4-tetrahydrobenzo[*h*][1,6]naphthyridines.

chloromethyl-4-methoxybenzene. In turn, acidic deprotection of **11b** afforded the target benzonaphthyridine **12b** in 76% yield.

Derivatization at position 9 was carried out following standard procedures. Thus, ethyl carboxylic esters **10a**, **11a** and **12b** were converted into the corresponding *N*-ethylcarboxamides **14a**, **15a** and **16b**, respectively, in moderate overall yields, by alkaline hydrolysis followed by reaction of the resulting carboxylic acids, isolated as naphthyridine hydrochlorides, with ethyl chloroformate in the presence of Et_3N, and reaction of the mixed anhydrides with ethylamine (Scheme 1). Finally, $LiAlH_4$ reduction of the amides **14a** and **16b** afforded the amines **17a** and **18b** in 44% and 51% yields, respectively, whereas reaction of the *N*-Boc-protected amide **15a** with $LiAlH_4$ proceeded with both *N*-Boc-deprotection and reduction of the amide, directly affording the target *N*-Boc-deprotected benzonaphthyridine **18a** in 35% yield, together with a small amount of the *N*-Boc-deprotected amide **16a** (14% yield).

2.2. Biological activity assays

The inhibitory activity of the novel 1,2,3,4-tetrahydrobenzo[*h*][1,6]naphthyridines against *Electrophorus electricus* AChE (EeAChE) and human recombinant (hAChE) was evaluated by the method of Ellman *et al.* [15]. Another cholinesterase that seems to play an important role in the cognitive decline associated to AD is butyrylcholinesterase (BChE). BChE exerts a compensatory effect in response to the decrease of AChE in CNS as AD progresses, thereby making dual inhibition of AChE and BChE a desirable property for anti-Alzheimer drugs [16]. Thus, the inhibitory activity of these compounds against human serum BChE (hBChE) was determined as well [15].

In general, the novel first-generation benzonaphthyridines were found to be moderately potent inhibitors of EeAChE, with IC_{50} values ranging from the submicromolar to the low micromolar range (Table 1). The best substitution pattern at position 1 clearly involves the presence of an unsubstituted secondary amino group, compound **12a** being 23- and >107-fold more potent EeAChE inhibitor than the *N*-benzylated and *N*-(4-methoxy)benzylated counterparts **10a** and **13a**, respectively. With the sole exception of **12a**, the rest of first generation benzonaphthyridines are *N*-benzylated derivatives, among which two additional structure–activity relationship (SAR) trends leading to a higher EeAChE inhibitory activity could be derived, namely the presence of a 3-pyridyl and an ethylaminomethyl substituent at positions 5 and 9, respectively. Thus, the 5-(3-pyridyl)-substituted ester **10b** is 3-fold more potent

Table 1
Inhibitory activity of 1,2,3,4-tetrahydrobenzo[*h*][1,6]naphthyridines against AChE and BChE.[a]

Compound	*Ee*AChE IC_{50} (μM)	hAChE IC_{50} (μM)	hBChE IC_{50} (μM) or % inhibition at 30 μM
First generation			
9a	5.21 ± 0.33	4.15 ± 0.16	8.41%
9b	>30[b]	13.0 ± 0.8	4.42%
9c	13.6 ± 1.8	>25[c]	5.54%
10a	6.33 ± 0.96	>25[d]	8.68%
10b	1.97 ± 0.17	1.06 ± 0.09	nd[e]
10c	6.62 ± 0.62	>25[f]	6.61%
12a	0.281 ± 0.031	>25[g]	20.3%
13a	>30[h]	>25[i]	12.4%
14a	5.48 ± 0.51	0.801 ± 0.069	25.3%
17a	0.147 ± 0.014	0.942 ± 0.038	nd[e]
Second generation			
12b	0.148 ± 0.017	22.8 ± 1.6	27.5%
16a	0.046 ± 0.006	0.065 ± 0.003	0.92 ± 0.03
18a	0.532 ± 0.030	0.556 ± 0.024	1.37 ± 0.07
18b	2.15 ± 0.20	15.8 ± 0.9	2.59 ± 0.14
Tacrine	nd[e]	0.424 ± 0.021[j]	0.046 ± 0.003[j]
Propidium	nd[e]	32.3 ± 2.2[j]	13.2 ± 0.4[j]

[a] IC_{50} inhibitory concentration (μM) of *Electrophorus electricus* or human recombinant AChE and IC_{50} inhibitory concentration (μM) or % inhibition at 30 μM of human serum BChE. IC_{50} values are expressed as mean ± standard error of the mean (SEM) of at least four experiments ($n = 4$), each performed in duplicate.
[b] 43.7% Inhibition of *Ee*AChE activity at 30 μM.
[c] 13.8% Inhibition of hAChE at 25 μM.
[d] 10.0% Inhibition of hAChE at 25 μM.
[e] Not determined.
[f] 15.7% Inhibition of hAChE at 25 μM.
[g] 17.8% Inhibition of hAChE at 25 μM.
[h] 33.7% Inhibition of *Ee*AChE activity at 30 μM.
[i] 10.2% Inhibition of hAChE at 25 μM.
[j] Data taken from Ref. [18], involving the same experimental conditions.

that its 5-(4-chlorophenyl)- and 5-(4-methoxycarbonylphenyl)-substituted analogues **10a** and **10c**, whereas the benzonaphthyridine **17a**, bearing an amine functionality in the side chain at position 9, is about 40-fold more potent than the ester and amide derivatives **10a** and **14a** (Table 1). Not unexpectedly, the benzonaphthyridines **10b**,**c** are more potent EeAChE inhibitors than their less basic lactam precursors **9b**,**c** (>15- and 2-fold, respectively), with the exception of compounds **10a** and **9a**, which were roughly equipotent.

In the light of the SAR derived from the first-generation benzonaphthyridines, starting from **10a** we designed a second generation of analogues bearing simultaneously several or all of the structural features that were found to lead to higher EeAChE inhibitory activity, all of them *N*-debenzylated at position 1 and additionally bearing either a 3-pyridyl group at position 5 (**12b**) or an ethylaminoethyl chain at position 9 (**18a**) or both groups (**18b**). To further explore the role of *N*-debenzylation at position 1, compound **16a**, the debenzylated analogue of the amide **14a**, was also included among the second generation benzonaphthyridines.

With the exception of **18a**, which is 4-fold less potent than its *N*-benzylated analogue **17a**, the second-generation *N*-debenzylated benzonaphthyridines **12b** and **16a** were clearly more potent than their *N*-benzylated counterparts **10b** and **14a** (13- and 119-fold, respectively). However, the two SAR trends seen for the first-generation *N*-benzylated benzonaphthyridines were not apparent in the second-generation *N*-debenzylated analogues, in which the presence of a 4-chlorophenyl group at position 5 and an amide functionality at the side chain in position 9 were the structural features leading to an optimal EeAChE inhibitory activity. These results seem to suggest a different orientation of the *N*-benzylated and *N*-debenzylated compounds within EeAChE. Worthy of note, divergent SARs and binding modes of the PAS-binding moiety of two similar structural classes of inhibitors featuring small changes in their aromatic rings have been recently reported [17].

Overall, amide **16a** turned out to be the most potent benzonaphthyridine of the whole series as EeAChE inhibitor, exhibiting a nanomolar IC_{50} value (46 nM).

When tested on hAChE, significant inter-species differences relative to EeAChE were found in some cases, even though similar general SAR trends were observed. Thus, benzonaphthyridines bearing an amide or an amine functionality in the side chain at position 9 were found to be potent inhibitors, with IC_{50} values in the submicromolar range in all cases except for the 5-(3-pyridyl)-substituted derivative **18b**, whereas most ester derivatives were weakly active (Table 1). Among the most potent derivatives, the higher hAChE inhibitory activity was associated to the presence of an unsubstituted secondary amino group at position 1 (**16a** and **18a** being 12- and 2-fold more potent than **14a** and **17a**), an amide at position 9 (**14a** and **16a** being 1.2- and 9-fold more potent than the amines **17a** and **18a**) and a 4-chlorophenyl substituent at position 5 (**18a** being 28-fold more potent than **18b**). Again, benzonaphthyridine **16a** turned out to be the most interesting compound of the series, emerging as a very potent inhibitor of hAChE (IC_{50} 65 nM). Noteworthy, **16a** is 500-fold more potent than the specific PAS inhibitor propidium and 6-fold more potent than the active site inhibitor tacrine, the second most potent hAChEI among the approved anti-Alzheimer drugs.

Regarding the inhibition of hBChE, most compounds displayed very weak inhibitory activity (4–28% inhibition at 30 μM). Interestingly, the *N*-debenzylated amide or amine derivatives **16a**, **18a**, and **18b** were found to be more potent inhibitors of hBChE, with IC_{50} values around 1–3 μM (Table 1), they being more potent than propidium but less potent than tacrine.

Inhibition of Aβ aggregation is another valuable property for anti-Alzheimer compounds, which is additionally investigated in many cholinesterase inhibitors [19]. Unfortunately, these benzonaphthyridines turned out to be rather weak inhibitors of Aβ42 self-aggregation, displaying percentages of inhibition up to 16% at 10 μM (data not shown).

Overall, benzonaphthyridine **16a** emerges as a promising anti-Alzheimer agent, by virtue of its dual potent hAChE and hBChE inhibitory activities. Because interactions of ligands at the PAS of AChE are not as tight as those that can be established at the active site, peripheral site AChEIs do not usually display high affinities and potencies [20]. Thus, the potent hAChE inhibitory activity of some of the benzonaphthyridines, particularly **16a**, which were designed as peripheral site AChEIs, was somehow astonishing. To shed light on the binding mode of these compounds within AChE, a set of mechanistic studies was performed, encompassing kinetic experiments (Lineweaver–Burk and Cornish–Bowden plots), propidium displacement assay, and molecular modelling studies (docking and molecular dynamics simulations, and Solvated Interaction Energy calculations).

2.3. Kinetic studies

To investigate the mode of inhibition of the most active AChEI benzonaphthyridine, **16a**, and its *N*-benzylated analogue **14a**, Lineweaver–Burk double reciprocal plots were generated. The interception of the lines in the Lineweaver–Burk plot above the *x*-axis (Fig. 2) demonstrated that both compounds serve as mixed-type inhibitors of AChE. Mixed-type of inhibition was further confirmed by Cornish–Bowden plots (*S*/*v versus* [I]) [21].

The inhibition constant (K_i) and the K'_i (dissociation constant for the enzyme–substrate–inhibitor complex) estimated for **14a** were 0.785 μM and 2.34 μM, respectively, and for **16a** were 0.065 μM and 0.073 μM, respectively. These findings show that introduction of a

benzyl substituent at position 1 decreases the affinity not only for the enzyme active site (12-fold higher dissociation constant of the EI complex) but likely also for the PAS (32-fold higher K'_i value). Moreover, the similar values of K_i and K'_i found for **16a** suggest that the high inhibitory potency of this compound might arise from the ability to tightly bind both sites, and not only at the PAS.

To get further insights into the mechanism of inhibition and confirm the ability to interact with the AChE PAS, the affinity of the four most interesting derivatives (**14a**, **16a**, **17a**, and **18a**) for the PAS of AChE was investigated by displacement studies with propidium iodide, using the method of Taylor *et al.* [22]. Propidium selectively associates with the PAS of AChE exhibiting an eight-fold enhancement of fluorescence [22a,23]. Back-titration experiments with increasing concentration of all selected compounds but **14a** showed a concentration-dependent decrease in the fluorescence intensity associated with the propidium–AChE complex, suggesting that they can effectively displace propidium from the AChE's PAS (Fig. 3A). Solubility of **14a** in the assay conditions was insufficient to allow a full back-titration experiment. At 1/1 ratio with propidium iodide **14a** was able to reduce fluorescence intensity associated with the AChE–propidium complex by only 5%, confirming a lower affinity for the PAS than the *N*-debenzylated analogue **16a**, as also suggested by the K'_i values. In general, the affinity trend was **16a** > **18a** > **17a** with concentrations required for decreasing initial fluorescence intensity of AChE–propidium complex ([propidium] = 8 μM) equal to 13, 23, and 33 μM, respectively.

Back-titration experiments for the most active derivative in the series, **16a**, predicted a dissociation constant of 1.76 μM (Fig. 3B). This value is consistent with a quite tight binding to the PAS, only 2.5-fold weaker than that of propidium (K_D on EeAChE = 0.7 μM [23]). Values for the other tested analogues were slightly higher, being 2.18 and 3.20 μM for **18a** and **17a**, respectively. The slightly lower value obtained for the *N*-benzylated derivative, **17a**, further confirms an unfavourable effect of the benzyl substituent at position 1.

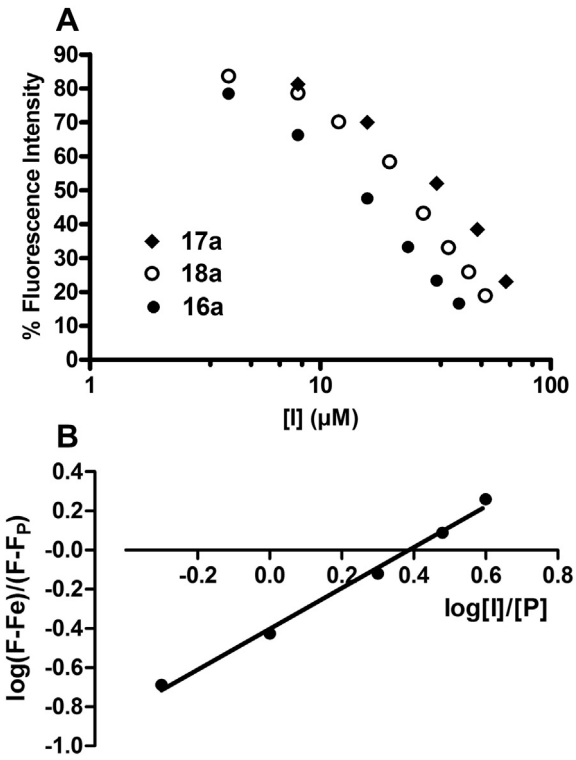

Fig. 3. (A) Back-titration of the propidium–AChE complex by compounds **16a**, **17a**, and **18a** (2.0 μM EeAChE, 8.0 μM propidium, Tris HCl 1.0 mM, pH 8.0); (B) determination of K_D value for most active derivative **16a**. K_D value is calculated from the antilog of the *Y*-intercept value [22b]. P stands for propidium iodide and I stands for tested inhibitor; Fe is the initial fluorescence intensity when enzyme sites are saturated with P, F_P is the fluorescence intensity when propidium is completely displaced from the enzyme, and F denotes the fluorescence intensity after adding a determined amount of displacing agent during the titration experiment.

2.4. Molecular modelling studies

The binding of compounds **16a** and **18a** to hAChE (Fig. 4) was firstly explored by docking calculations carried out with rDock [24]. It is worth noting that previous studies strongly support the performance of this docking program for predicting the binding mode of a number of AChE inhibitors to the enzyme [9]. Docking was performed using three models of hAChE that differ in the orientation of Trp286, which was arranged to reflect the three major conformations adopted by this residue upon inspection of the available X-ray crystallographic structures (see Experimental part) [25].

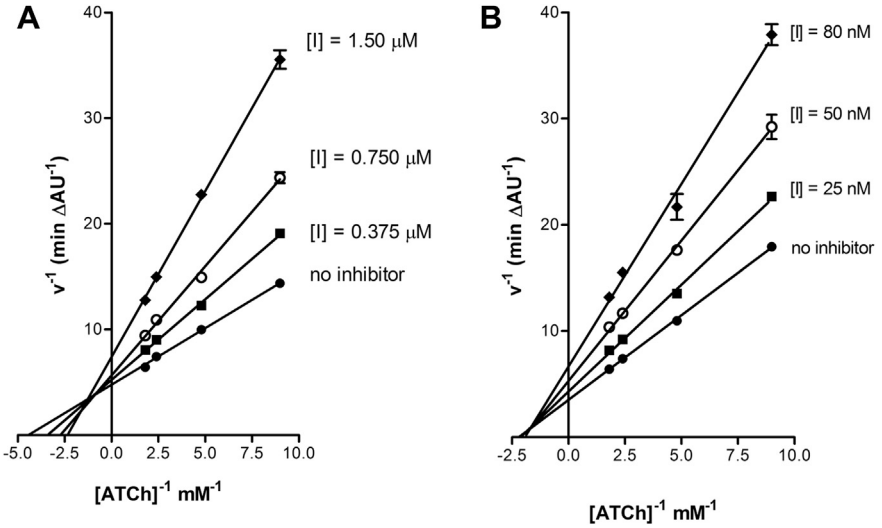

Fig. 2. Lineweaver–Burk plots illustrating mixed-type inhibition of AChE-mediated acetylthiocholine hydrolysis by compound (A) **14a** and (B) **16a**. ATCh = acetylthiocholine; *v* = initial velocity rate.

The docking results revealed a preferential binding to the AChE model where Trp286 retains the orientation found in the AChE–propidium complex (PDB ID 1N5R [20b]). This finding is not unexpected keeping in mind the size of the heteropolycyclic ring system present in compounds **16a** and **18a** and in propidium. Thus, a distinctive binding mode was clearly identified on the basis of the most populated cluster of docked poses and the docking score, where the 5-(4-chlorobenzyl) substituent of **16a** and **18a** stacks against the indole ring of Trp286 and the CONHEt (**16a**) and CH_2NH_2Et (**18a**) substituents penetrate along the gorge towards the catalytic site.

A 100 ns MD simulation was run to refine the binding mode of compounds **16a** and **18a**. Simulations yielded structurally and energetically stable trajectories, which showed an initial rearrangement of the ligand without significant alterations in the residues that shape the binding site (see Fig. S1 in Supplementary material). The results obtained for compound **16a** point out that the central pyridine ring of the benzonaphthyridine system stacks against Trp286 (average distance of 3.74 Å; Fig. 4A), thus enabling the cation–π interaction between the protonated pyridine nitrogen atom of **16a** and the indole system of Trp286. Furthermore, binding is assisted by the formation of hydrogen bonds between the pyridine nitrogen atom and the hydroxyl group of Tyr72 (average distance of 3.20 Å) and between the amide NH group and the hydroxyl group of Tyr124 (average distance of 3.17 Å). Compared to **16a**, binding of **18a** involves the formation of a water-mediated bridge between the protonated amine of the side chain at position 9 and Asp72 (average distance of 5.9 Å) and a cation–π interaction with the benzene ring of Tyr341 (average distance of 3.54 Å), besides the cation–π interaction with Trp286. Finally, the NH group at position 1 forms water-mediated hydrogen bonds with the carbonyl groups of Ser293 and Phe338. Clearly, the similar binding mode of compounds **16a** and **18a** (Fig. 4B) must be drastically perturbed by the attachment of the *N*-benzyl group at position 1 due to the steric clash with the neighbouring residues, which likely explains the weaker potency measured for compounds **14a** and **17a**. Overall, MD simulations show that compounds **16a** and **18a** are capable of forming a network of diverse interactions with residues at the PAS and midgorge sites.

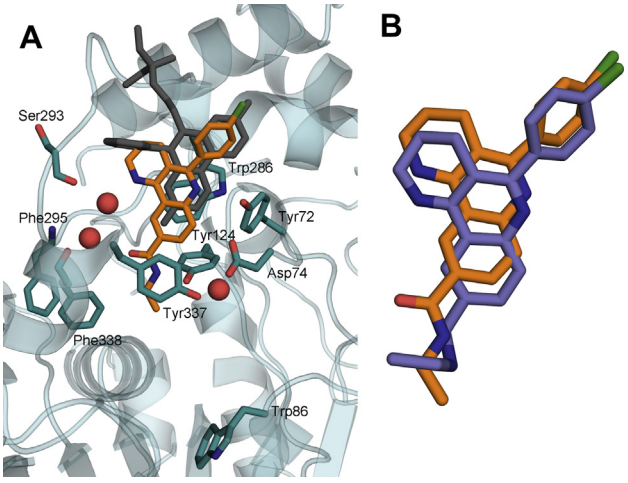

Fig. 4. (A) Representation of the binding mode of compound **16a** (in orange) obtained at the end of the 100 ns MD trajectory. The side chains or backbone units of the residues involved in interactions are shown as green-coloured sticks. Water molecules that mediate interactions of the ligand are shown as red spheres. Propidium is shown as grey sticks. (B) Superposition of the compounds **16a** (orange) and **18a** (cyan) as found at the end of the MD trajectories. (For interpretation of the references to colour in this figure legend, the reader is referred to the web version of this article.)

To further validate the binding mode of **16a** and **18a**, the binding affinities were determined using the Solvated Interaction Energy (SIE) calculations. The SIE method relies on MM/PBSA calculations of the ligand–receptor complex, but the free energy components are weighted by a scaling factor parameterized to reproduce the experimental binding affinities for a diverse set of protein–ligand complexes [26]. The predicted binding affinities for **16a** and **18a** are −8.5 ± 0.4 and −8.8 ± 0.6 kcal/mol (see Table S1 in Supplementary material), which compare with the experimental value determined from the inhibition constant for **16a** (−9.7 kcal/mol). Thus, within the uncertainty of the SIE method, the predicted binding affinities reflect the similar inhibitory potency of **16a** and **18a**. Since they exhibit a similar binding mode, it can be concluded that the large desolvation penalty of the protonated amine present in the side chain at position 9 counterbalances the enhanced coulombic stabilization found for **18a**, the net effect leading to an inhibitory potency close to the potency of the amide derivative **16a**.

2.5. Blood–brain barrier permeation assay

Brain penetration is an essential property for every anti-Alzheimer drug candidate. The ability of the synthesized benzonaphthyridines to cross the blood–brain barrier (BBB) and therefore to reach the CNS was assessed using the known parallel artificial membrane permeation assay (PAMPA-BBB) as an *in vitro* model of passive transcellular permeation [27]. The *in vitro* permeability (P_e) of the novel 1,2,3,4-benzo[*h*][1,6]naphthyridines through a lipid extract of porcine brain was determined using a mixture of phosphate-buffered saline (PBS)/EtOH (70:30). Assay validation was carried out by comparison of the experimental and reported permeability values of 14 commercial drugs (see Table S2 in Supplementary material), which provided a good linear correlation: P_e (exp) = 1.4974 P_e (lit) − 0.8434 (R^2 = 0.9428). Using this equation and the limits established by Di *et al.* for BBB permeation [27], the following ranges of permeability were established: P_e (10^{-6} cm s^{-1}) > 5.1 for compounds with high BBB permeation (CNS+); P_e (10^{-6} cm s^{-1}) < 2.15 for compounds with low BBB permeation (CNS−); and 5.1 > P_e (10^{-6} cm s^{-1}) > 2.15 for compounds with uncertain BBB permeation (CNS+/−). All the tested benzonaphthyridines were predicted to be able to cross the BBB, with the exception of amine **18b**, for which an uncertain brain penetration was predicted. Indeed, amines **18b** and **18a**, whose permeability value was near the minimum threshold for high BBB permeation, seemed to be the most polar benzonaphthyridines of the series, which, as mentioned above might account for the apparently high desolvation penalty detrimental for their AChE inhibitory potencies (Table 2).

3. Conclusion

We have carried out the optimization of the AChE PAS-binding affinity of the initial hit **1**, ethyl 5-(4-chlorophenyl)-3,4-dihydro-2*H*-pyrano[3,2-*c*]quinoline-9-carboxylate, neutral at physiological pH, by replacement of the oxygen atom at position 1 by a nitrogen atom [of a N–H, *N*-benzyl or *N*-(4-methoxybenzyl) group]. The main aim of this structural change was to increase the basicity, and therefore the protonation ability, of the resulting 1,2,3,4-tetrahydrobenzo[*h*][1,6]naphthyridine derivatives, thereby making it possible the establishment of cation–π interactions besides π–π stacking with the PAS residue Trp286. Moreover, the effect on the AChE inhibitory activity of replacements of the 4-chlorophenyl and ethyl carboxylate groups at positions 5 and 9, present in **1**, by 4-(methoxycarbonyl)phenyl or 3-pyridyl groups at position 5 and by *N*-ethylcarboxamido or ethylaminomethyl groups at position 9 were investigated to explore potential additional interactions

nearby the PAS. Despite some significant inter-species differences, the substitution pattern leading to a higher inhibitory activity both in EeAChE and hAChE involves the presence of a debenzylated nitrogen atom at position 1, and 4-chlorophenyl and *N*-ethylcarboxamido groups at positions 5 and 9, respectively. Overall, the hit-to-lead optimization process from **1** to **16a** simply involves a double bioisosteric O → NH replacement at position 1 and in the side chain at position 9, but results in a dramatic increase in EeAChE (>217-fold) and hAChE (>154-fold) inhibitory activities. Interestingly, such a change also leads to a noticeable increase in hBChE inhibitory activity (>11-fold). Because most AChE PAS inhibitors exhibit potencies in the micromolar range, the very potent hAChE inhibitory activity of the lead **16a** (IC_{50} = 65 nM) might arise from additional interactions other than those established with PAS residues, as supported by the results derived from a comprehensive mechanistic study. On the one hand, kinetic studies and propidium displacement studies have confirmed the ability of **16a** to tightly bind the AChE PAS. On the other hand, molecular modelling studies have suggested the ability of the heteroaromatic system of **16a** to establish cation–π and π–π interactions with the PAS residue Trp286 but also the ability of the amide functionality at position 9 to penetrate along the gorge towards the catalytic site and to establish additional hydrogen bond interactions with AChE midgorge residues. The tight binding of **16a** to the AChE PAS and the additional midgorge interactions seem to account for its very potent hAChE inhibitory activity. Overall, the potent dual hAChE and hBChE inhibitory activities of **16a** make it a very interesting anti-Alzheimer lead compound.

4. Experimental part

4.1. Chemistry. General methods

Melting points were determined in open capillary tubes with a MFB 595010M Gallenkamp melting point apparatus. 400 MHz ^{1}H/100.6 MHz ^{13}C NMR spectra were recorded on a Varian Mercury 400 spectrometer. The chemical shifts are reported in ppm (δ scale) relative to internal tetramethylsilane, and coupling constants are reported in Hertz (Hz). Assignments given for the NMR spectra of the new compounds have been carried out by comparison with the NMR data of **9c**, **10c**, **11a**, **17a**, and **18b**, which in turn, were assigned on the basis of DEPT, COSY ^{1}H/^{1}H (standard procedures), and COSY ^{1}H/^{13}C (gHSQC or gHMBC sequences) experiments. IR spectra were run on a Perkin–Elmer Spectrum RX I or on a Thermo Nicolet Nexus spectrophotometer. Absorption values are expressed as wave-numbers (cm^{-1}); only significant absorption bands are given. Column chromatography was performed on silica gel 60 AC.C (35–70 mesh, SDS, ref 2000027).

Table 2
Permeability values and predicted brain penetration of the novel 1,2,3,4-benzo[*h*][1,6]naphthyridines from the PAMPA-BBB assay.

Compound	P_e (10^{-6} cm s^{-1})[a]	Prediction
9a	13.3 ± 3.75	CNS+
9b	12.2 ± 1.54	CNS+
9c	16.8 ± 1.29	CNS+
10a	8.10 ± 1.13	CNS+
10c	9.50 ± 1.05	CNS+
12a	9.70 ± 1.03	CNS+
12b	14.6 ± 1.15	CNS+
13a	26.0 ± 3.87	CNS+
14a	7.70 ± 0.94	CNS+
16a	22.9 ± 0.78	CNS+
18a	5.60 ± 0.58	CNS+
18b	2.40 ± 0.73	CNS+/–

[a] Values are expressed as the mean ± SD of three independent experiments.

Thin-layer chromatography was performed with aluminium-backed sheets with silica gel 60 F_{254} (Merck, ref 1.05554), and spots were visualized with UV light and 1% aqueous solution of $KMnO_4$. NMR spectra of all of the new compounds were performed at the Centres Científics i Tecnològics of the University of Barcelona (CCiTUB), while elemental analyses and high resolution mass spectra were carried out at the Mycroanalysis Service of the IIQAB (CSIC, Barcelona, Spain) with a Carlo Erba model 1106 analyzer, and at the CCiTUB with a LC/MSD TOF Agilent Technologies spectrometer, respectively. The HPLC measurements were performed using a HPLC Waters Alliance HT apparatus comprising a pump (Edwards RV12) with degasser, an autosampler, a diode array detector and a column as specified below. The reverse phase HPLC determinations were carried out on a YMC-Pack ODS-AQ column (50 × 4.6 mm, D S. 3 μm, 12 nm). Solvent A: water with 0.1% formic acid; Solvent B: acetonitrile with 0.1% formic acid. Gradient: 5% of B to 100% of B within 3.5 min. Flux: 1.6 mL/min at 50 °C. The analytical samples of all of the compounds that were subjected to pharmacological evaluation were dried at 65 °C/2 Torr (standard conditions) and possess a purity ≥95% as evidenced by their elemental analyses and/or HPLC measurements. The synthetic procedures for the preparation of the intermediate and target compounds are exemplified through the synthesis of the most potent compound of the series, **16a**. The synthesis of the rest of compounds is included in the Supplementary material.

4.1.1. Ethyl 1-(tert-butoxycarbonyl)-5-(4-chlorophenyl)-1,2,3,4,4a,5,6,10b-octahydrobenzo[h][1,6]naphthyridine-9-carboxylate, diastereomeric mixture ***8a***

To a stirred solution of *p*-chlorobenzaldehyde, **4a** (1.36 g, 9.67 mmol) and ethyl 4-aminobenzoate, (1.60 g, 9.69 mmol) in anhydrous CH_3CN (25 mL), 4 Å molecular sieves and $Sc(OTf)_3$ (0.95 g, 1.93 mmol) were added. The mixture was stirred at room temperature under argon atmosphere for 5 min and then treated with a solution of enamine **7** (1.80 mL, 1.78 g, 9.70 mmol) in anhydrous CH_3CN (12 mL). The resulting suspension was stirred at room temperature under argon atmosphere for 3 days. Then, the resulting mixture was diluted with sat. aq. $NaHCO_3$ (150 mL) and extracted with EtOAc (3 × 200 mL). The combined organic extracts were dried over anhydrous Na_2SO_4, filtered and evaporated under reduced pressure to give a solid residue (4.75 g), which was purified by column chromatography (35–70 μm silica gel, hexane/EtOAc mixtures, gradient elution). On elution with hexane/EtOAc 80:20 to 70:30, the diastereomeric mixture **8a** (2.86 g, 63% yield, 3:1 diastereomeric ratio (^{1}H NMR)) was isolated as a white solid.

4.1.2. Ethyl 1-(tert-butoxycarbonyl)-5-(4-chlorophenyl)-1,2,3,4-tetrahydrobenzo[h][1,6]naphthyridine-9-carboxylate ***11a***

To a solution of diastereomeric mixture **8a** (1.41 g, 2.99 mmol) in anhydrous $CHCl_3$ (37 mL), DDQ (1.36 g, 5.99 mmol) was added. The reaction mixture was stirred at room temperature under argon atmosphere overnight, diluted with CH_2Cl_2 (150 mL) and washed with sat. aq. $NaHCO_3$ (3 × 200 mL). The combined organic extracts were dried over anhydrous Na_2SO_4, filtered and evaporated under reduced pressure to give an orange solid residue (1.46 g), which was purified through column chromatography (35–70 μm silica gel, hexane/EtOAc mixtures, gradient elution). On elution with hexane/EtOAc 80:20, compound **11a** (1.25 g, 90% yield) was isolated as a white solid; R_f 0.61 (hexane/EtOAc 1:1).

A solution of **11a** (100 mg, 0.21 mmol) in CH_2Cl_2 (8 mL) was filtered through a 0.2 μm PTFE filter and evaporated at reduced pressure. The solid was washed with pentane (3 × 4 mL) to give, after drying under standard conditions, the analytical sample of **11a** (97 mg): mp 154–155 °C (CH_2Cl_2); IR (KBr) ν 1713, 1697 (C=O st),

1618, 1592, 1577, 1566 (Ar–C–C and Ar–C–N st) cm^{-1}; ^1H NMR (400 MHz, $CDCl_3$) δ 1.39 [s, 9H, $C(CH_3)_3$], 1.43 (t, $J = 7.2$ Hz, 3H, $CO_2CH_2CH_3$), 2.00 (br signal, 2H, 3-H_2), 2.80 (m, 2H, 4-H_2), 3.20–3.60 (br signal, 2H, 2-H_2), 4.45 (q, $J = 7.2$ Hz, 2H, $CO_2CH_2CH_3$), 7.48 [ddd, $J = 8.4$ Hz, $J' \approx J'' \approx 2.0$ Hz, 2H, 5-Ar–C3(5)–H], 7.55 [ddd, $J \approx 8.4$ Hz, $J' \approx J'' \approx 2.0$ Hz, 2H, 5-Ar–C2(6)–H], 8.08 (d, $J \approx 8.8$ Hz, 1H, 7-H), 8.24 (dd, $J = 8.8$ Hz, $J' = 1.6$ Hz 1H, 8-H), 8.59 (d, $J = 1.6$ Hz, 1H, 10-H); ^{13}C NMR (100.6 MHz, $CDCl_3$) δ 14.3 (CH_3, $CO_2CH_2CH_3$), 24.1 (CH_2, C3), 25.4 (CH_2, C4), 27.9 [$3CH_3$, $C(CH_3)_3$], 44.7 (CH_2, C2), 61.3 (CH_2, $CO_2CH_2CH_3$), 82.1 [C, $C(CH_3)_3$], 122.9 (C, C10a), 123.8 (C, C4a), 127.0 (C, C9), 127.6 (CH, C10), 128.2 (CH, C8), 128.6 [2CH, 5-Ar–C3(5)], 129.7 (CH, C7), 130.3 [2CH, 5-Ar–C2(6)], 134.8 (C, 5-Ar–C4), 138.3 (C, 5-Ar–C1), 145.7 (C, C10b), 148.8 (C, C6a), 153.9 (C, NCOO), 160.5 (C, C5), 166.3 (C, $CO_2CH_2CH_3$); HRMS (ESI), calcd for $[C_{26}H_{27}{}^{35}ClN_2O_4 + H^+]$ 467.1732, found 467.1723.

4.1.3. 1-(tert-Butoxycarbonyl)-5-(4-chlorophenyl)-N-ethyl-1,2,3,4-tetrahydrobenzo[h][1,6]naphthyridine-9-carboxamide **15a**

A suspension of ester **11a** (2.54 g, 5.44 mmol) and KOH (85% purity, 1.08 g, 16.3 mmol) in MeOH (140 mL) was stirred under reflux for 24 h. The resulting solution was cooled down at room temperature and concentrated under reduced pressure. The solid residue (3.35 g) was treated with a solution of HCl in Et_2O (0.8 N, 138 mL, 110 mmol) and the resulting suspension was concentrated under reduced pressure to give the corresponding aminoquinoline carboxylic acid, in the form of hydrochloride, as a white solid (3.77 g). This crude product was used in the next step without further purification.

A solution of this crude product (3.60 g) in anhydrous CH_2Cl_2 (45 mL) was cooled to 0 °C with an ice bath and treated dropwise with freshly distilled Et_3N (2.89 mL, 2.10 g, 20.7 mmol) and $ClCO_2Et$ (0.49 mL, 556 mg, 5.12 mmol). The resulting suspension was thoroughly stirred at 0 °C for 30 min and treated with $EtNH_2 \cdot HCl$ (0.42 g, 5.15 mmol). The reaction mixture was stirred at room temperature for 3 days, diluted with 10% aq. Na_2CO_3 (200 mL), and extracted with CH_2Cl_2 (3 × 300 mL). The combined organic extracts were washed with H_2O (3 × 200 mL), dried over anhydrous Na_2SO_4, filtered and concentrated under reduced pressure to give a solid residue (2.36 g), which was purified through column chromatography (35–70 μm silica gel, hexane/EtOAc mixtures, gradient elution). On elution with hexane/EtOAc 60:40, amide **15a** (1.22 g, 50% overall yield) was obtained as a white solid; R_f 0.23 (hexane/EtOAc 1:1).

A solution of **15a** (50 mg, 0.11 mmol) in CH_2Cl_2 (4 mL) was filtered through a 0.2 μm PTFE filter and evaporated at reduced pressure. The solid was washed with pentane (3 × 4 mL) to give, after drying under standard conditions, the analytical sample of **15a** (45 mg) as a white solid: mp 203–204 °C (CH_2Cl_2); IR (ATR) ν 3391, 3316 (NH st), 1711, 1687, 1654, 1639, 1617, 1597, 1583, 1568, 1532 (C=O, Ar–C–C and Ar–C–N st) cm^{-1}; ^1H NMR (400 MHz, $CDCl_3$) δ 1.27 (t, $J = 7.2$ Hz, 3H, $CONHCH_2CH_3$), 1.40 [s, 9H, $C(CH_3)_3$], 1.99 (br signal, 2H, 3-H_2), 2.79 (t, $J = 6.4$ Hz, 2H, 4-H_2), 3.10–3.50 (br signal, 2H, 2-H_2), 3.54 (tt, $J = 7.2$ Hz, $J' \approx 5.2$ Hz, 2H, $CONHCH_2CH_3$), 6.27 (t, $J = 5.2$ Hz, 1H, $CONHCH_2CH_3$), 7.47 [ddd, $J = 8.4$ Hz, $J' \approx J'' \approx 2.0$ Hz, 2H, 5-Ar–C3(5)–H], 7.53 [ddd, $J \approx 8.4$ Hz, $J' \approx J'' \approx 2.0$ Hz, 2H, 5-Ar–C2(6)–H], 7.96 (dd, $J = 8.4$ Hz, $J' = 2.0$ Hz, 1H, 8-H), 8.08 (d, $J \approx 8.4$ Hz, 1H, 7-H), 8.25 (br s, 1H, 10-H); ^{13}C NMR (100.6 MHz, $CDCl_3$) δ 14.9 (CH_3, $CONHCH_2CH_3$), 24.0 (CH_2, C3), 25.4 (CH_2, C4), 28.0 [$3CH_3$, $C(CH_3)_3$], 35.1 (CH_2, $CONHCH_2CH_3$), 44.8 (CH_2, C2), 82.1 [C, $C(CH_3)_3$], 123.0 (C, C10a), 124.0 (C, C4a), 124.2 (CH), 126.3 (CH) (C8 and C10), 128.6 [2CH, 5-Ar–C3(5)], 129.9 (CH, C7), 130.3 [2CH, 5-Ar–C2(6)], 131.4 (C, C9), 134.7 (C, 5-Ar–C4), 138.3 (C, 5-Ar–C1), 145.4 (C, C10b), 148.0 (C, C6a), 154.0 (C, NCOO), 159.9 (C, C5), 167.0 (C, $CONHCH_2CH_3$); HRMS (ESI), calcd for $[C_{26}H_{28}{}^{35}ClN_3O_3 + H^+]$ 466.1892, found 466.1887.

4.1.4. N-{{5-(4-Chlorophenyl)-1,2,3,4-tetrahydrobenzo[h][1,6]naphthyridin-9-yl}methyl}ethanamine **18a** and 5-(4-chlorophenyl)-N-ethyl-1,2,3,4-tetrahydrobenzo[h][1,6]naphthyridine-9-carboxamide **16a**

A solution of amide **15a** (0.65 g, 1.39 mmol) in anhydrous THF (32 mL) was cooled to 0 °C with an ice bath, and treated portionwise with $LiAlH_4$ (0.17 g, 4.48 mmol). The resulting suspension was stirred under reflux overnight, cooled to 0 °C with an ice bath and treated dropwise with 1 N NaOH (20 mL), then diluted with H_2O (25 mL), and extracted with EtOAc (3 × 30 mL). The combined organic extracts were dried over anhydrous Na_2SO_4, filtered and evaporated under reduced pressure to give a solid residue (0.51 g), which was purified through column chromatography (35–70 μm silica gel, CH_2Cl_2/MeOH/50% aq. NH_4OH mixtures, gradient elution). On elution with CH_2Cl_2/MeOH/50% aq. NH_4OH 99:1:0.2, *N*-Boc-deprotected amide **16a** (72 mg, 14% yield) was isolated as a yellowish solid. On elution with CH_2Cl_2/MeOH/50% aq. NH_4OH 97:3:0.2 to 95:5:0.2, *N*-Boc-deprotected amine **18a** (170 mg, 35% yield) was isolated as a yellowish solid; $R_{f(\mathbf{16a})}$ 0.15 (CH_2Cl_2/MeOH/NH_4OH 9:1:0.05); $R_{f(\mathbf{18a})}$ 0.49 (CH_2Cl_2/MeOH/NH_4OH 9:1:0.05).

A solution of **16a** (64 mg, 0.17 mmol) in CH_2Cl_2 (5 mL) was filtered through a 0.2 μm PTFE filter and treated with a methanolic solution of HCl (0.75 N, 2.2 mL, 1.65 mmol). The resulting solution was evaporated at reduced pressure and the solid was washed with pentane (3 × 4 mL) to give, after drying under standard conditions, **16a**·HCl (57 mg) as a brown solid: mp 320–321 °C (CH_2Cl_2/MeOH 69:31); IR (ATR) ν 3500–2500 (max at 3395, 3231, 3090, 3028, 2929, 2865, 2810, 2640, $^+$NH, NH, OH and CH st), 1655, 1647, 1629, 1586, 1545 (C=O, Ar–C–C and Ar–C–N st) cm^{-1}; ^1H NMR (400 MHz, CD_3OD) δ 1.29 (t, $J = 7.2$ Hz, 3H, $CONHCH_2CH_3$), 1.99 (tt, $J \approx J' \approx 6.0$ Hz, 2H, 3-H_2), 2.75 (t, $J \approx 6.0$ Hz, 2H, 4-H_2), 3.49 (q, $J = 7.2$ Hz, 2H, $CONHCH_2CH_3$), 3.71 (t, $J = 5.6$ Hz, 2H, 2-H_2), 4.84 (s, NH and $^+$NH), 7.66 [complex signal, 4H, 5-Ar–C2(6)–H and 5-Ar–C3(5)–H], 7.85 (d, $J \approx 9.2$ Hz, 1H, 7-H), 8.24 (dd, $J = 9.2$ Hz, $J' = 1.6$ Hz, 1H, 8-H), 8.86 (d, $J = 1.6$ Hz, 1H, 10-H); ^{13}C NMR (100.6 MHz, CD_3OD) δ 14.8 (CH_3, $CONHCH_2CH_3$), 20.0 (CH_2, C3), 25.0 (CH_2, C4), 36.2 (CH_2, $CONHCH_2CH_3$), 43.0 (CH_2, C2), 109.8 (C, C4a), 116.2 (C, C10a), 120.9 (CH, C7), 123.6 (CH, C10), 130.4 (2CH), 131.8 (2CH) [5-Ar–C2(6) and 5-Ar–C3(5)], 132.3 (C, 5-Ar–C1), 132.5 (CH, C8), 133.8 (C, C9), 138.3 (C, 5-Ar–C4), 140.2 (C, C6a), 151.5 (C, C5), 155.8 (C, C10b), 168.1 (C, $CONHCH_2CH_3$); HRMS (ESI), calcd for $\left[C_{21}H_{20}{}^{35}ClN_3O + H^+\right]$ 366.1368, found 366.1364; Elemental analysis, calcd for $C_{21}H_{20}ClN_3O \cdot HCl \cdot H_2O$ C 60.01%, H 5.52%, N 10.00%, Cl 16.87%, found C 60.35%, H 5.81%, N 8.93%, Cl 16.05%. HPLC purity: 94%.

A solution of **18a** (106 mg, 0.30 mmol) in CH_2Cl_2 (8 mL) was filtered through a 0.2 μm PTFE filter and treated with a methanolic solution of HCl (0.75 N, 3.6 mL, 2.70 mmol). The resulting solution was evaporated at reduced pressure and the solid was washed with pentane (3 × 4 mL) to give, after drying under standard conditions, **18a**·2HCl (96 mg) as a yellowish solid: mp 323–324 °C (CH_2Cl_2/MeOH 69:31); IR (KBr) ν 3500–2400 (max at 3379, 3198, 3095, 3028, 2926, 2863, 2767, 2667, 2552, 2422, $^+$NH, NH and CH st), 1639, 1587, 1504 (Ar–C–C and Ar–C–N st) cm^{-1}; ^1H NMR (400 MHz, CD_3OD) δ 1.41 (t, $J = 7.6$ Hz, 3H, 9-$CH_2NHCH_2CH_3$), 1.99 (tt, $J \approx J' \approx 6.0$ Hz, 2H, 3-H_2), 2.76 (t, $J = 6.0$ Hz, 2H, 4-H_2), 3.23 (q, $J = 7.6$ Hz, 2H, 9-$CH_2NHCH_2CH_3$), 3.73 (t, $J = 5.6$ Hz, 2H, 2-H_2), 4.44 (s, 2H, 9-$CH_2NHCH_2CH_3$), 4.84 (s, NH and $^+$NH), 7.67 [complex signal, 4H, 5-Ar–C2(6)-H and 5-Ar–C3(5)–H], 7.92 (d, $J = 8.8$ Hz, 1H, 7-H), 8.06 (dd, $J = 8.8$ Hz, $J' = 1.6$ Hz, 1H, 8-H), 8.58 (d, $J = 1.6$ Hz, 1H, 10-H); ^{13}C NMR (100.6 MHz, CD_3OD) δ 11.6 (CH_3, 9-$CH_2NHCH_2CH_3$), 20.0 (CH_2, C3), 25.1 (CH_2, C4), 43.0 (CH_2, C2), 44.2 (CH_2, 9-$CH_2NHCH_2CH_3$), 51.5 (CH_2, 9-$CH_2NHCH_2CH_3$), 109.8 (C, C4a), 116.7 (C, C10a), 121.7 (CH, C7), 126.0 (CH, C10), 130.4 (2CH), 131.8 (2CH) [5-Ar–C2(6) and 5-Ar–C3(5)], 131.0 (C, C9), 132.3 (C, 5-

Ar–C1), 135.5 (CH, C8), 138.2 (C, 5-Ar–C4), 139.1 (C, C6a), 151.4 (C, C5), 155.2 (C, C10b); HRMS (ESI) calcd for $[C_{21}H_{22}{}^{35}ClN_3 + H^+]$ 352.1575, found 352.1574; Elemental analysis, calcd for $C_{21}H_{22}ClN_3 \cdot 1.5HCl \cdot 2.75H_2O$ C 55.30%, H 6.41%, N 9.21%, Cl 19.43%, found C 55.23%, H 6.16%, N 8.93%, Cl 19.10%. HPLC purity >99%.

4.2. Biological assays

4.2.1. Determination of inhibitory effect on AChE and BChE activity

The inhibitory activity against *E. electricus* (*Ee*) AChE (Sigma–Aldrich) and human serum BChE (Sigma–Aldrich) was evaluated spectrophotometrically by the method of Ellman *et al.* [15]. The reactions took place in a final volume of 300 μL of 0.1 M phosphate-buffered solution pH 8.0, containing EeAChE (0.03 u/mL) or hBChE (0.02 u/mL) and 333 μM 5,5′-dithiobis(2-nitrobenzoic) acid (DTNB; Sigma–Aldrich) solution used to produce the yellow anion of 5-thio-2-nitrobenzoic acid. Inhibition curves were performed in duplicates using at least 10 increasing concentrations of inhibitors and pre-incubated for 20 min at 37 °C before adding the substrate [28]. One duplicate sample without inhibitor was always present to yield 100% of AChE or BChE activities. Then substrates, acetylthiocholine iodide (450 μM; Sigma–Aldrich) or butyrylthiocholine iodide (300 μM; Sigma–Aldrich), were added and the reaction was developed for 5 min at 37 °C. The colour production was measured at 414 nm using a labsystems Multiskan spectrophotometer.

Data from concentration–inhibition experiments of the inhibitors were calculated by non-linear regression analysis, using the GraphPad Prism program package (GraphPad Software; San Diego, USA), which gave estimates of the IC_{50} (concentration of drug producing 50% of enzyme activity inhibition). Results are expressed as mean ± S.E.M. of at least 4 experiments performed in duplicate.

The inhibitory activity against human recombinant AChE was also assessed using the method of Ellman *et al.* [15]. Initial rate assays were performed at 37 °C with a Jasco V-530 double beam Spectrophotometer. The rate of increase in the absorbance at 412 nm was followed for 240 s. AChE stock solution was prepared by dissolving human recombinant AChE (E.C.3.1.1.7) lyophilized powder (Sigma–Aldrich) in 0.1 M phosphate buffer (pH = 8.0) containing Triton X-100 0.1%. Stock solutions of inhibitors (1–3 mM) were prepared in methanol and diluted in methanol. Inhibitors were first screened at a single concentration (25 μM). Then, for compounds showing a percentage of inhibition higher than 50% at the screening concentration (25 μM), the IC_{50} values were determined. In this case, five/six increasing concentrations of the inhibitor were used, able to give an inhibition of the enzymatic activity in the range of 20–80%. The assay solution consisted of a 0.1 M phosphate buffer pH 8.0, with the addition of 340 μM DTNB, 0.02 unit/mL of human recombinant AChE and 550 μM of substrate (acetylthiocholine iodide, ATCh). 50 μL aliquots of increasing concentration of the tested inhibitor (or methanol) were added to the assay solution and pre-incubated with the enzyme for 20 min at 37 °C before the addition of the substrate. Assays were carried out with a blank containing all components except AChE in order to account for the non-enzymatic hydrolysis of the substrate. The reaction rates were compared and the percent inhibition due to the presence of inhibitor was calculated. Each concentration was analyzed in duplicate, and IC_{50} values were determined graphically from log concentration–inhibition curves (GraphPad Prism 4.03 software, GraphPad Software Inc.). Two/three independent experiments were performed for the determination of each IC_{50} value.

4.2.2. Kinetic inhibition studies

To estimate the mode of inhibition of compound **16a** and the corresponded benzylated analogue **14a**, Lineweaver–Burk double reciprocal plots were constructed at relatively low concentration of substrate (0.11–0.55 mM) and using the same experimental conditions reported for the hAChE assay at Section 4.2.1. The plots were assessed by a weighted least square analysis that assumed the variance of v to be a constant percentage of v for the entire data set. To confirm the mode of inhibition, Cornish–Bowden plots were obtained by plotting S/v (substrate/velocity ratio) *versus* inhibitor concentration [21]. Data analysis was performed with GraphPad Prism 4.03 software (GraphPad Software Inc.).

Calculation of the inhibitor constant (K_i) value was carried out by re-plotting slopes of lines from the Lineweaver–Burk plot *versus* the inhibitor concentration and K_i was determined as the intersect on the negative *x*-axis. K'_i (dissociation constant for the enzyme–substrate–inhibitor complex) value was determined by plotting the apparent $1/v_{max,\ app}$ *versus* inhibitor concentration [29].

4.2.3. Propidium displacement studies

The affinity of selected inhibitors for the peripheral binding site of EeAChE (type VI-S, Sigma–Aldrich) was tested using propidium iodide (P) (Sigma–Aldrich), a known PAS-specific ligand as previously described by Taylor *et al.* [22]. A shift in the excitation wavelength follows the complexation of propidium iodide and AChE [22a]. Fluorescence intensity was monitored by a Jasco 6200 spectrofluorometer (Jasco Europe, Italy) using a 0.5 mL quartz cuvette at room temperature. EeAChE (2 μM, assuming 82,000 molecular mass subunits) was first incubated with 8 μM propidium iodide in 1 mM Tris–HCl, pH 8.0 at room temperature. Stock solutions (4 mM) of each inhibitor were prepared in methanol. In the back titration experiments of the propidium–AChE complex by the tested inhibitor, aliquots of inhibitor (2–40 μM, 4–68 μM and 2–44 μM for **16a**, **18a** and **14a**, respectively) were added successively, and fluorescence emission was monitored at 602 nm upon excitation at 535 nm. Blanks containing propidium alone, inhibitor plus propidium and EeAChE alone were prepared and fluorescence emission determined. Raw data were processed following the method of Taylor and Lappi [22b] to estimate K_D values assuming a dissociation constant value for propidium for acetylcholinesterase from *E. electricus* equals to 0.7 μM [23].

4.2.4. PAMPA-BBB assay

To evaluate the brain penetration of the synthesized compounds, a parallel artificial membrane permeation assay for blood–brain barrier was used, following the method described by Di *et al.* [27]. The *in vitro* permeability (P_e) of fourteen commercial drugs through lipid extract of porcine brain membrane together with the test compounds was determined. Commercial drugs and the synthesized compounds were tested using a mixture of PBS:EtOH (70:30). Assay validation was made by comparing the experimental permeability of the different compounds with the reported bibliography values of the commercial drugs, which showed a good correlation: P_e (exp) = 1.4974 P_e (lit) − 0.8434 ($R^2 = 0.9428$). From this equation and taking into account the limits established by Di *et al.* for BBB permeation, we established the ranges of permeability as compounds of high BBB permeation (CNS+): P_e (10^{-6} cm s^{-1}) > 5.1; compounds of low BBB permeation (CNS−): P_e (10^{-6} cm s^{-1}) < 2.15, and compounds of uncertain BBB permeation (CNS+/−): 5.1 > P_e (10^{-6} cm s^{-1}) > 2.15.

4.3. Molecular modelling

4.3.1. Setup of the system

Molecular modelling was performed using the X-ray crystallographic structure of the recombinant human AChE (PDB ID: 3LII) [30]. The structure was refined by removal of *N*-acetyl-D-glucosamine and sulphate anions and addition of missing hydrogen

atoms. Furthermore, the missing loop that comprises residues 259–263 (PGGTG) was modelled from the X-ray structure of hAChE complexed with huprine W (PDB ID: 4BDT) [31].

The enzyme was modelled in its physiological active form with neutral His447 and deprotonated Glu334, which together with Ser203 form the catalytic triad. The ionization state for the rest of ionizable residues was assessed from PROPKA3 calculations [32]. Accordingly, the standard ionization state at neutral pH was considered but for residues Glu285, Glu450 and Glu452, which were protonated. Finally, three disulfide bridges were defined between Cys residues 257–272, 529–409, and 69–96, respectively. Structural waters were retrieved from those found in the AChE–donepezil complex 1EVE [33].

Since Trp286 can adopt three main conformations in the peripheral binding site [9], three models were built up by re-orienting the side chain of Trp286 as found in the X-ray structures of the AChE complexes with propidium, *bis*(7)-tacrine and *syn*-TZ2PA6 (PDB ID: 1N5R, 2CKM and 1Q83, respectively). These models were energy minimized using the AMBER force field (see below).

4.3.2. Docking

Docking of AChE inhibitors was performed using the rDock program, which is an extension of the program RiboDock and utilizes an empirical scoring function calibrated on the basis of protein–ligand complexes [24]. It is worth noting that previous studies strongly support the excellent performance of rDock for predicting the binding mode of a variety of AChE inhibitors to the enzyme gorge [9]. A cavity of radius 17 Å, centred on the structure of a superligand containing huprine X, donepezil and propidium (as found in the X-ray structures 1E66 [34], 1EVE and 1N5R) was used to define the docking volume. Since huprine X and propidium are bound to the catalytic and peripheral binding sites, and donepezil is aligned along the gorge, this definition guarantees the exploration of the binding mode along the whole volume accessible for binding. Calculations were performed with no structural waters. Conformational flexibility around rotatable bonds of the ligand was allowed. Docking calculations were performed separately for the three models of the human enzyme, which differ in the relative orientation of the side chain of Trp286 (see above). Conformational adjustments of other residues in the binding site were accounted for indirectly by rescaling (by a factor of 0.9) the van der Waals volume of atoms. Each compound was subjected to 100 docking runs and the poses were sorted according to its docking score. The top 50 best scored poses were clustered and further analyzed by visual inspection.

4.3.3. Molecular dynamics simulations

Molecular dynamics (MD) simulations were run to further check the stability of the proposed binding mode of AChE inhibitors. Starting from the initial poses obtained from docking calculations, a 100 ns MD simulation was performed using the PMEMD module of AMBER12 [35] software package and the parm99SB [36] force field for the protein and GAFF [37]-derived parameters for the ligand. The geometry of the ligand was optimized at the B3LYP/6-31G(d) level [38]. The charge distribution of the inhibitors was defined from the electrostatic charges determined by fitting the B3LYP/6-31G(d) electrostatic potential using the RESP procedure [39]. Na^+ cations were added to neutralize the negative charge of the system with the XLEAP module of AMBER12. The system was immersed in an octahedral box of TIP3P water molecules [40], preserving the crystallographic waters inside the binding cavity. The final system contained around 53,000 atoms.

The geometry of the system was minimized in four steps. First, water molecules and counterions were refined through 7000 steps of conjugate gradient and 3000 steps of steepest descent algorithm. Then, the position of hydrogen atoms was optimized using 4500 steps of conjugate gradient and 500 steps of steepest descent algorithm. At the third stage, hydrogen atoms, water molecules and counterions were further optimized using 11,500 steps of conjugate gradient and 3500 steps of steepest descent algorithm. Finally, the whole system was optimized using 8500 steps of conjugate gradient and 2500 steps of steepest descent algorithm. Thermalization of the system was performed in five steps of 25 ps, increasing the temperature from 50 to 298 K. Concomitantly, the residues that define the binding site were restrained during thermalization using a variable restraining force. Thus, a force constant of 25 kcal mol^{-1} $Å^{-2}$ was used in the first stage of the thermalization and was subsequently decreased by increments of 5 kcal mol^{-1} $Å^{-2}$ in the next stages. Then, an additional step of 250 ps was performed in order to equilibrate the system density at constant pressure (1 bar) and temperature (298 K). Finally, a 100 ns trajectory was run using a time step of 2 fs. SHAKE was used for those bonds containing hydrogen atoms in conjunction with periodic boundary conditions at constant volume and temperature, particle mesh Ewald for the treatment of long range electrostatic interactions, and a cutoff of 10 Å for nonbonded interactions.

The structural analysis was performed using in-house software and standard codes of AMBER12. The solvent interaction energies (SIE) technique developed by Purisima and co-workers was used to estimate the interaction free energies for the AChE inhibitors [26]. Calculations were performed for a set of 150 snapshots taken along the last 30 ns of the MD trajectory.

Acknowledgements

This work was supported by Ministerio de Ciencia e Innovación (MICINN) (CTQ2011-22433, CTQ2012-30930, SAF2011-27642, SAF2009-10553) and Generalitat de Catalunya (GC) (2009SGR1396, 2009SGR1024, 2009SGR249). This work was supported by MIUR (PRIN 2009Z8YTYC-003). Fellowship from GC to E.V. and from Leonardo da Vinci Project Unipharma-Graduates 6 to O.D.P. are gratefully acknowledged. The Center for Scientific and Academic Services of Catalonia (CESCA) is acknowledged for providing access to computational facilities. We thank Dr. Marc Revés (Universitat de Barcelona) for his helpful assistance in the HPLC purity measurements.

Appendix A. Supplementary data

Supplementary data related to this article can be found at http://dx.doi.org/10.1016/j.ejmech.2013.12.008.

References

[1] N.L. Batsch, M.S. Mittelman, World Alzheimer Report 2012. Overcoming the Stigma of Dementia, Alzheimer's Disease International, London, 2012. http://www.alz.co.uk.
[2] Alzheimer's Association, Alzheimer's disease facts and figures, Alzheimers Dementia 9 (2013) 208–245.
[3] S.W. Pimplikar, Reassessing the amyloid cascade hypothesis of Alzheimer's disease, Int. J. Biochem. Cell Biol. 41 (2009) 1261–1268.
[4] (a) W.J. Geldenhuys, C.J. Van der Schyf, Rationally designed multi-targeted agents against neurodegenerative diseases, Curr. Med. Chem. 20 (2013) 1662–1672;
(b) X. Chen, M. Decker, Multi-target compounds acting in the central nervous system designed from natural products, Curr. Med. Chem. 20 (2013) 1673–1685;
(c) P. Russo, A. Frustaci, A. Del Bufalo, M. Fini, A. Cesario, Multitarget drugs of plants origin acting on Alzheimer's disease, Curr. Med. Chem. 20 (2013) 1686–1693;
(d) A. Rampa, F. Belluti, S. Gobbi, A. Bisi, Hybrid-based multi-target ligands for the treatment of Alzheimer's disease, Curr. Top. Med. Chem. 11 (2011) 2716–2730;
(e) A. Cavalli, M.L. Bolognesi, A. Minarini, M. Rosini, V. Tumiatti, M. Recanatini,

C. Melchiorre, Multi-target-directed ligands to combat neurodegenerative diseases, J. Med. Chem. 51 (2008) 347–372.
[5] (a) R.A. Sperling, J. Karlawish, K.A. Johnson, Preclinical Alzheimer disease – the challenges ahead, Nat. Rev. Neurol. 9 (2013) 54–58;
(b) D.C. Anderson, Alzheimer's disease biomarkers: more than molecular diagnostics, Drug Dev. Res. 74 (2013) 92–111;
(c) S.J. Teipel, O. Sabri, M. Grothe, H. Barthel, D. Prvulovic, K. Buerger, A.L. Bokde, M. Ewers, W. Hoffmann, H. Hampel, Perspectives for multimodal neurochemical and imaging biomarkers in Alzheimer's disease, J. Alzheimers Dis. 33 (Suppl. 1) (2013) S329–S347;
(d) J.F. Quinn, Biomarkers for Alzheimer's disease; showing the way or leading us astray? J. Alzheimers Dis. 33 (Suppl. 1) (2013) S371–S376;
(e) R.J. Caselli, E.M. Reiman, Characterizing the preclinical stages of Alzheimer's disease and the prospect of presymptomatic intervention, J. Alzheimers Dis. 33 (Suppl. 1) (2013) S405–S416;
(f) V.T. Papaliagkas, The role of cerebrospinal fluid biomarkers for Alzheimer's disease diagnosis. Where are we now? Recent Patents CNS Drug Discov. 8 (2013) 70–78.
[6] (a) L. Cheewakriengkrai, S. Gauthier, A 10-year perspective on donepezil, Expert Opin. Pharmacother. 14 (2013) 331–338;
(b) J.L. Cummings, S.J. Banks, R.K. Gary, J.W. Kinney, J.M. Lombardo, R.R. Walsh, K. Zhong, Alzheimer's disease drug development: translational neuroscience strategies, CNS Spectr. 18 (2013) 128–138;
(c) M.B. Colovic, D.Z. Krstic, T.D. Lazarevic-Pasti, A.M. Bondzic, V.M. Vasic, Acetylcholinesterase inhibitors: pharmacology and toxicology, Curr. Neuropharmacol. 11 (2013) 315–335;
(d) P. Anand, B. Singh, A review on cholinesterase inhibitors for Alzheimer's disease, Arch. Pharm. Res. 36 (2013) 375–399.
[7] J.L. Sussman, M. Harel, F. Frolow, C. Oefner, A. Goldman, L. Toker, I. Silman, Atomic structure of acetylcholinesterase from Torpedo californica – a prototypic acetylcholine-binding protein, Science 253 (1991) 872–879.
[8] (a) M.L. Bolognesi, A. Minarini, M. Rosini, V. Tumiatti, C. Melchiorre, From dual binding site acetylcholinesterase inhibitors to multi-target-directed ligands (MTDLs): a step forward in the treatment of Alzheimer's disease, Mini-Rev. Med. Chem. 8 (2008) 960–967;
(b) A. Castro, P. Muñoz, A. Martínez, Dual binding site acetylcholinesterase inhibitors: design, SAR, and potential role as new disease-modifying agents for Alzheimer's disease, in: A. Martínez Gil (Ed.), Medicinal Chemistry of Alzheimer's Disease, Transworld Research Network, Kerala, 2008, pp. 21–44;
(c) D. Muñoz-Torrero, Acetylcholinesterase inhibitors as disease-modifying therapies for Alzheimer's disease, Curr. Med. Chem. 15 (2008) 2433–2455.
[9] P. Camps, X. Formosa, C. Galdeano, D. Muñoz-Torrero, L. Ramírez, E. Gómez, N. Isambert, R. Lavilla, A. Badia, M.V. Clos, M. Bartolini, F. Mancini, V. Andrisano, M.P. Arce, M.I. Rodríguez-Franco, O. Huertas, T. Dafni, F.J. Luque, Pyrano[3,2-*c*]quinoline-6-chlorotacrine hybrids as a novel family of acetylcholinesterase- and β-amyloid-directed anti-Alzheimer compounds, J. Med. Chem. 52 (2009) 5365–5379.
[10] L.S. Povarov, α,β-Unsaturated ethers and their analogues in reactions of diene synthesis, Russ. Chem. Rev. 36 (1967) 656–670.
[11] (a) E. Vicente-García, F. Catti, R. Ramón, R. Lavilla, Unsaturated lactams: new inputs for Povarov-type multicomponent reactions, Org. Lett. 12 (2010) 860–863;
(b) D.A. Powell, R.A. Batey, Total synthesis of the alkaloids martinelline and martinellic acid via a hetero Diels–Alder multicomponent coupling reaction, Org. Lett. 4 (2002) 2913–2916.
[12] O. Jiménez, G. de la Rosa, R. Lavilla, Straightforward access to a structurally diverse set of oxacyclic scaffolds through a four-component reaction, Angew. Chem., Int. Ed. 44 (2005) 6521–6525.
[13] E. Vicente-García, R. Ramón, S. Preciado, R. Lavilla, Multicomponent reaction access to complex quinolines via oxidation of the Povarov adducts, Beilstein J. Org. Chem. 7 (2011) 980–987.
[14] S. Das, D. Addis, S. Zhou, K. Junge, M. Beller, Zinc-catalyzed reduction of amides: unprecedented selectivity and functional group tolerance, J. Am. Chem. Soc. 132 (2010) 1770–1771.
[15] G.L. Ellman, K.D. Courtney, V. Andres Jr., R.M. Featherstone, A new and rapid colorimetric determination of acetylcholinesterase activity, Biochem. Pharmacol. 7 (1961) 88–95.
[16] R.M. Lane, S.G. Potkin, A. Enz, Targeting acetylcholinesterase and butyrylcholinesterase in dementia, Int. J. Neuropsychopharmacol. 9 (2006) 101–124.
[17] C.D. Anderson, N. Forsgren, C. Akfur, A. Allgardsson, L. Berg, C. Engdahl, W. Qian, F.J. Ekström, A. Linusson, Divergent structure–activity relationships of structurally similar acetylcholinesterase inhibitors, J. Med. Chem. 56 (2013) 7615–7624.
[18] M.L. Bolognesi, V. Andrisano, M. Bartolini, R. Banzi, C. Melchiorre, Propidium-based polyamine ligands as potent inhibitors of acetylcholinesterase and acetylcholinesterase-induced amyloid-β aggregation, J. Med. Chem. 48 (2005) 24–27.
[19] E. Viayna, R. Sabate, D. Muñoz-Torrero, Dual inhibitors of β-amyloid aggregation and acetylcholinesterase as multi-target anti-Alzheimer drug candidates, Curr. Top. Med. Chem. 13 (2013) 1820–1842.
[20] (a) Z. Radić, P. Taylor, Interaction kinetics of reversible inhibitors and substrates with acetylcholinesterase and its fasciculin 2 complex, J. Biol. Chem. 276 (2001) 4622–4633;
(b) Y. Bourne, P. Taylor, Z. Radić, P. Marchot, Structural insights into ligand interactions at the acetylcholinesterase peripheral anionic site, EMBO J. 22 (2003) 1–12;
(c) B. Kaboudin, S. Emadi, M.R. Faghihi, M. Fallahi, V. Sheik-Hasani, Synthesis of α-oxycarbanilinophosphonates and their anticholinesterase activities: the most potent derivative is bound to the peripheral site of acetylcholinesterase, J. Enzyme Inhib. Med. Chem. 28 (2013) 576–582;
(d) S. Young, K. Fabio, C. Guillon, P. Mohanta, T.A. Halton, D.E. Heck, R.A. Flowers II, J.D. Laskin, N.D. Heindel, Peripheral site acetylcholinesterase inhibitors targeting both inflammation and cholinergic dysfunction, Bioorg. Med. Chem. Lett. 20 (2010) 2987–2990;
(e) P. de la Torre, L. Astudillo Saavedra, J. Caballero, J. Quiroga, J.H. Alzate-Morales, M. Gutiérrez Cabrera, J. Trilleras, A novel class of selective acetylcholinesterase inhibitors: synthesis and evaluation of (*E*)-2-(benzo[*d*]thiazol-2-yl)-3-heteroarylacrylonitriles, Molecules 17 (2012) 12072–12085.
[21] A. Cornish-Bowden, A simple graphical method for determining the inhibition constants of mixed, uncompetitive and non-competitive inhibitors, Biochem. J. 137 (1974) 143–144.
[22] (a) P. Taylor, J. Lwebuga-Mukasa, S. Lappi, J. Rademacher, Propidium – a fluorescent probe for a peripheral anionic site on acetylcholinesterase, Mol. Pharmacol. 10 (1974) 703–708;
(b) P. Taylor, S. Lappi, Interaction of fluorescence probes with acetylcholinesterase, the site and specificity of propidium binding, Biochemistry 14 (1975) 1989–1997.
[23] N. Nunes-Tavares, A. Nery da Matta, C.M. Batista e Silva, G.M. Araújo, S.R. Louro, A. Hassón-Voloch, Inhibition of acetylcholinesterase from *Electrophorus electricus* (L.) by tricyclic antidepressants, Int. J. Biochem. Cell Biol. 34 (2002) 1071–1079.
[24] (a) S.D. Morley, M. Afshar, Validation of an empirical RNA-ligand scoring function for fast flexible docking using RiboDock, J. Comput. Aided Mol. Des. 18 (2004) 189–208;
(b) X. Barril, R.E. Hubbard, S.D. Morley, Virtual screening in structure-based drug discovery, Mini-Rev. Med. Chem. 4 (2004) 779–791.
[25] C. Galdeano, E. Viayna, P. Arroyo, A. Bidon-Chanal, J.R. Blas, D. Muñoz-Torrero, F.J. Luque, Structural determinants of the multifunctional profile of dual binding site acetylcholinesterase inhibitors as anti-Alzheimer agents, Curr. Pharm. Des. 16 (2010) 2818–2836.
[26] (a) M. Naïm, S. Bhat, K.N. Rankin, S. Dennis, S.F. Chowdhury, I. Siddiqi, P. Drabik, T. Sulea, C.I. Bayly, A. Jakalian, E.O. Purisima, Solvated interaction energy (SIE) for scoring protein–ligand binding affinities. 1. Exploring the parameter space, J. Chem. Inf. Model. 47 (2007) 122–133;
(b) Q. Cui, T. Sulea, J.D. Schrag, C. Munger, M.-N. Hung, M. Naïm, M. Cygler, E.O. Purisima, Molecular dynamics-solvated interaction energy studies of protein–protein interactions: the MP1-p14 scaffolding complex, J. Mol. Biol. 379 (2008) 787–802.
[27] L. Di, E.H. Kerns, K. Fan, O.J. McConnell, G.T. Carter, High throughput artificial membrane permeability assay for blood-brain barrier, Eur. J. Med. Chem. 38 (2003) 223–232.
[28] E. Viayna, T. Gómez, C. Galdeano, L. Ramírez, M. Ratia, A. Badia, M.V. Clos, E. Verdaguer, F. Junyent, A. Camins, M. Pallàs, M. Bartolini, F. Mancini, V. Andrisano, M.P. Arce, M.I. Rodríguez-Franco, A. Bidon-Chanal, F.J. Luque, P. Camps, D. Muñoz-Torrero, Novel huprine derivatives with inhibitory activity toward β-amyloid aggregation and formation as disease-modifying anti-Alzheimer drug candidates, ChemMedChem 5 (2010) 1855–1870.
[29] R.B. Silverman, The Organic Chemistry of Enzyme-catalyzed Reactions, Academic Press, San Diego, 2000.
[30] H. Dvir, I. Silman, M. Harel, T.L. Rosenberry, J.L. Sussman, Acetylcholinesterase: from 3D structure to function, Chem. Biol. Interact. 187 (2010) 10–22.
[31] F. Nachon, E. Carletti, C. Ronco, M. Trovaslet, Y. Nicolet, L. Jean, P.-Y. Renard, Crystal structures of human cholinesterases in complex with huprine W and tacrine: elements of specificity for anti-Alzheimer's drugs targeting acetyl- and butyrylcholinesterase, Biochem. J. 453 (2013) 393–399.
[32] M.H.M. Olsson, C.R. Sondergard, M. Rostkowski, J.H. Jensen, PROPKA3: consistent treatment of internal and surface residues in empirical pKa predictions, J. Chem. Theor. Comput. 7 (2011) 525–537.
[33] G. Kryger, I. Silman, J.L. Sussman, Structure of acetylcholinesterase complexed with E2020 (Aricept): implications for the design of new anti-Alzheimer drugs, Structure 7 (1999) 297–307.
[34] H. Dvir, D.M. Wong, M. Harel, X. Barril, M. Orozco, F.J. Luque, D. Muñoz-Torrero, P. Camps, T.L. Rosenberry, I. Silman, J.L. Sussman, 3D structure of *Torpedo californica* acetylcholinesterase complexed with huprine X at 2.1 Å resolution: kinetic and molecular dynamics correlates, Biochemistry 41 (2002) 2970–2981.
[35] D.A. Case, T.A. Darden, T.E. Cheatham III, C.L. Simmerling, J. Wang, R.E. Duke, R. Luo, R.C. Walker, W. Zhang, K.M. Merz, B. Roberts, S. Hayik, A. Roitberg, G. Seabra, J. Swails, A.W. Goetz, I. Kolossváry, K.F. Wong, F. Paesani, J. Vanicek, R.M. Wolf, J. Liu, X. Wu, S.R. Brozell, T. Steinbrecher, H. Gohlke, Q. Cai, X. Ye, J. Wang, M.-J. Hsieh, G. Cui, D.R. Roe, D.H. Mathews, M.G. Seetin, R. Salomon-

Ferrer, C. Sagui, V. Babin, T. Luchko, S. Gusarov, A. Kovalenko, P.A. Kollman, AMBER 12, University of California, San Francisco, 2012.
[36] V. Hornak, R. Abel, A. Okur, B. Strockbine, A. Roitberg, C. Simmerling, Comparison of multiple Amber force fields and development of improved protein backbone parameters, Proteins 65 (2006) 712–725.
[37] J. Wang, R.M. Wolf, J.W. Caldwell, P.A. Kollman, D.A. Case, Development and testing of a general AMBER force field, J. Comput. Chem. 25 (2004) 1157–1174.
[38] (a) A.D. Becke, Density-functional thermochemistry. III. The role of exact exchange, J. Chem. Phys. 98 (1993) 5648–5652;
(b) C. Lee, W. Yang, R.G. Parr, Development of the Colle–Salvetti correlation-energy formula into a functional of the electron density, Phys. Rev. B 37 (1988) 785–789.
[39] C.I. Bayly, P. Cieplak, W.D. Cornell, P.A. Kollman, A well-behaved electrostatic potential based method using charge restraints for deriving atomic charges, J. Phys. Chem. 97 (1993) 10269–10280.
[40] W.L. Jorgensen, J. Chandrasekhar, J.D. Madura, R.W. Impey, M.L. Klein, Comparison of simple potential functions for simulating liquid water, J. Chem. Phys. 79 (1983) 926–935.

Suppementary material

1,2,3,4-Tetrahydrobenzo[*h*][1,6]naphthyridines as a new family of potent peripheral-to-midgorge-site inhibitors of acetylcholinesterase: synthesis, pharmacological evaluation and mechanistic studies

Ornella Di Pietro[a], Elisabet Viayna[a], Esther Vicente-García[b], Manuela Bartolini[c], Rosario Ramón[b], Jordi Juárez-Jiménez[d], M. Victòria Clos[e], Belén Pérez[e], Vincenza Andrisano[f], F. Javier Luque[d], Rodolfo Lavilla[b,g,*], Diego Muñoz-Torrero[a,*]

[a] *Laboratori de Química Farmacèutica (Unitat Associada al CSIC), Facultat de Farmàcia, and Institut de Biomedicina (IBUB), Universitat de Barcelona, Av. Joan XXIII, 27-31, E-08028, Barcelona, Spain*

[b] *Barcelona Science Park, Baldiri Reixac 10-12, E-08028, Barcelona, Spain*

[c] *Department of Pharmacy and Biotechnology, Alma Mater Studiorum University of Bologna, Via Belmeloro 6, I-40126, Bologna, Italy*

[d] *Departament de Fisicoquímica, Facultat de Farmàcia, and IBUB, Universitat de Barcelona, Prat de la Riba 171, E-08921, Santa Coloma de Gramenet, Spain*

[e] *Departament de Farmacologia, de Terapèutica i de Toxicologia, Institut de Neurociències, Universitat Autònoma de Barcelona, E-08193, Bellaterra, Barcelona, Spain*

[f] *Department for Life Quality Studies, University of Bologna, Corso d'Augusto 237, I-47921, Rimini, Italy*

[g] *Laboratori de Química Orgànica, Facultat de Farmàcia, Universitat de Barcelona, Av. Joan XXIII, 27-31, E-08028, Barcelona, Spain*

Ethyl 1-benzyl-5-(4-chlorophenyl)-1,2,3,4,4a,5,6,10b-octahydro-2-oxobenzo[h] [1,6]naphthyridine-9-carboxylate, diastereomeric mixture ***6a***

To a stirred solution of *p*-chlorobenzaldehyde, **4a** (1.50 g, 10.7 mmol) and ethyl 4-aminobenzoate, **5** (1.76 g, 10.7 mmol) in anhydrous CH_3CN (40 mL), 4 Å molecular sieves and $Sc(OTf)_3$ (1.05 g, 2.13 mmol) were added. The mixture was stirred at room temperature under argon atmosphere for 5 min and then treated with a solution of lactam **3** (2.00 g, 10.7 mmol) in anhydrous CH_3CN (20 mL). The resulting suspension was stirred at room temperature under argon atmosphere for 3 days. Then, additional $Sc(OTf)_3$ (0.53 g, 1.07 mmol) was added and the reaction mixture was stirred one more day. The resulting mixture was diluted with sat. aq. $NaHCO_3$ (35 mL) and extracted with EtOAc (3 × 45 mL). The combined organic extracts were dried over anhydrous Na_2SO_4, filtered and evaporated under reduced pressure to give a yellow oil (4.89 g), which was purified through column chromatography (35–70 μm silica gel, hexane/EtOAc mixtures, gradient elution). On elution with hexane/EtOAc 30:70 to 0:100, the diastereomeric mixture **6a** (3.36 g, 66% yield, 1.4:1 diastereomeric ratio (^{1}H NMR)) was isolated as a white solid.

Ethyl 1-benzyl-1,2,3,4,4a,5,6,10b-octahydro-2-oxo-5-(3-pyridyl)benzo[h] [1,6]naphthyridine-9-carboxylate, diastereomeric mixture ***6b***

It was prepared as decribed for **6a**. From 3-pyridinecarboxaldehyde, **4b** (1.00 mL, 1.14 g, 10.7 mmol), **5** (1.76 g, 10.7 mmol), $Sc(OTf)_3$ (1.05 g, 2.14 mmol + 0.53 g, 1.07 mmol), and lactam **3** (2.00 g, 10.7 mmol), a brown solid (5.20 g) was obtained and purified by column chromatography (35–70 μm silica gel, hexane/EtOAc/MeOH mixtures, gradient elution). On elution with 0:95:5 to 0:80:20, the diastereomeric mixture **6b** (2.53 g, 54% yield, 1:1 diastereomeric ratio (^{1}H NMR)) was isolated as a white solid.

Ethyl 1-benzyl-5-(4-methoxycarbonylphenyl)-1,2,3,4,4a,5,6,10b-octahydro-2-oxobenzo[h][1,6]naphthyridine-9-carboxylate, diastereomeric mixture ***6c***

It was prepared as described for **6a**. From methyl 4-formylbenzoate, **4c** (1.75 g, 10.7 mmol), **5** (1.76 g, 10.7 mmol), $Sc(OTf)_3$ (1.05 g, 2.14 mmol + 0.53 g, 1.07 mmol), and lactam **3** (2.00 g, 10.7 mmol), a solid residue (6.40 g) was obtained and purified by column chromatography (35–70 μm silica gel, hexane/EtOAc mixtures, gradient

elution). On elution with 40:60 to 0:100, the diastereomeric mixture **6c** (3.91 g, 73% yield, 1.7:1 diastereomeric ratio (^{1}H NMR)) was isolated as a white solid.

Ethyl 1-(tert-butoxycarbonyl)-1,2,3,4,4a,5,6,10b-octahydro-5-(3-pyridyl)benzo[h][1,6]naphthyridine-9-carboxylate, diastereomeric mixture ***8b***

It was prepared as described for **6a**. From **4b** (584 mg, 5.46 mmol), **5** (901 mg, 5.46 mmol), $Sc(OTf)_3$ (537 mg, 1.09 mmol), and enamine **7** (1.01 mL, 1.00 g, 5.46 mmol), a solid residue (2.85 g) was obtained and purified by column chromatography (35–70 μm silica gel, hexane/EtOAc mixtures, gradient elution). On elution with hexane/EtOAc 20:80, the diastereomeric mixture **8b** (1.21 g, 51% yield, 5:1 diastereomeric ratio (^{1}H NMR)) was isolated as a pale yellow solid.

Ethyl 1-benzyl-5-(4-chlorophenyl)-1,2,3,4-tetrahydro-2-oxobenzo[h][1,6] naphthyridine-9-carboxylate ***9a***

To a solution of diastereomeric mixture **6a** (2.69 g, 5.66 mmol) in anhydrous $CHCl_3$ (88 mL), DDQ (2.57 g, 11.3 mmol) was added. The reaction mixture was stirred at room temperature under argon atmosphere overnight, diluted with sat. aq. $NaHCO_3$ (150 mL) and extracted with CH_2Cl_2 (2 × 100 mL). The combined organic extracts were dried over anhydrous Na_2SO_4, filtered and evaporated under reduced pressure to give an orange solid (3.50 g), which was purified through column chromatography (35–70 μm silica gel, hexane/EtOAc mixtures, gradient elution). On elution with hexane/EtOAc 85:15 to 20:80, compound **9a** (1.94 g, 73% yield) was isolated as a beige solid; R_f 0.93 (hexane/EtOAc 1:1).

A solution of **9a** (91 mg, 0.19 mmol) in CH_2Cl_2 (3 mL) was filtered through a polytetrafluoroethylene (PTFE) 0.2 μm filter and washed with pentane (3 × 4 mL) to give, after drying under standard conditions, the analytical sample of **9a** (89 mg) as a white solid: mp 192–193 ºC (CH_2Cl_2); IR (KBr) ν 1706, 1689, 1566 (C=O, Ar–C–C and Ar–C–N st) cm^{-1}; ^{1}H NMR (400 MHz, $CDCl_3$) δ 1.34 (t, J=7.0 Hz, 3H, $CO_2CH_2CH_3$), 2.65 (br t, J=6.8 Hz, 2H, 4-H_2), 2.96 (br t, J=6.8 Hz, 2H, 3-H_2), 4.35 (q, J≈7.0 Hz, 2H, $CO_2CH_2CH_3$), 5.41 (s, 2H, 1–CH_2–Ar), 7.14 [dd, J=6.4 Hz, J'=1.6 Hz, 2H, 1–CH_2–Ar–C2(6)-*H*], 7.22–7.29 [complex signal, 3H, 1–CH_2–Ar–C4-*H* and 1–CH_2–Ar–C3(5)-*H*], 7.49 [dt, J≈8.4 Hz, J'≈2.0 Hz, 2H, 5–Ar–C3(5)-H_2], 7.56 [d, J=8.4 Hz, J'=2.0 Hz, 2H, 5–Ar–C2(6)-H_2], 8.14 (d, J=8.8 Hz, 1H, 7-H), 8.27 (dd, J=8.8

Hz, *J'*=1.6 Hz, 1H, 8-H), 8.74 (d, *J*=1.6 Hz, 1H, 10-H); ^{13}C NMR (100.6 MHz, $CDCl_3$) δ 14.5 (CH_3, $CO_2CH_2\mathit{C}H_3$), 23.8 (CH_2, C3), 32.8 (CH_2, C4), 52.7 (CH_2, 1–$\mathit{C}H_2$–Ar), 61.6 (CH_2, $CO_2\mathit{C}H_2CH_3$), 119.4 (C, C10a), 122.1 (C, C4a), 126.1 (CH, C7), 127.3 [2CH, 1–CH_2–Ar–*C*2(6)], 127.7 (CH, C10), 128.0 (C, C9), 128.7 (CH, 1–CH_2–Ar–*C*4), 128.9 (2CH), 129.0 (2CH) and 130.6 (2CH) [1–CH_2–Ar–*C*3(5), 5–Ar–*C*2(6) and 5–Ar–*C*3(5)], 130.9 (CH, C8), 135.5 (C, 1–CH_2–Ar–*C*1), 137.2 (C) and 137.8 (C) (5–Ar–*C*1 and 5–Ar–*C*4), 148.1 (C, C6a), 150.4 (C, C5), 159.1 (C, C10b), 166.0 (C, $\mathit{C}O_2CH_2CH_3$), 172.6 (C, C2); HRMS (ESI), calcd for [$C_{28}H_{23}{}^{35}ClN_2O_3 + H^+$]: 471.1470, found 471.1469; Elemental analysis, calcd for $C_{28}H_{23}ClN_2O_3$ C 71.41%, H 4.92%, N 5.95%, Cl 7.53%, found C 71.44%; H 4.94%; N 5.68%; Cl 7.36%. HPLC purity > 99%.

Ethyl 1-benzyl-1,2,3,4-tetrahydro-2-oxo-5-(3-pyridyl)benzo[h][1,6]naphthyridine-9-carboxylate ***9b***

It was prepared as described for **9a**. From diastereomeric mixture **6b** (2.53 g, 5.73 mmol) and DDQ (2.42 g, 10.7 mmol), an orange solid residue (1.22 g) was obtained and purified through column chromatography (35–70 μm silica gel, hexane/EtOAc/Et_3N mixtures, gradient elution). On elution with hexane/EtOAc/Et_3N 10:90:0.2, compound **9b** (110 mg, 5% yield) was isolated as a beige solid; R_f 0.60 (hexane/EtOAc 1:1).

A solution of **9b** (51 mg, 0.12 mmol) in CH_2Cl_2 (4 mL) was filtered through a 0.2 μm PTFE filter and treated with a methanolic solution of HCl (0.53 N, 2.00 mL, 1.06 mmol). The resulting solution was evaporated at reduced pressure and the solid was washed with pentane (3 × 4 mL) to give, after drying under standard conditions, **9b**·HCl (53 mg) as a white solid: mp 185–186 ºC (CH_2Cl_2/MeOH 67:33); IR (KBr) *v* 3500–2500 (max at 3404, 3051, 2982, 3008, 2384, $^+$NH and CH st), 2095, 1974, 1691, 1587, 1596, 1553 (C=O, Ar–C–C and Ar–C–N st) cm^{-1}; ^{1}H NMR (400 MHz, $CDCl_3$) δ 1.31 (t, *J*=7.2 Hz, 3H, $CO_2CH_2C\mathit{H}_3$), 2.76 (br s, 2H, 4-H_2), 3.09 (br s, 2H, 3-H_2), 4.32 (q, *J*=7.2 Hz, 2H, $CO_2C\mathit{H}_2CH_3$), 5.42 (s, 2H, 1–CH_2–Ar), 7.13 [d, *J*=7.2 Hz, 2H, 1–CH_2–Ar–C2(6)-*H*], 7.21–7.29 [complex signal, 3H, 1–CH_2–Ar–C3(5)-*H* and 1–CH_2–Ar–C4-*H*], 8.09 (br s, 1H 5–Ar–C5-H), 8.27–8.33 (complex signal, 2H, 7-H and 8-H), 8.66–8.78 (complex signal, 2H, 5–Ar–C4-H and 10-H), 8.97 (br s, 1H, 5–Ar–C6-H), 9.24 (br s, 1H, 5–Ar–C2-H); ^{13}C NMR (100.6 MHz, $CDCl_3$) δ 14.4 (CH_3, $CO_2CH_2\mathit{C}H_3$), 23.3 (CH_2, C3), 32.1 (CH_2, C4), 53.2 (CH_2, 1–$\mathit{C}H_2$–Ar), 61.9 (CH_2, $CO_2\mathit{C}H_2CH_3$), 119.8 (C, C10a), 121.8 (C, C4a), 126.4 (CH, C7), 126.7 (CH, C10),

127.0 [2CH, 1–CH_2–Ar–*C*2(6)], 127.9 (CH, 1–CH_2–Ar–*C*4), 128.9 [2CH, 1–CH_2–Ar–*C*3(5)], 129.3 (C, C9), 129.5 (CH, 5–Ar–*C*5) 130.7 (CH, C8), 136.5 (2C, 1–CH_2–Ar–*C*1 and 5–Ar–*C*3), 142.6 (CH), 143.1 (CH) and 145.2 (CH) (5–Ar–*C*2, 5–Ar–*C*4 and 5–Ar–*C*6), 148.7 (C, C6a), 150.8 (C, C5), 151.4 (C, C10b), 165.3 (C, *C*$O_2CH_2CH_3$), 171.6 (C, C2); HRMS (ESI), calcd for [$C_{27}H_{23}N_3O_3$ + H^+] 438.1812, found 438.1804; Elemental analysis, calcd for $C_{27}H_{23}N_3O_3$·HCl·2.5H_2O C 62.49%, H 5.63%, N 8.10%, Cl 6.83%, found C 62.53%, H 5.12%, N 8.02%, Cl 7.00%. HPLC purity: 95%.

Ethyl 1-benzyl-5-(4-methoxycarbonylphenyl)-1,2,3,4-tetrahydro-2-oxobenzo[h] [1,6]naphthyridine-9-carboxylate ***9c***

It was prepared as described for **9a**. From diastereomeric mixture **6c** (3.40 g, 6.80 mmol) and DDQ (3.06 g, 13.6 mmol), an orange solid residue (3.53 g) was obtained and purified through column chromatography (35–70 μm silica gel, hexane/EtOAc mixtures, gradient elution). On elution with hexane/EtOAc 70:30 to 60:40, compound **9c** (1.20 g, 36% yield) was isolated as a white solid; R_f 0.89 (hexane/EtOAc 1:1).

A solution of **9c** (145 mg, 0.29 mmol) in CH_2Cl_2 (10 mL) was filtered through a 0.2 μm PTFE filter and treated with a methanolic solution of HCl (0.53 N, 1.70 mL, 0.90 mmol). The resulting solution was evaporated at reduced pressure and the solid was washed with pentane (3 × 4 mL) to give, after drying under standard conditions, **9c**·HCl (150 mg) as a white solid: mp 223–224 ºC (CH_2Cl_2 / MeOH 85:15); IR (KBr) *v* 3500–2500 (max at 3409, 3126, 3101, 3033, 2981, 2954, 2917, 2847, $^+$NH and CH st), 1721, 1633, 1611, 1571, 1554, 1512 (C=O, Ar–C–C and Ar–C–N st) cm^{-1}; ^{1}H NMR (400 MHz, $CDCl_3$ + CD_3OD) δ 1.24 (t, *J*=7.0 Hz, 3H, $CO_2CH_2CH_3$), 2.75 (br t, *J*=7.0 Hz, 2H, 4-H_2), 3.00 (br t, *J*=6.8 Hz, 2H, 3-H_2), 3.92 (s, 3H, CO_2CH_3), 4.26 (q, *J*=7.2 Hz, 2H, $CO_2CH_2CH_3$), 5.43 (s, 2H, 1–CH_2–Ar), 7.12 [d, *J*=6.8 Hz, 2H, 1–CH_2–Ar–C2(6)-*H*], 7.23–7.31 [complex signal, 3H, 1–CH_2–Ar–C4-*H* and 1–CH_2–Ar–C3(5)-*H*], 7.75 [d, *J*=8.4 Hz, 2H, 5–Ar–C2(6)-H], 8.21 [d, *J*=8.4 Hz, 2H, 5–Ar–C3(5)-H], 8.42 (d, *J*=8.8 Hz, 1H, 8-H), 8.81–8.83 (complex signal, 2H, 7-H and 10-H); ^{13}C NMR (100.6 MHz, $CDCl_3$ + CD_3OD) δ 14.2 (CH_3, $CO_2CH_2CH_3$), 22.6 (CH_2, C3), 31.2 (CH_2, C4), 52.6 (CH_3, CO_2CH_3), 53.8 (CH_2, 1–CH_2–Ar), 62.2 (CH_2, $CO_2CH_2CH_3$), 119.1 (C, C10a), 122.2 (C, C4a), 124.0 (CH, C7), 126.6 (CH, C10), 126.7 [2CH, 1–CH_2–Ar–*C*2(6)], 128.1 (CH, 1–CH_2–Ar–*C*4), 129.0 [2CH, 1–CH_2–Ar–*C*3(5)], 130.1 [2CH, 5–Ar–*C*(2)6], 130.1 (C, C9), 130.2 [2CH, 5–Ar–*C*3(5)], 133.0 (C, 5–Ar–*C*4), 133.2 (CH,

C8), 134.7 (C, 5–Ar–*C*1), 135.7 (C, 1–CH_2–Ar–*C*1), 142.6 (C, C6a), 154.4 (C, C5), 154.9 (C, C10b) 164.6 (C, *C*$O_2CH_2CH_3$), 166.1 (*C*O_2CH_3), 171.1 (C, C2); HRMS (ESI), calcd for [$C_{30}H_{26}N_2O_5$ + H^+] 495.1914, found 495.1910; Elemental analysis, calcd for $C_{30}H_{26}N_2O_5$·HCl C 67.86%, H 5.13%, N 5.28%, Cl 6.68%, found C 67.82%, H 5.21%, N 5.09%, Cl 6.14%. HPLC purity: 99%.

Ethyl 1-benzyl-5-(4-chlorophenyl)-1,2,3,4-tetrahydrobenzo[h][1,6]naphthyridine-9-carboxylate ***10a***

A suspension of $Zn(OAc)_2$ (35 mg, 0.19 mmol) and $(EtO)_3SiH$ (0.77 mL, 685 mg, 4.17 mmol) in anhydrous THF (5 mL) was stirred at room temperature for 30 min and then treated with a solution of lactam **9a** (0.90 g, 1.91 mmol) in anhydrous THF (15 mL). The reaction mixture was stirred at 65 ºC for 48 h. The resulting mixture was poured onto 1N NaOH (15 mL), cooled to 0 ºC with an ice bath and thoroughly stirred for 30 min. Then, EtOAc was added (15 mL) and the phases were separated. The aqueous phase was extracted with EtOAc (2 × 15 mL). The combined organic extracts were dried over anhydrous Na_2SO_4, filtered and concentrated under reduced pressure to give a yellow solid (1.80 g), which was purified through column chromatography (35–70 μm silica gel, hexane/EtOAc mixtures, gradient elution). On elution with hexane/EtOAc 85:15, compound **10a** (0.45 g, 52% yield) was isolated as a yellowish solid. On elution with hexane/EtOAc 80:20 to 70:30, unreacted **9a** was recovered (0.29 g).

10a: R_f 0.76 (hexane/EtOAc 1:1).

A solution of **10a** (90 mg, 0.20 mmol) in CH_2Cl_2 (3 mL) was filtered through a 0.2 μm PTFE filter and treated with a methanolic solution of HCl (0.53 N, 1.10 mL, 0.58 mmol). The resulting solution was evaporated at reduced pressure and the solid was washed with pentane (3 × 4 mL) to give, after drying under standard conditions, **10a**·HCl (92 mg) as a white solid: mp 227–228 ºC (CH_2Cl_2 / MeOH 73:27); IR (KBr) *v* 3500–2500 (max at 3402, 3029, 2930, 2909, 2860, 2600, $^+$NH and CH st), 1716, 1653, 1626, 1595, 1576, 1560, 1521 (C=O, Ar–C–C and Ar–C–N st) cm^{-1}; ^{1}H NMR (400 MHz, $CDCl_3$) δ 1.03 (t, *J*=7.0 Hz, 3H, $CO_2CH_2CH_3$), 2.00 (tt, *J*≈*J'*≈4.0 Hz, 2H, 3-H_2), 2.87 (br t, *J*=6.0 Hz, 2H, 4-H_2), 3.70 (br t, *J*=5.4 Hz, 2H, 2-H_2), 4.10 (q, *J*≈7.0 Hz, 2H, $CO_2CH_2CH_3$), 5.18 (s, 2H, 1–CH_2–Ar), 7.34 [d, *J*=8.4 Hz, 2H, 5–Ar–C3(5)-H], 7.39–7.45 [complex signal, 3H, 1–CH_2–Ar–C4-*H* and 1–CH_2–Ar–C2(6)-*H*], 7.52 [dd, *J*≈*J'*≈7.4 Hz, 2H, 1–CH_2–Ar–C3(5)-*H*], 7.65 [d, *J*=8.4 Hz, 2H, 5–Ar–C2(6)-H], 8.18

(dd, *J*=8.8 Hz, *J'*=1.6 Hz 1H, 8-H), 8.63 (d, *J*=1.6 Hz, 1H, 10-H), 8.82 (d, *J*=8.8 Hz, 1H, 7-H); ^{13}C NMR (100.6 MHz, $CDCl_3$) δ 14.0 (CH_3, $CO_2CH_2\mathit{C}H_3$), 20.7 (CH_2, C3), 26.0 (CH_2, C4), 51.8 (CH_2, C2), 61.0 (CH_2, 1−*C*H_2−Ar), 61.5 (CH_2, $CO_2\mathit{C}H_2CH_3$), 114.1 (C, C4a), 116.0 (C, C10a), 121.1 (CH, C7), 126.5 [2CH, 1−CH_2−Ar−C2(6)], 127.1 (CH, C10), 128.5 (CH, 1−CH_2−Ar−*C*4), 129.0 [2CH, 1−CH_2−Ar−*C*3(5)], 129.2 (C, C9), 129.7 [2CH, 5−Ar−*C*3(5)], 131.6 [2CH, 5−Ar−*C*2(6)] 132.2 (CH, C8), 134.8 (2C) and 137.4 (C) (5−Ar−*C*1, 5−Ar−*C*4 and 1−CH_2−Ar−*C*1), 141.8 (C, C6a), 150.0 (C, C5), 158.5 (C, C10b), 164.9 (C, *C*$O_2CH_2CH_3$); HRMS (ESI), calcd for [$C_{28}H_{25}{}^{35}ClN_2O_2$ + H^+] 457.1677, found 457.1673; Elemental analysis, calcd for $C_{28}H_{25}ClN_2O_2\cdot HCl\cdot 1.25H_2O$ C 65.18%, H 5.57%, N 5.43%, Cl 13.74%, found C 65.31%, H 5.52%, N 5.20%, Cl 10.50%. HPLC purity: 95%.

Ethyl 1-benzyl-1,2,3,4-tetrahydro-5-(3-pyridyl)benzo[h][1,6]naphthyridine-9-carboxylate ***10b***

It was prepared as described for **10a**. From $Zn(OAc)_2$ (4.4 mg, 0.02 mmol), $(EtO)_3SiH$ (0.1 mL, 8.9 mg, 0.54 mmol), and lactam **9b** (115 mg, 0.26 mmol) a brown solid residue (160 mg) was obtained and purified through column chromatography (35-70 μm silica gel, CH_2Cl_2/MeOH/50% aq. NH_4OH mixtures, gradient elution). On elution with CH_2Cl_2/MeOH/50% aq. NH_4OH 99.5:0.5:0.2, impure **10b** (21 mg) was isolated. This product was taken in EtOAc (0.2 mL) and precipitated with hexane (0.8 mL). After drying of the precipitate under standard conditions, pure **10b** (16 mg, 15% yield) was obtained as a white solid; R_f 0.55 (CH_2Cl_2/MeOH/50% aq. NH_4OH 9:1:0.05).

A solution of **10b** (16 mg, 0.04 mmol) in CH_2Cl_2 (2 mL) was filtered through a 0.2 μm PTFE filter and treated with a methanolic solution of HCl (0.53 N, 0.60 mL, 0.32 mmol). The resulting solution was evaporated at reduced pressure and the solid was washed with pentane (3 × 4 mL) to give, after drying under standard conditions, **10b**·2HCl (17 mg) as a white solid: ^{1}H NMR (400 MHz, $CDCl_3$) δ 1.06 (t, *J*=7.0 Hz, 3H, $CO_2CH_2C\mathit{H}_3$), 2.13 (br s, 2H, 3-H_2), 2.92 (br s, 2H, 4-H_2), 3.74 (br s, 2H, 2-H_2), 4.13 (q, *J*=7.0 Hz, 2H, $CO_2C\mathit{H}_2CH_3$), 5.23 (br s, 2H, 1−CH_2−Ar), 7.38 [tt, *J*≈*J'*≈7.2 Hz, 2H, 1−CH_2−Ar−C3(5)-*H*], 7.38−7.48 [complex signal, 4H, 5−Ar−C5-H, 1−CH_2−Ar−C2(6)-*H* and 1−CH_2−Ar−C4-*H*], partially overlapped 8.12 (br s, 1H, 5−Ar−C5-H), 8.26 (d, *J*=9.2 Hz, 1H, 7-H), 8.67 (br d, 1H, 8-H), 8.71 (br signal, 2H, 10-H and 5−Ar−C4-H), 8.94 (br s, 1H, 5−Ar−C6-H), 9.38 (br s, 5−Ar−C2-H); HRMS (ESI), calcd for

[$C_{27}H_{25}N_3O_2$ + H^+] 424.2020, found 424.2013; Elemental analysis, calcd for $C_{27}H_{25}N_3O_2 \cdot 2HCl \cdot 3.5H_2O$ C 57.96%, H 6.13%, N 7.51%, found C 58.13%, H 5.80%, N 7.70%.

*Ethyl 1-benzyl-1,2,3,4-tetrahydro-5-(4-methoxycarbonylphenyl)benzo[h][1,6] naphthyridine-9-carboxylate **10c***

It was prepared as described for **10a**. From $Zn(OAc)_2$ (39 mg, 0.21 mmol), $(EtO)_3SiH$ (0.87 mL, 774 mg, 4.71 mmol), and lactam **9c** (1.06 g, 2.14 mmol) a yellow solid residue (1.20 g) was obtained and purified through column chromatography (35-70 μm silica gel, hexane/EtOAc mixtures, gradient elution). On elution with hexane/EtOAc 70:30, compound **10c** (0.40 g, 39% yield) was isolated as a yellow solid. On elution with hexane/EtOAc 70:30 to 60:40, unreacted **9c** (0.22 g) was recovered.

10c: R_f 0.89 (hexane/EtOAc 1:1).

A solution of **10c** (190 mg, 0.39 mmol) in CH_2Cl_2 (10 mL) was filtered through a 0.2 μm PTFE filter and treated with a methanolic solution of HCl (0.53 N, 2.20 mL, 1.17 mmol). The resulting solution was evaporated at reduced pressure and the solid was washed with pentane (3 × 4 mL) to give, after drying under standard conditions, **10c**·HCl (150 mg) as a white solid: mp 156–158 ºC (CH_2Cl_2/MeOH 82:18); IR (KBr) *v* 3500–2500 (max at 3406, 3219, 3102, 3043, 2985, 2950, 2844, 2656, $^+$NH and CH st), 1716, 1628, 1608, 1578, 1564 (C=O, Ar–C–C and Ar–C–N st) cm^{-1}; ^{1}H NMR (400 MHz, $CDCl_3$) δ 1.03 (t, *J*=7.2 Hz, 3H, $CO_2CH_2CH_3$), 2.00 (br s, 2H, 3-H_2), 2.92 (br s, 2H, 4-H_2), 3.76–3.82 (complex signal, 5H, 2-H_2 and CO_2CH_3), 4.11 (q, *J*=7.2 Hz, 2H, $CO_2CH_2CH_3$), 5.30 (s, 2H, 1–CH_2–Ar), 7.40–7.46 [complex signal, 3H, 1–CH_2–Ar–C2(6)-*H* and 1–CH_2–Ar–C4-*H*], 7.53 [dd, *J*≈*J'*≈7.6 Hz, 2H, 1–CH_2–Ar–C3(5)-*H*] 7.82 [d, *J*=7.2 Hz, 2H 5–Ar–C2(6)-H], 7.91 [d, *J*=7.2 Hz, 2H 5–Ar–C3(5)-H], 8.15 (dd, *J*=9.2 Hz, *J'*=1.6 Hz, 1H, 8-H), 8.61 (d, *J*=9.2 Hz, 1H, 7-H), 8.65 (d, *J*=1.6 Hz, 1H, 10-H); ^{13}C NMR (100.6 MHz, $CDCl_3$) δ 13.9 (CH_3, $CO_2CH_2CH_3$), 20.6 (CH_2, C3), 25.7 (CH_2, C4), 51.8 (CH_2, C2), 52.1 [CH_3, CO_2CH_3), 60.8 (CH_2, 1–CH_2–Ar), 61.3 (CH_2, $CO_2CH_2CH_3$), 114.0 (C, C4a), 115.8 (C, C10a), 121.8 (CH, C7), 126.2 [2CH, 1–CH_2–Ar–*C*2(6)], 126.9 (C, C9), 127.2 (CH, C10), 128.3 (CH, 1–CH_2–Ar–*C*4), 129.5 [4CH, 5–Ar–*C*3(5) and 1–CH_2–Ar–*C*3(5)], 130.2 [2CH, 5–Ar–*C*(2)6], 131.7 (C, 5–Ar–*C*4), 132.0 (CH, C8), 134.8 (2C, 5–Ar–*C*1 and 1–CH_2–Ar–*C*1), 141.5 (C, C6a), 149.4 (C, C5), 158.4 (C, C10b), 164.8 (C, $CO_2CH_2CH_3$), 165.6 (C, CO_2CH_3); HRMS (ESI), calcd

for [$C_{30}H_{28}N_2O_4$ + H^+] 481.2122, found 481.2111; Elemental analysis, calcd for $C_{30}H_{28}N_2O_4 \cdot HCl \cdot 1.75H_2O$ C 65.43%, H 5.52%, N 4.99%, Cl 6.69%, found C 65.69%, H 5.97%, N 5.11%, Cl 6.46%.

Ethyl 1-(tert-butoxycarbonyl)-1,2,3,4-tetrahydro-5-(3-pyridyl)benzo[h][1,6]naphthyridine-9-carboxylate ***11b***

From diastereomeric mixture **8b** (1.35 g, 3.09 mmol) in toluene (150 mL), pyridine (1.44 mL) and MnO_2 (Wako) (27 mg, 0.31 mmol) were added, and the mixture was stirred in an open vessel at 55 ^oC during 3 h. The crude mixture was filtered through Celite, and the filtrate was concentrated *in vacuo*. A yellow solid residue (1.26 g) was obtained and purified through column chromatography (35–70 μm silica gel, hexane/EtOAc mixtures, gradient elution). On elution with EtOAc, compound **11b** (643 mg, 48% yield) was isolated as a yellow pale solid. ^1H NMR δ 1.30–1.43 [complex signal, 12H, $CO_2CH_2CH_3$, $C(CH_3)_3$], 1.62–1.81 (m, 2H, 3-H_2), 1.95–2.09 (m, 2H, 4-H_2), 2.84 (t, *J*=6.6 Hz, 2H, 2-H_2), 4.45 (q, *J*=7.1 Hz, 2H, $CO_2CH_2CH_3$), 7.46–7.50 (m, 1H, 5-Ar–C5–H), 7.99 (dd, *J*=7.9 Hz, *J'*=1.9 Hz, 1H, 8-H), 8.10 (d, *J*=8.8 Hz, 1H, 7-H), 8.28 (d, *J*=1.9 Hz, 1H, 10-H), 8.60–8.62 (m, 1H, 5–Ar–C4-H), 8.71–8.74 (m, 1H, 5–Ar–C2-H), 8.88–8.90 (m, 1H, 5–Ar–C2-H); HPLC-MS (ES+), for [$C_{25}H_{27}N_3O_4$ + H^+] 434.

Ethyl 5-(4-chlorophenyl)-1,2,3,4-tetrahydrobenzo[h][1,6]naphthyridine-9-carboxylate ***12a***

Ester **11a** (1.30 g, 2.78 mmol) was dissolved in 4M HCl/dioxane solution (15 mL) at 0 ºC. The mixture was stirred at room temperature for 18 h and concentrated *in vacuo*. The residue was diluted in water (8 mL), treated with sat. aq. Na_2CO_3 until pH 9, and the aqueous phase was extracted with a 10% MeOH/$CHCl_3$ mixture (3 × 10 mL). The combined organic extracts were dried over anhydrous Na_2SO_4, filtered, and evaporated at reduced pressure to give **12a** (983 mg, 97% yield) as a white solid; IR (film) *v* 3421, 3065 (NH st), 1708, 1607, 1572 (C=O, Ar–C–C and Ar–C–N st) cm^{-1}; ^1H NMR (400 MHz, $CDCl_3$) δ 1.31 (t, *J*=7.1 Hz, 3H, $CO_2CH_2CH_3$), 1.73–1.91 (m, 2H, 3-H_2), 2.64 (t, *J*=6.1 Hz, 2H, 4-H_2), 3.37–3.51 (m, 2H, 2-H_2), 4.32 (q, *J*=7.1 Hz, 2H, $CO_2CH_2CH_3$), 5.72 (br s, 1H, NH), 7.32 (d, *J*=8.4 Hz, 2H, 5–Ar–C3(5)-H), 7.41 (d, *J*=8.4 Hz, 2H, 5-Ar–C2(6)-H), 7.85 (t, *J*=9.2 Hz, 1H, 7-H), 8.06 (dt, *J*=9.2, *J'*=1.4 Hz, 1H, 8-H), 8.45 (d, *J*=1.4 Hz, 1H, 10-H); ^{13}C NMR (100.6 MHz, $CDCl_3$) δ 14.5 (CH_3, $CO_2CH_2CH_3$), 20.8 (CH_2, C3), 25.6 (CH_2, C4), 41.6 (CH_2, C2), 61.2 (CH_2, $CO_2CH_2CH_3$), 108.1 (C, C4a),

116.4 (C, C10a), 122.8 (C, C10), 125.8 (C, C9), 128.3 (CH, C8), 128.4 [2CH, 5–Ar–*C*3(5)], 129.9 (CH, C7), 130.3 [2CH, 5–Ar–*C*2(6)], 134.2 (C, 5–Ar–*C*4), 139.5 (C, 5–Ar–*C*1), 147.7 (C, C10b), 149.1 (C, C6a), 160.4 (C, C5), 166.6 (C, $CO_2CH_2CH_3$); HRMS (ESI) calcd for [$C_{21}H_{19}{}^{35}ClN_2O_2 + H^+$] 367.1213, found 367.1208. HPLC purity > 99%.

Ethyl 5-(3-pyridyl)-1,2,3,4-tetrahydrobenzo[h][1,6]naphthyridine-9-carboxylate ***12b***

It was prepared as decribed for **12a**. From **11b** (562 mg, 1.30 mmol) and 4M HCl/dioxane solution (9 mL), a yellow residue (411 mg) was obtained and purified through column chromatography (35–70 μm silica gel, hexane/EtOAc mixtures, gradient elution). On elution with EtOAc, compound **12b** (329 mg, 76% yield) was isolated as a pale yellow powder: IR (film) *v* 3417, 3070 (NH st), 1708, 1621, 1558 (C=O, Ar–C–C and Ar–C–N st) cm^{-1}; ^1H NMR (400 MHz, CD_3OD) δ 1.46 (t, *J*=7.1 Hz, 3H, $CO_2CH_2CH_3$), 1.96–2.09 (m, 2H, 3-H_2), 2.74–2.84 (m, 2H, 4-H_2), 3.68–3.79 (m, 2H, 2-H_2), 4.47 (q, *J*=7.1 Hz, 2H, $CO_2CH_2CH_3$), 7.93 (d, *J*=8.8 Hz, 1H, 7-H), 8.25 (dd, *J*=7.7 Hz, *J'*=5.8 Hz, 1H, 5–Ar–C5-H), 8.40 (dd, *J*=8.8 Hz, *J'*=1.5 Hz, 1H, 8-H), 8.84 (d, *J*=8.0 Hz, 1H, 5–Ar–C4-H), 9.05 (d, *J*=1.5 Hz, 1H, 10-H), 9.11 (m, 1H, 5–Ar–C6-H), 9.30 (s, 1H, 5–Ar–C2-H); ^{13}C NMR (100.6 MHz, CD_3OD) δ 14.6 (CH_3, $CO_2CH_2CH_3$), 19.7 (CH_2, C3), 24.6 (CH_2, C4), 43.2 (CH_2, C2), 62.9 (CH_2, $CO_2CH_2CH_3$), 111.2 (C, C4a), 116.3 (C, C10a), 121.3 (CH, C10), 126.2 (C, C9), 128.2 (CH, C8), 129.8 (CH, C7), 132.5 (CH, 5–Ar–*C*5), 134.2 (C, 5–Ar–*C*3), 141.2 (CH), 145.3 (CH) and 145.9 (CH) (5–Ar–*C*2, 5–Ar–*C*4 and 5–Ar–*C*6), 146.5 (C, C6a), 146.7 (C, C5), 156.2 (C, C10b), 166.3 (C, $CO_2CH_2CH_3$); HRMS (ESI), calcd for [$C_{20}H_{19}N_3O_2 + H^+$] 334.1550, found 334.1558. HPLC purity: 97%.

Ethyl 5-(4-chlorophenyl)-1,2,3,4-tetrahydro-1-(4-methoxybenzyl)benzo[h][1,6]naphthyridine-9-carboxylate ***13a***

A mixture of **12a** (364 mg, 0.99 mmol), 1-chloromethyl-4-methoxybenzene (148 μL, 171 mg, 1.09 mmol) and NaH (26 mg, 1.08 mmol) in DMSO (10 mL) was stirred at room temperature for 18 h. The resulting mixture was treated at 0 ºC with 1N HCl (10 mL) and then with aq. $NaHCO_3$ until pH 7-8, and extracted with CH_2Cl_2 (3 × 10 mL). The combined organic extracts were washed with water (8 mL), dried over anhydrous Na_2SO_4, filtered, and evaporated at reduced pressure, to give a residue, which was

purified through column chromatography (35–70 μm silica gel, hexane/EtOAc mixtures), to afford compound **13a** (186 mg, 40% yield) as a white solid.

IR (film) *v* 1720, 1610, 1559, 1502 (C=O, Ar–C–C and Ar–C–N st) cm^{-1}; ^1H NMR (400 MHz, $CDCl_3$) δ 1.17 (t, *J*=7.1 Hz, 3H, $CO_2CH_2CH_3$), 1.80–1.92 (m, 2H, 3-H_2), 2.74 (t, *J*=6.2 Hz, 2H, 4-H_2), 3.25–3.32 (m, 2H, 2-H_2), 3.86 (s, 3H, 1–CH_2–Ar–OCH_3), 4.23 (q, *J*=7.1 Hz, 2H, $CO_2CH_2CH_3$), 4.64 (br s, 2H, 1–CH_2–Ar), 7.00 [dd, *J*=9.1 Hz, *J'*=2.5 Hz, 2H, 1–CH_2–Ar–C3(5)-*H*], 7.51–7.39 [complex signal, 5H, 7-H, 5–Ar–C3(5)-H, 1–CH_2–Ar–C2(6)-*H*], 7.53 [d, *J*=8.4 Hz, 2H, 5–Ar–C2(6)-H], 8.17 (d, *J*=8.3 Hz, 1H, 8-H), 8.81 (s, 1H, 10-H); ^{13}C NMR (100.6 MHz, $CDCl_3$) δ 14.2 (CH_3, $CO_2CH_2CH_3$), 19.3 (CH_2, C3), 27.2 (CH_2, C4), 48.8 (CH_2, C2), 55.5 (CH_2, 1–CH_2–Ar), 60.5 (CH_2, $CO_2CH_2CH_3$), 61.0 (CH_3, 1–CH_2–Ar–OCH_3), 114.4 (C, C4a), 117.3 [2CH, 1–CH_2–Ar– C3(5)], 120.7 (C, C10a), 126.2 (CH, C8), 126.7 (CH, C10), 128.4 (C, C9), 128.7 [2CH, 5–Ar–C3(5)], 128.8 [2CH, 1-CH_2–Ar–C2(6)], 130.1 (CH, C7), 130.3 (CH, 5–Ar–C2(6)], 134.5 (C, 5–Ar–C4), 139.4 (C, 5–Ar–C1), 149.9 (C, C6a), 153.9 (C, C10b), 159.3 (C, 1–CH_2–Ar–C4), 160.6 (C, C5), 166.6 (C, $CO_2CH_2CH_3$); HRMS (ESI), calcd for [$C_{29}H_{27}{}^{35}ClN_2O_3 + H^+$] 487.1783, found 487.1795. HPLC purity: 98%.

1-Benzyl-5-(4-chlorophenyl)-N-ethyl-1,2,3,4-tetrahydrobenzo[h][1,6] naphthyridine-9-carboxamide ***14a***

A suspension of ester **10a** (0.20 g, 0.42 mmol) and KOH (85% purity, 0.09 g, 1.36 mmol) in MeOH (11 mL) was stirred under reflux for 24 h. The resulting solution was cooled down at room temperature and concentrated under reduced pressure. The solid residue (0.38 g) was treated with a solution of HCl in Et_2O (0.5 N, 18 mL, 9,00 mmol) and the resulting suspension was concentrated under reduced pressure to give the corresponding aminoquinolino carboxylic acid, in the form of hydrochloride, as a white solid (0.34 g). This crude product was used in the next step without further purification.

A solution of this crude product (0.34 g) in anhydrous CH_2Cl_2 (5 mL) was cooled to 0º C with an ice bath and treated dropwise with freshly distilled Et_3N (0.25 mL, 0.18 g, 1.78 mmol) and $ClCO_2Et$ (0.04 mL, 45.6 mg, 0.42 mmol). The resulting suspension was thoroughly stirred at 0º C for 30 min and treated with $EtNH_2 \cdot HCl$ (0.04 g, 0.49 mmol). The reaction mixture was stirred at room temperature for 3 days, diluted with 10% aq. Na_2CO_3 (15 mL), and extracted with CH_2Cl_2 (3 × 10 mL). The combined organic extracts were washed with H_2O (2 × 50 mL), dried over anhydrous Na_2SO_4, filtered and

concentrated under reduced pressure to give a white solid (220 mg), which was purified through column chromatography (35–70 μm silica gel, CH_2Cl_2/MeOH/50% aq. NH_4OH mixtures, gradient elution). On elution with CH_2Cl_2/MeOH/50% aq. NH_4OH 98:2:0.2, amide **14a** (100 mg, 44% overall yield) was isolated as a white solid; R_f 0.54 (CH_2Cl_2/MeOH/50% aq. NH_4OH 9:1:0.05).

A solution of **14a** (40 mg, 0.09 mmol) in CH_2Cl_2 (3 mL) was filtered through a 0.2 μm PTFE filter and treated with a methanolic solution of HCl (0.53 N, 0.50 mL, 0.27 mmol). The resulting solution was evaporated at reduced pressure and the solid was washed with pentane (3 × 4 mL) to give, after drying under standard conditions, **14a**·HCl (43 mg) as a white solid: mp 149–151 ºC (CH_2Cl_2/MeOH 73:27); IR (KBr) ν 3500–2500 (max at 3415, 3229, 3144, 3058, 3034, 2953, 2922, 2868, 2709, 2636, $^+$NH, NH and CH st), 1659, 1625, 1607, 1595, 1577, 1563, 1531 (C=O, Ar–C–C and Ar–C–N st) cm^{-1}; ^{1}H NMR (400 MHz, CD_3OD) δ 1.06 (t, J≈7.2 Hz, 3H, $CONHCH_2CH_3$), 2.08 (tt, J≈J'≈4.8 Hz, 2H, 3-H_2), 2.77 (t, J=5.8 Hz, 2H, 4-H_2), 3.25 (q, J=7.2 Hz, 2H, $CONHCH_2CH_3$), 3.68 (t, J=5.2 Hz, 2H, 2-H_2), 4.80 (s, NH and $^+$NH), 5.28 (s, 2H, 1–CH_2–Ar), partially overlapped 7.42–7.47 [complex signal, 3H, 1–CH_2–Ar–C2(6)-*H* and 1–CH_2– Ar–C4-*H*], partially overlapped 7.47–7.53 [dd, J≈J'≈7.2 Hz, 2H, 1–CH_2–Ar–C3(5)-H], 7.63–7.68 [complex signal, 4H, 5–Ar–C2(6)-H and 5–Ar–C3(5)-H], 7.91 (d, J=8.8 Hz, 1H, 7-H), 8.15 (dd, J=8.8 Hz, J'=1.6 Hz, 1H, 8-H), 8.51 (d, J≈1.6 Hz, 1H, 10-H); ^{13}C NMR (100.6 MHz, CD_3OD) δ 14.6 (CH_3, $CONHCH_2CH_3$), 21.1 (CH_2, C3), 26.4 (CH_2, C4), 35.8 (CH_2, C2), 53.1 (CH_2, $CONHCH_2CH_3$), 61.6 (CH_2, 1–CH_2–Ar), 115.0 (C, C4a), 117.3 (C, C10a), 121.1 (CH, C7), 126.9 (CH, C10), 127.7 [2CH, 1–CH_2–Ar–*C*2(6)], 129.2 (CH, 1–CH_2–Ar–*C*4), 130.37 (CH, C8), 130.42 [2CH, 1–CH_2–*C*3(5)], 131.6 [2CH, 5–Ar–*C*3(5)], 132.0 (C, C9), 132.2 [2CH, 5–Ar–*C*2(6)], 132.8 (C, 5–Ar–*C*4), 136.2 (C, 5–Ar–*C*1), 138.2 (C, 1–CH_2–Ar–*C*1], 141.6 (C, C6a), 150.3 (C, C5), 159.8 (C, C10b), 168.1 (C, $CONHCH_2CH_3$); HRMS (MALDI), calcd for [$C_{28}H_{26}{}^{35}ClN_3O$ + H^+] 456.2, found 456.3; Elemental analysis, calcd for $C_{28}H_{26}ClN_3O$·1.1HCl·0.25H_2O C 66.58%, H 5.62%, N 8.32%, Cl 14.74%, found C 66.77%, H 5.74%, N 7.74%, Cl 15.04%. HPLC purity: 95%.

N-ethyl-1,2,3,4-tetrahydro-5-(3-pyridyl)benzo[h][1,6]naphthyridine-9-carboxamide ***16b***

It was prepared as described for **14a**. From ester **12b** (328 mg, 0.98 mmol) crude aminoquinolino carboxylic acid (300 g), in the form of hydrochloride, was obtained and directly used in the next step without further purification. From the above crude carboxylic acid (300 mg), freshly distilled Et_3N (653 μL, 474 mg, 4.69 mmol), $ClCO_2Et$ (287 μL, 326 mg, 3.00 mmol), and $EtNH_2 \cdot HCl$ (222 mg, 2.72 mmol), a solid residue (406 mg) was obtained and purified through column chromatography (35-70 μm silica gel, hexane/EtOAc mixtures, gradient elution). On elution with EtOAc, amide **16b** (192 mg, 59% overall yield) was obtained as a pale yellow solid.

^{1}H NMR (400 MHz, CD_3OD) δ 1.28 (t, *J*=7.3 Hz, 3H, $CONHCH_2CH_3$), 1.88–1.97 (m, 2H, 3-H_2), 2.71 (t, *J*=6.2 Hz, 2H, 4-H_2), 3.48 (q, *J*=7.3 Hz, 2H, $CONHCH_2CH_3$), 3.54–3.59 (m, 2H, 2-H_2], 7.58 (ddd, *J*=7.8 Hz, *J'*=5.0 Hz, *J''*=0.8 Hz, 1H, 5–Ar–C5-H), 7.83 (m, 1H, 7-H), 7.97 (dd, *J*=8.8 Hz, *J'*=2.0 Hz, 1H, 8-H), 8.02 (ddd, *J*=7.8 Hz, *J'*=2.2 Hz, *J''*=1.6 Hz, 1H, 5–Ar–C4-H), 8.54 (m, 1H, 10-H), 8.63 (dd, *J*=5.0 Hz, *J'*=1.6 Hz, 1H, 5–Ar–C6-H), 8.71 (dd, *J*=2.2 Hz, *J'*=0.8 Hz, 1H, 5–Ar–C2-H); ^{13}C NMR (100.6 MHz, CD_3OD) δ 20.1 (CH_3, $CONHCH_2CH_3$), 24.9 (CH_2, C3), 34.0 ($2CH_2$, C4, $CONHCH_2CH_3$), 40.8 (CH_2, C2), 116.5 (C, C4a), 120.9 (C, C10a), 123.5 (CH, C10), 126.6 (C, C9), 126.9 (CH, C8), 127.6 (CH, C7), 130.1 (CH, 5–Ar–*C*5), 136.9 (C, 5-Ar-*C*3), 137.2 (CH, 5–Ar–*C*4), 147.7 (CH), 148.3 (CH) (5–Ar–*C*2 and 5–Ar–*C*6), 148.6 (C, C6a), 149.1 (C, C5), 156.8 (C, C10b), 163.2 (C, $CONHCH_2CH_3$).

N-{{1-benzyl-5-(4-chlorophenyl)-1,2,3,4-tetrahydrobenzo[h][1,6]naphthyridin-9-yl}methyl}ethanamine ***17a***

A solution of amide **14a** (100 mg, 0.22 mmol) in anhydrous THF (5 mL) was cooled to 0 ºC with an ice bath, and treated portionwise with $LiAlH_4$ (30 mg, 0.77 mmol). The resulting suspension was stirred under reflux overnight, cooled to 0 ºC with an ice bath and treated dropwise with 1N NaOH (3 mL), then diluted with H_2O (8 mL), and extracted with EtOAc (3 × 8 mL). The combined organic extracts were dried over anhydrous Na_2SO_4, filtered and evaporated under reduced pressure to give a yellow solid (120 mg), which was purified through column chromatography (35–70 μm silica gel, CH_2Cl_2/MeOH/50% aq. NH_4OH mixtures, gradient elution). On elution with CH_2Cl_2/MeOH/50% aq. NH_4OH 99.5:0.5:0.2, unreacted **14a** (14 mg) was recovered. On elution with CH_2Cl_2/MeOH/50% aq. NH_4OH 99:1:0.2 to 95:5:0.2, amine **17a** (43

mg, 44% yield) was isolated as a white solid; R_f 0.44 (CH_2Cl_2/MeOH/50% aq. NH_4OH 9:1:0.05).

A solution of **17a** (35 mg, 0.08 mmol) in CH_2Cl_2 (3 mL) was filtered through a 0.2 μm PTFE filter and treated with a methanolic solution of HCl (0.43 N, 1.70 mL, 0.73 mmol). The resulting solution was evaporated at reduced pressure and the solid was washed with pentane (3 × 4 mL) to give, after drying under standard conditions, **17a**·2HCl (38 mg) as a white solid: mp 149–151 ºC (CH_2Cl_2/MeOH 73:27); IR (KBr) *v* 3500–2500 (max at 3380, 2924, 2853, 2662, 2522, $^+$NH, NH and CH st), 1631, 1596, 1578, 1563, 1518 (Ar–C–C and Ar–C–N st) cm^{-1}; ^{1}H NMR (400 MHz, CD_3OD) δ 1.29 (t, *J*=7.2 Hz, 3H, 9-$CH_2NHCH_2CH_3$), 2.05 (tt, *J*≈*J'*≈5.0 Hz, 2H, 3-H_2), 2.75 (t, *J*=5.8 Hz, 2H, 4-H_2), 3.00 (q, *J*=7.2 Hz, 2H, 9-$CH_2NHCH_2CH_3$), 3.65 (t, *J*=5.2 Hz, 2H, 2-H_2), 4.14 (s, 2H, 9-$CH_2NHCH_2CH_3$), 4.87 (s, NH and $^+$NH), 5.35 (s, 2H, 1–CH_2–Ar), 7.42 [dd, *J*≈*J'*≈6.8 Hz, 2H, 1–CH_2–C3(5)-*H*], 7.47–7.53 [complex signal, 3H, 1–Ar–C4-*H* and 1–CH_2–Ar–C2(6)-*H*], 7.66–7.71 [complex signal, 4H, 5–Ar–C2(6)-H and 5–Ar–C3(5)-H], 7.98 (d, *J*=8.4 Hz, 1H, 7-H), 8.04 (d, *J*=8.8 Hz, 1H, 8-H), 8.24 (s, 1H, 10-H); ^{13}C NMR (100.6 MHz, CD_3OD) δ 11.4 (CH_3, 9-$CH_2NHCH_2CH_3$), 21.3 (CH_2, C3), 26.5 (CH_2, C4), 43.8 (CH_2, C2), 51.4 (CH_2, 9-$CH_2NHCH_2CH_3$), 53.0 (CH_2, 9-$CH_2NHCH_2CH_3$), 61.7 (CH_2, 1–CH_2–Ar), 115.5 (C, C4a), 118.1 (C, C10a), 121.9 (CH, C7), 128.4 [2CH, 1–CH_2–Ar–*C*2(6)], 129.4 (CH, C10), 129.5 (C, C9), 129.6 (CH, 1–CH_2–Ar–*C*4), 130.4 [2CH, 1–CH_2–Ar–*C*3(5)], 130.5 [2CH, 5–Ar–*C*3(5)], 131.9 [2CH, 5–Ar–*C*2(6)], 132.5 (C, 5–Ar–*C*4), 135.2 (CH, C8), 137.1 (C, 1–CH_2–Ar–*C*1), 138.2 (C, 5–Ar–*C*1), 140.9 (C, C6a), 150.4 (C, C5), 159.8 (C, C10b); HRMS (ESI), calcd for [$C_{28}H_{28}{}^{35}ClN_3 + H^+$] 442.2045, found 442.2048; Elemental analysis, calcd for $C_{28}H_{28}ClN_3$·1.6HCl·2.6H_2O C 61.46%, H 6.41%, N 7.68%, Cl 16.85%, found C 61.81%, H 6.28%, N 7.06%, Cl 16.90%. HPLC purity: 98%.

N-{{1,2,3,4-tetrahydro-5-(3-pyridyl)benzo[h][1,6]naphthyridin-9-yl}methyl}ethanamine ***18b***

It was prepared as described for **17a**. From **16b** (91 mg, 0.27 mmol) and $LiAlH_4$ (156 mg, 4.11 mmol), a solid residue (65 g) was obtained and purified through column chromatography (35-70 μm silica gel, CH_2Cl_2/EtOH mixtures, gradient elution). On elution with CH_2Cl_2/EtOH 9:1, amine **18b** (44 mg, 51% yield) was isolated as a white solid.

18b·3HCl: IR (film) *v* 3500–2500 (max at 3415, 3363, 3035, 2969, 2930, 2841, $^{+}$NH, NH and CH st), 1611, 1561 (Ar–C–C and Ar–C–N st) cm^{-1}; ^{1}H NMR (400 MHz, CD_3OD) δ 1.39 (t, *J*=7.3 Hz, 3H, 9-$CH_2NHCH_2CH_3$), 1.99 (m, 2H, 3-H_2), 2.78 (m, 2H, 4-H_2), 3.19 (q, *J*=7.3 Hz, 2H, 9-$CH_2NHCH_2CH_3$), 3.76 (m, 2H, 2-H_2), 4.44 (s, 2H, 9-$CH_2NHCH_2CH_3$), 7.71 (dd, *J*=7.9 Hz, *J'*=5.0 Hz, 1H, 5–Ar–C5-H), 7.90 (d, *J*=8.7 Hz, 1H, 7-H), 8.02 (m, 1H, 8-H), 8.18 (dt, *J*=7.9 Hz, *J'*=1.8 Hz, 1H, 5–Ar–C4-H), 8.43 (m, 1H, 10-H), 8.81 (m, 1H), 8.88 (m, 1H) (5–Ar–C2-H and 5–Ar–C6-H); ^{13}C NMR (100.6 MHz, CD_3OD) δ 11.6 (CH_3, 9-$CH_2NHCH_2CH_3$), 19.9 (CH_2, C3), 24.7 (CH_2, C4), 43.1 (CH_2, C2), 44.2 (CH_2, 9-$CH_2NHCH_2CH_3$), 51.5 (CH_2, 9-$CH2NHCH_2CH_3$), 110.7 (C, C4a), 116.8 (C, C10a), 121.9 (CH, C7), 125.9 (CH, C10), 127.4 (CH, 5–Ar–*C*5), 131.4 (C, C9), 131.7 (C, 5–Ar–*C*3), 135.8 (CH, C8), 139.2 (C, C6a), 144.1 (CH, 5–Ar–*C*2 or 5–Ar–*C*6), 146.7 (C, C5), 148.4 (CH, 5–Ar–*C*4), 155.5 (C, C10b); HRMS (ESI) calcd for [$C_{20}H_{22}N_4 + H^+$] 319.1917, found, 319.1922. HPLC purity: 97%.

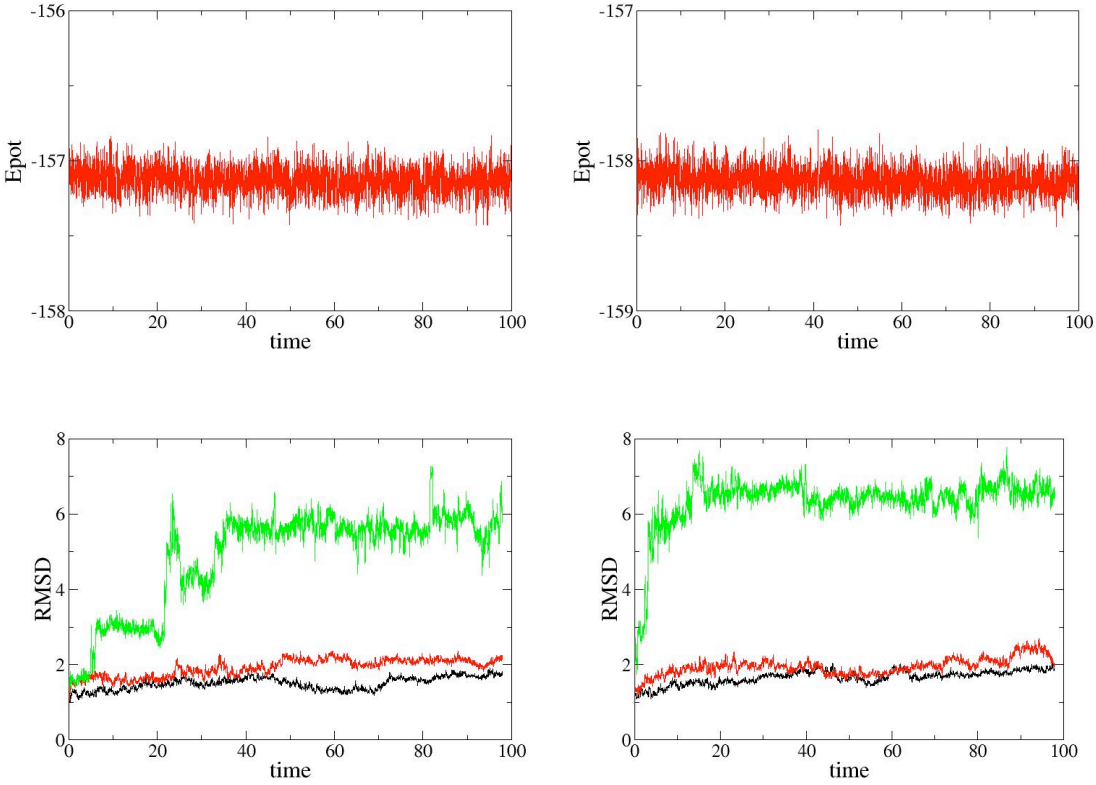

Fig. S1. (Top) Time evolution of the potential energy (× 10^3; kcal/mol) determined for the simulations of the AChE complexes with compounds **16a** (right) and **18a** (left). (Bottom) Time evolution of the rmsd (Å) determined for the backbone (black), the heavy atoms of the residues that define the binding site (red) and the ligand (green) for the simulations of the AChE complexes with compounds **16a** (right) and **18a** (left).

Table S1
Free energy components determined from Solvent Interaction Energy (SIE) computations for the binding of compounds **16a** and **18a**.[a]

Component	**16a**	**18a**
van der Waals (ΔE_{vW})	–44.1 ± 2.8	–42.2 ± 2.8
Coulombic (ΔE_{Coul})	–93.6 ± 5.7	–198.8 ± 6.1
Reaction Field (ΔG_{RF})	92.6 ± 5.0	192.2 ± 4.9
Cavity (γ ΔSA)	–8.1 ± 0.5	–7.7 ± 0.5
Total (ΔG) [a]	–8.5 ± 0.4	–8.8 ± 0.6

[a] Evaluated from the expression $\Delta G = \alpha\left[\Delta E_{vW} + \Delta E_{Coul} + \Delta G_{RF} + \gamma \Delta SA\right] + C$, where the parameters α (0.1048) and C (–2.89 kcal/mol) were fitted to the absolute binding free energies of 99 protein–ligand complexes.

Table S2

Reported and experimental permeability values (P_e 10^{-6} cm s^{-1}) of 14 commercial drugs used for the PAMPA-BBB assay validation.

Compound	Literature value[a]	Experimental value[b]
Verapamil	16	25.4 ± 0.78
Testosterone	17	24.0 ± 0.14
Corticosterone	5.1	6.70 ± 0.10
Clonidine	5.3	6.50 ± 0.05
Ofloxacin	0.8	0.97 ± 0.01
Lomefloxacin	1.1	0.75 ± 0.02
Progesterone	9.3	16.8 ± 0.30
Promazine	8.8	13.8 ± 0.30
Imipramine	13	12.3 ± 0.10
Hydrocortisone	1.9	1.40 ± 0.05
Piroxicam	2.5	1.71 ± 0.02
Desipramine	12	17.8 ± 0.10
Cimetidine	0.0	0.70 ± 0.03
Norfloxacin	0.1	0.90 ± 0.02

[a] Taken from ref. [1].

[b] Values are expressed as the mean ± SD of three independent experiments.

References

[1] L. Di, E.H. Kerns, K. Fan, O.J. McConnell, G.T. Carter, High throughput artificial membrane permeability assay for blood-brain barrier, Eur. J. Med. Chem. 38 (2003) 223–232.

Ethyl 1-benzyl-5-(4-chlorophenyl)-1,2,3,4-tetrahydro-2-oxobenzo[*h*][1,6]naphthyridine-9-carboxylate (**9a**)
^{1}H NMR (400 MHz, $CDCl_3$)

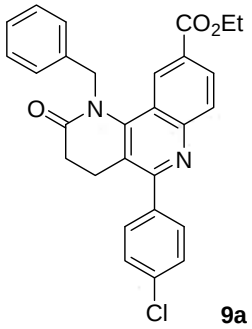

9a

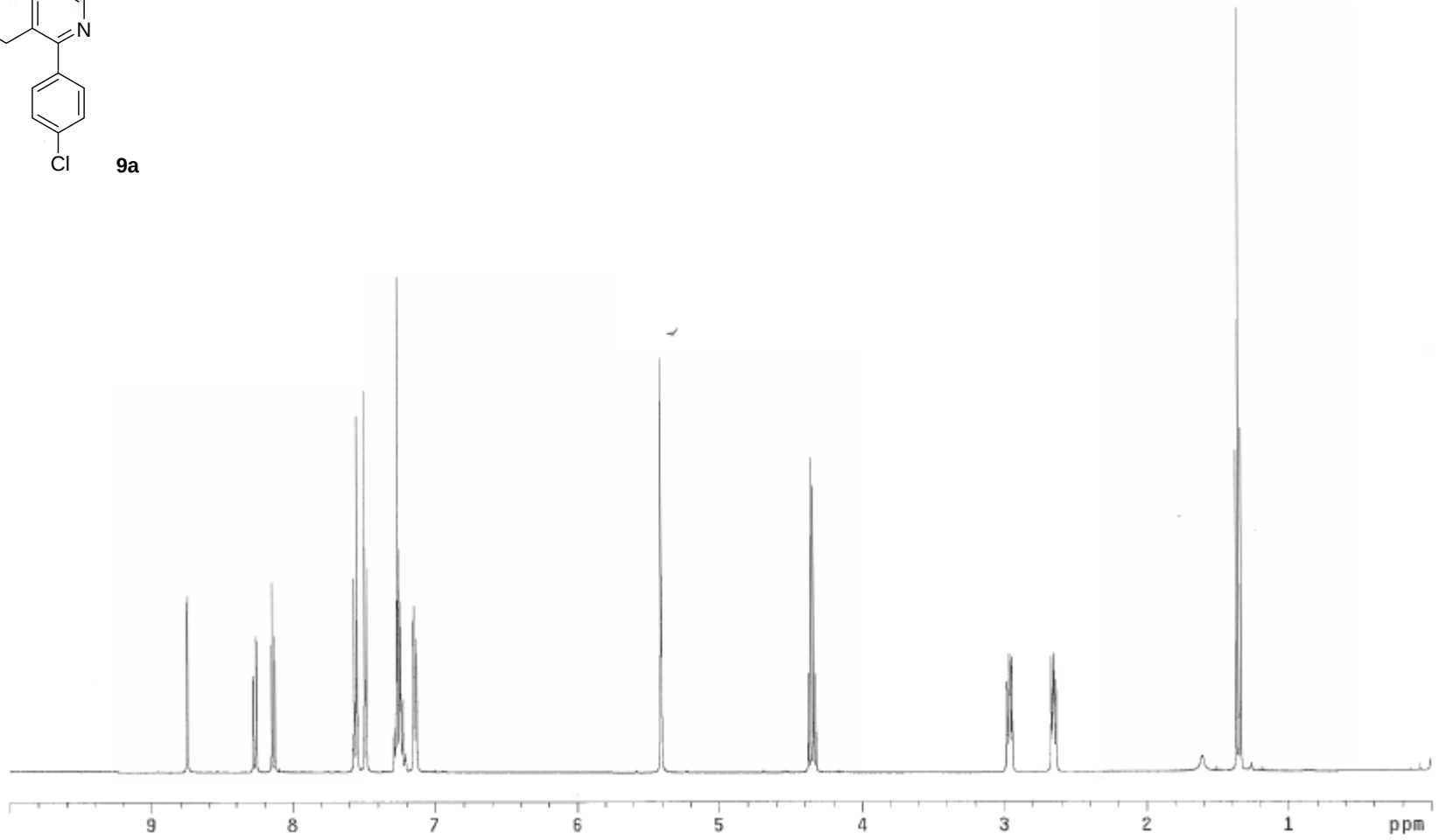

Ethyl 1-benzyl-5-(4-chlorophenyl)-1,2,3,4-tetrahydro-2-oxobenzo[*h*][1,6]naphthyridine-9-carboxylate (**9a**)
^{13}C NMR (100.6 MHz, $CDCl_3$)

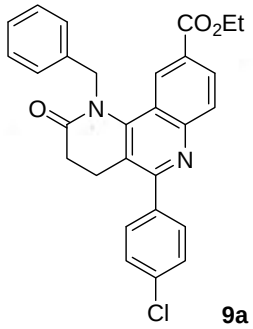

9a

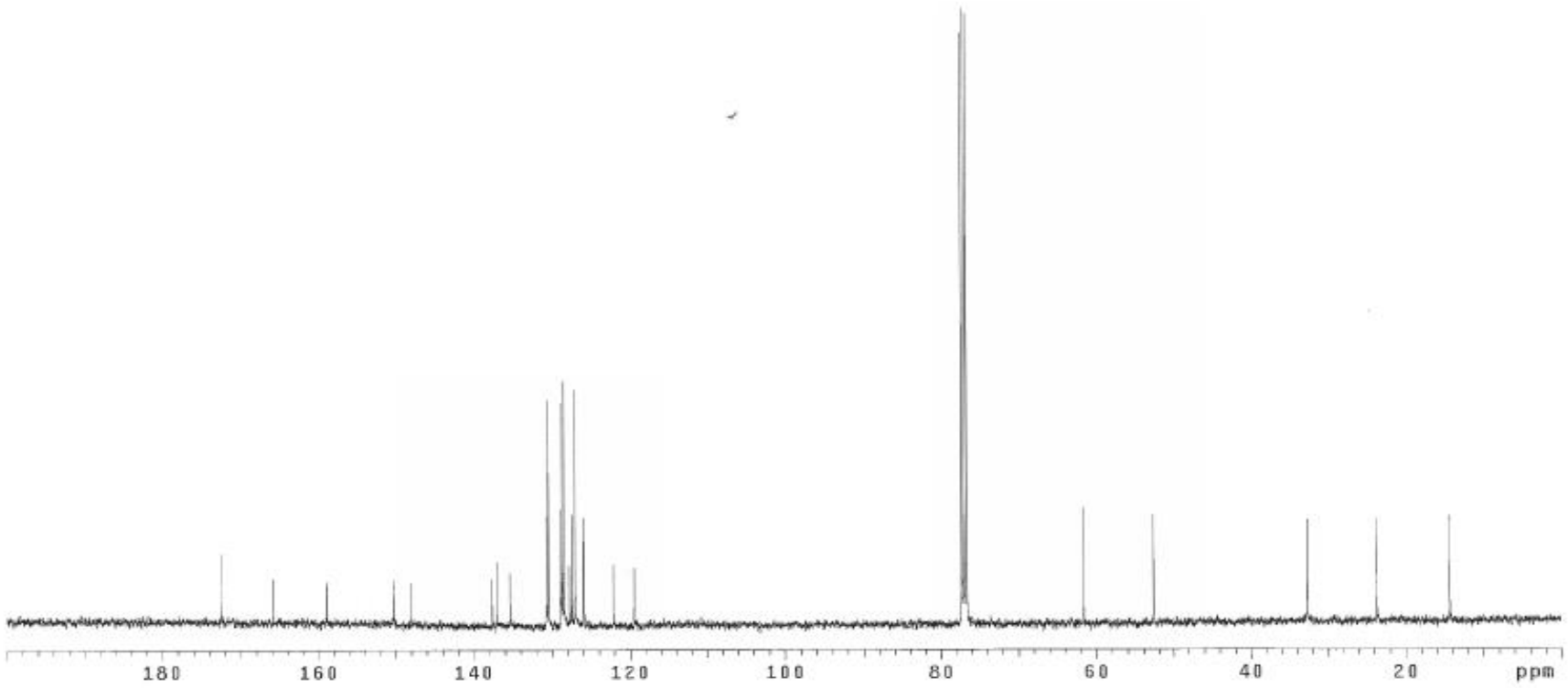

Ethyl 1-benzyl-1,2,3,4-tetrahydro-2-oxo-5-(3-pyridyl)benzo[*h*][1,6]naphthyridine-9-carboxylate (**9b**)
^{1}H NMR (400 MHz, $CDCl_3$)

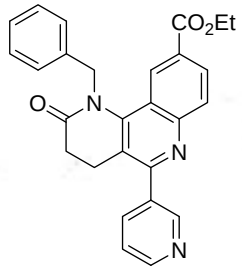

9b

Ethyl 1-benzyl-1,2,3,4-tetrahydro-2-oxo-5-(3-pyridyl)benzo[*h*][1,6]naphthyridine-9-carboxylate (**9b**)
^{13}C NMR (100.6 MHz, $CDCl_3$)

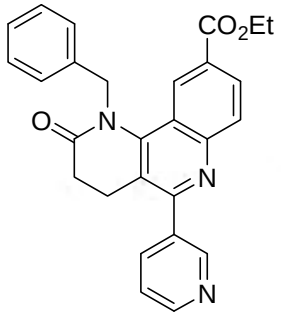

9b

Ethyl 1-benzyl-5-(4-methoxycarbonylphenyl)-1,2,3,4-tetrahydro-2-oxobenzo[*h*][1,6]naphthyridine-9-carboxylate (**9c**)
^{1}H NMR (400 MHz, $CDCl_3$ + CD_3OD)

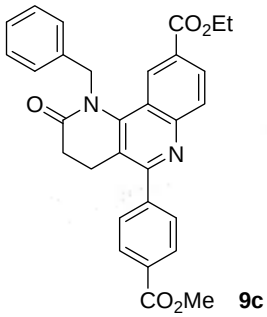

9c

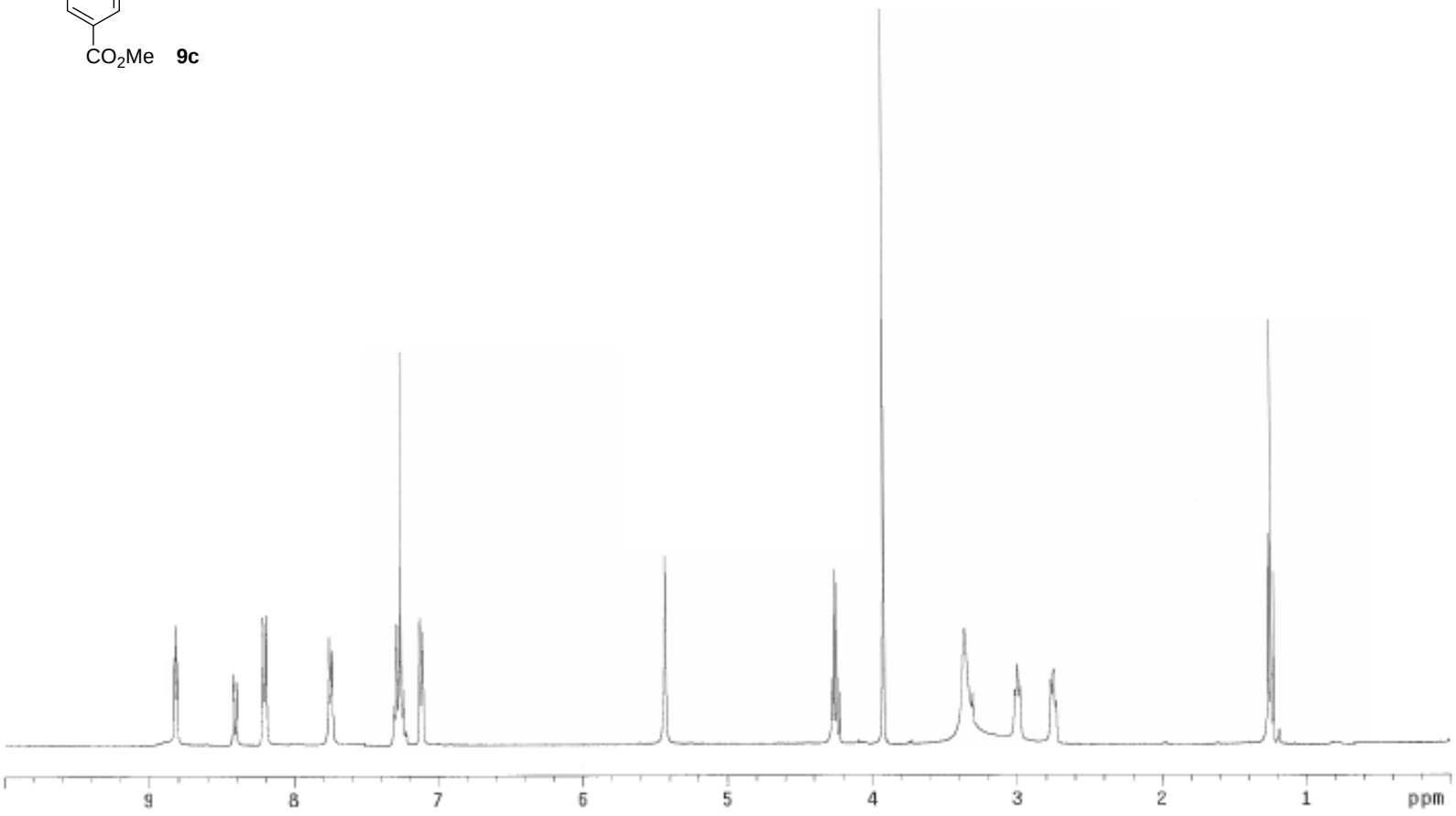

Ethyl 1-benzyl-5-(4-methoxycarbonylphenyl)-1,2,3,4-tetrahydro-2-oxobenzo[h] [1,6]naphthyridine-9-carboxylate (**9c**).
^{13}C-NMR (100.6 MHz, $CDCl_3$ + CD_3OD)

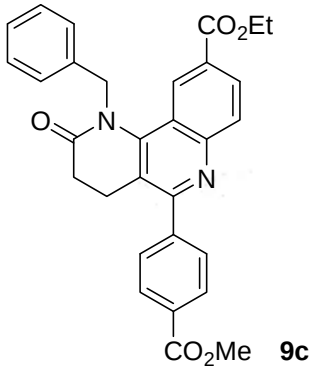

9c

Ethyl 1-benzyl-5-(4-chlorophenyl)-1,2,3,4-tetrahydrobenzo[*h*][1,6]naphthyridine-9-carboxylate (**10a**)
^{1}H NMR (400 MHz, $CDCl_3$)

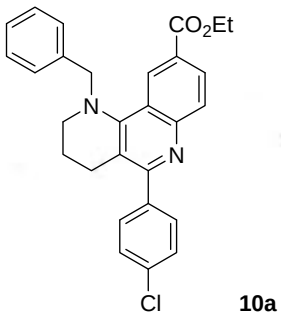

10a

Ethyl 1-benzyl-5-(4-chlorophenyl)-1,2,3,4-tetrahydrobenzo[*h*][1,6]naphthyridine-9-carboxylate (**10a**)
^{13}C NMR (100.6 MHz, $CDCl_3$)

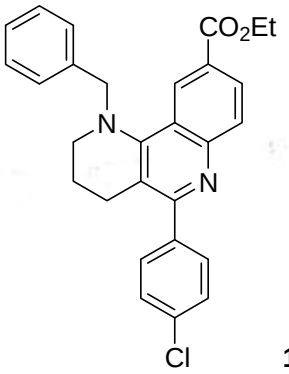

10a

Ethyl 1-benzyl-1,2,3,4-tetrahydro-5-(3-pyridyl)benzo[*h*][1,6]naphthyridine-9-carboxylate (**10b**)
^{1}H NMR (400 MHz, $CDCl_3$)

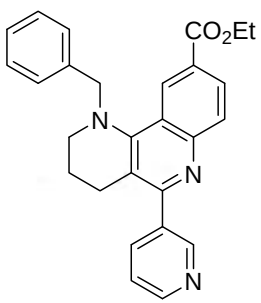

10b

Ethyl 1-benzyl-1,2,3,4-tetrahydro-5-(4-methoxycarbonylphenyl)benzo[*h*][1,6]naphthyridine-9-carboxylate (**10c**)
^{1}H NMR (400 MHz, $CDCl_3$)

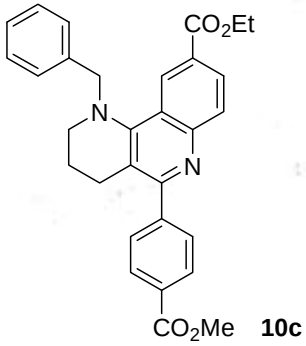

10c

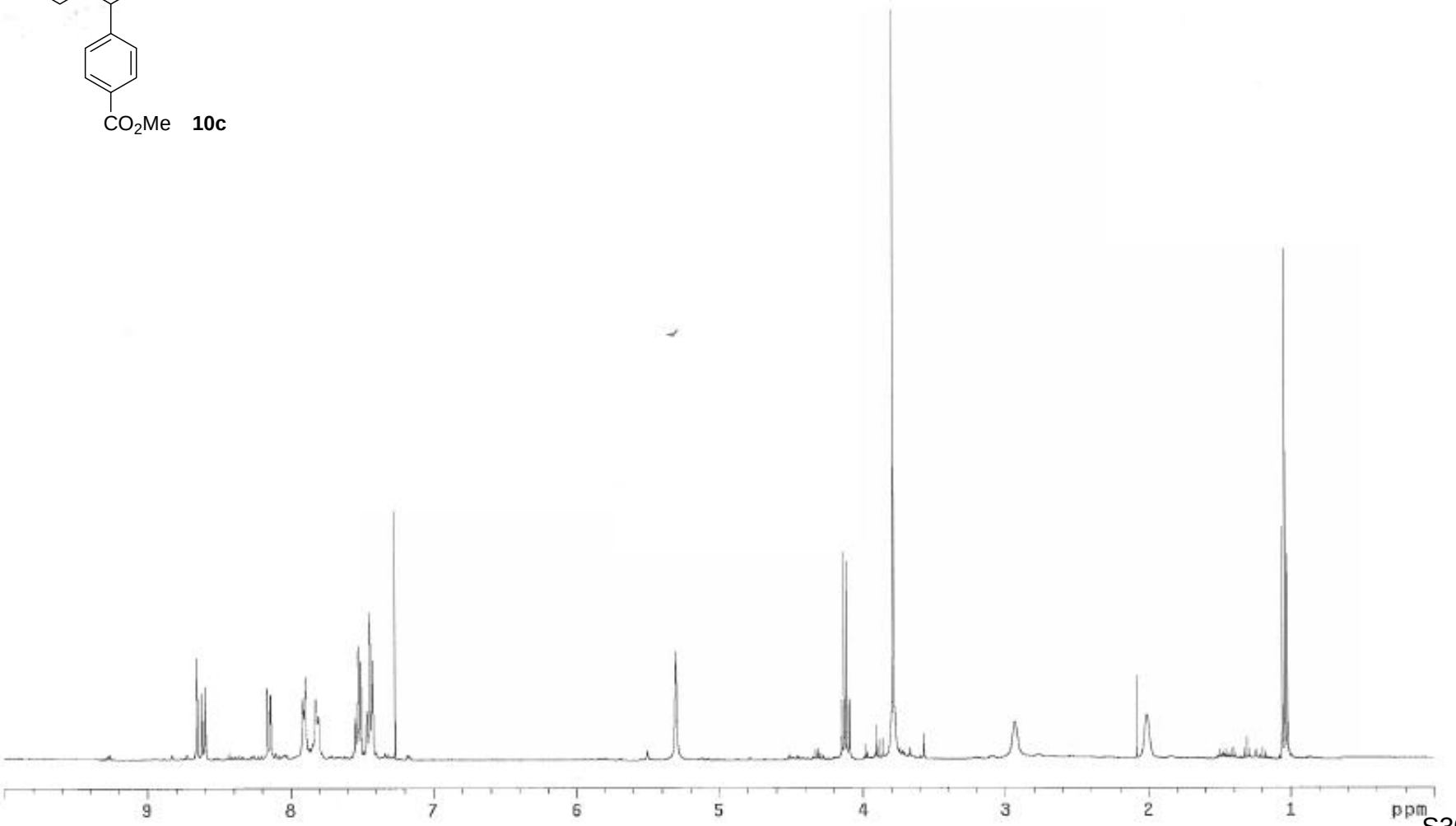

Ethyl 1-benzyl-1,2,3,4-tetrahydro-5-(4-methoxycarbonylphenyl)benzo[*h*][1,6]naphthyridine-9-carboxylate (**10c**)
^{13}C NMR (100.6 MHz, $CDCl_3$)

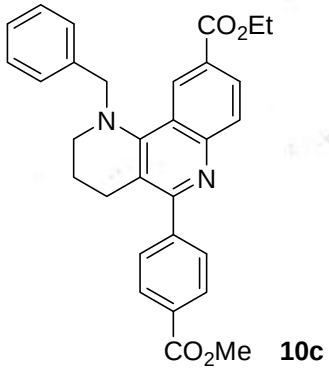

10c

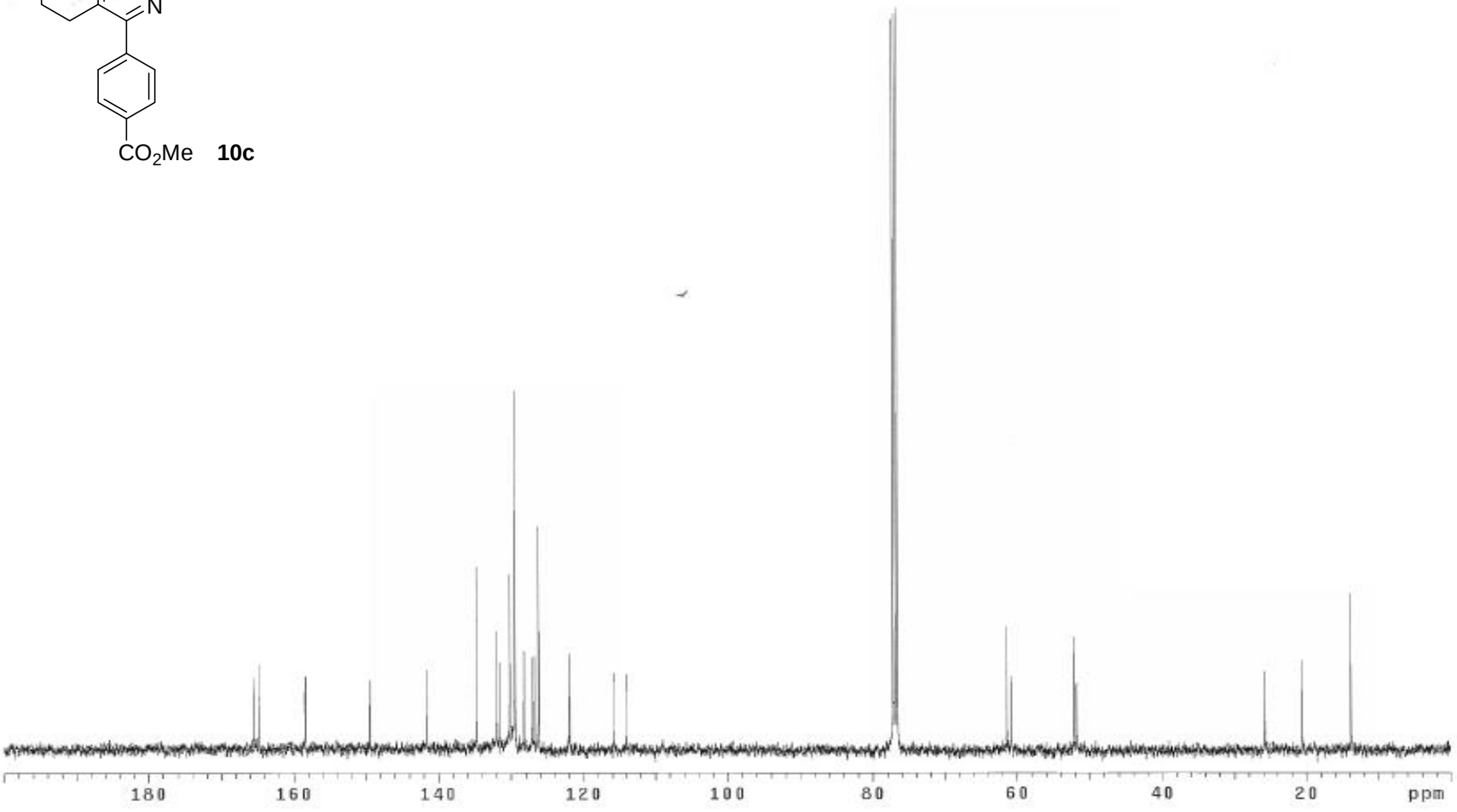

Ethyl 5-(4-chlorophenyl)-1,2,3,4-tetrahydrobenzo[*h*][1,6]naphthyridine-9-carboxylate (**12a**)
^{1}H NMR (400 MHz, $CDCl_3$)

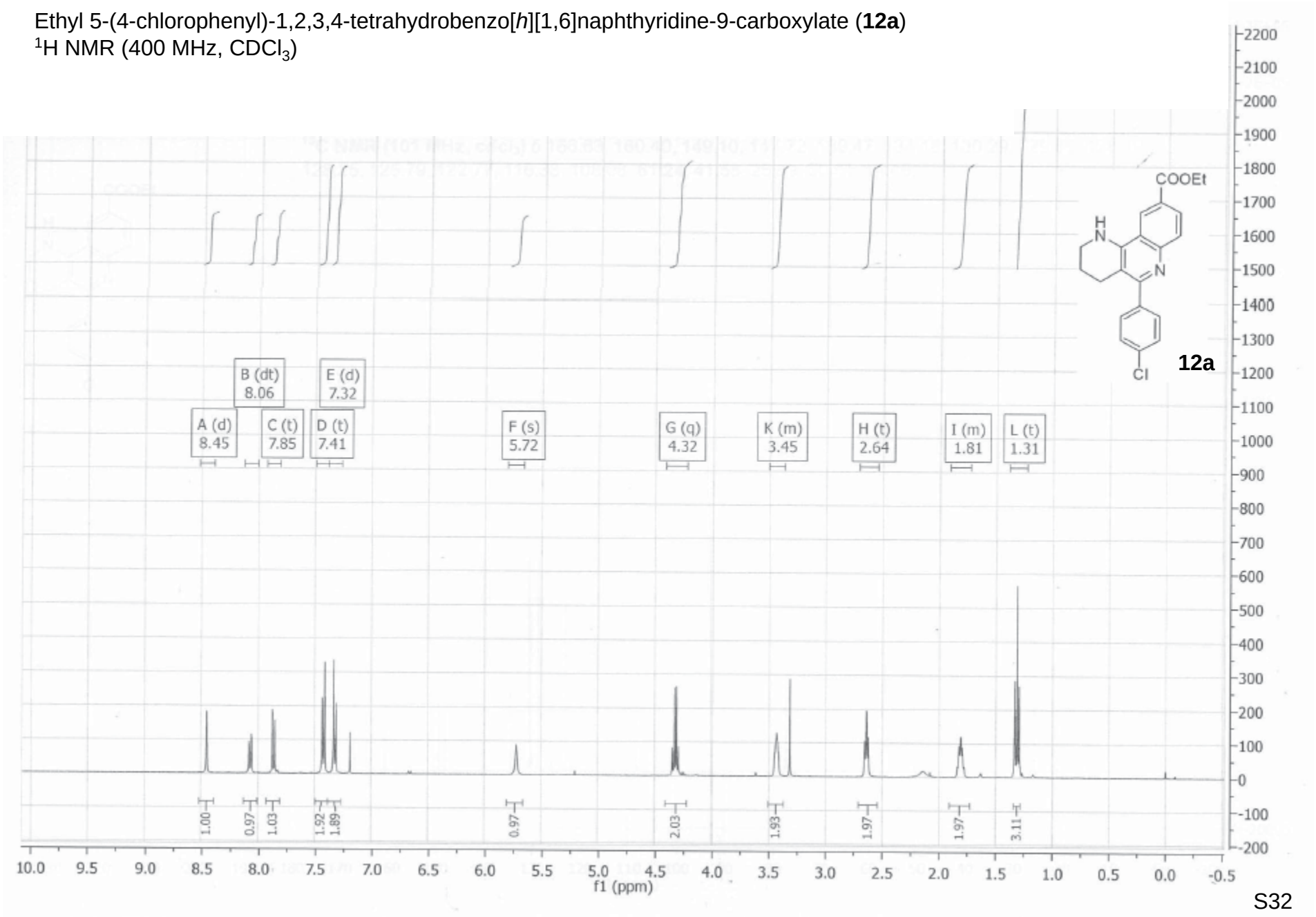

Ethyl 5-(4-chlorophenyl)-1,2,3,4-tetrahydrobenzo[*h*][1,6]naphthyridine-9-carboxylate (**12a**)
^{13}C NMR (100.6 MHz, $CDCl_3$)

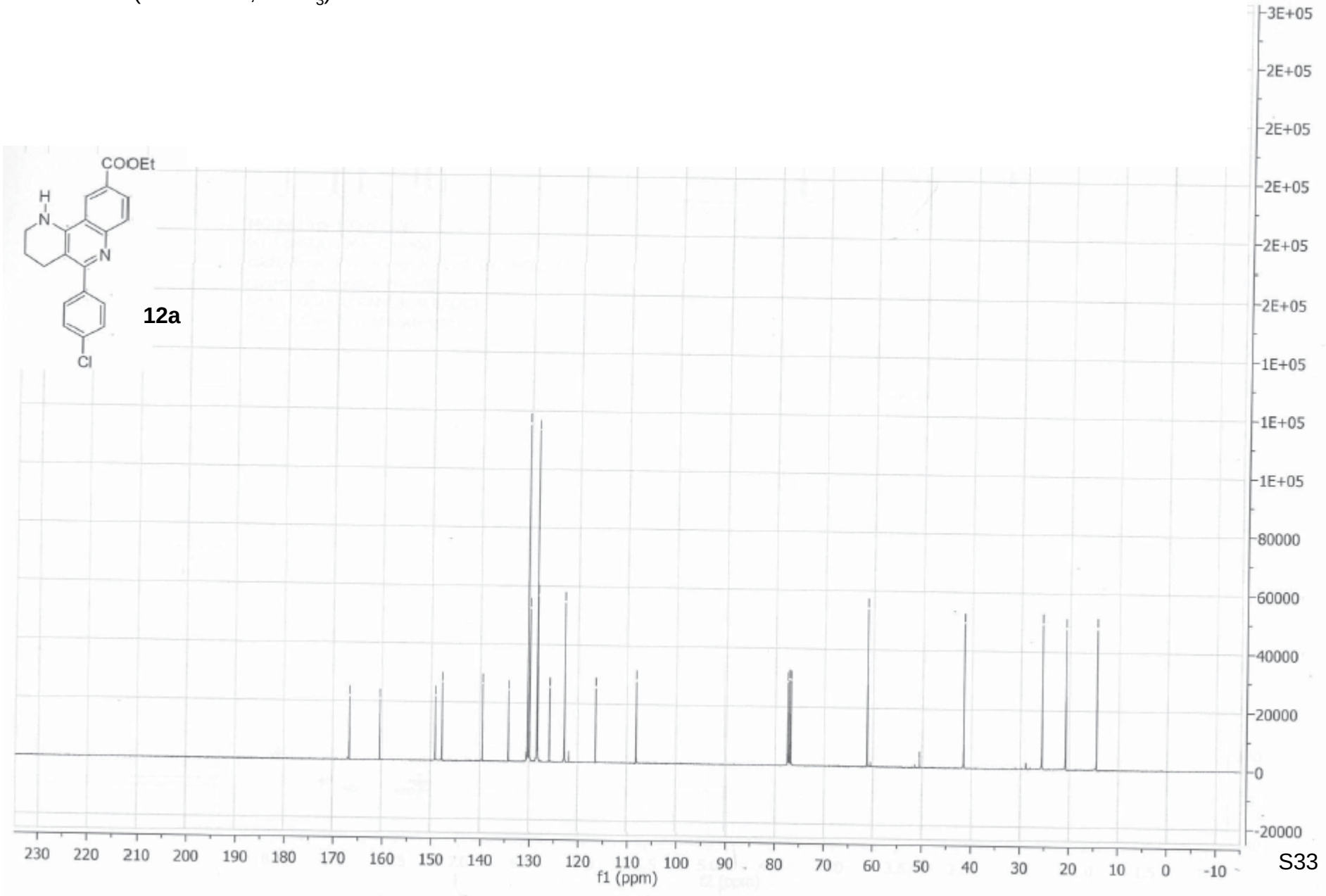

Ethyl 5-(3-pyridyl)-1,2,3,4-tetrahydrobenzo[*h*][1,6]naphthyridine-9-carboxylate (**12b**)
^{1}H NMR (400 MHz, CD_3OD)

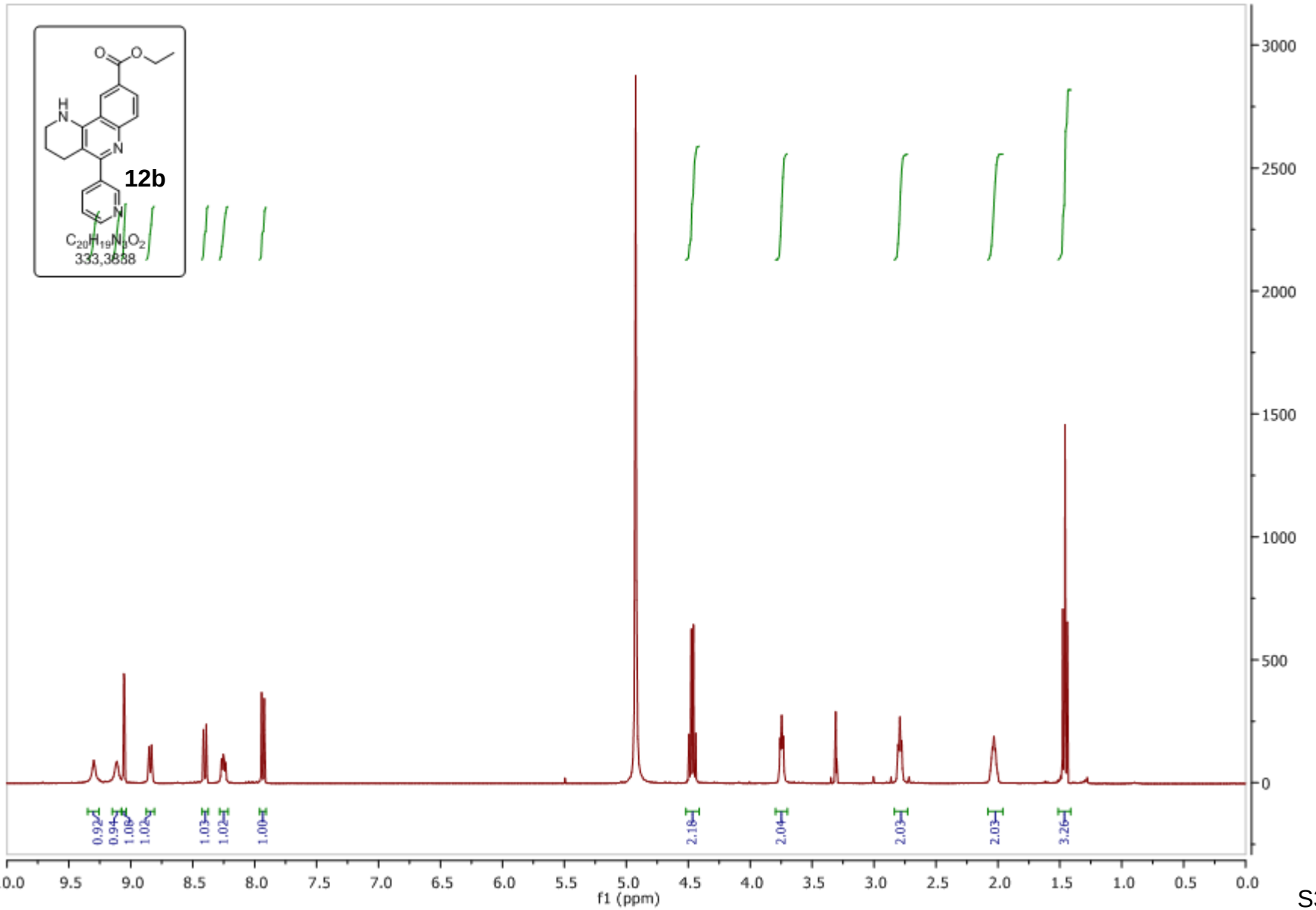

Ethyl 5-(3-pyridyl)-1,2,3,4-tetrahydrobenzo[*h*][1,6]naphthyridine-9-carboxylate (**12b**)
^{13}C NMR (100.6 MHz, CD_3OD)

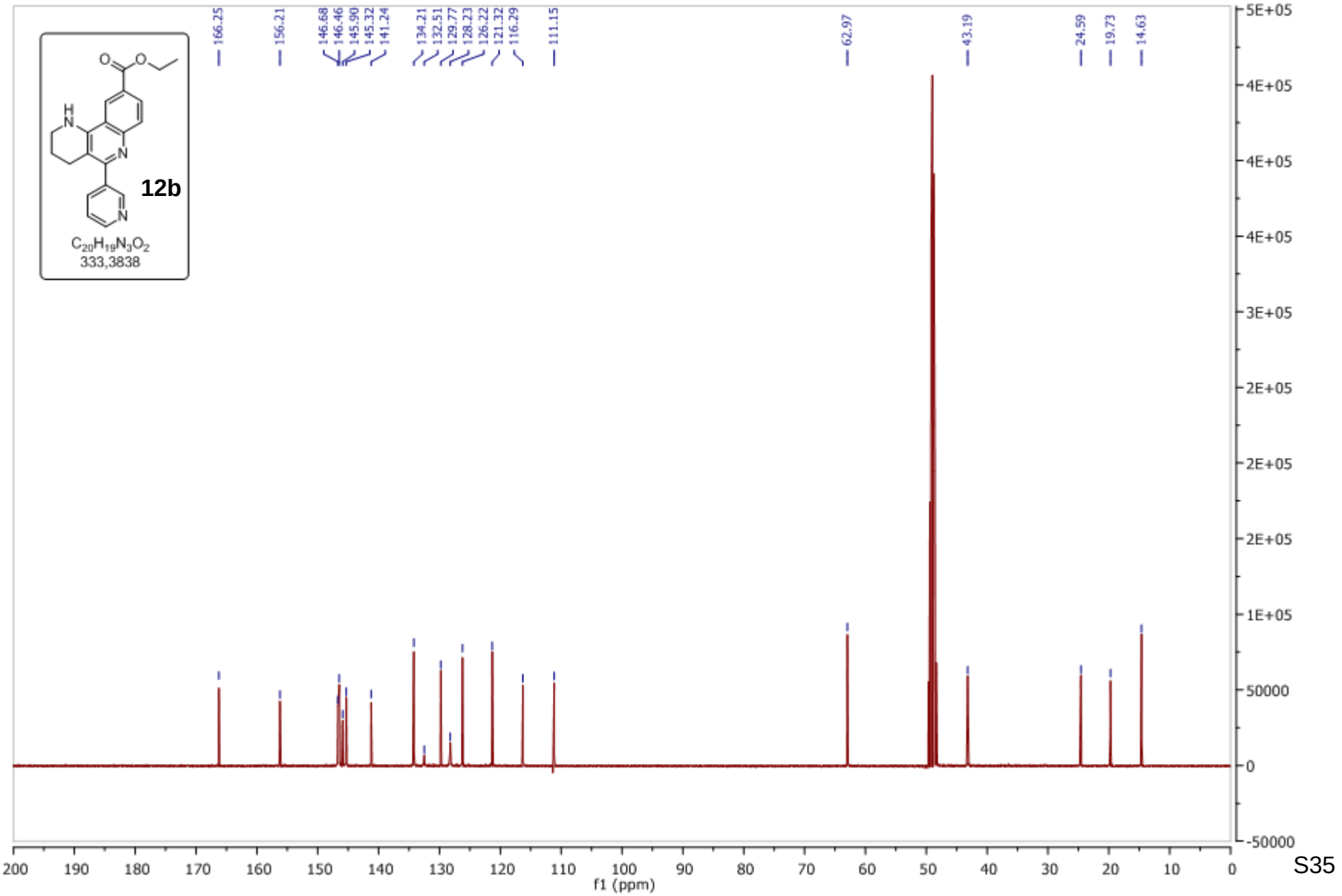

Ethyl 5-(4-chlorophenyl)-1,2,3,4-tetrahydro-1-(4-methoxybenzyl)benzo[*h*][1,6]naphthyridine-9-carboxylate (**13a**)
^{1}H NMR (400 MHz, $CDCl_3$)

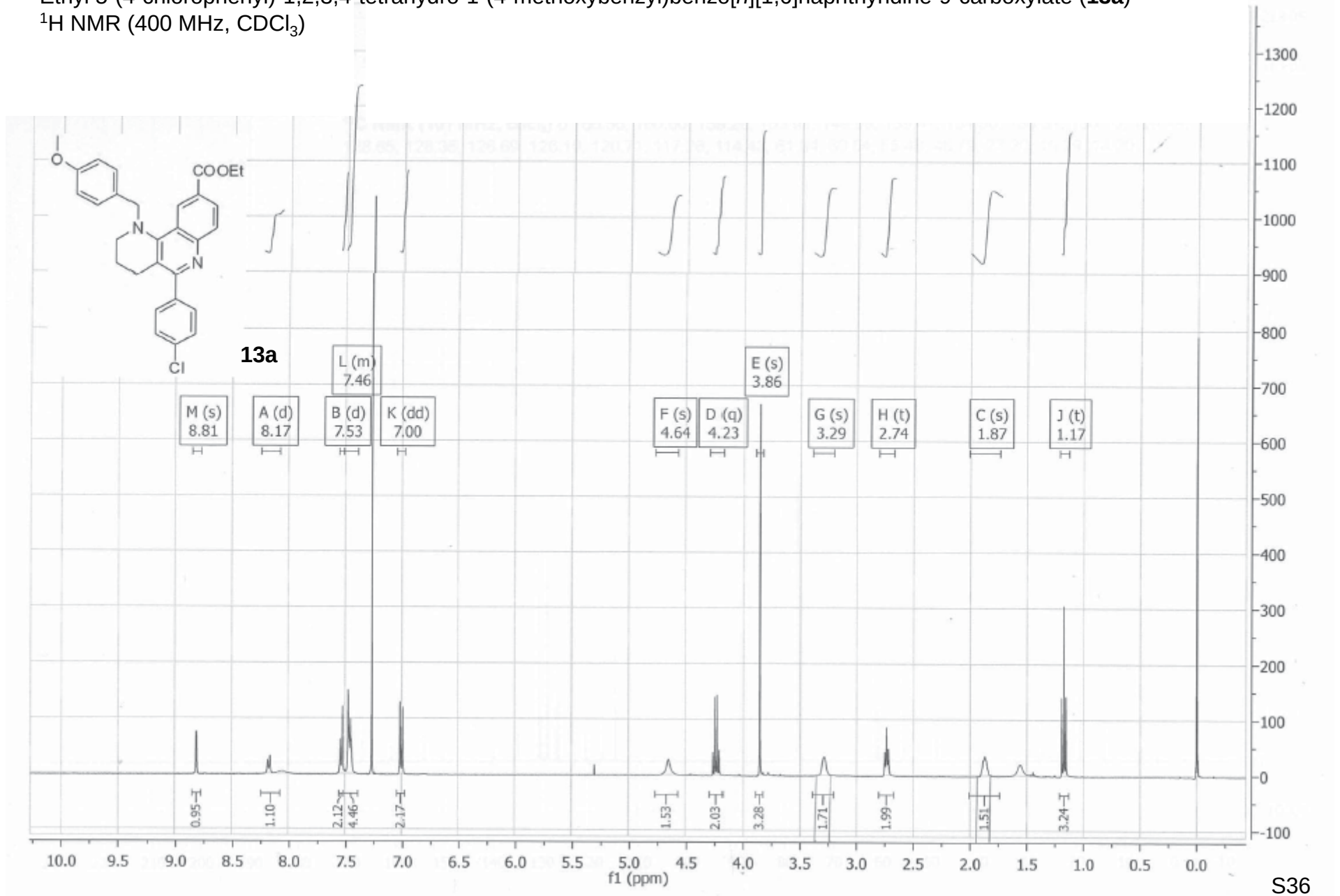

Ethyl 5-(4-chlorophenyl)-1,2,3,4-tetrahydro-1-(4-methoxybenzyl)benzo[*h*][1,6]naphthyridine-9-carboxylate (**13a**)
^{13}C NMR (100.6 MHz, $CDCl_3$)

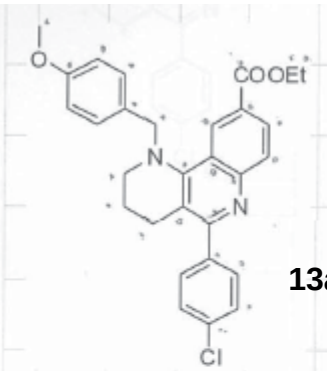

13a

1-Benzyl-5-(4-chlorophenyl)-*N*-ethyl-1,2,3,4-tetrahydrobenzo[*h*][1,6]naphthyridine-9-carboxamide (**14a**)
^{1}H NMR (400 MHz, CD_3OD)

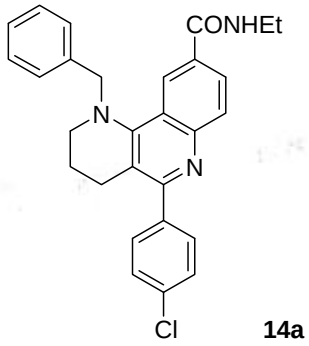

14a

1-Benzyl-5-(4-chlorophenyl)-*N*-ethyl-1,2,3,4-tetrahydrobenzo[*h*][1,6]naphthyridine-9-carboxamide (**14a**)
^{13}C NMR (100.6 MHz, CD_3OD)

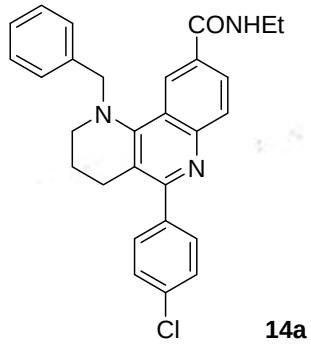

14a

5-(4-chlorophenyl)-*N*-ethyl-1,2,3,4-tetrahydrobenzo[*h*][1,6]naphthyridine-9-carboxamide (**16a**)
^{1}H NMR (400 MHz, CD_3OD)

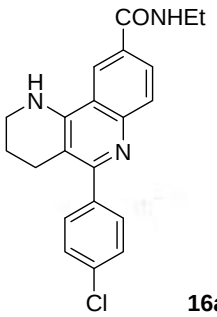

16a

5-(4-chlorophenyl)-*N*-ethyl-1,2,3,4-tetrahydrobenzo[*h*][1,6]naphthyridine-9-carboxamide (**16a**)
^{13}C NMR (100.6 MHz, CD_3OD)

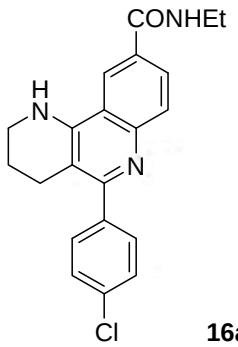

16a

N-{{1-benzyl-5-(4-chlorophenyl)-1,2,3,4-tetrahydrobenzo[*h*][1,6]naphthyridin-9-yl}methyl}ethanamine (**17a**)
^{1}H NMR (400 MHz, CD_3OD)

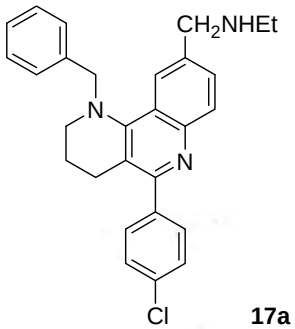

17a

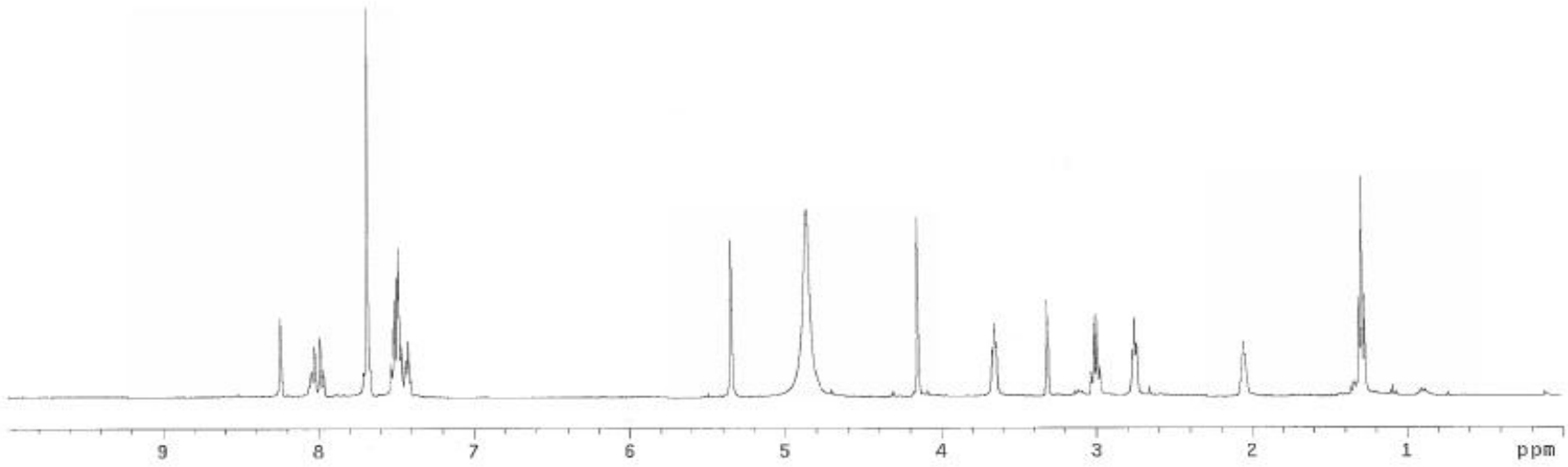

N-{{1-benzyl-5-(4-chlorophenyl)-1,2,3,4-tetrahydrobenzo[*h*][1,6]naphthyridin-9-yl}methyl}ethanamine (**17a**)
^{13}C NMR (100.6 MHz, CD_3OD)

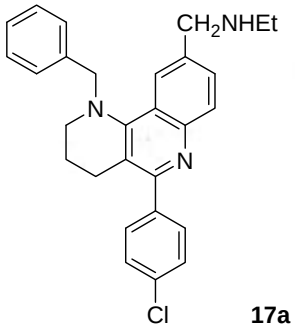

17a

N-{{5-(4-chlorophenyl)-1,2,3,4-tetrahydrobenzo[*h*][1,6]naphthyridin-9-yl}methyl}ethanamine (**18a**)
^{1}H NMR (400 MHz, CD_3OD)

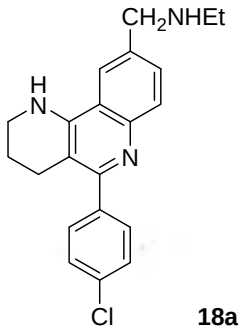

18a

N-{{5-(4-chlorophenyl)-1,2,3,4-tetrahydrobenzo[*h*][1,6]naphthyridin-9-yl}methyl}ethanamine (**18a**)
^{13}C NMR (100.6 MHz, CD_3OD)

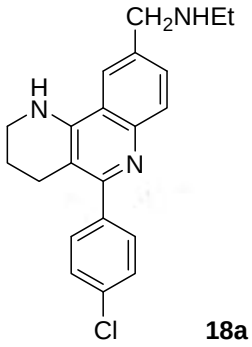

18a

N-{{1,2,3,4-tetrahydro- 5-(3-pyridyl)benzo[*h*][1,6]naphthyridin-9-yl}methyl}ethanamine (**18b**)
^{1}H NMR (400 MHz, CD_3OD)

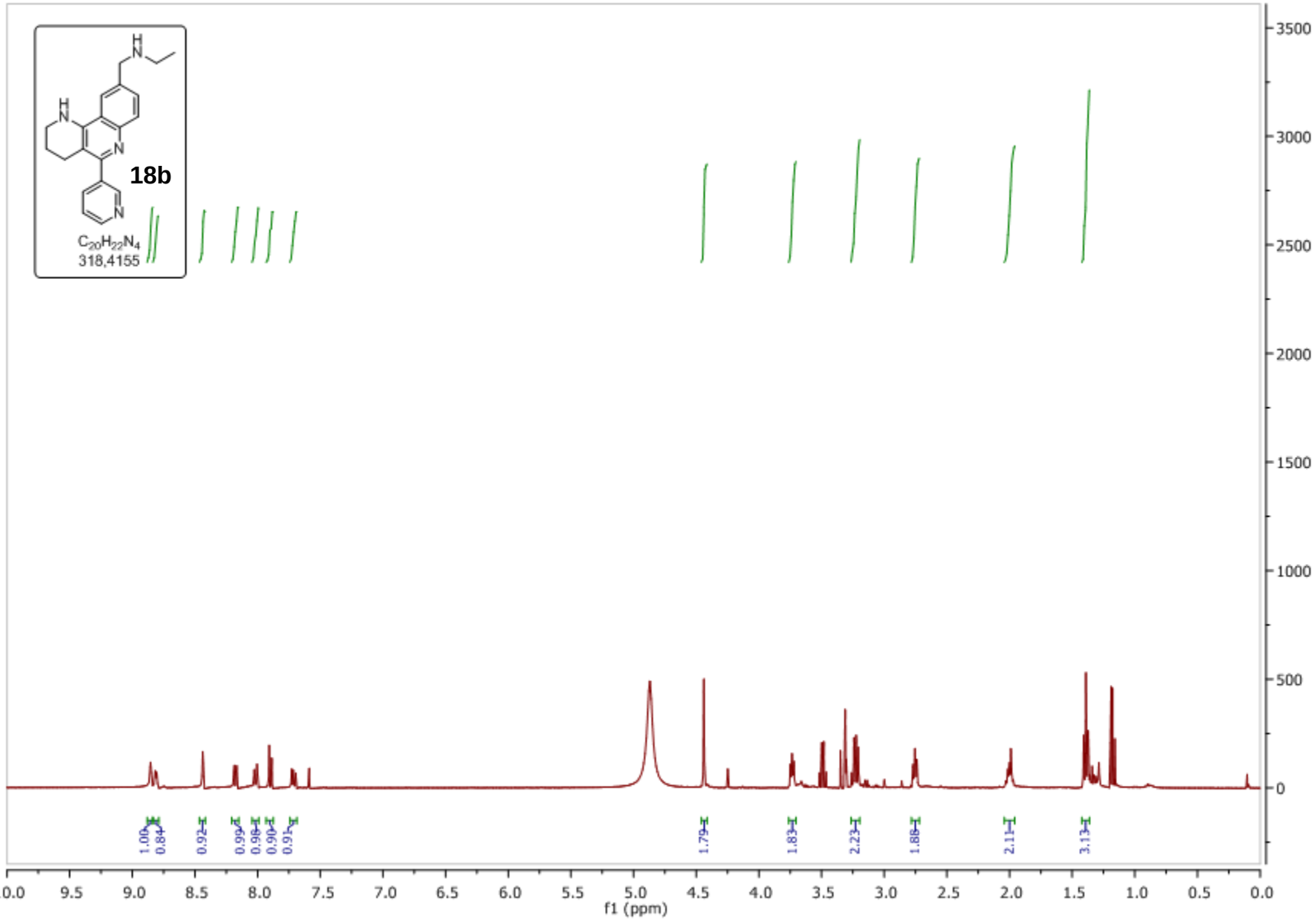

N-{{1,2,3,4-tetrahydro- 5-(3-pyridyl)benzo[*h*][1,6]naphthyridin-9-yl}methyl}ethanamine (**18b**)
^{13}C NMR (100.6 MHz, CD_3OD)

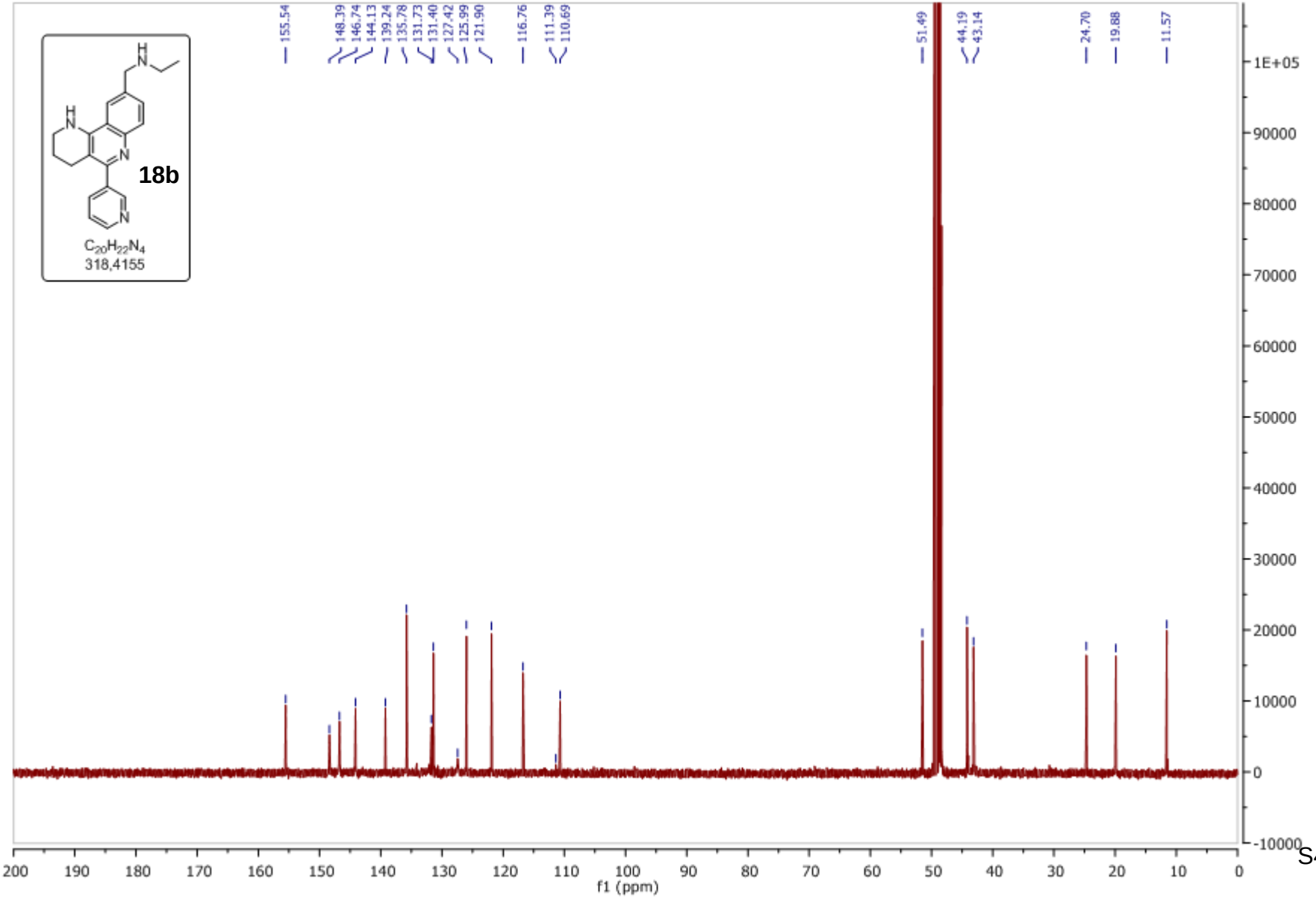

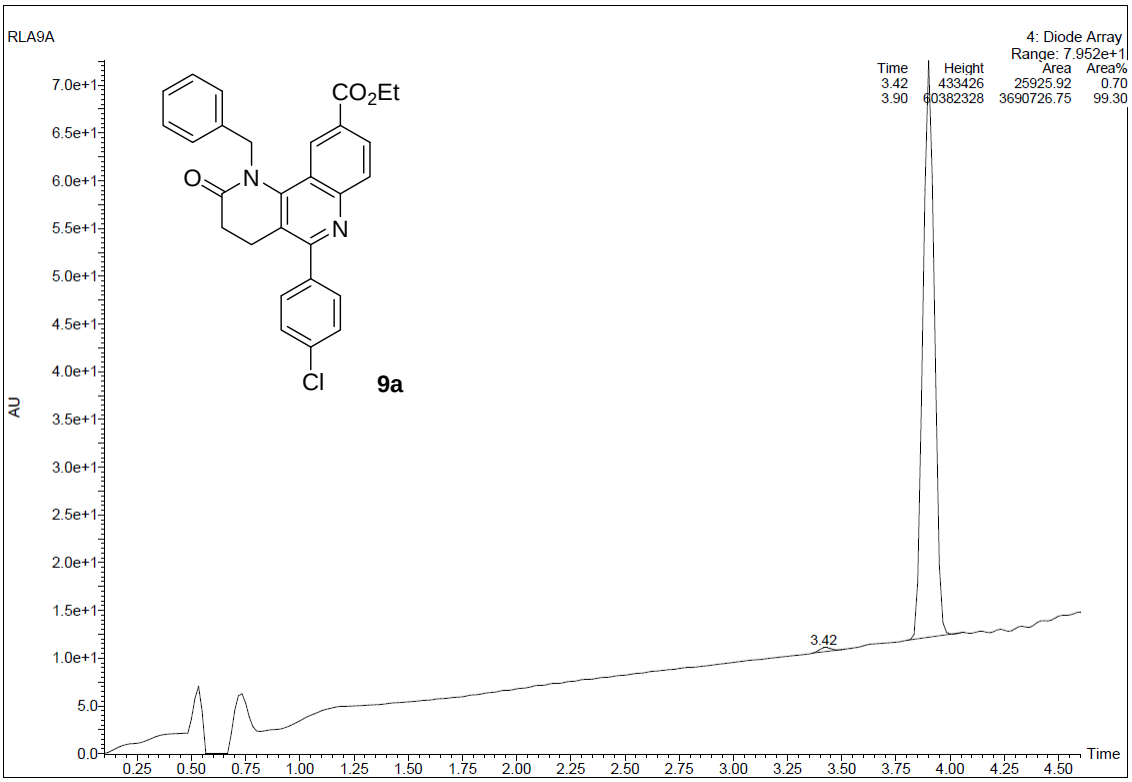
RLA9A
4: Diode Array
Range: 7.952e+1
Time Height Area Area%
3.42 433426 25925.92 0.70
3.90 60382328 3690726.75 99.30
CO2Et
O
N
N
Cl
9a
AU
3.42
Time

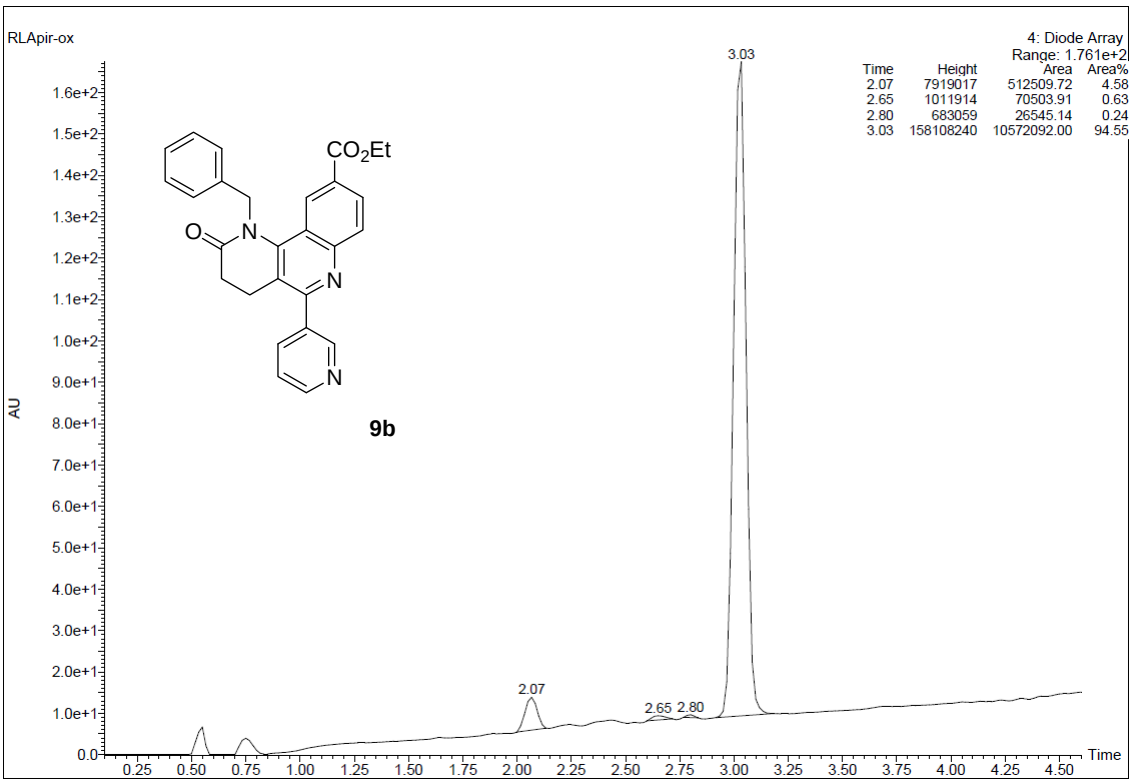
RLApir-ox
4: Diode Array
Range: 1.761e+2
Time Height Area Area%
2.07 7919017 512509.72 4.58
2.65 1011914 70503.91 0.63
2.80 683059 26545.14 0.24
3.03 158108240 10572092.00 94.55
CO2Et
O
N
N
N
9b
AU
3.03
2.07
2.65 2.80
Time

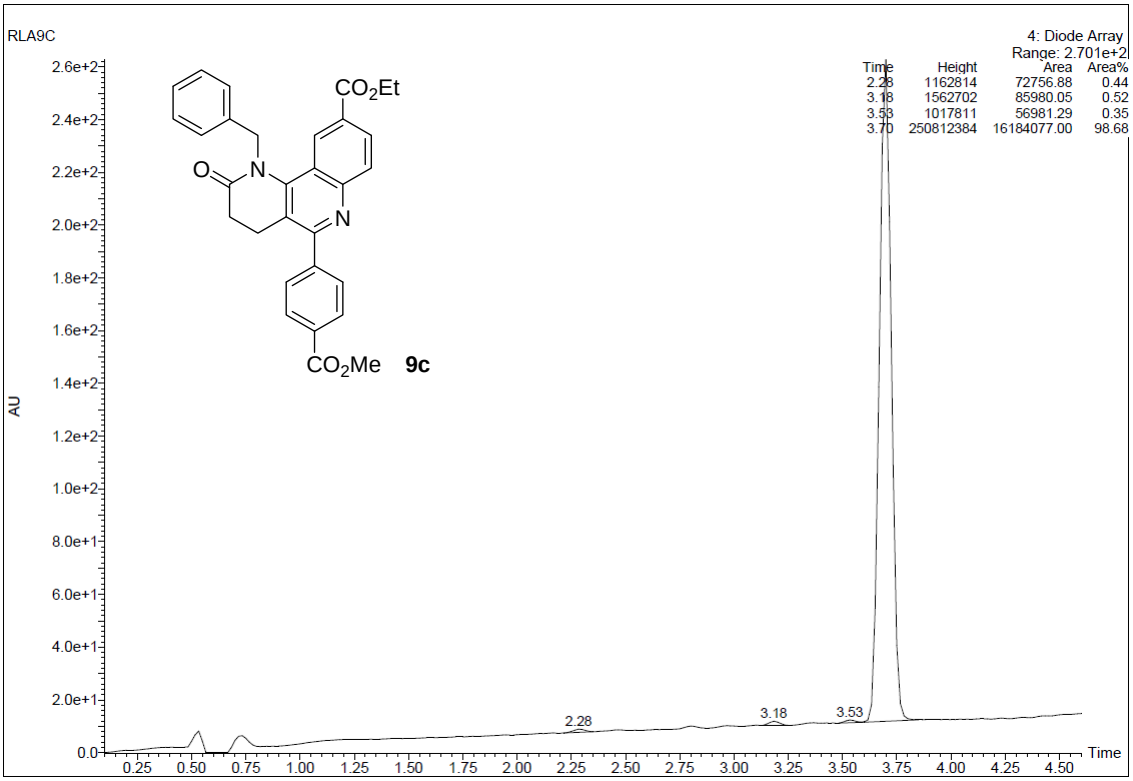
RLA9C
4: Diode Array
Range: 2.701e+2
Time Height Area Area%
2.28 1162814 72756.88 0.44
3.18 1562702 85980.05 0.52
3.53 1017811 56981.29 0.35
3.70 250812384 16184077.00 98.68
CO2Et
O
N
N
CO2Me
9c
AU
Time
2.28
3.18
3.53

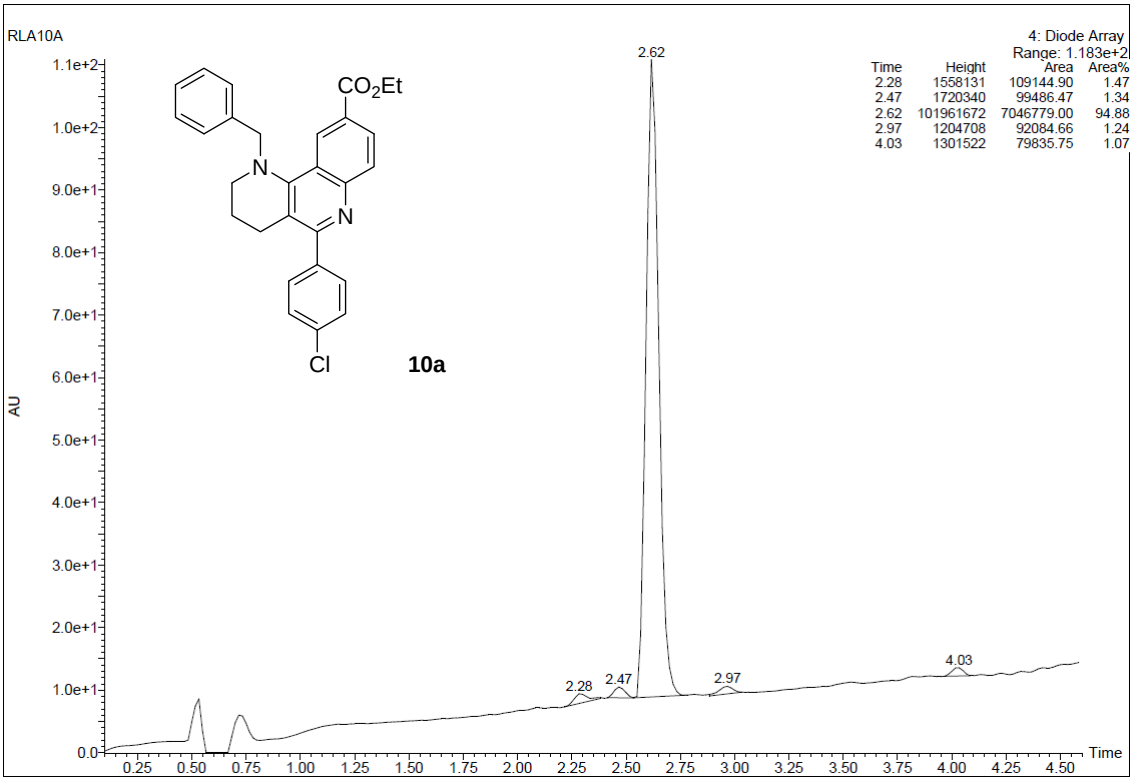
RLA10A
4: Diode Array
Range: 1.183e+2
Time Height Area Area%
2.28 1558131 109144.90 1.47
2.47 1720340 99486.47 1.34
2.62 101961672 7046779.00 94.88
2.97 1204708 92084.66 1.24
4.03 1301522 79835.75 1.07
CO2Et
N
N
Cl
10a
AU
Time
2.62
2.28
2.47
2.97
4.03

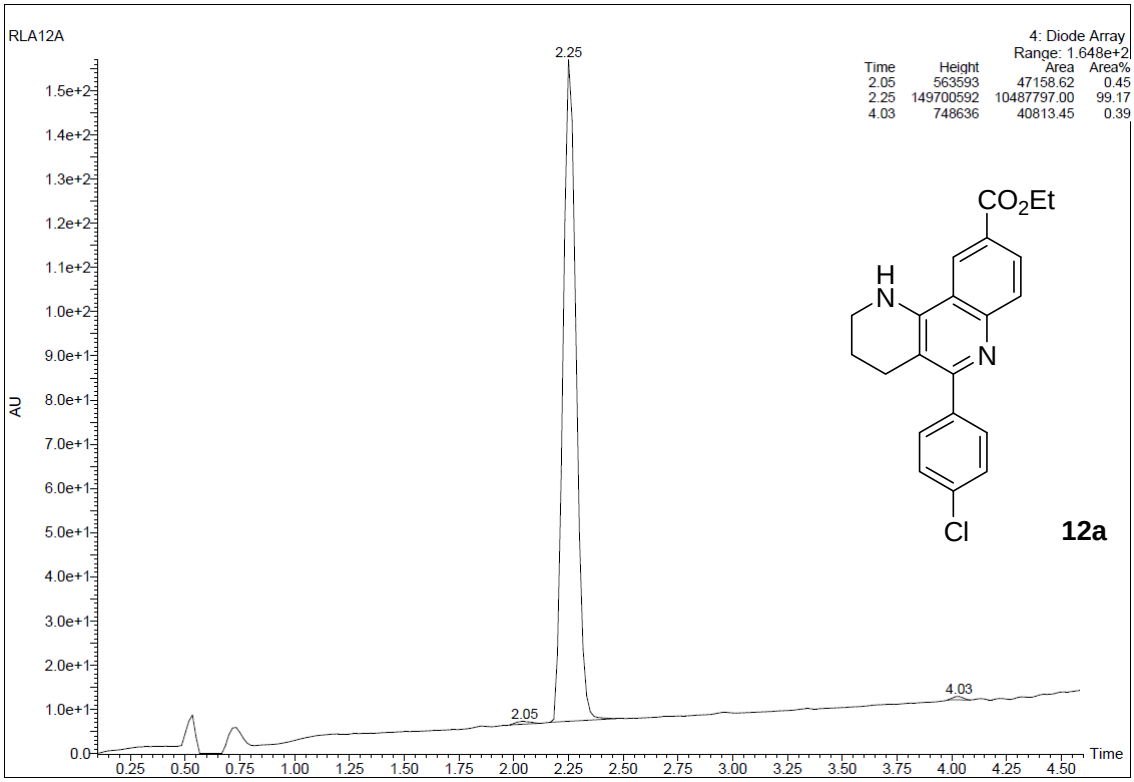
RLA12A
4: Diode Array
Range: 1.648e+2
Time Height Area Area%
2.05 563593 47158.62 0.45
2.25 149700592 10487797.00 99.17
4.03 748636 40813.45 0.39
2.25
2.05
4.03
AU
Time
CO2Et
H
N
N
Cl
12a

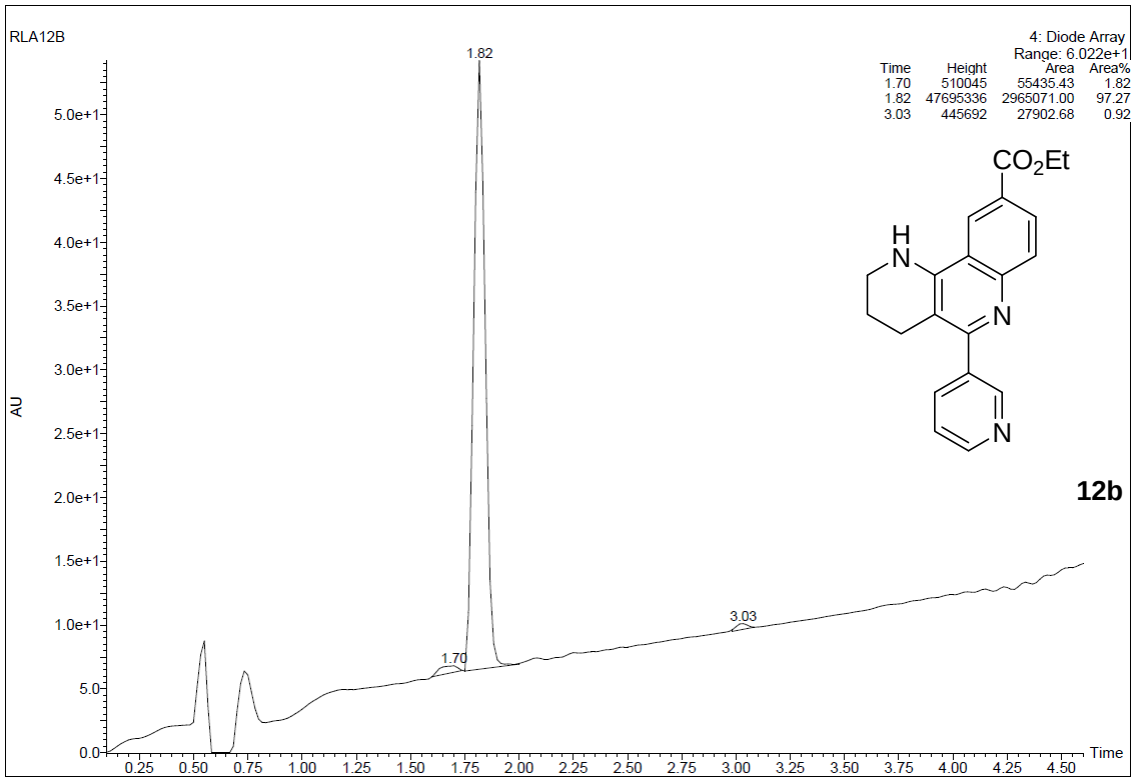
RLA12B
4: Diode Array
Range: 6.022e+1
Time Height Area Area%
1.70 510045 55435.43 1.82
1.82 47695336 2965071.00 97.27
3.03 445692 27902.68 0.92
1.82
1.70
3.03
AU
Time
CO2Et
H
N
N
N
12b

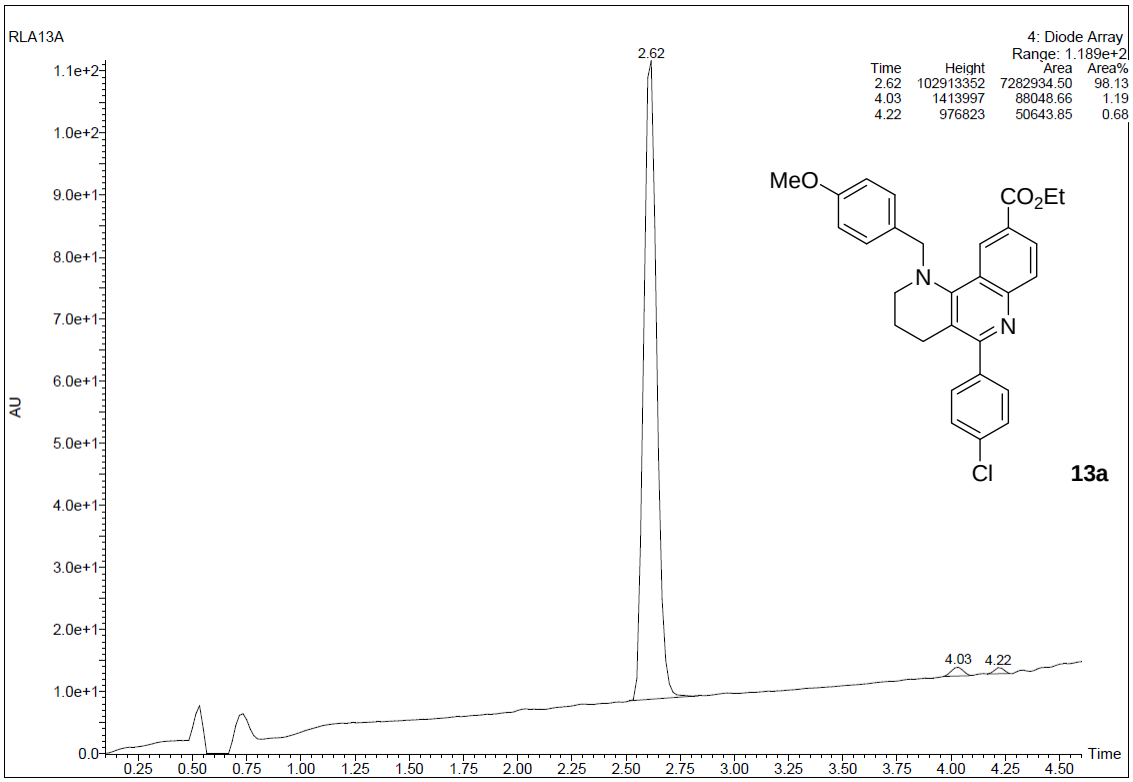
RLA13A
4: Diode Array
Range: 1.189e+2
Time Height Area Area%
2.62 102913352 7282934.50 98.13
4.03 1413997 88048.66 1.19
4.22 976823 50643.85 0.68
2.62
4.03
4.22
AU
Time
MeO
CO2Et
N
N
Cl
13a

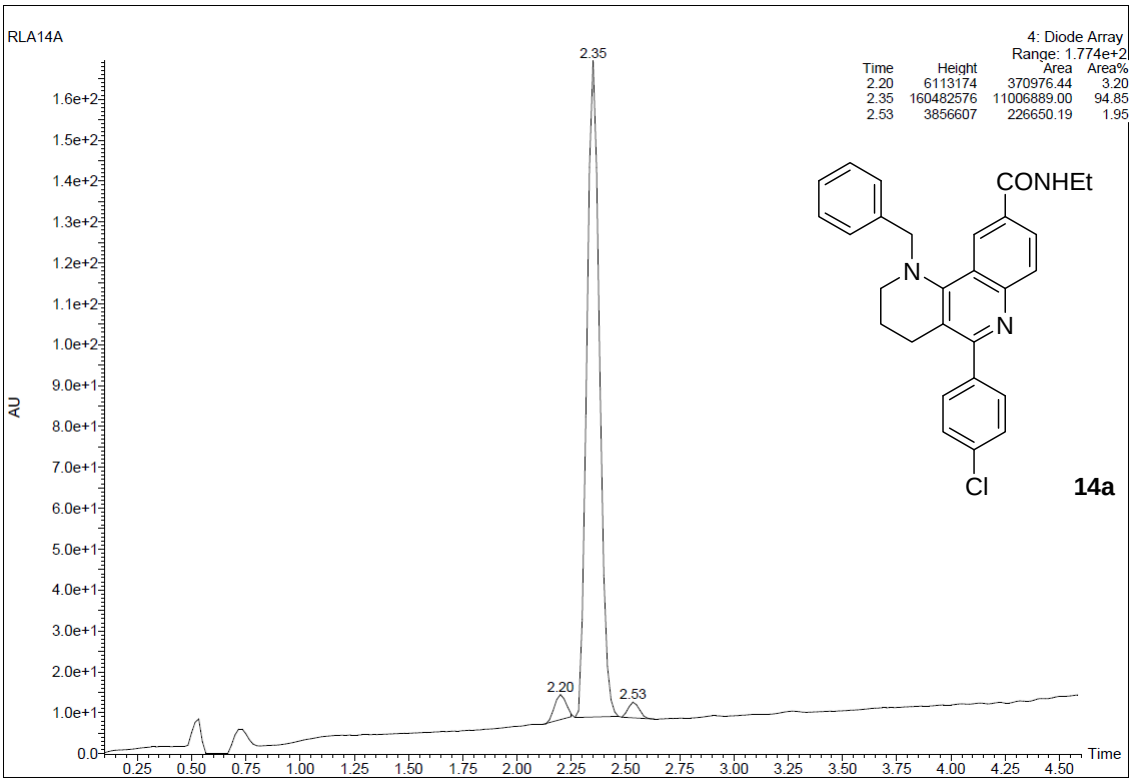
RLA14A
4: Diode Array
Range: 1.774e+2
Time Height Area Area%
2.20 6113174 370976.44 3.20
2.35 160482576 11006889.00 94.85
2.53 3856607 226650.19 1.95
2.35
2.20
2.53
AU
Time
CONHEt
N
N
Cl
14a

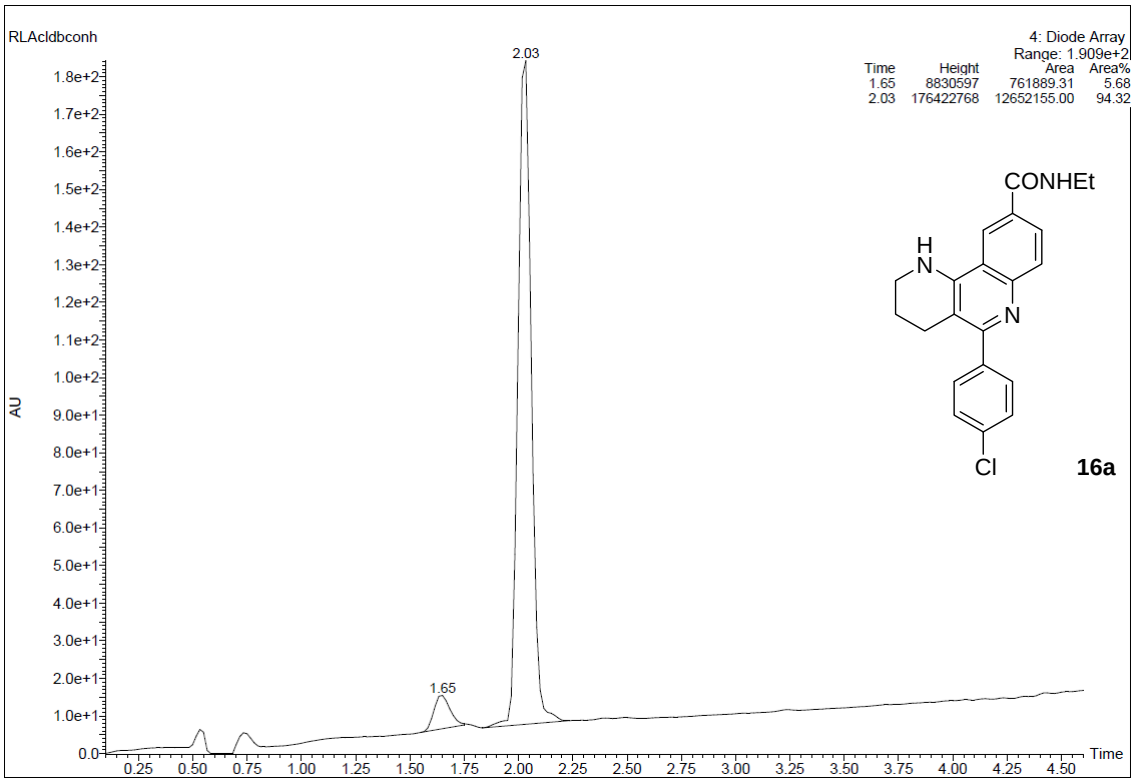
RLAcldbconh
4: Diode Array
Range: 1.909e+2
Time Height Area Area%
1.65 8830597 761889.31 5.68
2.03 176422768 12652155.00 94.32
2.03
1.65
AU
Time
CONHEt
H
N
N
Cl
16a

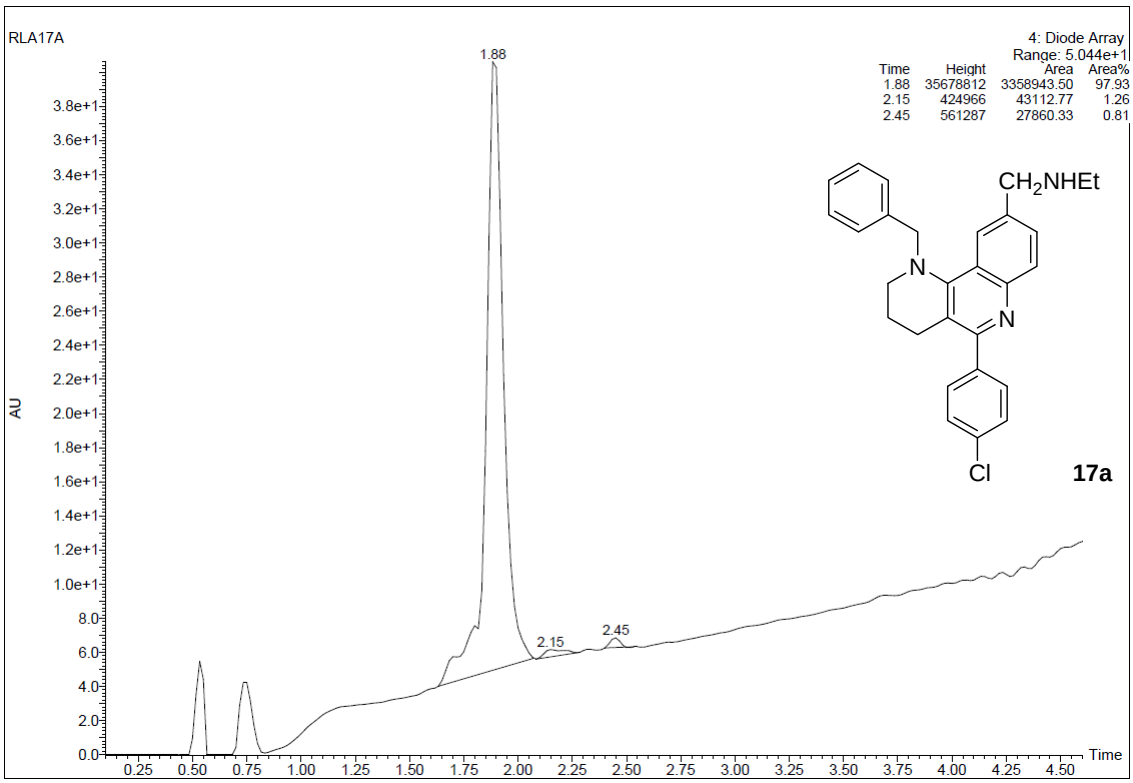
RLA17A
4: Diode Array
Range: 5.044e+1
Time Height Area Area%
1.88 35678812 3358943.50 97.93
2.15 424966 43112.77 1.26
2.45 561287 27860.33 0.81
1.88
2.15
2.45
AU
Time
CH2NHEt
N
N
Cl
17a

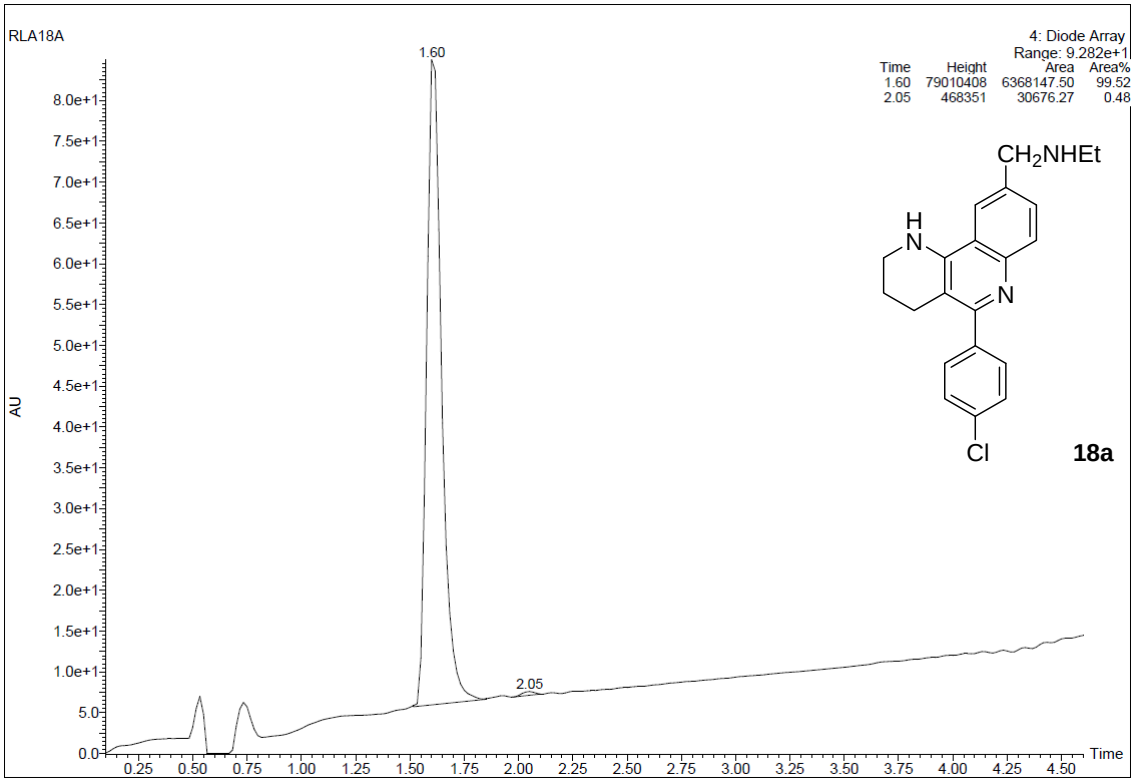
RLA18A
4: Diode Array
Range: 9.282e+1
Time Height Area Area%
1.60 79010408 6368147.50 99.52
2.05 468351 30676.27 0.48
1.60
2.05
AU
Time
CH2NHEt
H
N
N
Cl
18a

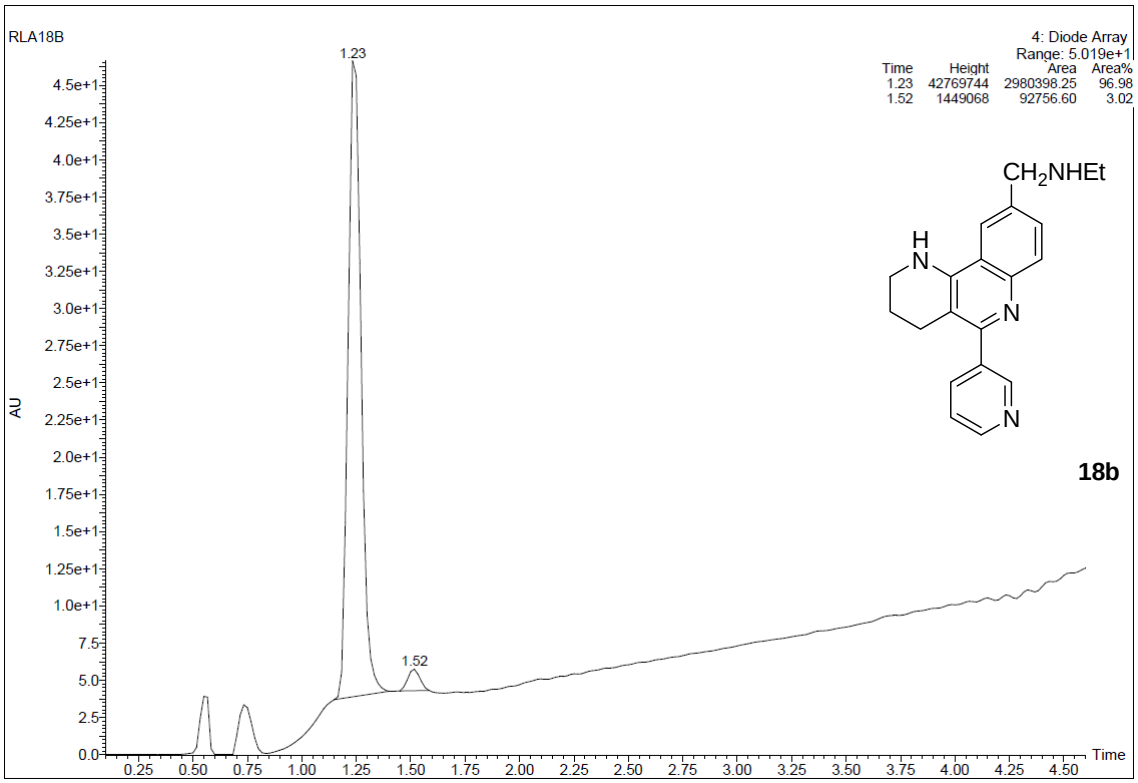
RLA18B
4: Diode Array
Range: 5.019e+1
Time Height Area Area%
1.23 42769744 2980398.25 96.98
1.52 1449068 92756.60 3.02
1.23
1.52
AU
Time
CH2NHEt
H
N
N
N
18b

5 Dual binding site AChE inhibitors

Chapter

(*Eur. J. Med. Chem.* **2014**, *84*, 107)

5.1 Design of a novel family of tetrahydrobenzo[h][1,6]naphthyridine–6-chlorotacrine hybrids as dual binding site AChEIs

In the frame of the MTDLs strategy,[85, 87,88,89,192,193] the design of dual binding site AChEIs provides an efficient alternative for simultaneously achieving, with a single chemical entity, multiple biological effects just targeting one single biological target.[60,61]

The experience of our research group in the design and synthesis of various families of dual binding site AChEIs,[2] and the recent *hit-to-lead* optimization successfully leading to the nanomolar PAS binding ligand **68** (*Chapter 4*) prompted us to combine the molecular hybridization with the MD-driven linker's optimization strategy for the structure-based design of a novel tetrahydrobenzo[*h*][1,6]naphthyridine–6-chlorotacrine hybrid, as potential anti-Alzheimer agent.

With this scope in mind, the binding mode predicted for **68** by the previous computational studies allowed us, after superimposition with the X-ray structure of the *Torpedo californica* AChE-tacrine complex (**Figure 5.1**), to rationally design the trimethylene-linked hybrid **81a** as a multisite AChE inhibitor.

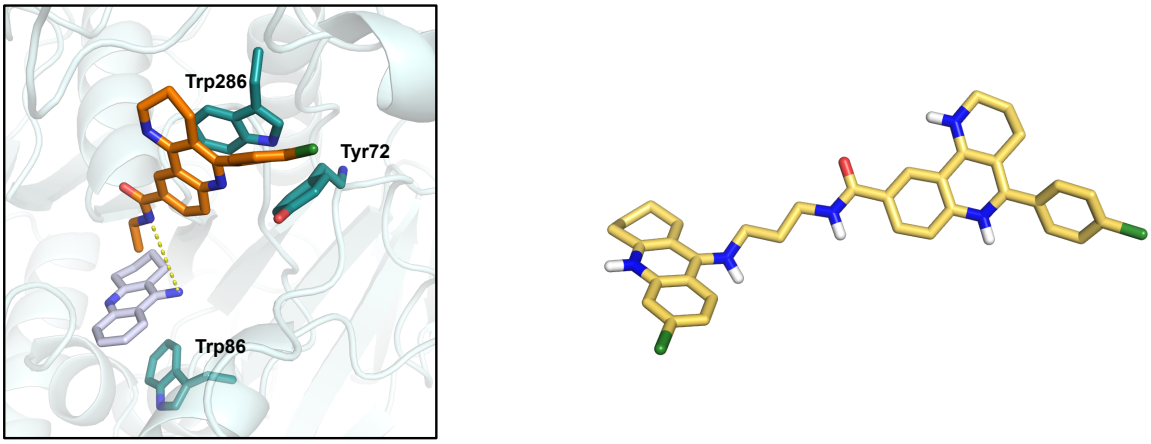

Figure 5.1 Superimposition of the MD-predicted binding mode of **68** in AChE with the X-ray structure of the complex *Torpedo californica* AChE-tacrine (PDB ID: 1ACJ) (left). Structure of the three methylene-linked hybrid **81a** (right).

[85]Hopkins, A.L. *Nat. Chem. Biol.* **2008**, *4*, 682.
[87]Janga, S.C.; Tzakos, A. *Mol. BioSyst.* **2009**, *5*, 1536.
[88]Bianchi, M.T. *Medical Hypoheses* **2010**, *74*, 297.
[89]Viayna, E.; Sola, I.; Di Pietro, O.; Muñoz-Torrero, D. *Curr. Med. Chem.* **2013**, *20*, 1621.
[192]Bolognesi, M.L. *Curr. Med. Chem.* **2013**, *20*, 1639.
[193]Pau, A.; Catto, M.; Pinna, G.; Frau, S.; Murineddu, G.; Asproni, B.; Curzu, M.M.; Pisani, L.; Leonetti, F.; Loza, M.I.; Brea, J.; Pinna, G.A.; Carotti, A. ChemMedChem **2015**, *10*, 1054.
[60]Pang, Y.-P.; Quiram, P.; Jelacic, T.; Hong, F.; Brimijoin, S. *J. Biol. Chem.* **1996**, *271*, 23646.
[61]Carlier, P.R.; Han, Y.F.; Chow, E.S.-H.; Li, C.P.-L-; Wang, H.; Lieu, T.X.; Wong, H.S.; Pang, Y.-P. *Bioorg. Med. Chem.* **1999**, *7*, 351.
[2]Muñoz-Torrero, D. *Curr. Med. Chem.* **2008**, *15*, 2433.

Additionally, also the longer tetra-, penta- and octa-methylene-linked homologues **81b**-**d** were synthesized and their *h*AChE, *h*BChE inhibitory activities, and $A\beta_{42}$ and tau protein antiaggregating activity evaluated.

The pharmacological results revealed that the rational design led to the development of a picomolar *h*AChE inhibitor, **81a**, one of the most potent non-covalent AChEIs so far reported in literature (IC_{50} 0.006 nM). Additionally, it had high and moderate potency against *h*BChE (IC_{50} 120 nM), and $A\beta_{42}$ (52.5% inhibition at 10 μM) and tau protein aggregation (40.7% inhibition at 10 μM), respectively.

Indeed, the optimization of the essentially inactive 3,4-dihydro-2*H*-pyrano[3,2-*c*]quinoline, **45**, through a double O → NH bioisosteric replacement (*Chapter 4*), together with the combined application of the molecular hybridization and MD-driven tether's optimization, successfully resulted in the novel hybrid compound **81a**, displaying roughly 1000-fold and more than 10000-fold enhanced potency compared to its fragment precursors 6-chlorotacrine (*h*AChE IC_{50} 5.9 nM) and benzonaphthyridine **68** (*h*AChE IC_{50} 65 nM), respectively, and also being more than 3200-fold more potent than hybrid **83** (*h*AChE IC_{50} 19.3 nM, **Scheme 5.5**), previously synthesized in our research group in the PhD thesis of Dr. Carles Galdeano.[184,67]

5.2 Synthesis of the novel tetrahydrobenzo[h][1,6]naphthyridine–6-chlorotacrine hybrids 81a-d and the pyrano[3,2-c]quinoline–6-chlorotacrine hybrid 83

For the synthesis of hybrid compounds **81a**-**d** and **83**, according to the retrosynthetic analysis proposed below (**Scheme 5.1**), it was envisaged an amidation coupling reaction between esters **45** or **68**, obtained through *Povarov* MCR,[174] and the ω-aminoalkyl–6-chlorotacrines **79a**-**d**, easily available through aromatic nucleophilic substitution of the known 6,9-dichloroacridine **77** with appropriate commercially available α,ω-diaminoalkanes.

[184]Galdeano, C. PhD thesis. *Unitat de Química Farmacèutica, Departament de Farmacologia i Química Terapèutica, Universitat de Barcelona*, **2012**.
[67]Camps, P.; Formosa, X.; Galdeano, C.; Muñoz-Torrero, D.; Ramírez, L.; Gómez, E.; Isambert, N.; Lavilla, R.; Badia, A.; Clos, M.V.; Bartolini, M.; Mancini, F.; Andrisano, V.; Arce, M.P.; Rodríguez-Franco, M.I.; Huertas, O.; Dafni, T.; Luque, F.J. *J. Med. Chem.* **2009**, *52*, 5365.
[174]Povarov, L.S. *Russ. Chem. Rev.* **1967**, *36*, 656.

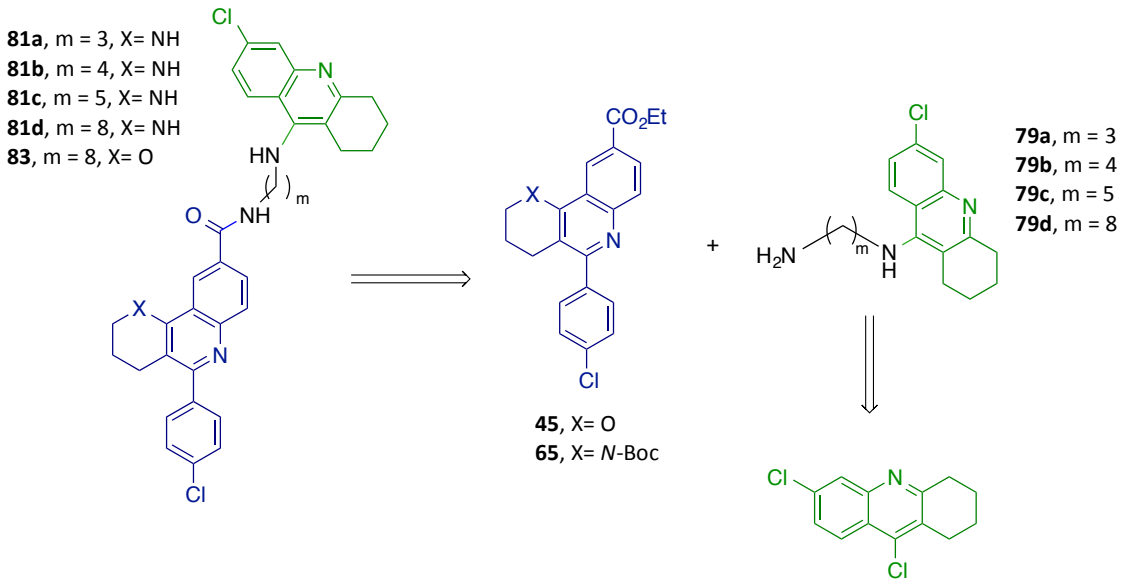

Scheme 5.1

5.2.1 Synthesis of the ω-aminoalkyl–6-chlorotacrines 79a-d

Following a synthetic strategy previously used in our research group, the preparation of the aminoalkyl–6-chlorotacrines **79a**-**d** was envisioned starting from the dichloroacridine intermediate **77**. This intermediate was obtained in 81% yield, with no necessity of column chromatography purification, through a described procedure that involved the reaction between 4-chloroanthranilic acid, **76**, and cyclohexanone, **75**, in the presence of an excess of $POCl_3$, stirring for 2 h under reflux (**Scheme 5.2**).

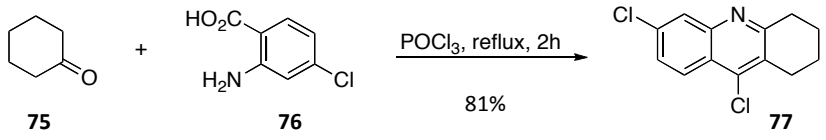

Scheme 5.2

Next, according to a synthetic procedure already employed by Carlier and Pang for the preparation of different tacrine-based AChEIs,[61,194] **77** was treated with an excess of the diamines **78a**-**d**, and stirred overnight at the reflux temperature of 1-pentanol (136-138 °C).

[61]Carlier, P.R.; Han, Y.F.; Chow, E.S.-H.; Li, C.P.-L-; Wang, H.; Lieu, T.X.; Wong, H.S.; Pang, Y.-P. *Bioorg. Med. Chem.* **1999**, *7*, 351.
[194]Carlier, P.R.; Chow, E.S.-H.; Han, Y.; Liu, J.; El Yazal, J.; Pang, Y.-P. *J. Med. Chem.* **1999**, *42*, 4225.

The following acid-base treatment of the reaction mixtures and subsequent silica gel column chromatography purification of the corresponding crudes provided the desired aminoalkyl-6-chlorotacrines **79a**-**d** in moderate to good yields (36-82%, **Scheme 5.3**). It is worth noting that the variability in the yield of the aromatic nucleophilic substitution reaction might be ascribed to the formation of secondary products resulting from the dimerization of **77** with the diamines, as already described in previous works carried out within our research group.[184,195,196]

Among the four aminoalkyl–6-chlorotacrines synthesized, only **79a** had not been previously described. Hence, it was subjected to a complete chemical characterization (spectroscopic data and elemental analysis), while the other amine intermediates, which were later converted into the corresponding dihydrochloride salts upon treatment with a HCl/MeOH solution and crystallized from a MeOH/EtOAc mixture, were characterized only by means of their spectroscopic data.

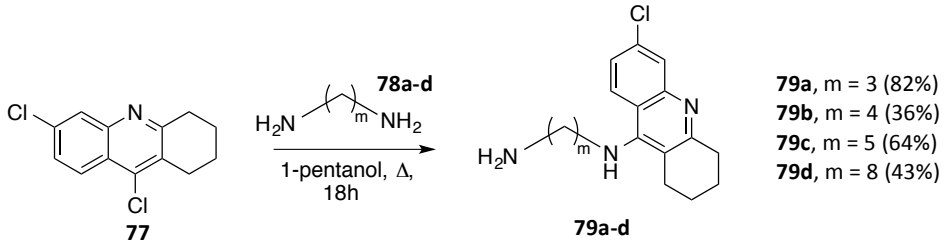

Scheme 5.3

5.2.2 Synthesis of the novel tetrahydrobenzo[h][1,6]naphthyridine–6-chlorotacrine hybrids 81a-d

The amidation coupling reaction preliminary required the preparation of ester **65** according to the synthetic strategy already described in *Chapter 4*, and the subsequent basic hydrolysis to the corresponding carboxylate, to be then converted into its acid form upon treatment with a HCl/Et_2O solution.

[184]Galdeano, C. PhD thesis. *Unitat de Química Farmacèutica, Departament de Farmacologia i Química Terapèutica, Universitat de Barcelona*, **2012**.
[195]Galdeano, C. Experimental Master. *Unitat de Química Farmacèutica, Departament de Farmacologia i Química Terapèutica, Universitat de Barcelona*, **2006**.
[196]Ramírez, L. Experimental Master. *Unitat de Química Farmacèutica, Departament de Farmacologia i Química Terapèutica, Universitat de Barcelona*, **2008**.

In this work, in contrast to the synthetic strategy described in *Chapter 4*, for the preparation of the amide derivatives **81a**-**d** from the carboxylic acid precursor, **66**·HCl, an alternative method, broadly employed in peptide synthesis, was preferred to the more tedious and low yield (15-48%) three-day reaction with $EtCO_2Cl$ and freshly distilled Et_3N as the base. The alternative amidation reaction involved the use of Et_3N as the base, 1-ethyl-3-(3-dimethylaminopropyl)carbodiimide (EDC) as the electrophilic agent activating the carboxylic group of **66**·HCl, and 1-hydroxybenzotriazole (HOBt) as the nucleophilic auxiliary activating the ester, stirring overnight at r.t. in a 10:1 AcOEt/DMF mixture.[197, 198] After column chromatography purification of the resulting crudes, the *N*-Boc protected hybrid compounds **80a**-**d** were obtained in moderate to good yields (34-81%), and subsequently subjected to acidic deprotection upon overnight treatment with a 4M HCl/dioxane solution, to finally provide the desired hybrids **81a**-**d** in quantitative yield. It is worth noting that in the case of compounds **81a** and **81c** it was not necessary to resort to the acidic deprotection reaction of the *N*-Boc group, since the final deprotected compounds were directly obtained from the silica gel column chromatography purification of their precursors **80a** and **80c**, respectively (**Scheme 5.4**).

[197]Chan, L.C.; Cox, B.G. *J.Org. Chem.* **2007**, *72*, 8863.
[198]Valeur, E.; Bradley, M. *Chem. Soc. Rev.* **2009**, *38*, 606.

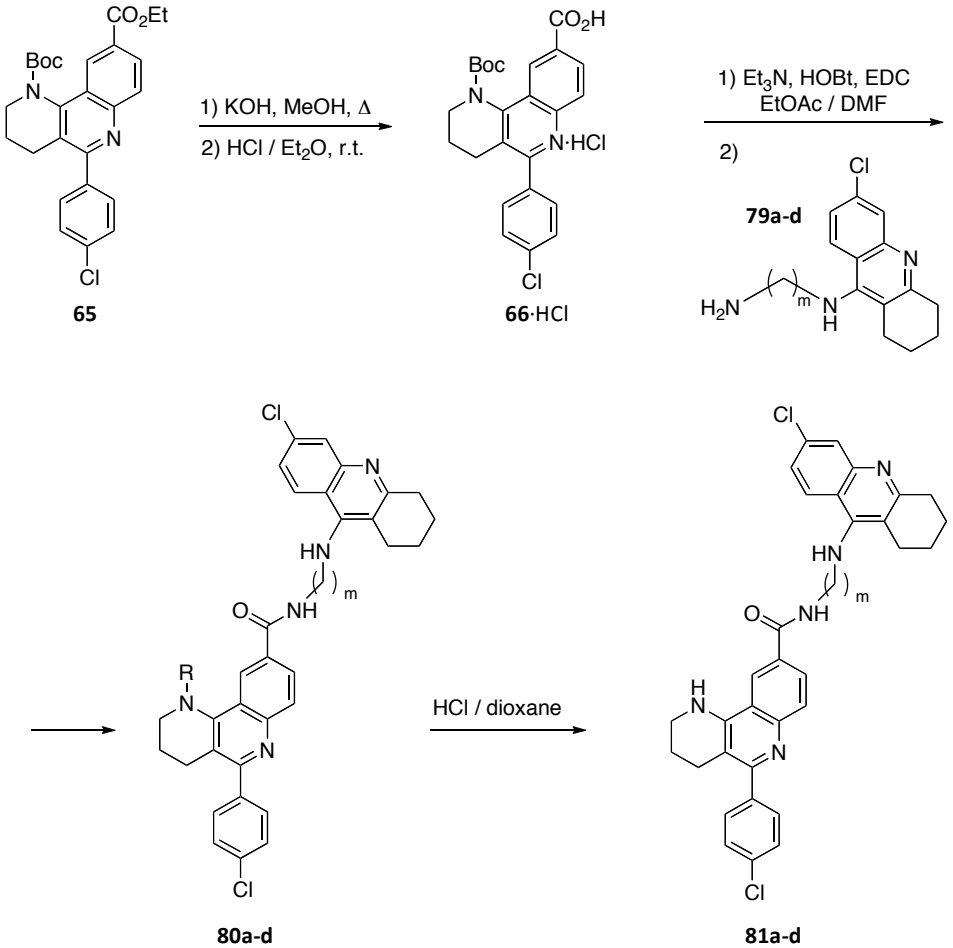

80a, m = 3, R = Boc (42%) + **81a**, m = 3, R = H (39%)
80b, m = 4, R = Boc (69%)
80c, m = 5, R = Boc (0%) + **81c**, m = 5, R = H (34%)
80d, m = 8, R = Boc (63%)

81a, m = 3, R = H (quantitative)
81b, m = 4, R = H (quantitative)
81d, m = 8, R = H (quantitative)

Scheme 5.4

5.2.3 Synthesis of the pyrano[3,2-c]quinoline–6-chlorotacrine 83

Since the pyrano-based hybrids, previously synthesized by Dr. Carles Galdeano during his PhD thesis, had been evaluated against erythrocytic *h*AChE, it was considered necessary to re-synthesize the most potent octamethylene-linked hybrid **83** (erythrocyte *h*AChE IC_{50} 7.03 nM) and to evaluate its inhibitory potency in the same experimental conditions as the novel benzonaphthyridines using recombinant human AChE, in order to facilitate the SAR analysis between the two sets of 6-chlorotacrine-based hybrid compounds.

The use of the same synthetic strategy previously described for hybrids **81a**-**d** afforded the desired compound **83** in 60% overall yield from ester **45** (**Scheme 5.5**), in contrast to the 16%

yield obtained by Dr. Carles Galdeano through reaction of **82**·HCl with $EtCO_2Cl$ in presence of freshly distilled Et_3N.[184]

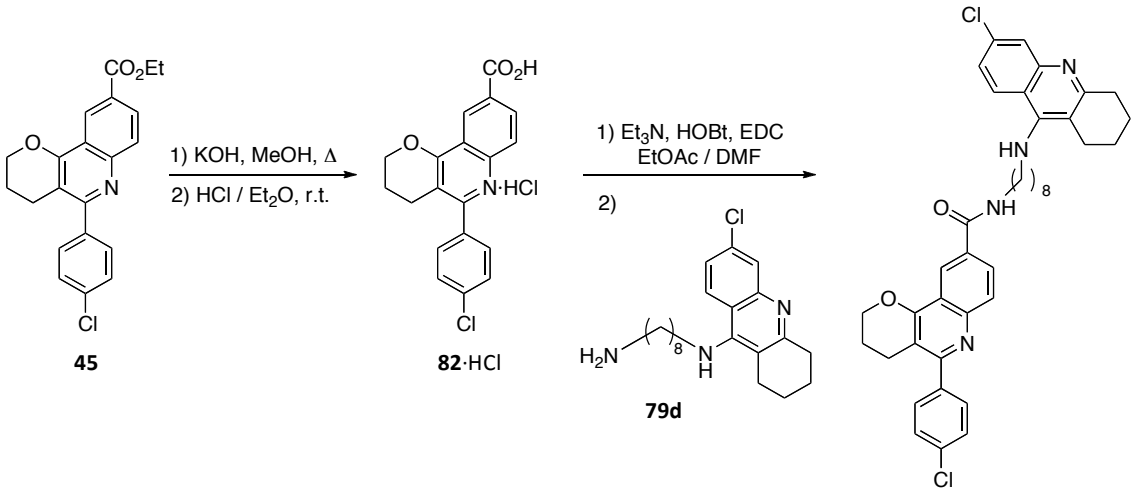

Scheme 5.5

5.3 Molecular modelling studies on hybrid 81a

The *in vitro* *h*AChE inhibitory activity of this novel series of tetrahydrobenzo[*h*][1,6]naphthyridine–6-chlorotacrine hybrids was evaluated by Prof. Victòria Clos (*Universitat Autonoma de Barcelona*). The pharmacological results disclosed a surprisingly high dependency of the inhibitory potency on the tether's length, with the tri-methylene linked compound, **81a** (IC_{50} 0.006 nM), being almost 2400-, 2400- and 350-fold more potent than the tetra-, the penta-, and the octa-methylene linked derivatives, respectively.

A 100 ns MD simulation was run in order to rationalize the outstanding pharmacological profile displayed by **81a**. The X-ray structure of the *h*AChE complex with huprine W (PDB ID 4BDT) was used to model the enzyme, while the initial coordinates of the ligand inside the binding cavity were retrieved from the structural information provided by the binding mode of huprine X to *Tc*AChE (PDB ID 1E66), together with the binding mode recently described for **68** (Chapter 4). In order to avoid possible artefactual rearrangements of 6-chlorotacrine moiety

[184]Galdeano, C. PhD thesis. *Unitat de Química Farmacèutica, Departament de Farmacologia i Química Terapèutica, Universitat de Barcelona*, **2012**.

inside the CAS, during the first 20 ns of the simulation a pharmacophoric restraint was applied to the distance between the protonated nitrogen atom of the 6-chlorotacrine moiety of the ligand and the carbonyl oxygen of His447 (**Figure 5.2**).

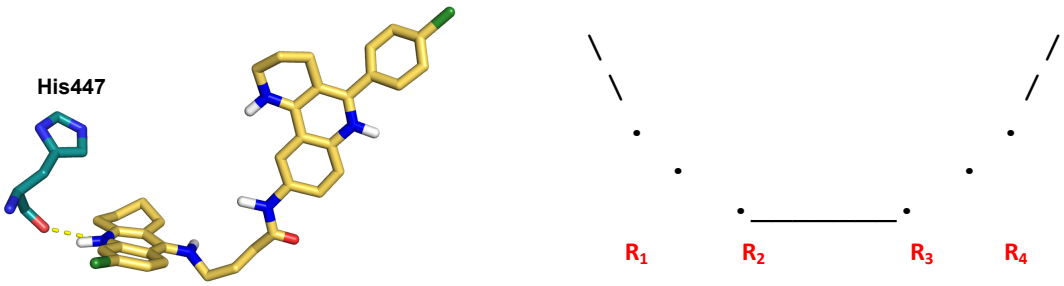

Figure 5.2 Left: Representation of the distance constrained (dotted yellow line) between the carbonyl oxygen atom of His447 and the protonated quinoline nitrogen atom of **81a**. Right: Representative plot of the constraint applied. R_1 = 2.80 Å; R_2 = 3.00 Å; R_3 = 3.30 Å; R_4 = 3.60 Å; "\": lower bound linear response; "/": lower bound linear response;"·": parabola; "_": flat region.

The simulation yielded a structurally and energetically stable trajectory, with the sole exception of a slight reorientation of the benzonaphthyridine moiety of the inhibitor in the PAS, due to a conformational change in the loop defined by residues 289-292. However, the ligand remained fully stable during the last 60 ns of the simulation (**Figure 5.3**).

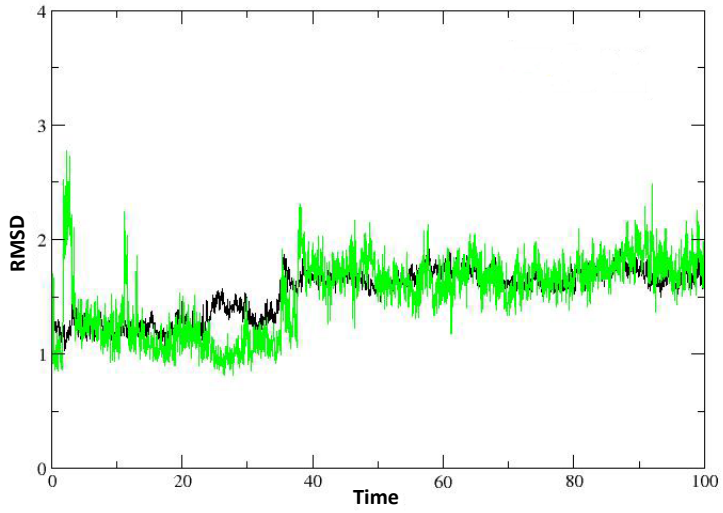

Figure 5.3 Time evolution of the root-mean square deviation (RMSD; Å) determined for the heavy atoms of the residues that define the binding site (black) and the ligand (green) for the simulation of the *h*AChE complex with hybrid **81a**.

The 6-chlorotacrine moiety of the ligand bound the CAS through a cation-π interaction with the aromatic rings of Trp86 and Tyr337, and an additional hydrogen bond between the protonated quinoline nitrogen atom and the carbonyl oxygen of His447. On the other hand, the benzonaphthyridine moiety established a π-π stacking interaction, reinforced by an additional cation-π interaction through its protonated quinoline nitrogen atom, with Trp286 at the PAS. This binding mode was further stabilized by the formation of transient hydrogen bond interactions between the NH group of the ligand and Tyr72. However, the most relevant finding was the network of interactions formed by the amide group in the tether and several midgorge residues of the protein. Indeed, the amide NH group formed a hydrogen bond with Asp74, which was in turn hydrogen-bonded with the hydroxyl group of Tyr341, and the carbonyl oxygen was involved either directly or through a water molecule in hydrogen bond interactions with the hydroxyl group of Tyr337 (**Figure 5.4**).

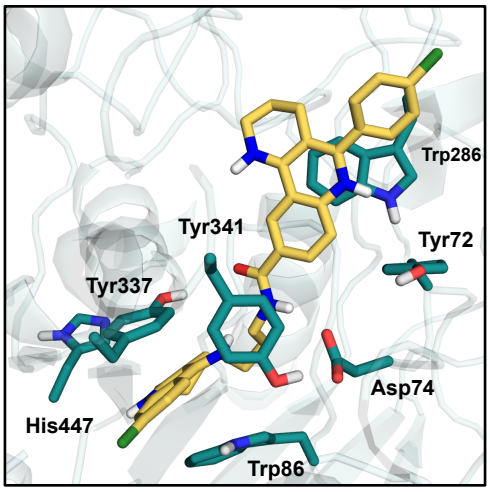

Figure 5.4 Representation of the binding mode of the benzo[*h*][1,6]naphthyridine–6-chlorotacrine hybrid **81a** (yellow) in the average structure obtained from the snapshots sampled in the last 5 ns of the trajectory. The side chains or backbone units of the residues involved in interactions are shown as cyan-coloured sticks.

The binding free energy of compound **81a**, through the Solvated Interaction Energy (SIE) method, supported the binding mode predicted by MD simulations, since the SIE bonding affinity calculated for **81a** (–12.5 kcal/mol) resulted 4 kcal/mol lower than that predicted for the PAS binding inhibitor **68** (–8.5 kcal/mol), a result that perfectly matches with the 10^4 ratio between the IC_{50} values of **81a** and **68** (**Table 5.1**).

Overall, the computational studies provided a rational explanation to the significant enhancement of the inhibitory potency of **81a** compared to **81b**-**d**, as the elongation of the

oligomethylene chain between the CAS- and PAS-binding fragments would have altered the network of interactions with midgorge residues, a hypothesis also reinforced by a similar case reported in literature by Muñoz-Ruiz *et al.* remarking the important contribution played by the midgorge region of AChE in modulating the affinity of some tacrine-indole heterodimers.[199]

Table 5.1
Free energy components determined from Solvent Interaction Energy (SIE) computations for the binding of compounds **81a** and **68**.[a]

Component	81a	68
van der Waals (ΔE_{vW})	–77.4 ± 4.1	–44.1 ± 2.8
Coulombic (ΔE_{Coul})	–154.2 ± 7.7	–93.6 ± 5.7
Reaction Field (ΔG_{RF})	153.3 ± 5.4	92.6 ± 5.0
Cavity (γ ΔSA)	–13.8 ± 0.6	–8.1 ± 0.5
Total (ΔG) [a]	–12.5 ± 0.7	–8.5 ± 0.4

[a]Evaluated from the expression $\Delta G = \alpha\left[\Delta E_{vW} + \Delta E_{Coul} + \Delta G_{RF} + \gamma \Delta SA\right] + C$, where the parameters α (0.1048) and C (–2.89 kcal/mol) were fitted to the absolute binding free energies of 99 protein–ligand complexes.

[199]Muñoz-Ruiz, P.; Rubio, L.; García-Palomero, E.; Dorronsoro, I.; del Monte-Millán, M.; Valenzuela, R.; Usan, P.; de Austria, C.; Bartolini, M.; Andrisano, V.; Bidon-Chanal, A.; Orozco, M.; Luque, F.J.; Medina, M.; Martínez, A. *J. Med. Chem.* **2005**, *48*, 7223.

European Journal of Medicinal Chemistry 84 (2014) 107–117

Contents lists available at ScienceDirect

European Journal of Medicinal Chemistry

journal homepage: http://www.elsevier.com/locate/ejmech

Original article

Tetrahydrobenzo[*h*][1,6]naphthyridine-6-chlorotacrine hybrids as a new family of anti-Alzheimer agents targeting β-amyloid, tau, and cholinesterase pathologies

Ornella Di Pietro [a], F. Javier Pérez-Areales [a], Jordi Juárez-Jiménez [b], Alba Espargaró [c], M. Victòria Clos [d], Belén Pérez [d], Rodolfo Lavilla [e], Raimon Sabaté [c], F. Javier Luque [b, *], Diego Muñoz-Torrero [a, **]

[a] *Laboratori de Química Farmacèutica (Unitat Associada al CSIC), Facultat de Farmàcia, and Institut de Biomedicina (IBUB), Universitat de Barcelona, Av. Joan XXIII, 27-31, E-08028 Barcelona, Spain*
[b] *Departament de Fisicoquímica, Facultat de Farmàcia (Campus Torribera), and IBUB, Universitat de Barcelona, Prat de la Riba 171, E-08921 Santa Coloma de Gramenet, Spain*
[c] *Departament de Fisicoquímica, Facultat de Farmàcia, and Institut de Nanociència i Nanotecnologia (IN²UB), Universitat de Barcelona, Av. Joan XXIII, 27-31, E-08028 Barcelona, Spain*
[d] *Departament de Farmacologia, de Terapèutica i de Toxicologia, Institut de Neurociències, Universitat Autònoma de Barcelona, E-08193 Bellaterra, Barcelona, Spain*
[e] *Laboratori de Química Orgànica, Facultat de Farmàcia, Universitat de Barcelona, and Barcelona Science Park, Baldiri Reixac 10-12, E-08028 Barcelona, Spain*

ARTICLE INFO

Article history:
Received 4 March 2014
Received in revised form
18 June 2014
Accepted 6 July 2014
Available online 7 July 2014

Keywords:
Tetrahydrobenzo[*h*][1,6]naphthyridines
Multitarget compounds
Dual binding site AChE inhibitors
Aβ aggregation inhibitors
Tau aggregation inhibitors

ABSTRACT

Optimization of an essentially inactive 3,4-dihydro-2*H*-pyrano[3,2-*c*]quinoline carboxylic ester derivative as acetylcholinesterase (AChE) peripheral anionic site (PAS)-binding motif by double O → NH bioisosteric replacement, combined with molecular hybridization with the AChE catalytic anionic site (CAS) inhibitor 6-chlorotacrine and molecular dynamics-driven optimization of the length of the linker has resulted in the development of the trimethylene-linked 1,2,3,4-tetrahydrobenzo[*h*][1,6]naphthyridine–6-chlorotacrine hybrid **5a** as a picomolar inhibitor of human AChE (hAChE). The tetra-, penta-, and octamethylene-linked homologues **5b**–**d** have been also synthesized for comparison purposes, and found to retain the nanomolar hAChE inhibitory potency of the parent 6-chlorotacrine. Further biological profiling of hybrids **5a**–**d** has shown that they are also potent inhibitors of human butyrylcholinesterase and moderately potent Aβ42 and tau anti-aggregating agents, with IC_{50} values in the submicromolar and low micromolar range, respectively. Also, *in vitro* studies using an artificial membrane model have predicted a good brain permeability for hybrids **5a**–**d**, and hence, their ability to reach their targets in the central nervous system. The multitarget profile of the novel hybrids makes them promising leads for developing anti-Alzheimer drug candidates with more balanced biological activities.

1. Introduction

Alzheimer's disease (AD) currently represents one of the most important unmet medical needs worldwide. Worryingly, because prevalence and mortality figures associated with AD will keep increasing, this condition will be even more pronounced in the upcoming decades, unless efficient disease-modifying drugs become available [1].

Current treatments for AD involve the use of acetylcholinesterase (AChE) inhibitors (donepezil, rivastigmine and galantamine) or NMDA receptor antagonists (memantine), which restore neurotransmitter deficits that are responsible for the symptomatic phase of the disease (cognitive, functional, and neuropsychiatric deficits) that appears a decade or more after the onset of the neurodegenerative process.

It is becoming increasingly apparent that the simultaneous modulation of several crucial targets that play early roles in the neuropathogenic process is a promising approach to derive

* Corresponding author.
** Corresponding author.
E-mail addresses: fjluque@ub.edu (F.J. Luque), dmunoztorrero@ub.edu (D. Muñoz-Torrero).

http://dx.doi.org/10.1016/j.ejmech.2014.07.021
0223-5234/

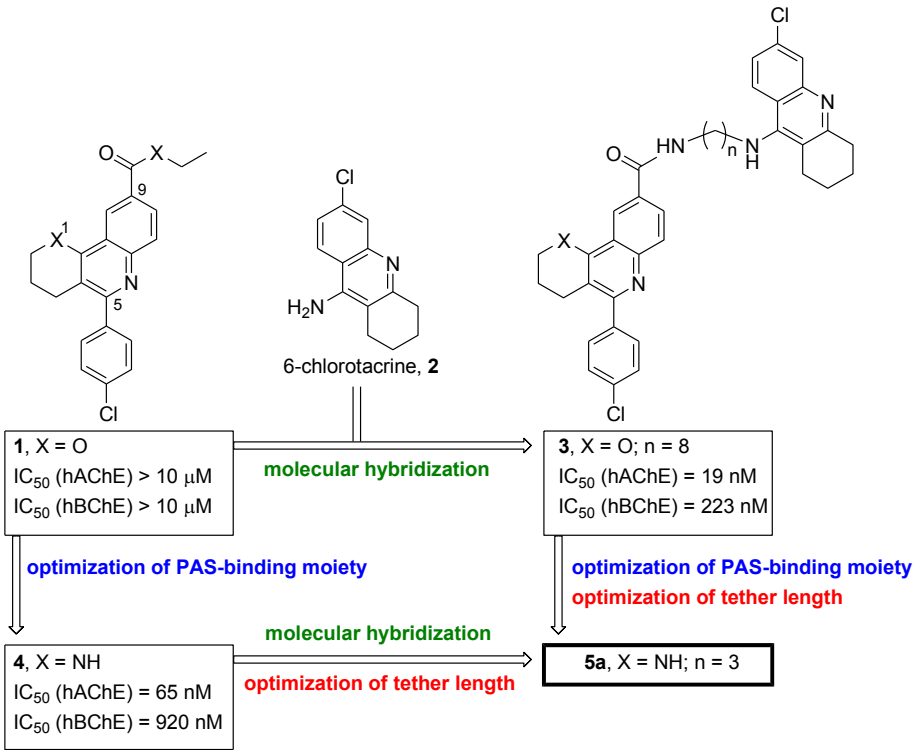

Fig. 1. Rational design of the tetrahydrobenzo[*h*][1,6]naphthyridine-6-chlorotacrine hybrid **5a**.

effective drugs that can modify the course of AD [3,4]. Obviously, administration of these multitarget drugs depends on a precise knowledge of the timing of the critical neuropathologies to be hit and on the development of suitable biomarkers that enable timely therapeutic interventions and the assessment of their impact on AD progression. Whereas these important issues are addressed [2,5,6], the parallel development of multitarget drugs hitting different combinations of key biological targets should be actively pursued.

Neuropathologies related to the β-amyloid peptide (Aβ) and tau protein are thought to be at the root of the neurodegenerative process [2]. Also, AChE seems to play a role in the early phases of the disease, inasmuch as it can bind to Aβ, thereby accelerating its aggregation into oligomers and fibrils and increasing the neurotoxicity of Aβ aggregates [7]. The Aβ proaggregating action of AChE has been reported to reside in its peripheral anionic site (PAS) [7c], which is located at the mouth of a 20 Å deep gorge that leads to the catalytic anionic site (CAS) of the enzyme [8].

We have recently developed a new family of potent AChE inhibitors able to simultaneously bind at the CAS and PAS of the enzyme, i.e. dual binding site inhibitors, which were designed by molecular hybridization of the novel 3,4-dihydro-2*H*-pyrano[3,2-*c*]quinoline scaffold of ester **1** and the potent AChE CAS inhibitor 6-chlorotacrine, **2** (Fig. 1) [9]. The most potent hybrid of the series, compound **3** (Fig. 1) retained the high human AChE inhibitory activity of the parent 6-chlorotacrine (**3**: IC_{50} = 7 nM in human erythrocyte AChE; IC_{50} = 19 nM in human recombinant AChE (hAChE)), and additionally exhibited a potent inhibitory activity of human butyrylcholinesterase (hBChE) and a weak Aβ anti-aggregating activity (29% inhibition of AChE-induced Aβ40 aggregation at 100 μM and 21% inhibition of self-induced Aβ42 aggregation at 50 μM) [9].

Even though the 5-(4-chlorophenyl)-3,4-dihydro-2*H*-pyrano[3,2-*c*]quinoline moiety of **3** might establish π–π stacking interactions with the aromatic PAS residues Trp286 and Tyr72 (hAChE numbering), concomitant to the interactions of the 6-chlorotacrine unit at the CAS, the 5-(4-chlorophenyl)-3,4-dihydro-2*H*-pyrano[3,2-*c*]quinoline ester **1**, used as synthetic precursor of **3**, was found to be essentially inactive as AChE inhibitor. With the aim of optimizing this tricyclic scaffold as a PAS-binding moiety, we recently designed a family of tetrahydrobenzo[*h*][1,6]naphthyridines, which mainly resulted from the substitution of the oxygen atom at position 1 of the 3,4-dihydro-2*H*-pyrano[3,2-*c*]quinoline system of ester **1** by an amine nitrogen atom [10]. The rationale behind this structural modification was that the increased basicity of the pyridine nitrogen atom would enable i) its protonation at physiological pH, and hence, ii) the establishment of cation–π interactions, apart from π–π stacking, with the aromatic PAS residues. Indeed, the most potent compound of the series, **4** (Fig. 1), resulting from a double O → NH bioisosteric replacement from ester **1** at position 1 and at the side chain in position 9, exhibited a nanomolar hAChE inhibitory activity (IC_{50} = 65 nM) [10]. Molecular dynamics (MD) simulations confirmed the expected binding of the tricyclic moiety of **4** at the AChE PAS (cation–π/π–π interactions with Trp286) and hydrogen bond between the protonated pyridine nitrogen atom and the hydroxyl group of the PAS residue Tyr72) as well as additional interactions of the amide function at position 9 with midgorge residues (hydrogen bond between the amide NH group and the hydroxyl group of Tyr124) [10].

Once the PAS-binding moiety had been optimized, we inferred that molecular hybridization with the CAS binder 6-chlorotacrine should provide further improvement of the AChE inhibitory activity. The disposition of the amide chain at position 9 of the tetrahydrobenzo[*h*][1,6]naphthyridine **4** along the midgorge, with its nitrogen atom at a distance of ~6 Å from the position occupied by the exocyclic amino group of tacrine in its complex with *Torpedo californica* AChE (Fig. 2) [11], suggested that a linker of 3 methylenes should be optimal to connect both moieties retaining all their interactions with AChE residues all along the enzyme gorge. Thus, the tetrahydrobenzo[*h*][1,6]naphthyridine-6-chlorotacrine hybrid **5a**

(Fig. 1) was rationally designed as a novel multiple-site AChE inhibitor, bearing optimized PAS-binding moiety and tether length.

Herein, we describe the synthesis of the tetrahydrobenzo[*h*][1,6]naphthyridine–6-chlorotacrine hybrid **5a** and its longer tetra-, penta-, and octa-methylene-linked homologues **5b**–**d**, the evaluation of their inhibitory activities against hAChE and hBChE, and the study of their binding mode to hAChE by MD simulations. To further expand the potential multitarget profile of hybrids **5a**–**d**, their inhibitory activities against the aggregation of Aβ42 and tau protein in intact *Escherichia coli* cells, as a simplified *in vivo* model of aggregation of amyloidogenic proteins, were also evaluated. Moreover, the brain penetration of these hybrids, and therefore the ability to reach their targets at the central nervous system (CNS), was assessed by a parallel artificial membrane permeation assay (PAMPA-BBB).

2. Results and discussion

2.1. Synthesis of the tetrahydrobenzo[h][1,6]naphthyridine-6-chlorotacrine hybrids

Apart from the rationally designed trimethylene-linked hybrid **5a**, we planned the synthesis of the longer tetra- and penta-methylene homologues **5b** and **5c**, still bearing relatively short linkers. We also envisioned the synthesis of the octamethylene-linked analogue **5d**, mainly for comparison with the octamethylene-linked 3,4-dihydro-2*H*-pyrano[3,2-*c*]quinoline-based hybrid **3**, to gain further insight into the effect of the O → NH bioisosteric replacement at position 1 of the tricyclic system, while keeping the same tether length.

For the synthesis of hybrids **5a**–**d**, we used as starting material the *N*-Boc-protected tetrahydrobenzo[*h*][1,6]naphthyridine **6**, readily available by a multicomponent Povarov reaction between 4-chlorobenzaldehyde, ethyl 4-aminobenzoate and *N*-Boc-3,4-dihydro-2*H*-pyridine under the catalysis of $Sc(OTf)_3$ in acetonitrile [12], followed by DDQ oxidation [13] of the resulting diastereomeric mixture of octahydrobenzo[*h*][1,6]naphthyridines [10].

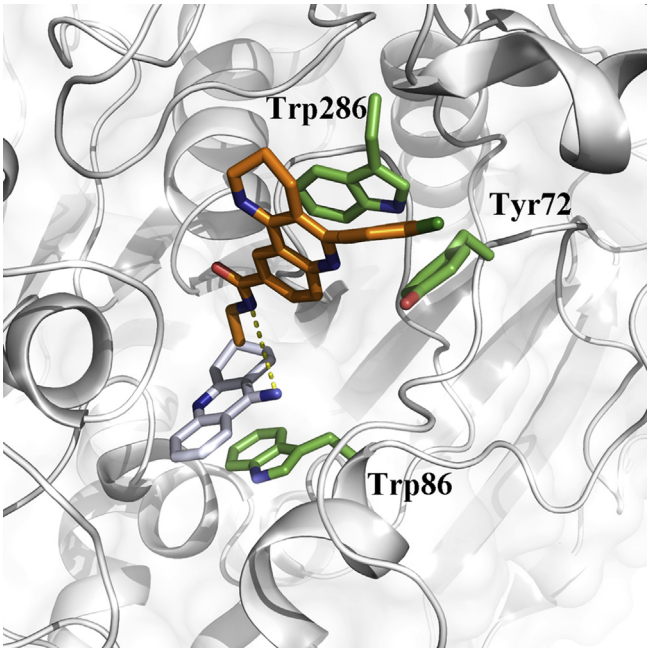

Fig. 2. Superimposition of the MD-predicted binding mode of tetrahydrobenzo[*h*][1,6]naphthyridine **4** in AChE with the X-ray structure of the complex *Torpedo californica* AChE–tacrine.

Saponification of ester **6**, followed by treatment of the resulting carboxylate with an Et_2O solution of HCl afforded the corresponding carboxylic acid, which was isolated as the naphthyridine hydrochloride. Coupling of the carboxylic acid with the known aminoalkyltacrine derivatives **7a**–**d** [14], using HOBt and EDC in the presence of Et_3N in a 10:1 mixture EtOAc/DMF, followed by silica gel column chromatography purification afforded the expected *N*-Boc-protected amides, in some cases together with directly deprotected amides (**5a** and **5c**). Treatment of the *N*-Boc-protected amides with 4 M HCl in dioxane at room temperature afforded the target amides **5a**–**d** in 34–80% total overall yields from ester **6** (Scheme 1).

The novel tetrahydrobenzonaphthyridine-6-chlorotacrine hybrids **5a**–**d** were fully characterized in the form of dihydrochloride salts through their spectroscopic data (IR, ^1H and ^{13}C NMR) and HRMS and their purity was assessed by elemental analysis and HPLC measurements. The biological characterization was also performed with the dihydrochloride salts.

2.2. Acetylcholinesterase inhibition

2.2.1. Evaluation of AChE inhibitory activity

The inhibitory activity of the novel hybrids **5a**–**d** against hAChE was evaluated by the method of Ellman et al. [15]. The 3,4-dihydro-2*H*-pyrano[3,2-*c*]quinoline derivatives **1** and **3**, as well as 6-chlorotacrine, **2**, were also evaluated under the same assay conditions as reference compounds. Also, the reported activity of compound **4** [10] was considered for comparison purposes.

All the tetrahydrobenzonaphthyridine-6-chlorotacrine hybrids turned out to be very potent inhibitors of hAChE (Table 1). Indeed, in agreement with the rational design strategy, the trimethylene-linked hybrid **5a** was the most potent hAChE inhibitor of the series, exhibiting a surprising picomolar IC_{50} value (IC_{50} = 6.27 pM). The highly potent inhibitory activity of **5a** is indicative of the success of the rational design strategy, in terms of both the molecular hybridization and the optimization of the tether length. On the one hand, molecular hybridization has been successful because **5a** is roughly 1000-fold and >10000-fold more potent than the parent compounds 6-chlorotacrine, **2**, and **4**, respectively (Table 1). On the other hand, the MD-driven optimization of the tether length has been also successful, inasmuch as the trimethylene-linked hybrid **5a** is much more potent than the tetra-, penta-, and octamethylene-linked counterparts (>2000-fold more potent than **5b** and **5c** and >300-fold more potent than **5d**).

The O → NH bioisosteric replacement, which had proven to be successful in the optimization from the 3,4-dihydro-2*H*-pyrano[3,2-*c*]quinoline ester **1** to the tetrahydrobenzo[*h*][1,6]naphthyridine amide **4** [10], has been also successful in the corresponding hybrids with 6-chlorotacrine, the tetrahydrobenzo[*h*][1,6]naphthyridine-based hybrid **5d** being roughly 10-fold more potent than the 3,4-dihydro-2*H*-pyrano[3,2-*c*]quinoline-based hybrid **3**, with the same tether length (Table 1).

Overall, hybrid **5a** constitutes one of the most potent non-covalent inhibitors of hAChE so far reported, even though a few examples of other picomolar or even femtomolar inhibitors of AChE have also been described [14a,16].

2.2.2. Binding mode within AChE: molecular modelling studies

To shed light on the structural basis of the surprisingly high AChE inhibitory activity determined for compound **5a**, the binding mode to hAChE was explored by means of MD simulations, taking advantage of the X-ray crystallographic structure of the hAChE complex with huprine W (PDB entry 4BDT [17]). The initial pose of the ligand was guided by the structural information available for the binding mode of huprine X to *T. californica* AChE (PDB entry

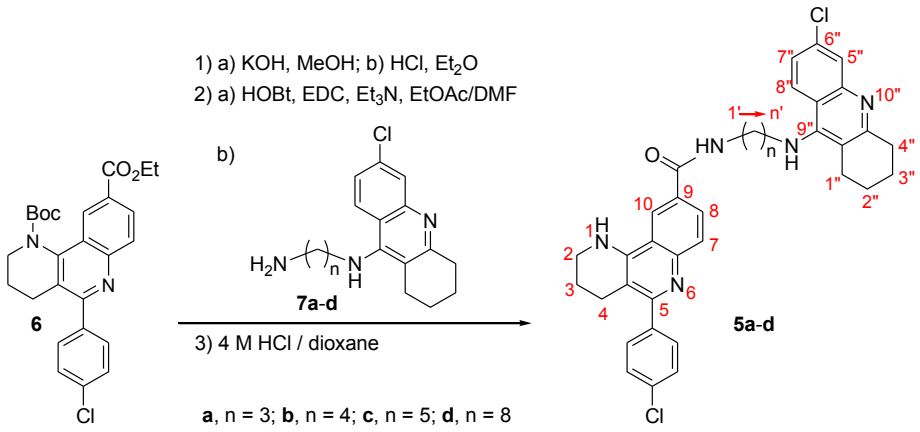

Scheme 1. Synthesis of the target tetrahydrobenzo[*h*][1,6]naphthyridine-6-chlorotacrine hybrids.

1E66 [18]), which matches well the structure of huprine W bound to hAChE, and by the recently reported binding mode of compound **4** [10].

The analysis of the 100 ns MD trajectory supported the structural integrity and stability of the ligand bound to the hAChE gorge. Thus, with the sole exception of a slight reorientation of the tetrahydrobenzo[*h*][1,6]naphthyridine moiety in the PAS, which was originated from a conformational change in the loop defined by residues 289–292, the RMSD of the ligand remained fully stable during the last 60 ns of the trajectory (Fig. S1, Supplementary Material). The hybrid **5a** establishes a complex network of interactions with the residues of the binding site (Fig. 3). As expected, the 6-chlorotacrine moiety was tightly bound in the CAS due to the cation–π interactions with the aromatic rings of Trp86 and Tyr337 (average distances of 3.9 Å between the indole or phenol rings and the aminoacridine unit) and the hydrogen bond of the protonated acridine nitrogen atom with the carbonyl oxygen of His447 (average distance of 2.9 Å). On the other hand, the tetrahydrobenzo[*h*][1,6]naphthyridine moiety was firmly stacked against Trp286, thus enabling the formation of a cation–π interaction between the protonated quinoline nitrogen atom and the indole ring of Trp286. The binding of this moiety was also assisted by transient hydrogen bond interactions between the NH group and the hydroxyl oxygen of Tyr72. The most remarkable finding concerns the interactions formed by the amide group in the tether, as the amide NH group is involved in a hydrogen bond with Asp74 (average distance of 3.6 Å), which is in turn hydrogen-bonded to the hydroxyl group of Tyr341 (average distance of 2.8 Å), while the amide carbonyl oxygen forms either direct or water-mediated interactions with the hydroxyl group of Tyr337 (average distance of 4.9 Å). As a further test, the binding free energy of compound **5a** was determined with the Solvated Interaction Energy (SIE) method [19], which relies on MM/PBSA calculations in conjunction with weighting scaling factors for the free energy components suitably parameterized to reproduce the experimental binding affinities for a diverse set of protein–ligand complexes. The SIE binding affinity obtained for compound **5a** is −12.5 kcal/mol (Table S1, Supplementary Material), which is 4 kcal/mol lower than that determined for compound **4** (−8.5 kcal/mol [10]), which is in agreement with the ~10^4 ratio between the IC_{50} values reported in Table 1.

These findings provide a basis to explain the abrupt change in inhibitory activity between compounds **5a** and **5b**, as the enlargement of the oligomethylene chain between tacrine and the amide group would disrupt the interactions with the midgorge residues. On the other hand, the amide group that is present in the tether of some tacrine–indole heterodimers reported by Muñoz-Ruiz et al. as picomolar AChE inhibitors was also suggested to participate in a complex network of interactions with midgorge residues [14a]. In

Table 1
Inhibitory activities of 1,2,3,4-tetrahydrobenzo[*h*][1,6]naphthyridine-6-chlorotacrine hybrids and reference compounds against AChE, BChE, Aβ42 and tau aggregation, and BBB predicted permeabilities.

Compd	hAChE IC_{50} (nM)[a]	hBChE IC_{50} (nM)[a]	Aβ42 aggregation in *E. coli* (% inhib. at 10 μM)[b]	Tau protein aggregation in *E. coli* (% inhib. at 10 μM)[b]	*Pe* (10^{-6} cm s^{-1})[c] (prediction)
5a	0.006 ± 0.002	120 ± 13	52.5 ± 0.4	40.7 ± 0.5	10.5 ± 0.7 (CNS+)
5b	14.2 ± 1.7	205 ± 16	55.8 ± 0.7	58.9 ± 0.4	13.8 ± 0.4 (CNS+)
5c	14.2 ± 1.9	337 ± 30	54.3 ± 0.7	57.7 ± 0.5	14.3 ± 1.3 (CNS+)
5d	2.06 ± 0.3	286 ± 35	77.5 ± 0.9	68.7 ± 0.5	19.2 ± 1.3 (CNS+)
1	na[d]	na[d]	41.8 ± 0.4	27.9 ± 1.2	9.9 ± 1.4 (CNS+)
2	5.9 ± 0.6	114 ± 4	11.0 ± 0.6	1.4 ± 0.7	19.8 ± 0.4 (CNS+)[e]
3	19.3 ± 1.4	223 ± 35	54.6 ± 0.5	37.8 ± 0.5	13.9 ± 0.8 (CNS+)
4	65.0 ± 3.0[f]	920 ± 30[f]	nd[g]	nd[g]	22.9 ± 0.8 (CNS+)[f]

[a] IC_{50} inhibitory concentration (nM) of human recombinant AChE and human serum BChE. IC_{50} values are expressed as mean ± standard error of the mean (SEM) of at least four experiments ($n = 4$), each performed in duplicate.
[b] % Inhibition of Aβ42 and tau protein aggregation at 10 μM in intact *E. coli* cells. Values are expressed as mean ± SEM of four independent experiments ($n = 4$).
[c] Permeability values from the PAMPA-BBB assay. Values are expressed as the mean ± SD of three independent experiments ($n = 3$).
[d] Not active.
[e] Data from Ref. [9].
[f] Data from Ref. [10].
[g] Not determined.

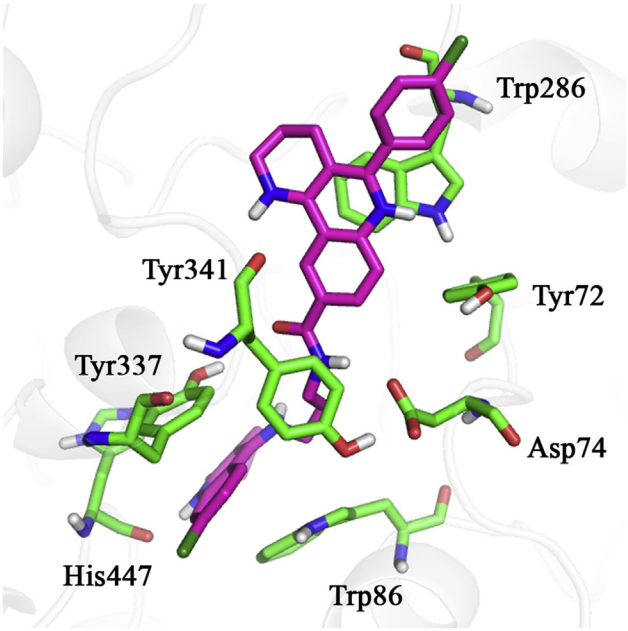

Fig. 3. Representation of the binding mode of the tetrahydrobenzo[*h*][1,6]naphthyridine-6-chlorotacrine hybrid **5a** (magenta) in the average structure obtained from the snapshots sampled in the last 5 ns of the trajectory. The residues involved in interactions are shown as green-coloured sticks. (For interpretation of the references to colour in this figure legend, the reader is referred to the web version of this article.)

the most potent tacrine–indole heterodimer the amide group, located at six methylene groups from the tacrine unit, was suggested to interact with Tyr124 and Tyr337. In hybrid **5a** the shortening of the chain to three methylenes enables the formation of a distinct interaction pattern with Asp74 and Tyr337. Overall, these findings reinforce the significant contribution played by the midgorge in complementing both PAS and CAS and modulating the affinity of AChE inhibitors.

2.3. Butyrylcholinesterase inhibition

BChE is partly responsible for acetylcholine hydrolysis and hence, for the cholinergic deficit of AD patients, especially in advanced stages of the disease, when the levels of AChE in CNS markedly decrease. Thus, BChE also represents a biological target of interest for AD treatment [20]. The BChE inhibitory activity of hybrids **5a**–**d** against hBChE was evaluated by the method of Ellman et al. [15].

The parent compounds 6-chlorotacrine, **2**, and **4** are selective inhibitors of hAChE, albeit still exhibiting a moderately potent hBChE inhibitory activity, with IC_{50} values in the submicromolar range. Not unexpectedly, hybrids **5a**–**d** were also more potent against hAChE than hBChE, displaying submicromolar IC_{50} values for hBChE inhibition (Table 1). In this case, molecular hybridization resulted in an increased hBChE inhibitory activity relative to the parent compound **4** (3–8-fold) but in a slightly decreased potency relative to 6-chlorotacrine, **2**, with the exception of hybrid **5a**, which was equipotent to 6-chlorotacrine.

The length of the linker has little influence on the hBChE inhibitory activity. Only a slight trend toward decreased potency with increased tether length was observed, the shorter homologue **5a** being 1.7-, 2.8-, and 2.4-fold more potent than the longer counterparts **5b**, **5c**, and **5d**, respectively. Finally, the O → NH bioisosteric replacement had little influence on the hBChE inhibitory activity, the octamethylene-linked 3,4-dihydro-2*H*-pyrano [3,2-*c*]quinoline- and tetrahydrobenzo[*h*][1,6]naphthyridine-based hybrids **3** and **5d** roughly displaying the same potency (Table 1).

2.4. Aβ42 and tau aggregation inhibition

The aggregation of the amyloidogenic proteins Aβ, especially the most aggregation-prone and neurotoxic 42 amino acid form thereof (Aβ42), and tau are widely thought to constitute early pathogenic events in AD, and hence, they are the target of many drug candidates purported to modify the natural course of the disease [21].

We have recently developed a new methodology for the evaluation of the effects of putative inhibitors on the aggregation and subsequent formation of insoluble inclusion bodies of any amyloidogenic protein that can be overexpressed in *E. coli* cells [22]. The method relies on monitoring the changes in the fluorescence of Thioflavin S (Th–S) that are produced upon binding to amyloid aggregates rich in β-sheet structures. Compounds that are able to cross the membranes of *E. coli* cells and inhibit the aggregation of overexpressed amyloidogenic proteins will lead to a decrease in the fluorescence of Th–S. This method is fast, simple and inexpensive, as it avoids the use of synthetic peptides. We have successfully used this method for the evaluation of inhibitors of Aβ42 and tau aggregation. Interestingly, the results obtained in the screening of Aβ42 aggregation inhibitors correlated very well with the results previously reported from *in vitro* assays using synthetic peptides, thereby validating this methodology [22].

The inhibitory activity of hybrids **5a**–**d** against Aβ42 and tau aggregation was assessed using this methodology. In general, very similar results and SAR trends were found for both activities. At 10 μM, hybrids **5a**–**d** exhibited percentages of inhibition in the ranges 52–77% and 41–69% against Aβ42 and tau aggregation, respectively (Table 1).

Molecular hybridization led to increased Aβ42 and tau anti-aggregating activities, hybrids **5a**–**d** being more potent than 6-chlorotacrine (5–7-fold more potent against Aβ42 aggregation and 30–50-fold more potent against tau aggregation). The parent compound **4** could not be tested in these assays, but in *in vitro* tests it had been found to be a weak inhibitor of Aβ42 aggregation (15% inhibition at 10 μM) [10], so presumably hybrids **5a**–**d** are also more potent than **4**.

The length of the linker seemed to have a subtle effect on Aβ42 and tau anti-aggregating activities. These activities slightly increased with the tether length so that the longer homologue **5d** was 1.5-fold more potent than the shorter counterpart **5a** for both activities. On the other hand, the O → NH bioisosteric replacement had a similar effect on both activities, the tetrahydrobenzo[*h*][1,6] naphthyridine-based hybrid **5d** being roughly 1.5-fold more potent than the 3,4-dihydro-2*H*-pyrano[3,2-*c*]quinoline-based hybrid **3** for Aβ42 and tau aggregation inhibition.

The parallel results obtained for these hybrids against both Aβ42 and tau aggregation further support the notion that diseases based on the pathological aggregation of one or several amyloidogenic proteins might share common mechanisms and might be confronted with common therapeutic interventions [23].

Overall, hybrids **5a**–**d** can be considered as moderately potent dual Aβ42 and tau anti-aggregating compounds, with IC_{50} values that must lie around or below 10 μM. Because these anti-aggregating activities have been determined without involving the presence of AChE, the high AChE inhibitory activity of hybrids **5a**–**d** cannot be responsible for their Aβ42 and tau anti-aggregating activities, which might be ascribed, instead, to a direct interaction with Aβ42 and tau. The precise mechanisms through which these hybrids bind Aβ42 and tau and/or exert their anti-aggregating activities are unknown, even though it has been reported that the

presence of several aromatic moieties with extended π-conjugated systems (including biphenyls and phenyl-substituted benzoheteroaromatic systems, similar to the phenylquinoline moiety present in hybrids **5a**–**d**) may enable binding to Aβ42 [24].

The dual Aβ42 and tau anti-aggregating profile is of much interest for disease-modifying anti-Alzheimer agents. However, it must be recognized that the anti-aggregating activities of hybrids **5a**–**d** are not well balanced relative to their cholinesterase inhibitory activities, especially AChE and particularly in the case of its picomolar inhibitor **5a**, which represents an important issue in multitarget compounds.

2.5. Blood–brain barrier permeation assay

Anti-Alzheimer drug candidates, like any other CNS drug, must be able to efficiently enter into the brain, which requires a good ability to cross the blood–brain barrier (BBB) and a low P-glycoprotein efflux liability [25]. The large molecular weight of hybrids **5a**–**d** (>500) might compromise their ability to cross biological membranes, including BBB [26]. However, a number of distinct anti-Alzheimer hybrid compounds with molecular weights over 500 have shown good oral availability and/or brain permeability in *ex vivo* and *in vivo* studies in mice [27]. Indeed, the positive results obtained for the hybrids **5a**–**d** in the aggregation studies in *E. coli* cells were already indicative of their ability to cross biological membranes, but a more accurate determination of their ability to cross the BBB was necessary. In this light, the brain permeability of the hybrids **5a**–**d** was predicted using an *in vitro* model of passive transcellular permeation, namely the widely known PAMPA-BBB assay [28]. Thus, the *in vitro* permeability (P_e) through a lipid extract of porcine brain was determined using a mixture of phosphate-buffered saline (PBS)/EtOH (70:30). Assay validation was made by comparing the experimental and reported permeability values of 14 commercial drugs (Table S2, Supplementary Material), which provided a good linear correlation: P_e (exp) = 1.5010 P_e (lit) − 0.8618 (R^2 = 0.9199). Using this equation and the limits established by Di et al. for BBB permeation [28], the following ranges of permeability were established: P_e (10^{-6} cm s^{-1}) > 5.1 for compounds with high BBB permeation (CNS+); P_e (10^{-6} cm s^{-1}) < 2.1 for compounds with low BBB permeation (CNS−); and 5.1 > P_e (10^{-6} cm s^{-1}) > 2.1 for compounds with uncertain BBB permeation (CNS±). All the tetrahydrobenzo[*h*][1,6]naphthyridine-6-chlorotacrine hybrids, **5a**–**d**, were predicted to be able to cross the BBB. The measured P_e values for **5a**–**d** were found to slightly increase with the tether length, and hence, with lipophilicity, and were clearly above the threshold for high BBB permeation (Table 1), thereby anticipating their ability to enter the brain and reach their different CNS targets.

Of note, the predicted *in vitro* ability of the novel hybrids to cross the BBB was also confirmed through the BBB permeation index obtained using a recently reported *in silico* multiclassification method (Table 2), which was developed utilizing a comprehensive data set containing around 12,000 diverse compounds [29]. This method was also used to assess the intestinal absorption of the novel compounds, which was predicted to be positive in all cases. Finally, the predicted rat acute toxicity of the hybrids was clearly lower than that predicted for the anti-Alzheimer AChE inhibitor tacrine, thereby supporting the safety of these compounds (Table 2).

Table 2
In silico prediction of ADMET properties for hybrids **5a**–**d** and the reference compound tacrine.

Compd	Blood–brain barrier permeation	Intestinal absorption	Rat acute toxicity LD_{50} (mg/kg)
5a	+	+	566
5b	+	+	449
5c	+	+	803
5d	+	+	493
Tacrine	+	+	75 (70)[a]

[a] Taken from ref. [30].

3. Conclusion

In this work we have further advanced in the hit-to-lead optimization process that, starting from the 3,4-dihydro-2*H*-pyrano[3,2-*c*]quinoline carboxylic ester **1**, had led to the potent hAChE inhibitors **3** [9] and **4** [10] by molecular hybridization with 6-chlorotacrine and by double O → NH bioisosteric replacement, respectively. Herein, combination of the optimized AChE PAS-binding moiety present in **4**, molecular hybridization with 6-chlorotacrine, and an MD-driven optimization of the tether length has led to the discovery of the 1,2,3,4-tetrahydrobenzo[*h*][1,6]naphthyridine-6-chlorotacrine hybrid **5a** as a picomolar inhibitor of hAChE.

Apart from **5a**, other three longer homologues, i.e. **5b**–**d**, have been also synthesized and found to be potent inhibitors of hAChE, exhibiting IC_{50} values in the low nanomolar range. Like the parent compounds 6-chlorotacrine, **2**, and the tetrahydrobenzo[*h*][1,6]naphthyridine **4**, hybrids **5a**–**d** have been found to be selective for hAChE *vs.* hBChE inhibition, albeit still keeping a potent hBChE inhibitory activity. Very interestingly, these hybrids turned out to be moderately potent dual inhibitors of Aβ42 and tau aggregation in intact *E. coli* cells, with IC_{50} values in the low micromolar range. Taking into account all the tested activities, hybrid **5d**, with the most potent Aβ42 and tau anti-aggregating activities, is likely the hybrid of the series with the most interesting multitarget profile. Notwithstanding that better balanced potencies at their different targets would have been desirable, the multitarget profile of the novel hybrids, together with their predicted ability to cross the BBB, make them interesting anti-Alzheimer lead compounds.

4. Experimental part

4.1. Chemistry

4.1.1. General methods

Melting points were determined in open capillary tubes with an MFB 595010M Gallenkamp melting point apparatus. Recrystallization solvents from which the analytical samples have been obtained are indicated after the melting points. 400 MHz ^{1}H NMR and 500 MHz ^{1}H/125.8 MHz ^{13}C NMR spectra were recorded on Varian Gemini 400 and Varian Mercury 500 spectrometers, respectively. The chemical shifts are reported in ppm (δ scale) and coupling constants are reported in Hertz (Hz). Assignments given for the NMR spectra of the new compounds have been carried out by comparison with the NMR data of the precursor ester **6** and the hybrid compound **5d** which in turn, were assigned on the basis of DEPT, COSY ^{1}H/^{1}H (standard procedures), and COSY ^{1}H/^{13}C (gHSQC or gHMBC sequences) experiments. IR spectra were run on a Perkin–Elmer Spectrum RX I spectrophotometer, using the Attenuated Total Reflectance (ATR) technique. Absorption values are expressed as wave-numbers (cm^{-1}); only significant absorption bands are given. Column chromatography was performed on silica gel 60 AC.C (35–70 μM, SDS, ref 2000027). Thin-layer chromatography was performed with aluminium-backed sheets with silica gel 60 F_{254} (Merck, ref 1.05554), and spots were visualized with UV light and 1% aqueous solution of $KMnO_4$. NMR spectra of all of the new compounds were performed at the Centres Científics i Tecnològics of the University of Barcelona (CCiTUB), while elemental analyses

and high resolution mass spectra were carried out at the Microanalysis Service of the IIQAB (CSIC, Barcelona, Spain) with a Carlo Erba model 1106 analyzer, and at the CCiTUB with an LC/MSD-TOF Agilent Technologies spectrometer, respectively. The HPLC measurements were performed using an HPLC Waters Alliance HT apparatus comprising a pump (Edwards RV12) with degasser, an autosampler, a diode array detector and a column as specified below. The reverse phase HPLC determinations were carried out on a YMC-Pack ODS-AQ column (50 × 4.6 mm, DS. 3 μm, 12 nm). Solvent A: water with 0.1% formic acid; Solvent B: acetonitrile with 0.1% formic acid, or solvent A: water with NH_4HCO_3, 10 mM pH 9.0; Solvent B: acetonitrile. Gradient: 5% of B to 100% of B within 3.5 min. Flux: 1.6 mL/min at 50 °C. The analytical samples of all of the compounds that were subjected to pharmacological evaluation were dried at 65 °C/2 Torr (standard conditions) at least for 2 days and possess a purity ≥95% as evidenced by their elemental analyses and HPLC measurements. Of note, as previously reported for some tacrine-related dimeric compounds [31], the new hybrids herein described have the ability to retain molecules of water, which cannot be removed after drying the analytical samples under the aforementioned standard conditions. Thus, the elemental analyses of these compounds showed the presence of variable amounts of water, which have been indicated in the corresponding compound formulae.

4.1.2. *N*-{3-[(6-chloro-1,2,3,4-tetrahydroacridin-9-yl)amino] propyl}-5-(4-chlorophenyl)-1,2,3,4-tetrahydrobenzo[h][1,6] naphthyridine-9-carboxamide **5a**

A solution of ester **6** (4.79 g, 10.2 mmol) and KOH pellets (85% purity, 2.04 g, 30.9 mmol) in MeOH (260 mL) was stirred under reflux for 24 h. The resulting mixture was cooled to room temperature and evaporated to dryness. The solid residue was treated with an Et_2O solution of HCl (1.2 N, 171 mL, 205 mmol) for 30 min and the resulting suspension was evaporated at reduced pressure, to give the corresponding tetrahydrobenzo[*h*][1,6]naphthyridinecarboxylic acid, in the form of its hydrochloride salt (6.54 g), which was directly used in the next step without further purification: IR (ATR) *ν* 3500–2500 (max at 3316, 2966, O–H, $^+$N–H, C–H st), 1679, 1584, 1574 (C=O, Ar–C–C, Ar–C–N st) cm^{-1}; ^{1}H NMR (400 MHz, CD_3SO) *δ* 1.28 [s, 9H, NCOO–C(CH_3)$_3$], 1.76 (m, 2H, 3-H_2), 2.66 (t, *J* = 5.6 Hz, 2H, 4-H_2), 3.41 (m, 2H, 2-H_2), 7.49 (d, *J* ≈ 8.4 Hz, 2H), 7.64 (d, *J* = 8.4 Hz, 2H) [2(6)-H and 3(5)-H 4-chlorophenyl], 7.78 (d, *J* = 8.8 Hz, 1H, 7-H), 8.17 (br d, *J* ≈ 8.8 Hz, 1H, 8-H), 8.34 (br s, 1H, 10-H); HRMS (ESI), calcd for [$C_{24}H_{23}^{35}ClN_2O_4$+$H^+$] 439.1419, found 439.1410.

To a solution of crude tetrahydrobenzo[*h*][1,6]naphthyridinecarboxylic acid (298 mg) in EtOAc/DMF 10:1 (21 mL), Et_3N (0.19 mL, 138 mg, 1.36 mmol), EDC (146 mg, 0.94 mmol), and HOBt (128 mg, 0.94 mmol) were added, and the mixture was stirred at room temperature for 5 min. To the resulting mixture, amine **7a** (200 mg, 0.69 mmol) was added and the reaction mixture was stirred at room temperature for 18 h and concentrated at reduced pressure, to give a semisolid residue (1.18 g), which was purified by column chromatography (35–70 μm silica gel, CH_2Cl_2/MeOH/50% aq. NH_4OH mixtures, gradient elution). On elution with CH_2Cl_2/MeOH/50% aq. NH_4OH 99.5:0.5:0.2 to 99.2:0.8:0.2, N^1-Boc-protected amide (141 mg, 43% overall yield from **6**) and the final amide **5a** (111 mg, 39% overall yield from **6**) were successively isolated as yellowish solids.

A solution of the N^1-Boc-protected amide (141 mg, 0.20 mmol) in 4 M HCl/dioxane (2.41 mL, 9.64 mmol) was stirred thoroughly at room temperature for 18 h, and was evaporated at reduced pressure. The resulting solid residue was diluted with H_2O (3 mL) and alkalinized with 10% aqueous Na_2CO_3 (2 mL). The alkaline solution was extracted with $CHCl_3$/MeOH 9:1 (4 × 25 mL) and the combined organic extracts were dried over anhydrous Na_2SO_4, and evaporated at reduced pressure to give amide **5a** (115 mg, 41% overall yield from **6**, 80% total overall yield of **5a**) as a yellowish solid; R_f 0.65 (CH_2Cl_2/MeOH/50% aq. NH_4OH 9:1:0.05).

A solution of amide **5a** (95 mg, 0.16 mmol) in MeOH (5 mL) was filtered through a 0.45 μm PTFE filter and treated with a methanolic solution of HCl (0.53 N, 2.6 mL, 1.38 mmol). The resulting solution was evaporated at reduced pressure and the solid was washed with pentane to give, after drying under standard conditions, **5a**·2HCl (95 mg) as a yellowish solid: mp 295–297 °C (MeOH); IR (ATR) *ν* 3500–2500 (max at 3315, 3231, 3084, 3034, 2941, 2865, 2772, N–H, $^+$N–H, C–H st), 1643, 1632, 1578, 1553, 1514 (C=O, Ar–C–C, Ar–C–N st) cm^{-1}; ^{1}H NMR (500 MHz, CD_3OD) *δ* 1.94–2.02 (complex signal, 4H, 2″-H_2, 3″-H_2), superimposed in part 2.00 (tt, *J*=*J*′ = 6.0 Hz, 2H, 3-H_2), 2,20 (tt, *J*=*J*′ = 6.5 Hz, 2H, 2'-H_2), 2.76 (t, *J* = 6.0 Hz, 2H, 4-H_2), superimposed in part 2.78 (m, 2H, 1″-H_2), 2.99 (t, *J* = 6.5 Hz, 2H, 4″-H_2), 3.61 (t, *J* = 6.5 Hz, 2H, 1′-H_2), 3.73 (t, *J* = 6.0 Hz, 2H, 2-H_2), 4.13 (t, *J* = 6.5 Hz, 2H, 3′-H_2), 4.85 (s, NH, $^+$NH), 7.47 (dd, *J* = 9.0 Hz, *J*′ = 2.0 Hz, 1H, 7″-H), 7.64 (d, *J* = 2.0 Hz, 1H, 5″-H), 7.65 (dm, *J* = 9.0 Hz, 2H) and 7.68 (dm, *J* = 9.0 Hz, 2H) [2(6)-H and 3(5)-H 4-chlorophenyl], 7.85 (d, *J* = 8.5 Hz, 1H, 7-H), 8.20 (dd, *J* = 8.5 Hz, *J*′ = 1.5 Hz, 1H, 8-H), 8.41 (d, *J* = 9.0 Hz, 1H, 8″-H), 8.96 (d, *J* = 1.5 Hz, 1H, 10-H); ^{13}C NMR (125.8 MHz, CD_3OD) *δ* 20.0 (CH_2, C3), 21.7 (CH_2, C3″), 22.9 (CH_2, C2″), 24.9 (CH_2, C1″), 25.0 (CH_2, C4), 29.4 (CH_2, C4″), 31.1 (CH_2, C2′), 37.9 (CH_2, C1′), 43.0 (CH_2, C2), 46.3 (CH_2, C3′), 110.0 (C, C4a), 113.7 (C, C9a″), 115.5 (C, C8a″), 116.1 (C, C10a) 119.0 (CH, C5″), 121.0 (CH, C7), 123.8 (CH, C10), 126.7 (CH, C7″), 128.7 (CH, C8″), 130.5 (2CH) and 131.8 (2CH) [C2(6) and C3(5) 4-chlorophenyl], 132.3 (C, C1 4-chlorophenyl), 132.5 (CH, C8), 132.8 (C, C9), 138.3 (C, C4 4-chlorophenyl), 139.9 (C, C6″), 140.3 (C, C6a), 140.4 (C, C10a″), 151.6 (C, C5), 152.3 (C, C4a″), 155.8 (C, C10b), 158.2 (C, C9″), 168.2 (C, CONH); HRMS (ESI), calcd for [$C_{35}H_{33}^{35}Cl_2N_5O$ + H^+] 610.2135, found 610.2129; Anal. $C_{35}H_{33}Cl_2N_5O \cdot 2HCl \cdot 1.5H_2O$ (C, H, N).

4.1.3. *N*-{4-[(6-chloro-1,2,3,4-tetrahydroacridin-9-yl)amino]butyl}-5-(4-chlorophenyl)-1,2,3,4-tetrahydrobenzo[h][1,6]naphthyridine-9-carboxamide **5b**

It was prepared as described for **5a**. Starting from crude tetrahydrobenzo[*h*][1,6]naphthyridinecarboxylic acid (570 mg) and amine **7b** (401 mg, 1.32 mmol), a semisolid residue (2.54 g) was obtained and purified by column chromatography (35–70 μm silica gel, CH_2Cl_2/MeOH/50% aq. NH_4OH mixtures, gradient elution). On elution with CH_2Cl_2/MeOH/50% aq. NH_4OH 99:1:0.2, N^1-Boc-protected amide (307 mg, 48% overall yield from **6**) and a 1:1 mixture of this amide with starting amine **7b** (^{1}H NMR) (234 mg, 18% overall yield of the protected amide from **6**; 66% total overall yield of protected amide from **6**) were successively isolated.

Treatment of the N^1-Boc-protected amide (272 mg, 0.38 mmol) with 4 M HCl/dioxane (2.51 mL, 10.0 mmol) as described for **5a** afforded amide **5b** (237 mg, 66% overall yield from **6**) as a yellowish solid; R_f 0.67 (CH_2Cl_2/MeOH/50% aq. NH_4OH 9:1:0.05).

A solution of amide **5b** (237 mg, 0.38 mmol) in CH_2Cl_2 (10 mL) was filtered through a 0.45 μm PTFE filter and treated with a methanolic solution of HCl (0.53 N, 6.3 mL, 3.34 mmol). The resulting solution was evaporated at reduced pressure and the solid was washed with pentane to give, after drying under standard conditions, **5b**·2HCl (285 mg) as a yellowish solid: mp 276–279 °C (CH_2Cl_2/MeOH 5:3); IR (ATR) *ν* 3500–2500 (max. at 3226, 3062, 3028, 2937, 2871, 2803, N–H, $^+$N–H, C–H st), 1651, 1632, 1586, 1573, 1538 (C=O, Ar–C–C, Ar–C–N st) cm^{-1}; ^{1}H NMR (500 MHz, CD_3OD) *δ* 1.84 (tt, *J*=*J*′ = 7.0 Hz, 2H, 2′-H_2), 1.92–2.03 (complex signal, 8H, 3-H_2, 3′-H_2, 2″-H_2 and 3″-H_2), 2.71 (t, *J* = 6.0 Hz, 2H, 1″-H_2), 2.76 (t, *J* = 6.0 Hz, 2H, 4-H_2), 2.98 (t, *J* = 6.0 Hz, 2H, 4″-H_2), 3.52 (t, *J* = 7.0 Hz, 2H, 1′-H_2), 3.72 (t, *J* = 6.0 Hz, 2H, 2-H_2), 4.05 (t, *J* = 7.0 Hz, 2H, 4′-H_2), 4.85 (s, NH, $^+$NH), 7.50 (dd, *J* = 9.5 Hz,

J' = 2.5 Hz, 1H, 7″-H), 7.66–7.70 [complex signal, 5H, 2(6)-H and 3(5)-H 4-chlorophenyl, and 5″-H], 7.84 (d, J = 9.0 Hz, 1H, 7-H), 8.22 (dd, J = 9.0 Hz, J' = 2.0 Hz, 1H, 8-H), 8.40 (d, J = 9.5 Hz, 1H, 8″-H), 8.98 (d, J = 2.0 Hz, 1H, 10-H); ^{13}C NMR (125.8 MHz, CD_3OD) δ 20.0 (CH_2, C3), 21.7 (CH_2, C3″), 22.9 (CH_2, C2″), 24.7 (CH_2, C1″), 25.0 (CH_2, C4), 27.3 (CH_2) and 28.7 (CH_2) (C2', C3'), 29.3 (CH_2, C4″), 40.7 (CH_2, C1'), 43.0 (CH_2, C2), 48.8 (CH_2, C4'), 109.9 (C, C4a), 113.6 (C, C9a″), 115.5 (C, C8a″), 116.2 (C, C10a), 119.0 (CH, C5"), 120.9 (CH, C7), 123.7 (CH, C10), 126.8 (CH, C7″), 128.9 (CH, C8″), 130.4 (2CH) and 131.8 (2CH) [C2(6) and C3(5) 4-chlorophenyl], 132.3 (C, C1 4-chlorophenyl), 132.5 (CH, C8), 133.2 (C, C9), 138.3 (C, C4 4-chlorophenyl), 140.0 (C, C6"), 140.3 (C, C6a), 140.5 (C, C10a"), 151.6 (C, C5), 152.1 (C, C4a"), 155.7 (C, C10b), 157.9 (C, C9"), 167.9 (C, CONH); HRMS (ESI), calcd for [$C_{36}H^{35}_{35}Cl_2N_5O$+$H^+$] 624.2291, found 624.2274; Anal. $C_{36}H_{35}Cl_2N_5O\cdot 2HCl\cdot 1.5H_2O$ (C, H, N).

4.1.4. *N-{5-[(6-chloro-1,2,3,4-tetrahydroacridin-9-yl)amino] pentyl}-5-(4-chlorophenyl)-1,2,3,4-tetrahydrobenzo[h][1,6] naphthyridine-9-carboxamide* ***5c***

It was prepared as described for **5a**. Starting from crude tetrahydrobenzo[*h*][1,6]naphthyridinecarboxylic acid (190 mg) and amine **7c** (141 mg, 0.44 mmol), a semisolid residue (1.34 g) was obtained and purified by column chromatography (35–70 μm silica gel, CH_2Cl_2/MeOH/50% aq. NH_4OH mixtures, gradient elution). On elution with CH_2Cl_2/MeOH/50% aq. NH_4OH 99.2:0.8:0.2 to 99:1:0.2, impure N^1-Boc-protected amide (51 mg) and deprotected amide **5c** (65 mg, 34% overall yield from **6**) were successively isolated as yellowish solids; R_f 0.71 (CH_2Cl_2/MeOH/50% aq. NH_4OH 9:1:0.05).

A solution of amide **5c** (65 mg, 0.10 mmol) in CH_2Cl_2 (10 mL) was filtered through a 0.45 μm PTFE filter and treated with a methanolic solution of HCl (0.53 N, 1.6 mL, 0.85 mmol). The resulting solution was evaporated at reduced pressure and the solid was washed with pentane to give, after drying under standard conditions, **5c**·2HCl (32 mg) as a yellowish solid: mp 207–208 °C (CH_2Cl_2/MeOH 20:3); IR (ATR) ν 3500–2500 (max. at 3376, 3062, 2927, 2860, N–H, $^+$N–H, C–H st), 1625, 1614, 1587, 1541, 1519 (C=O, Ar–C–C, Ar–C–N st) cm^{-1}; ^{1}H NMR (500 MHz, CD_3OD) δ 1.30 (m, 2H, 3'-H_2), 1.58 (tt, $J \approx J' \approx$ 6.5 Hz, 2H, 2'-H_2), 1.77 (m, 2H, 4'-H_2), 1.90–2.02 (complex signal, 4H, 2"-H_2, 3"-H_2), superimposed in part 1.99 (tt, $J \approx J' \approx$ 5.0 Hz, 2H, 3-H_2), 2.69 (m, 2H, 1"-H_2), 2.76 (t, J = 6.0 Hz, 2H, 4-H_2), 2.98 (m, 2H, 4"-H_2), 3.49 (td, J = 7.0 Hz, J' = 6.5 Hz, 2H, 1'-H_2), 3.72 (t, J = 5.0 Hz, 2H, 2-H_2), 3.98 (t, J = 7.0 Hz, 2H, 5'-H_2), 4.84 (s, NH, $^+$NH), 7.50 (br d, $J \approx$ 9.0 Hz, 1H, 7"-H), 7.66–7.72 [complex signal, 4H, 2(6)-H and 3(5)-H 4-chlorophenyl], 7.73 (d, J = 1.5 Hz, 1H, 5"-H), 7.86 (d, J = 9.0 Hz, 1H, 7-H), 8.24 (d, J = 9.0 Hz, 1H, 8-H), 8.39 (d, J = 9.0 Hz, 1H, 8"-H), 8.66 (m, 1H, CONH), 9.02 (br s, 1H, 10-H); ^{13}C NMR (125.8 MHz, CD_3OD) δ 20.0 (CH_2, C3), 21.7 (CH_2, C3"), 22.9 (CH_2, C2"), 24.9 (CH_2, C1"), 25.0 (CH_2, C4), 25.6 (CH_2, C3'), 29.4 (CH_2, C4"), 29.9 (CH_2) and 30.9 (CH_2) (C2', C4'), 40.8 (CH_2, C1'), 43.0 (CH_2, C2), 49.0 (CH_2, C5'), 109.8 (C, C4a), 113.4 (C, C9a"), 115.5 (C, C8a"), 116.1 (C, C10a), 119.0 (CH, C5"), 120.9 (CH, C7), 123.6 (CH, C10), 126.8 (CH, C7"), 128.7 (CH, C8"), 130.4 (2CH) and 131.9 (2CH) [C2(6) and C3(5) 4-chlorophenyl], 132.3 (C, C1 4-chlorophenyl), 132.7 (CH, C8), 133.3 (C, C9), 138.3 (C, C4 4-chlorophenyl), 140.0 (C, C6"), 140.2 (C, C6a), 140.4 (C, C10a"), 151.5 (C, C5), 152.2 (C, C4a"), 155.7 (C, C10b), 157.8 (C, C9"), 167.9 (C, CONH), an extra peak at 40.1 ppm was observed; HRMS (ESI), calcd for [$C_{37}H^{35}_{37}Cl_2N_5O + H^+$] 638.2448, found 638.2435; Anal. $C_{37}H_{37}Cl_2N_5O\cdot 2HCl\cdot 3H_2O$ (C, H, N).

4.1.5. *N-{8-[(6-chloro-1,2,3,4-tetrahydroacridin-9-yl)amino]octyl}-5-(4-chlorophenyl)-1,2,3,4-tetrahydrobenzo[h][1,6]naphthyridine-9-carboxamide* ***5d***

It was prepared as described for **5a**. Starting from crude tetrahydrobenzo[*h*][1,6]naphthyridinecarboxylic acid (480 mg) and amine **7d** (400 mg, 1.11 mmol), a semisolid residue (2.45 g) was obtained and purified by column chromatography (35–70 μm silica gel, CH_2Cl_2/MeOH/50% aq. NH_4OH mixtures, gradient elution). On elution with CH_2Cl_2/MeOH/50% aq. NH_4OH 100:0:1, N^1-Boc-protected amide (370 mg, 63% overall yield from **6**) was isolated as a yellowish solid.

Treatment of the N^1-Boc-protected amide (370 mg, 0.47 mmol) with 4 M HCl/dioxane (3.10 mL, 12.4 mmol) as described for **5a** afforded amide **5d** (359 mg, 63% overall yield from **6**) as a yellowish solid; R_f 0.78 (CH_2Cl_2/MeOH/50% aq. NH_4OH 9:1:0.05).

A solution of amide **5d** (359 mg, 0.53 mmol) in CH_2Cl_2 (10 mL) was filtered through a 0.45 μm PTFE filter and treated with a methanolic solution of HCl (0.53 N, 8.73 mL, 4.63 mmol). The resulting solution was evaporated at reduced pressure and the solid was washed with pentane to give, after drying under standard conditions, **5d**·2HCl (283 mg) as a yellowish solid: mp 203–204 °C (CH_2Cl_2/MeOH 5:4); IR (ATR) ν 3500–2500 (max. at 3228, 3039, 2929, 2860, N–H, $^+$N–H, C–H st), 1731, 1631, 1573 (C=O, Ar–C–C, Ar–C–N st) cm^{-1}; ^{1}H NMR (500 MHz, CD_3OD) δ 1.38–1.50 (complex signal, 8H, 3'-H_2, 4'-H_2, 5'-H_2, 6'-H_2), 1.69 (tt, J=J' = 7.5 Hz, 2H, 2'-H_2), 1.85 (tt, $J \approx J' \approx$ 7.5 Hz, 2H, 7'-H_2), 1.92–2.00 (complex signal, 6H, 3-H_2, 2"-H_2, 3"-H_2), 2.68 (t, J = 6.0 Hz, 2H, 1"-H_2), 2.75 (t, J = 6.5 Hz, 2H, 4-H_2), 3.01 (t, J = 6.0 Hz, 2H, 4"-H_2), 3.43 (t, J = 7.5 Hz, 2H, 1'-H_2), 3.71 (t, J = 6.0 Hz, 2H, 2-H_2), 3.95 (t, J = 7.5 Hz, 2H, 8'-H_2), 4.85 (s, NH, $^+$NH), 7.55 (dd, J = 9.5 Hz, J' = 2.0 Hz, 1H, 7"-H), 7.67 [complex signal, 4H, 2(6)-H and 3(5)-H 4-chlorophenyl], 7.78 (d, J = 2.0 Hz, 1H, 5"-H), 7.87 (d, J = 9.0 Hz, 1H, 7-H), 8.25 (dd, J = 9.0 Hz, J' = 2.0 Hz, 1H, 8-H), 8.38 (d, J = 9.5 Hz, 1H, 8"-H), 8.99 (d, $J \approx$ 2.0 Hz, 1H, 10-H); ^{13}C NMR (125.8 MHz, CD_3OD) δ 20.0 (CH_2, C3), 21.8 (CH_2, C3"), 22.9 (CH_2, C2"), 24.8 (CH_2, C1"), 25.0 (CH_2, C4), 27.6 (CH_2, C6'), 28.0 (CH_2, C3'), 29.3 (CH_2, C4"), 30.1 (CH_2) and 30.2 (CH_2) (C4', C5'), 30.4 (CH_2, C2'), 31.3 (CH_2, C7'), 41.3 (CH_2, C1'), 43.0 (CH_2, C2), 49.2 (CH_2, C8'), 109.8 (C, C4a), 113.3 (C, C9a"), 115.4 (C, C8a"), 116.1 (C, C10a), 119.1 (CH, C5"), 120.9 (CH, C7), 123.6 (CH, C10), 126.7 (CH, C7"), 128.8 (CH, C8"), 130.4 (2CH) and 131.9 (2CH) [C2(6) and C3(5) 4-chlorophenyl], 132.2 (C, C1 4-chlorophenyl), 132.6 (CH, C8), 133.5 (C, C9), 138.3 (C, C4 4-chlorophenyl), 140.1 (C, C6"), 140.2 (C, C6a), 140.5 (C, C10a"), 151.4 (C, C5), 152.1 (C, C4a"), 155.7 (C, C10b), 157.8 (C, C9"), 167.9 (C, CONH); HRMS (ESI), calcd for [$C_{40}H^{35}_{43}Cl_2N_5O$ + H^+] 680.2917, found 680.2900; Anal. $C_{40}H_{43}Cl_2N_5O\cdot 2HCl\cdot 2.5H_2O$ (C, H, N).

4.2. Biological assays

4.2.1. *Determination of AChE and BChE inhibitory activities*

The inhibitory activities against human recombinant AChE (Sigma–Aldrich) and human serum BChE (Sigma–Aldrich) were evaluated spectrophotometrically by the method of Ellman et al. [15]. The reactions took place in a final volume of 300 μL of 0.1 M phosphate-buffered solution pH 8.0, containing hAChE (0.02 u/mL) or hBChE (0.02 u/mL) and 333 μM 5,5'-dithiobis(2-nitrobenzoic) acid (DTNB; Sigma–Aldrich) solution used to produce the yellow anion of 5-thio-2-nitrobenzoic acid. Inhibition curves were performed in duplicates using at least 10 increasing concentrations of inhibitors and preincubated for 20 min at 37 °C before adding the substrate [32]. One duplicate sample without inhibitor was always present to yield 100% of AChE or BChE activities. Then substrates, acetylthiocholine iodide (450 μM; Sigma–Aldrich) or butyrylthiocholine iodide (300 μM; Sigma–Aldrich), were added and the reaction was developed for 5 min at 37 °C. The colour production was measured at 414 nm using a labsystems Multiskan spectrophotometer.

Data from concentration–inhibition experiments of the inhibitors were calculated by non-linear regression analysis, using the GraphPad Prism program package (GraphPad Software; San

Diego, USA), which gave estimates of the IC_{50} (concentration of drug producing 50% of enzyme activity inhibition). Results are expressed as mean ± S.E.M. of at least 4 experiments performed in duplicate.

4.2.2. Determination of Aβ42 and tau aggregation inhibitory activities in intact E. coli cells

Cloning and overexpression of Aβ42 peptide: *E. coli* competent cells BL21 (DE3) were transformed with the pET28a vector (Novagen, Inc., Madison, WI, USA) carrying the DNA sequence of Aβ42. Because of the addition of the initiation codon ATG in front of both genes, the overexpressed peptide contains an additional methionine residue at its N terminus. For overnight culture preparation, 10 mL of lysogeny broth (LB) medium containing 50 μg mL^{-1} of kanamycin were inoculated with a colony of BL21 (DE3) bearing the plasmid to be expressed at 37 °C. After overnight growth, the OD600 was usually 2–2.5. For expression of Aβ42 peptide, 20 μL of overnight culture were transferred into eppendorf tubes of 1.5 mL containing 960 μL of LB medium with 50 μg mL^{-1} of kanamycin, 1 mM of isopropyl 1-thio-β-D-galactopyranoside (IPTG), 10 μL of a 10 μM solution of each hybrid **5** or reference compound in DMSO, and 10 μL of a 25 μM solution of Th–S in water. The samples were grown for 24 h at 37 °C and 1400 rpm using a Thermomixer (Eppendorf, Hamburg, Germany). In the negative control (without drug) the same amount of DMSO was added in the sample.

Cloning and overexpression of tau protein: *E. coli* BL21 (DE3) competent cells were transformed with pTARA containing the RNA-polymerase gen of T7 phage (T7RP) under the control of the promoter pBAD. *E. coli* BL21 (DE3) with pTARA competent cells were transformed with pRKT42 vector encoding four repeats of tau protein in two inserts. For overnight culture preparation, 10 mL of M9 medium containing 0.5% of glucose, 50 μg mL^{-1} of ampicillin and 12.5 μg mL^{-1} of chloramphenicol were inoculated with a colony of BL21 (DE3) bearing the plasmids to be expressed at 37 °C. After overnight growth, the OD600 was usually 2–2.5. For expression of tau protein, 20 μL of overnight culture were transferred into eppendorf tubes of 1.5 mL containing 970 μL of M9 medium containing 0.25% of arabinose, 0.5% of glucose, 50 μg mL^{-1} of ampicillin and 12.5 μg mL^{-1} of chloramphenicol, 10 μL of a 10 μM solution of each hybrid **5** or reference compound in DMSO, and 10 μL of a 25 μM solution of Th–S in water. The samples were grown for 24 h at 37 °C and 1400 rpm using a Thermomixer (Eppendorf, Hamburg, Germany). In the negative control (without drug) the same amount of DMSO was added in the sample.

Th–S steady-state fluorescence: Th–S (T1892) and other chemical reagents were purchased from Sigma (St. Louis, MO). Th–S stock solution (2.5 mM) was prepared in double-distilled water purified through a Milli-Q system (Millipore, USA). Fluorescent spectral scans of Th–S were analyzed using an Aminco Bowman Series 2 luminescence spectrophotometer (Aminco-Bowman AB2, SLM Aminco, Rochester, NY, USA). Excitation and emission slit widths of 4 nm were used. Finally, the fluorescence emission at 455 nm, when exciting at 375 nm, was recorded. In order to normalize the Th–S fluorescence as a function of the bacterial concentration, OD_{600} was obtained using a Shimadzu UV-2401 PC UV–Vis spectrophotometer (Shimadzu, Japan). The final fluorescence data were obtained considering as 100% the Th–S fluorescence of the bacterial cells expressing the peptide or protein in the absence of drug and 0% the Th–S fluorescence of the bacterial cells non-expressing the peptide or protein. Final data are the average of ten independent experiments.

4.2.3. PAMPA-BBB assay

To evaluate the brain penetration of hybrids **5**, a parallel artificial membrane permeation assay for blood–brain barrier was used, following the method described by Di et al. [28]. The *in vitro* permeability (P_e) of fourteen commercial drugs through lipid extract of porcine brain membrane together with the test compounds was determined. Commercial drugs and the synthesized compounds were tested using a mixture PBS:EtOH 70:30. Assay validation was made by comparing the experimental permeability of the different compounds with the reported bibliography values of the commercial drugs, which showed a good correlation: P_e (exp) = 1.5010 P_e (lit) − 0.8618 (R^2 = 0.9199). From this equation and taking into account the limits established by Di et al. for BBB permeation, we established the ranges of permeability as compounds of high BBB permeation (CNS+): P_e (10^{-6} cm s^{-1}) > 5.1; compounds of low BBB permeation (CNS−): P_e (10^{-6} cm s^{-1}) < 2.1, and compounds of uncertain BBB permeation (CNS ±): 5.1 > P_e (10^{-6} cm s^{-1}) > 2.1.

4.3. Molecular modelling

4.3.1. Setup of the system

Molecular modelling was performed using the X-ray crystallographic structure of hAChE in complex with huprine W (PDB ID: 4BDT [15]). The structure was refined by removal of *N*-acetyl-D-glucosamine and sulphate anions and addition of missing hydrogen atoms. The enzyme was modelled in its physiological active form with neutral His447 and deprotonated Glu334, which together with Ser203 form the catalytic triad. The ionization state for the rest of ionizable residues was assessed from PROPKA3 [33] calculations. Accordingly, the standard ionization state at neutral pH was considered but for residues Glu285, Glu450 and Glu452, which were protonated. Finally, three disulfide bridges were defined between Cys residues 257–272, 529–409, and 69–96, respectively.

4.3.2. Molecular dynamics simulations

The binding mode of hybrid **5a** to hAChE was explored by means of MD simulations. Starting from that proposed initial pose, a 100 ns MD simulation was performed using the PMEMD module of AMBER12 [34] software package, the parm99SB [35] force field for the protein and the GAFF-derived parameters [36] for the ligand, whose geometrical parameters were optimized at the B3LYP/6-31G(d) level [37] and its charge distribution was described by using electrostatic potential charges with the RESP procedure [38]. Na^+ cations were added to neutralize the negative charge of the system with the XLEAP module of AMBER12. The system was immersed in an octahedral box of TIP3P [39] water molecules, preserving the crystallographic waters inside the binding cavity. The final system contained around 52,000 atoms.

The geometry of the system was minimized in four steps. First, water molecules and counterions were refined through 7000 steps of conjugate gradient and 3000 steps of steepest descent algorithm. Then, the position of hydrogen atoms was optimized using 4500 steps of conjugate gradient and 500 steps of steepest descent algorithm. At the third stage, hydrogen atoms, water molecules and counterions were further optimized using 11500 steps of conjugate gradient and 2500 steps of steepest descent algorithm. Thermalization of the system was performed in five steps of 25 ps, increasing the temperature from 50 to 298 K. Concomitantly, the residues that define the binding site were restrained during thermalization using a variable restraining force. Thus, a force constant of 25 kcal mol^{-1} $Å^{-2}$ was used in the first stage of the thermalization and was subsequently decreased by increments of 5 kcal mol^{-1} $Å^{-2}$ in the next stages. Then, an additional step of 250 ps was performed in order to equilibrate the system density at constant pressure (1 bar) and temperature (298 K). Finally, a 100 ns trajectory was run using a time step of 2 fs. SHAKE was used for those bonds containing hydrogen atoms in conjunction with periodic boundary

conditions at constant volume and temperature, particle mesh Ewald for the treatment of long electrostatic interactions, and a cutoff of 10 Å for nonbonded interactions. Moreover, in the initial 20 ns of the simulation the distance between the protonated nitrogen in the 6-chlorotacrine moiety of the inhibitor and the carbonyl oxygen of His447 was constrained to avoid artefactual rearrangements in the CAS of the enzyme.

The structural analysis was performed using in-house software and standard codes of AMBER12. The solvent interaction energies (SIE) technique developed by Purisima and co-workers [19] was used to estimate the interaction free energies for the AChE inhibitor. Calculations were performed for a set of 200 snapshots taken along the last 40 ns of the MD trajectory.

Acknowledgements

This work was supported by Ministerio de Ciencia e Innovación (MICINN) (CTQ2011-22433, CTQ2012-30930, SAF2011-27642, SAF2009-10553, start-up grant of the Ramón y Cajal program for R.S.), Generalitat de Catalunya (GC) (2009SGR1396, 2009SGR1024, 2009SGR249), and Xarxa de Recerca en Química Teòrica i Computacional (XRQTC). Fellowships from GC to O.D.P. and F.J.P.A., a contract from the Ramón y Cajal program of MICINN to R.S., a contract from the Juan de la Cierva program of Ministerio de Economía y Competitividad to A.E., and the ICREA Academia support to F.J.L. are gratefully acknowledged. The Center for Scientific and Academic Services of Catalonia (CESCA) is acknowledged for providing access to computational facilities. We are grateful to Dr. Marc Revés and Dr. F. Spyrakis for their technical assistance in the HPLC purity measurements and in predicting safety data, respectively.

Appendix A. Supplementary data

Supplementary data related to this article can be found at http://dx.doi.org/10.1016/j.ejmech.2014.07.021.

References

[1] Alzheimer's Association, Alzheimer's disease facts and figures, Alzheimers Dement. 9 (2013) 208–245.
[2] R.E. Becker, N.H. Greig, E. Giacobini, L.S. Schneider, L. Ferruci, A new roadmap for drug development for Alzheimer's disease, Nat. Rev. Drug. Discov. 13 (2014) 156.
[3] S.W. Pimplikar, Reassessing the amyloid cascade hypothesis of Alzheimer's disease, Int. J. Biochem. Cell. Biol. 41 (2009) 1261–1268.
[4] (a) Y. Bansal, O. Silakari, Multifunctional compounds: smart molecules for multifactorial diseases, Eur. J. Med. Chem. 76 (2014) 31–42;
(b) W.J. Geldenhuys, C.J. Van der Schyf, Rationally designed multi-targeted agents against neurodegenerative diseases, Curr. Med. Chem. 20 (2013) 1662–1672;
(c) X. Chen, M. Decker, Multi-target compounds acting in the central nervous system designed from natural products, Curr. Med. Chem. 20 (2013) 1673–1685;
(d) P. Russo, A. Frustaci, A. Del Bufalo, M. Fini, A. Cesario, Multitarget drugs of plants origin acting on Alzheimer's disease, Curr. Med. Chem. 20 (2013) 1686–1693;
(e) A. Rampa, F. Belluti, S. Gobbi, A. Bisi, Hybrid-based multi-target ligands for the treatment of Alzheimer's disease, Curr. Top. Med. Chem. 11 (2011) 2716–2730;
(f) A. Cavalli, M.L. Bolognesi, A. Minarini, M. Rosini, V. Tumiatti, M. Recanatini, C. Melchiorre, Multi-target-directed ligands to combat neurodegenerative diseases, J. Med. Chem. 51 (2008) 347–372.
[5] A. Mullard, Sting of Alzheimer's failures offset by upcoming prevention trials, Nat. Rev. Drug. Discov. 11 (2012) 657–660.
[6] C.R. Jack Jr., D.M. Holtzman, Biomarker modeling of Alzheimer's disease, Neuron 80 (2013) 1347–1358.
[7] (a) N.C. Inestrosa, A. Alvarez, C.A. Pérez, R.D. Moreno, M. Vicente, C. Linker, O.I. Casanueva, C. Soto, J. Garrido, Acetylcholinesterase accelerates assembly of amyloid-β-peptides into Alzheimer's fibrils: possible role of the peripheral site of the enzyme, Neuron 16 (1996) 881–891;
(b) N.C. Inestrosa, M.C. Dinamarca, A. Alvarez, Amyloid-cholinesterase interactions. Implications for Alzheimer's disease, FEBS J. 275 (2008) 625–632;
(c) G.V. De Ferrari, M.A. Canales, I. Shin, L.M. Weiner, I. Silman, N.C. Inestrosa, A structural motif of acetylcholinesterase that promotes amyloid beta-peptide fibril formation, Biochemistry 40 (2001) 10447–10457.
[8] J.L. Sussman, M. Harel, F. Frolow, C. Oefner, A. Goldman, L. Toker, I. Silman, Atomic structure of acetylcholinesterase from Torpedo californica – a prototypic acetylcholine-binding protein, Science 253 (1991) 872–879.
[9] P. Camps, X. Formosa, C. Galdeano, D. Muñoz-Torrero, L. Ramírez, E. Gómez, N. Isambert, R. Lavilla, A. Badia, M.V. Clos, M. Bartolini, F. Mancini, V. Andrisano, M.P. Arce, M.I. Rodríguez-Franco, O. Huertas, T. Dafni, F.J. Luque, Pyrano[3,2-*c*]quinoline-6-chlorotacrine hybrids as a novel family of acetylcholinesterase- and β-amyloid-directed anti-Alzheimer compounds, J. Med. Chem. 52 (2009) 5365–5379.
[10] O. Di Pietro, E. Viayna, E. Vicente-García, M. Bartolini, R. Ramón, J. Juárez-Jiménez, M.V. Clos, B. Pérez, V. Andrisano, F.J. Luque, R. Lavilla, D. Muñoz-Torrero, 1,2,3,4-Tetrahydrobenzo[*h*][1,6]naphthyridines as a new family of potent peripheral-to-midgorge-site inhibitors of acetylcholinesterase: synthesis, pharmacological evaluation and mechanistic studies, Eur. J. Med. Chem. 73 (2014) 141–152.
[11] M. Harel, I. Schalk, L. Ehret-Sabatier, F. Bouet, M. Goeldner, C. Hirth, P.H. Axelsen, I. Silman, J.L. Sussman, Quaternary ligand binding to aromatic residues in the active-site gorge of acetylcholinesterase, Proc. Natl. Acad. Sci. USA 90 (1993) 9031–9035.
[12] E. Vicente-García, F. Catti, R. Ramón, R. Lavilla, Unsaturated lactams: new inputs for Povarov-type multicomponent reactions, Org. Lett. 12 (2010) 860–863.
[13] E. Vicente-García, R. Ramón, S. Preciado, R. Lavilla, Multicomponent reaction access to complex quinolines via oxidation of the Povarov adducts, Beilstein J. Org. Chem. 7 (2011) 980–987.
[14] (a) P. Muñoz-Ruiz, L. Rubio, E. García-Palomero, I. Dorronsoro, M. del Monte-Millán, R. Valenzuela, P. Usán, C. de Austria, M. Bartolini, V. Andrisano, A. Bidon-Chanal, M. Orozco, F.J. Luque, M. Medina, A. Martínez, Design, synthesis, and biological evaluation of dual binding site acetylcholinesterase inhibitors: new disease-modifying agents for Alzheimer's disease, J. Med. Chem. 48 (2005) 7223–7233;
(b) P.R. Carlier, Y.F. Han, E.S.-H. Chow, C.P.-L. Li, H. Wang, T.X. Lieu, H.S. Wong, Y.-P. Pang, Evaluation of short-tether bis-THA AChE inhibitors. A further test of the dual binding site hypothesis, Bioorg. Med. Chem. 7 (1999) 351–357;
(c) M. Rosini, V. Andrisano, M. Bartolini, M.L. Bolognesi, P. Hrelia, A. Minarini, A. Tarozzi, C. Melchiorre, Rational approach to discover multipotent anti-Alzheimer drugs, J. Med. Chem. 48 (2005) 360–363.
[15] G.L. Ellman, K.D. Courtney, V. Andres Jr., R.M. Featherstone, A new and rapid colorimetric determination of acetylcholinesterase activity, Biochem. Pharmacol. 7 (1961) 88–95.
[16] (a) W.G. Lewis, L.G. Green, F. Grynszpan, Z. Radić, P.R. Carlier, P. Taylor, M.G. Finn, K.B. Sharpless, Click chemistry in situ: acetylcholinesterase as a reaction vessel for the selective assembly of a femtomolar inhibitor from an array of building blocks, Angew. Chem. Int. Ed. 41 (2002) 1053–1057;
(b) P. Camps, B. Cusack, W.D. Mallender, R. El Achab, J. Morral, D. Muñoz-Torrero, T.L. Rosenberry, Huprine X is a novel high-affinity inhibitor of acetylcholinesterase that is of interest for the treatment of Alzheimer's disease, Mol. Pharmacol. 57 (2000) 409–417.
[17] F. Nachon, E. Carletti, C. Ronco, M. Trovaslet, Y. Nicolet, L. Jean, P.-Y. Renard, Crystal structures of human cholinesterases in complex with huprine W and tacrine: elements of specificity for anti-Alzheimer's drugs targeting acetyl- and butyrylcholinesterase, Biochem. J. 453 (2013) 393–399.
[18] H. Dvir, D.M. Wong, M. Harel, X. Barril, M. Orozco, F.J. Luque, D. Muñoz-Torrero, P. Camps, T.L. Rosenberry, I. Silman, J.L. Sussman, 3D Structure of *Torpedo californica* acetylcholinesterase complexed with huprine X at 2.1 Å resolution: kinetic and molecular dynamics correlates, Biochemistry 41 (2002) 2970–2981.
[19] M. Naïm, S. Bhat, K.N. Rankin, S. Dennis, S.F. Chowdhury, I. Siddiqi, P. Drabik, T. Sulea, C.I. Bayly, A. Jakalian, E.O. Purisima, Solvated interaction energy (SIE) for scoring protein–ligand binding affinities. 1. Exploring the parameter space, J. Chem. Inf. Model 47 (2007) 122–133.
[20] R.M. Lane, S.G. Potkin, A. Enz, Targeting acetylcholinesterase and butyrylcholinesterase in dementia, Int. J. Neuropsychopharmacol. 9 (2006) 101–124.
[21] (a) E. Viayna, R. Sabate, D. Muñoz-Torrero, Dual inhibitors of β-amyloid aggregation and acetylcholinesterase as multi-target anti-Alzheimer drug candidates, Curr. Top. Med. Chem. 13 (2013) 1820–1842;
(b) B. Bulic, M. Pickhardt, B. Schmidt, E.-M. Mandelkow, H. Waldmann, E. Mandelkow, Development of tau aggregation inhibitors for Alzheimer's disease, Angew. Chem. Int. Ed. 48 (2009) 1740–1752.
[22] S. Pouplana, A. Espargaró, C. Galdeano, E. Viayna, I. Sola, S. Ventura, D. Muñoz-Torrero, R. Sabate, Thioflavin-S staining of bacterial inclusion bodies for the fast, simple, and inexpensive screening of amyloid aggregation inhibitors, Curr. Med. Chem. 21 (2014) 1152–1159.
[23] (a) Y. Porat, A. Abramowitz, E. Gazit, Inhibition of amyloid fibril formation by polyphenols: structural similarity and aromatic interactions as a common inhibition mechanism, Chem. Biol. Drug. Des. 67 (2006) 27–37;
(b) H.-Y. Zhang, Same causes, same cures, Biochem. Biophys. Res. Commun. 351 (2006) 578–581.
[24] M. Cui, Past and recent progress of molecular imaging probes for β-amyloid plaques in the brain, Curr. Med. Chem. 21 (2014) 82–112.
[25] K. Lu, Y. Jiang, B. Chen, E.M. Eldemenky, G. Ma, M. Packiarajan, G. Chandrasena, A.D. White, K.A. Jones, B. Li, S.-P. Hong, Strategies to lower the

Pgp efflux liability in a series of potent indole azetidine MCHR1 antagonists, Bioorg. Med. Chem. Lett. 21 (2011) 5310–5314.
[26] (a) C.A. Lipinski, F. Lombardo, B.W. Dominy, P.J. Feeney, Experimental and computational approaches to estimate solubility and permeability in drug discovery and development settings, Adv. Drug. Deliv. Rev. 23 (1997) 3–25;
(b) R. Morphy, Z. Rankovic, Designing multiple ligands – medicinal chemistry strategies and challenges, Curr. Pharm. Des. 15 (2009) 587–600.
[27] (a) E. García-Palomero, P. Muñoz, P. Usan, P. Garcia, C. De Austria, R. Valenzuela, L. Rubio, M. Medina, A. Martínez, Potent β-amyloid Modulators, Neurodegener. Dis. 5 (2008) 153–156;
(b) C. Spuch, D. Antequera, M.I. Fernandez-Bachiller, M.I. Rodríguez-Franco, E. Carro, A new tacrine–melatonin hybrid reduces amyloid burden and behavioral deficits in a mouse model of Alzheimer's disease, Neurotox. Res. 17 (2010) 421–431;
(c) C. Galdeano, E. Viayna, I. Sola, X. Formosa, P. Camps, A. Badia, M.V. Clos, J. Relat, M. Ratia, M. Bartolini, F. Mancini, V. Andrisano, M. Salmona, C. Minguillón, G.C. González-Muñoz, M.I. Rodríguez-Franco, A. Bidon-Chanal, F.J. Luque, D. Muñoz-Torrero, Huprine–tacrine heterodimers as anti-amyloidogenic compounds of potential interest against Alzheimer's and prion diseases, J. Med. Chem. 55 (2012) 661–669;
(d) V. Capurro, P. Busquet, J.P. Lopes, R. Bertorelli, G. Tarozzo, M.L. Bolognesi, D. Piomelli, A. Reggiani, A. Cavalli, Pharmacological characterization of memoquin, a multi-target compound for the treatment of Alzheimer's disease, PLoS One 8 (2013) e56870;
(e) E. Viayna, I. Sola, M. Bartolini, A. De Simone, C. Tapia-Rojas, F.G. Serrano, R. Sabaté, J. Juárez-Jiménez, B. Pérez, F.J. Luque, V. Andrisano, M.V. Clos, N.C. Inestrosa, D. Muñoz-Torrero, Synthesis and multitarget biological profiling of a novel family of rhein derivatives as disease-modifying anti-Alzheimer agents, J. Med. Chem. 57 (2014) 2549–2567.
[28] L. Di, E.H. Kerns, K. Fan, O.J. McConnell, G.T. Carter, High throughput artificial membrane permeability assay for blood-brain barrier, Eur. J. Med. Chem. 38 (2003) 223–232.
[29] X. Li, L. Chen, F. Cheng, Z. Wu, H. Bian, C. Xu, W. Li, G. Li, X. Shen, Y. Tang, In Silico prediction of chemical acute oral toxicity using multi-classification methods, J. Chem. Inf. Model 54 (2014) 1061–1069.
[30] A. Villalobos, T.W. Butler, D.S. Chapin, Y.L. Chen, S.B. DeMattos, J.L. Ives, S.B. Jones, D.R. Liston, A.A. Nagel, 5,7-Dihydro-3-[2-[1-(phenylmethyl)-4-piperidinyl]ethyl]-6*H*-pyrrolo[3,2-*f*]-1,2-benzisoxazol-6-one: a potent and centrally-selective inhibitor of acetylcholinesterase, J. Med. Chem. 38 (1995) 2802–2808.
[31] F. Aguado, A. Badía, J.E. Baños, F. Bosch, C. Bozzo, P. Camps, J. Contreras, M. Dierssen, C. Escolano, D.M. Görbig, D. Muñoz-Torrero, M.D. Pujol, M. Simón, M.T. Vázquez, N.M. Vivas, Synthesis and evaluation of tacrine-related compounds for the treatment of Alzheimer's disease, Eur. J. Med. Chem. 29 (1994) 205–221.
[32] E. Viayna, T. Gómez, C. Galdeano, L. Ramírez, M. Ratia, A. Badia, M.V. Clos, E. Verdaguer, F. Junyent, A. Camins, M. Pallàs, M. Bartolini, F. Mancini, V. Andrisano, M.P. Arce, M.I. Rodríguez-Franco, A. Bidon-Chanal, F.J. Luque, P. Camps, D. Muñoz-Torrero, Novel huprine derivatives with inhibitory activity toward β-amyloid aggregation and formation as disease-modifying anti-Alzheimer drug candidates, ChemMedChem 5 (2010) 1855–1870.
[33] M.H.M. Olsson, C.R. Sondergard, M. Rostkowski, J.H. Jensen, PROPKA3: consistent treatment of internal and surface residues in empirical pKa predictions, J. Chem. Theory Comput. 7 (2011) 525–537.
[34] D.A. Case, T.A. Darden, T.E. Cheatham III, C.L. Simmerling, J. Wang, R.E. Duke, R. Luo, R.C. Walker, W. Zhang, K.M. Merz, B. Roberts, S. Hayik, A. Roitberg, G. Seabra, J. Swails, A.W. Goetz, I. Kolossváry, K.F. Wong, F. Paesani, J. Vanicek, R.M. Wolf, J. Liu, X. Wu, S.R. Brozell, T. Steinbrecher, H. Gohlke, Q. Cai, X. Ye, J. Wang, M.-J. Hsieh, G. Cui, D.R. Roe, D.H. Mathews, M.G. Seetin, R. Salomon-Ferrer, C. Sagui, V. Babin, T. Luchko, S. Gusarov, A. Kovalenko, P.A. Kollman, AMBER 12, University of California, San Francisco, 2012.
[35] V. Hornak, R. Abel, A. Okur, B. Strockbine, A. Roitberg, C. Simmerling, Comparison of multiple Amber force fields and development of improved protein backbone parameters, Proteins 65 (2006) 712–725.
[36] J. Wang, R.M. Wolf, J.W. Caldwell, P.A. Kollman, D.A. Case, Development and testing of a general AMBER force field, J. Comput. Chem. 25 (2004) 1157–1174.
[37] (a) A.D. Becke, Density-functional thermochemistry. III. The role of exact exchange, J. Chem. Phys. 98 (1993) 5648–5652;
(b) C. Lee, W. Yang, R.G. Parr, Development of the Colle-Salvetti correlation-energy formula into a functional of the electron density, Phys. Rev. B 37 (1988) 785–789.
[38] C.I. Bayly, P. Cieplak, W.D. Cornell, P.A. Kollman, A well-behaved electrostatic potential based method using charge restraints for deriving atomic charges, J. Phys. Chem. 97 (1993) 10269–10280.
[39] W.L. Jorgensen, J. Chandrasekhar, J.D. Madura, R.W. Impey, M.L. Klein, Comparison of simple potential functions for simulating liquid water, J. Chem. Phys. 79 (1983) 926–935.

Suppementary material

Tetrahydrobenzo[*h*][1,6]naphthyridine–6-chlorotacrine hybrids as a new family of anti-Alzheimer agents targeting β-amyloid, tau, and cholinesterase pathologies

Ornella Di Pietro[a], F. Javier Pérez-Areales[a], Jordi Juárez-Jiménez,[b] Alba Espargaró[c], M. Victòria Clos[d], Belén Pérez[d], Rodolfo Lavilla[e], Raimon Sabaté[c], F. Javier Luque[b,*], Diego Muñoz-Torrero[a,**]

[a] *Laboratori de Química Farmacèutica (Unitat Associada al CSIC), Facultat de Farmàcia, and Institut de Biomedicina (IBUB), Universitat de Barcelona, Av. Joan XXIII, 27-31, E-08028, Barcelona, Spain*

[b] *Departament de Fisicoquímica, Facultat de Farmàcia (Campus Torribera), and IBUB, Universitat de Barcelona, Prat de la Riba 171, E-08921, Santa Coloma de Gramenet, Spain*

[c] *Departament de Fisicoquímica, Facultat de Farmàcia, and Institut de Nanociència i Nanotecnologia (IN^{2}UB), Universitat de Barcelona, Av. Joan XXIII, 27-31, E-08028, Barcelona, Spain*

[d] *Departament de Farmacologia, de Terapèutica i de Toxicologia, Institut de Neurociències, Universitat Autònoma de Barcelona, E-08193, Bellaterra, Barcelona, Spain*

[e] *Laboratori de Química Orgànica, Facultat de Farmàcia, Universitat de Barcelona, and Barcelona Science Park, Baldiri Reixac 10-12, E-08028, Barcelona, Spain*

Elemental analysis data of hybrids 5a–d

Compound	**Molecular Formula**	**Calculated (%)**			**Found (%)**		
		C	H	N	C	H	N
5a·2HCl·1.5H_2O	$C_{35}H_{33}Cl_2N_5O$·2HCl·1.5H_2O	59.17	5.39	9.86	59.31	5.05	9.57
5b·2HCl·1.5H_2O	$C_{36}H_{35}Cl_2N_5O$·2HCl·1.5H_2O	59.68	5.56	9.67	59.96	5.39	9.43
5c·2HCl·3H_2O	$C_{37}H_{37}Cl_2N_5O$·2HCl·3H_2O	58.05	5.92	9.15	58.11	6.05	8.94
5d·2HCl·2.5H_2O	$C_{40}H_{43}Cl_2N_5O$·2HCl·2.5H_2O	60.15	6.31	8.77	60.51	6.24	8.40

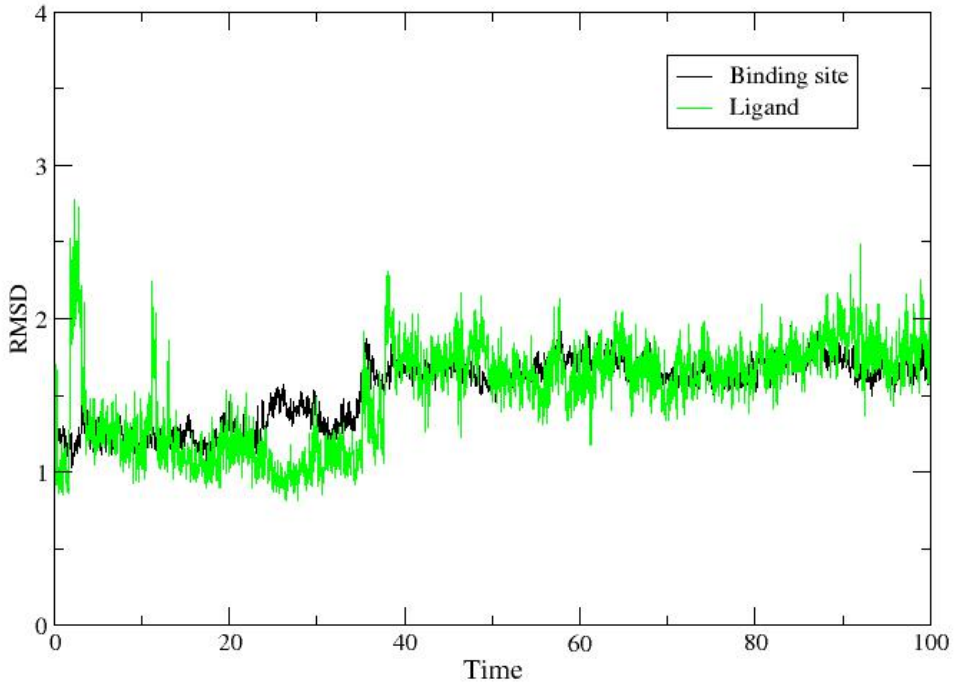

Fig. S1. Time evolution of the root-mean square deviation (RMSD; Å) determined for the heavy atoms of the residues that define the binding site (black) and the ligand (green) for the simulations of the hAChE complex with hybrid **5a**.

Table S1
Free energy components (kcal/mol) determined from Solvent Interaction Energy (SIE) computations for the binding of compounds **5a** and **4**.[a]

Component	**5a**	**4**
van der Waals (ΔE_{vW})	–77.4 ± 4.1	–44.1 ± 2.8
Coulombic (ΔE_{Coul})	–154.2 ± 7.7	–93.6 ± 5.7
Reaction Field (ΔG_{RF})	153.3 ± 5.4	92.6 ± 5.0
Cavity (γ ΔSA)	–13.8 ± 0.6	–8.1 ± 0.5
Total (ΔG) [a]	–12.5 ± 0.7	–8.5 ± 0.4

[a] Evaluated from the expression $\Delta G = \alpha\left[\Delta E_{vW} + \Delta E_{Coul} + \Delta G_{RF} + \gamma \Delta SA\right] + C$, where the parameters α (0.1048) and C (–2.89 kcal/mol) were fitted to the absolute binding free energies of 99 protein–ligand complexes.

Table S2

Reported and experimental permeability values (P_e 10^{-6} cm s^{-1}) of 14 commercial drugs used for the PAMPA-BBB assay validation.

Compound	Literature value[a]	Experimental value[b]
Verapamil	16	25.2 ± 1.07
Testosterone	17	24.3 ± 0.46
Corticosterone	5.1	6.70 ± 0.10
Clonidine	5.3	6.50 ± 0.05
Ofloxacin	0.8	0.98 ± 0.02
Lomefloxacin	1.1	0.75 ± 0.02
Progesterone	9.3	16.8 ± 0.30
Promazine	8.8	13.8 ± 0.30
Imipramine	13	12.3 ± 0.10
Hydrocortisone	1.9	1.40 ± 0.05
Piroxicam	2.5	1.83 ± 0.19
Desipramine	12	17.8 ± 0.10
Cimetidine	0.0	0.70 ± 0.03
Norfloxacin	0.1	0.90 ± 0.02

[a] Taken from ref. [1].

[b] Values are expressed as the mean ± SD of three independent experiments.

References

[1] L. Di, E.H. Kerns, K. Fan, O.J. McConnell, G.T. Carter, High throughput artificial membrane permeability assay for blood-brain barrier, Eur. J. Med. Chem. 38 (2003) 223–232.

N-{3-[(6-chloro-1,2,3,4-tetrahydroacridin-9-yl)amino]propyl}-5-(4-chlorophenyl)-1,2,3,4-tetrahydrobenzo[*h*][1,6]naphthyridine-9-carboxamide (**5a**) – ^{1}H NMR (500 MHz, CD_3OD)

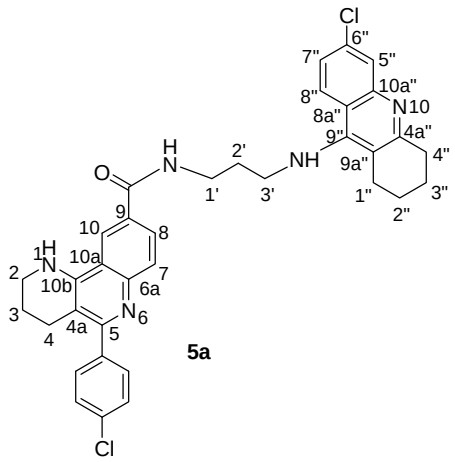

5a

N-{3-[(6-chloro-1,2,3,4-tetrahydroacridin-9-yl)amino]propyl}-5-(4-chlorophenyl)-1,2,3,4-tetrahydrobenzo[*h*][1,6]naphthyridine-9-carboxamide (**5a**) - ^{13}C NMR (125.8 MHz, CD_3OD)

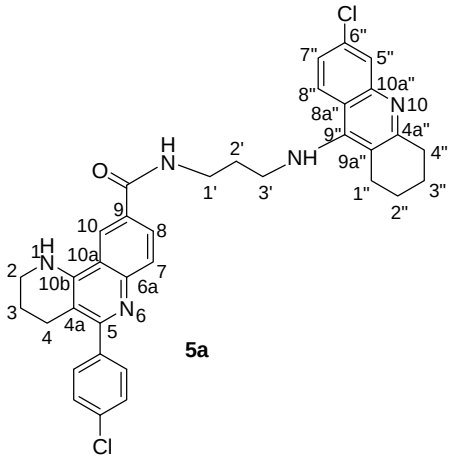

5a

N-{4-[(6-chloro-1,2,3,4-tetrahydroacridin-9-yl)amino]butyl}-5-(4-chlorophenyl)-1,2,3,4-tetrahydrobenzo[*h*][1,6]naphthyridine-9-carboxamide (**5b**) – ^{1}H NMR (500 MHz, CD_3OD)

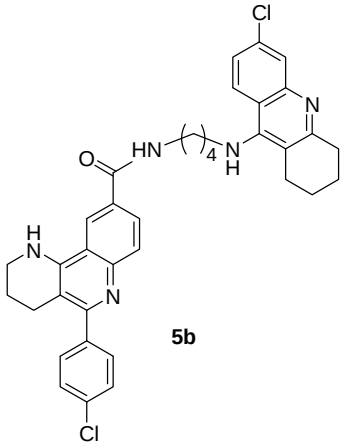

5b

N-{4-[(6-chloro-1,2,3,4-tetrahydroacridin-9-yl)amino]butyl}-5-(4-chlorophenyl)-1,2,3,4-tetrahydrobenzo[*h*][1,6]naphthyridine-9-carboxamide (**5b**) - ^{13}C NMR (125.8 MHz, CD_3OD)

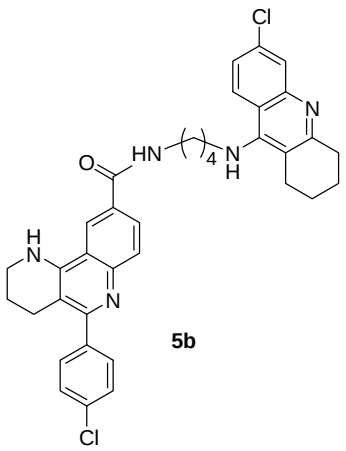

5b

N-{5-[(6-chloro-1,2,3,4-tetrahydroacridin-9-yl)amino]pentyl}-5-(4-chlorophenyl)-1,2,3,4-tetrahydrobenzo[*h*][1,6]naphthyridine-9-carboxamide (**5c**) – ^{1}H NMR (500 MHz, CD_3OD)

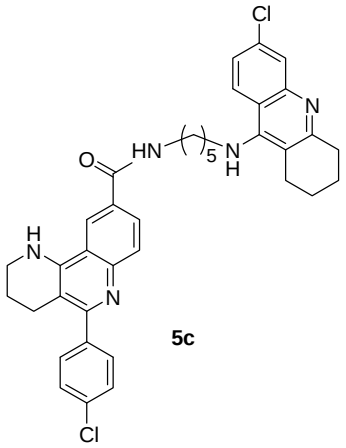

5c

N-{5-[(6-chloro-1,2,3,4-tetrahydroacridin-9-yl)amino]pentyl}-5-(4-chlorophenyl)-1,2,3,4-tetrahydrobenzo[*h*][1,6]naphthyridine-9-carboxamide (**5c**) - ^{13}C NMR (125.8 MHz, CD_3OD)

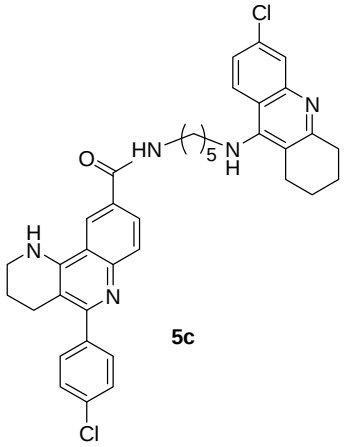

5c

N-{8-[(6-chloro-1,2,3,4-tetrahydroacridin-9-yl)amino]octyl}-5-(4-chlorophenyl)-1,2,3,4-tetrahydrobenzo[*h*][1,6]naphthyridine-9-carboxamide (**5d**) – ^{1}H NMR (500 MHz, CD_3OD)

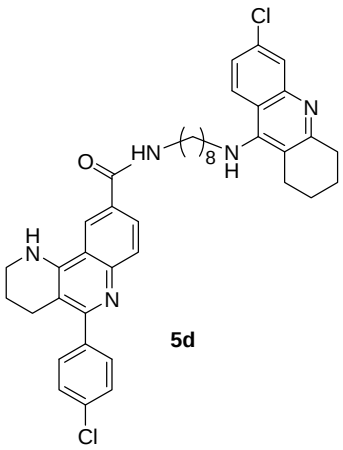

5d

N-{8-[(6-chloro-1,2,3,4-tetrahydroacridin-9-yl)amino]octyl}-5-(4-chlorophenyl)-1,2,3,4-tetrahydrobenzo[*h*][1,6]naphthyridine-9-carboxamide (**5d**) - ^{13}C NMR (125.8 MHz, CD_3OD)

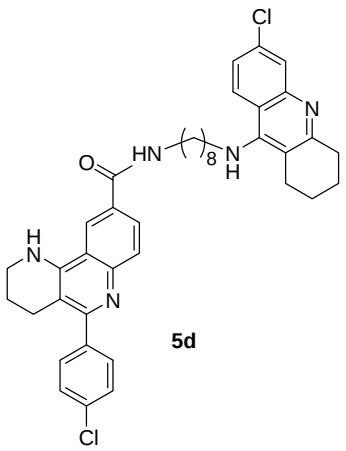

5d

N-{8-[(6-chloro-1,2,3,4-tetrahydroacridin-9-yl)amino]octyl}-5-(4-chlorophenyl)-1,2,3,4-tetrahydrobenzo[*h*][1,6]naphthyridine-9-carboxamide (**5d**) - ^{13}C NMR - DEPT (125.8 MHz, CD_3OD)

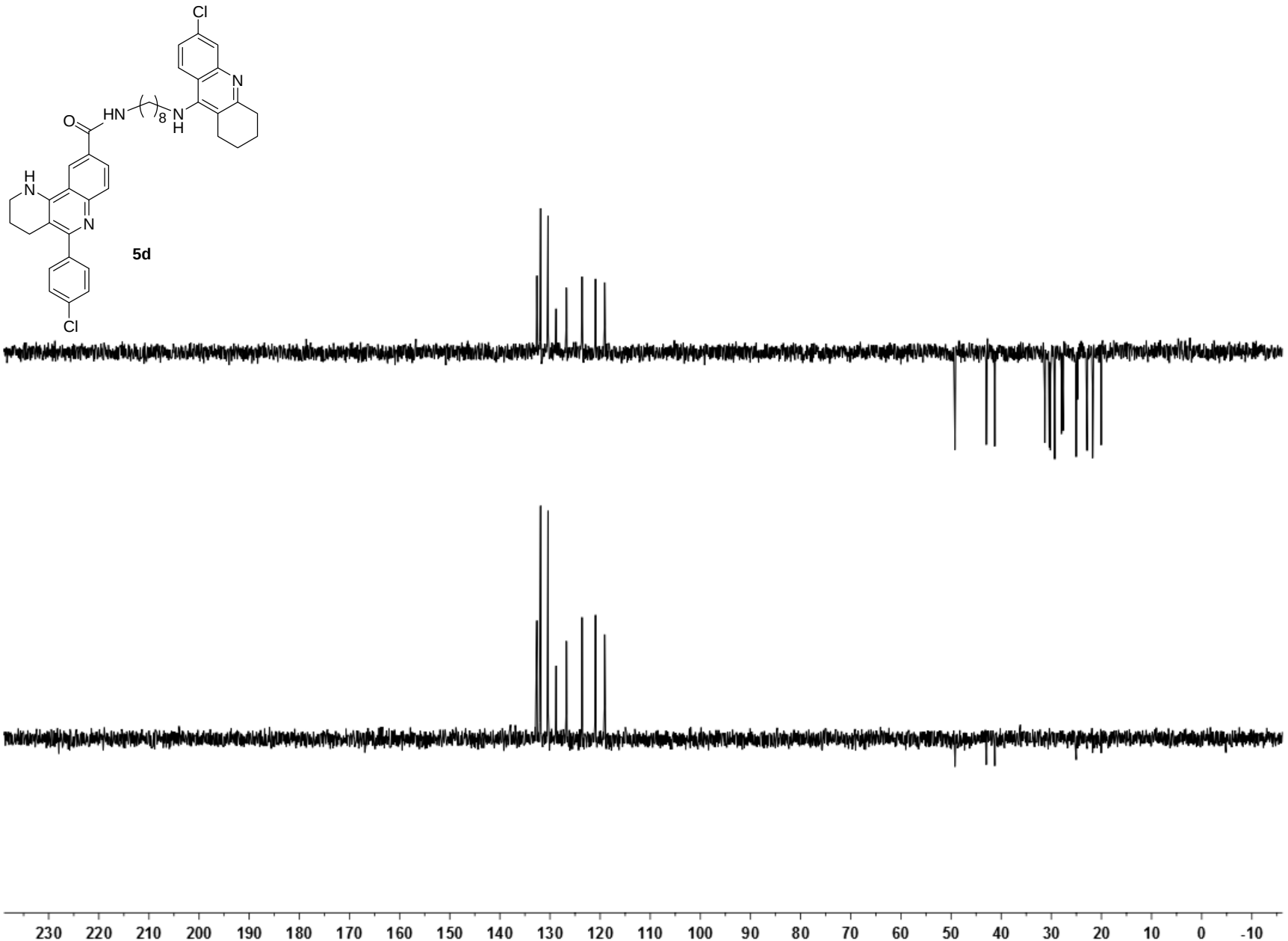

N-{8-[(6-chloro-1,2,3,4-tetrahydroacridin-9-yl)amino]octyl}-5-(4-chlorophenyl)-1,2,3,4-tetrahydrobenzo[*h*][1,6]naphthyridine-9-carboxamide (**5d**) – COSY $^{1}H/^{1}H$

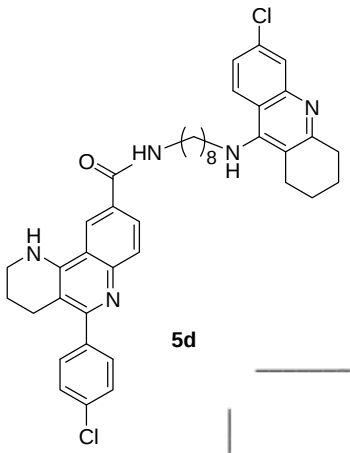

5d

N-{8-[(6-chloro-1,2,3,4-tetrahydroacridin-9-yl)amino]octyl}-5-(4-chlorophenyl)-1,2,3,4-tetrahydrobenzo[*h*][1,6]naphthyridine-9-carboxamide (**5d**) – COSY $^{1}H/^{1}H$

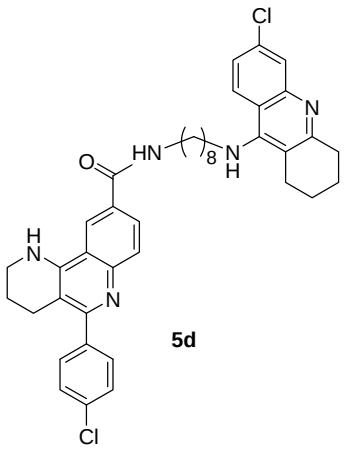

5d

N-{8-[(6-chloro-1,2,3,4-tetrahydroacridin-9-yl)amino]octyl}-5-(4-chlorophenyl)-1,2,3,4-tetrahydrobenzo[*h*][1,6]naphthyridine-9-carboxamide (**5d**) – COSY $^{1}H/^{1}H$

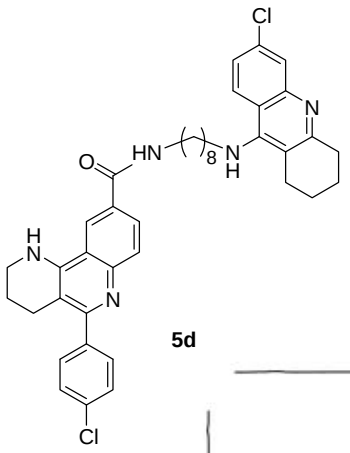

5d

N-{8-[(6-chloro-1,2,3,4-tetrahydroacridin-9-yl)amino]octyl}-5-(4-chlorophenyl)-1,2,3,4-tetrahydrobenzo[*h*][1,6]naphthyridine-9-carboxamide (**5d**) – COSY $^{1}H/^{13}C$ (HSQC)

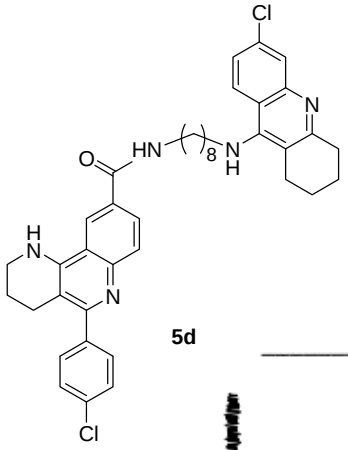

5d

N-{8-[(6-chloro-1,2,3,4-tetrahydroacridin-9-yl)amino]octyl}-5-(4-chlorophenyl)-1,2,3,4-tetrahydrobenzo[*h*][1,6]naphthyridine-9-carboxamide (**5d**) – COSY $^{1}H/^{13}C$ (HSQC)

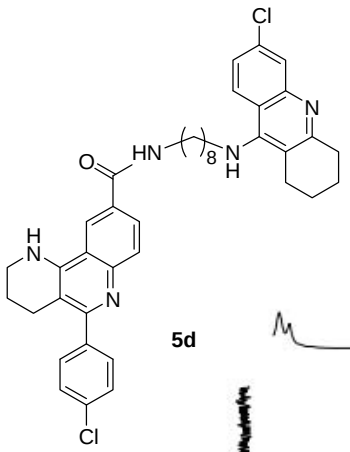

5d

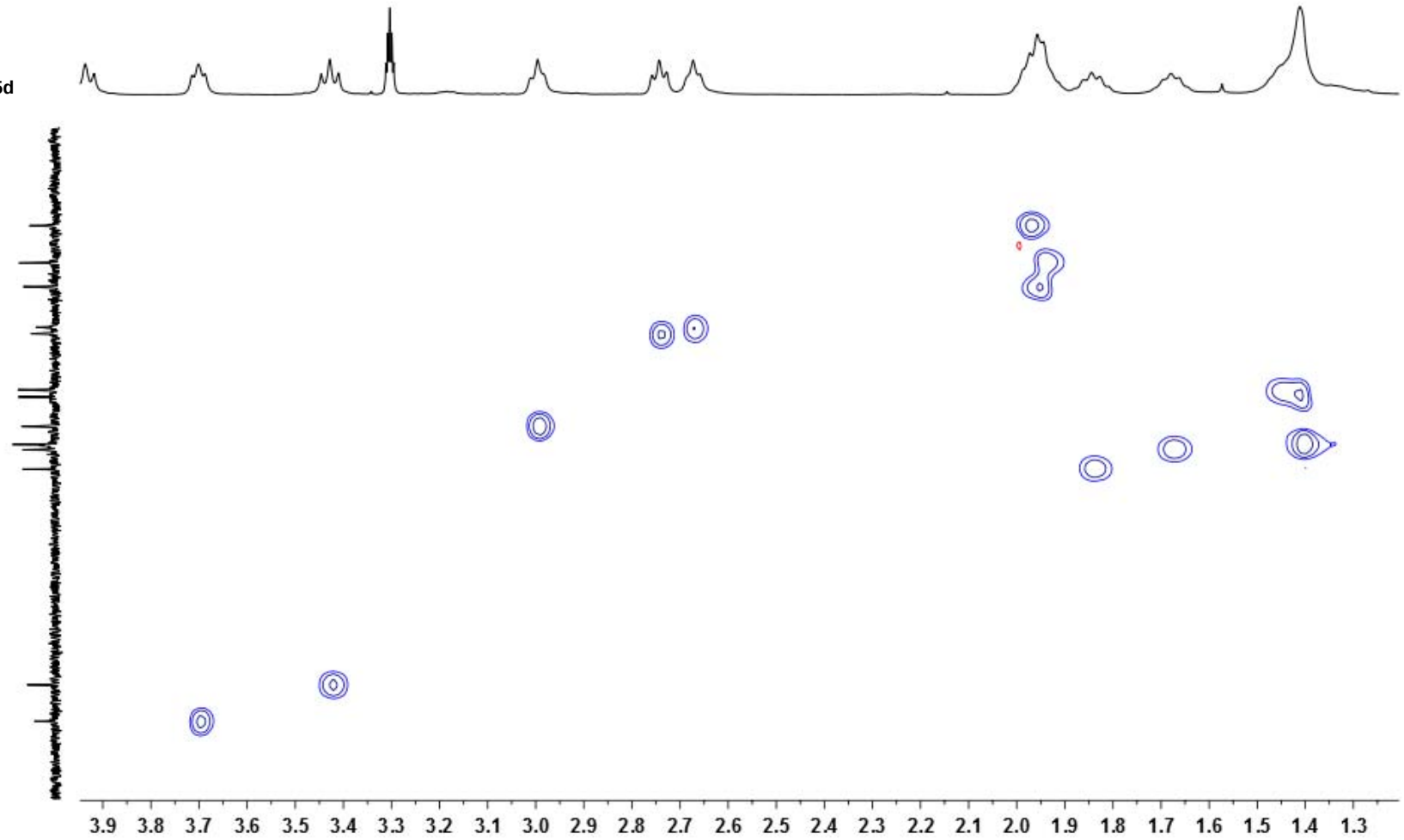

N-{8-[(6-chloro-1,2,3,4-tetrahydroacridin-9-yl)amino]octyl}-5-(4-chlorophenyl)-1,2,3,4-tetrahydrobenzo[*h*][1,6]naphthyridine-9-carboxamide (**5d**) – COSY $^{1}H/^{13}C$ (HSQC)

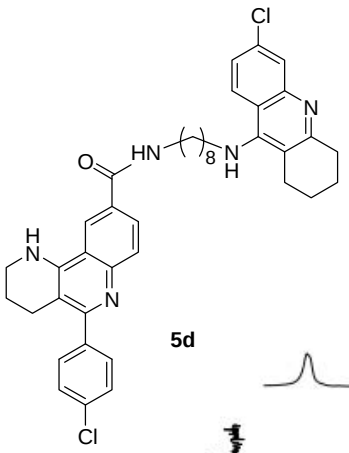

5d

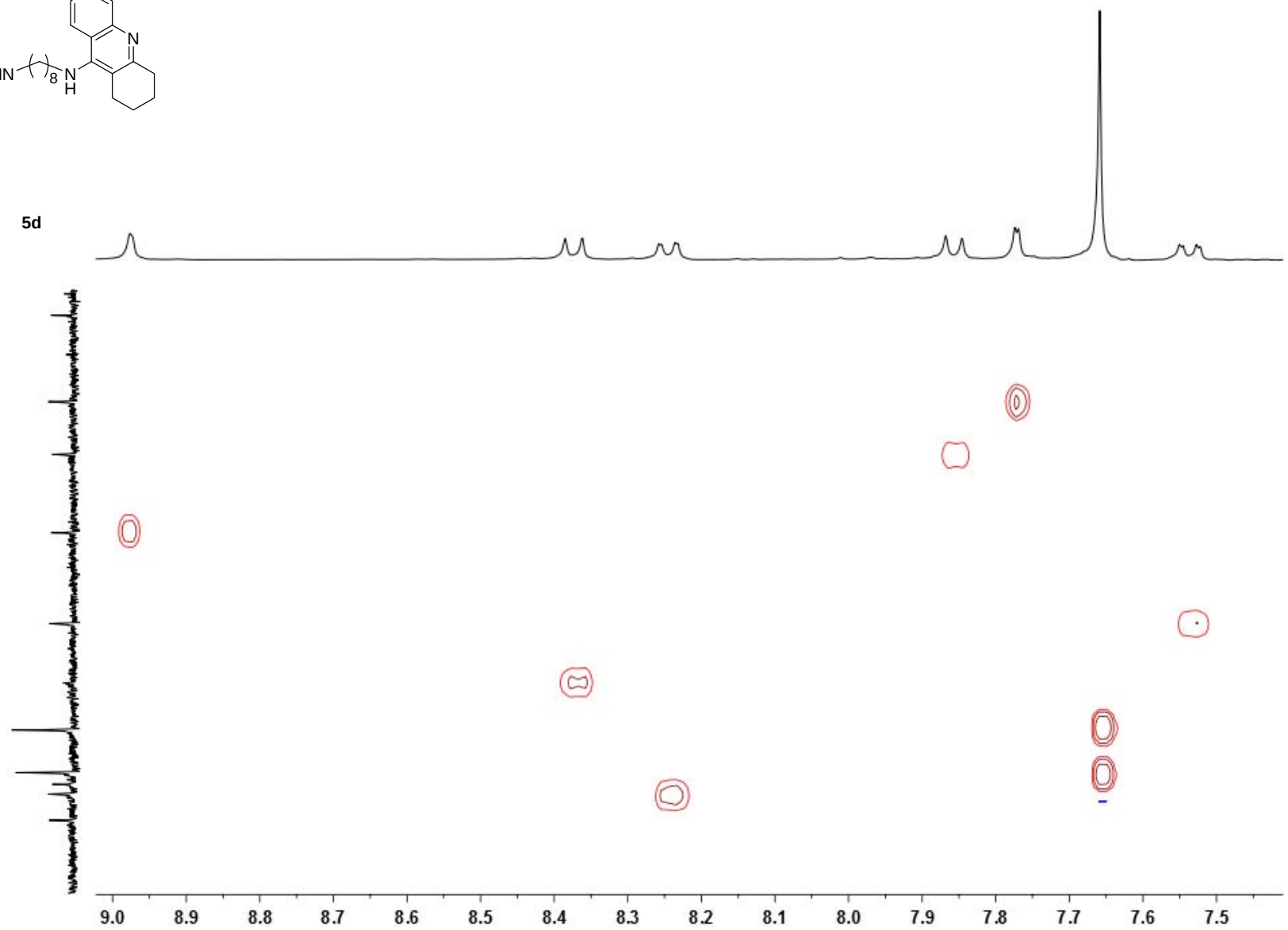

N-{8-[(6-chloro-1,2,3,4-tetrahydroacridin-9-yl)amino]octyl}-5-(4-chlorophenyl)-1,2,3,4-tetrahydrobenzo[*h*][1,6]naphthyridine-9-carboxamide (**5d**) – COSY $^{1}H/^{13}C$ (HMBC)

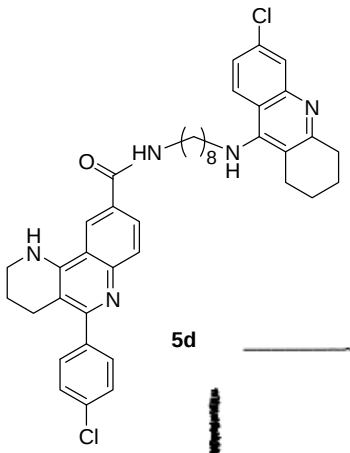

5d

N-{8-[(6-chloro-1,2,3,4-tetrahydroacridin-9-yl)amino]octyl}-5-(4-chlorophenyl)-1,2,3,4-tetrahydrobenzo[*h*][1,6]naphthyridine-9-carboxamide (**5d**) – COSY $^{1}H/^{13}C$ (HMBC)

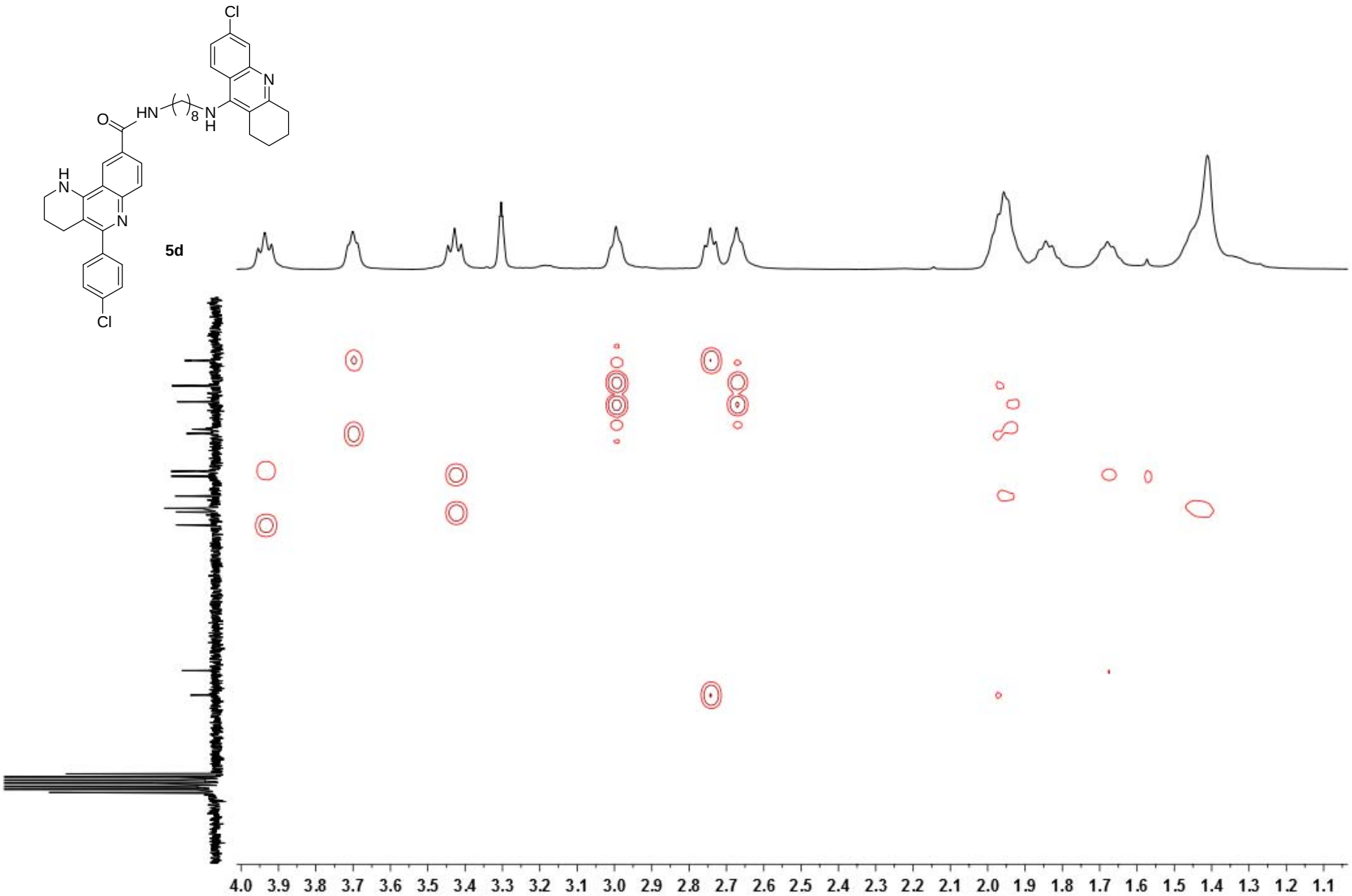

N-{8-[(6-chloro-1,2,3,4-tetrahydroacridin-9-yl)amino]octyl}-5-(4-chlorophenyl)-1,2,3,4-tetrahydrobenzo[*h*][1,6]naphthyridine-9-carboxamide (**5d**) – COSY $^{1}H/^{13}C$ (HMBC)

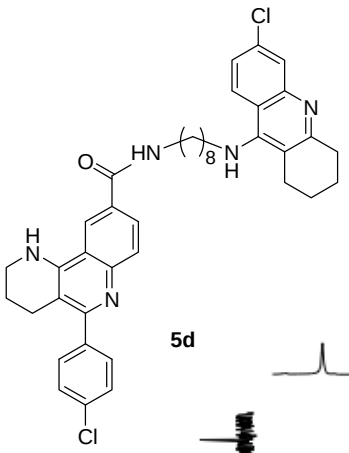

5d

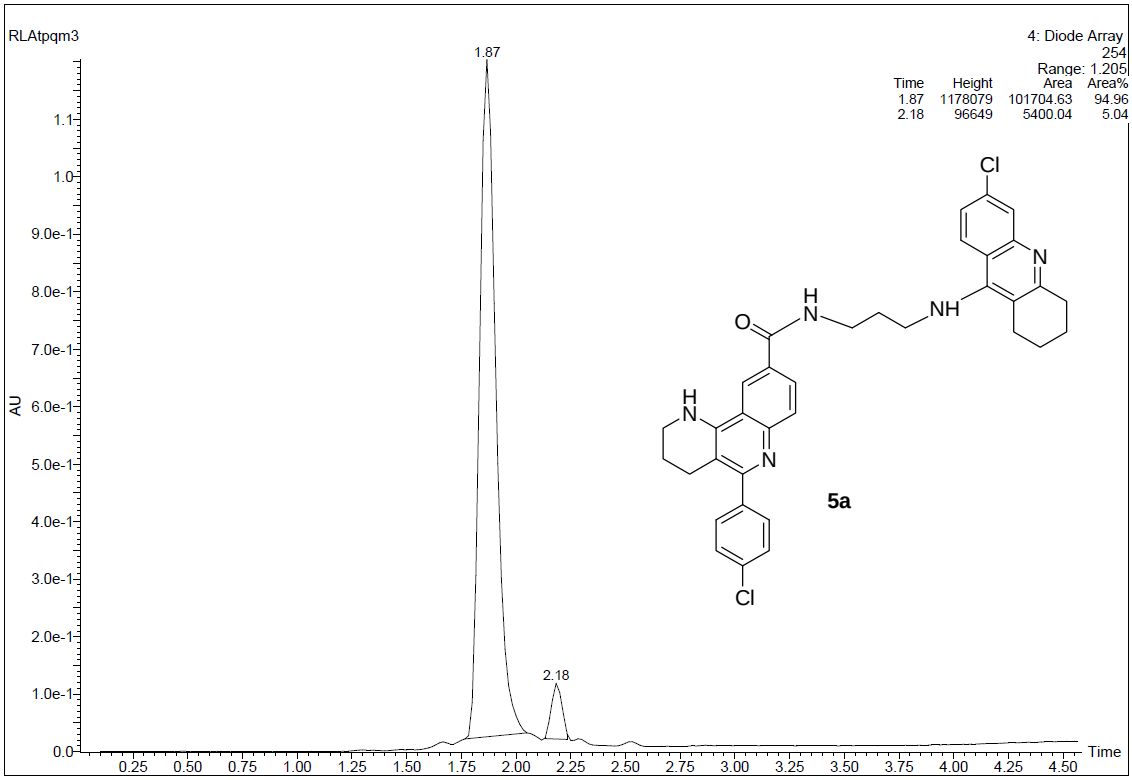
RLAtpqm3
4: Diode Array
254
Range: 1.205
Time Height Area Area%
1.87 1178079 101704.63 94.96
2.18 96649 5400.04 5.04
1.87
2.18
AU
Time
5a

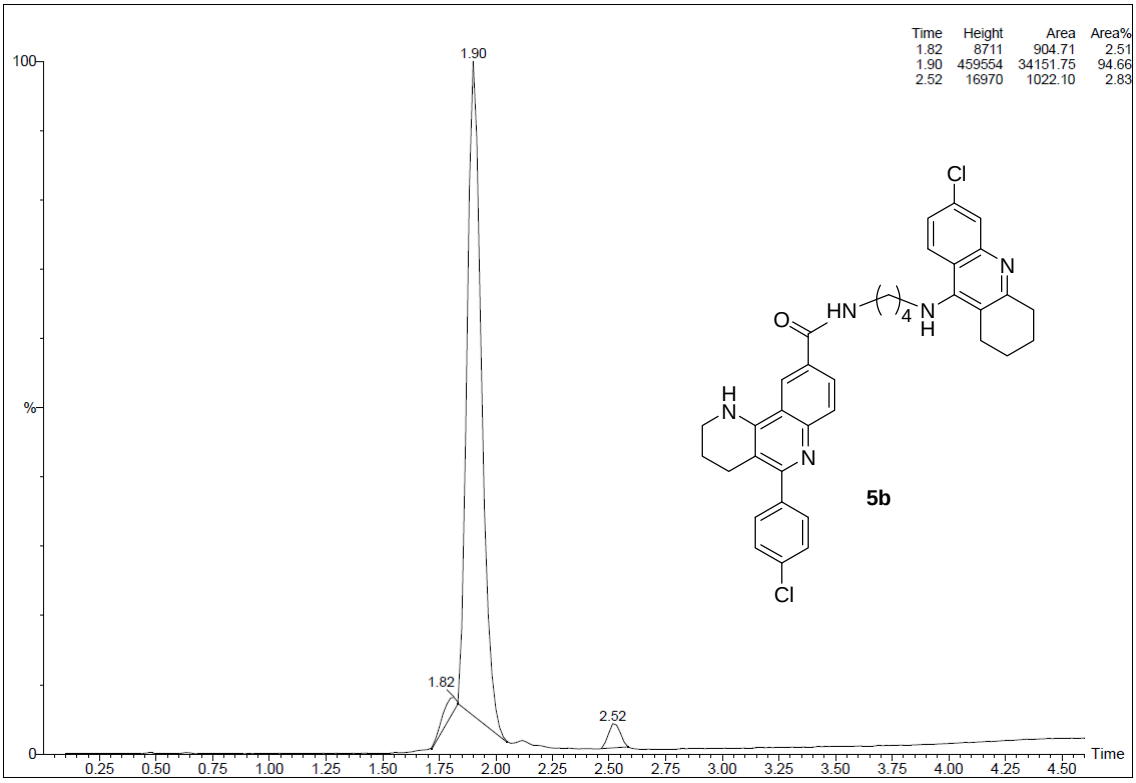
Time Height Area Area%
1.82 8711 904.71 2.51
1.90 459554 34151.75 94.66
2.52 16970 1022.10 2.83
1.90
1.82
2.52
%
Time
5b

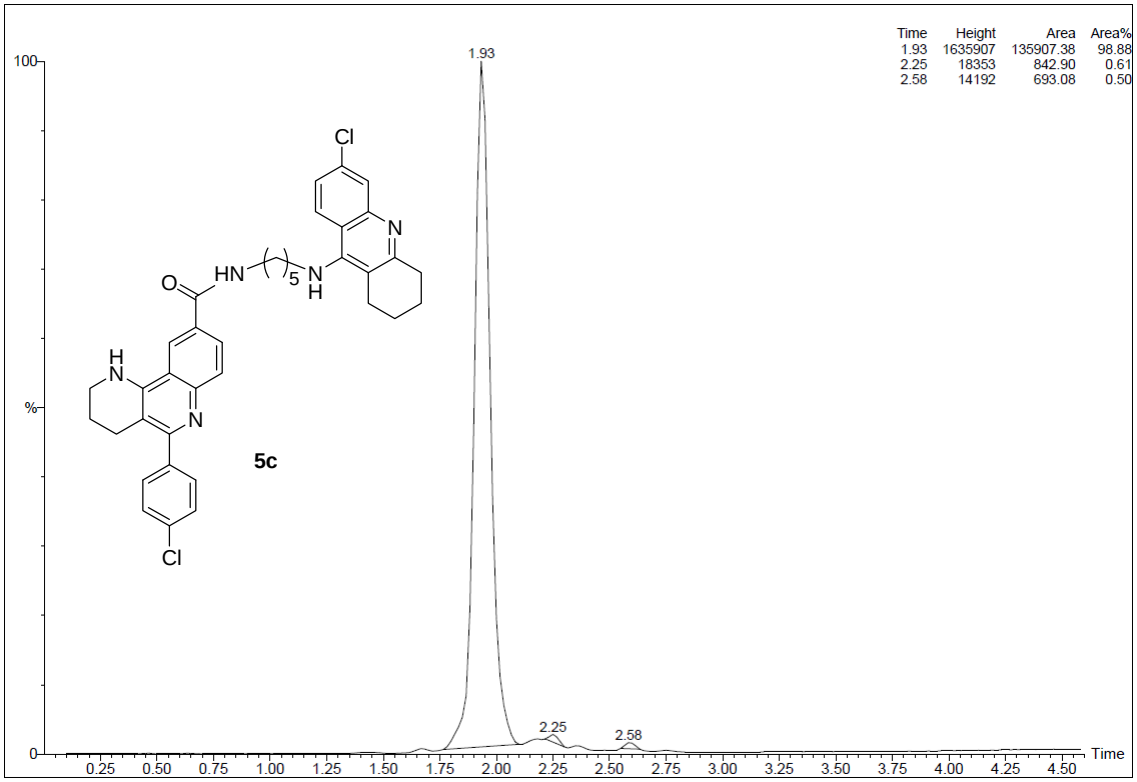
Time Height Area Area%
1.93 1635907 135907.38 98.88
2.25 18353 842.90 0.61
2.58 14192 693.08 0.50
100
%
0
1.93
2.25
2.58
Time
0.25 0.50 0.75 1.00 1.25 1.50 1.75 2.00 2.25 2.50 2.75 3.00 3.25 3.50 3.75 4.00 4.25 4.50
Cl
HN
5
N
H
O
N
H
N
Cl
5c

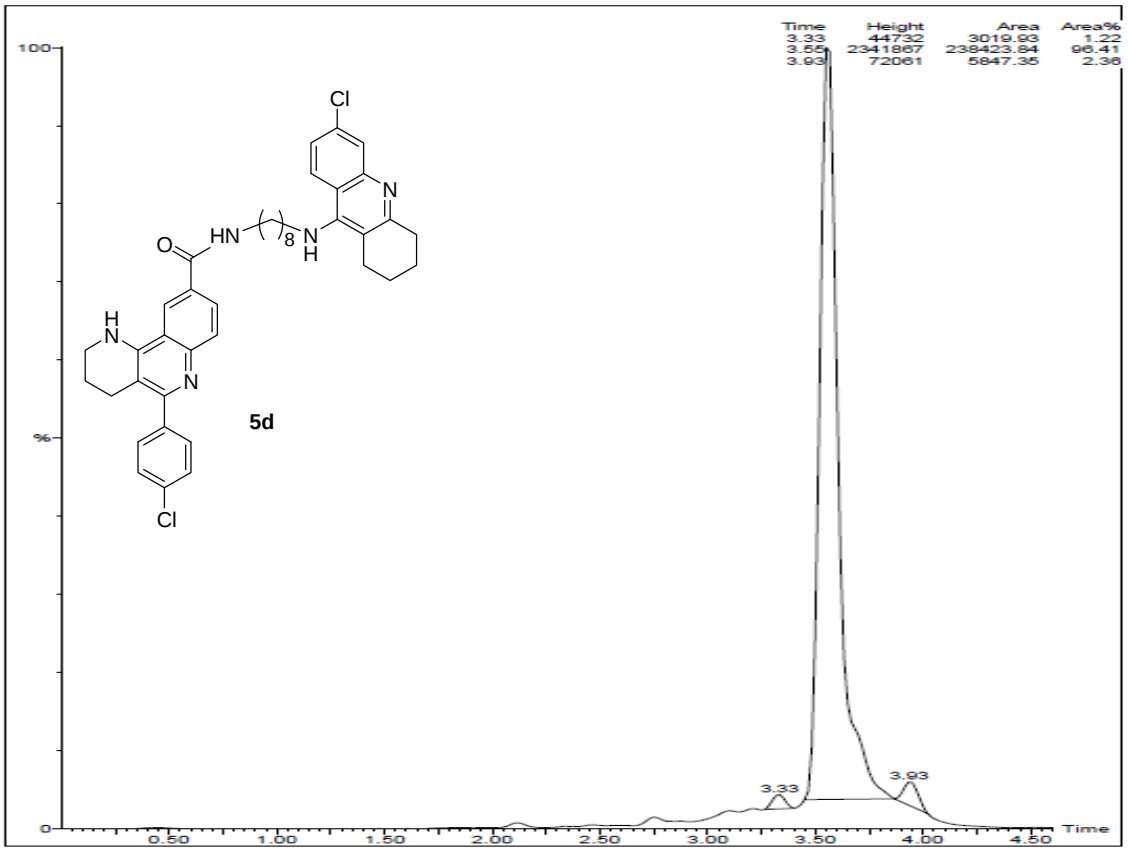
Time Height Area Area%
3.33 44732 3019.93 1.22
3.56 2341867 238423.84 96.41
3.93 72061 5847.35 2.36
100
%
0
3.33
3.93
Time
0.50 1.00 1.50 2.00 2.50 3.00 3.50 4.00 4.50
Cl
HN
8
N
H
O
N
H
N
Cl
5d

6 Propargylamine-based MAO-B inhibitors

Chapter

(Draft manuscript)

6.1 Selective targeting of MAO-B, an alternative strategy for the treatment of AD

As already discussed in section ***1.6.3***, selective targeting of MAO-B has recently emerged as an alternative strategy in the search for novel disease-modifying anti-Alzheimer drug candidates.[200,201] Within the FDA-approved irreversible MAO inhibitors, such as the anti-Parkinson's agents rasagiline and selegiline, and the antidepressant clorgiline, the incorporation of a terminal propargylamine group is a feature conserved to guarantee the enzymatic inhibition through the formation of a covalent bond with FAD,[202,203,204] according to the reaction shown below (**scheme 6.1**):

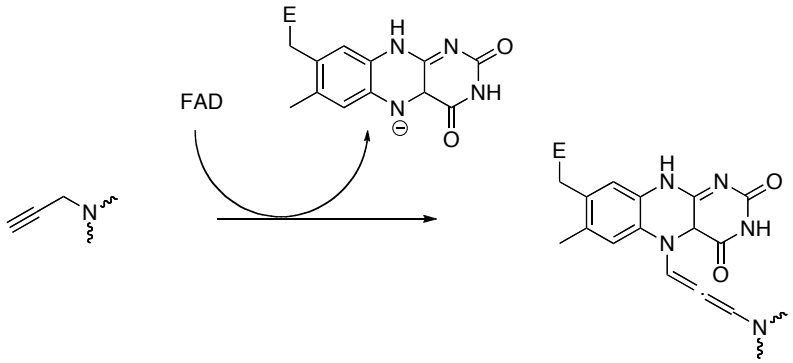

Scheme 6.1 Putative mechanism of the covalent bonding of the propargylamine group to FAD cofactor.

Multiple actions, independent from the mere restoration of the physiological levels of dopamine and serotonin due to MAO-B inhibition, including prevention of the reactive oxygen species formation as byproducts of the oxidative deamination reaction,[92,205,206] inhibition of apoptosis,[207,208] and enhancement of the release of the sAPPα (**Figure 6.1**),[209] have been postulated as the molecular determinants behind the neuroprotective effects displayed by the propargylamine-containing MAO-B inhibitors.

[200]Xie, S.S.; Wang, X.; Jiang, N.; Yu, W.; Wang, K.D.G.; Lan, J.S. *Eur. J. Med. Chem.***2015**, *95*, 153.
[201]Novaroli, L.; Reist, M.; Favre, E.; Carotti, A.; Catto, M.; Carrupt, P.-A. *Bioorg. Med. Chem.* **2005**, *13*, 6212.
[202]Bolea, I.; Gella, A.; Unzeta, M. *J Neural Transm.* **2013**, *120*, 893.
[203]Szewczuk, L.M.; Culhane, C., Yang, M.; Majumdar, A.; Yu, H.; Cole, P.A. *Biochemistry* **2007**, *46*, 6892.
[204] Yang, M.; Culhane, J.C.; Szewczuk, L.M.; Gocke, C.B.; Brautingam, C.A.; Tomchick, D.R.; Machius, M.; Cole, P.A.; Yu, H. *Nat. Struct. Mol. Biol.* **2007**, *14*, 535.
[92]Sterling, J.; Herzig, Y.; Goren, T.; Finkelstein, N., Lerner, D.; Goldenberg, W.; Miskolczi, I.; Molnar, S.; Rantal, F.; Tamas, T.; Toth, G.; Zagyva, A.; Zekany, A.; Finberg, J.; Lavian, G.; Gross, A.; Friedman, R.; Razin, M.; Huang, W.; Krais, B.; Chorev, M.; Youdim, M.B.; Weinstock, M. *J. Med. Chem.* **2002**, *45*, 5260.
[205]Song, M.S.; Matveychuk, D.; MacKenzie, E.M.; Duchcherer, M.; Mousseau, D.D.; Baker, G.B. *Neuropsychopharmacol. Biol. Psychiatry* **2013**, *44*, 118.
[206]Riederer, P.; Danielczyk, W.; Grunblatt, E. *Neurotoxicology* **2004**, *25*, 271.
[207]Tatton, W.; Chalmers-Redman, R.; Tatton, N. *J. Neural Transm.* **2003**, *110*, 509.
[208]Weinreb, O.; Amit, T.; Bar-Am, O.; Sagi, Y.; Mandel, S.; Youdim, M.B. *J. Neural Transm. Suppl.* **2006**, *70*, 457.
[209]Youdim, M.B.H.; Weinstock, M. *Cell. Mol. Neurobiol.* **2001**, *21*, 555.

In this PhD Thesis, following the research project developed in a preliminary phase by Drs. Elisabet Viayna and Jordi Juárez-Jiménez during their PhD, the combination of propargylamine group, as key structural feature for selectively addressing irreversible MAO-B inhibition, with a 1,2,3-triazole scaffold, a very attractive structure in medicinal chemistry,[210] led to the design of a novel family of *N1*-substituted triazole-based MAO-B inhibitors, which might be further hybridized with other pharmacophoric moieties to provide multipotentanti-Alzheimer drug candidates targeting both MAO-B and AChE.

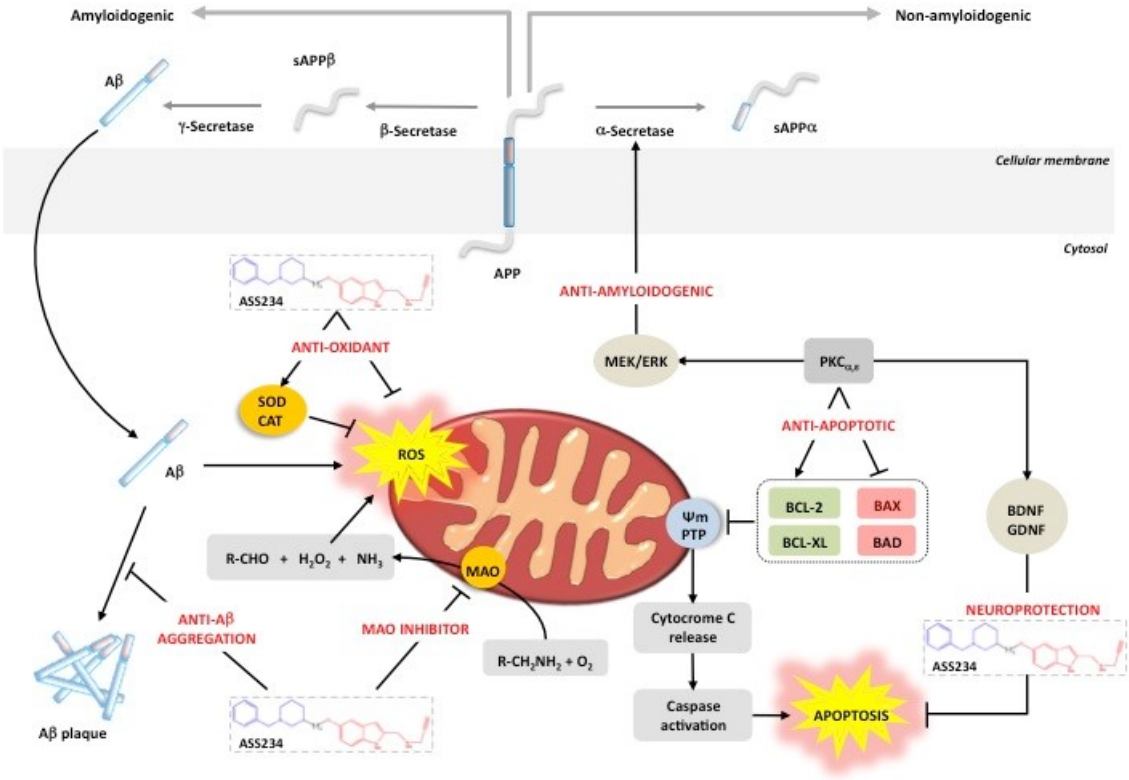

Figure 6.1 Schematic representation of the sites of action of a propargylamine-derived multipotent compound developed by Bolea *et al.* (*J. Neural Transm.* **2013**, 893).

6.2 1,2,3-Triazole scaffold: from click chemistry synthetic strategy to applications in drug discovery

In the light of the facile and modular synthesis allowing steric and electronic fine-tuning, the 1,4-disubstituted 1,2,3-triazoles constitute a virtually unlimited source of ligand architectures provided with multiple of applications in several scientific fields.[211]

[210] Mindt, T.L.; Struthers, H.; Brans, L.; Anguelov, T.; Schweinsberg, C.; Maes, V.; Tourwé, D.; Schibli, R. *J. Am. Chem. Soc.* **2005**, *127*, 10824.
[211] Schulze, B.; Schubert, U.S. *Chem. Soc. Rev.* **2014**, *43*, 2522.

This interesting scaffold is readily available through click chemistry, a synthetic approach introduced for the first time in 2001 by Prof. K. B. Sharpless to describe a category of reactions that are simple to perform, afford products in good yields and high stereoselectivities, do not need chromatographic purifications, and allow the use of easily removable and benign solvents.[212]

Likely the most popular click chemistry reaction is based on the Huisgen 1,3-dipolar cycloaddition of azides to alkynes,[213] whose recourse is, however, strictly limited due to the elevated temperatures required and the mixtures of the two regioisomers afforded when using asymmetric alkynes. Interestingly, a *Cu*-catalyzed version of this reaction, performed under aqueous conditions and r.t., and specifically affording the 1,4-disubstituted regioisomer,[214,215] was discovered concurrently and independently by the groups of Prof. V. V. Fokin and Prof. B. K. Sharpless at the Scripts Institute, California,[109] and Prof. M. Meldal at the Carlsberg Laboratory, Denmark (**Scheme 6.2**).[110]

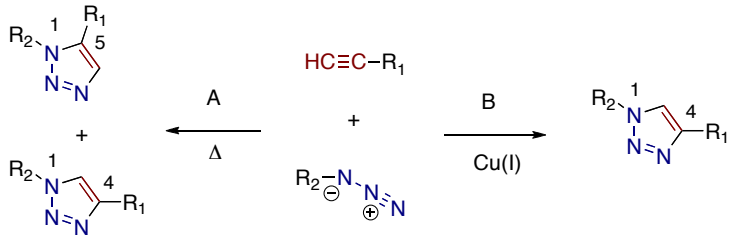

Scheme 6.2 A) Uncatalyzed version of the Huisgen 1,3-dipolar azide-alkyne cycloaddition; **B)** *Cu*-catalyzed version of azide-alkyne cycloaddition

Mechanistically different from the classical Huisgen 1,3-dipolar cycloaddition, the *Cu*-catalyzed azide-alkyne cycloaddition (CuAAC) implies the initial formation of a copper acetylide species (**I**), after which the azide displaces another ligand and binds to the copper (**II**). Then, an unusual six-membered Cu(III) metallacycle (**III**), calculated to possess a considerably lower energy barrier than the transition state coming from the uncatalyzed reaction, is formed.

[212]Kolb, H.C.; Finn, M.G.; Sharpless, K.B. *Angew.Chem. Int. Ed.* **2001**, *40*, 2004.
[213]Huisgen, P.; Padwa, A. *Ed. Wiley*: New York **1984**, *1*.
[214]Rostovtsev, V.V.; Green, L.G.; Fokin, V.V. Sharpless, K.B. *Angew. Chem. Int. Ed.* **2002**, *41*, 2596.
[215]Tornoe, C.W.; Christensen, C.; Meldal, M. *J. Org. Chem.* **2002**, *67*, 3057.

Finally, ring contraction to a triazolyl-copper derivative (**IV**) and following protonolysis close the catalytic cycle delivering the final triazole product (**V**) (**Scheme 6.3**).[216]

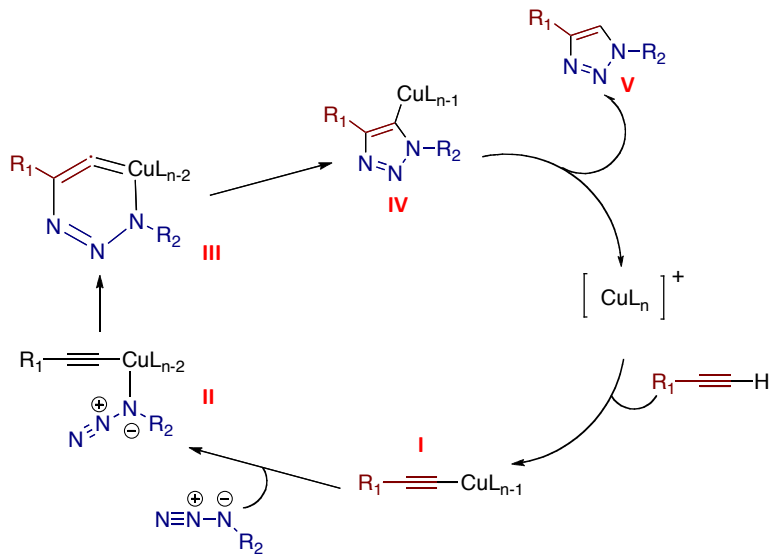

Scheme6.3

Examples of successful applications of click chemistry synthetic strategy in drug discovery have been already reported in the literature. Particularly worthy of note is an *in situ* click chemistry approach used by Sharpless and co-workers for assembling the 1,2,3-triazole scaffold inside the AChE binding cavity, leading to one of the most potent dual binding site AChEI reported so far (**84**, Figure **6.2**).[217]

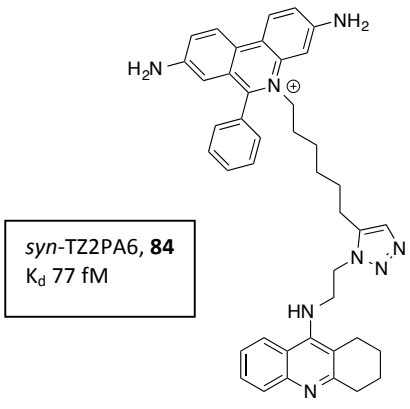

syn-TZ2PA6, **84**
K_d 77 fM

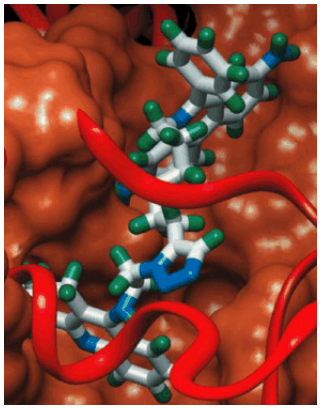

Figure 6.2 Left: Structure of *in situ* generated dual binding site AChEI *syn*-TZ2PA6, **84**. Right: Representation of inhibitor **84** complexed with mouse AChE (Source: Warren, G. *et al. Angew. Chem. Int. Ed.* **2002**, *41*, 1053).

[216]Himo, F.; Lovell, T.; Hilgraf, R.; Rostovtsev, V.V.; Noodleman, L.; Sharpless, K.B.; Fokin, V.V. *J. Am. Chem. Soc.* **2005**, *127*, 210.
[217]Manetsch, R.; Krasinski, A.; Radic, Z.; Raushel, J.; Taylor, P.; Sharpless, K.B.; Kolb, H.C. *J. Am. Chem. Soc.* **2004**, *126*, 12809.

6.3 Design and synthesis, via click chemistry, of a novel family of propargylamine-containing 1,2,3-triazole derivatives targeting MAO-B

In the present PhD thesis, the CuAAC has been used for the fast preparation of a novel series of 1,4-disubstituted 1,2,3-triazole derivatives in which a propargylamine group has been further incorporated to provide irreversible inhibition of MAO enzyme (**Figure 6.3**). The main goal was the exploration of a broad spectrum of chemical modifications on this common skeleton, aimed at identifying key structural features capable of discriminating between the two differently shaped binding cavities of MAO-A and MAO-B and selectively binding to this latter isoform, thus avoiding the occurrence of severe side effects due to MAO-A inhibition.

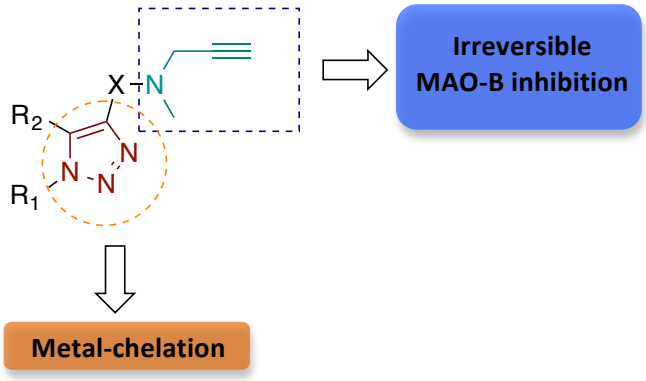

Figure 6.3 Design of a novel family of 1,2,3-triazoles

Because of the low inhibitory activity displayed by triazole derivatives **85**-**88** (**Table 6.1**), previously synthesized by Dr. Elisabet Viayna as simple prototypes to validate the CuAAC-assisted synthetic methodology, in this PhD thesis different patterns of chemical modifications at positions *N1* and *C5*, and spacers between the propargylamine nitrogen atom and *C4* of the triazole ring have been explored in collaboration with the Erasmus PhD student Natalia Guzior. The main objective was to increase the lipophilicity of the quite polar "*probe*"-compounds **85**-**88** (miLogP 0.43-1.06) for a more suitable fitting into the hydrophobic substrate cavity of MAO enzyme (**Table 6.2**).

Table 6.1 *h*MAO-A and *h*MAO-B inhibitory activities of triazoles **85**-**88.**

	R_1	R_2	X	IC_{50} (μM) *h*MAO-A[a]	IC_{50} (μM) *h*MAO-B[a]
85	Et	H	$-CH_2-$	135 ± 22	249 ± 94
86	Et	Me	$-CH_2-$	267 ± 31	105 ± 27
87	Et	H	$-(CH_2)_2-$	553 ± 84	374 ± 119
88	Et	Me	$-(CH_2)_2-$	91 ± 14	238 ± 52

[a]Values are expressed as the mean ± SEM of at least three experiments performed in quadruplicate.

In vitro evaluation of the biological activity of all the synthesized compounds against both MAO-A and MAO-B, together with further rationalization through SAR studies and considerations about some physicochemical properties relevant for understanding the binding affinity and selectivity, led to the identification of two interesting *hit* compounds, **121** and **102**, displaying the best inhibitory potency (*h*MAO-B IC_{50} 0.607 μM) and selectivity index (SI 0.036), respectively. Compound **102**, by virtue of its very well balanced inhibitory potency (IC_{50} 3.54 μM) and MAO-B selectivity, was further selected to carry out reversibility and time-dependent inhibition studies, which overall attested an irreversible slow time-dependent mode of MAO-B inhibition.

Table 6.2 Triazole derivatives synthesize in this PhD thesis.

	R_1	R_2	X	IC_{50} (μM) *h*MAO-A[a]	IC_{50} (μM) *h*MAO-B[a]
101	Me	*n*-Bu	$-CH_2-$	< 300	94.73 ± 16.3
102	Bn	H	$-(CH_2)_2-$	97.12 ± 30.1	3.54 ± 0.44
103	$Ph(CH_2)_2-$	H	$-(CH_2)_2-$	56.1 ± 8.7	172.8 ± 47.8
120	Me	H	*m*-xylenediyl	2.12 ± 0.32	64.96 ± 15.4
121	Me	H	*p*-xylenediyl	0.526 ± 0.06	0.607 ± 0.08
131	PhCH(Me)-	Me	$-(CH_2)_2-$	47.0 ± 6.9	134.2 ± 25.5
140	Ph	Et	$-(CH_2)_2-$	7.5 ± 1.1	213.4 ± 54.0
141	Ph	*n*-Pr	$-(CH_2)_2-$	26.1 ± 4.0	156.8 ± 31.9
142	Ph	*n*-Bu	$-(CH_2)_2-$	17.3 ± 4.5	155.5 ± 25.0

[a]Values are expressed as the mean ± SEM of at least three experiments performed in quadruplicate.

These promising results have recently boosted the design of an optimized generation of triazole derivatives in the frame of another PhD thesis of our research group, expected to be more potent and selective towards MAO-B. Moreover, metal-chelation, a property reported in the literature for other structurally similar 1,2,3-triazoles,[218] will be additionally tested, thus providing, if confirmed, a structurally innovative family of small molecule drug-like compounds provided with intrinsic multipotent biological profile, a trait traditionally associated with high molecular weight molecules (**Figure 6.3**).

6.4 Synthesis of the novel series of 1,2,3-triazole derivatives

6.4.1 Synthesis of triazole-based compounds 101-103

For the preparation of the target triazoles **101**-**103** a CuAAC was envisioned as the key step. Thus, reaction of methyl azide, benzyl azide or phenethylazide, generated *in situ* through reaction of ethyl bromide, benzyl bromide or phenethyl bromide, respectively, with NaN_3, and *N*-Boc-propargylamine **89** or *N*-Boc-butynylamine **90**, in the presence of an excess of Na_2CO_3 and catalytic $CuSO_4{\cdot}5H_2O$ and ascorbic acid in H_2O and DMF at r. t. overnight [219] afforded triazoles **91**-**93** in 49-71% yield and with no need of purification. Triazoles **91**-**93** were treated with an excess of NaH and MeI at r. t. for 3 h to afford **94**-**96** in 81-95% yield, after washing with pentane (**Scheme 6.4**).

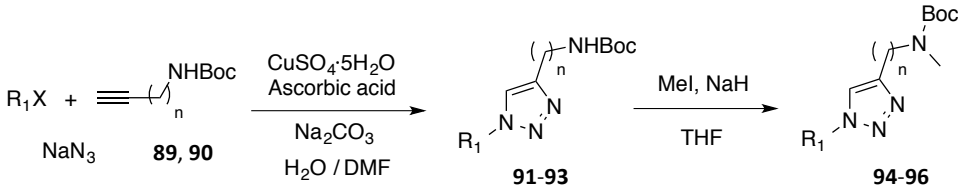

R_1X = *n*-BuBr, BnBr, or $Ph(CH_2)_2Br$
89, n = 1
90, n = 2

91, n = 1, R_1 = Me, 69%
92, n = 2, R_1 = Bn, 71%
93, n = 2, R_1 = $Ph(CH_2)_2$-, 49%

94, n = 1, R_1 = Me, 95%
95, n = 2, R_1 = Bn, 95%
96, n = 2, R_1 = $Ph(CH_2)_2$-, 81%

Scheme 6.4

[218] Struthers, H.; Mindt, T.; Schibli, R. *Dalton Trans.* **2010**, *39*, 675.
[219] Crowley, J.D.; Bandeen, P.H. *Dalton Trans.* **2010**, *39*, 612.

A butyl substituent was further introduced at position 5 of triazole **94** by reaction of this compound with *n*-BuLi at –78 °C followed by treatment with *n*-butyl bromide, at –78 °C for 1 h and at r. t. for 2h, to give **97** in 97% yield and again with no need of purification (**Scheme 6.5**).

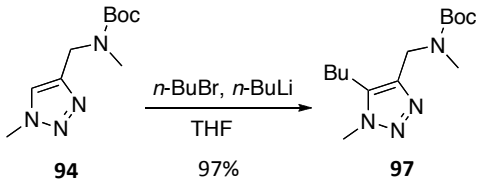

Scheme 6.5

Compounds **95**-**97** were deprotected by treatment with an excess of 85% H_3PO_4 in CH_2Cl_2 at r. t. for 1.5-2 h to give the desired deprotected triazoles **98**-**100** in 94% to quantitative yield without necessity of purification. Finally, **98**-**100** were treated with Cs_2CO_3 and 1 equivalent of propargyl bromide in acetone at 0 °C from 2 to 3.5 h to give the desired propargylamines **101**-**103** in 65-71% yields without any column chromatography purification (**Scheme 6.6**).

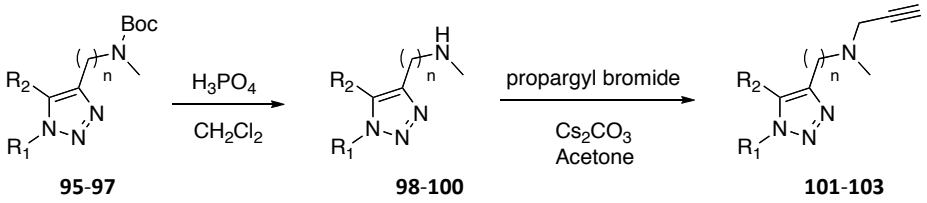

98, n = 1, R_1 = Me, R_2 = *n*-Bu, quantitative
99, n = 2, R_1 = Bn, R_2 = H, 94%
100, n = 2, R_1 = $Ph(CH_2)_2$-, R_2 = H, 98%
101, n = 1, R_1 = Me, R_2 = *n*-Bu, 65%
102, n = 2, R_1 = Bn, R_2 = H, 71%
103, n = 2, R_1 = $Ph(CH_2)_2$-, R_2 = H, 66%

Scheme 6.7

6.4.2 Synthesis of triazole-based compounds 120 and 121

The synthesis of the target triazoles **120** and **121** required the preliminary preparation of alkynes **108** and **109** through a two step sequence involving an initial *Negishi* coupling of benzyl bromides **104** or **105** with trimethylsilyl acetylene in the presence of *n*-BuLi and $ZnBr_2$, using $Pd(PHEphos)Cl_2$ as catalyst,[220] which afforded the corresponding silylated alkynes **106**

[220]Shi, Z.-J.; Yu, D.-G. *Comprehensive Org. Chem.* **2013**, *II 6*, 47.

and **107** in 83% and 63% yield, respectively, after column chromatography purification (**Scheme 6.8**).

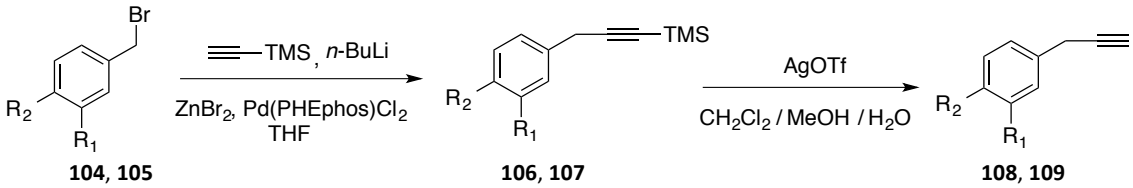

104, **105** **106**, **107** **108**, **109**

104, R_1 = H, R_2 = CN
105, R_1 = CN, R_2 = H

106, R_1 = H, R_2 = CN, 83%
107, R_1 = CN, R_2 = H, 63%

108, R_1 = H, R_2 = CN, 63%
109, R_1 = CN, R_2 = H, 68%

Scheme 6.8

This step was followed by a desilylation reaction of **106** and **107** by treatment with an excess of AgOTf in a mixture of MeOH, H_2O and CH_2Cl_2,[221] which afforded the unprotected alkynes **108** and **109** in 63% and 68% yield, respectively, after column chromatography purification. Alkynes **108** and **109** were subjected to the CuAAC with MeN_3, generated *in situ* through reaction of NaN_3 with MeI, to afford triazoles **110** and **111** in 94% and 95% yield, respectively, with no need of purification. Subsequent $LiAlH_4$ reduction of nitriles **110** and **111** to the corresponding amines afforded triazole derivatives **112** and **113** in 80% and 49% yield, respectively, again without any purification process (**Scheme 6.9**).

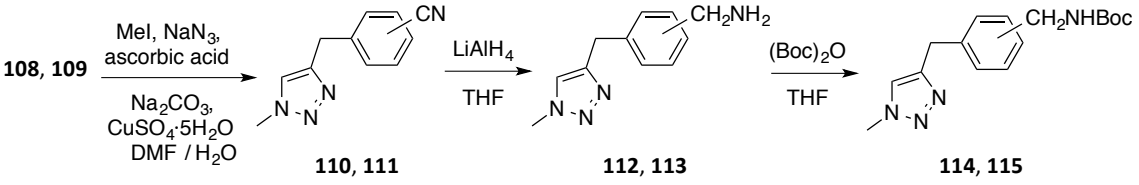

110, **111** **112**, **113** **114**, **115**

110, -CN (*para*), 94%
111, -CN (*meta*), 95%

112, -CH_2NH_2 (*para*), 80%
113, -CH_2NH_2 (*meta*), 49%
114, -CH_2NHBoc (*para*), quantitative
115, -CH_2NHBoc (*meta*), quantitative

Scheme 6.9

[221]Orsini, A.; Vitérisi, A.; Bodlenner, A.; Weibel, J.-M.; Pale, P. *Tetrahedron Lett.* **2005**, *46*, 2259.

After previous protection of amine groups of **112** and **113** through treatment at 0 °C with 1 equivalent of $(Boc)_2O$ in THF, the resulting *N*-Boc-protected triazoles **114** and **115** were methylated by treatment with an excess of NaH and MeI at r. t. or 60 °C from 4 h to overnight to afford triazoles **116** and **117** in 84% and 80% yield, after washing with pentane. Compounds **116** and **117** were deprotected by treatment with an excess of 85% H_3PO_4 in CH_2Cl_2 at r. t. for 1.5 h to 3 h to give the desired unprotected triazoles **118** and **119** in quantitative and 96% yield, respectively, without any purification. Finally, **118** and **119** were treated with Cs_2CO_3 and propargyl bromide in acetone at 0 °C from 3 to 3.5 h to give the desired propargylamines **120** in 65%, with no need of purification, and **121** in 40% yield after column chromatography purification (**Scheme 6.10**).

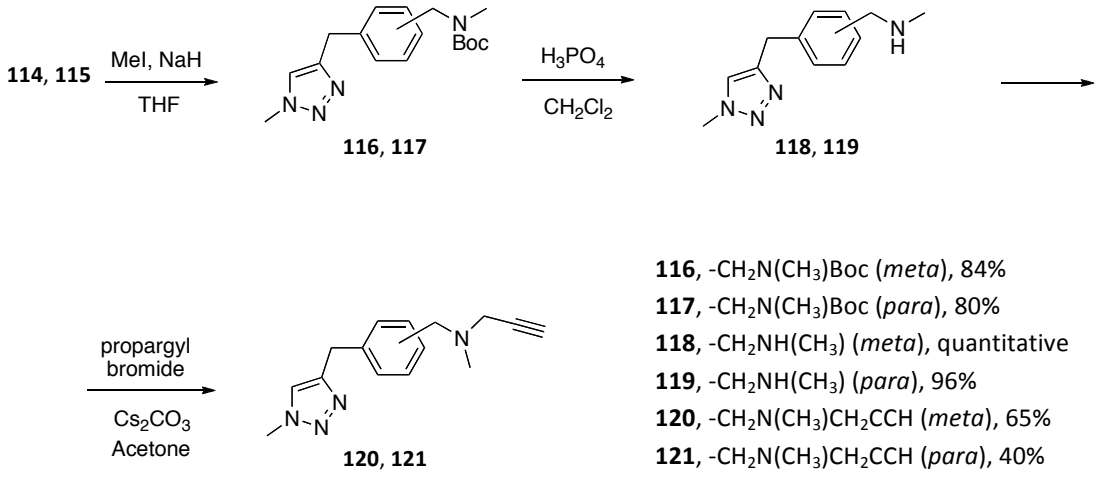

Scheme 6.10

6.4.3 Synthesis of triazole-based compounds 122-126

According to the initial design, scaffold **95** was selected for further alkylation at position 5 with different alkyl halides (MeI, EtBr, PrBr and BuBr). Surprisingly, all the attempts to reach selective alkylation of substrate **95** at its *C5*, using stoichiometric amounts of *n*-BuLi or, alternatively, the more sterically hindered *tert*-BuLi, resulted ineffective. Indeed, even thoughit was not apparent from TLC analysis and ^{1}H-NMR spectra, MS spectra and DEPT experiments revealed that mixtures of the desired monoalkylated triazoles **124**-**126** with the corresponding dialkylated derivatives **127**-**129** were obtained when using EtBr, *n*-PrBr or *n*-BuBr as the alkylating agent. Unfortunately, any attempt of purification through gradient elution column chromatography was fruitless.

Alkylation reaction of **95** with MeI, using *n*-BuLi as the base, afforded only the dialkylated compound **122** as a racemic mixture in 79% yield, after washing with pentane (**Scheme 6.11**).

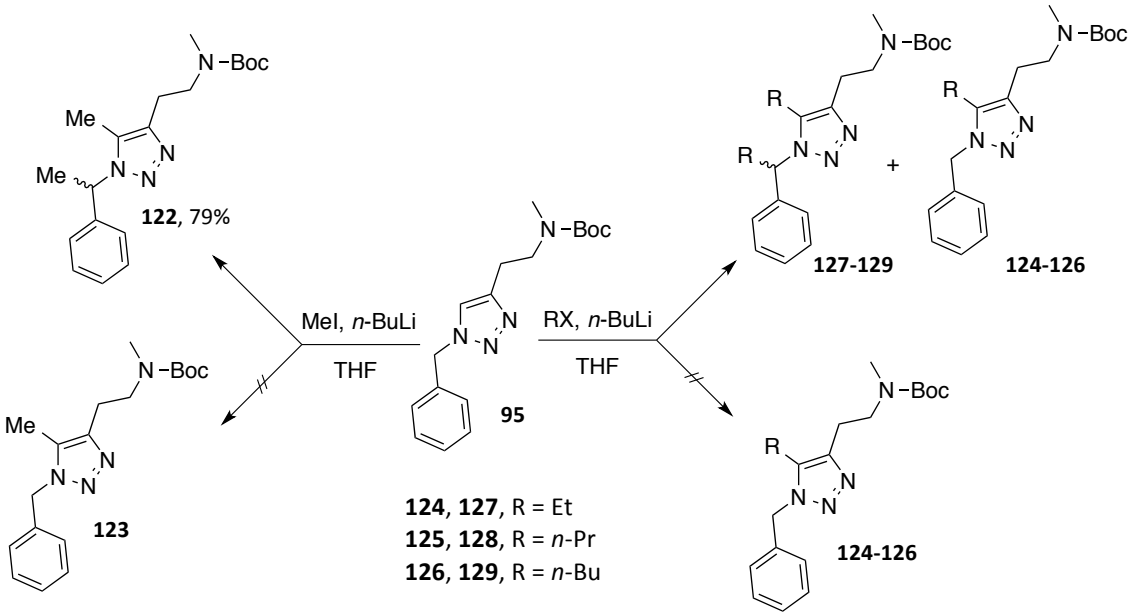

Scheme 6.11

Triazole **122** was subjected to acidic deprotection by treatment with an excess of 85% H_3PO_4 in CH_2Cl_2, affording the unprotected triazole **130** in quantitative yield. The final propargylation reaction of **130** with Cs_2CO_3 and propargyl bromide in acetone at 0 °C for 3.5 h provided the desired propargylamine **131** in 53% yield, after column chromatography purification (**Scheme 6.12**).

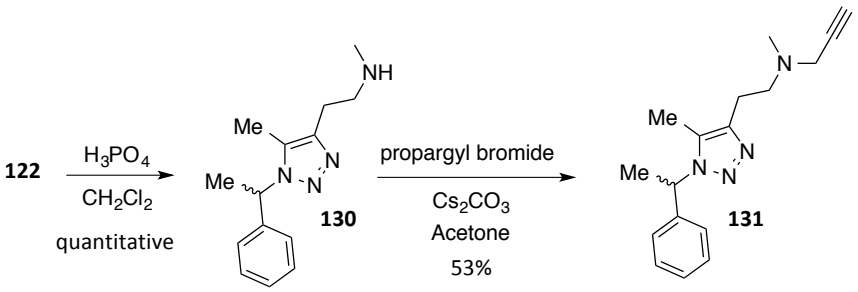

Scheme 6.12

6.4.4 Synthesis of triazole-based compounds 140-142

Elimination of the slightly acidic benzylic position of triazole **95**, through substitution of the benzyl by a phenyl group was considered an affordable chemical modification that should not affect, in principle, the putative biological activity of the resulting compounds. Thus, the triazole derivative **132** was prepared through CuAAC of the commercially available PhN_3 to alkyne **90** in 56% yield, after precipitation with isopropanol. Compound **132** was further methylated at its *N*-Boc-protected nitrogen atom with the same procedure previously described, affording **133** in 95% yield (**Scheme 6.13**).

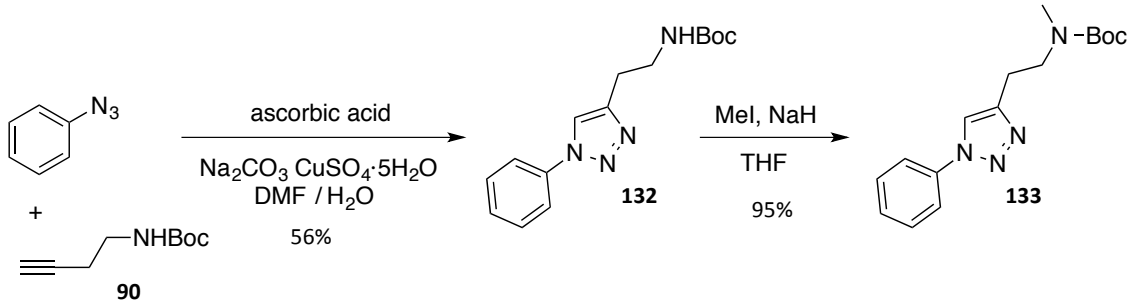

Scheme 6.13

Compound **133** was alkylated at position 5 using EtBr, *n*-PrBr and *n*-BuBr and *n*-BuLi in excess at −78 °C in THF, affording triazoles **134** and **135** in 98% and 96% yield, respectively, with no need of purification, and **136** in 43% yield after column chromatography. Then, acidic deprotection of **134**-**136** afforded triazoles **137** and **138** in 89% and 67% yield, respectively, after column chromatography purification, and **139** in 92% yield with no need of purification. Finally, propargylation reaction of **137**-**139** in the same conditions as described before, afforded the desired propargylamines **140**-**142** in 95%, 88% and 91% yield, respectively, after column chromatography purification (**Scheme 6.14**).

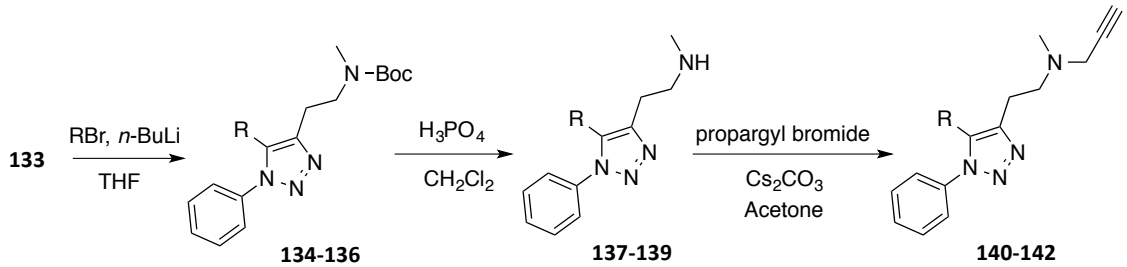

134, R = Et, 98%
135, R = *n*-Pr, 96%
136, R = *n*-Bu, 43%

137, R = Et, 89%
138, R = *n*-Pr, 67%
139, R = *n*-Bu, 92%

140, R = Et, 95%
141, R = *n*-Pr, 88%
142, R = *n*-Bu, 91%

Scheme 6.14

Design, synthesis and biological evaluation of *N*-methyl-*N*-[(1,2,3-triazol-4-yl)alkyl]propargylamines as novel monoamine oxidase B inhibitors

Ornella Di Pietro,[a] Nelson Alencar,[b] Jordi Juárez-Jiménez,[b] Javier Vázquez,[b] Elisabet Viayna,[a] Natalia Guzior,[a] Irene Sola,[a] Gerard Esteban,[c] Mercedes Unzeta,[c] Diego Muñoz-Torrero,*[a] F. Javier Luque*[b]

[a] Laboratori de Química Farmacèutica (Unitat Associada al CSIC), Facultat de Farmàcia and Institut de Biomedicina (IBUB), Universitat de Barcelona, Av. Joan XXIII 27-31, E-08028 Barcelona, Spain

[b] Departament de Fisicoquímica, Facultat de Farmàcia and Institut de Biomedicina (IBUB), Universitat de Barcelona, Av. Prat de la Riba 171, E-08921 Santa Coloma de Gramenet, Spain

[c] Departament de Bioquímica i Biologia Molecular, Facultat de Medicina and Institut de Neurociències, Universitat Autònoma de Barcelona, E-08193 Bellaterra, Spain

* E-mail: dmunoztorrero@ub.edu; fjluque@ub.edu

Abstract

Different azides and alkynes have been coupled via Cu-catalyzed 1,3-dipolar Huisgen cycloaddition to afford a novel family of N_1- and C_5-substituted 1,2,3-triazole derivatives that feature the propargylamine group typical of irreversible MAO-B inhibitors at the *C4*-side chain of the triazole ring. All the synthesized compounds were evaluated against human MAO-A and MAO-B (*h*MAO-A, *h*MAO-B). Structure-activity relationships and molecular modelling were utilized to gain insight into the structural features that enhance the binding affinity and selectivity between the two enzyme isoforms. Two promising *hit* candidates, in terms of potency and MAO-B selective recognition, respectively, were identified. The one displaying the best pharmacological profile (*h*MAO-B IC_{50} of 3.54 μM, selectivity MAO-B/MAO-A index of 0.04) was further subjected to reversibility and time-dependence inhibition studies, which disclosed a slow and irreversible inhibition of *h*MAO-B. Overall, the results support the suitability of the 4-triazolylalkyl propargylamine scaffold for exploring the design of multipotent anti-Alzheimer compounds endowed with irreversible MAO-B inhibitory activity.

Keywords

Click-chemistry; monoamine oxidase B; Alzheimer's disease; irreversible inhibition

1. Introduction

Alzheimer's disease (AD) is one of the most relevant age-related neurodegenerative disorders currently representing the fourth leading cause of death and afflicting over 36 million people worldwide.[1,2] Its clinical manifestation is mainly reflected in a progressive loss of memory and cognitive functions, often in association with behavioral disturbances and depression.[3] Its complex and multifaceted etiopathology, which involves massive loss of cholinergic neurons,[4] oxidative stress,[5-7] metal dyshomeostasis,[8] excitotoxicity,[9] neurofibrillary tangles and β-amyloid aggregate deposition,[10,11] has precluded so far the discovery of effective disease-modifying drugs. The low efficacy, confined to symptomatic effects, of the currently approved drugs, namely, three acetylcholinesterase (AChE) inhibitors (rivastigmine, galantamine, and donepezil),[12-14] and an *N*-methyl-*D*-aspartate receptor antagonist (memantine),[15] and the failure of a number of drug candidates targeting one of the targets involved mainly in β-amyloid biology to show efficacy over placebo in clinical trials, has shifted drug discovery efforts toward the development of compounds hitting less explored biological targets alone or in combination with other key targets, i.e. the so-called multi-target-directed ligands (MTDLs).[16-18]

In this context, monoamine oxidase (MAO, E.C.1.4.3.4) has emerged as a promising target because of the neuroprotective properties exerted by their inhibitors.[2,19-21] MAO is a flavin adenine dinucleotide (FAD)-containing enzyme that catalyzes the degradation of biogenic and xenobiotic amines. MAO is found in two isoforms, namely MAO-A and MAO-B, which have been characterized by their amino acid sequence, tissue distribution, substrate specificity and inhibitor sensitivity.[22-24] Thus MAO-A, preferentially degrading serotonin, adrenaline and noradrenaline, is irreversibly inhibited by clorgyline, whereas MAO-B, specifically responsible for the oxidative deamination of ethylamine and benzylamine, is irreversibly inhibited by *R*-(−)-deprenyl (Figure 1). These trends reflect the structural differences in the binding sites as revealed by high-resolution X-ray structures.[25-29] In particular, a key structural feature in shaping the substrate cavity is the replacement of the pair Phe208/Ile335 in MAO-A by Ile199/Tyr326 in MAO-B, leading to the distinction between "substrate" and "entrance" sites in MAO-B. The replacement of Ile180/Asn181 and Val210 in MAO-A by Leu17/Cys172 and Thr201 in MAO-B are additional differences in the binding sites, which may modulate the selective inhibition by certain MAO inhibitors.[30]

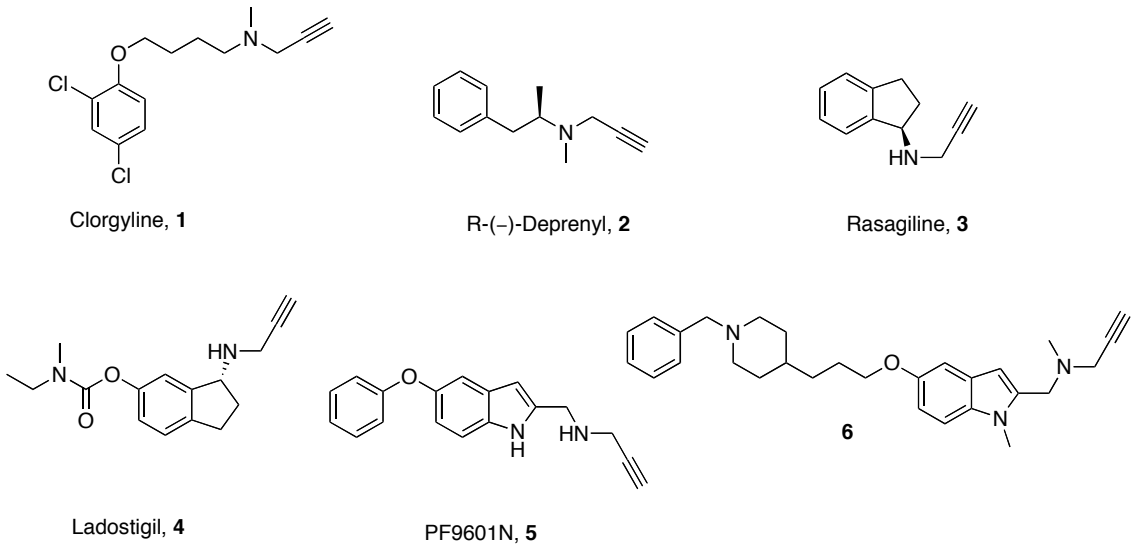

Figure 1. Chemical structures of MAO inhibitors.

The neuroprotection exerted by MAO inhibitors may result not only from the increased amine neurotransmission, but also from the prevention of the formation of neurotoxic species, which may ultimately lead to neuronal damage,[31,32] and from the anti-apoptotic properties of the propargylamine group present in some MAO inhibitors.[33,34] Interestingly, the levels of MAO-B increase with age and its activity is elevated in AD patients, which results in increased brain levels of neurotoxic free radicals.[20] In this context, the development of MAO-B inhibitors and MAO-B-inhibitor-based MTDLs emerges as a promising strategy for the design of neuroprotective agents with potential disease-modifying activity towards AD and other neurodegenerative disorders, such as Parkinson disease.[35,36]

Most efforts have been addressed toward the design of MTDLs targeting AChE and/or butyrylcholinesterase (BuChE) and MAO. A successful example is ladostigil (Figure 1), a dual inhibitor of MAO-B and AChE, which is undergoing phase II clinical trials.[37] Ladostigil combines the carbamate moiety of the AChE inhibitor rivastigmine with the indolamine moiety of the selective MAO-B inhibitor rasagiline, and shows neuroprotective and anti-apoptotic activities.[38] A novel series of MAO/ChE inhibitors that combine the *N*-benzylpiperidine moiety of the AChE inhibitor donepezil with the indolyl propargylamine of the potent MAO-B inhibitor PF9601N has been reported,[39] with the most promising compound (**1**, Figure 1) being also able to inhibit the

aggregation of the β-amyloid peptide. Other strategies have relied on the hybridization of coumarins with either *N*-benzyl-*N*-alkyloxy groups[40] or tacrine,[41] leading to multipotent inhibitors of both MAO and ChEs, or alternatively have pursued the development of MTDLs targeting both MAO inhibition and additional activities, such as metal chelation.[42,43] Also, natural products endowed with MAO and ChEs inhibitory activities have been recently reported.[44]

Although the development of MAO-inhibitor-based MTDLs is very attractive, it is challenged by the need to keep a good balance among potencies against multiple targets and optimal ADME-T properties.[45-47] Furthermore, the success of this strategy depends on the suitability of an efficient synthetic approach, which should afford the fusion or linkage of chemical scaffolds without introducing drastic alterations in the activity against the multiple targets. In this context, the Cu(I)-catalyzed azide-alkyne cycloaddition (CuAAC) enables the synthesis of a virtually unlimited source of ligands containing the 1,4-disubstituted 1,2,3-triazole core.[48-51] The CuAAC reaction between libraries of azides and alkynes featuring different pharmacophoric moieties has been used for the synthesis of triazole-linked hybrid compounds as multisite enzyme inhibitors and MTDLs.[52-62] Also, azide-alkyne cycloaddition reactions have been successfully used for the synthesis of high-affinity multisite enzyme inhibitors inside the biological target, in the absence of copper catalysis, i.e. the so-called *in situ* click chemistry.[63-67] In these hybrid compounds not only the triazole ring is used as a non-hydrolyzable, non-oxidizable, and non-reducible robust linker between their two pharmacophoric moieties, but it can also provide favourable physicochemical properties and potential interactions with the biological target, i.e. hydrogen bond, dipole-dipole, and π-stacking interactions.[68]

In this context, as the first step of a program directed to the synthesis of MAO-B-inhibitor-based anti-Alzheimer MTDLs, here we have explored the CuAAC-mediated synthesis of a series of 1,2,3-triazole derivatives, featuring the propargylamine group of typical irreversible MAO-B inhibitors in the side chain at position 4 and different lipophilic substituents at positions 1 and 5 (Scheme 1). To determine the therapeutic potential of the target compounds and their usefulness as the MAO-B pharmacophoric moiety of novel families of MTDLs, we have assessed the *in vitro* inhibitory activity of the novel compounds against human MAO-B and MAO-A and their brain penetration, through the widely used parallel artificial membrane permeability assay (PAMPA-BBB). The mechanism of action of these compounds has been studied by reversibility

and time-dependence inhibition studies. Molecular modelling studies have been performed to rationalize the differences in inhibitory potency and selectivity between the two MAO isoforms of the novel compounds.

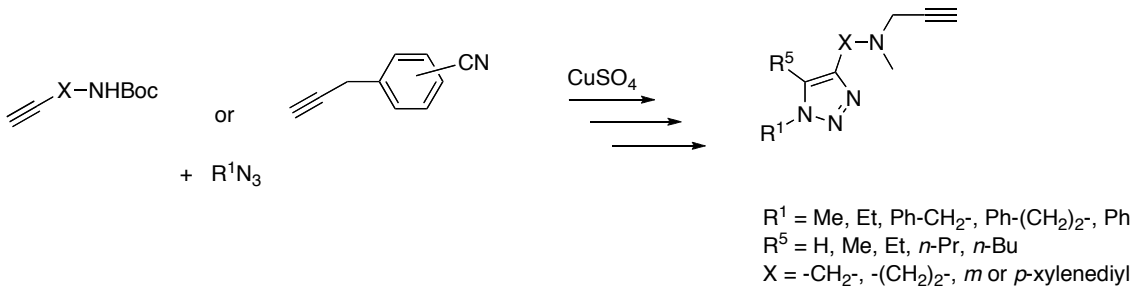

Scheme 1. General structure of the target *N*-methyl-*N*-[(1,2,3-triazol-4-yl)alkyl]propargylamines.

2. Results and Discussion

2.1. Design and synthesis of the target N-methyl-N-[(1,2,3-triazol-4-yl)alkyl]propargylamines

We initially planned the synthesis of the 1-ethyltriazolylmethyl and 1-ethyltriazolylethyl propargylamines **25** and **26**, unsubstituted at position 5 of the triazole ring, and their 5-methyl-substituted analogues **43** and **44**, as the early simple prototypes to validate the suitability of the CuAAC-assisted synthetic methodology to deliver 1,4-disubstituted and 1,4,5-trisubstituted 1,2,3-triazole scaffolds featuring the propargylamine group of irreversible MAO inhibitors. These compounds are quite polar (miLogP 0.43, 0.84, 0.65, and 1.06, respectively) due to the presence of the triazole ring. However, the substrate cavity of MAO is highly hydrophobic, and accordingly MAO inhibitors are usually more lipophilic molecules (miLogP in the range 2-4 for compounds depicted in Figure 1). Thus, to counterbalance the high polarity conferred by the triazole ring, we envisaged the introduction of more lipophilic benzyl or phenethyl substituents at position 1 (i.e. compounds **27** and **28**, respectively, Scheme 2) or at position 5 of the triazole ring (i.e. the 1-methyl-5-butyl-substituted compound **46**). We also planned the synthesis of derivatives of the 1-benzyl-substituted compound **27** bearing different alkyl groups at position 5. However, the moderate acidity of the α-nitrogen benzylic protons of the substituent at position 1 of the triazole ring interfered with the alkylation of the position 5 (see below). To avoid these synthetic issues, we envisaged the synthesis of

compounds **47**, **48** and **49** (Scheme 2), bearing a phenyl group instead of a benzyl group at position 1 of the triazole ring and ethyl, propyl, or butyl substituents at position 5. Finally, we also explored the isomerization of the benzene ring of compound **27** from the substituent at position 1 of the triazole ring to the side chain at position 4, i.e. between the triazole ring and the propargylamine moiety (compounds **66** and **67**, Scheme 3).

The synthesis of the target compounds was envisaged through synthetic sequences involving as the key step a CuAAC reaction[69-72] between alkyl or phenyl azides and alkynes bearing an amino or a cyano group to enable the subsequent installation of the propargylamine moiety (Scheme 1). The synthesis of the 5-unsubstituted triazolylmethyl and triazolylethyl propargylamines **25-28** was carried out through a four-step synthetic sequence, starting from the copper-catalyzed Huisgen 1,3-dipolar cycloaddition of the known *N*-Boc-protected amines **7** and **8** with ethyl, benzyl, and phenethyl azide, generated *in situ* by reaction of NaN_3 with the corresponding alkyl halide,[73] which afforded the 1-substituted triazole derivatives **9-12** in moderate to good yields (49-78%, Scheme 2). Subsequent methylation of the *N*-Boc-protected aliphatic nitrogen atom of compounds **9-12** with MeI in anhydrous THF, in the presence of NaH, followed by acidic deprotection of the resulting compounds **15-18** afforded the secondary amines **21-24** in excellent yields. The final propargylation of amines **21-24** on reaction with propargyl bromide in acetone in the presence of Cs_2CO_3 led to propargylamines **25-28** in 59-89% yield (Scheme 2). Thus, the target compounds **25-28** were obtained in 26-58% overall yield without the need of any column chromatography purification, with the sole exception of the last step for **25**.

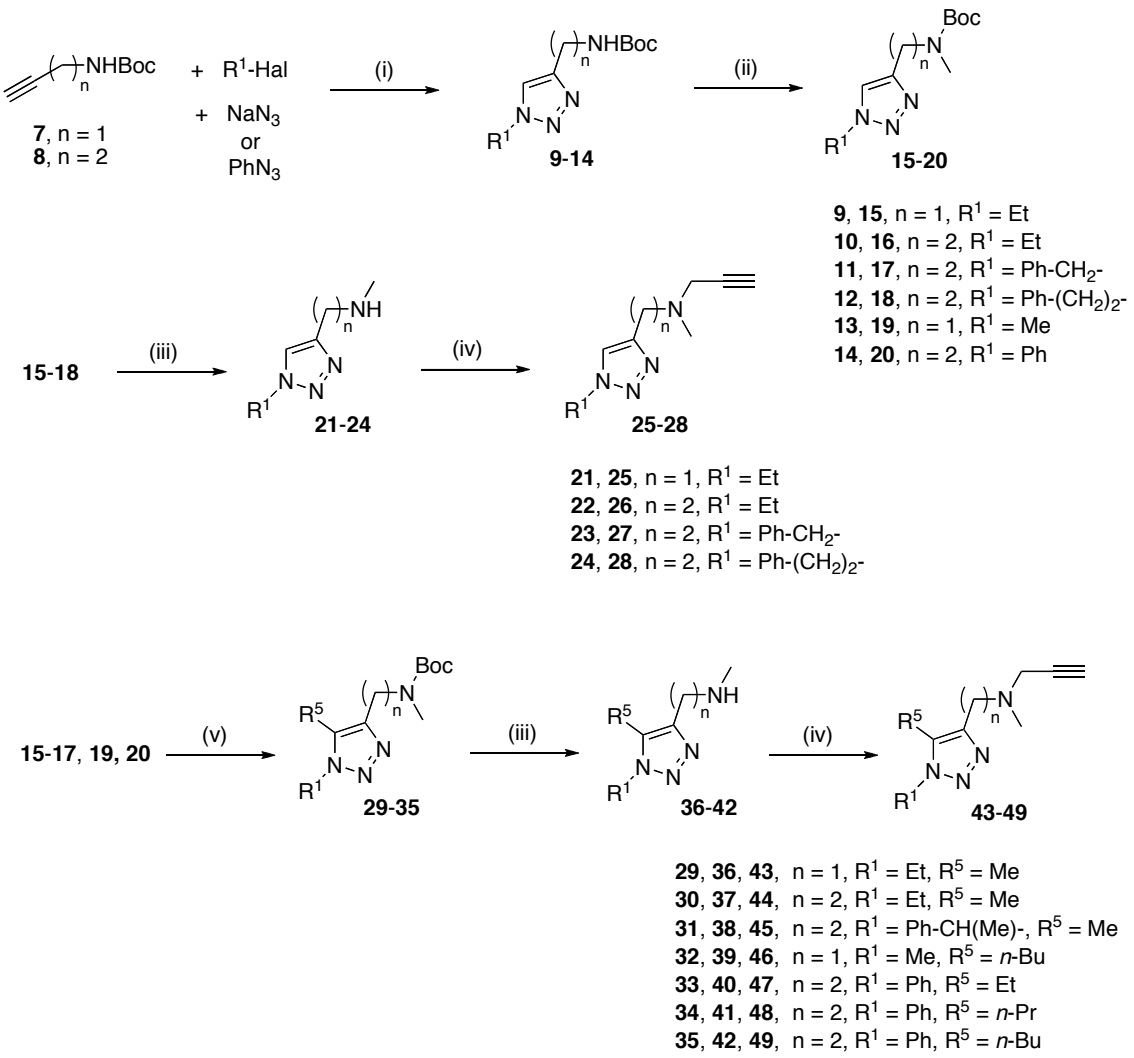

Scheme 2. Reagents and conditions: (i) $CuSO_4 \cdot 5H_2O$, ascorbic acid, Na_2CO_3, H_2O/DMF, rt, overnight: **9** (78%), **10** (78%), **11** (71%), **12** (49%), **13** (69%), **14** (56%); (ii) MeI, NaH, THF, rt, 1.5-15 h: **15** (97%), **16** (95%), **17** (95%), **18** (81%), **19** (95%), **20** (95%); (iii) H_3PO_4, CH_2Cl_2, rt, 1.5-4 h: **21** (86%), **22** (90%), **23** (94%), **24** (98%), **36** (91%), **37** (89%), **38** (quant.), **39** (quant.), **40** (89%), **41** (67%), **42** (92%); (iv) propargyl bromide, Cs_2CO_3, acetone, rt for 2-15 h, or 0 ºC for 2-2.5 h, or 0 ºC for 30 min and then rt for 3 h: **25** (89%), **26** (59%), **27** (71%), **28** (66%), **43** (62%), **44** (54%), **45** (53%), **46** (65%), **47** (95%), **48** (88%), **49** (91%); (v) R^5-Hal, *n*-BuLi, THF, -78 ºC, 1 h, then -78 ºC → rt, and rt, 2 h: **29** (96%), **30** (90%), **31** (79%), **32** (97%), **33** (98%), **34** (96%), **35** (43%).

For the synthesis of the 5-alkyl-substituted triazolylmethyl and triazolylethyl propargylamines **43**, **44** and **46**, apart from the intermediates **15** and **16**, the triazole derivative **19** was also prepared in good yield using the same CuAAC-*N*-methylation

protocol (Scheme 2). Alkylation of compounds **15**, **16** and **19** with the appropriate alkyl halide using *n*-BuLi as the base afforded the corresponding 5-alkylated compounds **29**, **30** and **32**, respectively, in excellent yields (90-97%). However, when we subjected the 1-benzyl-substituted intermediate **17** to the same alkylation reaction conditions with methyl iodide as the alkylating agent we did not obtain the expected 1-benzyl-5-methyl-substituted derivative but the 1-(α-methylbenzyl)-5-methyl-substituted derivative **31** in 79% yield, resulting from the double alkylation at the position 5 of the triazole ring and at the moderately acidic α-nitrogen benzylic position of the substituent at position 1 (Scheme 2). Treatment of intermediate **17** with ethyl bromide or *n*-butyl bromide as the alkylating agents and *n*-BuLi or the more hindered *t*-BuLi as the base yielded inseparable mixtures of 5-monoalkylated and α,5-dialkylated products. To avoid double alkylation, we prepared the 1-phenyl-substituted intermediate **20**, which was alkylated with ethyl bromide, *n*-propyl bromide, and *n*-butyl bromide using *n*-BuLi as the base, to afford the expected 5-alkyl-substituted derivatives **33**, **34** and **35** in 98%, 96%, and 43% yield, respectively (Scheme 2). The acidic *N*-Boc deprotection of 5-alkyl-substituted compounds **29**-**35** afforded the secondary amines **36**-**42** in good yields (67% to quantitative yield). Propargylation of amines **36**-**42** had to be performed by monitoring the reaction course at different reaction temperatures and times to avoid the formation of dipropargylated products. For example, reaction of amine **36** with propargyl bromide in the presence of Cs_2CO_3 at rt overnight yielded the dipropargylated derivative as the major reaction product (92% yield), whereas on reaction at 0 ºC for 2 h only the desired monopropargylated product, **43**, was obtained, in 62% yield. Thus, by selecting the most appropriate reaction temperature and time, the target 5-alkyl-substituted triazolylmethyl and triazolylethyl propargylamines **43**-**49** were synthesized (19-44% overall yield over the five-step sequence).

The synthesis of the triazolyl-*m*-xylyl and triazolyl-*p*-xylyl propargylamines **66** and **67** was carried out through the eight-step sequence depicted in Scheme 3. First, the alkynes **54** and **55**, necessary for the CuAAC, were prepared by an initial Negishi coupling[73] between benzyl bromides **50** and **51** and trimethylsilylacetylene in the presence of *n*-BuLi and $ZnBr_2$, under Pd(0) catalysis, followed by desilylation of the protected alkyne derivatives **52** and **53** with AgOTf in a mixture of CH_2Cl_2/MeOH/H_2O,[74] and silica gel column chromatography purification. The CuAAC of methyl azide to alkynes **54** and **55** afforded the corresponding triazole derivatives **56** and **57** in excellent yield (95%). $LiAlH_4$ reduction of the nitrile group of **56** and **57** to the corresponding amines **58** and

59, followed by *N*-Boc protection of the primary amino group afforded the intermediates **60** and **61**, from which the target propargylamines **66** and **67** were synthesized in good yields through the standard *N*-methylation-acidic deprotection-propargylation protocol, without the need of any additional column chromatography purification (Scheme 3).

All the compounds to be subjected to biological evaluation were transformed into the corresponding hydrochloride salts and were chemically characterized through IR, ^{1}H and ^{13}C NMR spectra, and elemental analysis and/or HRMS.

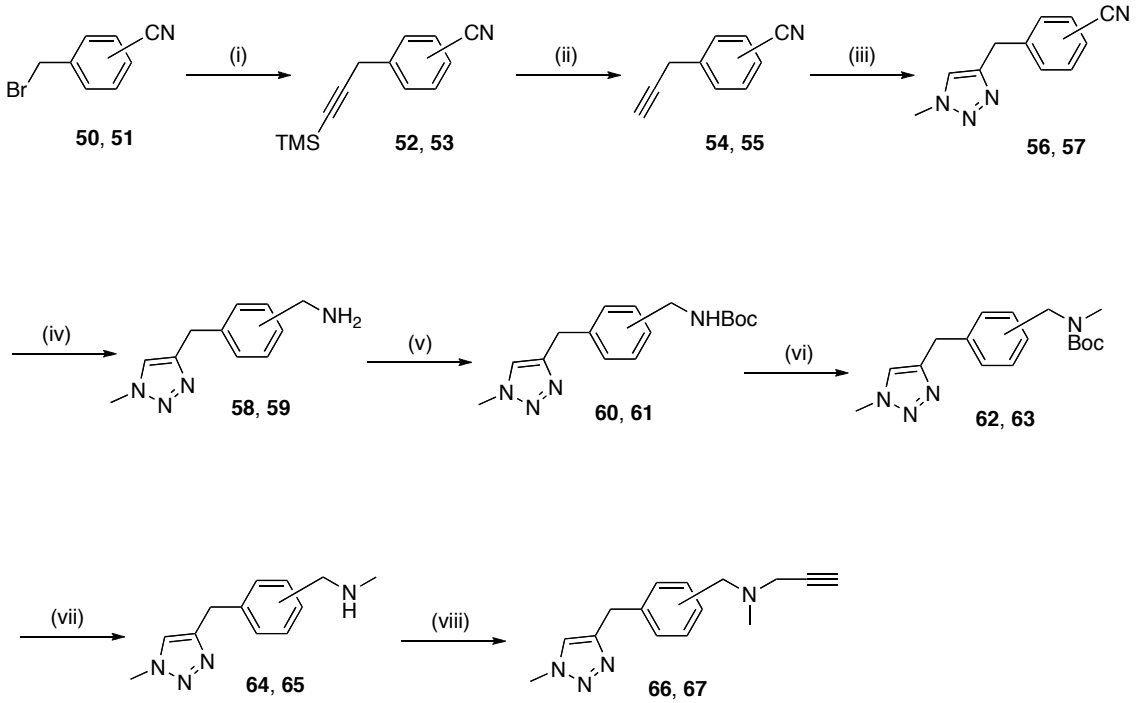

Series *meta* : **50**, **52**, **54**, **56**, **58**, **60**, **62**, **64**, **66**
Series *para* : **51**, **53**, **55**, **57**, **59**, **61**, **63**, **65**, **67**

Scheme 3. Reagents and conditions: (i) trimethylsilylacetylene, THF, *n*-BuLi, -78 ºC, 30 min, then, $ZnBr_2$, THF, -78 ºC → 0 ºC, then, **50** or **51**, $Cl_2Pd(PPh_3)_2$, rt, overnight: **52** (63%), **53** (83%); (ii) AgOTf, CH_2Cl_2/MeOH/H_2O, rt, overnight: **54** (68%), **55** (63%); (iii) $CuSO_4 \cdot 5H_2O$, ascorbic acid, Na_2CO_3, H_2O/DMF, rt, overnight: **56** (95%), **57** (94%); (iv) $LiAlH_4$, THF, reflux, 2 h: **58** (49%), **59** (80%); (v) $(Boc)_2O$, THF, rt, 3 h: **60** (quantitative), **61** (quantitative); (vi) MeI, NaH, THF, 60 ºC, 4 h: **62** (84%), **63** (80%); (vii) H_3PO_4, CH_2Cl_2, rt, 1.5-3 h: **64** (quantitative), **65** (96%); (viii) propargyl

bromide, Cs_2CO_3, acetone, 0 ºC for 3.5 h or 0 ºC for 30 min and then rt for 3 h: **66** (65%), **67** (31%).

2.2. Molecular modelling and MAO inhibitory activity of the target compounds

The novel *N*-methyl-*N*-[(1,2,3-triazol-4-yl)alkyl]propargylamines **25**-**28**, **43**-**49**, **66** and **67** were evaluated *in vitro* against human recombinant MAO-A and MAO-B (*hr*MAO-A and *hr*MAO-B), and the corresponding IC_{50} values and selectivity indices (SI; defined as the ratio IC_{50}(MAO-B)/IC_{50}(MAO-A)) were determined (Table 1).

Table 1. MAO-A and MAO-B inhibitory activities, selectivity indices, and BBB permeability

Compound	*hr*MAO-A[a] IC_{50} (μM)	*hr*MAO-B[a] IC_{50} (μM)	SI[b]	*Pe* (10^{-6} cm s^{-1})[c]
25	134.7 ± 21.8	248.6 ± 94.5	1.8	nd[d]
26	553.5 ± 83.6	373.9 ± 119	0.7	nd[d]
43	267.4 ± 30.8	104.7 ± 27.1	0.4	nd[d]
44	91.2 ± 13.6	237.6 ± 51.8	2.6	nd[d]
27	97.12 ± 30.1	3.54 ± 0.44	0.036	15.6 ± 1.5 (CNS+)
28	56.1 ± 8.7	172.8 ± 47.8	3.1	14.8 ± 0.85 (CNS+)
45	47.0 ± 6.9	134.2 ± 25.5	2.9	20.0 ± 0.7 (CNS+)
46	<300	94.73 ± 16.3	<0.32	29.9 ± 0.8 (CNS+)
47	7.5 ± 1.1	213.4 ± 54.0	28.5	17.0 ± 1.9 (CNS+)
48	26.1 ± 4.0	156.8 ± 31.9	6.0	17.2 ± 0.6 (CNS+)
49	17.3 ± 4.5	155.5 ± 25.0	9.0	21.4 ± 1.3 (CNS+)
66	2.12 ± 0.32	64.96 ± 15.4	30.6	15.6 ± 1.5 (CNS+)
67	0.526 ± 0.06	0.607 ± 0.08	1.15	14.8 ± 0.85 (CNS+)
***L*-Deprenyl**	nd[d]	0.018 ± 0.003		
Clorgyline	0.020 ± 0.003			

[a] *In vitro* inhibitory activities against *hr*-MAO-A and *hr*-MAO-B. Experiments performed with Amplex Red fluorimetric method in 96-well plates. Data are the mean of duplicate experiments ± SEM.

[b] SI = IC_{50} (MAO-B) / IC_{50} (MAO-A).

[c] Permeability values from the PAMPA-BBB assay. Values are expressed as the mean ± SD of three independent experiments.

[d] Not determined.

The novel compounds turned out to be in most cases moderate to weak MAO inhibitors, with 2-3-digit micromolar IC_{50} values, with the exceptions of compounds **27**, **47**, **66** and **67**, which exhibited submicromolar or low micromolar potencies against one of both MAO isoforms.

The prototype compound **25**, **26**, **43** and **44** were weak inhibitors and showed no selectivity. These trends were not unexpected due to the large polarity of the triazole ring and the small size of these fragment-like compounds. Accordingly, several strategies were explored to modulate both the molecular size and hydrophobicity of the triazole derivatives. The first approach involved the substitution of the ethyl group at position 1 of the triazole ring of the initial prototypes by benzyl and phenethyl groups, which led to increased inhibitory potencies. Thus, the 1-phenethyl-derivative **28** was 2- and 10-fold more potent MAO-A inhibitor than the 1-benzyl- and 1-ethyl-analogues **27** and **26**, respectively. In contrast, for MAO-B inhibition, the optimal substitution pattern involved the presence of a 1-benzyl group, with compound **27** being 49- and 106-fold more potent than the 1-phenethyl- and 1-ethyl-analogues **28** and **26**, respectively. This latter findings suggests that the size of compound **27** is better suited to fill the binding cavity in MAO-B, as confirmed by the results obtained from restrained docking calculations, where the amine nitrogen atom of the propargylamine unit was imposed to overly the position of the corresponding atom fin the X-ray structures of covalently-bound L-deprenyl and rasagiline (PDB entries 2BYB and 2BK4),[28,75] following the strategy used in our previous studies.[39] Thus, Figure 1 shows that **27** superposes well with the structures of the irreversible inhibitor **6** (PDB entry 4CRT)[76] and the reversible inhibitor 1,4-diphenyl-2-butene (PDB entry 1OJ9).[26] In turn, docking of the phenethyl derivative **28** made it necessary to adopt a folded conformation, reflecting some degree of internal strain due to clashes within the cavity (data not shown).

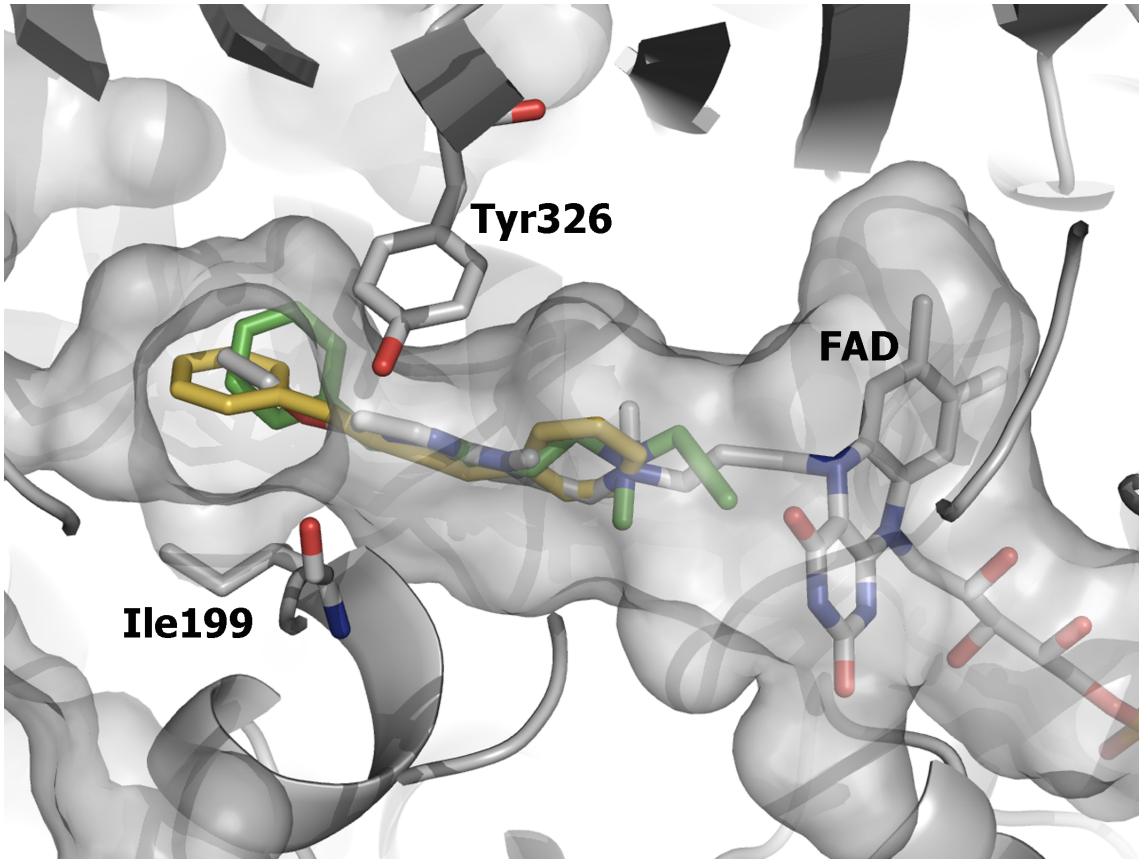

Figure 1. Representation of the docked pose of compound **27** (shown as green-coloured sticks) in the binding cavity of MAO-B (shown as gray cartoon). The surface of the binding cavity is depicted as a gray isocontour. The structures of inhibitor **6** (PDB entry 4CRT; covalently-bound to FAD, also shown as gray-coloured sticks) and the reversible inhibitor 1,4-diphenyl-2-butene (PDB entry 1OJ9) are shown as white-colored and yellow sticks, respectively.

An alternative strategy explored to modulate the hydrophobicity distribution of triazole derivatives relied on the alkylation of position 5 of the triazole ring (compounds **45**-**49**). However, alkylation did not seem to have a clear effect on MAO inhibitory potency, although this chemical modification was generally beneficial for MAO-A selectivity for compounds bearing large substituents at position 1 (Ph-CH(Me)- or Ph), with selectivity indices in the range 2.9-28.5. Finally, we also envisaged the isomerization of the benzene ring of compound **27** from the substituent at position 1 of the triazole ring to the side chain at position 4. This approach led to increased MAO-A inhibitory potencies, with compounds **66** and **67** being 46- and 183-fold more potent than **27**, and also to increased MAO-B inhibitory activity in the case of **67** (6-fold more potent than **27**), bearing a *para*-disubstituted benzene ring in the side chain at position 4. Docking

calculations also led to a binding pose that filled the binding cavity of MAO-B (Figure 2).

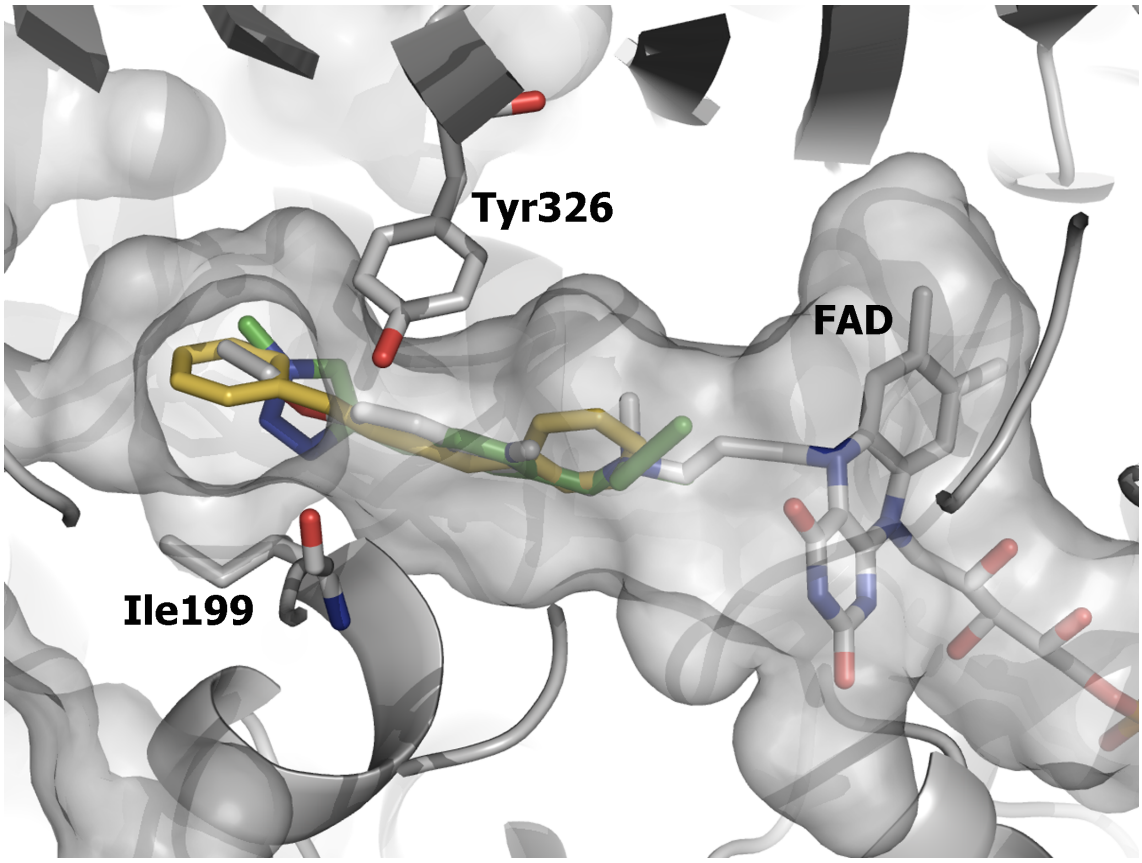

Figure 2. Representation of the docked pose of compound **67** (shown as green-coloured sticks) in the binding cavity of MAO-B (shown as gray cartoon). The surface of the binding cavity is depicted as a gray isocontour. The structures of inhibitor **6** (PDB entry 4CRT; covalently-bound to FAD, also shown as gray-coloured sticks) and the reversible inhibitor 1,4-diphenyl-2-butene (PDB entry 1OJ9) are shown as white-colored and yellow sticks, respectively.

Overall, compound **67** emerges as the most potent MAO inhibitor of the series, with submicromolar potencies against both MAO-A and MAO-B, and hence, essentially without selectivity, whereas compound **27** emerges as a moderately potent and the most selective MAO-B inhibitor.

2.3. Reversibility and time-dependent inhibition studies

The triazole derivative **27**, the most promising compound of the series by virtue of its one-digit micromolar inhibitory potency and MAO-B selectivity, was subjected to further studies to gain insight into the type of inhibition of MAO-B. First, we investigated whether the propargylamino group present in **27** led to the irreversible inhibition of the enzyme. As shown in Figure 4, the reversibility assays confirmed that **27** irreversibly inhibited MAO-B, since the inhibition was not reverted after various cycles of consecutive centrifugations and washings with buffer. Furthermore, this finding is in agreement with the time-dependent inhibition of MAO-B resulting from incubation with **27**, as shown in Figure 3. Thus, after pre-incubation of *hr*MAO-B with a 10 μM concentration of **27** for different times ranging from 5 to 360 min, the enzymatic activity showed a slow time-dependent inhibition of MAO-B. This result suggests that a previous conformational rearrangement of the inhibitor is required for the structural adaptation to the peculiar shape of MAO-B binding pocket and the consequent proper alignment of the propargylamine moiety to finally provide an efficient enzymatic inactivation.

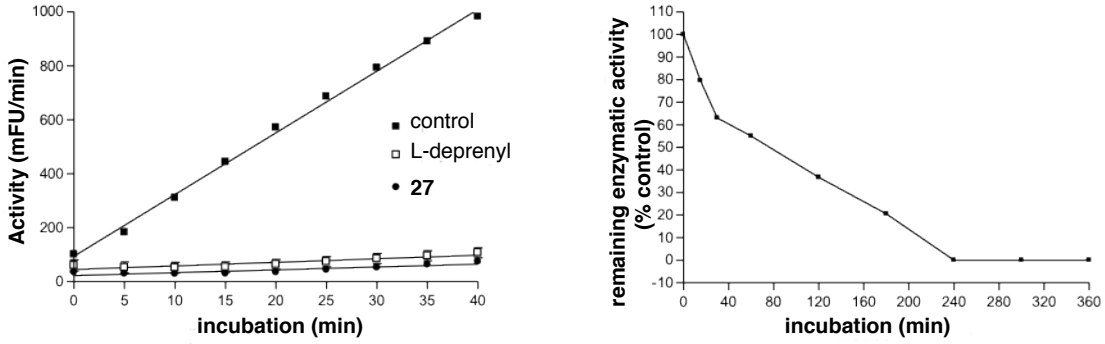

Figure 3. Plot of the enzymatic activity (mFU/min) *versus* pre-incubation time (min) (left) and plot of the remaining enzymatic activity (as % of control sample) *versus* pre-incubation time (right) in the study of reversibility of *hr*MAO-B inhibition by **27**.

2.4. Blood-brain barrier permeation assay

Because an essential feature of anti-neurodegenerative drug candidates is the ability to cross the blood-brain barrier (BBB), all the novel compounds were subjected to the well-established PAMPA-BBB assay, as an *in vitro* model of passive permeation.[75] The *in vitro* permeability (*Pe*) of the novel compounds through a lipid extract of porcine

brain was determined using a mixture of phosphate-buffered saline (PBS)/EtOH 70:30. Assay validation was carried out by comparison of the experimental and reported permeability values of 14 commercial drugs (see Table S1 in Supplementary Material), which provided a good linear correlation: *Pe* (exp) = 1.003 *Pe* (lit) - 0.783 (R^2=0.9278). Using this equation and the limits established by Di *et al.* for BBB permeation,[76] the following ranges of permeability were established: *Pe* (10^{-6} cm s^{-1}) > 5.185 for compounds with high BBB permeation(CNS+); *Pe* (10^{-6} cm s^{-1}) < 2.06 for compounds with low BBB permeation (CNS-); and 5.185 > *Pe* (10^{-6} cm s^{-1}) > 2.06 for compounds with uncertain BBB permeation (CNS±). As shown in Table 1, all the tested compounds had *Pe* values well above the threshold for high BBB permeation, so that they were predicted to be able to cross the BBB and reach their biological target in the CNS.

3. Conclusion

The results reported in this study support the feasibility of the CuAAC-mediated synthesis of 1,2,3-triazole derivatives featuring the propargylamine group of typical irreversible MAO-B inhibitors as suitable templates for the design of MAO-B inhibitor-based MTDLs. The synthetic procedures of the 1,4-disubstituted or 1,4,5-trisubstituted 1,2,3-triazole scaffolds involve 4-6-step sequences from the CuAAC of alkyl or phenyl azides with an alkyne bearing an *N*-Boc-protected primary amino or a cyano group as precursors of the propargylamine warhead. Nevertheless, introduction of lipophilic substitutents were necessary to counterbalance the high polarity conferred by the triazole ring and to modulate the inhibitory activity against the two MAO isoforms. The triazolyl-*p*-xylyl propargylamine **67** has been found to be a moderately potent nonselective MAO inhibitor, with submicromolar potencies against both human MAO-A and MAO-B. On the other hand, the isomeric 1-benzyltriazolylethyl propargylamine **27** has emerged as a moderately potent and selective MAO-B inhibitor with a low micromolar potency and a selectivity index of 0.04, with an appropriate hydrophilic-lipophilic balance (miLogP = 2.1, i.e. in the range of classical MAO inhibitors) and a relatively low molecular weight (254). Further work will be focused on refining the MAO-B inhibitory potency of these scaffolds while enabling the linkage to a second pharmacophoric moiety to derive novel MTDLs as potential anti-Alzheimer drug candidates.

4. Experimental part

4.1. Chemistry. General methods

Melting points were determined in open capillary tubes with a MFB 595010M Gallenkamp melting point apparatus. 400 MHz ^{1}H/100.6 MHz ^{13}C NMR spectra were recorded on a Varian Mercury 400 spectrometer. The chemical shifts are reported in ppm (δ scale) relative to solvent signals (CD_3OD at 3.31 and 49.0 ppm in the ^{1}H and ^{13}C NMR spectra, respectively; $CDCl_3$ at 7.26 and 77.00 ppm in the ^{1}H and ^{13}C NMR spectra, respectively), and coupling constants are reported in Hertz (Hz). Assignments given for the NMR spectra of the new compounds have been carried out by comparison with the NMR data of compounds **10**, **21**, **28**, **29**, **44** and **66**, which in turn, were assigned on the basis of DEPT, COSY ^{1}H/^{1}H (standard procedures), and COSY ^{1}H/^{13}C (gHSQC or gHMBC sequences) experiments. IR spectra were run on a Perkin-Elmer Spectrum RX I spectrophotometer. Absorption values are expressed as wavenumbers (cm^{-1}); only significant absorption bands are given. Column chromatography was performed on silica gel 60 AC.C (40–60 mesh, SDS, ref 2000027). Thin-layer chromatography was performed with aluminum-backed sheets with silica gel 60 F_{254} (Merck, ref 1.05554), and spots were visualized with UV light and 1% aqueous solution of $KMnO_4$. NMR spectra of all of the new compounds were performed at the Centres Científics i Tecnològics of the University of Barcelona (CCiTUB), while elemental analyses and high resolution mass spectra were carried out at the Mycroanalysis Service of the IIQAB (CSIC, Barcelona, Spain) with a Carlo Erba model 1106 analyzer, and at the CCiTUB with a LC/MSD TOF Agilent Technologies spectrometer, respectively. The analytical samples of all of the compounds that were subjected to pharmacological evaluation were dried at 65 ºC / 2 Torr (standard conditions).

*4.1.1. N-(tert-Butoxycarbonyl)-N-[(1-ethyl-1H-1,2,3-triazol-4-yl)methyl]amine **9***

To a solution of bromoethane (0.53 mL, 774 mg, 7.10 mmol) in H_2O / DMF 1:4 (50 mL), NaN_3 (502 mg, 7.72 mmol), Na_2CO_3 (2.05 g, 19.3 mmol), ascorbic acid (907 mg, 5.15 mmol), $CuSO_4 \cdot 5H_2O$ (641 mmg, 2.57 mmol) and *N*-Boc-propargylamine, **7** (1.00 g, 6.44 mmol) were added. The reaction mixture was stirred at rt overnight, diluted with 20% aq. NH_4OH (200 mL), treated with solid EDTA (ca 5 g) and extracted with EtOAc (2 × 150 mL). The combined organic extracts were washed with H_2O (3 × 100 mL),

dried over anhydrous Na_2SO_4, and concentrated under reduced pressure. The resulting residue was washed with pentane (3 × 10 mL) and dried under vacuum, to give compound **9** (1.14 g, 78% yield) as a white solid; R_f 0.57 (CH_2Cl_2 / MeOH 9:1); mp 77-78 ºC; IR (neat) ν 3318 (NH st), 1685, 1675, 1528 (C=O, Ar–C–C and Ar–C–N st), 1249 (N–N=N st) cm^{-1}; ^1H NMR (400 MHz, $CDCl_3$) δ 1.40 [s, 9H, $C(CH_3)_3$], 1.51 (t, J = 7.2 Hz, 3H, N–CH_2–CH_3), 4.33–4.38 (complex signal, 4H, N–CH_2–CH_3 and 4–CH_2–NH), 5.21 (broad s, 1H, NH), 7.50 (s, 1H, 5-H); ^{13}C NMR (100.6 MHz, $CDCl_3$) δ 15.5 (CH_3, N–CH_2–*C*H_3), 28.4 [CH_3, $C(CH_3)_3$], 36.2 (CH_2, 4–*C*H_2–NH), 45.3 (CH_2, N–*C*H_2–CH_3), 79.7 [C, *C*$(CH_3)_3$], 121.3 (CH, C5), 145.6 (C, C4), 156.0 (C, C=O); HRMS (ESI), calcd for ($C_{10}H_{18}N_4O_2$ + H^+) 227.1503, found 227.1493.

*4.1.2. N-(tert-Butoxycarbonyl)-N-[2-(1-ethyl-1H-1,2,3-triazol-4-yl)ethyl]amine **10***

It was prepared as described for **9**. From bromoethane (0.65 mL, 949 mg, 8.71 mmol), NaN_3 (618 mg, 9.51 mmol), Na_2CO_3 (2.52 g, 23.8 mmol), ascorbic acid (1.12 g, 6.36 mmol), $CuSO_4 \cdot 5H_2O$ (790 mg, 3.16 mmol), and *N*-Boc-3-butynylamine, **8** (1.34 g, 7.92 mmol), compound **10** (1.48 g, 78% yield) was obtained as a white solid; R_f 0.50 (CH_2Cl_2 / MeOH 9:1); mp 78-80 ºC; IR (neat) ν 3341 (NH st), 1692, 1512, 1504 (C=O, Ar–C–C and Ar–C–N st), 1249 (N–N=N st) cm^{-1}; ^1H NMR (400 MHz, $CDCl_3$) δ 1.40 [s, 9H, $C(CH_3)_3$], 1.51 (t, J = 7.2 Hz, 3H, N–CH_2–CH_3), 2.87 (t, $J \approx$ 6.8 Hz, 2H, 4–CH_2–CH_2–NH), 3.44 (dt, $J \approx J' \approx$ 6.4 Hz, 2H, 4–CH_2–CH_2–NH), 4.35 (q, J = 7.2 Hz, 2H, N–CH_2–CH_3), 5.04 (broad s, 1H, NH), 7.35 (s, 1H, 5-H); ^{13}C NMR (100.6 MHz, $CDCl_3$) δ 15.6 (CH_3, N–CH_2–*C*H_3), 26.3 (CH_2, 4–*C*H_2–CH_2–NH), 28.5 [CH_3, $C(CH_3)_3$], 39.9 (CH_2, 4–CH_2–*C*H_2–NH), 45.2 (CH_2, N–*C*H_2–CH_3), 79.2 [C, $C(CH_3)_3$], 120.8 (CH, C5), 145.5 (C, C4), 156.1 (C, C=O); HRMS (ESI) calcd for ($C_{11}H_{20}N_4O_2$ + H^+) 241.1659, found 241.1654.

*4.1.3. N-(tert-Butoxycarbonyl)-N-[2-(1-benzyl-1H-1,2,3-triazol-4-yl)ethyl]amine **11***

It was prepared as described for **9**. From benzyl bromide (0.75 mL, 1.08 g, 6.31 mmol), NaN_3 (462 mg, 7.11 mmol), Na_2CO_3 (1.88 g, 17.7 mmol), ascorbic acid (834 mg, 4.74 mmol), $CuSO_4 \cdot 5H_2O$ (590 mg, 2.36 mmol), and *N*-Boc-3-butynylamine, **8** (1.00 g, 5.91 mmol), compound **11** (1.27 g, 71% yield) was obtained as a white solid; R_f 0.58 (CH_2Cl_2 / MeOH / 50% aq. NH_4OH 9.5:0.5:0.05); mp 103-105 ºC; IR (ATR) ν 3500-2000 (max at 3407, 3116, 3069, 2972, 2930, 2157, 2025, 2000, C-H, N-H st), 1687, 1520 (CO, Ar-

C-C, Ar-C-N st) cm^{-1}; ^1H NMR (400 MHz, $CDCl_3$) δ 1.38 [s, 9H, $(CH_3)_3C$], 2.85 (t, J = 6.8 Hz, 2H, 4-CH_2CH_2-N), 3.41 (q, J = 6.8 Hz, 2H, 4-CH_2CH_2-N), 5.04 [broad s, 1H, 4-CH_2CH_2-*NH*(BOC)], 5.46 (s, 2H, N1-CH_2-Ar), 7.22-7.24 [complex signal, 2H, N1-CH_2-Ar-C2(6)-H_2], 7.26 (s, 1H, 5-*H*), 7.31-7.37 [complex signal, 3H, N1-CH_2-Ar-C3(5)-H_2 and N1-CH_2-Ar-C4-*H*]; ^{13}C NMR (100.6 MHz, $CDCl_3$) δ 26.27 (CH_2, 4-CH_2CH_2N), 28.44 [3CH_3, $(CH_3)_3C$], 39.84 (CH_2, 4-CH_2CH_2N), 54.12 (CH_2, N1-CH_2-Ar), 79.20 [C, $(CH_3)_3C$], 121.40 (CH, *C5*), 128.11 [2CH, N1-CH_2-Ar-*C2(6)* or N1-CH_2-Ar-*C3(5)*], 128.76 (CH, N1-CH_2-Ar-*C4*), 129.16 [2CH, N1-CH_2-Ar-*C2(6)* or N1-CH_2-Ar-*C3(5)*], 134.80 (C, *C4*), 145.92 (C, N1-CH_2-Ar-*C1*), 156.02 (C, *CO*); HRMS (ESI) calcd for ($C_{16}H_{22}N_4O_2$ + H^+) 303.1816; found 303.1813.

4.1.4. N-(tert-Butoxycarbonyl)-N-[2-(1-phenethyl-1H-1,2,3-triazol-4-yl)ethyl]amine ***12***

It was prepared as described for **9**. From phenethyl bromide (0.89 mL, 1.21 g, 6.52 mmol), NaN_3 (462 mg, 7.11 mmol), Na_2CO_3 (1.88 g, 17.7 mmol), ascorbic acid (834 mg, 4.74 mmol), $CuSO_4 \cdot 5H_2O$ (590 mg, 2.36 mmol), and *N*-Boc-3-butynylamine, **8** (1.00 g, 5.91 mmol), compound **12** (908 mg, 49% yield) was obtained as a white solid; R_f 0.52 (CH_2Cl_2 / MeOH / 50% aq. NH_4OH 9.5:0.5:0.05); mp 123-125 ºC; IR (ATR) ν 3400-2500 (max at 3392, 3111, 3062, 2976, 2919, C-H, N-H st), 1688, 1602, 1518 (CO, Ar-C-C, Ar-C-N st) cm^{-1}; ^1H NMR (400 MHz, $CDCl_3$) δ 1.43 [s, 9H, $(CH_3)_3C$], 2.85 (t, J = 6.8 Hz, 2H, 4-CH_2CH_2N), 3.19 (t, J = 7.2 Hz 2H, N1-CH_2CH_2-Ar), 3.41 (q, $J \approx$ 6.4 Hz, 2H, 4-CH_2CH_2N), 4.55 (t, J = 7.2 Hz, 2H, N1-CH_2CH_2-Ar), 4.95 [broad s, 1H, 4-CH_2CH_2*NH*(BOC)], 7.09 [d, J = 6.8 Hz, 2H, N1-CH_2CH_2-Ar-*C2(6)*-H_2 or N1-CH_2CH_2-Ar-*C3(5)*-H_2], 7.23-7.32 [complex signal, 3H, N1-CH_2CH_2-Ar-*C2(6)*-H_2 or N1-CH_2CH_2-Ar-*C3(5)*-H_2 and N1-CH_2CH_2-Ar-*C4-H*]; ^{13}C NMR (100.6 MHz, $CDCl_3$) δ 26.22 (CH_2, 4-CH_2CH_2N), 28.51 [3CH_3, $(CH_3)_3C$], 36.88 (CH_2, N1-CH_2CH_2-Ar), 39.98 (CH_2, 4-CH_2CH_2N), 51.64 (CH_2, N1-CH_2CH_2-Ar), 79.30 [C, $(CH_3)_3C$], 121.85 (CH, *C5*), 127.22 (CH, N1-CH_2CH_2-Ar-*C4*), 128.77 [2CH, N1-CH_2CH_2-Ar-*C2(6)* or N1-CH_2CH_2-Ar-*C3(5)*], 128.90 [2CH, N1-CH_2CH_2-Ar-*C2(6)* or N1-CH_2CH_2-Ar-*C3(5)*], 137.18 (C, *C4*), 145.06 (C, CO); HRMS (ESI) calcd for ($C_{17}H_{24}N_4O_2$ + H^+) 317.1972, found 317.1968.

4.1.5. N-(tert-Butoxycarbonyl)-N-[(1-methyl-1H-1,2,3-triazol-4-yl)methyl]amine ***13***

It was prepared as described for **9**. From iodomethane (0.44 mL, 1.00 g, 7.07 mmol), NaN_3 (502 mg, 7.72 mmol), Na_2CO_3 (2.05 g, 19.3 mmol), ascorbic acid (907 mg, 5.15

mmol), $CuSO_4 \cdot 5H_2O$ (641 mg, 2.57 mmol), and *N*-Boc-propargylamine, **7** (1.00 g, 6.44 mmol), compound **13** (938 mg, 69% yield) was obtained as a white solid; R_f 0.87 (CH_2Cl_2 / MeOH / 50% aq. NH_4OH 9.5:0.5:0.05); mp 102-104 ºC; IR (ATR) *v* 3400-2500 (max at 3379, 3152, 2969, 2950, C-H st), 1678, 1553, 1512 (CO, Ar-C-C, Ar-C-N st) cm^{-1}; ^1H NMR (400 MHz, $CDCl_3$) δ 1.41 [s, 9H, $(CH_3)_3C$], 4.05 [s, 3H, N1(CH_3)], 4.35 (d, J = 6.0 Hz, 2H, 4-CH_2N), 5.17 [broad s, 1H, 4-CH_2NH(BOC)], 7.48 (s, 1H, *5-H*); ^{13}C NMR (100.6 MHz, $CDCl_3$) δ: 28.31 [3CH_3, $(CH_3)_3C$], 36.01 (CH_2, 4-CH_2N), 36.58 [CH_3, N1(CH_3)], 78.59 [C, $(CH_3)_3C$], 122.79 (CH, *C5*), 145.71 (C, *C4*), 155.81 (C, *CO*); HRMS (ESI) calcd for ($C_9H_{16}N_4O_2$ – *tert*-Bu + H^+) 157.0720, found 157.0721.

4.1.6. N-(tert-Butoxycarbonyl)-N-[2-(1-phenyl-1H-1,2,3-triazol-4-yl)ethyl]amine ***14***

It was prepared as described for **9**. From phenyl azide (0.5 M solution in *tert*-butyl methyl ether, 26.2 mL, 13.1 mmol), Na_2CO_3 (3.47 g, 32.7 mmol), ascorbic acid (1.54 g, 8.74 mmol), $CuSO_4 \cdot 5H_2O$ (1.09 mmg, 4.36 mmol), and *N*-Boc-3-butynylamine, **8** (2.00 g, 11.8 mmol), compound **14** (1.89 g, 56% yield) was obtained as a yellow solid; R_f 0.90 (CH_2Cl_2 / MeOH / 50% aq. NH_4OH 9:1:0.05); mp 127-129 ºC; IR (ATR) *v* 3300-2900 (max at 3297, 2973, C-H, N-H st), 1712, 1528, 1500 (CO, Ar-C-C, Ar-C-N st) cm^{-1}; ^1H NMR (400 MHz, $CDCl_3$) δ 1.43 [s, 9H, $(CH_3)_3C$], 3.00 (t, J = 6.8 Hz, 2H, 4-CH_2CH_2N), 3.54 (q, $J \approx$ 6.4 Hz, 2H, 4-CH_2CH_2N), 5.02 [broad s, 1H, 4-CH_2CH_2NH(BOC)], 7.41-7.45 (tt, $J \approx$ 7.6 Hz, $J' \approx$ 1.2 Hz, 1H, N1-Ar-*C4-H*), 7.50-7.55 [tt, $J \approx$ 7.6 Hz, $J' \approx$ 1.6 Hz, 2H, N1-Ar-*C3(5)-H*$_2$], 7.70-7.73 [complex signal, 2H, N1-Ar-*C2(6)-H*$_2$], 7.81 (s, 1H, 5-H); ^{13}C NMR (100.6 MHz, $CDCl_3$) δ 26.23 (CH_2, 4-CH_2CH_2N), 28.35 [3CH_3, $(CH_3)_3C$], 39.72 (CH_2, 4-CH_2CH_2N), 79.25 [C, $(CH_3)_3C$], 119.62 (CH, *C5*), 120.37 (CH, N1-Ar-*C4*), 128.58 [2CH, N1-Ar-*C2(6)*], 129.70 [2CH, N1-Ar-*C3(5)*], 137.07 (C, *C4*), 146.10 (C, N1-Ar-*C1*), 155.99 (C, *CO*); HRMS (ESI) calcd for ($C_{15}H_{19}N_4O_2$ – *BOC* + H^+) 189.1135, found 189.1137.

4.1.7. N-(tert-Butoxycarbonyl)-N-[(1-ethyl-1H-1,2,3-triazol-4-yl)methyl]-N-methylamine ***15***

A solution of **9** (634 mg, 2.80 mmol) in anhydrous THF (6.5 mL) was cooled to 0 ºC and treated with NaH (60% suspension in mineral oil, 246 mg, 6.15 mmol) and iodomethane (0.19 mL, 433 mg, 3.05 mmol). The reaction mixture was stirred at rt for 3 h, cooled to 0 ºC, diluted dropwise with sat. aq. NH_4Cl (40 mL), and extracted with EtOAc (3 × 40 mL). The combined organic extracts were dried over anhydrous Na_2SO_4

and evaporated under reduced pressure. The resulting residue was washed with pentane (3 × 10 mL) and dried under vacuum, to give **15** (654 mg, 97% yield) as a colorless oil; R_f 0.64 (CH_2Cl_2 / MeOH 9:1); IR (neat) ν 1688 (C=O), 1245 (N–N=N st) cm^{-1}; ^1H NMR (400 MHz, $CDCl_3$) δ 1.42 [s, 9H, $C(CH_3)_3$], 1.51 (t, J = 7.2 Hz, 3H, N–CH_2–CH_3), 2.87 (s, 3H, N–CH_3), 4.32–4.38 (m, 2H, N–CH_2–CH_3), 4.44 (s, 2H, 4–CH_2–N), 7.37–7.49 (m, 1H, 5-H); ^{13}C NMR (100.6 MHz, $CDCl_3$) δ 17.5 (CH_3, N–CH_2–CH_3), 30.5 [CH_3, $C(CH_3)_3$], 36.5 (CH_3, N–CH_3), 38.2 (CH_2, 4–CH_2–N), 47.3 (CH_2, N–CH_2–CH_3), 81.8 [C, $C(CH_3)_3$], 123.7 (CH, C5), 147.0 (C, C4), 157.9 (C, C=O); HRMS (ESI) calcd for ($C_{11}H_{20}N_4O_2$ + H^+) 241.1659, found 241.1654.

*4.1.8. N-(tert-Butoxycarbonyl)-N-[2-(1-ethyl-1H-1,2,3-triazol-4-yl)ethyl]-N-methylamine **16***

It was prepared as described for **15**. From compound **10** (1.70 g, 7.08 mmol), NaH (60% supension in mineral oil, 424 mg, 10.6 mmol), and iodomethane (0.48 mL, 1.09 g, 7.71 mmol), stirring at rt for 2 h, compound **16** (1.71 mg, 95% yield) was obtained as a colorless oil; R_f 0.58 (CH_2Cl_2 / MeOH 9:1); IR (neat) ν 1690 (C=O, st), 1249 (N–N=N st) cm^{-1}; ^1H NMR (400 MHz, $CDCl_3$) δ 1.41 [s, 9H, $C(CH_3)_3$], 1.51 (t, J = 7.2 Hz, 3H, N–CH_2–CH_3), 2.82 (s, 3H, N–CH_3), 2.93 (broad s, 2H, 4–CH_2–CH_2–N), 3.52 (broad t, J ≈ 6.8 Hz, 2H, 4–CH_2–CH_2–N), 4.35 (q, J = 7.2 Hz, 2H, N–CH_2–CH_3), 7.28–7.41 (m, 1H, 5-H); ^{13}C NMR (100.6 MHz, $CDCl_3$) δ 15.6 (CH_3, N–CH_2–CH_3), 24.5 (CH_2, 4–CH_2–CH_2–N), 28.5 [CH_3, $C(CH_3)_3$], 34.4 (CH_3, N–CH_3), 45.2 (CH_2, 4–CH_2–CH_2–N), 48.9 (CH_2, N–CH_2–CH_3), 79.5 [C, $C(CH_3)_3$], 120.8 (CH, C5), 145.2 (C, C4), 155.8 (C, C=O); HRMS (ESI) calcd for ($C_{12}H_{22}N_4O_2$ + H^+) 255.1816, found 255.1815.

*4.1.9. N-(tert-Butoxycarbonyl)-N-[2-(1-benzyl-1H-1,2,3-triazol-4-yl)ethyl]-N-methylamine **17***

It was prepared as described for **15**. From compound **11** (3.67 g, 12.1 mmol), NaH (60% supension in mineral oil, 0.73 g, 18.2 mmol), and iodomethane (0.83 mL, 1.89 g, 13.3 mmol), stirring at rt for 3 h, compound **17** (3.64 g, 95% yield) was obtained as a yellowish oil; R_f 0.60 (CH_2Cl_2 / MeOH / 50% aq. NH_4OH 9.5:0.5:0.05); IR (ATR) ν 3200-2000 (max at 3134, 2971, 2923, 2105, C-H st), 1686, 1541 (CO, Ar-C-C, Ar-C-N st) cm^{-1}; ^1H NMR (400 MHz, $CDCl_3$) δ 1.37 [s, 9H, $(CH_3)_3C$], 2.78 (s, 3H, 4-$(CH_2)_2$-N(CH_3)BOC], 2.90 (broad s, 2H, 4-CH_2CH_2-N), 3.48 (t, J ≈ 7.2 Hz, 2H, 4-CH_2CH_2N),

5.46 (s, 2H, N1-*CH*$_2$-Ar), 7.22-7.23 [complex signal, 2H, N1-CH$_2$-Ar-C2(6)-*H*$_2$], 7.26 (s, 1H, 5-*H*), 7.29-7.36 (complex signal, 3H, N1-CH$_2$-Ar-C3(5)-*H*$_2$ and N1-CH$_2$-Ar-C4-*H*]; ^{13}C NMR (100.6 MHz, $CDCl_3$) δ 24.23/24.67 (CH_2 of the two possible isomers, 4-*CH*$_2$CH$_2$N), 28.44 [3CH$_3$, (*CH*$_3$)$_3$C], 34.44 [CH$_3$, 4-CH$_2$CH$_2$-N(*CH*$_3$)BOC], 48.01/48.74 (CH_2 of the two possible isomers, 4-CH$_2$*CH*$_2$-N), 54.10 (CH2, N1-*CH*$_2$-Ar), 79.46 [C, (CH$_3$)$_3$*C*], 121.44 (CH, *C5*), 128.06 (2CH, N1-CH$_2$-Ar-*C2(6)* or N1-CH$_2$-Ar-*C3(5)*], 128.73 (CH, N1-CH$_2$-Ar-*C4*), 129.14 [2CH, N1-CH$_2$-Ar-*C2(6)* or N1-CH$_2$-Ar-*C3(5)*], 134.88 (C, *C4*), 145.59 (C, N1-CH$_2$-Ar-*C1*), 155.74 (C, *CO*); HRMS (ESI) calcd for ($C_{17}H_{24}N_4O_2$ + H^+) 317.1972, found 317.1964.

4.1.10. N-(tert-Butoxycarbonyl)-N-methyl-N-[2-(1-phenethyl-1H-1,2,3-triazol-4-yl)ethyl]amine ***18***

It was prepared as described for **15**. From compound **12** (876 mg, 2.77 mmol), NaH (60% supension in mineral oil, 167 mg, 4.17 mmol), and iodomethane (0.19 mL, 433 mg, 3.05 mmol), stirring at rt for 1.5 h, compound **18** (738 mg, 81% yield) was obtained as a yellowish oil; R_f 0.57 (CH_2Cl_2 / MeOH / 50% aq. NH_4OH 9.5:0.5:0.05); mp 58-60 ºC; IR (ATR) *v* 3100-2500 (max at 3111, 3066, 2971, 2950, 2931, 2857, C-H st), 1685, 1604, 1580, 1549 (CO, Ar-C-C, Ar-C-N st) cm^{-1}; ^{1}H NMR (400 MHz, $CDCl_3$) δ 1.41 [s, 9H, (*CH*$_3$)$_3$C], 2.80 [s, 3H, 4-CH$_2$CH$_2$N(*CH*$_3$)], 2.90 (broad signal, 2H, 4-*CH*$_2$CH$_2$N), 3.18 (t, *J* = 7.2 Hz, 2H, N1-CH$_2$*CH*$_2$-Ar), 3.48 (broad signal, 2H, 4-CH$_2$*CH*$_2$N), 4.54 (t, *J* = 7.2 Hz, 2H, N1-*CH*$_2$CH$_2$-Ar), 7.10 [d, *J* ≈ 7.6 Hz, 2H, N1-CH$_2$CH$_2$-Ar-*C2(6)-H*$_2$], 7.22-7.32 (complex signal, 4H, N1-CH$_2$CH$_2$-Ar-*C3(5)-H*$_2$ and N1-CH$_2$CH$_2$-Ar-*C4-H* and *5-H*]; ^{13}C NMR (100.6 MHz, $CDCl_3$) δ 24.22/24.61 (CH_2, 4-*CH*$_2$CH$_2$N), 28.48 (3CH$_3$, (*CH*$_3$)$_3$C], 34.48 [CH$_3$, 4-CH$_2$CH$_2$N(*CH*$_3$)], 36.87 (CH_2, N1-CH$_2$*CH*$_2$-Ar), 48.06/48.87 (CH_2, 4-CH$_2$*CH*$_2$N), 51.55 (CH_2, N1-*CH*$_2$CH$_2$-Ar), 79.46 [C, (CH$_3$)$_3$*C*], 121.77 (CH, *C5*), 127.15 (CH, N1-CH$_2$CH$_2$-Ar-*C4*), 128.74 [2CH, N1-CH$_2$CH$_2$-Ar-*C2(6)* or N1-CH$_2$CH$_2$-Ar-*C3(5)*], 128.87 [2CH, N1-CH$_2$CH$_2$-Ar-*C2(6)* or N1-CH$_2$CH$_2$-Ar-*C3(5)*], 137.16 (C, *C4*), 144.80 (C, N1-CH$_2$CH$_2$-Ar-*C1*), 155.75 (C, *CO*); HRMS (ESI) calcd for ($C_{18}H_{26}N_4O_2$ + H^+) 331.2129, found 331.2122.

4.1.11. N-(tert-Butoxycarbonyl)-N-methyl-N-[(1-methyl-1H-1,2,3-triazol-4-yl)methyl]amine ***19***

It was prepared as described for **15**. From compound **13** (928 mg, 4.38 mmol), NaH (60% supension in mineral oil, 263 mg, 6.57 mmol), and iodomethane (0.30 mL, 684

mg, 4.82 mmol), stirring at rt for 1.5 h, compound **19** (945 mg, 95% yield) was obtained as a yellowish oil; R_f 0.31 (CH_2Cl_2 / MeOH / 50% aq. NH_4OH 9.5:0.5:0.05); IR (ATR) *v* 3200-2000 (max at 3126, 2974, 2925, 2098, C-H st), 1686, 1542 (CO, Ar-C-C, Ar-C-N st) cm^{-1}; ^1H NMR (400 MHz, $CDCl_3$) δ 1.45 [s, 9H, $(CH_3)_3C$], 2.89 [s, 3H, 4-$CH_2N(CH_3)$], 4.07 [s, 3H, N1(CH_3)], 4.47 (s, 2H, 4-CH_2N), 7.49 (broad s, 1H, *5-H*); ^{13}C NMR (100.6 MHz, $CDCl_3$) δ 28.58 [3CH_3, $(CH_3)_3C$], 34.64 (CH_3, 4-$CH_2N(CH_3)$], 36.79 [CH_3, N1(CH_3)], 43.83/44.51 (CH_2, 4-CH_2N), 79.92 [C, $(CH_3)_3C$], 122.56/123.52 (CH, *C5*), 145.34 (C, *C4*), 155.78 (C, *CO*); HRMS (ESI) calcd for ($C_{10}H_{18}N_4O_2$ – *tert*-Bu + H^+) 171.0877; found 171.0880.

4.1.12. N-(tert-Butoxycarbonyl)-N-methyl-N-[2-(1-phenyl-1H-1,2,3-triazol-4-yl)ethyl]amine ***20***

It was prepared as described for **15**. From compound **14** (1.82 g, 6.32 mmol), NaH (60% supension in mineral oil, 0.76 g, 19.0 mmol), and iodomethane (1.96 mL, 4.47 g, 31.5 mmol), stirring at rt overnight, compound **20** (1.82 g, 95% yield) was obtained as a yellowish oil; R_f 0.86 (CH_2Cl_2 / MeOH / 50% aq. NH_4OH 9:1:0.05); IR (ATR) *v* 3000-2000 (max at 2976, 2926, 2315, 2098, C-H st), 1681, 1598, 1502 (CO, Ar-C-C, Ar-C-N st) cm^{-1}; ^1H NMR (400 MHz, $CDCl_3$) δ 1.44 [s, 9H, $(CH_3)_3C$], 2.88 [s, 3H, 4-$CH_2CH_2NH(CH_3)$], 3.04 (broad signal, 2H, 4-CH_2CH_2N), 3.61 (broad signal, 2H, 4-CH_2CH_2N), 7.40-7.46 (complex signal, 1H, N1-Ar-*C4-H*), 7.49-7.54 [complex signal, 2H, N1-Ar-*C3(5)-H*$_2$], 7.69-7.72 [complex signal, 2H, N1-Ar-*C2(6)-H*$_2$], 7.87 (s, 1H, *5-H*); HRMS (ESI) calcd for ($C_{16}H_{22}N_4O_2$ + H^+) 303.1816, found 303.1809.

4.1.13. N-[(1-Ethyl-1H-1,2,3-triazol-4-yl)methyl]-N-methylamine ***21***

To a solution of **15** (411 mg, 1.71 mmol) in CH_2Cl_2 (6 mL), H_3PO_4 (85% purity, 2.96 mL, 25.7 mmol) was added. The reaction mixture was stirred at rt for 2 h, cooled to 0 ºC, diluted with H_2O (15 mL), alkalinized dropwise to pH = 14 with 5 N NaOH, and extracted with CH_2Cl_2 (2 × 30 mL). The combined organic extracts were dried over anhydrous Na_2SO_4 and evaporated under reduced pressure to give amine **21** (205 mg, 86% yield) as a colorless oil; R_f 0.07 (CH_2Cl_2 / MeOH / 50% aq. NH_4OH 9:1:0.05).

A solution of amine **21** (25 mg, 0.18 mmol) in CH_2Cl_2 (4 mL) was filtered through a PTFE filter (0.2 μm), treated with a HCl / MeOH solution (0.75 N, 0.71 mL, 0.53 mmol), and evaporated under reduced pressure. The resulting residue was washed with pentane (3 × 2 mL) to give, after drying under standard conditions, **21**·HCl (28 mg) as a

beige sticky solid; IR (neat) ν 3500–2500 (max. at 3386, 3126, 3080, 3028, 2981, 2935, 2756, 2695, $^{+}$NH, NH and CH st), 1234, (N–N=N st) cm^{-1}; ^{1}H NMR (400 MHz, CD_3OD) δ 1.55 (t, $J \approx 7.6$ Hz, 3H, N–CH_2–CH_3), 2.76 (s, 3H, NH–CH_3), 4.35 (s, 2H, 4–CH_2–NH), 4.50 (q, $J = 7.6$ Hz, 2H, N–CH_2–CH_3), 4.96 (s, NH and $^{+}$NH), 8.22 (s, 1H, 5-H); ^{13}C NMR (100.6 MHz, CD_3OD) δ 15.8 (CH_3, N–CH_2–*C*H_3), 33.1 (CH_3, NH–CH_3), 44.2 (CH_2, 4–*C*H_2–NH), 46.8 (CH_2, N–*C*H_2–CH_3), 126.2 (CH, C5), 139.3 (C, C4); HRMS (ESI) calcd for ($C_6H_{12}N_4 + H^+$) 141.1135, found 141.1133.

4.1.14. N-[2-(1-Ethyl-1H-1,2,3-triazol-4-yl)ethyl]-N-methylamine ***22***

It was prepared as described for **21**. From **16** (263 mg, 1.03 mmol) and H_3PO_4 (85% purity, 1.80 mL, 15.6 mmol), and stirring at rt for 4 h, amine **22** (143 mg, 90% yield) was obtained as a colorless oil; R_f 0.07 (CH_2Cl_2 / MeOH / 50% aq. NH_4OH 9:1:0.05).

22·HCl: beige sticky solid, IR (neat) ν 3500–2500 (max. at 3395, 3116, 3064, 2976, 2936, 2752, 2691, 2446, $^{+}$NH, NH and CH st), 1252 (N–N=N st) cm^{-1}; ^{1}H NMR (400 MHz, CD_3OD) δ 1.54 (t, $J = 7.2$ Hz, 3H, N–CH_2–CH_3), 2.76 (s, 3H, NH–CH_3), 3.17 (t, $J = 7.2$ Hz, 2H, 4–CH_2–CH_2–NH), 3.37 (t, $J = 7.2$ Hz, 2H, 4–CH_2–CH_2–NH), 4.47 (q, $J = 7.2$ Hz, 2H, N–CH_2–CH_3), 4.87 (s, NH and $^{+}$NH), 8.07 (s, 1H, 5-H); ^{13}C NMR (100.6 MHz, CD_3OD) δ 15.6 (CH_3, N–CH_2–*C*H_3), 22.9 (CH_2, 4–*C*H_2–CH_2–NH), 33.7 (CH_3, NH–CH_3), 47.1 (CH_2, 4–CH_2–*C*H_2–NH), 47.9 (CH_2, N–*C*H_2–CH_3), 124.6 (CH, C5), 143.3 (C, C4); HRMS (ESI) calcd for ($C_7H_{14}N_4 + H^+$) 155.1291, found 155.1297.

4.1.15. N-[2-(1-Benzyl-1H-1,2,3-triazol-4-yl)ethyl]-N-methylamine ***23***

It was prepared as described for **21**. From **17** (1.12 g, 3.54 mmol) and H_3PO_4 (85% purity, 6.08 mL, 52.7 mmol), amine **23** (721 mg, 94% yield) was obtained as a yellow oil; R_f 0.23 (CH_2Cl_2 / MeOH / 50% aq. NH_4OH 9.5:0.5:0.05).

23·HCl: beige solid, mp 189-190 ºC; IR (ATR) ν 3100-2000 (max at 3064, 3013, 2927, 2868, 2735, 2685, 2446, 2356, 2320, 2253, C-H, $^{+}$N-H_2, O-H st), 1907, 1598 (Ar-C-C, Ar-C-N st) cm^{-1}; ^{1}H NMR (400 MHz, CD_3OD) δ 2.75 [s, 3H, 4-CH_2CH_2-NH(*C*H_3)], 3.24 (t, $J \approx 7.4$ Hz, 2H, 4-*C*H_2CH_2-N), 3.38 (t, $J \approx 7.4$ Hz, 2H, 4-CH_2*C*H_2-N), 4.98 (s, $^{+}NH_2$), 5.72 (s, 2H, N1-*C*H_2-Ar), 7.38-7.45 (complex signal, 5H, N1-CH_2-*Ar*), 8.30 (s, 1H, 5-*H*); ^{13}C NMR (100.6 MHz, CD_3OD) δ 22.38 (CH_2, 4-*C*H_2CH_2-N), 33.73 [CH_3, 4-CH_2CH_2-NH(*C*H_3)], 48.60 (CH_2, 4-CH_2*C*H_2-N), 56.46 (CH_2, N1-*C*H_2-Ar), 126.57 (CH, *C5*), 129.78 [2CH, N1-CH_2-Ar-*C2(6)* or N1-CH_2-Ar-*C3(5)*], 130.15 (CH, N1-CH_2-Ar-

C4), 130.20 [2CH, N1-CH_2-Ar-*C2(6)* or N1-CH_2-Ar-*C3(5)*], 135.27 (C, *C4*), 142.63 (C, N1-CH_2-Ar-*C1*); HRMS (ESI) calcd for ($C_{12}H_{16}N_4$ + H^+) 217.1448, found 217.1442.

4.1.16. N-Methyl-N-[2-(1-phenethyl-1H-1,2,3-triazol-4-yl)ethyl]amine ***24***

It was prepared as described for **21**. From **18** (693 mg, 2.10 mmol) and H_3PO_4 (85% purity, 3.61 mL, 31.3 mmol), amine **24** (472 mg, 98% yield) was obtained as a yellow oil; R_f 0.26 (CH_2Cl_2 / MeOH / 50% aq. NH_4OH 9.5:0.5:0.05).

24·HCl: beige solid, mp 160-162 ºC; IR (ATR) ν 3500-2000 (max at 3413, 3354, 3126, 3092, 2953, 2783, 2702, 2444, 2103, C-H, $^+$N-H_2, O-H st), 1903, 1622, 1599, 1568 (Ar-C-C, Ar-C-N st) cm^{-1}; ^{1}H NMR (400 MHz, CD_3OD) δ 2.75 (s, 3H, 4-$CH_2CH_2NH(CH_3)$], 3.24-3.31 (partilly overlapped signal, 4H, 4-CH_2CH_2N and N1-CH_2CH_2-Ar), 3.37 (t, $J \approx$ 7.2 Hz, 2H, 4-CH_2CH_2N), 4.80 (t, J = 7.2 Hz, 2H, N1-CH_2CH_2-Ar), 4.99 (s, $^+NH_2$), 7.19-7.30 (complex signal, 5H, N1-CH_2CH_2-*Ar*), 8.31 (s, 1H, *5-H*); ^{13}C NMR (100.6 MHz, CD_3OD) δ 22.08 (CH_2, 4-CH_2CH_2N), 33.77 (CH_3, 4-$CH_2CH_2NH(CH_3)$], 36.68 (CH_2, N1-CH_2CH_2-Ar), 48.43 (CH_2, 4-CH_2CH_2N), 54.60 (CH_2, N1-CH_2CH_2-Ar), 127.54 (CH, *C5*), 128.19 (CH, N1-CH_2CH_2-Ar-*C4*), 129.83 (4CH, N1-CH_2CH_2-Ar-*C2(6)* and N1-CH_2CH_2-Ar-*C3(5)*], 137.87 (C, C4), 141.57 (C, N1-CH_2CH_2-Ar-*C1*); HRMS (ESI) calcd for ($C_{13}H_{18}N_4$ + H^+) 231.1604; found 231.1604.

4.1.17. N-[(1-Ethyl-1H-1,2,3-triazol-4-yl)methyl]-N-methyl-N-propargylamine ***25***

A solution of amine **21** (85 mg, 0.61 mmol) in anhydrous acetone (20 mL) was cooled to 0 ºC and treated with Cs_2CO_3 (199 mg, 0.61 mmol) and propargyl bromide (80% solution in toluene, 0.09 mL, 0.61 mmol). The reaction mixture was stirred at rt overnight, then filtered, and evaporated under reduced pressure to give an oily residue (161 mg), which was purified through column chromatography (40–60 μm silica gel, CH_2Cl_2 / MeOH / 50% aq. NH_4OH mixtures, gradient elution). On elution with CH_2Cl_2 / MeOH / 50% aq. NH_4OH 98:2:0.2, propargylamine **25** (97 mg, 89% yield) was isolated as a colorless oil; R_f 0.33 (CH_2Cl_2 / MeOH / 50% aq. NH_4OH 9:1:0.05).

25·HCl: beige sticky solid, IR (neat) ν 3500–2300 (max. at 3412, 3205, 3126, 2987, 2941, 2568, 2477, 2381, $^+$NH and CH st), 2125 (C≡C st), 1213 (N–N=N st) cm^{-1}; ^{1}H NMR (400 MHz, CD_3OD) δ 1.56 (t, $J \approx$ 7.2 Hz, 3H, N–CH_2–CH_3), 2.94 (s, 3H, N–CH_3), 3.39 (t, $J \approx$ 2.0 Hz, 1H, propargyl CH), 4.11 (d, J = 2.0 Hz, 2H, propargyl

CH_2), partially overlapped 4.50 (q, J = 7.2 Hz, 2H, N–CH_2–CH_3), partially overlapped 4.54 (s, 2H, 4–CH_2–N), 4.87 (s, $^+$NH), 8.26 (s, 1H, 5-H); ^{13}C NMR (100.6 MHz, CD_3OD) δ 15.7 (CH_3, N–CH_2–CH_3), 40.3 (CH_3, N–CH_3), 45.6 (CH_2, propargyl CH_2), 46.7 (CH_2, N–CH_2–CH_3), 50.3 (CH_2, 4–CH_2–N), 73.3 (C, propargyl C), 81.2 (CH, propargyl CH), 127.4 (CH, C5), 137.8 (C, C4); HRMS (ESI) calcd for ($C_9H_{14}N_4$ + H^+) 179.1291, found 179.1289; Elemental analysis, calcd for $C_9H_{14}N_4$·HCl·1/2H_2O C 48.32%, H 7.21%, N 25.04%, found C 48.82%, H 7.41%, N 23.33%.

4.1.18. N-[2-(1-Ethyl-1H-1,2,3-triazol-4-yl)ethyl]-N-methyl-N-propargylamine ***26***

It was prepared as described for **25**. From amine **22** (299 mg, 1.94 mmol), Cs_2CO_3 (630 mg, 1.93 mmol), and propargyl bromide (80% solution in toluene, 0.29 mL, 1.95 mmol), and stirring at 0 ºC for 2.5 h, propargylamine **26** (220 mg, 59% yield) was obtained as a yellow oil, without the need of chromatographic purification; R_f 0.55 (CH_2Cl_2 / MeOH / 50% aq. NH_4OH 9:1:0.05).

26·HCl: yellow sticky solid, IR (neat) ν 3500–2300 (max. at 3417, 3191, 2937, 2521, 2434, 2359, $^+$NH and CH st), 2121 (C≡C st), 1214 (N–N=N st) cm^{-1}; ^{1}H NMR (400 MHz, CD_3OD) δ 1.53 (t, J = 7.2 Hz, 3H, N–CH_2–CH_3), 3.05 (s, 3H, N–CH_3), 3.24 (t, J = 7.6 Hz, 2H, 4–CH_2–CH_2–N), 3.41 (t, $J \approx$ 2.8 Hz, 1H, propargyl CH), 3.62 (broad t, $J \approx$ 7.6 Hz, 2H, 4–CH_2–CH_2–N), 4.24 (d, J = 2.8 Hz, 2H, propargyl CH_2), 4.46 (q, J = 7.2 Hz, 2H, N–CH_2–CH_3), 4.87 (s, $^+$NH), 8.01 (s, 1H, 5-H); ^{13}C NMR (100.6 MHz, CD_3OD) δ 15.7 (CH_3, N–CH_2–CH_3), 21.6 (CH_2, 4–CH_2–CH_2–N), 40.7 (CH_3, N–CH_3), 46.3 (CH_2, propargyl CH_2), 46.8 (CH_2, N–CH_2–CH_3), 55.4 (CH_2, 4–CH_2–CH_2–N), 72.6 (C, propargyl C), 81.6 (CH, propargyl CH), 124.2 (CH, C5), 143.1 (C, C4); HRMS (ESI) calcd for ($C_{10}H_{16}N_4$ + H^+) 193.1448, found 193.1440; Elemental analysis, calcd for $C_{10}H_{16}N_4$·HCl·1.5H_2O C 46.96%, H 7.88%, N 21.91%, found C 47.44%, H 7.68%, N 21.85%.

4.1.19. N-[2-(1-Benzyl-1H-1,2,3-triazol-4-yl)ethyl]-N-methyl-N-propargylamine ***27***

It was prepared as described for **25**. From amine **23** (690 mg, 3.19 mmol), Cs_2CO_3 (1.04 g, 3.19 mmol), and propargyl bromide (80% solution in toluene, 0.47 mL, 3.16 mmol), and stirring at rt for 2 h, propargylamine **27** (577 mg, 71 % yield) was obtained as a yellow oil, without the need of chromatographic purification; R_f 0.48 (CH_2Cl_2 / MeOH / 50% aq. NH_4OH 9.5:0.5:0.05).

27·HCl: brown solid, mp 97-99 ºC; IR (ATR) *v* 3200-2000 (max at 3193, 2947, 2521, 2123, C-H, $^{+}$N-H, O-H st), 1887, 1716, 1597 (Ar-C-C, Ar-C-N st) cm^{-1}; ^{1}H NMR (400 MHz, CD_3OD) δ 3.03 [s, 3H, 4-CH_2CH_2-N(CH_3)], 3.29-3.33 (t overlapped to the signal of CD_3OD, J = 7.8 Hz, 2H, 4-CH_2CH_2-N), 3.39 [t, $J \approx$ 2.6 Hz, 1H, 4-$CH_2CH_2N(CH_3)CH_2CCH$], 3.60 (broad signal, 2H, 4-CH_2CH_2-N), 4.23 [d, J = 2.4 Hz, 2H, 4-$CH_2CH_2N(CH_3)CH_2CCH$], 5.00 (s, $^{+}$NH), 5.68 (s, 2H, N1-CH_2-Ar), 7.34-7.41 (complex signal, 5H, N1-CH_2-*Ar*), 8.24 (s, 1H, 5-*H*); ^{13}C NMR (100.6 MHz, CD_3OD) δ 21.19 (CH_2, 4-CH_2CH_2N), 40.70 [CH_3, 4-$CH_2CH_2N(CH_3)$], 46.35 (CH_2, 4-CH_2CH_2-N), 54.80 [CH_2, 4-CH_2CH_2-N(CH_3)CH_2C], 56.05 (CH_2, N1-CH_2-Ar), 72.58 (C, 4-CH_2CH_2-N(CH_3)CH_2C], 81.70 [CH, 4-CH_2CH_2-N(CH_3)CH_2CCH], 126.09 (CH, *C5*), 129.62 [2CH, N1-CH_2-Ar-*C2(6)* or N1-CH_2-Ar-*C3(5)*], 129.99 (CH, N1-CH_2-Ar-*C4*), 130.14 [2CH, N1-CH_2-Ar-*C2(6)* or N1-CH_2-Ar-*C3(5)*], 135.62 (C, *C4*), 142.59 (C, N1-CH_2-Ar-*C1*); HRMS (ESI) calcd for ($C_{15}H_{18}N_4 + H^+$) 255.1604, found 255.1607; Elemental analysis, calcd for $C_{15}H_{18}N_4$·HCl·H_2O C 58.34%, H 6.85%, N 18.14%, found C 57.90%, H 6.80%, N 17.55%.

4.1.20. N-Methyl-N-[2-(1-phenethyl-1H-1,2,3-triazol-4-yl)ethyl]-N-propargylamine ***28***

It was prepared as described for **25**. From amine **24** (384 mg, 1.67 mmol), Cs_2CO_3 (543 mg, 1.67 mmol), and propargyl bromide (80% solution in toluene, 0.25 mL, 1.68 mmol)), and stirring at rt for 2 h, propargylamine **28** (295 mg, 66% yield) was obtained as a yellow oil, without the need of chromatographic purification; R_f 0.75 (CH_2Cl_2 / MeOH / 50% aq. NH_4OH 9.5:0.5:0.05).

28·HCl: brown solid, mp 157-159 ºC; IR (ATR) *v* 3500-2000 (max at 3470, 3354, 3363, 3202, 3093, 3059, 3023, 2924, 2842, 2532, 2125, C-H, $^{+}$N-H, O-H st), 1889, 1603 (Ar-C-C, Ar-C-N st) cm^{-1}; ^{1}H NMR (400 MHz, CD_3OD) δ 3.03 [s, 3H, 4-$CH_2CH_2N(CH_3)$], 3.26-3.34 (partially overlapped signal, 4H, 4-CH_2CH_2N and N1-CH_2CH_2-Ar), 3.42 [t, J = 2.4 Hz, 1H, 4-$CH_2CH_2N(CH_3)CH_2CCH$], 3.61 (broad signal, 2H, 4-CH_2CH_2N), 4.23 [d, J = 2.4 Hz, 2H, 4-$CH_2CH_2N(CH_3)CH_2C$], 4.78 (t, J = 7.2 Hz, 2H, N1-CH_2CH_2-Ar), 4.98 (s, $^{+}$NH), 7.17-7.30 (complex signal, 5H, N1-CH_2CH_2-*Ar*), 8.22 (s, 1H, *5-H*); ^{13}C NMR (100.6 MHz, CD_3OD) δ 20.85 (CH_2, 4-CH_2CH_2N), 36.79 (CH_2, N1-CH_2CH_2-Ar), 40.69 [CH_3, 4-$CH_2CH_2N(CH_3)$], 46.43 [CH_2, 4-$CH_2CH_2N(CH_3)CH_2C$], 54.30 (CH_2, N1-CH_2CH_2-Ar), 54.55 (CH_2, 4-CH_2CH_2N), 72.56 [C, 4-$CH_2CH_2N(CH_3)C$], 81.80 [CH, 4-$CH_2CH_2N(CH_3)CCH$], 127.10 (CH, *C5*), 128.16 (CH, N1-CH_2CH_2-Ar-*C4*), 129.82 (4CH, N1-CH_2CH_2-Ar-*C2(6)* and N1-CH_2CH_2-Ar-*C3(5)*], 138.00 (C, C4), 141.49 (C,

N1-CH_2CH_2-Ar-*C1*); HRMS (ESI) calcd for ($C_{16}H_{20}N_4$ + H^+) 269.1761; found 269.1758.

*4.1.21. N-(tert-Butoxycarbonyl)-N-[(1-ethyl-5-methyl-1H-1,2,3-triazol-4-yl)methyl]-N-methylamine **29***

A solution of **15** (420 mg, 1.75 mmol) in anhydrous THF (30 mL) was cooled to □78 ºC and then treated with *n*-BuLi (2.5 M solution in hexanes, 1.05 mL, 2.62 mmol) and iodomethane (0.43 mL, 980 mg, 6.91 mmol). The reaction mixture was stirred at –78 ºC for 1 h, then warmed to rt and stirred an additional 2 h. The resulting solution was diluted with H_2O (20 mL) and extracted with CH_2Cl_2 (2 × 40 mL). The combined organic extracts were dried over anhydrous Na_2SO_4 and evaporated under reduced pressure. The resulting residue was washed with pentane (3 × 10 mL) and dried under vacuum, to give compound **29** (427 mg, 96% yield) as a colorless oil; R_f 0.57 (CH_2Cl_2 / MeOH 9:1); IR (neat) ν 1686 (C=O, st), 1240 (N–N=N st) cm^{-1}; ^{1}H NMR (400 MHz, $CDCl_3$) δ partially overlapped 1.46 [s, 9H, $C(CH_3)_3$], overlapped 1.44–1.49 (t, J ≈ 7.2 Hz, 3H, N–CH_2–CH_3), 2.31 (s, 3H, 5–CH_3), 2.85 (s, 3H, N–CH_3), 4.26 (q, *J* = 7.2 Hz, 2H, N–CH_2–CH_3), 4.48 (s, 2H, 4–CH_2–N); ^{13}C NMR (100.6 MHz, $CDCl_3$) δ 7.8 (CH_3, 5–CH_3), 15.2 (CH_3, N–CH_2–*C*H_3), 28.5 [CH_3, $C(CH_3)_3$], 34.0 (CH_3, N–CH_3), 42.7 (CH_2, 4–*C*H_2–N), 43.1 (CH_2, N–*C*H_2–CH_3), 78.9 [C, *C*$(CH_3)_3$], 130.5 (C, C5), 142.0 (C, C4), 156.0 (C, C=O); HRMS (ESI) calcd for ($C_{12}H_{22}N_4O_2$ + H^+) 255.1816, found 255.1811.

*4.1.22. N-(tert-Butoxycarbonyl)-N-[2-(1-ethyl-5-methyl-1H-1,2,3-triazol-4-yl)ethyl]-N-methylamine **30***

It was prepared as described for **29**. From **16** (942 mg, 3.71 mmol), *n*-BuLi (2.5 M solution in hexanes, 2.97 mL, 7.42 mmol) and iodomethane (0.92 mL, 2.10 g, 14.8 mmol), compound **30** (895 mg, 90% yield) was obtained as a colorless oil; R_f 0.57 (CH_2Cl_2 / MeOH 9:1); IR (neat) ν 1685 (C=O st), 1249 (N–N=N st) cm^{-1}; ^{1}H NMR (400 MHz, $CDCl_3$) δ 1.40 [s, 9H, $C(CH_3)_3$], 1.44 (t, *J* = 7.2 Hz, 3H, N–CH_2–CH_3), 2.20 (broad s, 3H, 5–CH_3) , 2.77 (s, 2H, 4–CH_2–CH_2–N), partially overlapped 2.77–2.82 (broad s, 3H, N–CH_3), 3.43 (t, *J* ≈ 7.2 Hz, 4–CH_2–CH_2–N), 4.23 (q, *J* = 7.2 Hz, 2H, N–CH_2–CH_3); ^{13}C NMR (100.6 MHz, $CDCl_3$) δ 7.7 (CH_3, 5–CH_3), 15.3 (CH_3, N–CH_2–*C*H_3), 23.9 (CH_2, 4–*C*H_2–CH_2–N), 28.5 [CH_3, $C(CH_3)_3$], 34.9 (CH_3, N–CH_3), 43.0 (CH_2, 4–CH_2–*C*H_2–N), 48.9 (CH_2, N–*C*H_2–CH_3), 79.4 [C, *C*$(CH_3)_3$], 129.2 (C,

C5), 142.2 (C, C4), 155.7 (C, C=O), HRMS (ESI) calcd for ($C_{13}H_{24}N_4O_2$ + H^+) 269.1972, found 269.1974.

4.1.23. N-(tert-Butoxycarbonyl)-N-methyl-N-{2-[5-methyl-1-(α-methyl)benzyl-1H-1,2,3-triazol-4-yl]ethyl}amine ***31***

It was prepared as described for **29**. From **17** (356 mg, 1.13 mmol), *n*-BuLi (2.5 M solution in hexanes, 0.90 mL, 2.25 mmol) and iodomethane (0.28 mL, 638 mg, 4.50 mmol), compound **31** (306 mg, 79% yield) was obtained as a yellowish oil; IR (ATR) *v* 3000-2000 (max at 2974, 2914, 2351, 2087, C-H st), 1681, 1581 (CO, Ar-C-C, Ar-C-N st) cm^{-1}; ^1H NMR (400 MHz, $CDCl_3$) δ 1.41 [s, 9H, $(CH_3)_3C$], 2.02 [t, J ≈ 3.6 Hz, 6H, PhCH(*CH_3*) and 5-(*CH_3*)], 2.76 [s, 3H, N(BOC)*CH_3*], 2.81 [complex signal, 2H, *CH_2*N(BOC)], 3.47 [complex signal, 2H, 4-(*CH_2*)], 5.48 [q, J = 7.2 Hz, 1H, N1-*CH*(CH_3)], 7.14 [d, J = 7.2 Hz, 2H, N1-CH(CH_3)-Ar-*C2(6)-H_2*], 7.25-7.34 [complex signal, 3H, N1-CH(CH_3)-Ar-*C3(5)-H_2* and N1-CH(CH_3)-Ar-*C4-H*]; HRMS (ESI) calcd for ($C_{19}H_{28}N_4O_2$ + H^+) 345.2285, found 345.2285.

4.1.24. N-(tert-Butoxycarbonyl)-N-[(5-butyl-1-methyl-1H-1,2,3-triazol-4-yl)methyl]-N-methylamine ***32***

It was prepared as described for **29**. From **19** (945 mg, 4.18 mmol), *n*-BuLi (2.5 M solution in hexanes, 3.36 mL, 8.40 mmol) and 1-bromobutane (1.81 mL, 2.31 g, 16.9 mmol), compound **32** (1.14 g, 97% yield) was obtained as a yellowish oil; R_f 0.87 (CH_2Cl_2 / MeOH / 50% aq. NH_4OH 9.5:0.5:0.05); IR (ATR) *v* 3000-2000 (max at 2966, 2929, 2863, 2103, C-H st), 1688, 1478, 1457 (CO, Ar-C-C, Ar-C-N st) cm^{-1}; ^1H NMR (400 MHz, $CDCl_3$) δ 0.91 [t, *J* ≈ 7.2 Hz, 3H, 5-$(CH_2)_3$*CH_3*], 1.31/1.36 [sext., *J* ≈ 7.2 Hz, 2H, 5-$(CH_2)_2$*CH_2*CH_3], 2.69 (broad signal, 2H, 5-CH_2*CH_2*CH_2CH_3), 2.81/2.88 [s, 3H, 4-CH_2N(*CH_3*)], 3.93/4.06 [s, 3H, N1(*CH_3*)], 4.46/4.49 (s, 2H, 4-*CH_2*N); HRMS (ESI) calcd for ($C_{14}H_{26}N_4O_2$ + H^+) 283.2129; found 283.2123.

4.1.25. N-(tert-Butoxycarbonyl)-N-methyl-N-[2-(5-ethyl-1-phenyl-1H-1,2,3-triazol-4-yl)ethyl]amine ***33***

It was prepared as described for **29**. From **20** (542 mg, 1.79 mmol), *n*-BuLi (2.5 M solution in hexanes, 1.43 mL, 3.57 mmol) and bromoethane (0.53 mL, 774 mg, 7.10 mmol), compound **33** (578 mg, 98% yield) was obtained as a yellowish oil; R_f 0.86 (CH_2Cl_2 / MeOH / 50% aq. NH_4OH 9:1:0.05); IR (ATR) *v* 3000-2900 (max at 2973,

2935, C-H st), 1688, 1598, 1502 (CO, Ar-C-C, Ar-C-N st) cm^{-1}; ^1H NMR (400 MHz, $CDCl_3$) δ 1.05 (t, J = 7.6 Hz, 3H, 5-CH_2CH_3), 1.45 [s, 9H, $(CH_3)_3C$], 2.70 (broad signal, 2H, 4-CH_2CH_2N), 2.88 [s, 3H, 4-$CH_2CH_2N(CH_3)$], 2.94 (broad signal, 2H, 4-CH_2CH_2N), 3.58 (t, J = 7.6 Hz, 2H, 5-CH_2CH_3), 7.41-7.44 [complex signal, 2H, N1-Ar-*C3(5)-H*$_2$], 7.50-7.54 [complex signal, 3H, N1-Ar-*C2(5)-H*$_2$ and N1-Ar-*C4-H*]; HRMS (ESI) calcd for ($C_{18}H_{26}N_4O_2$ + H^+) 331.2129; found 331.2128.

4.1.26. N-(tert-Butoxycarbonyl)-N-methyl-N-[2-(1-phenyl-5-propyl-1H-1,2,3-triazol-4-yl)ethyl]amine ***34***

It was prepared as described for **29**. From **20** (577 mg, 1.91 mmol), *n*-BuLi (2.5 M solution in hexanes, 1.53 mL, 3.82 mmol) and 1-bromopropane (0.69 mL, 934 mg, 7.60 mmol), compound **34** (634 mg, 96% yield) was obtained as an orange oil; R_f 0.84 (CH_2Cl_2 / MeOH / 50% aq. NH_4OH 9:1:0.05); IR (ATR) ν 3000-2000 (max at 2966, 2930, 2868, 2351, 2098, C-H st), 1692, 1598, 1504 (CO, Ar-C-C, Ar-C-N st) cm^{-1}; ^1H NMR (400 MHz, $CDCl_3$) δ 0.75-0.88 (complex signal, 5H, 5-$CH_2CH_2CH_3$), 1.46 [s, 9H, $(CH_3)_3C$], 2.63 (broad signal, 2H, 5-$CH_2CH_2CH_3$), 2.88 [s, 3H, 4-$CH_2CH_2N(CH_3)$], 2.92 (broad signal, 2H, 4-CH_2CH_2N), 3.59 (t, J = 7.2 Hz, 2H, 4-CH_2CH_2N), 7.40-7.42 [complex signal, 2H, N1-Ar-*C3(5)-H*$_2$], 7.50-7.54 [complex signal, 3H, N1-Ar-*C2(6)-H*$_2$ and , N1-Ar-*C4-H*]; HRMS (ESI) calcd for ($C_{19}H_{28}N_4O_2$ + H^+) 345.2285, found 345.2286.

4.1.27. N-(tert-Butoxycarbonyl)-N-methyl-N-[2-(5-butyl-1-phenyl-1H-1,2,3-triazol-4-yl)ethyl]amine ***35***

It was prepared as described for **29**. From **20** (590 mg, 1.95 mmol), *n*-BuLi (2.5 M solution in hexanes, 1.56 mL, 3.90 mmol) and 1-bromobutane (0.84 mL, 1.07 g, 7.82 mmol), an oily residue (678 mg) was obtained. After column chromatography purification of the residue (40–60 μm silica gel, CH_2Cl_2 / 50% aq. NH_4OH 100:0.2), compound **35** (300 mg, 43% yield) was isolated as a yellow oil; R_f 0.82 (CH_2Cl_2 / MeOH / 50% aq. NH_4OH 9:1:0.05); IR (ATR) ν 3400-2800 (max at 2950, 2930, 2958, 2863, C-H st), 1692, 1598, 1576, 1502 (CO, Ar-C-C, Ar-C-N st) cm^{-1}; ^1H NMR (400 MHz, $CDCl_3$) δ 0.79 [t, J = 7.2 Hz, 3H, 5-$(CH_2)_3CH_3$], 1.16-1.25 [m, $J \approx$ 7.4 Hz, 2H, 5-$(CH_2)_2CH_2CH_3$], 1.35 (quint., $J \approx$ 7.6 Hz, 2H, 5-$CH_2CH_2CH_2CH_3$), 1.45 [s, 9H, $(CH_3)_3C$], 2.65 [broad signal, 2H, 5-$CH_2(CH_2)_2CH_3$], 2.87 [s, 3H, 4-$CH_2CH_2N(CH_3)$], 2.91 (broad signal, 2H, 4-CH_2CH_2N), 3.59 (t, J ≈ 7.4 Hz, 2H, 4-CH_2CH_2N), 7.40-7.42

[dd, $J \approx 7.6$ Hz, $J' \approx 1.6$ Hz, 2H, N1-Ar-*C2(6)-H*$_2$], 7.48-7.56 [complex signal, 3H, N1-Ar-*C3(5)-H*$_2$ and N1-Ar-*C4-H*]; HRMS (ESI) calcd for ($C_{20}H_{30}N_4O_2$ + H^+) 359.2442, found 359.2438.

4.1.28. N-[(1-Ethyl-5-methyl-1H-1,2,3-triazol-4-yl)methyl]-N-methylamine ***36***

It was prepared as described for **21**. From **29** (370 mg, 1.46 mmol) and H_3PO_4 (85% purity, 2.52 mL, 21.9 mmol), and stirring at rt for 4 h, amine **36** (205 mg, 91% yield) was obtained as a colorless oil; R_f 0.11 (CH_2Cl_2 / MeOH / 50% aq. NH_4OH 9:1:0.05).

36·HCl: beige sticky solid, IR (neat) ν 3500–2500 (max. at 3390, 2925, 2868, 2837, 2757, 2697, $^+$NH, NH and CH st), 1250 (N–N=N st) cm^{-1}; ^{1}H NMR (400 MHz, CD_3OD) δ 1.48 (t, J = 7.2 Hz, 3H, N–CH_2–C*H*$_3$), 2.41 (s, 3H, 5–CH_3), 2.76 (s, 3H, NH–C*H*$_3$), 4.27 (s, 2H, 4–C*H*$_2$–NH), 4.38 (q, J = 7.2 Hz, 2H, N–C*H*$_2$–CH_3), 4.87 (s, NH and $^+$NH); ^{13}C NMR (100.6 MHz, CD_3OD) δ 7.7 (CH_3, 5–CH_3), 15.2 (CH_3, N–CH_2–*C*H_3), 33.1 (CH_3, NH–CH_3), 43.6 (CH_2, 4–*C*H_2–NH), 44.4 (CH_2, N–*C*H_2–CH_3), 134.7 (C, C5), 136.8 (C, C4); HRMS (ESI) calcd for ($C_7H_{14}N_4$ + H^+) 155.1291, found 155.1288.

4.1.29. N-[2-(1-Ethyl-5-methyl-1H-1,2,3-triazol-4-yl)ethyl]-N-methylamine ***37***

It was prepared as described for **21**. From **30** (890 mg, 3.32 mmol) and H_3PO_4 (85% purity, 5.70 mL, 49.4 mmol), and stirring at rt for 1.5 h, amine **37** (495 mg, 89% yield) was obtained as a colorless oil; R_f 0.10 (CH_2Cl_2 / MeOH / 50% aq. NH_4OH 9:1:0.05).

37·HCl: beige sticky solid, IR (neat) ν 3500–2500 (max. at 3374, 2981, 2937, 2746, 2692, 2446, $^+$NH, NH and CH st), 1236 (N–N=N st) cm^{-1}; ^{1}H NMR (400 MHz, CD_3OD) δ 1.49 (t, J = 7.2 Hz, 3H, N–CH_2–C*H*$_3$), 2.38 (s, 3H, 5–CH_3), 2.76 (s, 3H, NH–C*H*$_3$), 3.09 (t, J = 7.2 Hz, 2H, 4–C*H*$_2$–CH_2–NH), 3.34 (t, J = 7.2 Hz, 2H, 4–CH_2–C*H*$_2$–NH), 4.39 (q, J = 7.2 Hz, 2H, N–C*H*$_2$–CH_3), 4.86 (s, NH and $^+$NH); ^{13}C NMR (100.6 MHz, CD_3OD) δ 7.6 (CH_3, 5–CH_3), 15.0 (CH_3, N–CH_2–*C*H_3), 22.1 (CH_2, 4–*C*H_2–CH_2–NH), 33.7 (CH_3, NH–CH_3), 45.0 (CH_2, 4–CH_2–*C*H_2–NH), 49.0 (CH_2, N–*C*H_2–CH_3), 133.4 (C, C5), 140.1 (C, C4); HRMS (ESI) calcd for ($C_8H_{16}N_4$ + H^+) 169.1448, found 169.1452.

*4.1.30. N-Methyl-N-{2-[5-methyl-1-(α-methyl)benzyl-1H-1,2,3-triazol-4-yl]ethyl}amine **38***

It was prepared as described for **21**. From **31** (306 mg, 0.89 mmol) and H_3PO_4 (85% purity, 1.60 mL, 13.9 mmol), amine **38** (215 mg, quantitative yield) was obtained as a yellow oil; R_f 0.33 (CH_2Cl_2 / MeOH / 50% aq. NH_4OH 9:1:0.05).

38·HCl: yellow sticky solid, IR (ATR) *v* 3400-2000 (max at 3373, 2950, 2709, 2434, 2108, C-H st), 1870, 1614, 1454 (Ar-C-C, Ar-C-N st) cm^{-1}; ^1H NMR (400 MHz, CD_3OD) δ 2.00 (d, J = 7.2 Hz, 3H, N1-CH(*CH_3*)], 2.30 (s, 3H, 5-*CH_3*), 2.76 (s, 3H, 4-CH_2CH_2NH(*CH_3*)], 3.19 (t, J = 7.2 Hz, 2H, 4-CH_2*CH_2*N), 3.36 (t, J = 7.2 Hz, 2H, 4-*CH_2*CH_2N), 4.94 (s, $^+NH_2$), 5.94 (complex signal, 1H, N1-*CH*(CH_3)-Ar), 7.29 [d, J ≈ 7.4 Hz, 2H, N1-CH(CH_3)-Ar-*C2(6)-H_2*], 7.34-7.41 (complex signal, 3H, N1-CH(CH_3)-Ar-*C3(5)-H_2* and N1-CH(CH_3)-Ar-*C4-H*]; ^{13}C NMR (100.6 MHz, CD_3OD) δ 8.23 [CH_3, 4-CH_2CH_2NH(*CH_3*)], 21.66 (CH_2, 4-CH_2*CH_2*N), 21.94 (CH_2, 4-*CH_2*CH_2N), 33.75 [CH_3, 5-(*CH_3*)], 53.81 (CH, N1-*CH*(CH_3)-Ar), 61.55 (CH_3, N1-CH(*CH_3*)-Ar], 127.48 [2CH, N1-CH(CH_3)-Ar-*C2(6)* or N1-CH(CH_3)-Ar-*C3(5)*], 129.71 (CH, N1-CH(CH3)-Ar-*C4*), 130.23 [2CH, N1-CH(CH_3)-Ar-*C2(6)* or N1-CH(CH_3)-Ar-*C3(5)*], 135.58 [C, *C5*), 139.27 (C, *C4*), 140.49 (C, N1-CH(CH_3)-Ar-*C1*); HRMS (ESI) calcd for ($C_{14}H_{20}N_4 + H^+$) 245.1761, found 245.1762.

*4.1.31. N-[(5-Butyl-1-methyl-1H-1,2,3-triazol-4-yl)methyl]-N-methylamine **39***

It was prepared as described for **21**. From **32** (954 mg, 3.38 mmol) and H_3PO_4 (85% purity, 5.84 mL, 50.7 mmol), amine **39** (620 mg, quantitative yield) was obtained as a yellow oil; R_f 0.06 (CH_2Cl_2 / MeOH / 50% aq. NH_4OH 9.5:0.5:0.05).

39·HCl: beige sticky solid, IR (ATR) *v* 3400-2000 (max at 3372, 2957, 2930, 2863, 2711, 2107, 2082, C-H, ^+N-H_2, O-H st), 1624, 1458 (Ar-C-C, Ar-C-N st) cm^{-1}; ^1H NMR (400 MHz, CD_3OD) δ 0.98 [t, J = 7.2 Hz, 3H, 5-$(CH_2)_3$*CH_3*], 1.41 [sext., J = 7.2 Hz, 2H, 5-$(CH_2)_2$*CH_2*CH_3], 1.58 (quint., J ≈ 7.7 Hz, 2H, 5-CH_2*CH_2*CH_2CH_3), 2.79 [s, 3H, 4-CH_2NH(*CH_3*)], 2.87 (t, J ≈ 7.6 Hz, 2H, 5-*CH_2*$CH_2CH_2CH_2CH_3$), 4.05 [s, 3H, N1(*CH_3*)], 4.31 (s, 2H, 4-*CH_2*N), 5.06 (s, $^+NH_2$); ^{13}C NMR (100.6 MHz, CD_3OD) δ 14.05 [CH_3, 5-$(CH_2)_3$*CH_3*], 22.87 [CH_2, 5-$(CH_2)_2$*CH_2*CH_3], 23.41 (CH_2, 5-CH_2*CH_2*CH_2CH_3), 31.60 [CH_2, 5-*CH_2*$(CH_2)_2CH_3$], 33.35 [CH_3, N1(*CH_3*)], 35.52 (CH_3, 4-CH_2NH(*CH_3*)], 43.50 (CH_2, 4-*CH_2*N), 136.50 (C, *C5*), 139.33 (C, *C4*); HRMS (ESI) calcd for ($C_9H_{18}N_4 + H^+$) 183.1604, found 183.1599.

*4.1.32. N-Methyl-N-[2-(5-ethyl-1-phenyl-1H-1,2,3-triazol-4-yl)ethyl]amine **40***

It was prepared as described for **21**. From **33** (517 mg, 1.57 mmol) and H_3PO_4 (85% purity, 2.68 mL, 23.2 mmol), and stirring at rt for 3 h, an orange oil (435 mg) was obtained and purified through column chromatography (40–60 μm silica gel, CH_2Cl_2 / MeOH / 50% aq. NH_4OH mixtures, gradient elution). On elution with CH_2Cl_2 / MeOH / 50% aq. NH_4OH 98:2:0.2 to 96:4:0.2, amine **40** (322 mg, 89% yield) was obtained as a yellowish oil; R_f 0.51 (CH_2Cl_2 / MeOH / 50% aq. NH_4OH 9:1:0.05).

40·HCl: yellow sticky solid, IR (ATR) *v* 3400-2000 (max at 3380, 2964, 2930, 2741, 2434, 2103, C-H, $^+$N-H, O-H st), 1615, 1596, 1500 (Ar-C-C, Ar-C-N st) cm^{-1}; ^1H NMR (400 MHz, CD_3OD) δ 1.05 (t, J = 7.6 Hz, 3H, 5-CH_2CH_3), 2.81 [partially overlapped signal, 5H, 5-CH_2CH_3 and 4-$CH_2CH_2NH(CH_3)$], 3.20 (t, J = 7.2 Hz, 2H, 4-CH_2CH_2N), 3.45 (t, J = 7.2 Hz, 2H, 4-CH_2CH_2N), 4.90 (s, $^+NH_2$), 7.52-7.56 [complex signal, 2H, N1-Ar-*C3(5)-H*$_2$], 7.62-7.66 [complex signal, 3H, N1-Ar-*C2(6)-H*$_2$ and N1-Ar-*C4-H*]; ^{13}C NMR (100.6 MHz, CD_3OD) δ 13.43 (CH_3, 5-CH_2CH_3), 16.93 (CH_2, 5-CH_2CH_3), 22.49 ($2CH_2$, 4-CH_2CH_2N), 33.86 [CH_3, 4-$CH_2CH_2NH(CH_3)$], 126.76 [2CH, N1-Ar-*C3(5)*], 130.91 [2CH, N1-Ar-*C2(6)*], 131.43 (CH, N1-Ar-*C4*), 137.52 (C, *C5*), 139.14 (C, *C4*), 140.54 (C, N1-Ar-*C1*); HRMS (ESI) calcd for ($C_{13}H_{18}N_4$ + H^+) 231.1604; found 231.1607.

*4.1.33. N-Methyl-N-[2-(1-phenyl-5-propyl-1H-1,2,3-triazol-4-yl)ethyl]amine **41***

It was prepared as described for **21**. From **34** (573 mg, 1.66 mmol) and H_3PO_4 (85% purity, 2.85 mL, 24.7 mmol), and stirring at rt for 3 h, an orange oil (564 mg) was obtained and purified through column chromatography (40–60 μm silica gel, CH_2Cl_2 / MeOH / 50% aq. NH_4OH mixtures, gradient elution). On elution with CH_2Cl_2 / MeOH / 50% aq. NH_4OH 99:1:0.2 to 95:5:0.2, amine **41** (270 mg, 67% yield) was obtained as a yellowish oil; R_f 0.52 (CH_2Cl_2 / MeOH / 50% aq. NH_4OH 9:1:0.05).

41·HCl: yellow sticky solid, IR (ATR) *v* 3400-2000 (max at 3350, 2960, 2935, 2863, 2721, 2430, 2098, C-H, $^+NH_2$, O-H st), 1597, 1500, 1462 (Ar-C-C, Ar-C-N st) cm^{-1}; ^1H NMR (400 MHz, CD_3OD) δ 0.76-0.85 (complex signal, 3H, 5-$CH_2CH_2CH_3$), 1.41 (q, J ≈ 7.6 Hz, 2H, 5-$CH_2CH_2CH_3$), 2.75 (t, J ≈ 7.8 Hz, 2H, 5-$CH_2CH_2CH_3$), 2.81 [d, J = 6.0 Hz, 3H, 4-$CH_2CH_2NH(CH_3)$], 3.16 (t, J ≈ 7.0 Hz, 2H, 4-CH_2CH_2N), 3.43 (t, J ≈ 7.0 Hz, 2H, 4-CH_2CH_2N), 4.86 (s, ^+NH), 7.49-7.53 [complex signal, 2H, N1-Ar-*C3(5)-H*$_2$], 7.61-7.64 [complex signal, 3H, N1-Ar-*C2(6)-H*$_2$ and N1-Ar-C4]; ^{13}C NMR (100.6

MHz, CD_3OD) δ 13.86 (CH_3, 5-CH_2CH_2*CH_3*), 22.59 (CH_2, 5-CH_2*CH_2*CH_3), 22.86 (CH_2, 5-*CH_2*CH_2CH_3), 25.23 ($2CH_2$, 4-*CH_2*CH_2*N*), 33.83 [CH_3, 4-CH_2CH_2NH(*CH_3*)], 126.80 [2CH, N1-Ar-*C3(5)* or N1-Ar-*C2(6)*], 130.87 [2CH, N1-Ar-*C3(5)* or N1-Ar-*C2(6)*], 131.33 (CH, N1-Ar-*C4*), 137.45 (C, *C5*), 137.70 (C, *C4*), 141.26 (C, N1-Ar-*C1*); HRMS (ESI) calcd for ($C_{14}H_{20}N_4 + H^+$) 245.1761, found 245.1761.

4.1.34. N-Methyl-N-[2-(5-butyl-1-phenyl-1H-1,2,3-triazol-4-yl)ethyl]amine ***42***

It was prepared as described for **21**. From **35** (265 mg, 0.74 mmol) and H_3PO_4 (85% purity, 1.27 mL, 11.0 mmol), and stirring at rt for 3 h, amine **42** (175 mg, 92% yield) was obtained as a yellowish oil; R_f 0.54 (CH_2Cl_2 / MeOH / 50% aq. NH_4OH 9:1:0.05).

42·HCl: yellow oil, IR (ATR) ν 3400-2000 (max at 3389, 2954, 2919, 2868, 2755, 2444, 2098, C-H, $^+$N-H, O-H st), 1638, 1597, 1502 (Ar-C-C, Ar-C-N st) cm^{-1}; ^1H NMR (400 MHz, CD_3OD) δ 0.80 [t, J = 7.2 Hz, 3H, 5$(CH_2)_3$*CH_3*], 1.18-1.27 [sext., J ≈ 7.2 Hz, 2H, 5-$(CH_2)_2$*CH_2*CH_3], 1.34-1.41 [quint., J ≈ 7.5 Hz, 2H, 5-CH_2*CH_2*CH_2CH_3], 2.77 [t, J ≈ 7.6 Hz, 2H, 5-*CH_2*$(CH_2)_2CH_3$], 2.81 [d, J = 5.6 Hz, 3H, 4-CH_2CH_2NH(*CH_3*)], 3.15 (t, J = 7.2 Hz, 2H, 4-*CH_2*CH_2*N*), 3.44 (t, J = 7.2 Hz, 2H, 4-CH_2*CH_2*N*), 4.86 (s, $^+NH_2$), 7.50-7.52 [complex signal, 2H, N1-Ar-*C2(6)-H_2*], 7.62-7.66 [complex signal, 2H, N1-Ar-*C3(5)-H_2* and N1-Ar-*C4-H*]; ^{13}C NMR (100.6 MHz, CD_3OD) δ 13.79 [CH_3, 5-$(CH_2)_3$*CH_3*], 22.59, 23.03, 23.15 [$4CH_2$, 5-(*CH_2*$)_3CH_3$ and 4-*CH_2*CH_2*N*], 31.62 (CH_2, 4-CH_2*CH_2*N*), 33.82 [CH_3, 4-CH_2CH_2NH(*CH_3*)], 126.79 [2CH, N1-Ar-*C2(6)* or N1-Ar-*C3(5)*], 130.87 [2CH, N1-Ar-*C2(6)* or N1-Ar-*C3(5)*], 131.31 (CH, N1-Ar-*C4*), 137.74 (C, *C5*), 137.74 (C, *C4*), 141.20 (C, N1-Ar-*C1*); HRMS (ESI) calcd for ($C_{15}H_{22}N_4 + H^+$) 259.1917; found 259.1922.

4.1.35. N-[(1-Ethyl-5-methyl-1H-1,2,3-triazol-4-yl)methyl]-N-methyl-N-propargylamine ***43***

It was prepared as described for **25**. From amine **36** (128 mg, 0.83 mmol), Cs_2CO_3 (270 mg, 0.83 mmol), and propargyl bromide (80% solution in toluene, 0.12 mL, 0.81 mmol), and stirring at 0 ºC for 2 h, propargylamine **43** (96 mg, 62% yield) was obtained as a yellow oil, without the need of chromatographic purification; R_f 0.55 (CH_2Cl_2 / MeOH / 50% aq. NH_4OH 9:1:0.05).

43·HCl: yellow sticky solid, IR (neat) ν 3500–2300 (max. at 3386, 3197, 2938, 2497, 2352, $^+$NH and CH st), 2123, (C≡C st), 1254 (N–N=N st) cm^{-1}; ^1H NMR (400 MHz,

CD_3OD) δ 1.50 (t, J = 7.2 Hz, 3H, N–CH_2–CH_3), 2.45 (s, 3H, 5–CH_3), 3.01 (s, 3H, N–CH_3), 3.44 (t, J = 2.4 Hz, 1H, propargyl CH), 4.16 (d, J = 2.4 Hz, 2H, propargyl CH_2), 4.39 (q, J = 7.2 Hz, 2H, N–CH_2–CH_3), 4.52 (s, 2H, 4–CH_2–N), 4.84 (s, $^+$NH); ^{13}C NMR (100.6 MHz, CD_3OD) δ 8.0 (CH_3, 5–CH_3), 15.1 (CH_3, N–CH_2–*C*H_3), 40.3 (CH_3, N–CH_3), 44.5 (CH_2, propargyl CH_2), 45.6 (CH_2, N–*C*H_2–CH_3), 49.8 (CH_2, 4–*C*H_2–N), 73.1 (C, propargyl C), 81.5 (CH, propargyl CH), 135.1 (C, C5), 136.3 (C, C4); HRMS (ESI) calcd for ($C_{10}H_{16}N_4$ + H^+) 193.1448, found 193.1450; Elemental analysis, calcd for $C_{10}H_{16}N_4$·HCl·1/2H_2O C 47.72%, H 7.33%, N 21.26%, found C 47.30%, H 7.86%, N 22.06%.

Note: From amine **36** (117 mg, 0.76 mmol), Cs_2CO_3 (362 mg, 1.11 mmol), and propargyl bromide (80% solution in toluene, 0.16 mL, 1.08 mmol), and stirring at rt overnight, an oily residue was obtained and purified through column chromatography (40–60 μm silica gel, CH_2Cl_2 / MeOH / 50% aq. NH_4OH mixtures, gradient elution). On elution with CH_2Cl_2 / MeOH / 50% aq. NH_4OH 99:1:0.2 to 98:2:0.2, propargylamine **43** (15 mg, 10% yield) was isolated as a colorless oil. On elution with CH_2Cl_2 / MeOH / 50% aq. NH_4OH 98:2:0.2, slightly impure *N*-[(1-ethyl-5-methyl-1*H*-1,2,3-triazol-4-yl)methyl]-*N*-methyl-*N*,*N*-dipropargylammonium bromide (223 mg) was isolated as a brown oil; R_f 0. 04 (CH_2Cl_2 / MeOH / 50% aq. NH_4OH 9:1:0.05).

A solution of the dipropargylated byproduct (223 mg) in CH_2Cl_2 (20 mL) was filtered through a PTFE filter (0.2 μm) and evaporated under reduced pressure. The resulting residue was washed with pentane (3 × 2 mL) to give, after drying under standard conditions, the analytical sample of the dipropargylated byproduct (213 mg) as a brownish oil; IR (neat) ν 2124 (C≡C st), 1258 (N–N=N st) cm^{-1}; ^{1}H NMR (400 MHz, CD_3OD) δ 1.53 (t, J = 7.6 Hz, 3H, N–CH_2–CH_3), 2.73 (s, 3H, 5–CH_3), 2.85 (t, J = 2.4 Hz, 2H, propargyl CH), 3.42 (s, 3H, $^+$N–CH_3), 4.34 (q, $J \approx$ 7.6 Hz, 2H, N–CH_2–CH_3), 4.83 (dd, J = 16.0 Hz, J' = 2.4 Hz, 2H) and 4.91 (dd, J = 16.0 Hz, J' = 2.4 Hz, 2H) (propargyl CH_2), 5.34 (s, 2H, 4–CH_2–N^+); ^{13}C NMR (100.6 MHz, CD_3OD) δ 8.8 (CH_3, 5–CH_3), 14.9 (CH_3, N–CH_2–*C*H_3), 43.6 (CH_2, N–*C*H_2–CH_3), 47.3 (CH_3, $^+$N–CH_3), 51.8 ($2CH_2$, propargyl CH_2), 55.7 (CH_2, 4–CH_2–N^+), 70.9 (2C, propargyl C), 80.3 (2CH, propargyl CH), 132.5 (C, C5), 136.5 (C, C4); HRMS (ESI) calcd for ($C_{13}H_{19}N_4$ + H^+) 231.1604, found 231.1613.

*4.1.36. N-[2-(1-Ethyl-5-methyl-1H-1,2,3-triazol-4-yl)ethyl]-N-methyl-N-propargylamine **44***

It was prepared as described for **25**. From amine **37** (490 mg, 2.91 mmol), Cs_2CO_3 (952 mg, 2.92 mmol), and propargyl bromide (80% solution in toluene, 0.43 mL, 2.89 mmol), and stirring at 0 ºC for 2.5 h, propargylamine **44** (319 mg, 54% yield) was obtained as a yellow oil, without the need of chromatographic purification; R_f 0.59 (CH_2Cl_2 / MeOH / 50% aq. NH_4OH 9:1:0.05).

44·HCl: yellow sticky solid, IR (neat) ν 3500–2300 (max. at 3406, 3181, 2981, 2932, 2583, 2518, 2461, 2408, 2366, $^+$NH and CH st), 2123 (C≡C st), 1215 (N–N=N st) cm^{-1}; ^{1}H NMR (400 MHz, CD_3OD) δ 1.56 (t, J = 7.2 Hz, 3H, N–CH_2–CH_3), 2.50 (s, 3H, 5–CH_3), 3.08 (s, 3H, N–CH_3), 3.35 (broad t, J = 7.8 Hz, 2H, 4–CH_2–CH_2–N), 3.45 (t, J ≈ 2.8 Hz, 1H, propargyl CH), 3.63 (t, J = 7.8 Hz, 2H, 4–CH_2–CH_2–N), 4.28 (d, J = 2.8 Hz, 2H, propargyl CH_2), 4.51 (q, J = 7.2 Hz, 2H, N–CH_2–CH_3), 4.94 (s, $^+$NH); ^{13}C NMR (100.6 MHz, CD_3OD) δ 8.0 (CH_3, 5-CH_3), 14.4 (CH_3, N–CH_2–CH_3), 20.0 (CH_2, 4–CH_2–CH_2–N), 40.7 (CH_3, N–CH_3), 46.3 (CH_2, propargyl CH_2), 46.4 (CH_2, N–CH_2–CH_3), 54.0 (CH_2, 4–CH_2–CH_2–N), 72.5 (C, propargyl C), 81.8 (CH, propargyl CH), 136.3 (C, C5), 137.8 (C, C4); HRMS (ESI) calcd for ($C_{11}H_{18}N_4$ + H^+) 207.1604, found 207.1609; Elemental analysis, calcd for $C_{11}H_{18}N_4$·HCl·1.75H_2O C 48.17%, H 8.27%, N 20.43%, found C 48.14%, H 7.96%, N 19.81%.

*4.1.37. N-Methyl-N-{2-[5-methyl-1-(α-methyl)benzyl-1H-1,2,3-triazol-4-yl]ethyl}-N-propargylamine **45***

It was prepared as described for **25**. From amine **38** (234 mg, 0.93 mmol), Cs_2CO_3 (0.30 g, 0.92 mmol), and propargyl bromide (80% solution in toluene, 0.10 mL, 0.67 mmol), and stirring at at 0 °C for 30 min and at rt for an additional 3 h, an orange oily residue (263 mg) was obtained and purified through column chromatography (40–60 µm silica gel, CH_2Cl_2 / MeOH / 50% aq. NH_4OH mixtures, gradient elution). On elution with CH_2Cl_2 / MeOH / 50% aq. NH_4OH 99.97:0.03:0.2, propargylamine **45** (100 mg, 53% yield) was obtained as a yellow oil; R_f 0.45 (CH_2Cl_2 / MeOH / 50% aq. NH_4OH 9:1:0.05).

45·HCl: beige sticky solid, IR (ATR) ν 3400-2000 (max at 3386, 3209, 2936, 2351, 2118, C-H, $^+$N-H, O-H st), 1886, 1613, 1453 (Ar-C-C, Ar-C-N st) cm^{-1}; ^{1}H NMR (400 MHz, CD_3OD) δ 2.00 [d, J = 6.8 Hz, 3H, 4-CH_2CH_2N(*CH3*)], 3.06 [s, 3H, 5-(*CH_3*)],

3.22 (t, J = 8.0 Hz, 2H, 4-CH_2CH_2N), 3.42 [t, $J \approx$ 2.6 Hz, 1H, 4-$CH_2CH_2N(CH_3)CH_2$-C*CH*], 3.59 (t, J = 7.6 Hz, 2H, 4-CH_2CH_2N), 4.25 [d, J = 2.0 Hz, 2H, 4-$CH_2CH_2N(CH_3)CH_2$C], 4.89 (s, $^+$NH), 5.86 [q, $J \approx$ 7.0 Hz, 1H, N1*CH*(CH_3)-Ar], 7.25-7.27 (complex signal, 2H, N1-CH(CH_3)-Ar-*C2(6)-H*$_2$], 7.30-7.39 (complex signal, 3H, N1-CH(CH_3)-Ar-*C3(5)-H*$_2$ and N1-CH(CH_3)-Ar-*C4-H*]; ^{13}C NMR (100.6 MHz, CD_3OD) δ 8.07 [CH_3, 4-$CH_2CH_2N(CH_3)$], 20.47 (CH_2, 4-CH_2CH_2N), 21.99 (CH_2, 4-CH_2CH_2N), 40.71 [CH_3, 5-(CH_3)], 46.26 [CH_2, 4-$CH_2CH_2N(CH_3)CH_2$C-CH], 54.65 [CH, N1-*CH*(CH_3)-Ar], 60.99 (CH_3, N1-CH(CH_3)-Ar], 72.59 [C, 4-$CH_2CH_2N(CH_3)CH_2$*C*CH], 81.72 [CH, 4-$CH_2CH_2N(CH_3)CH_2$C*CH*], 127.40 [2CH, N1-CH(CH_3)-Ar-*C2(6)-H*$_2$ or N1-CH(CH_3)-Ar-*C3(5)-H*$_2$], 129.55 [CH, N1-CH(CH_3)Ar-*C4-H*], 130.18 [2CH, N1-CH(CH_3)-Ar-*C2(6)-H*$_2$ or N1-CH(CH_3)-Ar-*C3(5)-H*$_2$], 134.49 (C, *C5*), 139.60 (C, *C4*), 141.06 [C, N1-CH(CH_3)-Ar-*C1*]; HRMS (ESI) calcd for ($C_{17}H_{22}N_4$ + H^+) 283.1917, found 283.1923.

4.1.38. N-[(5-Butyl-1-methyl-1H-1,2,3-triazol-4-yl)methyl]-N-methyl-N-propargylamine ***46***

It was prepared as described for **25**. From amine **39** (529 mg, 2.90 mmol), Cs_2CO_3 (946 mg, 2.90 mmol), and propargyl bromide (80% solution in toluene, 0.44 mL, 2.96 mmol), and stirring at rt for 3.5 h, propargylamine **28** (418 mg, 65% yield) was obtained as a yellow oil, without the need of chromatographic purification; R_f 0.29 (CH_2Cl_2 / MeOH / 50% aq. NH_4OH 9.5:0.5:0.05).

46·HCl: brown sticky solid, IR (ATR) v 3500-2000 (max at 3410, 3218, 2955, 2930, 2863, 2490, 2121, C-H, $^+$N-H, O-H st), 1717, 1633 (Ar-C-C, Ar-C-N st) cm^{-1}; ^{1}H NMR (400 MHz, CD_3OD) δ 0.98 [t, J = 7.2 Hz, 3H, 5-$(CH_2)_3CH_3$], 1.38-1.48 [sext., J = 7.6 Hz, 2H, 5-$(CH_2)_2CH_2CH_3$], 1.55-1.63 (quint., $J \approx$ 7.7 Hz, 2H, 5-$CH_2CH_2CH_2CH_3$), 2.89 (t, J ≈ 7.8 Hz, 2H, 5-$CH_2CH_2CH_2CH_3$), 3.03 [s, 3H, N1(CH_3)], 3.47 [t, J = 2.4 Hz, 1H, 4-$CH_2N(CH_3)CH_2$C*CH*], 4.05 [d, J = 5.2 Hz, 3H, 4-$CH_2N(CH_3)$], 4.21 [d, J = 2.4 Hz, 2H, 4-$CH_2N(CH_3)CH_2$C], 4.55 (s, 2H, 4-CH_2N), 4.92 (s, $^+$NH); ^{13}C NMR (100.6 MHz, CD_3OD) δ 14.07 [CH_3, 5-$(CH_2)_3CH_3$], 22.97 [CH_2, 5-$(CH_2)_2CH_2CH_3$], 23.45 (CH_2, 5-$CH_2CH_2CH_2CH_3$), 31.59 (2CH_2, 5-$CH_2(CH_2)_2CH_3$ and 4-CH_2N], 35.48 [CH_3, N1(CH_3)], 40.52 (CH_3, 4-$CH_2N(CH_3)$], 45.63 [CH_2, 4-$CH_2N(CH_3)CH_2$C], 73.15 [C, 4-$CH_2N(CH_3)CH_2$*C*], 81.15 (CH, 4-$CH_2N(CH_3)CH_2$C*CH*], 134.91 (C, *C5*), 140.53 (C, *C4*); HRMS (ESI) calcd for ($C_{12}H_{20}N_4$ + H^+) 221.1761, found 221.1762; Elemental

analysis, calcd for $C_{12}H_{20}N_4 \cdot HCl \cdot 0.7H_2O$ C 53.50%, H 8.38%, N 20.80%, found C 53.38%, H 7.95%, N 20.69%.

4.1.39. N-Methyl-N-[2-(5-ethyl-1-phenyl-1H-1,2,3-triazol-4-yl)ethyl]-N-propargylamine ***47***

It was prepared as described for **25**. From amine **40** (260 mg, 1.13 mmol), Cs_2CO_3 (0.37 g, 1.14 mmol), and propargyl bromide (80% solution in toluene, 0.13 mL, 0.87 mmol), and stirring at 0 ºC for 30 min and at rt for an additional 3 h, an orange oil (333 mg) was obtained and purified through column chromatography (40–60 μm silica gel, CH_2Cl_2 / MeOH / 50% aq. NH_4OH mixtures, gradient elution). On elution with CH_2Cl_2 / MeOH / 50% aq. NH_4OH 99.9:0.1:0.2, propargylamine **47** (222 mg, 95% yield) was obtained as a yellow oil; R_f 0.59 (CH_2Cl_2 / MeOH / 50% aq. NH_4OH 9:1:0.05).

47·HCl: yellow sticky solid, IR (ATR) *ν* 3400-2000 (max at 3395, 3193, 2958, 2925, 2518, 2459, 2397, 2123, C-H $^+$N-H, O-H st), 1599, 1502, 1455 (Ar-C-C, Ar-C-N st) cm^{-1}; ^{1}H NMR (400 MHz, CD_3OD) *δ* 1.06 (t, *J* ≈ 7.6 Hz, 3H, 5-CH_2CH_3), 2.81 (q, *J* = 7.6 Hz, 2H, 5-CH_2CH_3), 3.11 [d, *J* = 3,2 Hz, 3H, 4-$CH_2CH_2N(CH_3)$], 3.27 (t, *J* = 7.6 Hz, 2H, 4-CH_2CH_2N), 3.45 [t, *J* ≈ 2.8 Hz, 1H, 4-$CH_2CH_2N(CH_3)CH_2CCH$], 3.70 (broad signal, 2H, 4-CH_2CH_2N), 4.31 (d, *J* = 2.8 Hz, 2H, 4-$CH_2CH_2N(CH_3)CH_2CCH$), 4.88 (s, $^+$NH), 7.51-7.54 [complex signal, 2H, N1-Ar-*C3(5)-H*$_2$], 7.63-7.65 [complex signal, 3H, N1-Ar-*C2(6)-H*$_2$ and N1-Ar-*C4-H*]; ^{13}C NMR (100.6 MHz, CD_3OD) *δ* 13.44 (CH_3, 5-CH_2CH_3), 16.92 (CH_2, 5-CH_2CH_3), 21.05 (CH_2, 4-CH_2CH_2N), 40.84 [CH_3, 4-$CH_2CH_2N(CH_3)$], 46.31 (CH_2, 4-CH_2CH_2N), 55.26 [CH_2, 4-$CH_2CH_2N(CH_3)CH_2C$], 72.70 [C, 4-$CH_2CH_2N(CH_3)CH_2C$], 81.68 [CH, 4-$CH_2CH_2N(CH_3)CH_2CCH$], 126.74 [2CH, N1-Ar-*C3(5)*], 130.92 [2CH, N1-Ar-*C2(6)*], 131.42 [CH, N1-Ar-*C4*], 137.58 (C, *C5*), 139.06 (C, *C4*), 140.20 (C, N1-Ar-*C1*); HRMS (ESI) calcd for ($C_{16}H_{20}N_4 + H^+$) 269.1761; found 269.1766.

4.1.40. N-Methyl-N-[2-(1-phenyl-5-propyl-1H-1,2,3-triazol-4-yl)ethyl]-N-propargylamine ***48***

It was prepared as described for **25**. From amine **41** (168 mg, 0.69 mmol), Cs_2CO_3 (0.22 g, 0.68 mmol), and propargyl bromide (80% solution in toluene, 0.07 mL, 0.47 mmol), and stirring at 0 ºC for 30 min and at rt for an additional 3 h, an oily residue (278 mg) was obtained and purified through column chromatography (40–60 μm silica gel,

CH_2Cl_2 / MeOH / 50% aq. NH_4OH mixtures, gradient elution). On elution with CH_2Cl_2 / MeOH / 50% aq. NH_4OH 98:2:0.2, propargylamine **48** (117 mg, 88% yield) was obtained as a yellow oil; R_f 0.84 (CH_2Cl_2 / MeOH / 50% aq. NH_4OH 9:1:0.05).

48·HCl: orange sticky solid, IR (ATR) *v* 3400-2000 (max at 3400, 3197, 2958, 2930, 2873, 2354, 2121, C-H, $^+$N-H, O-H st), 1630, 1597, 1501 (Ar-C-C, Ar-C-N st) cm^{-1}; ^1H NMR (400 MHz, CD_3OD) δ 0.83 (complex signal, 3H, 5-$CH_2CH_2CH_3$), 1.44 (m, $J \approx$ 7.5 Hz, 2H, 5-$CH_2CH_2CH_3$), 2.76 (t, $J \approx$ 7.8 Hz, 2H, 5-$CH_2CH_2CH_3$), 3.11 [d, J = 3.6 Hz, 3H, 4-$CH_2CH_2N(CH_3)$], 3.45 [t, J = 2.4 Hz, 1H, 4-$CH_2CH_2N(CH_3)CH_2CCH$], 3.70 (broad signal, 2H, 4-CH_2CH_2N), 4.31 [d, J = 2.4 Hz, 2H, 4-$CH_2CH_2N(CH_3)CH_2CCH$], 4.85 (s, $^+$NH), 7.50-7.53 [complex signal, 2H, N1-Ar-*C3(5)-H*$_2$], 7.63-7.65 [complex signal, 3H, N1-Ar-*C2(6)-H*$_2$ and N1-Ar-*C4-H*]; ^{13}C NMR (100.6 MHz, CD_3OD) δ 13.88 (CH_3, 5-$CH_2CH_2CH_3$), 21.11 (CH_2, 5-$CH_2CH_2CH_3$), 22.85 (CH_2, 5-$CH_2CH_2CH_3$), 25.33 (CH_2, 4-CH_2CH_2N), 40.86 (CH_2, 4-CH_2CH_2N), 46.31 [CH_3, 4-$CH_2CH_2N(CH_3)$], 55.26 [CH_2, 4-$CH_2CH_2N(CH_3)CH_2C$], 72.70 (C, 4-$CH_2CH_2N(CH_3)CH_2C$), 81.68 (CH, 4-$CH_2CH_2N(CH_3)CH_2CCH$), 126.80 [2CH, N1-Ar-*C2(6)* or N1-Ar-*C3(5)*], 130.91 [2CH, N1-Ar-*C2(6)* or N1-Ar-*C3(5)*], 131.42 (CH, N1-Ar-*C4*), 137.63 (C, *C5*), 137.66 (C, *C4*), 140.70 (C, N1-Ar-*C1*); HRMS (ESI) calcd for ($C_{17}H_{22}N_4$ + H^+) 283.1917, found 283.1923.

*4.1.41. N-Methyl-N-[2-(5-butyl-1-phenyl-1H-1,2,3-triazol-4-yl)ethyl]-N-propargylamine **49***

It was prepared as described for **25**. From amine **42** (157 mg, 0.61 mmol), Cs_2CO_3 (0.22 g, 0.68 mmol), and propargyl bromide (80% solution in toluene, 0.07 mL, 0.47 mmol), and stirring at 0 ºC for 30 min and at rt for an additional 3 h, an oily residue (172 mg) was obtained and purified through column chromatography (40–60 μm silica gel, CH_2Cl_2 / MeOH / 50% aq. NH_4OH mixtures, gradient elution). On elution with CH_2Cl_2 / MeOH / 50% aq. NH_4OH 100:0:0.2 to 99:1:0.2, propargylamine **49** (164 mg, 91% yield) was obtained as a yellow oil; R_f 0.86 (CH_2Cl_2 / MeOH / 50% aq. NH_4OH 9:1:0.05).

49·HCl: yellow sticky solid, IR (ATR) *v* 3500-2000 (max at 3426, 3209, 2929, 2869, 2352, 2120, C-H, $^+$N-H, O-H st), 1633, 1597, 1576, 1501 (Ar-C-C, Ar-C-N st) cm^{-1}; ^1H NMR (400 MHz, CD_3OD) δ 0.80 [t, $J \approx$ 7.4 Hz, 3H, 5-$(CH_2)_3CH_3$], 1.18-1.28 [sext., $J \approx$ 7.4 Hz, 2H, 5-$(CH_2)_2CH_2CH_3$], 1.35-1.42 (quint., $J \approx$ 7.6 Hz, 2H, 5-$CH_2CH_2CH_2CH_3$), 2.78 [t, J = 7.6 Hz, 2H, 5-$CH_2(CH_2)_2CH_3$], 3.11 [s, 3H, 4-$CH_2CH_2N(CH_3)$], 3.22 (t, J =

7.6 Hz, 2H, 4-*CH*$_2$CH$_2$N), 3.46 [t, *J* ≈ 2.4 Hz, 1H, 4-CH$_2$CH$_2$N(CH$_3$)CH$_2$C*CH*], 3.69 (broad signal, 2H, 4-CH$_2$*CH*$_2$N), 4.30 [d, *J* = 2.4 Hz, 2H, 4-CH$_2$CH$_2$N(CH$_3$)*CH*$_2$C], 4.85 (s, $^+$NH), 7.49-7.52 [complex signal, 2H, N1-Ar-*C2(6)-H*$_2$], 7.62-7.66 [complex signal, 3H, N1-Ar-*C3(5)-H*$_2$ and N1-Ar-*C4-H*]; ^{13}C NMR (100.6 MHz, CD$_3$OD) *δ* 13.82 (CH$_3$, 5-(CH$_2$)$_3$*CH*$_3$], 21.13 [CH$_2$, 5-(CH$_2$)$_2$*CH*$_2$CH$_3$], 23.06 (CH$_2$, 5-CH$_2$*CH*$_2$CH$_2$CH$_3$), 23.18 (CH$_2$, 5-*CH*$_2$(CH$_2$)$_2$CH$_3$], 31.60 (CH$_2$, 4-*CH*$_2$CH$_2$N), 40.87 (CH$_2$, 4-CH$_2$*CH*$_2$N), 46.31 (CH$_3$, 4-CH$_2$CH$_2$N(*CH*$_3$)], 55.29 [CH$_2$, 4-CH$_2$CH$_2$N(CH$_3$)*CH*$_2$C], 72.70 [C, 4-CH$_2$CH$_2$N(CH$_3$)CH$_2$*C*],81.67 [CH, 4-CH$_2$CH$_2$N(CH$_3$)CH$_2$C*CH*], 126.80 [2CH, N1-Ar-*C2(6)* or N1-Ar-*C3(5)*], 130.90 [2CH, N1-Ar-*C2(6)* or N1-Ar-*C3(5)*], 131.38 (CH, N1-Ar-*C4*), 137.69 (C, *C5*), 137.72 (C, *C4*), 140.64 (C, N1-Ar-*C1*); HRMS (ESI) calcd for (C$_{18}$H$_{24}$N$_4$ + H$^+$) 297.2074; found 297.2085.

4.1.42. 3-[3-(Trimethylsilyl)-2-propynyl]benzonitrile ***52***

A solution of trimethylsilylacetylene (1.59 mL, 1.11 g, 11.3 mmol) in anhydrous THF (22 mL) was cooled to –78 ºC, treated dropwise with *n*-BuLi (2.5 M solution in hexanes, 4.59 mL, 11.5 mmol), and stirred at –78 ºC for 30 min. A solution of $ZnBr_2$ (2.59 g, 11.5 mmol) in anhydrous THF (8 mL) was then added and the resulting mixture was warmed to 0 ºC. 3-Bromomethylbenzonitrile, **51** (1.50 g, 7.65 mmol), and $Pd(PPh_3)_2Cl_2$ (290 mg, 0.41 mmol) were added and the reaction mixture was stirred at rt overnight. The reaction mixture was cooled to 0 ºC, treated with 1 N HCl (20 mL), and extracted with EtOAc (2 × 30 mL). The combined organic extracts were washed with sat. aq. $NaHCO_3$ (20 mL), dried over anhydrous Na_2SO_4, and evaporated under reduced pressure to give a residue (2.02 g), which was purified through column chromatography (40–60 *μ*m silica gel, hexane / EtOAc mixtures, gradient elution). On elution with hexane / EtOAc 95:5, compound **52** (1.03 g, 63% yield) was isolated as a colorless oil; R_f 0.73 (hexane / EtOAc 8:2); IR (ATR) *ν* 3000-2000 (max at 2958, 2230, 2178, C-H st), 1583, 1482, (CN, Ar-C-C st) cm^{-1}; ^{1}H NMR (400 MHz, $CDCl_3$) *δ* 0.20 [s, 9H, (*CH*$_3$)$_3$Si], 3.68 (s, 2H, 3-*CH*$_2$C), 7.42 (dd, *J'* ≈ *J''* ≈ 7.6 Hz, 1H, 4-*H*), 7.52-7.58 (complex signal, 2H, 5-*H* and 6-*H*), 7.65 (s, 1H, 2-*H*); ^{13}C NMR (100.6 MHz, $CDCl_3$) *δ* -0.05 [3CH$_3$, (*CH*$_3$)$_3$Si], 25.81 (CH$_2$, 3-*CH*$_2$C), 88.40 [C, 3-CH$_2$C*C*-Si(CH$_3$)$_3$], 102.19 [C, 3-CH$_2$*C*C-Si(CH$_3$)$_3$], 112.56 (C, *C1*), 118.74 (C, *CN*), 129.22 (CH, *C6*), 130.43 (CH, *C5*), 131.41 (CH, *C2*), 132.38 (CH, *C4*), 137.90 (C, *C3*); HRMS (ESI) calcd for (C$_{13}$H$_{15}$NSi + H$^+$) 214.1047, found 214.1048.

*4.1.43. 4-[3-(Trimethylsilyl)-2-propynyl]benzonitrile **53***

It was prepared as described for **52**. From trimethylsilylacetylene (1.06 mL, 737 mg, 7.50 mmol), *n*-BuLi (2.5 M solution in hexanes, 3.06 mL, 7.65 mmol), $ZnBr_2$ (1.72 g, 7.64 mmol), 4-bromomethylbenzonitrile, **51** (1.00 g, 5.10 mmol), and $Pd(PPh_3)_2Cl_2$ (183 mg, 0.26 mmol), a residue (1.38 g) was obtained and purified through column chromatography (40–60 μm silica gel, hexane / EtOAc mixtures, gradient elution). On elution with hexane / EtOAc 90:10, compound **53** (900 mg, 83% yield) was isolated as a colorless oil; R_f 0.77 (hexane / EtOAc 8:2); IR (ATR) *v* 3000-2000 (max at 2958, 2229, 2178, 2114, C-H st), 1608, 1507, (CN, Ar-C-C st) cm^{-1}; ^1H NMR (400 MHz, $CDCl_3$) δ 0.19 [s, 9H, $(CH_3)_3Si$], 3.71 (s, 2H, 4-CH_2C), 7.45 [d, J = 8.4 Hz, 2H, 3(*5*)-H_2], 7.61 [d, J = 8.4 Hz, 2H, 2(6)-H_2]; ^{13}C NMR (100.6 MHz, $CDCl_3$) δ -0.04 [$3CH_3$, $(CH_3)_3Si$], 26.36 (CH_2, 4-CH_2C), 88.43 [C, 4-CH_2CC-$Si(CH_3)_3$], 102.13 (C, 4-CH_2CC-$Si(CH_3)_3$], 110.62 (C, *C1*), 118.82 (C, *CN*), 128.66 [2CH, *C3(5)*], 132.30 [2CH, *C2(6)*], 141.93 (C, *C4*); HRMS (ESI) calcd for ($C_{13}H_{15}NSi + H^+$) 214.1047; found 214.1048.

*4.1.44. 3-(2-Propynyl)benzonitrile **54***

To a solution of **52** (1.60 g, 7.51 mmol) in CH_2Cl_2 (70 mL), a solution of AgOTf (193 mg, 0.75 mmol) in MeOH / H_2O 11:1 (50 mL) was added. The reaction mixture was stirred at rt for 7 h, treated with an additional amount of AgOTf (386 mg, 1.50 mmol), and stirred at rt overnight. The resulting mixture was diluted with sat. aq. NH_4Cl (50 mL) and extracted with CH_2Cl_2 (3 × 50 mL). The combined organic extracts were washed with H_2O (50 mL), dried over anhydrous Na_2SO_4, and evaporated under reduced pressure to give a crude (944 mg), which was purified through column chromatography (40–60 μm silica gel, hexane / EtOAc mixtures, gradient elution). On elution with hexane / EtOAc 95:5, alkyne **54** (690 mg, 65% yield) was isolated as a white solid; R_f 0.72 (hexane / EtOAc 8:2), mp 63-65 ºC; IR (ATR) *v* 3200-2200 (max at 3247, 2362, 2230, C-H st), 1584, 1484, (CN, Ar-C-C st) cm^{-1}; ^1H NMR (400 MHz, $CDCl_3$) δ 2.26 (t, J = 2.8 Hz, 1H, 3-CH_2CCH), 3.64 (d, J = 2.8 Hz, 2H, 3-CH_2C), 7.43 (dd, $J' \approx J'' \approx$ 7.8 Hz, 1H, 4-*H*), 7.53-7.55 (dt, J' = 8.0 Hz, $J'' \approx$ 1.2 Hz, 1H, 6-*H*), 7.57-7.60 (complex signal, 1H, 5-*H*), 7.67 (complex signal, 1H, 2-*H*); ^{13}C NMR (100.6 MHz, $CDCl_3$) δ 24.43 (CH_2, 3-CH_2C), 71.73 (CH, 3-CH_2CCH), 80.13 (C, 3-CH_2CCH), 112.63 (C, *C1*), 118.64 (C, *CN*), 129.27 (CH, *C6*), 130.53 (CH, *C5*), 131.37 (CH, *C2*), 132.35 (CH, *C4*), 137.54 (C, *C3*); HRMS (ESI) calcd for ($C_{10}H_7N + H^+$) 142.0651, found 142.0653.

*4.1.45. 4-(2-Propynyl)benzonitrile **55***

It was prepared as described for **54**. From **53** (642 mg, 3.01 mmol) and AgOTf [(80 mg, 0.31 mmol) × 2], a crude (548 mg) was obtained and purified through column chromatography (40–60 μm silica gel, hexane / EtOAc mixtures, gradient elution). On elution with hexane / EtOAc 80:20, alkyne **55** (346 mg, 81% yield) was isolated as a white solid; R_f 0.76 (hexane / EtOAc 8:2), mp 87-89 ºC; IR (ATR) *v* 3300-2000 (max at 3254, 2229, C-H st), 1605, 1504, (CN, Ar-C-C st) cm^{-1}; ^1H NMR (400 MHz, $CDCl_3$) δ 2.25 (t, *J* = 2.8 Hz, 1H, 4-CH_2C*CH*), 3.67 (d, *J* = 2.4 Hz, 2H, 4-*CH_2*C), 7.48 [dd, *J'* = 8.8 Hz, *J''* = 0.8 Hz, 2H, 3(5)-*H_2*], 7.62 [dd, *J'* = 6.8 Hz, *J''* = 2.0 Hz, 2H, 2(6)-*H_2*]; ^{13}C NMR (100.6 MHz, $CDCl_3$) δ 24.99 (CH_2, 4-*CH_2*C), 71.71 (CH, 4-CH_2C*CH*), 80.07 (C, 4-CH_2*C*), 110.80 (C, *C1*), 118.74 (C, *CN*), 128.66 [2CH, *C3(5)*], 132.35 [2CH, *C2(6)*], 141.53 (C, *C4*); HRMS (ESI) calcd for ($C_{10}H_7N + H^+$) 142.0651, found 142.0647.

*4.1.46. 3-[(1-Methyl-1H-1,2,3-triazol-4-yl)methyl]benzonitrile **56***

It was prepared as described for **9**. From iodomethane (0.30 mL, 0.68 g, 4.82 mmol), NaN_3 (342 mg, 5.26 mmol), Na_2CO_3 (1.39 g, 13.1 mmol), ascorbic acid (616 mg, 3.50 mmol), $CuSO_4 \cdot 5H_2O$ (436 mg, 1.75 mmol), and alkyne **54** (618 mg, 4.38 mmol), compound **56** (823 mg, 95% yield) was obtained as a yellowish solid; R_f 0.64 (CH_2Cl_2 / MeOH / 50% aq. NH_4OH 9.5:0.5:0.05); mp 85-87 ºC; IR (ATR) *v* 3200-2200 (max at 3123, 2949, 2361, 2229, C-H st), 1670, 1597, 1582, 1542, 1505, (CN, Ar-C-C Ar-C-N st) cm^{-1}; ^1H NMR (400 MHz, $CDCl_3$) δ 4.06 [s, 3H, N1(*CH_3*)], 4.10 (s, 2H, 4-*CH_2*-Ar), 7.27 (s, 1H, 5-*H*), 7.39 (t, *J* = 8.0 Hz, 1H, 4-CH_2-Ar-C5'-*H*), 7.49-7.53 (partially overlapped signal, 3H, 4-CH_2-Ar-C2'-*H*, 4-CH_2-Ar-C4'-*H*, 4-CH_2-Ar-C6'-*H*); ^{13}C NMR (100.6 MHz, $CDCl_3$) δ 31.54 [CH_3, N1(*CH_3*)], 36.61 (CH_2, 4-*CH_2*-Ar), 112.54 (C, 4-CH_2-Ar-*C3'*), 118.67 (C, *CN*), 122.46 (CH, *C5*), 129.34 (CH, 4-CH_2-Ar-*C4'*), 130.23 (CH, 4-CH_2-Ar-*C5'*), 132.04 (CH, 4-CH_2-Ar-*C2'*), 133.22 (CH, 4-CH_2-Ar-*C6'*), 140.57 (C, *C4*), 145.97 (C, 4-CH_2-Ar-*C1'*); HRMS (ESI) calcd for ($C_{11}H_{10}N_4 + H^+$) 199.0978, found 199.0980.

*4.1.47. 4-[(1-Methyl-1H-1,2,3-triazol-4-yl)methyl]benzonitrile **57***

It was prepared as described for **9**. From iodomethane (0.17 mL, 0.38 g, 2.70 mmol), NaN_3 (191 mg, 2.94 mmol), Na_2CO_3 (779 mg, 7.35 mmol), ascorbic acid (350 mg, 1.99 mmol), $CuSO_4 \cdot 5H_2O$ (250 mg, 1.00 mmol), and alkyne **55** (346 mg, 2.45 mmol),

compound **57** (459 mg, 95% yield) was obtained as a white solid; R_f 0.63 (CH_2Cl_2 / MeOH / 50% aq. NH_4OH 9.5:0.5:0.05); mp 116-118 ºC; IR (ATR) *v* 3200-2100 (max at 3128, 3083, 2948, 2905, 2227, C-H st), 1608, 1554, 1508 (CN, Ar-C-C, Ar-C-N st) cm^{-1}; ^1H NMR (400 MHz, $CDCl_3$) δ 4.05 [s, 3H, N1(*CH*$_3$)], 4.13 (s, 2H, 4-*CH*$_2$-Ar), 7.24 (s, 1H, 5-*H*), 7.35 [dd, *J* = 8.8 Hz, *J'* = 2.0 Hz, 2H, 4-CH_2-Ar-C2'(6')-*H*$_2$], 7.56-7.59 [dt, *J* = 8.4 Hz, *J'* ≈ *J''* ≈ 1.8 Hz, 2H, 4-CH_2-Ar-C3'(5')-*H*$_2$]; ^{13}C NMR (100.6 MHz, $CDCl_3$) δ 32.15 (CH_2, 4-*CH*$_2$-Ar), 36.63 [CH_3, N1(*CH*$_3$)], 110.44 (C, *C4'*), 118.78 (C, *CN*), 122.45 (CH, *C5*), 129.43 [2CH, 4-CH_2-*C2'(6')*], 132.37 [2CH, 4-CH_2-*C3'(5')*], 144.60 (C, *C4*), 145.91 (C, *C1'*); HRMS (ESI) calcd for ($C_{11}H_{10}N_4$ + H^+) 199.0978, found 199.0978.

4.1.48. 3-[(1-Methyl-1H-1,2,3-triazol-4-yl)methyl]benzylamine ***58***

A solution of nitrile **56** (739 mg, 3.73 mmol) in anhydrous THF (30 mL) was cooled to 0 ºC and treated dropwise with $LiAlH_4$ (4 M solution in Et_2O, 2.98 mL, 11.9 mmol). The reaction mixture was stirred under reflux for 2 h, cooled to 0 ºC, treated portionwise with 1 N NaOH (100 mL), diluted with H_2O (100 mL), and extracted with EtOAc (3 × 100 mL). The combined organic extracts were dried over anhydrous Na_2SO_4 and concentrated under reduced pressure to afford amine **58** (368 mg, 49% yield) as a yellow oil; R_f 0.28 (CH_2Cl_2 / MeOH / 50% aq. NH_4OH 9.5:0.5:0.05).

58·HCl: yellowish solid, mp 85-87 ºC; IR (ATR) *v* 3400-2200 (max at 3303, 3077, 2908, 2870, 2356, 2322, C-H, $^+NH_3$, O-H st), 1893, 1624, 1599, 1522, (Ar-C-C, Ar-C-N st) cm^{-1}; ^1H NMR (400 MHz, $CDCl_3$) δ 4.14 (s, 2H, 4-*CH*$_2$-Ar), 4.29 [s, 3H, N1(*CH*$_3$)], 4.30 (s, 2H, 4-CH_2-Ar-C3'-*CH*$_2$-N), 4.95 (s, $^+NH_3$), 7.39-7.49 (overlapped signal, 4H, 4-CH_2-*Ar*), 8.39 (s, 1H, 5-*H*); ^{13}C NMR (100.6 MHz, $CDCl_3$) δ 30.23 (CH_2, 4-*CH*$_2$-Ar), 39.80 [CH_3, N1(*CH*$_3$)], 44.09 (CH_2, 4-CH_2-Ar-C3'-*CH*$_2$-N), 129.06 (CH), 129.23 (CH), 130.67 (CH), 130.97 (CH), 135.34 (C, *C4*), 138.18 (C, *C1'*), 144.88 (C, *C3'*); HRMS (ESI) calcd for ($C_{11}H_{10}N_4$ + H^+) 199.0978, found 199.0980.

4.1.49. 4-[(1-Methyl-1H-1,2,3-triazol-4-yl)methyl]benzylamine ***59***

It was prepared as described for **58**. From nitrile **57** (310 mg, 1.56 mmol) and $LiAlH_4$ (4 M solution in Et_2O, 1.18 mL, 4.72 mmol), amine **59** (254 mg, 81% yield) was obtained as a yellow oil; R_f 0.27 (CH_2Cl_2 / MeOH / 50% aq. NH_4OH 9.5:0.5:0.05).

59·HCl: yellowish sticky solid, IR (ATR) *v* 3400-2000 (max at 3386, 2931, 2810, 2536, C-H, ^+N-H_3, O-H st), 1892, 1596, 1517, 1426 (Ar-C-C, Ar-C-N st) cm^{-1}; ^1H NMR (400

MHz, $CDCl_3$) δ 4.11 (s, 2H, 4-*CH_2*-Ar), 4.21 [s, 3H, N1(*CH_3*)], 4.89 (s, 5H, 4'-*CH_2*-NH_2 and $^+NH_3$), 7.38 [d, *J* = 8.0 Hz, 2H, 4-CH_2-Ar-C2'(6')-*H_2* or 4-CH_2-Ar-C2'(6')-*H_2*], 7.45 [d, *J* = 8.0 Hz, 2H, 4-CH_2-Ar-C2'(6')-*H_2* or 4-CH_2-Ar-C2'(6')-*H_2*], 8.16 (s, 1H, 5-*H*); ^{13}C NMR (100.6 MHz, $CDCl_3$) δ 30.64 [CH_3, N1(*CH_3*)], 38.95 (CH_2, 4-*CH_2*-Ar), 43.93 (CH_2, 4'-*CH_2*-N), 127.73 (CH, *C5*), 130.58 [2CH, 4-CH_2-Ar-*C3'(5')*], 130.69 [2CH, 4-CH_2-Ar-*C2'(6')*], 133.45 (C, *C4*), 139.28 (C, *C1'*), 145.81 (C, *C4'*); HRMS (ESI) calcd for ($C_{11}H_{14}N_4$ + H^+) 203.1291, found 203.1292.

4.1.50. N-(tert-Butoxycarbonyl)-3-[(1-methyl-1H-1,2,3-triazol-4-yl)methyl]benzylamine ***60***

To a solution of **58** (352 mg, 1.74 mmol) in anhydrous THF (6 mL), a solution of di-*tert*-butyl dicarbonate (380 mg, 1.74 mmol) in anhydrous THF (2 mL) was added at 0 ºC. The reaction mixture was stirred at rt for 3 h and evaporated under reduced pressure. The resulting residue was washed with pentane (3 × 10 mL) and dried under vacuum, to afford **60** (520 mg, quantitative yield) as a yellow oil; R_f 0.85 (CH_2Cl_2 / MeOH / 50% aq. NH_4OH 9.5:0.5:0.05); IR (ATR) *v* 3400-2000 (max at 3341, 2976, 2930, 2113, C-H, NH st), 1696, 1520, 1508, (CO, Ar-C-C, Ar-C-N st) cm^{-1}; ^{1}H NMR (400 MHz, $CDCl_3$) δ 1.55 [s, 9H, (*CH_3*)$_3$C], 4.12 [s, 3H, N1(*CH_3*)], 4.16 (s, 2H, 4-*CH_2*-Ar), 4.37 (d, *J* = 5.6 Hz, 2H, 4-CH_2-Ar-C3'-*CH_2*-N), 4.97 [broad s, 1H, 4-CH_2-Ar-C3'-CH_2-*NH*(BOC)], 7.23-7.26 (complex signal overlapped to the signal of $CDCl_3$, 3H, 2'-*H*, 6'-*H* and 4'-*H*), 7.34-7.38 (overlapped signal, 2H, 5-*H* and 5'-*H*); ^{13}C NMR (100.6 MHz, $CDCl_3$) δ 28.35 [3CH_3, (*CH_3*)$_3$C], 32.11 (CH_2, 4-*CH_2*-Ar), 36.53 [CH_3, N1(*CH_3*)], 44.51 (CH_2, 4-CH_2-Ar-C3'-*CH_2*-N), 79.46 [C, (CH_3)$_3$*C*], 122.40 (CH), 125.56 (CH), 125.56 (CH), 127.65 (2CH), 128.86 (CH), 139.29 (C, *C4*), 139.48 (C, *C1'*), 147.67 (C, *C3'*), 155.86 (C, *CO*); HRMS (ESI) calcd for ($C_{16}H_{22}N_4O_2$ + H^+) 303.1816, found 303.1812.

4.1.51. N-(tert-Butoxycarbonyl)-4-[(1-methyl-1H-1,2,3-triazol-4-yl)methyl]benzylamine ***61***

It was prepared as described for **60**. From **59** (90 mg, 0.45 mmol) and di-*tert*-butyl dicarbonate (98 mg, 0.45 mmol), **61** (133 mg, quantitative yield) was obtained as a beige solid; R_f 0.63 (CH_2Cl_2 / MeOH / 50% aq. NH_4OH 9.5:0.5:0.05).

The analytical sample of **61** was obtained by filtration of a dichloromethane solution through a PTFE filter (0.2 μm), evaporation of the filtrate under reduced pressure and washing of the resulting solid with pentane (3 × 2 mL); IR (ATR) *v* 3400-2500 (max at

3382, 2926, C-H, N-H st), 1690, 1502, (CO, Ar-C-C, Ar-C-N st) cm^{-1}; ^1H NMR (400 MHz, $CDCl_3$) δ 1.44 [s, 9H, $(CH_3)_3C$], 4.00 [s, 3H, N1(CH_3)], 4.04 (s, 2H, 4-CH_2-Ar), 4.26 (d, J = 5.6 Hz, 2H, 4-CH_2-Ar-C4'-CH_2N), 4.86 [broad s, 1H, *NH*(BOC)], 7.13 (s, 1H, 5-*H*), 7.20 (s, 4H, 4-CH_2-*Ar*); ^{13}C NMR (100.6 MHz, $CDCl_3$) δ 28.35 [3CH_3, $(CH_3)_3C$], 31.80 (CH_2, 4-CH_2-Ar), 36.51 [CH_3, N1(CH_3)], 44.27 (CH_2, 4'-CH_2-N), 79.42 [C, $(CH_3)_3C$], 122.35 (CH, *C5*), 127.68 [2CH, 4-CH_2-Ar-*C2'(6')* or 4-CH_2-Ar-*C3'('5)*], 128.87 [2CH, 4-CH_2-Ar-*C'2(6')* or 4-CH_2-Ar-*C'3('5)*], 137.16 (C, *C4*), 138.17 (C, *C1'*), 147.82 (C, *C4'*), 155.85 (C, *CO*); HRMS (ESI) calcd for ($C_{16}H_{22}N_4O_2$ + H^+) 303.1816, found 303.1817.

4.1.52. N-(tert-Butoxycarbonyl)-N-methyl-3-[(1-methyl-1H-1,2,3-triazol-4-yl)methyl]benzylamine ***62***

It was prepared as described for **15**. From compound **60** (480 mg, 1.59 mmol), NaH (60% supension in mineral oil, 96 mg, 2.40 mmol), and iodomethane (0.11 mL, 251 mg, 1.77 mmol), stirring at 60 ºC for 2 h, treating again with NaH (60% supension in mineral oil, 96 mg, 2.40 mmol), and iodomethane (0.11 mL, 251 mg, 1.77 mmol) and stirring at 60 ºC for an additional 2 h, compound **62** (422 mg, 84% yield) was obtained as an orange oil; R_f 0.85 (CH_2Cl_2 / MeOH / 50% aq. NH_4OH 9.5:0.5:0.05); IR (ATR) v 3000-2000 (max at 2973, 2105, 2930, 2113, C-H st), 1750, 1685, (CO, Ar-C-C, Ar-C-N st) cm^{-1}; ^1H NMR (400 MHz, $CDCl_3$) δ 1.48 [s, 9H, $(CH_3)_3C$], 2.83 [broad s, 3H, 4-CH_2-Ar-C3'-CH_2-N(CH_3)BOC], 4.04 [s, 3H, N1(CH_3)], 4.09 (s, 2H, 4-CH_2-Ar), 4.40 (broad s, 4-CH_2-Ar- CH_2-N), 7.09-7.18 (overlapped signal, 3H, 2'-*H*, 6'-*H* and 4'-*H*), 7.26-7.30 (overlapped signal, 2H, 5-*H* and 5'-*H*); ^{13}C NMR (100.6 MHz, $CDCl_3$) δ 28.39 [CH_3, $(CH_3)_3C$], 32.13 (CH_2, 4-CH_2-Ar), 33.94 [CH_3, N1(CH_3)], 36.53 [CH_3, 4-CH_2-Ar-C3'-CH_2-N(CH_3)BOC], 51.80/52.51 (CH_2, 4-CH_2-Ar-C3'-CH_2-N), 79.63 [C, $(CH_3)C$], 122.37 (CH, *C5*), 125.42 (CH), 127.52 (CH), 128.77 (2CH), 138.46 (C, *C4*), 139.38 (2C, *C1'* and *C3'*), 147.70 (C, *CO*); HRMS (ESI) calcd for [2 ($C_{17}H_{24}N_4O_2$) + H^+]: 633.3871, found 633.3864.

4.1.53. N-(tert-Butoxycarbonyl)-N-methyl-4-[(1-methyl-1H-1,2,3-triazol-4-yl)methyl]benzylamine ***63***

It was prepared as described for **15**. From compound **61** (140 mg, 0.46 mmol), NaH (60% supension in mineral oil, 28 mg, 0.70 mmol), and iodomethane (0.03 mL, 68 mg, 0.48 mmol), stirring at 60 ºC for 2 h, treating again with NaH (60% supension in

mineral oil, 28 mg, 0.70 mmol), and iodomethane (0.03 mL, 68 mg, 0.48 mmol) and stirring at 60 ºC for an additional 2 h, compound **63** (120 mg, 83% yield) was obtained as a brown oil; R_f 0.56 (CH_2Cl_2 / MeOH / 50% aq. NH_4OH 9.5:0.5:0.05); IR (ATR) *v* 3000-2500 (max at 2970, 2926, C-H st), 1686, 1512, (CO, Ar-C-C, Ar-C-N st) cm^{-1}; ^1H NMR (400 MHz, $CDCl_3$) δ 1.46 [s, 9H, $(CH_3)_3C$], 2.79 [broad signal, 3H, 4'-$CH_2N(CH_3)$BOC], 4.01 [s, 3H, N1(CH_3)], 4.05 (s, 2H, 4-CH_2-Ar), 4.37 (broad signal, 2H, 4'-CH_2-N), 7.14 (d, *J* = 7.20 Hz, 2H, 6'-*H* and 2'-*H*), 7.20-7.22 (partially overlapped signal, 3H, 3'-*H*, 5-*H* and 5'-*H*); ^{13}C NMR (100.6 MHz, $CDCl_3$) δ 28.41 [3CH_3, $(CH_3)_3C$], 31.80 (CH_2, 4-CH_2-Ar), 33.81 (CH_3, 4'-CH_2-N(CH_3)BOC], 36.52 [CH_3, N1(CH_3)], 51.53/52.24 (CH_2 of the two possible diastereomers, 4'-CH_2-N), 79.61 [C, $(CH_3)_3C$], 122.36 (CH, *C5*), 127.62/127.85 (2CH, 4-CH_2-Ar-*C2'(6')*], 128.79 [2CH, 4-CH_2-Ar-*C3'(5')*], 136.24 (C, *C4*), 138.03 (C, *C1'*), 147.82 (C, *C4'*), 155.75 (C, *CO*); HRMS (ESI) calcd for ($C_{17}H_{24}N_4O_2$ – *tert*-Bu + H^+) 261.1346, found 261.1341.

4.1.54. N-Methyl-3-[(1-methyl-1H-1,2,3-triazol-4-yl)methyl]benzylamine ***64***

It was prepared as described for **21**. From **62** (384 mg, 1.21 mmol) and H_3PO_4 (85% purity, 2.15 mL, 18.6 mmol), amine **64** (242 mg, quantitative yield) was obtained as an orange oil; R_f 0.30 (CH_2Cl_2 / MeOH / 50% aq. NH_4OH 9.5:0.5:0.05).

64·HCl: sticky solid, IR (ATR) *v* 3400-2000 (max at 3373, 2955, 2778, 2699, 2541, 2111, C-H, ^+N-H_2, O-H st), 1899, 1599, (Ar-C-C, Ar-C-N st) cm^{-1}; ^1H NMR (400 MHz, CD_3OD) δ 2.73 [s, 3H, N1(CH_3)], 3.35 (s, 2H, 4-CH_2-Ar), 4.21 (broad s, 2H, 3'-CH_2-N), 4.32 [d, *J* = 4.0 Hz, 3H, 3'-CH_2-NH(CH_3)], 4.99 (s, $^+NH_2$), 7.43-7.51 (complex signal, 3H, 4-CH_2-Ar-C4'-*H*, 4-CH_2-Ar-C5'-*H* and 4-CH_2-Ar-C6'-*H*), 7.55 (s, 1H, 4-CH_2-Ar-C2'-*H*), 8.47 (s, 1H, 5-*H*); ^{13}C NMR (100.6 MHz, CD_3OD) δ 29.96 (CH_2, 4-CH_2-Ar), 33.24 [CH_3, N1(CH_3)], 40.04 [CH_3, 3'-CH_2-NH(CH_3)], 53.27 (CH_2, 3'-CH_2-N), 129.51 (CH, *C5*), 130.26 (CH), 131.05 (CH), 131.15 (CH), 131.54 (CH), 133.55 (C, *C4*), 137.97 (C, *C1'*), 144.46 (C, *C3'*); HRMS (ESI) calcd for ($C_{12}H_{16}N_4$ + H^+): 217.1448, found 217.1446.

4.1.55. N-Methyl-4-[(1-methyl-1H-1,2,3-triazol-4-yl)methyl]benzylamine ***65***

It was prepared as described for **21**. From **63** (237 mg, 0.75 mmol) and H_3PO_4 (85% purity, 1.29 mL, 11.2 mmol), amine **65** (156 mg, 96% yield) was obtained as an orange oil; R_f 0.24 (CH_2Cl_2 / MeOH / 50% aq. NH_4OH 9.5:0.5:0.05).

65·HCl: sticky solid, IR (ATR) *v* 3400-2000 (max at 3339, 2931, 2744, 2708, 2547, 2415, 2351, 2098 C-H, $^{+}$N-H_2, O-H st), 1851, 1588, 1514 (Ar-C-C, Ar-C-N st) cm^{-1}; ^{1}H NMR (400 MHz, CD_3OD) δ 2.71 [s, 3H, N1(*CH_3*)], 4.19 (s, 2H, 4-*CH_2*-Ar), 4.23 [overlapped signal, 5H, 4'-CH_2-NH(*CH_3*) and 4'-*CH_2*-N], 4.90 (s, $^{+}NH_2$), 7.41 [d, *J* = 7.6 Hz, 2H, 4-CH_2-Ar-C2'(6')-*H_2*], 7.50 [d, *J* = 8.0 Hz, 2H, 4-CH_2-Ar-C3'(5')-*H_2*], 8.20 (s, 1H, 5-*H*); ^{13}C NMR (100.6 MHz, CD_3OD) δ 30.62 (CH_2, 4-*CH_2*-Ar), 33.13 [CH_3, N1(*CH_3*)], 39.04 [CH_3, 4'-CH_2-NH(*CH_3*)], 53.13 (CH_2, 4'-*CH_2*-N), 127.89 (CH, *C5*), 130.67 (2CH, 4-CH_2-Ar-*C2'(6')*], 131.63 [2CH, 4-CH2-Ar-*C3'(5')*], 133.01 (C, *C4*), 139.72 (C, *C4'*), 145.64 (C, *C1'*); HRMS (ESI) calcd for ($C_{12}H_{16}N_4$ + H^+) 217.1448, found 217.1448.

4.1.56. N-Methyl-N-{3-[(1-methyl-1H-1,2,3-triazol-4-yl)methyl]benzyl}-N-propargylamine ***66***

It was prepared as described for **25**. From amine **64** (236 mg, 1.09 mmol), Cs_2CO_3 (354 mg, 1.09 mmol), and propargyl bromide (80% solution in toluene, 0.16 mL, 1.08 mmol), and stirring at at 0 °C for 30 min and at rt for an additional 3 h, propargylamine **66** (180 mg, 66% yield) was obtained as a yellow oil, without the need of chromatographic purification; R_f 0.66 (CH_2Cl_2 / MeOH / 50% aq. NH_4OH 9.5:0.5:0.05). **66**·HCl: sticky solid; IR (ATR) *v* 3400-2000 (max at 3388, 3190, 3023, 2930, 2490, 2342, 2122, C-H, $^{+}$N-H, O-H st), 1889, 1593, 1457 (Ar-C-C, Ar-C-N st) cm^{-1}; ^{1}H NMR (400 MHz, CD_3OD) δ 2.94 [s, 3H, 3'-CH_2-N(*CH_3*)], 3.48 [t, *J* = 2.8 Hz, 1H, 3'-CH_2-N(CH_3)CH_2C*CH*], 4.08 (broad signal, 2H, 4-*CH_2*-Ar), 4.27 [s, 3H, N1(*CH_3*)], 4.30 (s, 2H, 3'-*CH_2*-N), 4.47 [broad signal, 2H, 3'-CH_2-N(CH_3)*CH_2*CCH], 5.04 (s, $^{+}$NH), 7.49-7.55 (complex signal, 3H, 4-CH_2-Ar-C4'-*H*, 4-CH_2-Ar-C5'-*H* and 4-CH_2-Ar-C6'-*H*), 7.61 (s, 1H, 4-CH_2-Ar-C2'-*H*), 8.33 (s, 1H, 5-*H*); ^{13}C NMR (100.6 MHz, CD_3OD) δ 30.51 (CH_2, 3'-*CH_2*-N), 39.29 [CH_3, 3'-CH_2-N(*CH_3*)], 40.12 [CH_3, N1(*CH_3*)], 45.39 (CH_2, 4-*CH_2*-Ar), 59.37 [CH_2, 3'-CH_2-N(CH_3)*CH_2*CCH], 72.80 [C, 3'-CH_2-N(CH_3)CH_2*C*CH], 81.94 [CH, 3'-CH_2-N(CH_3)CH_2C*CH*], 128.37 (CH, *C5*), 131.00 (CH), 131.17 (CH), 131.82 (CH), 132.63 (CH, *C2'*), 139.23 (2C, *C1'* and *C3'*), 145.17 (C, *C4*); HRMS (ESI) calcd for ($C_{15}H_{18}N_4$ + H^+) 255.1604, found 255.1600; Elemental analysis, calcd for $C_{15}H_{18}N_4$·HCl·$3H_2O$ C 52.25%, H 7.31%, N 16.25%, found C 52.51%, H 7.11%, N 14.14%.

*4.1.57. N-Methyl-N-{4-[(1-methyl-1H-1,2,3-triazol-4-yl)methyl]benzyl}-N-propargylamine **67***

It was prepared as described for **25**. From amine **65** (131 mg, 0.61 mmol), Cs_2CO_3 (0.20 g, 0.61 mmol), and propargyl bromide (80% solution in toluene, 0.07 mL, 0.47 mmol), and stirring at at 0 °C for 3.5 h, an orange oily residue (122 mg) was obtained and purified through column chromatography (40–60 μm silica gel, CH_2Cl_2 / 50% aq. NH_4OH 100:0.2), to afford propargylamine **67** (48 mg, 40% yield) as a yellow oil; R_f 0.67 (CH_2Cl_2 / MeOH / 50% aq. NH_4OH 9:1:0.05).

67·HCl: mp 156-158 ºC; IR (ATR) *v* 3200-2000 (max at 3178, 3095, 2923, 2692, 2501, 2357, 2120, C-H, $^+$N-H, O-H st), 1882, 1606, 1518 (Ar-C-C, Ar-C-N st) cm^{-1}; ^{1}H NMR (400 MHz, CD_3OD) δ 2.92 [s, 3H, 4'-CH_2-N(CH_3)], 3.47 (t, J = 2.4 Hz, 1H, 4'-CH_2-N(CH_3)CH_2C*CH*], 4.05 (broad signal, 2H, 4-CH_2-Ar), 4.19 (s, 3H, N1(CH_3)], 4.22 (s, 2H, 4'-CH_2N), 4.43 (broad signal, 2H, 4'-CH_2-N(CH_3)CH_2CCH), 4.86 (s, $^+$NH), 7.44 [d, J = 8.4 Hz. 2H, 4-CH_2-Ar-C2'(6')-H_2], 7.52 [d, J = 8.4 Hz. 2H, 4-CH_2-Ar-C3'(5')-H_2], 8.10 (s, 1H, 5-*H*); ^{13}C NMR (100.6 MHz, CD_3OD) δ 30.64 (CH_2, 4'-CH_2-N), 39.04 [CH_3, 4'-CH_2-N(CH_3)], 40.10 [CH_3, N1(CH_3)], 45.36 (CH_2, 4-CH_2-Ar), 59.31 [CH_2, 4'-CH_2-N(CH_3)CH_2CCH], 72.81 [C, 4'-CH_2-N(CH_3)CH_2CCH], 81.92 [CH, 4'-CH_2-N(CH_3)CH_2C*CH*], 127.97 (CH, *C5*), 129.39 (C, *C4*), 130.94 [2CH, 4-CH_2-Ar-*C2'(6')*], 132.89 [2CH, 4-CH_2-Ar-*C3'(5')*], 140.54 (C, *C1'*), 145.49 (C, *C4'*); HRMS (ESI) calcd for ($C_{15}H_{19}N_4$ + H^+) 255.1604, found 255.1599.

4.2. Biological assays

4.2.1. Inhibition of hrMAO-A and hrMAO-B

The activity of *hr*MAO-A and *hr*MAO-B (Sigma-Aldrich, Madrid, Spain) was determined using Amplex UltraRed fluorometric coupled method. For both MAO isoforms, tyramine hydrochloride was used as substrate and enzymatic assays were performed in 96-well black opaque microplates (OptiPlate-96F, PerkinElmer) in a final volume of 200 µL. Serial dilutions of each inhibitor were pre-incubated with either 0.36 U/mL *hr*MAO A or 0.0675 U/mL *hr*MAO B for 30 min at 37 ºC. Enzymatic reactions were started upon the addition of 100 µL of a mixture solution containing 1 mM tyramine, 0.04 U/mL horseradish peroxidase (HRP) and 25 mM Amplex UltraRed® reagent in 0.25 mM sodium phosphate (pH 7.4) as final concentrations. The

fluorescence production of resorufin was measured for at least 30 min at 530/590 nm in a spectrophotometric plate reader (FluoStar OPTIMA, BM G Labtech). The enzymatic activity in the absence of compound was used to determine 100% enzyme activity. The potential capacity of the compounds to interfere with the fluorescence generated in the reaction was determined by adding the compounds to solutions in the absence of MAO. From dose-response curves, IC_{50} values were accordingly calculated using the GraphPad 'PRISM' software (version 5.0). Data are expressed as mean ± SEM of at least three different experiments performed in duplicate. Clorgyline and *R*-deprenyl (Sigma-Aldrich) were used as reference compounds.

4.2.2. Reversibility of hrMAO-B inhibition

To study the reversibility of the inhibition of *hr*MAO-B by compound **27**, 100-fold enzyme concentration was inhibited by 200 nM *L*-deprenyl or 50 nM **27** (10-fold IC_{50} values) for 1 h at 37 ºC. Following pre-incubation times, enzyme solution was rapidly diluted (100-fold) in a mix solution containing 1 mM *p*-tyramine, HRP and Amplex UltraRed® reagent in 50 mM phosphate buffer pH 7.4. Next, *hr*MAO-B activity was followed at 530/590 nm for 40 min.

4.2.3. Time-dependent inhibition of hrMAO-B

To investigate the time-dependent inhibition of *hr*MAO-B activity by compound **27**, the enzyme was inhibited by 10 μM **27** for at different pre-incubation times (0-360 min). At the end of each pre-incubation, activity was measured as previously described and plotted as percentage of control samples *versus* pre-incubation time.

4.2.4. Determination of brain permeability: PAMPA-BBB assay

The *in vitro* permeability (P_e) of the novel 1,2,3-triazole-based compounds and fourteen known drugs (Table 2) through lipid extract of porcine brain membrane was determined by using a parallel artificial membrane permeation assay[77] using a mixture PBS:EtOH 70:30. Assay validation was made by comparison of the experimental P_e values of the known drugs with their reported values, which showed a good correlation: *Pe* (exp) = 1.003 *Pe* (lit) – 0.1783 (R^2 = 0.9278). From this equation and the limits established by Di *et al.* for BBB permeation,[77] three ranges of permeability were established:

compounds of high BBB permeation (CNS+): *Pe* (10^{-6} cm s^{-1}) > 5.185; compounds of low BBB permeation (CNS–): *Pe* (10^{-6} cm s^{-1}) < 2.06; compounds of uncertain BBB permeation (CNS±): and 5.185 > *P*e (10^{-6} cm s^{-1}) > 2.06.

Table 2. Reported and experimental permeability values (P_e 10^{-6} cm s^{-1}) of 14 commercial drugs used for the PAMPA-BBB assay validation

Compound	Literature value[a]	Experimental value[b]
Cimetidine	0.0	0.70 ± 0.03
Lomefloxacin	0.0	0.78 ± 0.044
Norfloxacin	0.1	0.90 ± 0.02
Ofloxacin	0.8	0.98 ± 0.057
Hydrocortisone	1.9	1.40 ± 0.05
Piroxicam	2.5	1.93 ± 0.114
Clonidine	5.3	6.50 ± 0.05
Corticosterone	5.1	6.70 ± 0.10
Imipramine	13	12.3 ± 0.10
Promazine	8.8	13.8 ± 0.30
Progesterone	9.3	16.8 ± 0.03
Desipramine	12	17.8 ± 0.10
Testosterone	17	24.0 ± 1.38
Verapamil	16	28.1 ± 1.63

[a] Taken from ref. [77].

[b] Values are expressed as the mean ± SD of three independent experiments.

4.3. Docking studies

The binding mode of selected 1,2,3-triazole derivatives was explored by means of docking calculations carried out with Glide, using an empirical scoring function calibrated on the basis of protein−ligand complexes.[78] Docking was performed using the MAO-B X-ray structure of the complex with inhibitor **6** (PDB entry 4CRT)[76] and deprenyl (PDB entry 2BYB),[28] but no significant differences were found for the best ligand poses. The protocol defined in our previous studies was adopted here.[39] Briefly, the docking volume was defined as the space covered by the binding cavity in MAO-B.

Suitable restraints were introduced to keep the amine nitrogen of the proargylamine unit close to the position found for the corresponding atom in deprenyl and rasagiline (PDB entry 2BK4)[75] in order to mimic the orientation after irreversible linkage with the FAD. Each compound was subjected to 100 docking runs. Whereas the protein was kept rigid, Glide accounts for the conformational flexibility of the ligand around rotatable bonds during docking calculations. The output docking modes were analyzed by visual inspection in conjunction with the docking scores.

Acknowledgements

We thank the financial support from Ministerio de Economía y Competitividad (SAF2014-57094-R) and the Generalitat de Catalunya (GC) (2014SGR52 and 2014SGR1189). We are grateful to the Consorci de Serveis Universitaris de Catalunya for computational resources. FJL acknowledges the support from ICREA Academia. Fellowships from GC to O.D.P., E.V., and I.S. are gratefully acknowledged.

References

[1] Wimo, A.; Jönsson, L.; Gustavsson, A.; McDaid, D.; Ersek, K.; Georges, J.; Gulácsi, L.; Karpati, K.; Kenigsberg, P.; Valtonen, H. The economic impact of dementia in Europe 2008-cost estimates from the Eurocode project. *Int. J. Geriatr. Psychiatry* **2011**, *26*, 825–32.

[2] Bolea, I.; Gella, A.; Unzeta, M. Propargylamine-derived mutitarget-directed ligands: fighting Alzheimer's disease with monoamine oxidase inhibitors. *J. Neural Transm.* **2013**, *120*, 893–902.

[3] Guzior, N.; Wieckowska, A.; Panek, D.; Malawska, B. Recent development of multifunctional agents as potential drug candidates for the treatment of Alzheimer's disease. *Curr. Med. Chem.* **2015**, *22*, 373–404.

[4] Perry, E.K.; Perry, R.H.; Blessed, G.; Tomlinson, B.E. Necropsy evidence of central cholinergic deficits in senile dementia. *Lancet* **1977**, *1*, 189–189.

[5] Coyle, J.T.; Puttfarcken, P. Oxidative stress, glutamate, and neurodegenerative disordes. *Science* **1993**, *262*, 689–695.

[6] Perry, G.; Raina, A.K.; Nunomura, A.; Wataya, T.; Sayre, L.M.; Smith, M.A. How important is oxidative damage? Lessons from Alzheimer's disease. *Free Radic. Biol. Med.* **2000**, *28*, 831–834.

[7] Gella, A.; Durany, N. Oxidative stress in Alzheimer's disease. *Cell. Adh. Migr.* **2009**, *3*, 88–93.

[8] Huang X.; Moir, R.D.; Tanzi, R.E.; Bush, A.I.; Rogers, J.T. Redox-active metals, oxidative stress, and Alzheimer's disease pathology. *Ann. N. Y. Acad. Sci.* **2004**, *1012*, 153–163.

[9] Mishizen-Eberz, A.J.; Rissman, R.A.; Carter, T.L.; Ikonomovic, M.D.; Wolfe, B.B.; Armstrong, D.M. Biochemical and molecular studies of NMDA receptor

subunits NR1/2A/2B in hippocampal subregions throughout progression of Alzheimer's disease pathology. *Neurobiol. Dis.* **2004**, *15*, 80–92.

[10] Goedert, M.; Spillantini, M.G.; Jakes, R.; Rutherford, D.; Crowther, R.A. Multiple isoforms of human microtubule-associated protein tau: sequences and localization in neurofibrillary tangles of Alzheimer's disease. *Neuron.* **1989**, *3*, 519–526.

[11] Glenner, G.G.; Murphy, M.A. Amyloidosis of the nervous system. *J. Neurol. Sci.* **1989**, *94*, 1–28.

[12] Birks, J.; Harvey, R. Donepezil for dementia due to Alzheimer's disease. *Cochrane Database Syst. Rev.* **2006**, *1*, CD001190.

[13] Birks, J.; Grimley, E.J.; Iakovidou, V.; Tsolaki, M. Rivastigmine for Alzheimer's disease. *Cochrane Database Syst. Rev.* **2000**, *4*, CD001191.

[14] Loy, C.; Schneider, L. Galantamine for Alzheimer's disease. *Cochrane Database Syst. Rev.* **2004**, *4*, CD001747.

[15] Areosa, S.A.; McShane, R.; Sheriff, F. Memantine for dementia. *Cochrane Database Syst. Rev.* **2005**, *4*, CD003154.

[16] Chen, X.; Decker, M. Multi-target compounds acting in the central nervous system designed from natural products. *Curr. Med. Chem.* **2013**, *20*, 1673–1685.

[17] Galdeano, C.; Viayna, E.; Arroyo, P.; Bidon-Chanal, A.; Blas, J.R.; Muñoz-Torrero, D.; Luque, F.J. Structural determinants of the multifactorial profile of dual binding site acetylcholinesterase inhibitors as anti-Alzheimer agents. *Curr. Pharm. Design* **2010**, *16*, 2818–2836.

[18] Matinez, A. Emerging drugs and targets for Alzheimer's disease. Vol. 1. Beta-Amyloid, tau protein and glucose metabolism. *(Ed.) RSC*, **2010**.

[19] Thomas, T. Monoamine oxidase B inhibitors in the treatment of Alzheimer's disease. *Neurobiol. Aging* **2000**, *21*, 343–348.

[20] Riederer, P.; Danyelczyk, W.; Grunblat, E. Monoamine oxidase inhibition in Alzheimer's disease. *Neurotoxicology* **2004**, *25*, 271–277.

[21] Kristal, B.S.; Conway, A.D.; Brown, A.M.; Jain, J.C.; Ulluci, P.A.; Li, S.W.; Burke, W.J. Selective dopaminergic vulnerability: 3,4-dihydroxyphenylacetaldehyde targets mitochondria. *Free Radic. Biol. Med.* **2001**, *30*, 924–931.

[22] Edmondson, D.E.; Binda, C.; Wang, J.; Upadhyay, A.K.; Mattevi, A. Molecular and mechanistic properties of the membrane-bound mitochondrial monoamine oxidases. *Biochemistry* **2009**, *48*, 4220–4230.

[23] Tripton, K.F.; Boyce, S.; O'Sullivan, J.; Davey, G.P.; Healy, J. Monoamine oxidases: certainties and uncertainties. *Curr. Med. Chem.* **2004**, *11*, 1965–1982.

[24] Chen, K.; Holschneider, D.P.; Wu, W.; Rebrin, I.; Shih, J.C. A spontaneous point mutation produces monoamine oxidase A/B knock-out mice with greatly elevated monoamines and anxiety-like behavior. *J. Biol. Chem.* **2004**, *279*, 39645–39652.

[25] Binda, C.; Newton-Vinson, P.; Hubálek, F.; Edmonson, D.E.; Mattevi, A. Structure of humane monoamine oxidase B, a drug target for the treatment of neurological disorders. *Nat. Struct. Biol.* **2002**, *9*, 22–26.

[26] Binda, C.; Li, M.; Hubálek, F.; Restelli, N.; Edmonson, D.E.; Mattevi, A. Insights into the mode of inhibition of human mitochondrial monoamine oxidase B from high-resolution crystal structures. *Proc. Natl. Acad. Sci. U.S.A.* **2003**, *100*, 9750–9755.

[27] Binda, C.; Hubálek, F.; Li, M.; Herzig, Y.; Sterling, J.; Edmonson, D.E.; Mattevi, A. Crystal structures of monoamine oxidase B in complex with four inhibitors of the *N*-propargylaminoindan class. *J. Med. Chem.* **2004**, *47*, 1767–1774.

[28] De Colibus, L.; Li, M.; Binda, C.; Lustig, A.; Edmonson, D.E.; Mattevi, A. Three-dimensional structure of human monoamine oxidase A (MAO A): relation to the structure of rat MAO A and human MAO B. Proc. *Natl. Acad. Sci. U.S.A.* **2005**, *102*, 12684–12689.

[29] Son, S.Y.; Ma, J.; Kondou, Y.; Yoshimura, M.; Yamashita, E.; Tsukihara, T. Structure of human monoamine oxidase A at 2.2-Å resolution: the control of opening the entry for substrates/inhibitors. *Proc. Natl. Acad. Sci. U.S.A.* **2008**, *105*, 5739–5744.

[30] Juárez-Jiménez, J.; Mendes, E.; Galdeano, C.; Martins, C.; Silva, D.B.; Marco-Contelles, J.; do Carmo Carreiras, M.; Luque, F.J.; Ramsay, R.R. Exploring the structural basis of the selective inhibition of monoamine oxidase A by dicarbonitrile aminoheterocycles: role of Asn181 and Ile335 validated by spectroscopic and computational studies. *Biochim. Biophys. Acta* **2014**, *1844*, 389–397.

[31] Song, M.S.; Matveychuk, D.; MacKenzie, E.M.; Duchcherer, M.; Mousseau, D.D.; Baker, G.B. An update of monoamine oxidase inhibitors: multifaceted drugs. *Prog. Neuropsychopharmacol. Biol. Psychiatry* **2013**, *44*, 118–124.

[32] Burke, W.J.; Li, S.W.; Chung, H.D.; Ruggiero, D.A.; Kristal, B.S.; Johnson, E.M.; Lampe, P.; Kumar, V.B.; Franko, M.; Williams, E.A.; Zahm, D.S. Neurotoxicity of MAO metabolites of catecholamine neurotransmitters: role in neurodegenerative diseases. *Neurotoxicology* **2004**, *25*, 101–115.

[33] Naoi, M.; Maruyama, W.; Yi, H.; Akao, Y.; Yamaoka, Y.; Shamoto-Nagai, M. Neuroprotection by propargylamines in Parkinson's disease: intracellular mechanism underlying the anti-apoptotic function and search for clinical markers. *J. Neural Transm. Suppl.* **2007**, *72*, 121–131.

[34] Weinreb, O.; Amit, T.; Bar-Am, O.; Sagi, Y.; Mandel, S.; Youdim, M.B. (2006) Involvement of multiple survival signal transduction pathways in the neuroprotective, neurorescue and APP processing activity of rasagiline and its propargyl moiety. *J. Neural Transm. Suppl.* **2006**, *70*, 457–465.

[35] Yáñez, M.; Viña, D. Dual inhibitors of monoamine oxidase and cholinesterase for the treatment of Alzheimer disease. *Curr. Top. Med. Chem.* **2013**, *13*, 1692–1706.

[36] Jo, S.; Yarishkin, O.; Hwang, Y.J.; Chun, Y.E.; Park, M.; Woo, D.H.; Bae, J.Y.; Kim, T.; Lee, J.; Chun, H.; Park, H.J.; Lee, D.Y.; Hong, J.; Kim, H.Y.; Oh, S.-J.; Park, S.J.; Lee, H.; Yoon, B.-E.; Kim, Y.S.; Jeong, Y.; Shim, I.; Bae, Y.C.; Cho, J.; Kowall, N.W.; Ryu, H.; Hwang, E.; Kim, D.; Lee, C.J. GABA from reactive astrocytes impairs memory in mouse models of Alzheimer's disease. *Nat. Med.* **2014**, *20*, 886–896.

[37] Weinreb, O.; Amit, T.; Bar-Am, O.; Youdim, M.B. Ladostigil: a novel multimodal neuroprotective drug with cholinesterase and brain-selective monoamine oxidase inhibitory activities for Alzheimer's disease treatment. *Curr. Drug Targets* **2012**, *13*, 483–494.

[38] Sterling, J.; Herzig, Y.; Goren, T.; Finkelstein, N.; Lerner, D.; Goldenberg, W.; Mikcolczi, I.; Molnar, S.; Rantal, F.; Tamas, T.; Toth, G.; Zagyva, A.; Zekany, A.; Finberg, J.; Lavian, G.; Gross, A.; Friedman, R.; Razin, M.; Huang, W.; Krais, B.; Chorev, M.; Youdim, M.B.; Weinstock, M. Novel dual inhibitors of

AChE and MAO derived from hydroxy aminoindan and phenethylamine as potential treatment for Alzheimer's disease. *J. Med. Chem.* **2002**, *54*, 5260–5279.

[39] Bolea, I.; Juárez-Jiménez, J.; de los Ríos, C.; Chioua, M.; Pouplana, R.; Luque, F.J.; Unzeta, M. Synthesis, biological evaluation and molecular modelling of donepezil and N-[(5-(benzyloxy)-1-methyl-1H-indol-2-yl) methyl]-N-methylprop-2-yn-1-amine hybrids as new multipotent cholinesterase/monoamine oxidase inhibitors for the treatment of Alzheimer's disease. *J. Med. Chem.* **2011**, *54*, 8251–8270.

[40] Farina, R.; Pisani, L.; Catto, M.; Nicolotti, O.; Gadaleta, D.; Denora, N.; Soto-Otero, R.; Mendez-Alvarez, E.; Passos, C. S.; Muncipinto, G.; Altomare, C. D.; Nurisso, A.; Carrupt, P.-A.; Carotti, A. Structure-based design and optimization of multitarget-directed 2*H*-chromen-2-one as potent inhibitors of monoamine oxidase B and cholinesterases. *J. Med. Chem.* **2015**, *58*, 5561–5578.

[41] Xie, S.S.; Wang, X.; Jiang, N.; Yu, W.; Wang, K.D.G.; Lan, J.S.; Li, Z.R.; Kong L.Y. Multi-target tacrine-coumarin hybrids: cholinesterase and monoamine oxidase B inhibition properties against Alzheimer's disease. *Eur. J. Med. Chem.* **2015**, *95*, 153–165.

[42] Zheng, H.; Youdim, M.B.H.; Fridkin, M. Site-activated multifunctional chelator with acetylcholinesterase and neuroprotective/neurorestorative moieties for Alzheimer's therapy. *J. Med. Chem.* **2009**, *52*, 4095–4098.

[43] Zheng, H.; Youdim, M.B.; Fridkin, M. Site-activated chelators targeting AChE and MAO for Alzheimer's therapy. *ACS Chem. Biol.* **2010**, *5*, 603–610.

[44] Passos, C.S.; Simões-Pires, C.A.; Nurisso, A.; Soldi, T.C.; Kato, L.; de Oliveira, C.M.; de Faria, E.O.; Marcourt, L.; Gottfried, C.; Carrupt, P.-A.; Henriques,

A.T. Indole alkaloids of psychotria as multifunctional cholinesterases and monoamine oxidases inhibitors. *Phytochemistry* **2013**, *86*, 8−20.

[45] Nicolotti, O.; Giangreco, I.; Introcaso, A.; Leonetti, F.; Stefanachi, A.; Carotti, A. Strategies of multi-objective optimization in drug discovery and development. *Expert Opin. Drug Discov.* **2011**, *6*, 871−884.

[46] Dias, K.S.T.; Viegas, C., Jr. Multi-target directed drugs: A Modern approach for design of new drugs for the treatment of Alzheimer's disease. *Curr. Neuropharmacol.* **2014**, *12*, 239−255.

[47] Prati, F.; Uliassi, E.; Bolognesi, M. L. Two diseases, one approach: Multitarget drug discovery in Alzheimer's and neglected tropical diseases. *MedChemComm* **2014**, *5*, 853−861.

[48] Rostovtsev, V.V.; Green, L.G.; Fokin, V.V.; Sharpless, K.B. A stepwise Huisgen cycloaddition process: Cu(I)-catalyzed regioselective "ligation" of azides and terminal alkynes. *Angew. Chem. Int. Ed.* **2002**, *41*, 2596−2599.

[49] Tornøe, C.W.; Christensen, C.; Meldal, M. *J. Org. Chem.* **2002**, *67*, 3057−3064.

[50] Struthers, H.; Mindt, T.L.; Schibli, R. Metal chelating systems synthesized using the copper(I) catalyzed azide-alkyne cycloaddition. *Dalton Trans.* **2010**, *39*, 675−696.

[51] Schulze, B.; Schubert, U.S. Beyond click chemistry − supramolecular interactions of 1,2,3-triazoles. *Chem. Soc. Rev.* **2014**, *43*, 2522−2571.

[52] Jiaranaikulwanitch, J.; Govitrapong, P.; Fokin, V.V.; Vajragupta, O. From BACE1 inhibitor to multifunctionality of tryptoline and tryptamine triazole derivatives for Alzheimer's disease, *Molecules* **2012**, *17*, 8312−8333.

[53] Lenhart, J.A.; Ling, X.; Gandhi, R.; Guo, T.L.; Gerk, P.M.; Brunzell, D.H.; Zhang, S. "Clicked" bivalent ligands containing curcumin and cholesterol as

multifunctional Aβ oligomerization inhibitors: Design, synthesis, and biological characterization. *J. Med. Chem.* **2010**, *53*, 6198−6209.

[54] Ramprasad, J.; Nayak, N.; Dalimba, U.; Yogeeswari, P.; Sriram, D. One-pot synthesis of new triazole-imidazo[2,1-b][1,3,4]thiadiazole hybrids via click chemistry and evaluation of their antitubercular activity. *Bioorg. Med. Chem. Lett.* **2015**, in press, DOI: 10.1016/j.bmcl.2015.08.009.

[55] Mishra, N.M.; Briers, Y.; Lamberigts, C.; Steenackers, H.; Robijns, S.; Landuyt, B.; Vanderleyden, J.; Schoofs, L.; Lavigne, R.; Luyten, W.; Van der Eycken, E.V. Evaluation of the antibacterial and anti-biofilm activities of novel CRAMP-vancomycin conjugates with diverse linkers. *Org. Biomol. Chem.* **2015**, *13*, 7477−7486.

[56] Ma, L.-Y.; Pang, L.-P.; Wang, B.; Zhang, M.; Hu, B.; Xue, D.-Q.; Shao, K.-P.; Zhang, B.-L.; Liu, Y.; Zhang, E.; Liu, H.-M. Design and synthesis of novel 1,2,3-triazole-pyrimidine hybrids as potential anticancer agents, *Eur. J. Med. Chem.* **2014**, *86*, 368−380.

[57] Fabbrizzi, P.; Bianchini, F.; Menchi, G.; Raspanti, S.; Guarna, A.; Trabocchi, A. Combination of click chemistry and sulfonamides to develop three-armed triazole compounds, *Tetrahedron* **2014**, *70*, 5439−5449.

[58] Brabez, N.; Saunders, K.; Nguyen, K.L.; Jayasundera, T.; Weber, C.; Lynch, R.M.; Chassaing, G.; Lavielle, S.; Hruby, V.J. Multivalent interactions: Synthesis and evaluation of melanotropin multimers-tools for melanoma targeting. *ACS Med. Chem. Lett.* **2013**, *4*, 98−102.

[59] Liu, K.; Gandhi, R.; Chen, J.; Zhang, S. Bivalent ligands targeting multiple pathological factors involved in Alzheimer's disease. *ACS Med. Chem. Lett.* **2012**, *3*, 942−946.

[60] Howell, L.A.; Bowater, R.A.; O'Connell, M.A.; Reszka, A.P.; Neidle, S.; Searcey, M. Synthesis of small molecules targeting multiple DNA structures using click chemistry. *ChemMedChem*, **2012**, *7*, 792−804.

[61] Ouberai, M.; Brannstrom, K.; Vestling, M.; Olofsson, A.; Dumy, P.; Chierici, S.; Garcia, J. Clicked tacrine conjugates as acetylcholinesterase and β-amyloid directed compounds. *Org. Biomol. Chem.* **2011**, *9*, 1140−1147.

[62] Ronco, C.; Carletti, E.; Colletier, J.-P.; Weik, M.; Nachon, F.; Jean, L.; Renard, P.-Y. Huprine derivatives as sub-nanomolar human acetylcholinesterase inhibitors: From rational design to validation by X-ray crystallography. *ChemMedChem* **2012**, *7*, 400−405.

[63] Lewis, W.G.; Green, L.K.; Grynszpan, F.; Radić, Z.; Carlier, P.R.; Taylor, P.; Finn, M.G.; Sharpless, K.B. Click chemistry in situ: Acetylcholinesterase as a reaction vessel for the selective assembly of a femtomolar inhibitor from an array of building blocks. *Angew. Chem. Int. Ed.* **2002**, *41*, 1053−1057.

[64] Krasiński, A.; Radić, Z.; Manetsch, R.; Raushel, J.; Taylor, P.; Sharpless, K.B.; Kolb, H.C. In situ selection of lead compounds by click chemistry: Target-guided optimization of acetylcholinesterase inhibitors, *J. Am. Chem. Soc.* **2005**, *127*, 6686−6692.

[65] Whiting, M.; Muldoon, J.; Lin, Y.-C.; Silverman, S.M.; Lindstrom, V.; Olson, A.J.; Kolb, H.C.; Finn, M.G.; Sharpless, K.B.; Elder, J.H.; Fokin, V.V. Inhibitors of HIV-1 protease by using in situ click chemistry. *Angew. Chem. Int. Ed.* **2006**, *45*, 1435−1439.

[66] Sharpless, K.B; Manetsch, R. In situ click chemistry: A powerful means for lead discovery. *Expert Opin. Drug Discovery* **2006**, *1*, 525−538.

[67] Oueis, E.; Santoni, G.; Ronco, C.; Syzgantseva, O.; Tognetti, V.; Joubert, L.; Romieu, A.; Weik, M.; Jean, L.; Sabot, C.; Nachon, F., Renard, P.-Y. Reaction site-driven regioselective synthesis of AChE inhibitors. *Org. Biomol. Chem.* **2014**, *12*, 156−161.

[68] Kolb, H.C.; Sharpless, K.B. The growing impact of click chemistry on drug discovery. Drug Discovery Today **2003**, *8*, 1128−1137.

[69] Hein, J.E.; Fokin, V.V. Copper-catalyzed azide-alkyne cycloaddition (CuAAC) and beyond: new reactivity of copper(I) acetylides. *Chem. Soc. Rev.* **2010**, *39*, 1302−1315.

[70] Díez-González, S. Well-defined copper(I) complexes for Click azide-alkyne cycloaddition reactions: one Click beyond. *Catal. Sci. Technol.* **2011**, *1*, 166−178.

[71] Mendal, M.; Tornøe, C.W. Cu-catalyzed azide-alkyne cycloaddition. *Chem. Rev.* **2008**, *108*, 2952−3015.

[72] Bock, V.D.; Hiemstra, H.; van Maarseveen, J.H. Cu^{I}-catalyzed azide-alkyne "Click" cycloadditions from a mechanistic and synthetic perspective. *Eur. J. Org. Chem.* **2006**, *2006*, 51−68.

[73] Shi, Z.-J.; Yu, D.-G. Cross-coupling reactions. *Comprehensive Inorg. Chem. II* **2013**, *6*, 47−77.

[74] Orsini, A.; Vitérisi, A.; Bodlenner, A.; Weibel, J.-M.; Pale, P. A chemoselective deprotection of trymethylsilyl acetylenes catalyzed by silver salts. *Tetrahedron Lett.* **2005**, *46*, 2259−2262.

[75] Hubálek, F.; Binda, C.; Khalil, A.; Li, M.; Mattevi, A.; Castagnoli, N.; Edmondson, D.E. Demonstration of isoleucine 199 as a structural determinant

for the selective inhibition of human monoamine oxidase B by specific reversible inhibitors. *J. Biol. Chem.* **2005**, *280*, 15761−15766.

[76] Esteban, G.; Allan, J.; Samadi, A.; Mattevi, A.; Unzeta, M.; Marco-Contelles, J.; Binda, C.; Ramsay, R.R. Kinetic and structural analysis of the irreversible inhibition of human monoamine oxidases by ASS234, a multi-target compound designed for use in Alzheimer's disease. *Biochim. Biophys. Acta* **2014**, *1844*, 1104−1110.

[77] Di, L.; Kerns, E.H.; Fan, K.; McConnell, O.J.; Carter, G.T. High throughput artificial membrane permeability assay for blood-brain barrier. *Eur. J. Med. Chem.* **2003**, *38*, 223–232.

[78] Friesner, R.A.; Murphy, R.B.; Repasky, M.P.; Frye, L.L.; Greenwood, J.R.; Halgren, T.A.; Sanschagrin, P.C.; Mainz, D.T. Extra Precision Glide: Docking and scoring incorporating a model of hydrophobic enclosure for protein-ligand complexes. *J. Med. Chem.* **2006**, *49*, 6177–6196.

7 New druggable pockets in BACE-1

Chapter

(Draft manuscript)

"Is there really a case where a drug that's on the market was designed by a computer?" "When asked this, I invoke the professoral mantra ("All questions are good questions."), while sensing that the desired answer is "no". Then, the inquisitor could go back to the lab with the reassurance that his or her choice to avoid learning about computational chemistry remains wise. The reality is that the use of computers and computational methods permits all aspects of drug discovery today. Those who are most proficient with the computational tools have the advantage for delivering new drug candidates more quickly and at lower cost than their competitors."

(William L. Jorgensen, from *Science*, **2004**, *303*, 1813-1818)

7.1 The many roles of computation in drug discovery

Computational methods play a crucial role in modern medicinal chemistry, presenting a unique potential for transforming the early phases of drug research, particularly in term of time and cost savings.[222] Most drugs now arise through discovery programs that begin with the identification of a biomolecular target of potential therapeutic value through biological studies including, for example, analysis of mice with gene knockout. A multidisciplinary project team is then assembled with the goal of finding clinical candidates, i.e., drug-like compounds that selectively bind to the molecular target and interfere with its biological activity. Molecular libraries are screened, and the resulting leads are optimized in a cycle that features design, synthesis and assaying of numerous analogues, and animal studies. Crystal structure determination for complexes of some analogues with the biomolecular target is often possible, which enables "structure-based" drug design (SBDD) and the efficient optimization of leads.[223] The success of SBDD is well documented;[224,225] it has contributed to the introduction of several chemical entities into clinical trials and to numerous drug approvals.

In this scenario, preliminary studies focused on attesting the druggability of a macromolecule have gradually become part of the target validation process, as limiting step in the very early stage of every SBDD process. While traditional target validation tries to assess whether or not alteration of the normal activity of a potential target can have some significant

[222]Guido, R.V.C.; Oliva, G.; Andricopulo, A.D. *Curr. Med. Chem.* **2008**, *15*, 37.
[223]Jorgensen, W.L. *Science* **2004**, *303*, 1813.
[224]Hardy, L.W.; Malikayil, A. *Curr. Med. Chem.* **2003**, *3*, 15.
[225]Maryanoff, B.E. *J. Med. Chem.* **2004**, *47*, 769.

therapeutic effect, conversely the druggability concept adds a structural dimension and evaluates the likelihood that small drug-like molecules can bind a given target with sufficient potency to alter its activity.[226]

Once a new druggable pocket is individuated, the availability of suitable crystallographic structures of the biomolecular target also opens the way towards virtual screening of libraries of known or constructed compounds, which in this way are optimally positioned in the binding site, and scored for potential activity. The top-scoring compounds can then be purchased or synthesized and subjected to experimental testing.[227,228,229]

However, it may happen that the information retrieved from the analysis of the available crystallographic structures is insufficient and leads to erroneously consider a given target as undruggable. In this case, a huge host of techniques can enable extensive computations of a protein conformational ensemble, thus allowing the identification of tractable conformations, which otherwise would risk to remain undisclosed upon a mere crystallographic analysis. This is particularly useful for individuating new druggable cavities lacking of known and well validated binders, and potentially susceptible to undergo induced-fits upon binding of a putative ligand.[230,231]

7.2 Conformational analysis and searching for novel druggable pockets in BACE-1

7.2.1 Overview of the structural features of BACE-1

As already extensively discussed in section ***1.6.1***, BACE-1 constitutes a prime target in the frame of a disease-modifying approach against AD.[232,233] For this reason, the design of a small-molecule inhibitor of BACE-1 has been pursued for nearly a decade.[234] The early availability of a crystal structure[76] promoted various computationally-guided drug discovery projects. However, the design of a small (< 500 molecular weight), brain penetrant, BACE-1 inhibitor has proven to be extremely difficult, as the active site is quite large (> 1000 $Å^3$) and the ability of a drug-like molecule to occupy such a large volume is a formidable task.[234] In fact, although a

[226]Schmidtke, P.; Barril, X. *J.Med. Chem.* **2010**, *53*, 5858.
[227]Shoicket, B.K.; McGovern, S.L.; Wei, B.; Irwin, J.J. *Curr. Opin. Chem. Biol.* **2002**, *6*, 439.
[228]Blake, J.F.; Laird, E.R. *Annu. Rep. Med. Chem.* **2003**, *38*, 305.
[229]Taylor, R.D.; Jewsbury, P.J.; Essex, J.W. *J. Comput. Aided Mol. Des.* **2002**, *16*, 151.
[230]Zhao, H.; Huang, D.; Caflisch, A. *ChemMedChem* **2012**, *7*, 1983.
[231]Cuchillo, R.; Pinto-Gil, K.; Michel, J. *J. Chem. Theory Comput.* **2015**, *11*, 1292.
[232]Cole, S.L.; Vassar, R. *Curr. Genomics* **2007**, *8*, 509.
[233]Vassar, R. *J. Mol. Neurosci.* **2001**, *17*, 157.
[234]McGaughey, G.B.; Holloway, M.K. *Expert Opin. Drug Discov.* **2007**, *2*, 1129.
[76]Hong, L.; Koelsch, G.; Lin, X.; Wu, S.; Terzyan, S.; Ghosh, A.K.; Zhang, X.C.; Tang, J. *Science* **2000**, *290*, 150.

variety of computational methods have been already undertaken, ranging from QM studies to MD calculations and scoring methods, all aimed at understanding the unique chemical features of the active site, BACE-1 has proven to be a difficult target, mainly due to its intrinsic flexibility. Apart from localized movements of side-chain residues as a result of specific ligand interactions, there are also large domain motions, mainly involving a β-hairpin loop, commonly referred to as the flap, and a short length region (residues 9-14) near the *N*-terminus of the protein, located between two strands at the base of the S_3 pocket, termed the 10s loop.[235]

As mentioned in section ***1.6.1***, the flap descends over the top of the active site to pin the substrate adjacent to the catalytic aspartic acids. It can exist either in a closed (*flap down*) or open (*flap up*) form, with a variety of intermediate positions depending on the binder, with an up to 6 Å displacement measured on the C_α of the flap residues between the closed and open conformation.[73] In the *apo* structure the flap region can adopt both forms, constantly switching between the two on a 10 ns timescale at room temperature.[236] Tyr71 has been individuated as a key residue for the stabilization of the flap region: indeed, it is involved in a network of H bonds with several residues in the substrate binding pocket, thus fixing the flap in a closed conformation upon inhibitor or substrate binding.[237] Unusual Tyr71 orientations have been also observed, where the Tyr71 side chain occupies the S_1 pocket in a self-inhibitory mode;[238] Tyr71 was also suggested to play a role in the capture and cleavage of substrates.[239]

As also attested by visual inspection of the available X-ray structures, the second region accounting for a significant portion of the overall protein motions is the 10s loop, observed in either an *up* and *down* conformation that appears to be governed by the ligand *via* induced-fit. As the 10s loop can vary by at least 10 Å, long timescales are required in a MD simulation to capture this motion.[234]

[235]Patel, S.; Vuillard, L.; Cleasby, A.; Murray, C.W.; Yon, J. *J. Mol. Biol.* **2004**, *343*, 407.
[73]Kacker, P.; Bottegoni, G, Cavalli, A. *Curr. Med. Chem.* **2012**, *19*, 6095.
[236]Gorfe, A.A.; Caflisch, A. *Structure* **2005**, *13*, 1487.
[237]Andreeva, N.S.; Rumsh, L.D. *Protein Sci.* **2001**, *10*, 2439.
[238]Andreeva, N.; Dill, J.; Gilliland, G.L. *Biochem. Biophys. Res. Commun.* **1992**, *184*, 1074.
[239]Tang, J.; Koelsch, G. *Peptide Lett.* **1995**, *2*, 257.
[234]McGaughey, G.B.; Holloway, M.K. *Expert Opin. Drug Discov.* **2007**, *2*, 1129.

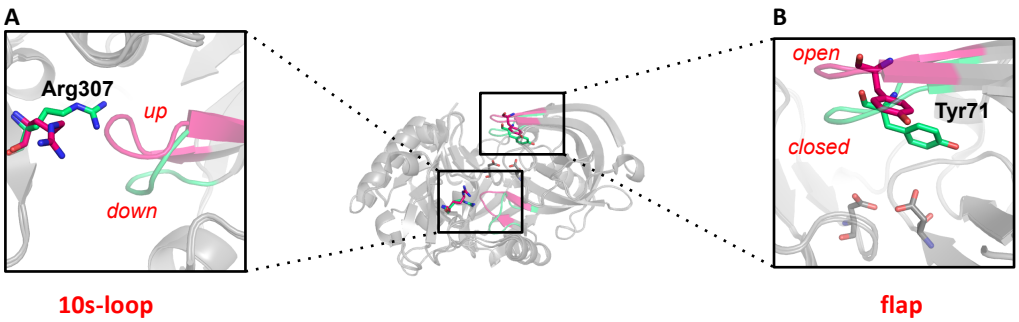

Figure 7.1 Representation of the "*up*" and "*down*" conformations of the 10s-loop and Arg307 (**A**) and the "*open*" and "*closed*" conformations of the flap and Tyr71 (**B**). (PDB ID: 1SGZ, magenta structure. PDB ID: 2P4J, green structure).

7.2.2 Insights of the high inhibitory potency of the rhein-huprine hybrid, 15, against BACE.1

A novel rhein-huprine hybrid (compound **15**, **Figure 7.2**) has been recently developed in our research group as multipotent anti-Alzheimer agent, displaying an unexpected high inhibitory potency against BACE-1 (IC_{50} 80 nM).[91] Strong dependency of the enzymatic inhibitory activity on the length and flexibility of the linker has been observed for this in-house family of rhein-huprine hybrids. On the other hand, the effect of chemical modifications introduced in the chromene unit of a structurally related family of tacrine-chromene hybrid compounds has been examined (general structure **VII**, **Figure 7.2**). Within the series of the decamethylene-linked derivatives, low micromolar K_i values against BACE-1 have been reported.[186]

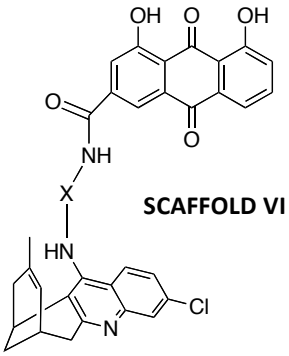

SCAFFOLD VI

15, X= $(-CH_2-)_9$
143, X= $-CH_2$-*p*-phenylene-CH_2-

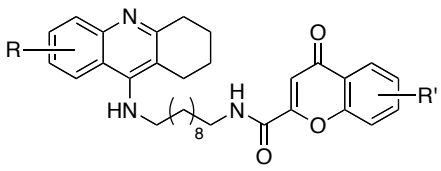

SCAFFOLD VII

144, R= H, R'= H

Figure 7.2

[91]Viayna, E.; Sola, I.; Bartolini, M.; De Simone, A., Tapia-Rojas, C.; Serrano, F.; Sabaté, R.; Juárez-Jiménez, J.; Pérez, B.; Luque, F.J.; Andrisano, V.; Clos, M.V.; Inestrosa, N.C.; Muñoz-Torrero, D. *J. Med. Chem.* **2014**, *57*, 2549.
[186]Fernández-Bachiller, M.I.; Pérez, C.; Monjas, L.; Rademann, J.; Rodríguez-Franco, M.I. *J. Med. Chem.* **2012**, *55*, 1303.

The experimental data above taken together with the structural information retrieved from previous computational studies carried out on the much less potent derivative **143** (**Figure 7.2**),[91] led us to hypothesize that the nonamethylene linker produces a considerable enhancement in the inhibitory potency due to the fact that it enables a simultaneous and cooperative binding of **15** to two different protein regions. Thus, while the huprine moiety interacts with the well-known catalytic aspartic dyad, it is likely that the 10s loop fluctuations support the induced fit-mediated formation of a secondary pocket never described before, which is supposed to be a suitable binding cleft for allocating the rhein moiety.

In a scenario where the available structural information is impaired, since almost the totality of the X-ray structures display a very low resolution of the region of interest, in this PhD thesis we have undertaken an exhaustive computation of the BACE-1 *apo* conformational ensemble in combination with the application of Principal Component Analysis (PCA) method,[240] in the perspective of future drug design purposes. It is worth noting that this part of the research project was developed during an internship at the Centre for Biomolecular Sciences (CBS) of the University of Nottingham, under the supervision of Prof. Charles Anthony Laughton. An extensive dissertation regarding the work carried out and the results obtained is provided in the draft manuscript, while some theoretical fundaments of the PCA method are presented in section ***7.2.3*.**

7.2.3 Theoretical fundaments of the Principal Component Analysis

Principal component analysis (PCA) of ensembles of structures is an orthogonal linear transformation, which enables the conversion of the data from the Cartesian coordinate system into a new system of collective coordinates.[240] The goal is to gain a simplified view of the structural variability in the examined data set by identifying the dominant directions of structural changes. The new coordinate system is such that the greatest variance in the data set lies along the first principal component (PC) axis, followed by the second PC axis, and so on. Taking into account an ensemble of *M* conformations of a protein of *N* interaction sites, each conformation, *k*, is described by a 3*N*-dimensional vector consisting of the position vectors

[91]Viayna, E.; Sola, I.; Bartolini, M.; De Simone, A., Tapia-Rojas, C.; Serrano, F.; Sabaté, R.; Juárez-Jiménez, J.; Pérez, B.; Luque, F.J.; Andrisano, V.; Clos, M.V.; Inestrosa, N.C.; Muñoz-Torrero, D. *J. Med. Chem.* **2014**, *57*, 2549.
[240]Bahar, I.; Lezon, T.R.; Bakan, A.; Shrivastava, I.H. *Chem. Rev.* **2010**, *110*, 1463.

$R_i^{(k)} = \left(x_i^{(k)}, y_i^{(k)}, z_i^{(k)}\right)^T$ of the *N* sites $(1 \leq i \geq N)$ in that particular conformation, organized as follows:

$$6q^{(k)} = \left[\left(R_1^{(k)}\right)^T, \ldots, \left(R_N^{(k)}\right)^T\right]^{\boldsymbol{T}} = \left(x_1^{(k)}, y_1^{(k)}, \ldots, x_N^{(k)}, y_N^{(k)}, z_N^{(k)}\right)^{\boldsymbol{T}} \quad \textbf{(1)}$$

Likewise, for each conformation a 3*N*-dimensional fluctuation vector $\Delta q^{(k)} = q^{(k)} - q^0$ can be defined, describing the departure $\Delta R_i^{(k)} = R_i^{(k)} - R_i^0$ in the position vectors of the *N* sites from their equilibrium position $R_i^0 = \left(x_i^0, y_i^0, z_i^0\right)^{\boldsymbol{T}}$. The equilibrium position may be identified by the average over all snapshots from MD trajectories. The cross-correlation between the components of the fluctuations vectors are given by the averages $< \Delta q_i . \Delta q_j >$ over all conformations, conveniently organized in a $3N * 3N$ covariance matrix, $\boldsymbol{C}$:

$$C = M^{-1} \sum_K \Delta q^{(k)} \Delta q^{(k)\boldsymbol{T}} \quad \textbf{(2)}$$

The elements of $\boldsymbol{C}$ may alternatively be viewed as $N * N$ blocks (or submatrices of size $3 * 3$), $\boldsymbol{C}_{ij}$, each of the form:

$$C_{ij} = \begin{matrix} \langle \Delta x_i \Delta x_j \rangle & \langle \Delta x_i \Delta y_j \rangle & \langle \Delta x_i \Delta z_j \rangle \\ \langle \Delta y_i \Delta x_j \rangle & \langle \Delta y_i \Delta y_j \rangle & \langle \Delta y_i \Delta z_j \rangle \\ \langle \Delta z_i \Delta x_j \rangle & \langle \Delta z_i \Delta y_j \rangle & \langle \Delta z_i \Delta z_j \rangle \end{matrix} \quad \textbf{(3)}$$

The fluctuations in the Cartesian space are mapped onto the space spanned by the 3N principal axes upon diagonalization of the covariance matrix $\bar{A}$ as

$$\overline{\boldsymbol{A}} = \boldsymbol{PSP^T} = \sum_{\boldsymbol{k=1}}^{\boldsymbol{3N}} \boldsymbol{\sigma \rho_k \rho_k^T} \quad \textbf{(4)}$$

where $\boldsymbol{P}$ is the unitary matrix of normalized displacements along the principal axes, also called *eigenvectors*, each given by a column $\boldsymbol{\rho_k}$, $(1 \leq k \geq 3N)$, and $\boldsymbol{S}$ is the diagonal matrix of eigenvalues $\sigma_1, \sigma_2, \ldots, \sigma_N$, usually ordered in descending order.

7.2.4 Recent outcomes and further perspectives

The exhaustive characterization of the structural and intrinsic flexibility features of this floppy secondary pocket recently allowed us to propose a novel pharmacophoric model provided with the following chemical elements (**Figure 7.3**):

1. Two hydrogen bond acceptors (HBA), instead of only one as in rhein, located at a mutual distance of approximately 2.5 Å (or alternatively a negatively charged group) to interact with Arg307;
2. A hydrogen bond donor (HBD), instead of the carbonyl group between the two hydroxyl groups of rhein, to interact with Glu310. It is thought that this would reduce *via* induced-fit the conformational preferences of the side chain of Glu310 in such a way as to enable the formation of a hydrogen bond with Ser10, a key feature to maintain the pocket closed and not totally exposed to solvent as it occurs in the *apo* form of the protein.

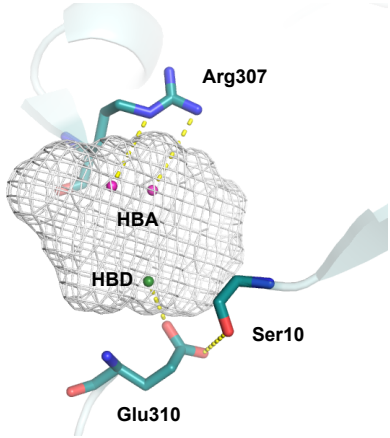

Figure 7.3 Schematic representation of the novel pharmacophore.

Preliminary docking calculations of the rhein fragment inside the putative binding cavity were performed in order to individuate, among several selected *apo* clusters, the most suitable protein structure for further virtual screening purposes. Thus, a library of 500.000 commercially available fragments, selected from the ZINC database according to their molecular weight, was virtually screened. As first step, all the compounds were preprocessed by LigPrep program in order to generate their corresponding 3D structures and assign the correct protonation state at physiological pH. Then, a pharmacophoric restraint was applied,

requiring as mandatory condition two HBA groups and, as optional one, a HBD group. Thus, all the compounds responding to these features were docked with rDock program.[241] For each of them, 100 poses were generated and sorted according to their score value. Next, for each docked compound, the best scored pose was selected and the molecules were sorted again according to their best score value. Finally, 340 compounds with a score value ≤ −40 kJ/mol were visually inspected and three fragments selected for the further hybridization with huprine Y (**Figure 7.4**-**7.6**). With this scope in mind, in the context of the present PhD thesis, linkers of suitable length have been already selected (**Figure 7.7**) and the synthetic route for the preparation of the desired novel huprine-based hybrid compounds designed (**Schemes 7.1**-**7.3**). The synthesis of the target novel BACE-1 inhibitors is currently in progress in our laboratory.

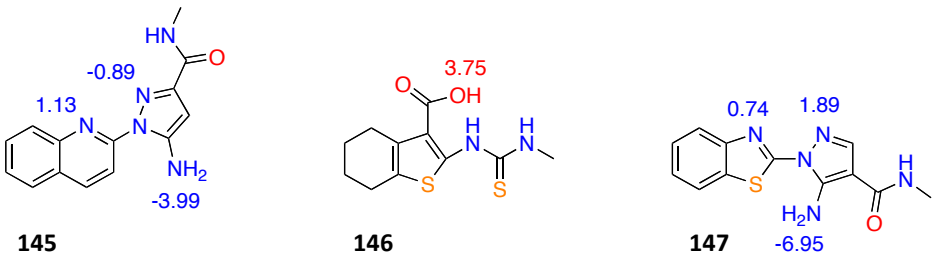

Figure 7.4 Structure of the three selected fragments for the further molecular hybridization with huprine Y and pk_a values predicted by MarvinSketch *5.12.0* software, **2013**, ChemAxon (http://www.chemaxon.com).

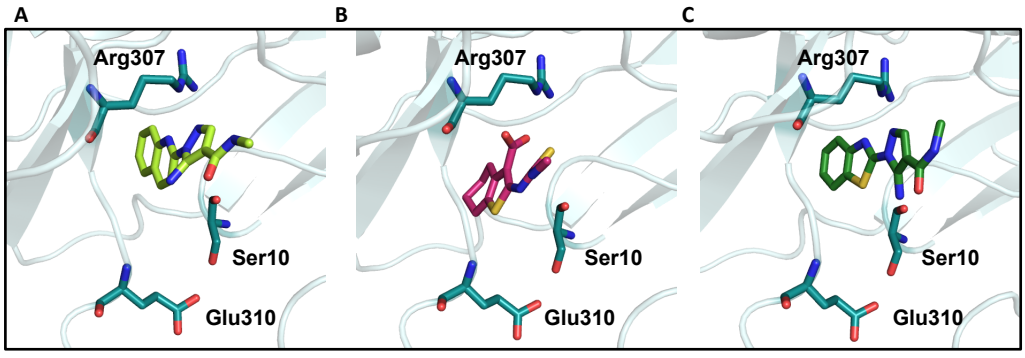

Figure 7.5 In order to corroborate the results of the virtual screening, additional unrestrained docking calculations were run for the three selected fragments using rDock program. The best scored poses for compounds **145** (**A**), **146** (**B**) and **147** (**C**) are shown above.

[241]Morley, S.D.; Afshar, M. *J. Comput. Aided Mol. Des.* **2004**, *187*, 10-22.

Table 7.1 Score values of the selected docking poses reported in **Figure 7.5**.

	Total score	Inter-	Intra-	VdW
145	-22.19	-20.39	-0.17	-20.91
146	-27.92	-20.70	-5.58	-22.40
147	-23.86	-20.60	-1.63	-21.82

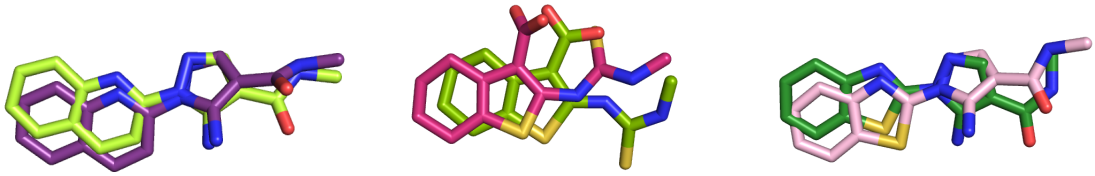

145 **146** **147**

Table 7.2A

	Total Score
rDock	-22.19 kJ/mol
GLIDE	-5.99 kcal/mol

Table 7.2B

	Total Score
rDock	-27.92 kJ/mol
GLIDE	-5.71 kcal/mol

Table 7.2C

	Total Score
rDock	-23.86 kJ/mol
GLIDE	-5.86 kcal/mol

Figure 7.6 The rDock-predicted binding modes were further cross-validated with GLIDE program.[242] The superimposition of the rDock- with the GLIDE-predicted docking poses and the comparison between the respective score values (**Tables 7.2 A**-**C**) are shown above.

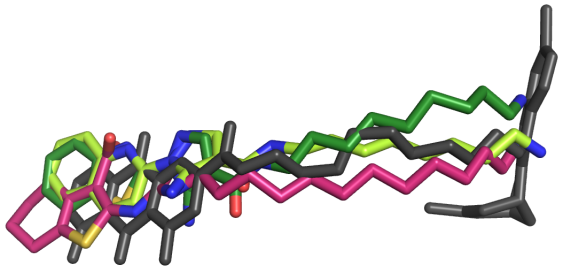

Figure 7.7 Superimposition of the selected docking poses of compounds **145**, **146** and **147** with the MD-predicted binding mode of the complex BACE-1/compound **15** (black structure). A nona-, a dodeca-, and a nona-methylene linkers have been predicted as the optimal tethers for the molecular hybridization of compounds **145**, **146** and **147**, respectively, with racemic huprine Y.

[242]Friesner, R.; Murphy, R.B.; Repasky, M.P.; Frye, L.L.; Greenwood, J.R.; Halgren, T.A.; Sanschagrin, P.C.; Mainz, D.T. *J. Med. Chem.* **2006**, *49*, 6177.

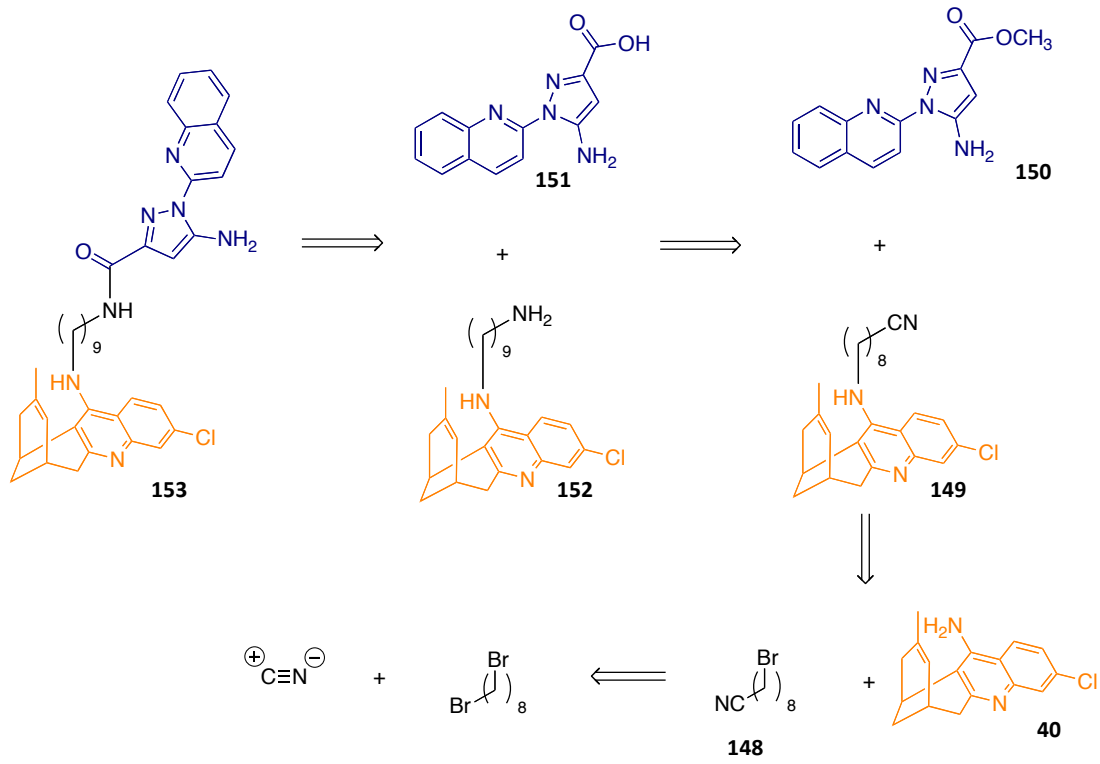

Scheme 7.1 Retrosynthetic analysis for compound **153**.

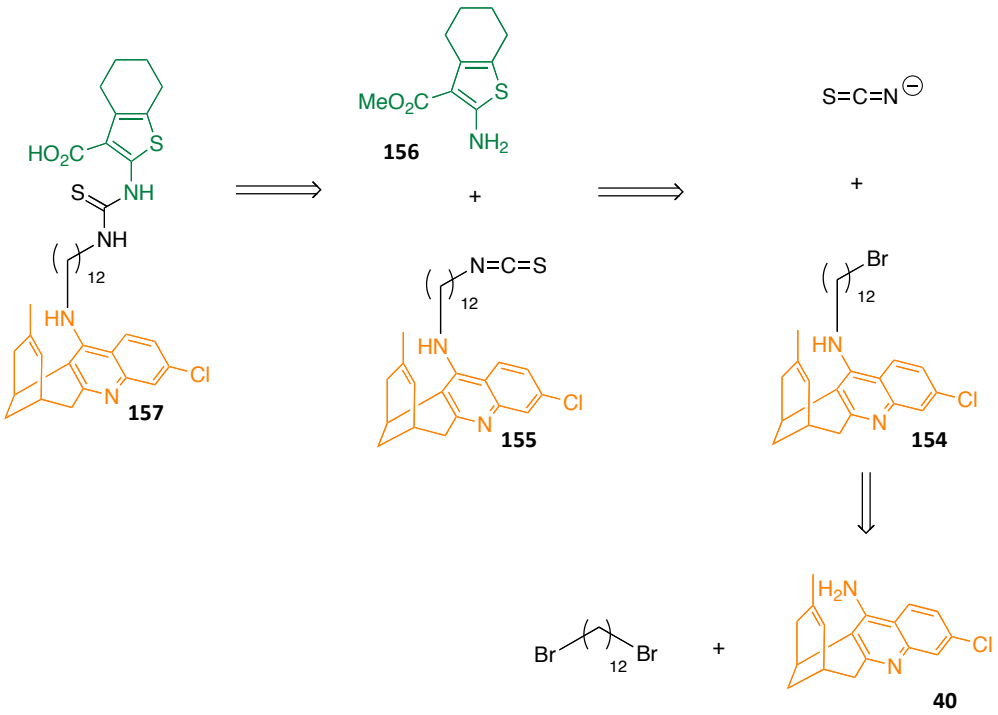

Scheme 7.2 Retrosynthetic analysis for compound **157**.

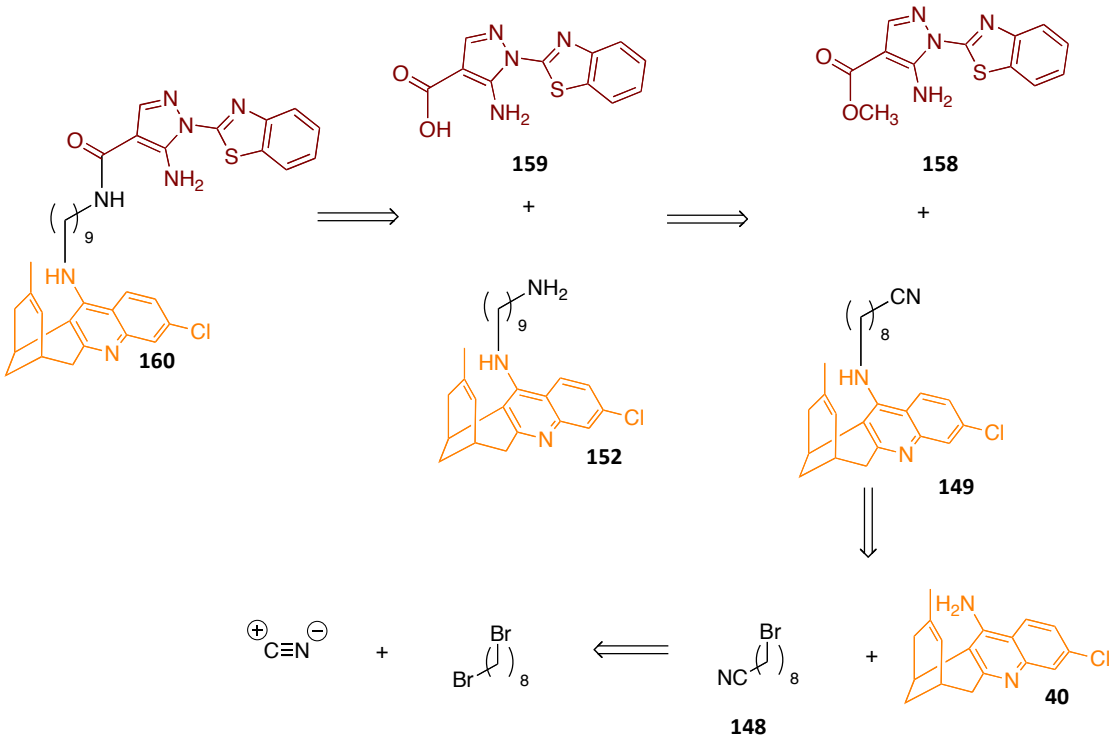

Scheme 7.3 Retrosynthetic analysis for compound **160**.

Searching for Novel Transient Druggable Pockets in BACE-1. Conformational Analysis and Design of Multitarget-Directed Ligands

Ornella Di Pietro,[a] Jordi Juárez-Jiménez, [b] Diego Muñoz-Torrero,[a] Charles A. Laughton,*[c] and F. Javier Luque*[b]

[1] Laboratorio de Química Farmacéutica (Unidad Asociada al CSIC), Facultad de Farmacia and Instituto de Biomedicina (IBUB), Universidad de Barcelona, Av. Joan XXIII, 27-31, 08028-Barcelona, Spain

[2] Departamento de Fisicoquímica, Facultad de Farmacia (Campus Torribera) and IBUB, UB, Prat de la Riba 171, E-08921, Santa Coloma de Gramenet, Spain

[3] Centre for Biomolecular Sciences, University Park, Nottingham, NG7 2RD, UK

Abstract

BACE-1 plays a critical role in the production of neurotoxic β-amyloid peptides in the brain. Hence, it is an attractive drug discovery target for the therapeutic intervention of Alzheimer's disease, though up to now the development of BACE-1 inhibitors has proved to be extremely challenging. In this study we report the results of extended molecular dynamics simulations conducted to explore the conformational flexibility of BACE-1. The analysis of the protein dynamics allows us to hypothesize the existence of a secondary « floppy » binding site defined by residues in loops 8-14, 154-169 and 307-318, which involve a highly flexible region in the enzyme. Conformational fluctuations allow the transient formation of a druggable binding pocket connected with the active site, which would allow the design of compounds targeting both active and secondary sites. The feasibility of this hypothesis is supported by molecular dynamics simulations of the enzyme bound to huprine-rhein and tacrine-chromene hybrids, which were determined to have nanomolar and submicromolar inhibitory potencies. Overall, these findings pave the way for the exploration of novel functionalities in the development of non-peptidomimetic compounds targeting BACE-1.

Introduction

BACE-1 (also known as *β*-secretase) is a membrane-associated, pepsin-like aspartic protease responsible for the cleavage of the amyloid precursor protein (APP), thus generating toxic β-amyloid (Aβ) peptides of various lengths, including the most pathogenic isoform, Aβ42, which is a key factor in the onset and progression of Alzheimer's disease (AD).[1] The early formation of Aβ in the AD neurotoxic pathogenic cascade, and the abolished Aβ production in BACE-1 knockout mice,[2,3] accompanied by slowed memory decline,[4,5] give support to the concept that BACE-1 is a pharmacologically target for a disease-modifying approach against AD.[6-8]

The more than 150 crystal structures so far deposited in the Protein Data Bank (PDB)[9] attest that the BACE-1 active site is an open, hydrophilic, nearly 20 Å long cavity of remarkable size (about 1000 $Å^3$), revolved around two catalytic Asp residues, Asp32 and Asp228, facing each other generally in a non-coplanar orientation.[10,11] The binding site cleft is partially covered by a highly flexible antiparallel hairpin-loop, known as "flap". The open conformation of the flap found in apo structures of the enzyme[12-14] would allow access of the substrate and release of hydrolytic products. Instead, a closed conformation is found in ligand-bound complexes, even though the degree of flap opening/closure varies among structures. [15]

Despite the huge research effort invested to gain insight into issues regarding the substrate specificity, the protonation state of the dyad, the presence of allosteric sites, and the enzyme's functional plasticity,[16-18] the impact in the design of novel drugs is limited, since no compound has still successfully passed clinical trials. The huge size of the active site cleft and the subcellular location of the enzyme in neurons challenge the development of non-peptidomimetic BACE-1 inhibitors.[19]

We have recently reported the outstanding *in vitro* and *in vivo* pharmacological profile displayed by the novel rhein-huprine hybrid compound, **1** (Figure 1), as a multipotent disease-modifying anti-Alzheimer agent, unexpectedly endowed with a remarkable inhibitory potency against BACE-1 (IC_{50} 80 nM).[20] Interestingly, no significant reduction of the enzymatic activity was reported for the two separate moieties, huprine and rhein, present in the hybrid compound. Moreover, the inhibitory potency was found to be highly dependent with the length of the methylenic chain, suggesting that linkage of huprine and rhein through a 9-mer methylene tether in **1** is optimal for a cooperative enhancement of the inhibitory potency upon binding to BACE-1.

Previous computational studies on a much less potent member of the same family, **2** (IC_{50} 2020 nM; Figure 1), pointed out that the protonated aminoquinoline ring of huprine interacts with the catalytic dyad, while forming multiple hydrophobic contacts between the heterocyclic ring and residues Leu30, Phe108, Ile110 and Ile118.[20] On the other hand, the evidence of the strict dependency of the inhibitory potency on the tether length prompted us to hypothesize that the rhein moiety of **1** is capable to fill a secondary "floppy" pocket in the region delimited by the highly flexible loops formed by residues 8-14, 154-169 and 307-318. The Arg307 residue located in this area was also envisaged as a key feature for the binding of rhein inside this putative secondary pocket.[20] On the other hand, the involvement of a "floppy" binding pocket was reinforced by the inhibitory potencies reported by Fernández-Bachiller *et al.*,[21] in which the homologous series of 10-mer methylene-linked derivatives displayed low micromolar IC_{50} values against BACE-1. Thus, while it is reasonable to expect that tacrine will bind to the catalytic dyad, mimicking the binding of huprine, it might be speculated that both rhein and chromene units could bind the same secondary pocket in the enzyme.

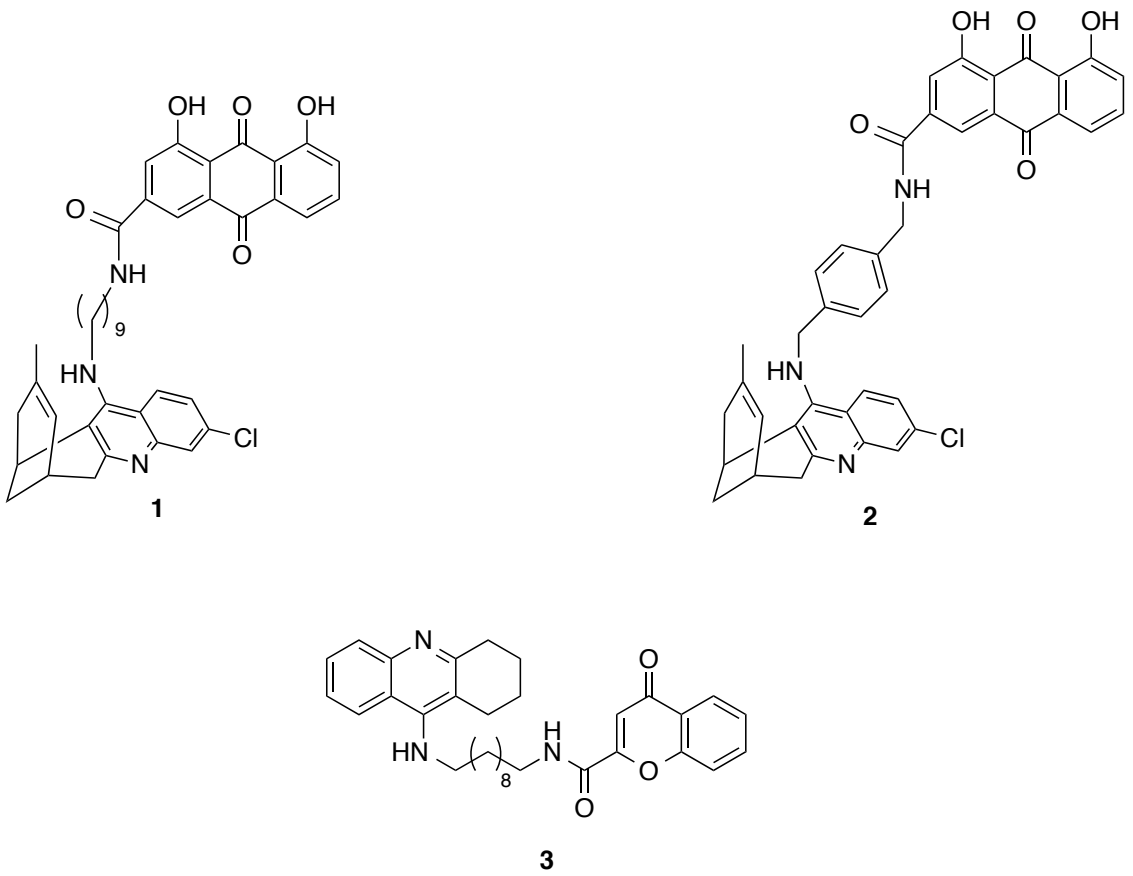

Figure 1. Representation of the huprine-rhein hybrids **1** and **2** and of the tacrine-chromene hybrid **3**.

In this study we report the results of the conformational analysis and clustering studies of the flexible region defined by loops 8-14, 154-169 and 307-318 in BACE-1. To this end, the conformational flexibility of this region in the *apo* form of the enzyme was studies by means of extended molecular dynamics (MD) simulations, and the conformational preferences were examined in order to identify the formation of a secondary pocket in this highly flexible region. The druggability analysis of the pocket supported the feasibility to bind the rhein/chromene moieties. Finally, the reliability of the secondary pocket was examined by MD simulations of the rhein-huprine and chromene-tacrine hybrids **1** and **3** bound to BACE-1.

Methods

Setup of the molecular system. Computational studies were performed using the X-ray crystallographic structures of human BACE-1 (PDB ID 1SGZ and 2P4J).[22] The structure was refined by removal of the complexed ligand and addition of missing hydrogen atoms. Two different protein conformations of the refined structure, bearing Arg307 and the neighboring loop defined by residues 8-14 modelled on the pdb structures 3QUW and 1SGZ, respectively, were generated. Furthermore, acetyl and N-methyl groups were added to the N-terminal and C-terminal residues, respectively.

The catalytic dyad of the enzyme was modelled with neutral Asp228 and deprotonated Asp32. The ionization state for the rest of ionizable residues was assessed from PROPKA3 calculations. Additionally, three disulfide bridges were defined between Cys residues 155-359, 217-382, and 269-319. Structural waters were retrieved from those found in the pdb structure 2P4J itself.

Molecular dynamics simulations. The conformational space of the *apo* form of BACE-1 was explored by means of extended MD simulations. To this end, the two main orientations of Arg307 and the neighbouring loops between residues 8-14, 154-169 and 307-318were sampled by means of 200 independent 100 ns MD replicas. Calculations were performed using GROMACS 4.7 software package.[23] Parameters for the protein were taken from parm99SB[24] force field. Na^+ cations were added to neutralize the negative charge of the system. The simulated systems were immersed in a cubic box of TIP3P water molecules,[25] preserving the crystallographic waters inside the binding cavity. Each of the two final systems contained around 44.500 atoms.

The geometry of the system was minimized in four steps. First, water molecules were refined through 3000 steepest descent algorithm followed by 7000 steps of conjugated

gradient. Then, protein and ligand hydrogen atoms positions were optimized using 500 steps of steepest descent and 4500 of conjugated gradient. Next, the ligand, water molecules, and counterions were further optimized with 2500 steps of descent and 11500 of conjugated gradient and, at the last step, the whole system was optimized with 2500 steps of steepest descent and 8500 of conjugate gradient. Thermalization of the system was performed in five steps of 25 ps, increasing the temperature from 50 to 298 K. Concomitantly, the residues that define the binding site were restrained during thermalization using a variable restraining force. Thus, a force constant of 25 kcal mol^{-1} $Å^{-2}$ was used in the first stage of the thermalization and was subsequently decreased by increments of 5 kcal mol^{-1} $Å^{-2}$ in the next stages. Then, prior to the production runs, a 10 ns simulation in the isothermal-isobaric ensemble was performed in order to reach a stable density. At this point, 100 independent replicas for each of the two systems were generated by randomly assigning different sets of velocities to the initial coordinates, fitting in all cases a Marxwell distribution for a temperature of 300 K. For each replica, a 100 ns trajectory was run using a time step of 2 fs. LINCS (LINear Constraint Solver) was used to constraint all bonds length in conjugation with periodic boundary conditions at constant volume and temperature, particle mesh Ewald was used for the treatment of long electrostatic interactions, and a cutoff of 10 Å was utilized for nonbonded interactions.

MD simulations of BACE-1 in complex with (+)-**1**, (−)-**1** and **3** were run using AMBER12 software package.[26] Parm99SB was used to assign parameters for the protein, while GAFF force field was used to assign parameters for the ligands. RESP charges at the B3LYP/6-31G(d) level were used for the ligands.[27] Preparation, minimization and Thermalization of the simulated systems followed the protocol outlined above for the *apo* form of the enzyme. The only difference was the

introduction of a suitable restraint to keep the distance between the carbonyl oxygen atom of rhein and the guanidine moiety of Arg307. After equilibration, five different replicas for each ligand were generated by randomly assigning different sets of velocities (at a temperature of 300 K) to the initial coordinates. Production runs consisted of 50 ns trajectories (accounting for a global simulation time of 250 ns for each ligand) using SHAKE for bonds involving hydrogen atoms, allowing for a time step of 2 fs, in conjunction with periodic boundary conditions at constant pressure and temperature, particle mesh Ewald for long-range electrostatic interactions, and a cutoff of 10 Å for nonbonded interactions.

Principal Component Analysis. Principal Component Analysis (PCA)[28] was chosen to study the conformational variability of the protein target using a locally modified version of pyPCAzip package.[29] The analysis was focused on the region shaping the pocket of interest, and included all the heavy atoms forming the three loops between residues 8-14, 154-176, and 308-318. Overall, fluctuations of a total amount of 484 atoms were examined. The analysis was performed for a total amount of 1.200.000 frames extracted from the simulations of the two forms of the *apo* enzyme taken over the last 50 ns of the trajectories. A total of 58 eigenvectors were required to capture 90% of the structural variance. PCA was also performed for a set of 17080 frames composed of *apo* and *holo* structures, where 41 eigenvectors were required to explain 90% of the structural variance. Finally, as an indirect validation of the method, an additional PCA, including all the heavy atoms forming the flap (residues 68-76; 500.000 frames, 35 eigenvectors accounting for 90% of the structural variance), was run in order to verify if the captured fluctuations were able to reflect the constitutive open and a closed conformations of the flap.

The pyPCAzip package also allowed further clusterization of the protein conformational ensemble. Parameters were set such that only the 2D space was considered for clusters generation.

Druggability predictions. The Epock program[30] was used to characterize the cavity volume. Calculations were run on selected protein structures representative of open and closed conformations of the *apo* enzyme, and the *holo*-conformation of the pocket, respectively. Parameters for grid generation were set as follows. Through the VMD plugin, an including-sphere of 6.0 Å radius, centered on a point of coordinates (-10.00, -3.61, -13.60), and several excluding-spheres were used to define the maximum region where the pocket lies. Grid-spacing, defining the distance between two grid points, was set to the default value (0.5 Å); contiguous-cutoff parameter, defining the "free space points" which lie within the grid space and distant from any atom less than the cutoff value itself, was also set for default to 4 Å. Thus, the cavity volume of each of the three representative pocket conformations resulted to be equal to 456.25 $Å^3$ (for the open *apo*-conformation), 194.75 $Å^3$ (for the closed *apo*-conformation), and 379.12 $Å^3$ (for the *holo*-conformation), respectively. Additionally, Epock also allowed us to calculate the ligand volume of the rhein moiety, which resulted to amount to 240.12 $Å^3$.

The fPocket program was used for binding pocket detection and characterization.[31] A list of the pdb structures generated by clusterization of the whole BACE-1 *apo* conformational ensemble was provided as input file. Parameters were set to the default values.

Docking calculations. Clusterization allowed to identify a pool of protein conformations supposed to be capable to recognize and bind the inhibitor. On the basis of the

topological and druggability features of the cluster, the suitability to accommodate the rhein unit was explored by docking calculations performed with the rDock program.[32] To this end, a cavity of radius 6 Å, centered on the structure of a superligand, containing rhein and an acetamide side chain, was defined as the docking volume. Calculations were performed with no structural waters. 100 docking poses were generated and sorted according to their score value. The top 50 best scored poses were further analyzed by visual inspection.

Results and Discussion

Analysis of X-ray structures in the PDB. Inspection of the available X-ray structures of BACE-1 shows that the spatial arrangement of the protein skeleton is well preserved, while conformational flexibility is primarily limited to two regions: i) the "flap" region at the binding site, and the loops located at a distant region shaped by loops 8-14, 154-169 and 307-318 (Figure 2). The high conformational flexibility of this latter region precludes the identification of the spatial arrangement in the largest part of X-ray structures deposited in the Protein Data Bank, but for the structure of the *apo* enzyme 1SGZ[12] and the holo species 2P4J [22] The loop 8-14 is found in two major arrangements, which will be denoted in and out hereafter (Figure 2). The adoption of these two conformations is dictated by the specific features of the inhibitors bound to BACE-1, which often promote the transition to the loop out conformation in order to accommodate small fragments, such as the benzene ring in the inhibitor found in PDB ID 2P4J. On the other hand, even though loops 154-169 and 307-318 show similar arrangements in X-ray structures 1SGZ and 2P4J (Figure 2), a much larger conformational variability is observed upon comparison with other structures deposited in the PDB.

Conformational sampling. In light of the preceding findings, one can speculate that the conformational flexibility of the loops might shape transient cavities well suited to accommodate the rhein unit in the huprine-rhein hybrid compound **1**. In order to check the feasibility of this hypothesis, extended MD simulations were performed in order to examine the conformational preferences of loops 8-14, 154-169 and 307-318 from the analysis of 250 independent 100 ns MD simulations.

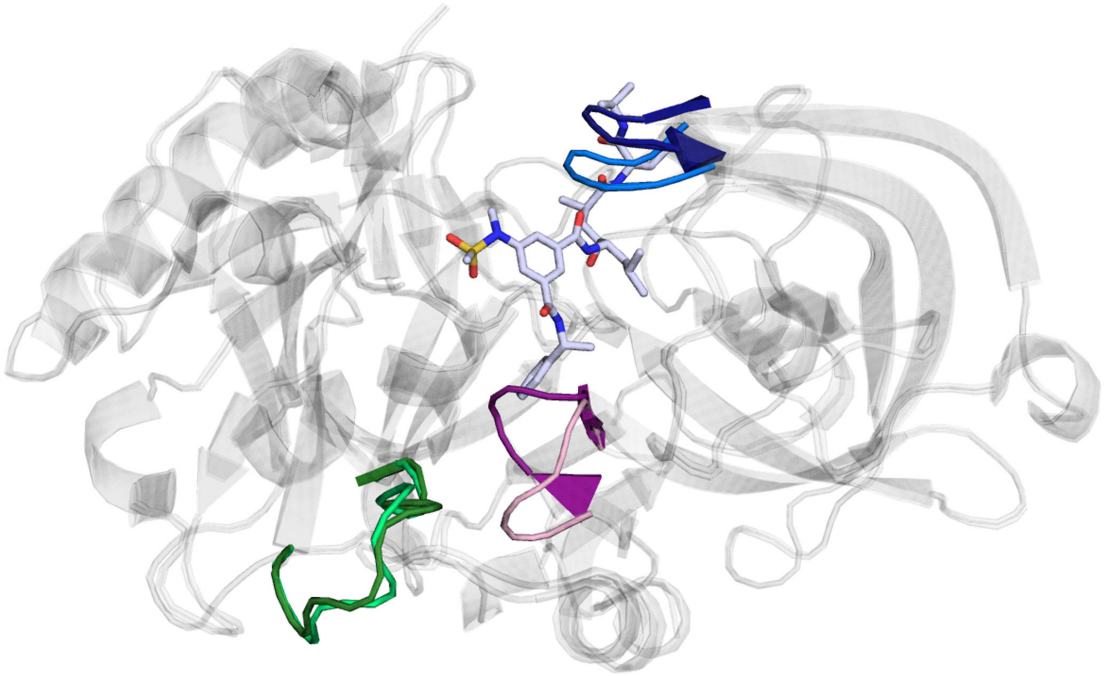

Figure 2. Representation of the highly flexible regions in BACE-1 as found in the PDB entries 1SGZ and 2P4J. The flap region (blue) shows the open and closed conformations typically found in *apo* and substrate-bound states. The other highly flexible region is shaped by residues 8-14 (magenta) and 307-318 (green) in a region located around 20 angstroms apart from the catalytic dyad (shown in green and magenta). The loop 154-156 is generally disordered in other PDB structures.

The PCA analysis of the collected frames allowed us to identify the major conformational deformations. Near 50% of the conformational variance is covered by

the first four eigenvectors, which point out a limited range of conformational flexibility. Indeed, the two first eigenvectors explain around 35% of the structural variance, with contributions of 22% and 13% for the first and second components, respectively. The projection of the sampled snapshots onto the bidimensional map defined by the two principal components in shown in Figure 3. The plots clearly identifies the existence of two clusterings, which denote the presence of protein structures with the loop 8-14 in the *in* (right) and *out* (left) conformations. Importantly, some snapshots are located in the region that defines the overlap between the two clusters, thus revealing the occurrence of a smooth transition between *in* and *out* arrangements.

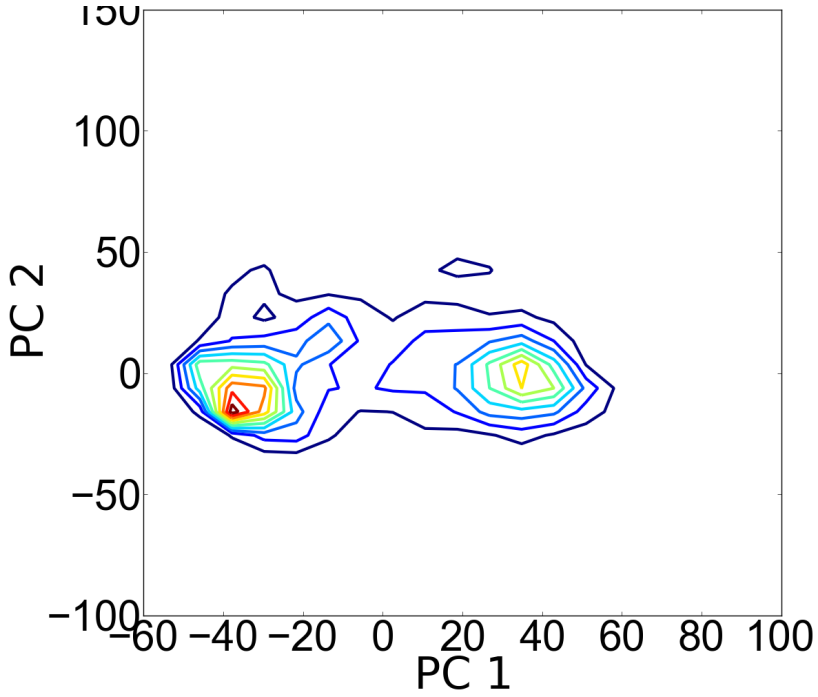

Figure 3. Projection of the MD trajectory on the space defined by the two major principal components.

Identification of pocket cavities and docking calculations. The collected snapshots were clustered in 14 major conformational families. Most of them fit two major clusters, as shown by the green and blue lines in Figure 4, which represent the major arrangements

of the loop *in* and *out*. However no cavity well suited to accommodate the rhein moiety could be identified. On the other hand, up to 12 additional less populated clusters were also identified, and in this case suitable pockets allowing recognition and binding of rhein could be identified. Some of them were found in conformations with a very large pocket, well accessible to bulk waters, such as cluster 26, as the volume determined from Epock calculations determined a size close to 1250 $Å^3$, which is exceedingly large to be tightly filled with small fragments. On the other hand, he population of this pocket, nevertheless, was very low, but this demonstrates the rather large fluctuations of the loop, covering a range of diverse cavities and the "floppy" nature of the secondary site.

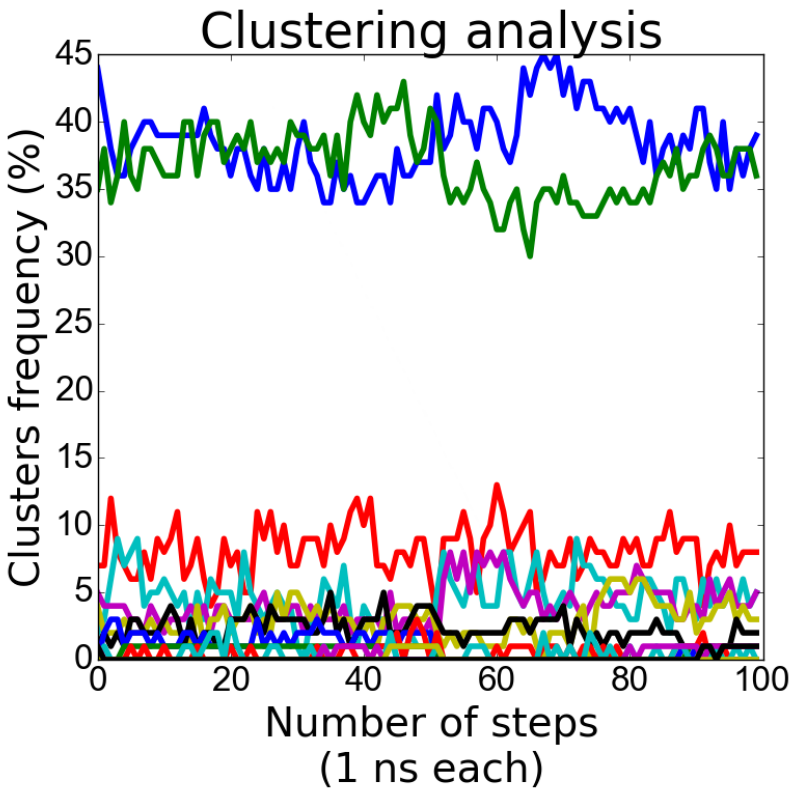

Figure 4. Representation of the conformational families obtained upon positional clustering of the snapshots collected from the trajectory.

Attention was paid to cluster with smaller pockets able to accommodate the rhein unit of compound **1**. The topological analysis of the different cluster revealed three potential cavities. The first was found in cluster 3, which included around 12% and 5% of the sampled structures starting from the loop *in* and loop *out* conformations, respectively. Epock calculations revealed that the volume of the pocket was close to 560 $Å^3$, which is around 2.3-fold larger than the molecular volume of rhein (estimated to be 240 $Å^3$). Two other clusters were found to have a smaller pocket, still able to accommodate the rhein unit: cluster 13, with a volume of 495 $Å^3$, and cluster 21, with a volume of 466 $Å^3$. Moreover, the distance between the centroids of these pockets from the catalytic dyad was comprised between 11 and 15 Å, thus satisfying the geometrical criteria required for the 9-mer methylenic tether in the rhein–huprine hybrid **1**.

The druggability of the pockets found in these clusters was examined with the fPocket program. For clusters 13 and 21 the results identified two druggable pockets, characterized with a druggability score ranging from 0.6 to 0.82 (Figure 5). The first correspond to the catalytic site, including the wide area around the catalytic dyad, which has been widely exploited for the design of several clases of BACE-1 inhibitors. The second one includes the secondary "floppy" site, thus giving support to its potential implication in the binding of fragments, such as the hydroxyanthraquinone moieties present in hybrid **1**.

As a final test, docking calculations were performed to check the feasibility of the pockets to bind the rhein unit. The results obtained for cluster 3 was unsuccessful, as the rhein unit was found to adopt multiple poses in the binding pocket. This is not surprising due to the lower volumen of rhein compared to the available volumen of the pocket. In contrast, the best results were obtained for the docking of rhein into the pocket of clusters 13 and 21. In the fomer case, 10 out of the first 13 scores were

docked with an scoring of -22 kcal/mol, whereas in the latter the first 24 poses were ranked with a scoring comprised between -22 and -21 kcal/mol. In all cases, a common feature is the interaction between Arg407 and the carbonyl unit of rhein, suggesting that this residue can be relevant for the binding of the chromene unit present in hybrid **3**. Overall, the result support the plasticity of the region defined by loops 8-14, 154-169 and 307-318, and the feasibility of adopting transient cavities that appear well suited to accommodate the rhein unit.

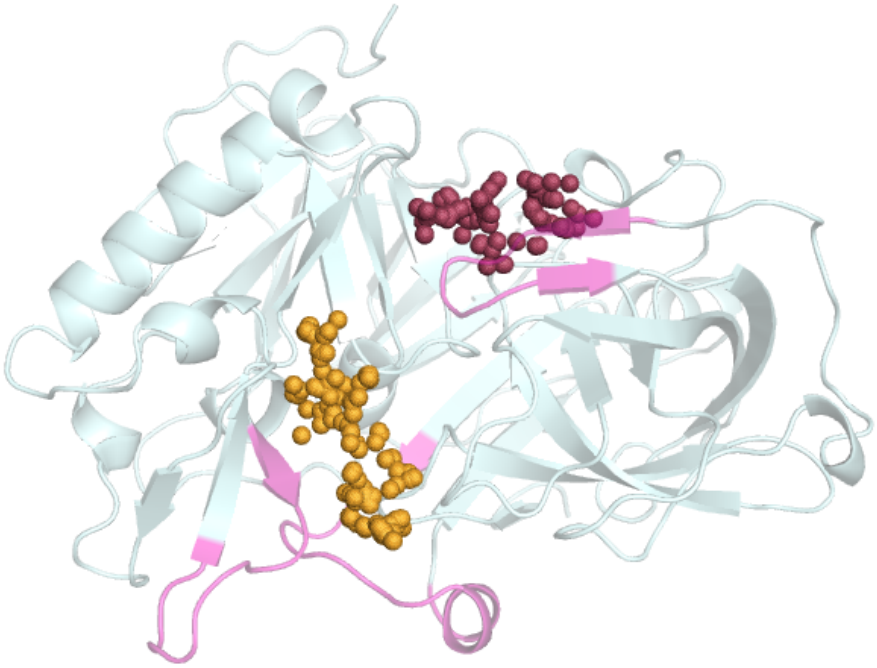

Figure 5. Representation of the two druggable sites identified from fPocket analysis. Red spheres denote the extension of the druggable cavity around the catalytic dyad, wheras orange spheres denote the transient secondary cavity defined by flexible loops.

Molecular dynamics simulations of the holo enzyme. The structural integrity of the binding mode disclosed in docking calculations was examined by means of MD simulations run for the BACE-1 complexes with hydrid compounds **1** and **3**. The

analysis of the set of independent simulations pointed out that the huprine moiety was tightly bound to the active site in all cases, as expected from the electrostatic stabilization between the protonated aminoquinoline system and the catalytic dyad. Furthermore, the aminoquinoline system of the huprine moiety fills the hydrophobic pocket formed by residues Leu30, Phe108, Ile110, and Ile118. On the other hand, the hydroxyanthraquinone moiety in the two enantiomeric forms of compound **1** was found to exhibit a well defined binding mode in the secondary cavity, which involves the electrostatic interaction with Ar407 (Figure 6).

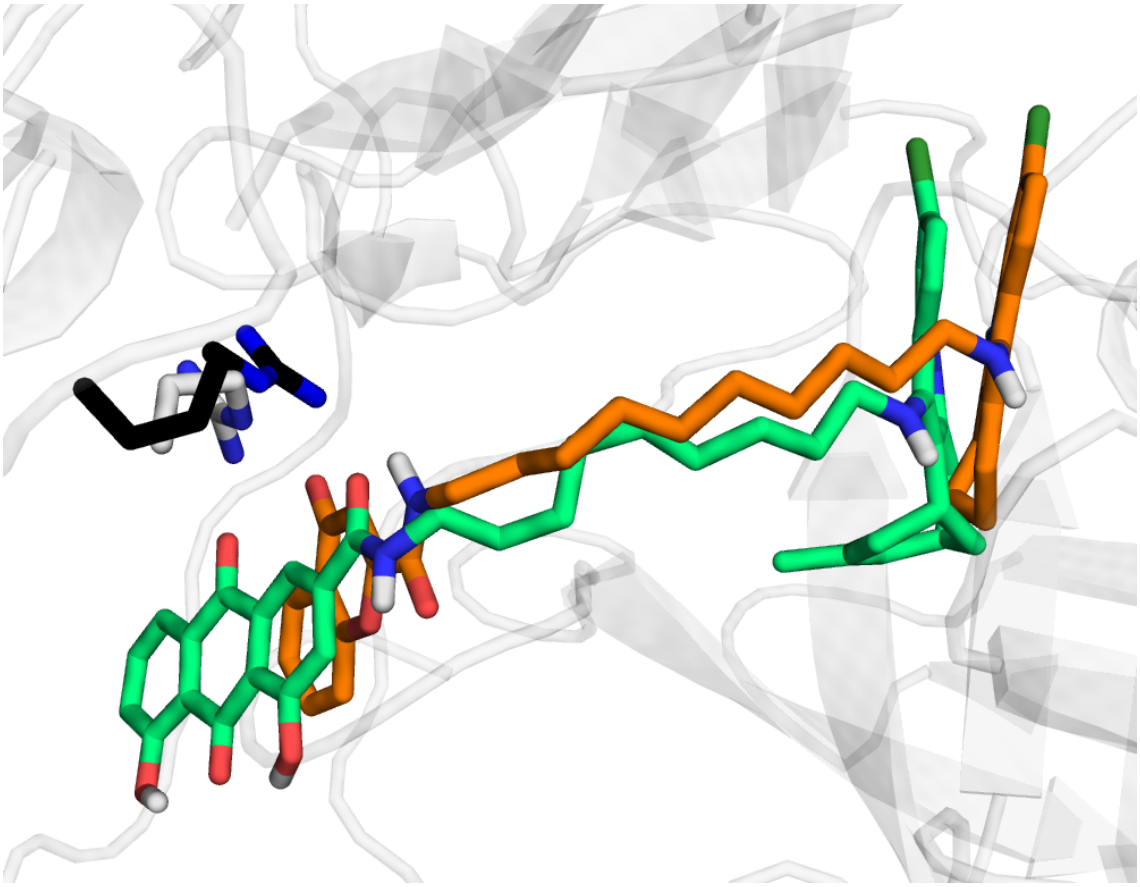

Figure 6. Superposition of representative snapshots collected at the end of the trajectories run for the BACE-1 complexes with hybrid compounds **1** and **3**. Fort he sake of clarity, only the relative location of Arg407 (shown as sticks) relative to the hydrid compounds is shown.

Noteworthy, similar arrangement is found for the tacrine-chromene hybrid **3**, and that the carbonyl unit of the chromene unit is also capable of forming electrostatic interactions with Arg407 (Figure 6). It is also worth noting that the methylenic tether adopt a similar arrangement in the substrate binding pocket, which permits both chromene and rhein moieties to fill similar regions in the secondary pocket. The only remarkable feature is that the presence of the two carbonyl units present in the huprine-rhein compound permits the formation of distinct electrostatic interactions with Arg407, which is found to adopt two major orientations in the binding pocket.

The binding model shown in Figure 6 allows us to rationalize the structure-activity relationships observed for the two hybrid compounds. First, regarding the huprine-rhein hybrid, the results reported in ref. 20 showed a notable dependence of the inhibitory activity with the legth of the tether. This trend can be easily explained by the expected alteration in the arrangement of the rhein unit, which would affect the electrostatic stabilization with Arg407. Thus, extension/reduction of the tether from 9-mer methylenic chain by a single methylene unit changes the inhibitory potency from an IC_{50} value of 80 nM to around 1 μM. On the other hand, the similar IC50 value obtained for both (+)-**1** and (–)-**1**, which is located at the catalytic site, is expected to have no impact on the binding of the rhein moiety to the secondary site.

With regard to the tacrine-chromene hybrid **3**, the dependence of the tether length on the inhibitory activity was not explicitly reported in the work by Fernández-Bachiller et al.[21] Present results suggest that these hybrid should exhibit a similar dependence as that found for the series of huprine-rhein compounds. Nevertheless, the authors checked the effect of different chemical modifications in positions 5', 6', and 7' of the chromene ring, finding that the inhibitory activity was nearly unaffected by changes involving different substituion pattern with hydroxyl and methxy groups in these positions (Ki

values ranging from 0.62 to 3.99 μM). The lack of sensitivity to these changes can be attributed to the solvent exposure of this face of the chromene ring in the binding mode reported in present MD simulations, which would not participate directly in contacts with the secondary pocket nor would affect the electrostatic interaction of the carbonyl unit with Arg407.

Conclusion

Within the plethora of the therapeutically useful proteins codified by the "druggable genome", *β*-secretase (BACE-1) has been classified in the subset of the target receptors considered of "difficult" addressability through small molecules. Hence, the identification of novel sites that could provide additional anchoring points could be highly valuable for increasing the chemical diversity of therapeutic drug candidates, enhancing the likelihood of finding suitable scaffolds for the design of therapeutically active BACE-1 inhibitors. In this context, the results presented in this work support the feasibility of formation of transient secondary pockets in th region shaped by the highly flexible loops 8-14, 154-169 and 307-318. The plasticity of these loops is revealed by the formation of pockets that cover a wide range of size and shapes, some with druggability features that would permit the binding of small fragments, such as the rhein and chromene units. Importantly, the results provide a basis to rationalize the trends in inhibitory potency observed for the two series of compounds, particularly the large dependence of the inhibitory potency with the tether length observed in huprine-rhein hybrids and the insensitivity to the substituents in the tacrine-chromene compounds. Overall, the results support the reliability of the computational methods to disclose "floopy" pockets hidden in highly flexible regions and to exploit these secondary pockets for the design of novel drugs hitting at challenging targets, such as BACE-1.

Acknowledgement

We thank the financial support from Ministerio de Economía y Competitividad (SAF2014-57094-R) and the Generalitat de Catalunya (2014-SGR-1189). We are grateful to the Consorci de Serveis Universitaris de Catalunya for computational resources. FJL acknowledges the support from ICREA Academia.

References

[1] D. J. Selkoe, *Nature* **1999**, *399*, A23-31.

[2] S. L. Roberds, J. Anderson, G. Basi, M. J. Bienkowski, D. G. Branstetter, K. S. Chen, S. B. Freedman, N. L. Frigon, D. Games, K. Hu, K. Johnson-Wood, K. E. Kappenman, T. T. Kawabe, I. Kola, R. Kuehn, M. Lee, W. Liu, R. Motter, N. F. Nichols, M. Power, D. W. Robertson, D. Schenk, M. Schoor, G. M. Shopp, M. E. Shuck, S. Sinha, K. A. Svensson, G. Tatsuno, H. Tintrup, J. Wijsman, S. Wright, L. McConlugue, *Hum. Mol. Genet.* **2001**, *10*, 1317-1324.

[3] L. McConlugue, M. Buttini, J. P. Anderson, E. F. Brigham, K. S. Chen, S. B. Freedman, D. Games, K. Johnson-Wood, M. Lee, M. Zeller, W. Liu, R. Motter, S. Sinha, *J. Biol. Chem*. **2007**, *282*, 26326-26334.

[4] M. S. Wolfe, *Curr. Alzheimer Res*. **2008**, *5*, 158-164.

[5] L. C. Walker, R. F. Rosen, *Age Ageing* **2006**, *35*, 332-335.

[6] R. Vassar, *J. Mol. Neurosci.* **2001**, *17*, 157-170.

[7] D. M. Skovronsky, V. M.-Y. Lee, J. Q. Trojanowski, *Annu. Rev. Pathol.* **2006**, *1*, 151-170.

[8] S. L. Cole, R. Vassar, *Curr. Genomics* **2007**, *8*, 509-530.

[9] H. M. Berman, J. Westbrook, Z. Feng, G. Gilliland, T. N. Bhat, H. Weissig, I. N. Shindyalov, P. E. Bourne, *Nuc. Acids Res.* **2000**, *28*, 235-242.

[10] M. Cascella, C. Micheletti, U. Rothlisberger, P. Carloni, *J. Am. Chem. Soc.* **2005**, *127*, 3734–3742.

[11] R. Friedman, A. Caflisch, *Proteins* **2010**, 78, 1575-1582.

[12] L. Hong, J. Tang, Biochemistry **2004**, *43*, 4689-4695.

[13] S. Patel, L. Vuillard, A. Cleasby, C. W. Murray, J. Yon, *J. Mol. Biol*. **2004**, *343*, 407-416.

[14] A. A. Gorfe, A. Caflisch, *Structure* **2005**, *13*, 1487-1498.

[15] D. R. Davies, *Annu. Rev. Biophys. Chem.* **1990**, *19*, 189-215.

[16] J. Y. Lee, S. A. Lee, J. K. Kim, C. B. Chae, Y. Kim, *Mol. Cells* **2009**, *27*, 651-656.

[17] L. J. Gutierrez, R. D. Enriz, H. A. Baldoni, *J. Phys. Chem. A.* **2010**, *114*, 10261-10269.

[18] H. Park, S. Lee, *J. Am. Chem. Soc.* **2003**, *125*, 16416-16422.

[19] P. Kacker, G. Bottegoni, A. Cavalli, *Curr. Med. Chem.* **2012**, *19*, 6095.

[20] E. Viayna, I. Sola, M. Bartolini, A. De Simone, C.Tapia-Rojas, F. Serrano, R. Sabaté, J. Juárez-Jiménez, B. Pérez, F. J. Luque, V. Andrisano, M. V. Clos, N. C. Inestrosa, D. Muñoz-Torrero, *J. Med. Chem.* **2014**, *57*, 2549-2567.

[21] M. I. Fernández-Bachiller, C. Pérez, L. Monjas, J. Rademann, M. I. Rodríguez-Franco, *J. Med. Chem.* **2012**, *55*, 1303-1317.

[22] A. K. Ghosh, N. Kumaragurubaran, L. Hong, S. S. Kulkarni, X. Xu, W. Chang, V. Weerasena, R. Turner, G. Koelsch, G. Blicer, J. Tang, J. Med. Chem. 2007, 50, 2399-2407.

[23] D. van der Spoel, E. Lindahl, B. Hess, A. R. van Buuren, E. Apol, P. J. Meulenhoff, D. P. Tieleman, A. L. T. M. Sijbers, K. A. Feenstra, R. van Drunen and H. J. C. Berendsen, *Gromacs User Manual version 4.0*, 2005. www.gromacs.org

[24] V. Hornak, R. Abel, A. Okur, B. Strockbine, A. Roitberg, C. Simmerling, *Proteins* **2006**, *65*, 712-725.

[25] W. L. Jorgensen, J. Chandrasekhar, J. D. Madura, R. W. Impey, M. L. Klein, *J. Chem. Phys.* **1983**, *79*, 926-935.

[26] Case, D. A.; Darden, T. A.; Cheatham, T. E.; Simmerling, C. L.; Wang, J.; Duke, R. E.; Luo, R.; Walker, R. C.; Zhang, W.; Merz, K. M.; Roberts, B.; Hayik, S.; Roitberg, A.; Seabra, G.; Swails, J.; Goetz, A. W.; Kolossváry, I.; Wong, K. F.; Paesani, F.; Vanicek, J.; Wolf, R. M.; Liu, J.; Wu, X.; Brozell, S. R.; Steinbrecher, T.; Gohlke, H.; Cai, Q.; Ye, X.; Wang, J.; Hsieh, M. J.; Cui, G.; Roe, D. R.; Mathews, D. H.; Seetin, M. G.; Salomon-Ferrer, R.; Sagui, C.; Babin, V.; Luchko, T.; Gusarov, S.; Kovalenko, A.; Kollman, P. A. AMBER 12, 2012.

[27] C. I. Bayly, P. Cieplak, W. Cornell, P. A. Kollman, *J. Phys. Chem.* **1993**, *97*, 1026-1028.

[28] I. Bahar, T. R. Lezon, A. Bakan, I. H. Shrivastava, *Chem. Rev.* **2010**, *110*, 1463-1497.

[29] T. Meyer, C. Ferrer-Costa, A. Pérez, M. Rueda, A. Bidon-Chanal, F. J. Luque, C. A. Laughton, M. Orozco, *J. Chem. Theory Comput.* **2006**, *2*, 251-258.

[30] B. Laurent, M. Chavent, T. Cragnolini, A. C. E. Dahl, S. Pasquali, P. Derreumaux, S. P. Sansom, M. Baaden, *Bioinformatics* 2014. DOI: 10.1093/bioinformatics/btu822

[31] P. Schmidtke, X. Barril, *J. Med. Chem.* **2010**, *53*, 5858-5867

8 Multi-trypanosomatid compounds

Chapter

(*Eur. J. Med. Chem.* **2015**)
accepted with minor revision

8.1 Design and synthesis of a small library of novel quinoline-based antiprotozoan compounds

A fruitful collaboration recently established with the research group of Prof. Rodolfo Lavilla allowed us to acquire experience on the *Povarov* MCR, a powerful synthetic strategy for the fast access, after oxidation of the resulting diastereomeric mixture of octahydroquinolines, to variously substituted heterofused quinoline derivatives, endowed with a broad spectrum of potential applications in medicinal chemistry. This chapter will discussed the wide and successful recourse to the *Povarov* reaction for the exploration of an ensemble of chemical modifications around the scaffold **VIII** (**Figure 8.1**), with the aim of synthesizing a small library of quinoline-based antiprotozoan *hit* compounds.

As noted in *Chapter 4*, this synthetic route has been already utilized in this PhD thesis for the synthesis of optimized AChE PAS inhibitors, as anti-Alzheimer agents. Surprisingly, we have found that **57**, one of these anticholinesterasic compounds (**Figure 8.1**),[182] shows moderate activity against *Trypanosoma brucei* (IC_{50} = 3.33 μM). This promising result, together with other results described in literature, remarking the antiprotozoan properties displayed by quinoline-based compounds, [243,149] prompted us to further investigate the possibility to exploit scaffold **VII** in the search for novel antiprotozoan agents.

Two new benzonaphthyridines (**167** and **161** in **Figure 8.1**) were synthesized in collaboration with Dr. Esther Vicente to explore the best substitution pattern at positions 5 and 9. The pharmacological results pointed out that the presence of 4-(aminomethyl)phenyl group and a chloro substituent at position 5 and 9, respectively, of the benzonaphthyridine moiety (compound **161**), respectively, led to slightly higher potency against *T. brucei* (IC_{50} = 1.00 μM).

[182]Di Pietro, O.; Viayna, E.; Vicente-García, E.; Bartolini, M.; Ramón, R.; Juárez-Jiménez, J.; Clos, M.V.; Pérez, B.; Andrisano, V.; Luque, F.J.; Lavilla, R.; Muñoz-Torrero, D. *Eur. J. Med. Chem.* **2014**, *73*, 141.
[243]Md. Mushtaque, S. *Eur. J. Med. Chem.* **2015**, *90*, 280.
[149]Bongarzone, S.; Bolognesi, M.L. *Expert Opin. Drug Discov.* **2011**, *6*, 251.

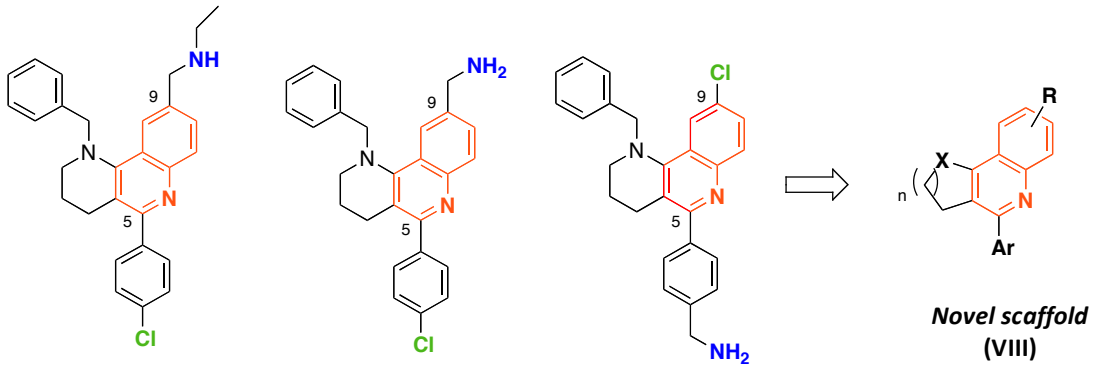

57 **167** **161**

T. brucei IC_{50} = 3.33 µM *T. brucei* IC_{50} = 2.10 µM *T. brucei* IC_{50} = 1.00 µM

Figure 8.1 Chemical structures of the benzonaphthyridines preliminarily evaluated against *T. brucei*, and designed novel derivatives with scaffold **VII** (n = 1, 2, 3; X = NH, O; R = *m*-Cl, *p*-Cl; Ar = 4-cianophenyl-, 4-aminomethylphenyl-, 2-furyl-, 2-thienyl-).

Then, a small library of various heterofused tricyclic quinoline derivatives was designed and synthesized, mainly exploring ring contraction, expansion or opening, *N*-debenzylation and bioisosteric replacements (**Table 8.1**). All the synthesized compounds were subjected to whole-cell phenotypic screening against bloodstream form of *T. brucei*, epimastigotes of *T. cruzi* and promastigotes of *Leishmania donovani*. Their cytotoxicity against rat myoblast L6 cells, AChE inhibitory activity as potential off-target effect, and capability to cross the blood-brain barrier (BBB) were also evaluated.

In a general overview, the screened compounds displayed trypanocidal activities in the micromolar range (IC_{50} 0.92-35.7 µM) against the bloodstream form of *T. brucei*; the most promising *hits* belong to the series of the 5-[4-(aminomethyl)phenyl]-derivatives, displaying from low- to sub-micromolar IC_{50} values (0.92-2.44 µM). With the sole exception of amines **185**, **187** and **195f**, for which a uncertain BBB penetration was predicted, the *hit* compounds turned out to be able to cross the BBB, thus being also potentially effective during the secondary stage of the infection. Moreover, although most compounds resulted to have rather weak efficacy against *T. cruzi*, a set of amine derivatives (**184**, **186**, **167** and **193**) showed moderate antileishmanial activity (IC_{50} 4.85-8.11 µM), being 3- to 5-fold more potent than the reference compound [potassium antimony (III) tartrate hydrate].

Despite the promising results obtained so far, cytotoxicity and potential cholinergic side effects still remain an important issue that should be dealt with in a future *lead* optimization.

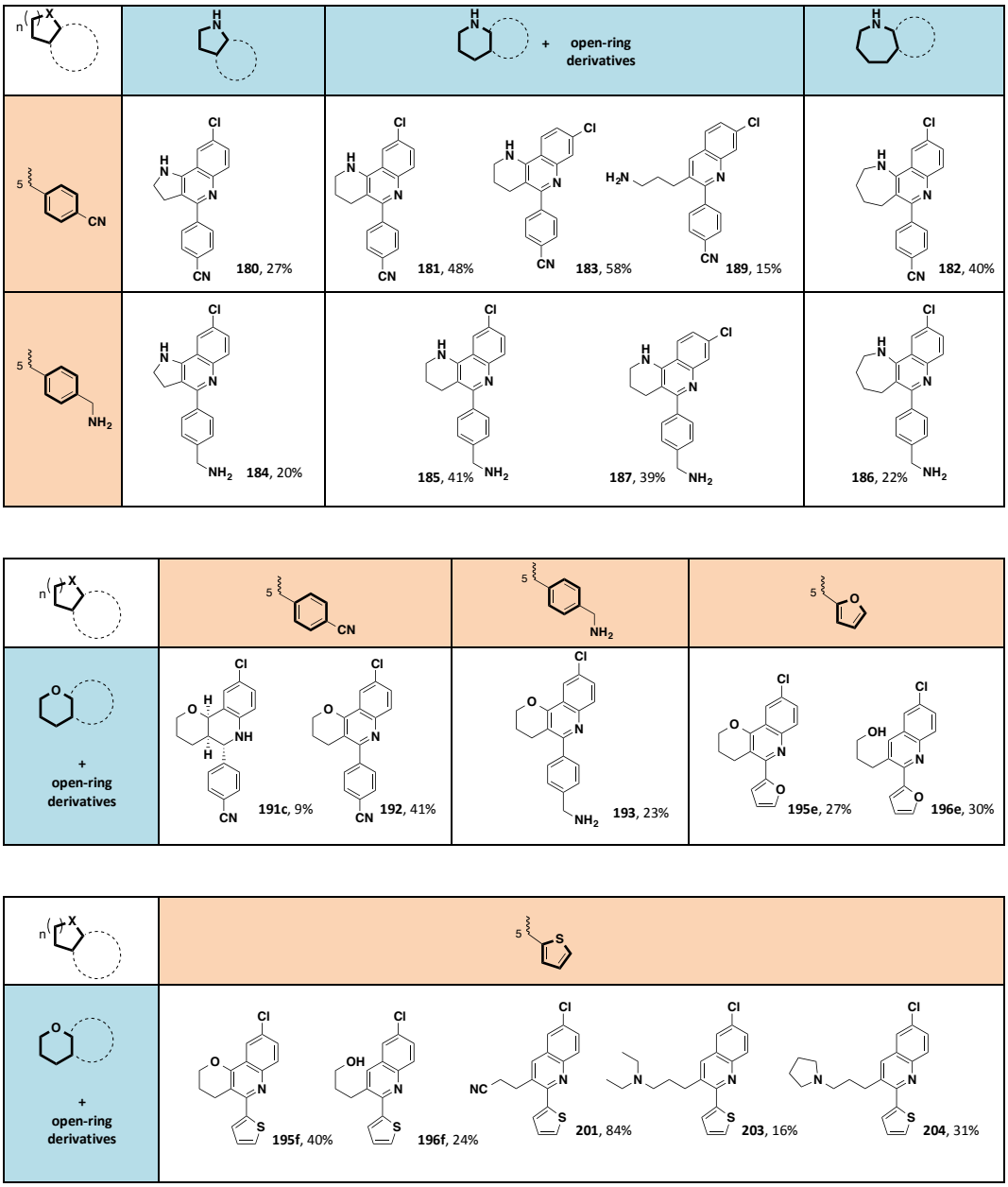

Table 8.1. Chemical structures and overall yields of the new quinoline-derivatives

8.2 Synthesis of the library of novel quinolines and tricyclic heterofused quinolines

8.2.1 Synthesis of the benzo[h][1,6]naphthyridine 167

For the synthesis of benzonaphthyridine **167**, a *Povarov* reaction between lactam **46**, already available in our laboratory, aldehyde **43**, and aniline **162** was performed under $Sc(OTf)_3$ catalysis in anhydrous CH_3CN. The resulting diastereomeric mixture was directly oxidized with DDQ and the crude subjected to silica gel column chromatography purification to provide byproduct **164** in 14% yield and the desired product, **163**, as a slightly impure fraction, which was submitted to two consecutive purifications through column chromatography and subsequent precipitation with a mixture of hexane/EtOAc (9:1) to finally obtain the desired product only in 8% overall yield (**Scheme 8.1**).

With the aim of improving the yield, the *Povarov* reaction was stirred at 50 °C for 72 h. The resulting diastereomeric mixture, without any further purification, was oxidized with an excess of MnO_2 (from Wako),[244] in the presence of pyridine and stirred at 55 °C in toluene for 5 h; then, after TLC control, the reaction mixture was heated up to 100 °C for the following 43 h. Unfortunately, after column chromatography purification of the crude, the desired product **163** was not detected (**Scheme 8.1**).

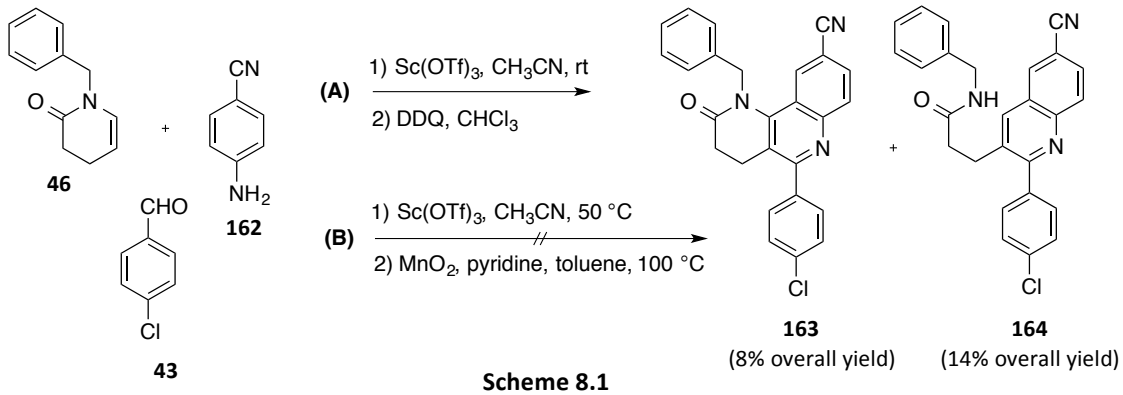

Scheme 8.1

In an alternative synthetic route, the *Povarov* reaction was performed with the *N*-Boc protected aniline **71**, aldehyde **43** and lactam **46**. DDQ oxidation of the corresponding diastereomeric mixture, followed by column chromatography purification, provided the *N*-Boc protected benzonaphthyridine **165** in 47% overall yield. Next, acidic deprotection with 4M HCl/dioxane and further column chromatography purification afforded amine **166** in 44% yield.

[244]Vicente-García, E.; Ramón, R.; Preciado, S.; Lavilla, R. *Beilstein J. Org. Chem.* **2011**, *7*, 980.

Finally, the $Zn(OAc)_2$ catalyzed reduction of the lactam group with $(EtO)_3SiH$, [245] and subsequent chromatography purification, provided the desired product **167** in 66% yield.

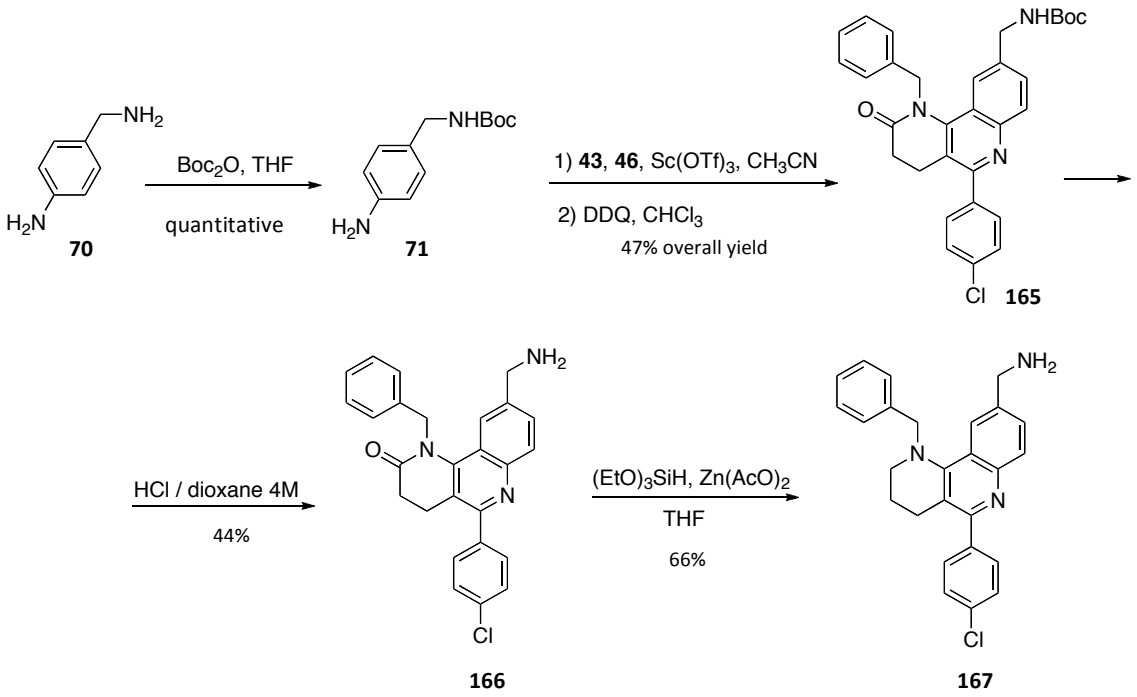

Scheme 8.2

8.2.2 Synthesis of the pyrrolo[3,2-c]quinolines, pyrano[3,2-c]quinolines, azepino[3,2-c]quinolines, and benzo[h][1,6]naphthyridines 180-183, 184-187, 189, 192 and 193

The *Povarov* reaction of the activated alkenes **58**, **168**, **169** and **42** with anilines **170a**,**b** and 4-cyanobenzaldehyde **171** afforded the diastereomeric mixture of compounds **172**-**175** and **191**. *Cis-cis* and *cis-trans* diastereomeric mixture of octahydronaphthyridine **191** was further subjected to two consecutive column chromatography purifications to finally isolate, in 9% yield, the *cis-cis* diastereomer **191c**.

DDQ oxidation of **172**-**175**, **191** and subsequent silica gel column chromatography purification provided the desired quinolines **176**-**179** and **192** in 41-79% yields (**Schemes 8.3** and **8.5**). Importantly, during the synthesis of compound **179**, the ring-open by-product **188** was also formed in 17% yield. Finally, the $LiAlH_4$ reduction of the nitrile group, preceded by the acidic deprotection of **176**-**179**, yielded the corresponding amines **184**-**187** and **193** in good

[245] Das, S.; Addis, D.; Zhou, S.; Junge, K.; Beller, M. *J. Am. Chem. Soc.* **2010**, *132*, 1770.

yields (55-87%), after column chromatography purification (**Schemes 8.3** - **8.5**). It is to be noted that amine **190**, even after silica gel chromatography purification and subsequent precipitation of the corresponding hydrochloride, could not be adequately purified for pharmacological evaluation purposes.

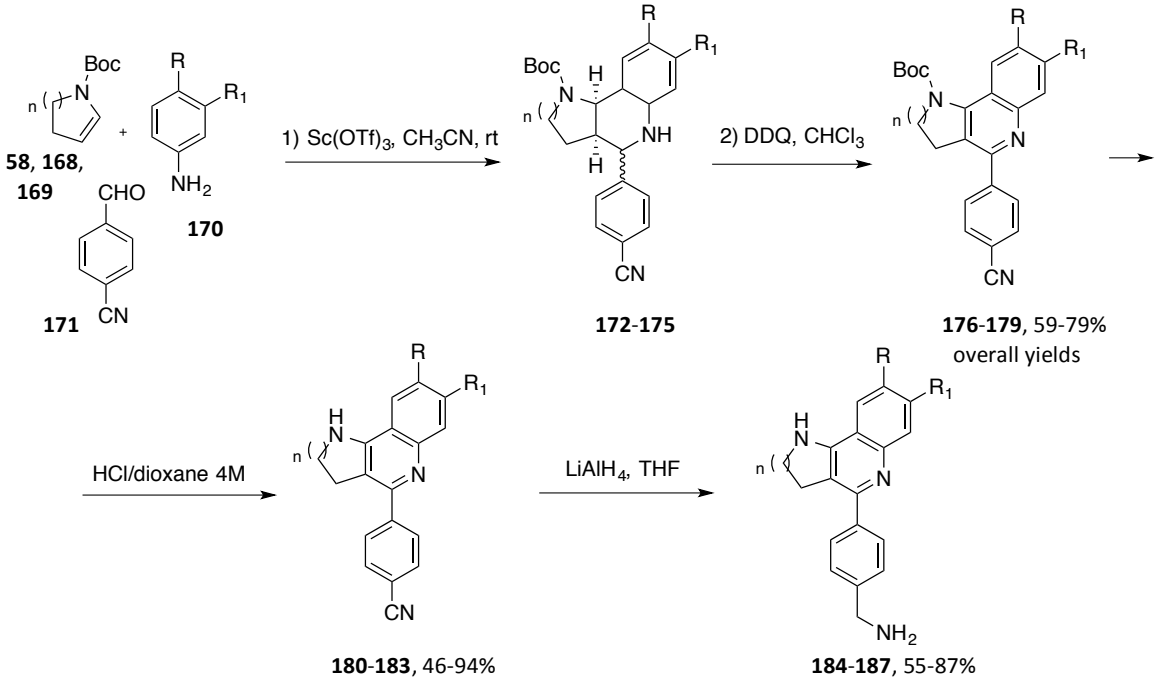

58 n= 2**; 168** n= 1**; 169** n= 3
170a R = Cl, R_1 = H
170b R = H, R_1 = Cl
172, **176**, **180**, **184** n = 1, R = Cl, R_1 = H
173, **177**, **181**, **185** n = 2, R = Cl, R_1 = H
174, **178**, **182**, **186** n = 3, R = Cl, R_1 = H
175, **179**, **183**, **187** n = 2, R = H, R_1 = Cl

Scheme 8.3

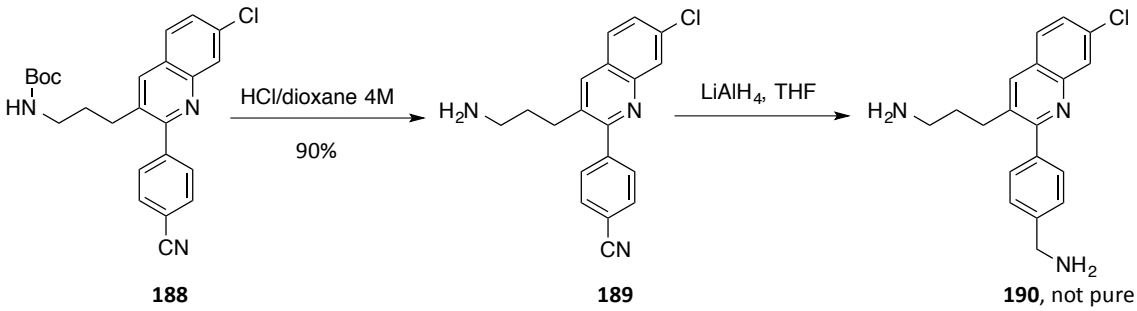

Scheme 8.4

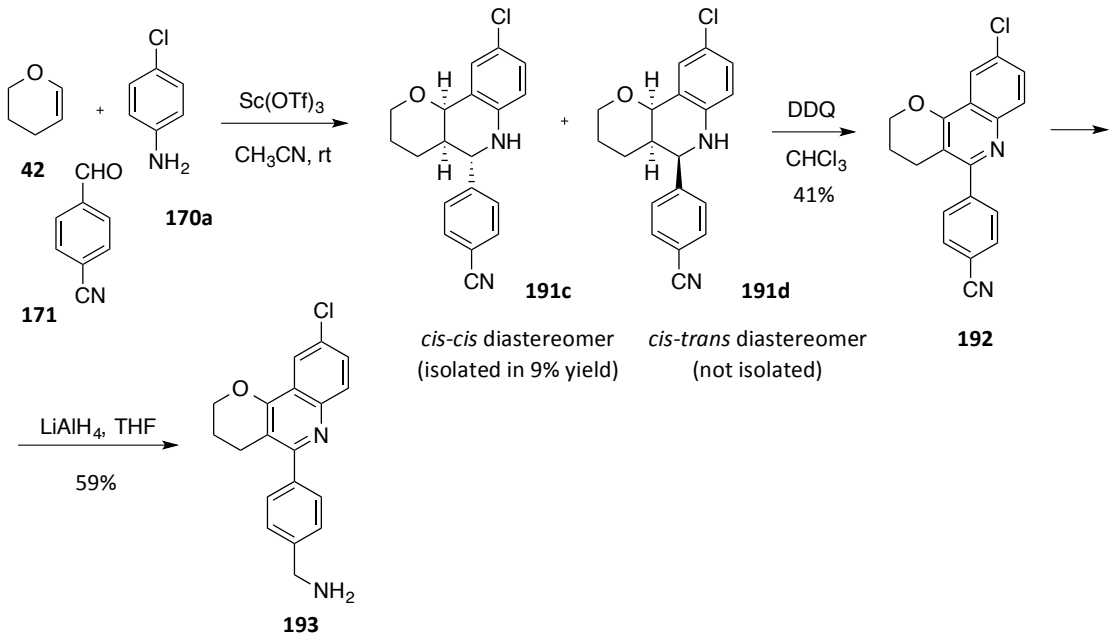

Scheme 8.5

8.2.3 Synthesis of the pyrano[3,2-c]quinolines 195e,f and alcohols 196e,f

The synthesis of pyrano[3,2-*c*]quinoline **195e** consisted of a two-step sequence involving the *Povarov* reaction of the commercially available dihydropyran **42**, aniline **170a** and aldehyde **194e**, stirring for 72 h at 50 °C, followed by DDQ oxidation and further column chromatography purification (27% overall yield). Worthy of note is the additional formation of alcohol **196e** (30% yield) as byproduct resulting from the opening of the pyran ring, according to the mechanism proposed in **Scheme 8.6** (as already shown in **Schemes 8.1** and **8.4,** similar byproducts [**164** and **188**] were also isolated during the preparation of quinolines **163** and **179**, respectively).

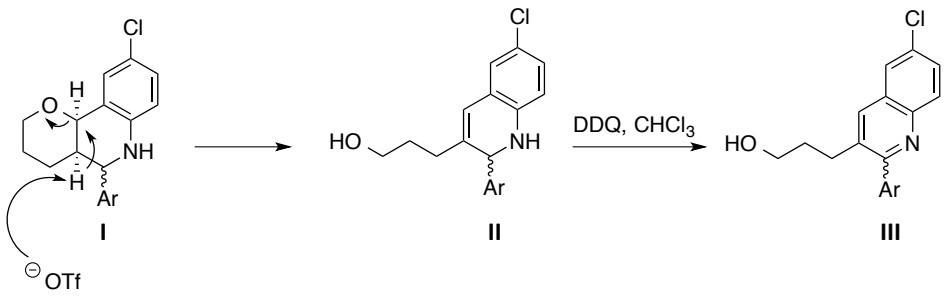

Scheme 8.6

Analogously, the *Povarov* reaction between the commercially available dihydropyran **42**, aniline **170a** and aldehyde **194f** was stirred at 80 °C for 72 h. After DDQ oxidation and further column chromatography purification, quinoline **195f** and alcohol derivative **196f** were isolated in 40% and 24% yield, respectively (**Scheme 8.7**).

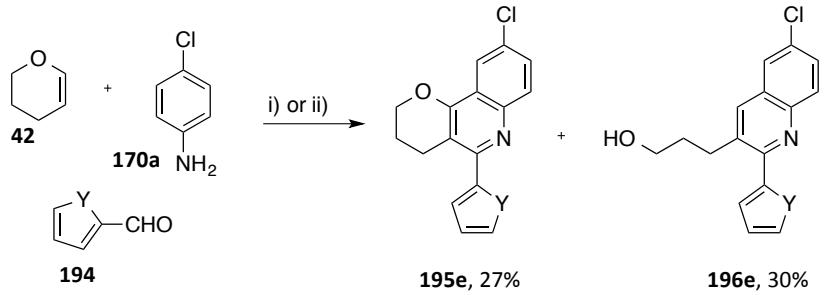

194e, **195e**, **196e** Y= O
194f, **195f**, **196f** Y= S
for **195e** and **196e** i): 1) $Sc(OTf)_3$, CH_3CN, 50 °C; 2) DDQ, $CHCl_3$
for **195f** and **196f** ii): 1) $Sc(OTf)_3$, CH_3CN, 80 °C; 2) DDQ, $CHCl_3$

Scheme 8.7

8.2.4 Synthesis of quinoline derivatives 201, 203, 204

Alcohol **196f** was also used as substrate for further functionalizations of the hydroxypropyl chain at position 3 of the quinoline ring. To this end, the pyrrolidino-, diethylamino-, and the cyano-derivatives **204**, **203**, and **200** were prepared in the context of the *graduate thesis* of the Erasmus student Anna Lanzoni.

The obtention of the cyano-derivative **201** occurred while attempting to replace the hydroxy group of **196f** by an oxime, through a *Mitsunobu* reaction.[246] The synthetic strategy required the preliminary preparation of *O*-*TBS*-*N*-tosylhydroxylamine, **198**, which was easily accessed following a synthetic method described in the literature.[247] Thus, alcohol **196f** was first treated with *O*-*TBS*-*N*-tosylhydroxylamine and PPh_3 in a mixture of THF/toluene, and, then, DEAD (40% in toluene) was added at 0 °C to afford, after column chromatography purification, slightly impure **199**. Subsequent desilylative elimination of *p*-toluenesulfinate by treatment

[246]Fletcher, S. *Org. Chem. Font.* **2015**, *2*, 739.
[247]Kitahara, K.; Toma, T.; Shimokawa, J.; Fukuyama, T. *Org. Lett.* **2008**, *10*, 2259.

with CsF did not proceed as initially expected, providing nitrile **201** (84% overall yield from alcohol **196f**) instead of the initially planned diastereomeric mixture of oximes **200** (**Scheme 8.8**).

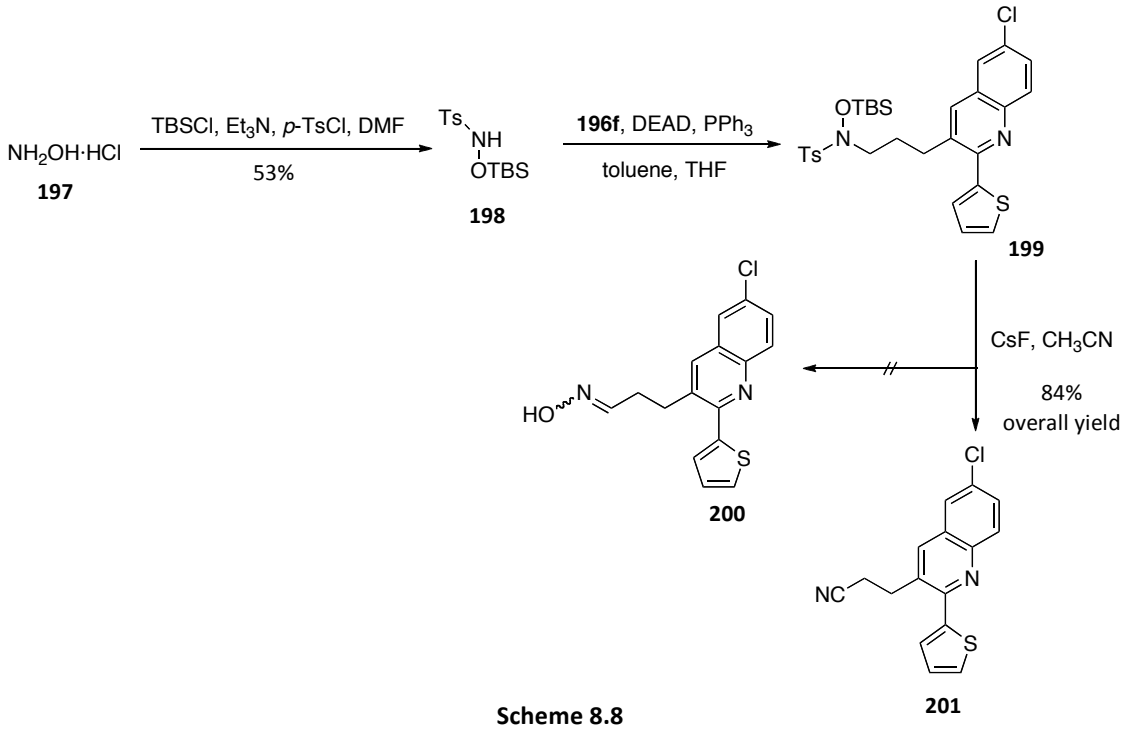

Scheme 8.8

Conversely, the initial attempt to analogously prepare the diethylamino-derivative **203** through *Mitsunobu* reaction was not successful, since it provided a solid residue consisting of a complex mixture not containing the desired amine **203**. Thus, as an alterative route to functionalize the side chain of **196f** with different amines, alcohol **196f** was quantitatively converted into the corresponding mesylate by treatment with Et_3N and MsCl in CH_2Cl_2. The subsequent nucleophilic substitution carried out by treatment of mesylate **202** at 0 °C with diethylamine in presence of Et_3N in anhydrous CH_2Cl_2 disappointingly revealed, after TLC control, only the presence of starting material. The desired amine **203** was finally obtained in 16% overall yield, after column chromatography purification, *via* overnight reaction of the mesylate with diethylamine using K_2CO_3 as the base in DMF at 85 °C.

With an analogous synthetic procedure, pyrrolidino-derivative **204** was obtained in 31% overall yield, after silica gel column chromatography purification (**Scheme 8.9**).

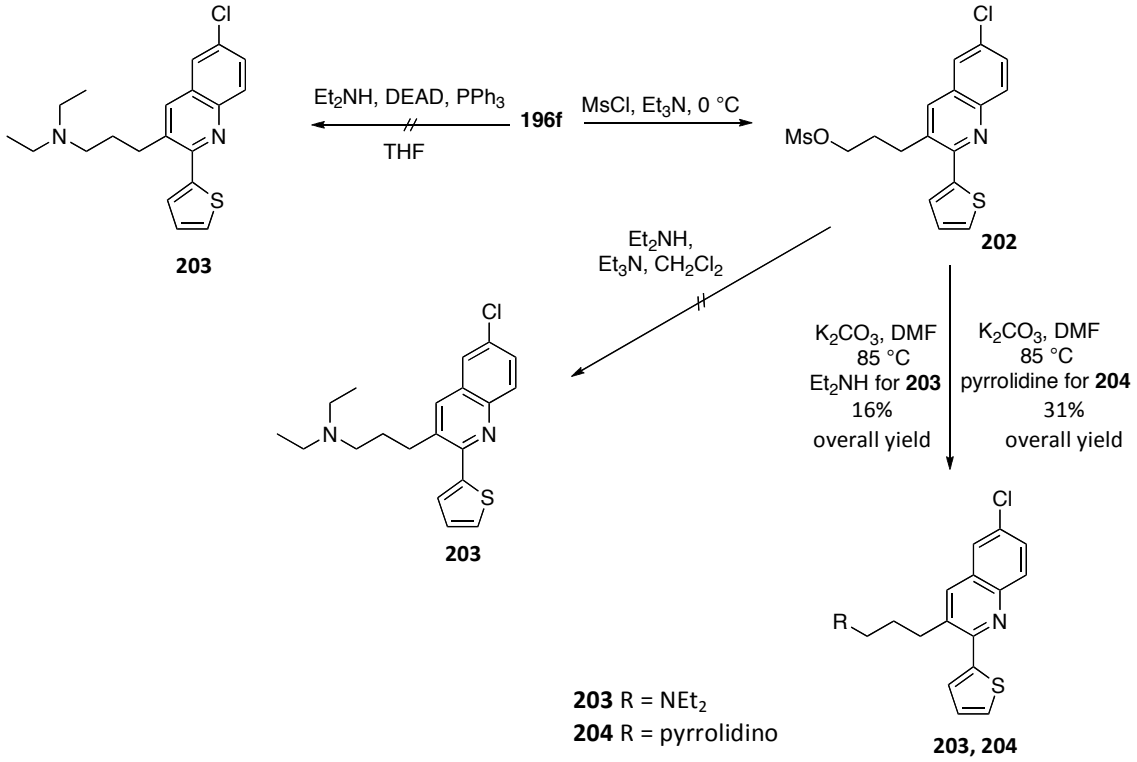
Cl
N
N
S
203
Et2NH, DEAD, PPh3
THF
196f
MsCl, Et3N, 0 °C
MsO
202
Et2NH,
Et3N, CH2Cl2
K2CO3, DMF
85 °C
Et2NH for 203
16%
overall yield
K2CO3, DMF
85 °C
pyrrolidine for 204
31%
overall yield
R
203 R = NEt2
204 R = pyrrolidino
203, 204

Scheme 8.9

Multicomponent reaction-based synthesis and biological evaluation of tricyclic heterofused quinolines with multi-trypanosomatid activity

Ornella Di Pietro[a], Esther Vicente-García[b], Martin C. Taylor[c], Diana Berenguer[d], Elisabet Viayna[a], Anna Lanzoni[a], Irene Sola[a], Helena Sayago[b], Cristina Riera[d], Roser Fisa[d], M. Victòria Clos[e], Belén Pérez[e], John M. Kelly[c], Rodolfo Lavilla[b,f], Diego Muñoz-Torrero[a,*]

[a] *Laboratori de Química Farmacèutica (Unitat Associada al CSIC), Facultat de Farmàcia, and Institut de Biomedicina (IBUB), Universitat de Barcelona, Av. Joan XXIII, 27-31, E-08028, Barcelona, Spain*

[b] *Barcelona Science Park, Baldiri Reixac 10-12, E-08028, Barcelona, Spain*

[c] *Department of Pathogen Molecular Biology, London School of Hygiene and Tropical Medicine, Keppel Street, London WC1E 7HT, United Kingdom*

[d] *Laboratori de Parasitologia, Departament de Microbiologia i Parasitologia Sanitàries, Facultat de Farmàcia, Universitat de Barcelona, Av. Joan XXIII, 27-31, E-08028, Barcelona, Spain*

[e] *Departament de Farmacologia, de Terapèutica i de Toxicologia, Institut de Neurociències, Universitat Autònoma de Barcelona, E-08193, Bellaterra, Barcelona, Spain*

[f] *Laboratori de Química Orgànica, Facultat de Farmàcia, Universitat de Barcelona, Av. Joan XXIII, 27-31, E-08028, Barcelona, Spain*

* Corresponding author. Tel.: +34 934024533; fax: +34 934035941.

E-mail address: dmunoztorrero@ub.edu (D. Muñoz-Torrero).

ABSTRACT

Human African trypanosomiasis (HAT), Chagas disease and leishmaniasis, caused by the trypanosomatids *Trypanosoma brucei*, *T. cruzi* and *Leishmania* species, are among the most deadly neglected tropical diseases. The development of drugs that are active against several trypanosomatids is appealing from a clinical and economic viewpoint, and seems feasible, as these parasites share alike metabolic pathways and hence they might be treatable by common drugs. From benzonapthyridine **1**, an inhibitor of acetylcholinesterase (AChE) for which we have found a remarkable trypanocidal activity, we have designed and synthesized novel benzo[*h*][1,6]naphthyridines, pyrrolo[3,2-*c*]quinolines, azepino[3,2-*c*]quinolines, and pyrano[3,2-*c*]quinolines through 2–4-step sequences featuring an initial multicomponent Povarov reaction as the key step. To assess the therapeutic potential of the novel compounds, we have evaluated their *in vitro* activity against *T. brucei*, *T. cruzi*, and *L. infantum*, as well as their brain permeability, of interest for the treatment of late-stage HAT. To assess their potential toxicity, we have determined their cytotoxicity against rat myoblast L6 cells and their AChE inhibitory activity. Several tricyclic heterofused quinoline derivatives have been found to display an interesting multi-trypanosomatid profile, with one-digit micromolar potencies against two of these parasites and two-digit micromolar potency against the other. Pyranoquinoline **39**, which displays IC_{50} values of 1.46 μM, 6.14 μM and 29.2 μM against *T. brucei*, *L. infantum* and *T. cruzi*, respectively, brain permeability, better drug-like properties (lower lipophilicity and molecular weight) than hit **1**, and the lowest AChE inhibitory activity of the series (IC_{50} > 30 μM), emerges as an interesting multi-trypanosomatid lead, amenable to further optimization particularly in terms of its selectivity index over mammalian cells.

Keywords: Benzo[*h*][1,6]naphthyridines
Pyrano[3,2-*c*]quinolines
Povarov reaction
Tripanocidal agents
Leishmanicidal agents
Brain permeability

1. Introduction

Neglected tropical diseases (NTDs) are a group of 17 infectious diseases that globally affect more than 1 billion people from 149 countries [1]. Not only do NTDs cause a huge health impact, both in terms of disability-adjusted life years (DALY, 26 million DALYs) and mortality (534,000 deaths annually), but they also have harmful effects on the overall economic productivity of developing countries where these diseases are endemic, which become inexorably trapped in an unbreakable cycle of poverty [2–4].

Among NTDs, vector-borne kinetoplastid diseases are particularly deadly, with leishmaniasis, Chagas disease (or American trypanosomiasis) and human African trypanosomiasis (HAT or sleeping sickness) ranking first, fifth and sixth, respectively, in number of associated deaths [2]. Their causative agents are trypanosomatid parasites that are transmitted to humans through the intervention of an infected insect vector: *Trypanosoma brucei gambiense* and *T. brucei rhodesiense* (accounting for 98% and 2% of cases of HAT, respectively) spread through the bite of blood-feeding tsetse flies; *Trypanosoma cruzi* (for Chagas disease) transmitted most commonly through contact with the faeces of a blood-sucking triatomine bug (the so-called kissing bug); and different *Leishmania* species, prominently *Leishmania donovani* and *L. infantum* (for visceral leishmaniasis), transmitted by the bite of female phlebotomine sand flies. In the absence of treatment, these diseases are frequently fatal, with their mortality being associated to particular stages or forms of the disease. In the case of HAT, after an initial hemo-lymphatic stage characterized by nonspecific clinical symptoms, parasites can cross the blood–brain barrier (BBB) and invade the central nervous system (CNS), giving rise to an array of severe neurological manifestations that include profound sleep disruptions and eventually coma and death. The initial phases of Chagas disease are usually asymptomatic or associated with non-specific symptoms of fever, malaise, or lymph node enlargement, but in about 30% of patients it evolves into a chronic phase, usually characterized by cardiomyopathy, and is a major cause of premature heart failure in Latin America. The most severe manifestation of leishmaniasis is visceral form, which leads to hepatosplenomegaly, progressive anemia, and ultimately death in most cases.

These diseases are usually confined to rural areas of endemic countries (sub-Saharan Africa for HAT, mainly Central and South America for Chagas disease, and Middle East and Asia, East Africa, Central and South America and Southern Europe for leishmaniasis). However, climate changes due to global warming, which may result in

an extension of the insect vector habitats, as well as international travel and immigration patterns may expand the geographical impact of these infectious diseases, thereby increasing the population at risk [5]. Travel to and immigration from endemic countries have made Chagas disease and several forms of leishmaniasis emerging infections in the United States (both infections), and Spain and Japan (Chagas disease) [6,7].

The current therapies against HAT, Chagas disease and leishmaniasis suffer from important shortcomings. HAT first-stage treatments rely on pentamidine and suramin, which require parenteral administration and are ineffective against the second stage. Stage 2 HAT can be treated by painful intravenous administration of the arsenical drug melarsoprol, which may lead to fatal reactive encephalopathy in 5–10% of patients, or with eflornithine, which is much safer but requires intravenous administration and hospitalization [8]. Toxicity is also a major issue with the approved drugs against Chagas disease, the nitroderivatives benznidazole and nifurtimox, and with some of the drugs used for the treatment of visceral leishmaniasis (pentavalent antimonials, amphotericin B, paromomycin and miltefosine). Apart from complicated long courses of treatment, in most cases parenteral administration is required. In addition, the emergence of resistance to these drugs in areas of high transmission further challenges their clinical application [6,8–13].

In the absence of preventive or therapeutic vaccines and rigorous control of insect vectors [5,14], the development of novel chemotherapies against these infectious diseases, with appropriate efficacy and safety profiles, is desperately needed [15,16]. Besides combinations of approved antiprotozoan drugs or repurposing of known drugs with other indications [8,14,15], increasing research efforts are being made to design novel chemical entities that hit one or several biological targets which play a key role in the biology of the parasite and are sufficiently different from those in the mammalian host cells as to enable selective toxicity [5,9,17–23]. However, while we are gaining a better understanding of the relevant parasite targets, phenotypic whole cell screening of novel compounds or chemical libraries remains a very successful approach for anti-protozoan drug discovery [8,24,25]. Thus, anti-protozoan drug pipelines are being enriched through drug discovery campaigns involving the synthesis of novel chemical entities and their biological evaluation against the selected parasites [26–28]. Of particular interest are those compounds that can be active against several protozoan parasites [25,29–31], as several NTDs usually coexist in endemic countries [1]. The trypanosomatid parasites that cause HAT, Chagas disease and leishmaniasis are

taxonomically related, have similar structural and biochemical features, and seem to share some of their metabolic pathways [14], thereby rendering them especially amenable to modulation by common drugs. Indeed, several structural families featuring a 4-aminoquinoline moiety have been recently reported to display a multi-protozoan profile, namely trypanocidal and antiplasmodial activity [32–35].

The use of multicomponent reactions [36] appears as a very useful strategy to rapidly build new hits in a modular manner. This approach is having a tremendous impact in modern medicinal chemistry. Apart from considerably speeding the process and manufacture of some drugs [37], it is especially relevant in drug discovery, allowing the preparation of new scaffolds and its straightforward decoration, also facilitating the hit to lead transition and pharmacogical issues [38,39]. We have recently reported the synthesis and acetylcholinesterase (AChE) inhibitory activity of a series of 1,2,3,4-tetrahydrobenzo[*h*][1,6]naphthyridines such as **1** (Fig. 1), which are prepared using a multicomponent Povarov reaction as the key step [40]. This transformation requires a cyclic enamide as an activated olefin, which affords the ring A of **1** (Fig. 1), an aromatic aldehyde, which affords the substituent at position 5, and an aniline, which affords the ring C with the substituent at position 9. Because the tricyclic scaffold of the benzo[*h*][1,6]naphthyridine system of **1** contains a 4-aminoquinoline motif and a side chain with a second protonatable nitrogen atom, we inferred that this compound might display some anti-protozoan activity. Indeed, the outstanding IC_{50} value of 3.33 μM against *Trypanosoma brucei* that we have found for **1** has confirmed our initial assumption. In light of this, and relying on the synthetic versatility of the multicomponent Povarov reaction [41,42], which might enable the modification of ring A and the substituents at positions 1, 5 and 9 of benzonaphthyridine **1** by simply changing the starting materials, we planned the synthesis of a series of analogues of **1** and their evaluation against the trypanosomatids that cause HAT, Chagas disease and leishmaniasis.

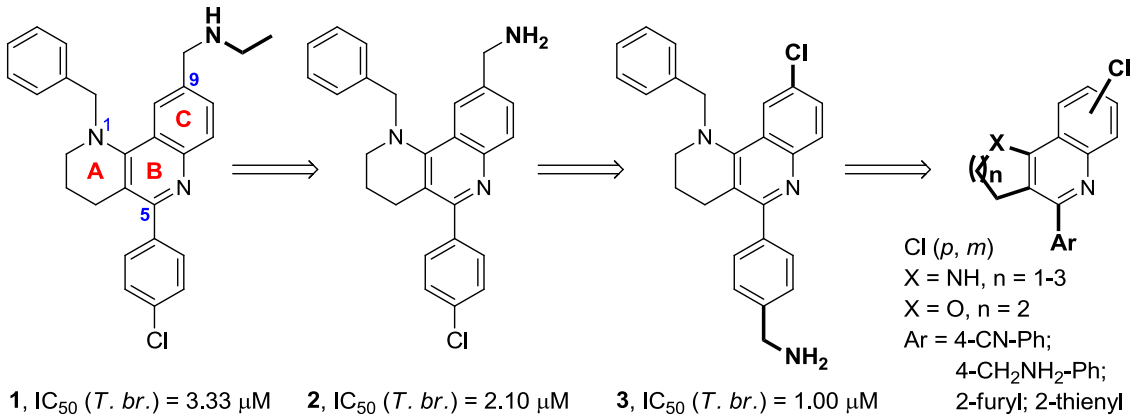

Fig. 1. Design of the novel benzonaphthyridines **2** and **3** and other heterofused quinoline analogues from compound **1**.

Here, we report i) the synthesis of novel benzo[*h*][1,6]naphthyridine-, pyrrolo[3,2-*c*]quinoline-, azepino[3,2-*c*]quinoline-, and pyrano[3,2-*c*]quinoline-based analogues of **1** with different substituents at rings A, B, and C, as well as some quinoline derivatives resulting from opening of ring A of some of these tricyclic scaffolds; ii) their evaluation against *T. brucei*, *T. cruzi* and *L. infantum*; iii) and the assessment of their cytotoxic activity against rat myoblast L6 cells and their AChE inhibitory activity. Also, to determine their potential usefulness for late-stage HAT, the ability to cross BBB of the novel compounds has been evaluated *in vitro* using a parallel artificial membrane permeability assay (PAMPA-BBB).

2. Results and discussion

2.1. Design and synthesis of the target compounds

Compound **1** is a rather quite lipophilic molecule, with a calculated log P value of 6.64 [43], hence clearly above the commonly accepted threshold for good oral bioavailability [44]. In order to decrease lipophilicity, we first envisaged the synthesis of compound **2**, i.e. the *N*-deethylated derivative of **1**, and its isomer **3** (Fig. 1 and Schemes 1 and 2), in which the chloro and aminomethyl substituents at the *para* position of the phenyl substituent and at position 9, respectively, were interchanged. Interestingly, both analogues turned out to be more potent against *T. brucei* than hit **1** (Fig. 1, see section 2.2), especially compound **3**, which was 3-fold more potent, albeit still too lipophilic (log P = 5.89).

In this regard, we next envisioned a series of modifications around the structure of compound **3**, aimed at improving drug likeness and deriving structure–activity relationships first against *T. brucei*, and then against *T. cruzi* and *L. infantum*. Because removal of the benzyl group at position 1 of compound **3** should lead to a significant decrease of both lipophilicity and molecular weight and, hence, to improved drug likeness, we planned the synthesis of the N_1-unsubstituted derivative **31** and its analogues resulting from ring contraction and ring expansion (**30** and **32**, respectively, Scheme 3), isomerization of the chlorine substituent from position 9 to position 8 (**33**, Scheme 3), and NH→O bioisosteric replacement (**39**, Scheme 5), using the corresponding nitriles as the immediate precursors. Moreover, to assess the relevance of the 4-aminomethylphenyl substituent at the B-ring, we decided to study the biological activity of the nitrile precursors (i.e. **26**–**29** and **38**, Schemes 3 and 5), as well as that of compounds **42** and **43**, in which the 4-aminomethylphenyl group at the B-ring of compound **39** was replaced by a 2-furyl- or 2-thienyl- substituent (Scheme 6). During the synthesis of the target tricyclic heterofused quinoline compounds some byproducts arising from opening of the A-ring were obtained (see below) and, eventually, converted into additional target compounds featuring cyano, hydroxy or amino groups at the side chain (i.e. **35**, **44**, **45**, **47**, **49** and **50**, Schemes 4, 6, and 7).

The synthesis of compound **2** was carried out by the four-step sequence depicted in Scheme 1. The multicomponent Povarov reaction between the known unsaturated lactam **4** as the activated olefin [45,46], and commercially available 4-chlorobenzaldehyde, **6**, and aniline **5**, bearing an *N*-Boc-protected aminomethyl side chain, under $Sc(OTf)_3$ catalysis in acetonitrile, followed by DDQ oxidation [47] of the resulting diastereomeric mixture of octahydrobenzonaphthyridines **7** afforded compound **8** in 47% overall yield, after silica gel column chromatography purification. *N*-Boc deprotection of **8**, followed by reduction of the resulting lactam **9** with $(EtO)_3SiH$ under $Zn(OAc)_2$ catalysis [48], and silica gel column chromatography purification afforded the target benzonaphthyridine **2**, in 29% overall yield for the last two steps (Scheme 1).

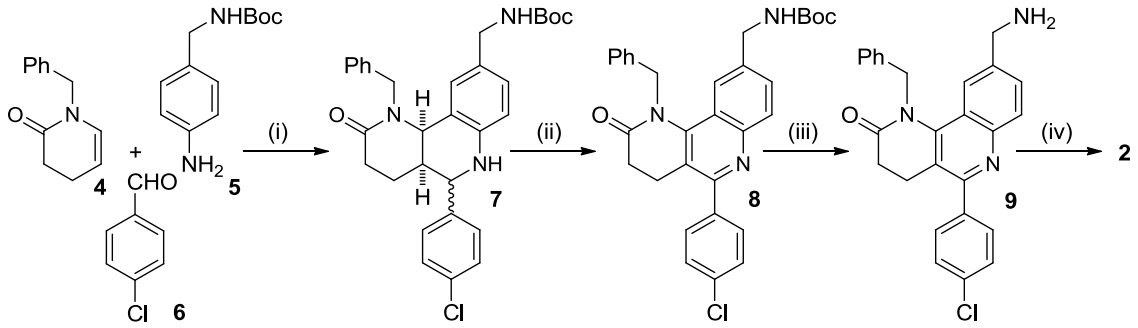

Scheme 1. Reagents and conditions: (i) **5**, **6**, $Sc(OTf)_3$, CH_3CN, rt, 5 min; then, **4**, CH_3CN, rt, 3 days; (ii) DDQ, $CHCl_3$, rt, overnight, 47% overall; (iii) 4M HCl/dioxane, rt, overnight, 44%; (iv) $(EtO)_3SiH$, $Zn(OAc)_2$, THF, rt, 30 min; then, **9**, THF, 65 ºC, 48 h, 66%.

The synthesis of compound **3** required only 3 steps, starting with a multicomponent Povarov reaction between the enamide **4**, 4-chloroaniline, **10**, and the aromatic aldehyde **11**, bearing a 4-cyano group as the precursor of the aminomethyl side chain. DDQ oxidation of the resulting diastereomeric mixture of octahydrobenzonaphthyridines **12**, followed by simultaneous $LiAlH_4$ reduction of the lactam and nitrile functionalities of compound **13** afforded the target benzonaphthyridine **3** in low overall yield, after silica gel column chromatography purification (Scheme 2).

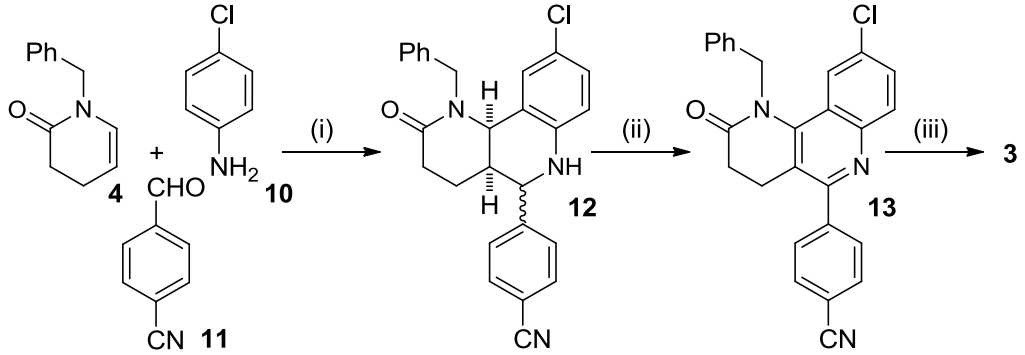

Scheme 2. Reagents and conditions: (i) **10**, **11**, $Sc(OTf)_3$, CH_3CN, rt, 5 min; then, **4**, CH_3CN, rt, 3 days; (ii) DDQ, $CHCl_3$, rt, overnight, 35% overall; (iii) $LiAlH_4$, THF, reflux, overnight, 22%.

For the synthesis of the N_1-debenzylated analogues **30**–**33** we used a 4-step protocol that involved an initial multicomponent Povarov reaction between chloroanilines **10** or **17**,

cyano aldehyde **11** and commercially available *N*-Boc-protected cyclic enamines **14**–**16**, followed by DDQ oxidation, *N*-Boc acidic deprotection, and final $LiAlH_4$ reduction of nitriles **26**–**29** (Scheme 3). After silica gel column chromatography purification, the target compounds **30**, **31**, **32**, and **33** were obtained in 20%, 41%, 22%, and 39% overall yield, respectively.

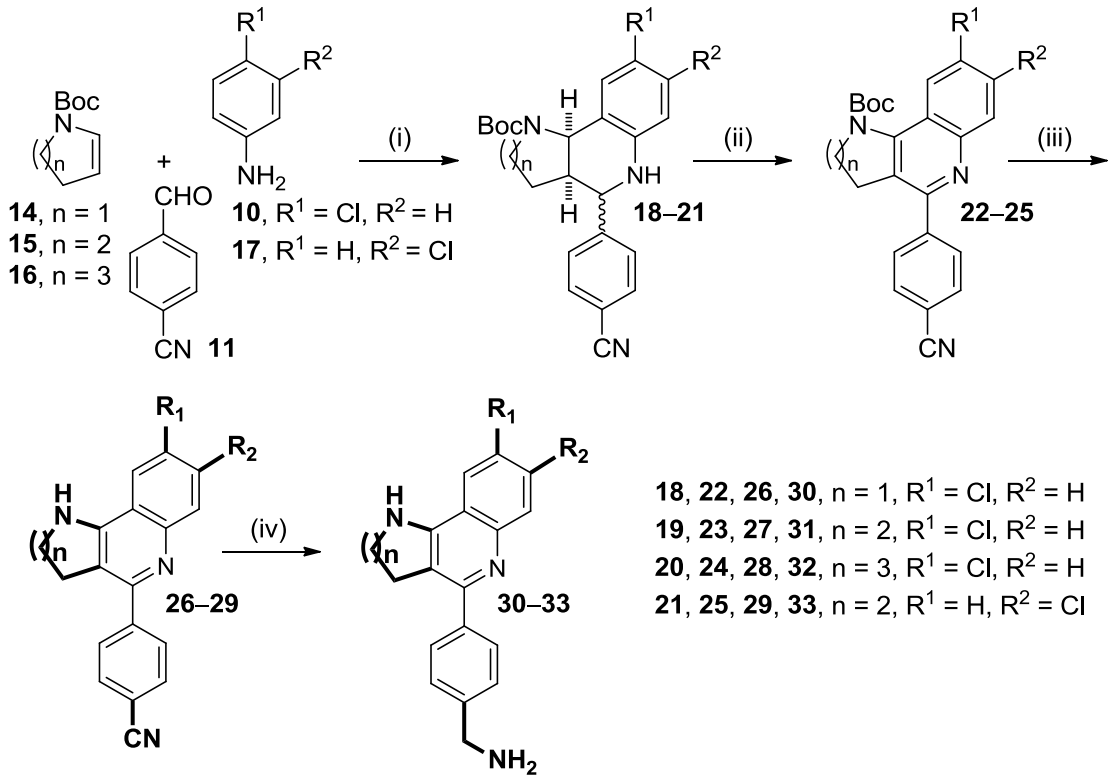

Scheme 3. Reagents and conditions: (i) **10** or **17**, **11**, $Sc(OTf)_3$, CH_3CN, rt, 5 min; then, **14**, **15** or **16**, CH_3CN, rt, 3 days; (ii) DDQ, $CHCl_3$, rt, overnight, 59% (**22**), 69% (**23**), 79% (**24**), and 62% (**25**) overall; (iii) 4M HCl/dioxane, rt, overnight, 46% (**26**), 68% (**27**), 51% (**28**), and 94% (**29**); (iv) $LiAlH_4$, THF, reflux, overnight, 74% (**30**), 87% (**31**), 55% (**32**), and 67% (**33**).

Of note, during the synthesis of compound **25**, a significant amount (17% yield) of ring-open by-product **34** (Scheme 4) was also formed. This compound was subjected to the standard acidic conditions for *N*-Boc deprotection, affording amine **35** in 90% yield (Scheme 4).

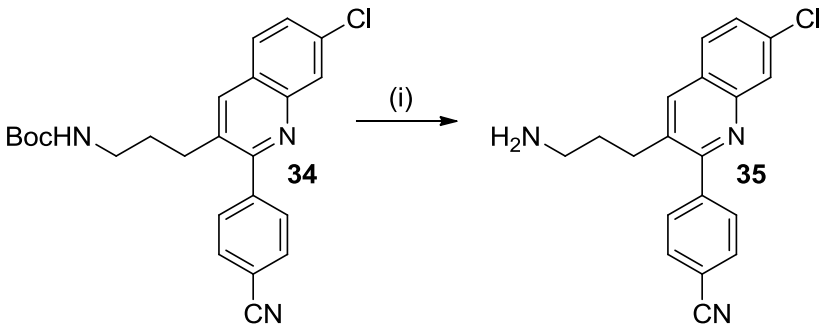

Scheme 4. Reagents and conditions: (i) 4M HCl/dioxane, rt, overnight, 90%.

The synthesis of pyranoquinoline **39** was envisaged through a three-step sequence, analogous to that used for compound **3**, but starting from 3,4-dihydro-2*H*-pyran, **36**, as the activated olefin for the Povarov reaction instead of the enamide **4** (Scheme 5).

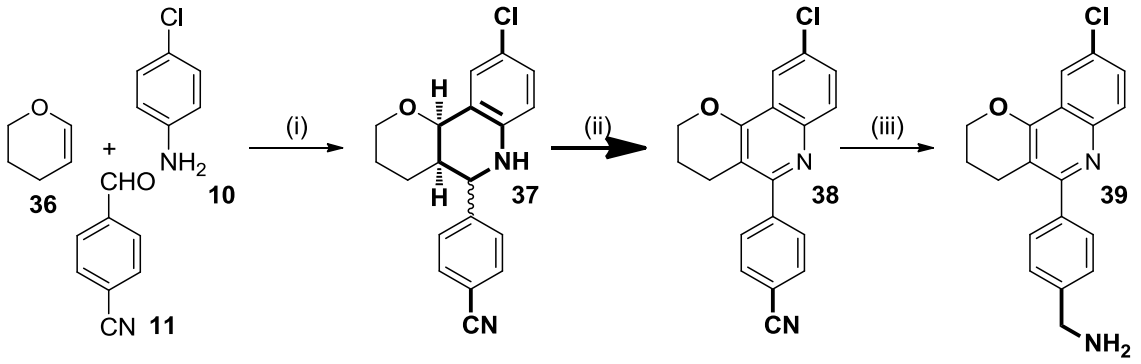

Scheme 5. Reagents and conditions: (i) **10**, **11**, $Sc(OTf)_3$, CH_3CN, rt, 5 min; then, **36**, CH_3CN, rt, 3 days, 95% (1:1 diastereomeric mixture); (ii) DDQ, $CHCl_3$, rt, overnight, 41%; (iii) $LiAlH_4$, THF, reflux, overnight, 59%.

Because we wanted to assess the influence on anti-protozoan activity of the degree of oxidation of the B-ring of the heterofused quinoline compounds, at this point we decided to isolate the tetrahydroquinoline compound resulting from the Povarov reaction, before performing the oxidation to the final quinoline derivative. Thus, after the reaction between the cyclic enol ether **36**, the aniline **10** and the aldehyde **11**, the crude product was purified by silica gel column chromatography to obtain a 1:1 diastereomeric mixture **37** in 95% yield. After a second column chromatography from this material, a sample of the all-*cis*-diastereoisomer, all-*cis*-**37**, was isolated to be subjected to biological evaluation (see below). Eventually, the pyranoquinoline **39** was

obtained in 23% overall yield by DDQ oxidation of the diastereomeric mixture **37** to the quinoline derivative **38**, followed by $LiAlH_4$ reduction of the nitrile to an aminomethyl group (Scheme 5).

Analogously to the synthesis of **39**, starting from the cyclic enol ether **36** and aniline **10** but changing now the aromatic aldehyde to furan-2-carboxaldehyde and thiophene-2-carboxaldehyde, **40**, and **41**, respectively, the target pyranoquinoline derivatives **42** and **43**, substituted at position 5 with a 2-furyl or 2-thienyl group instead of an aminomethylphenyl substituent, were obtained in 27% and 40% yield, respectively, together with significant amounts of the ring-open byproducts **44** (30% yield) and **45** (24% yield), respectively (Scheme 6).

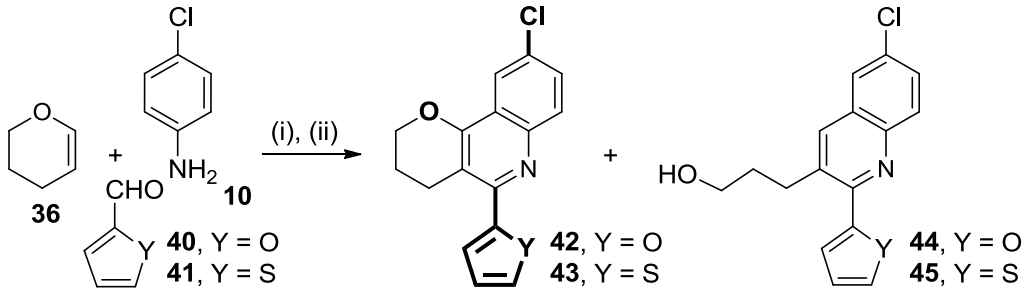

Scheme 6. Reagents and conditions: (i) **10**, **40** or **41**, $Sc(OTf)_3$, CH_3CN, rt, 5 min; then, **36**, CH_3CN, 50 ºC (for **42**) or 80 ºC (for **43**), 3 days; (ii) DDQ, $CHCl_3$, rt, overnight, 27% (**42**) and 30% (**44**), 40% (**43**) and 24% (**45**) overall.

Finally, the Mitsunobu reaction of compound **45** with *N*-(*tert*-butyldimethylsilyloxy)-4-methylbenzenesulfonamide followed by treatment with CsF in acetonitrile afforded nitrile **47** in 84% overall yield, after silica gel column chromatography purification. Moreover, alcohol **45** was converted *via* mesylate into the corresponding amines **49** and **50** in 31% and 16% overall yield, respectively (Scheme 7).

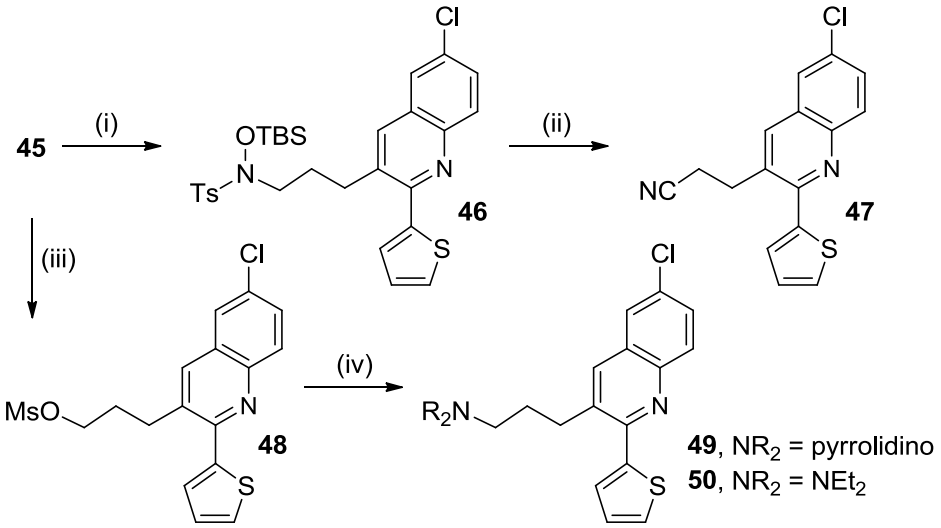

Scheme 7. Reagents and conditions: (i) *N*-(*tert*-butyldimethylsilyloxy)-4-methylbenzenesulfonamide, PPh_3, DEAD, toluene, THF, rt, 5 min; (ii) CsF, CH_3CN, 60 ºC, 2.5 h, 84% overall; (iii) MsCl, Et_3N, 0 ºC, 30 min; (iv) pyrrolidine or Et_2NH, K_2CO_3, DMF, 85 ºC, overnight, 31% (**49**), 16% (**50**) overall.

All the compounds to be subjected to biological evaluation, except **37**, were transformed into the corresponding hydrochloride or dihydrochloride salts, and were chemically characterized through IR, ^1H and ^{13}C NMR spectra, HRMS and HPLC purity analysis and elemental analysis.

2.2. Biological profiling of the novel heterofused quinoline compounds and ring-open analogues

2.2.1. In vitro activity against T. brucei

As previously mentioned, we first evaluated the activity of **1**, a compound that we had developed as an inhibitor of AChE [40], and the novel heterofused quinoline and ring-open analogues *in vitro* against cultured bloodstream forms of *T. brucei*. We also investigated their brain permeability to assess their potential usefulness in late-stage HAT. To determine potential toxic effects, their cytotoxicity against rat skeletal myoblast L6 cells and AChE inhibitory activity, which might result in cholinergic side-effects, were also evaluated.

Table 1

Trypanocidal (*T. brucei*), cytotoxic and anticholinesterase activity and BBB permeability of the novel heterofused quinolines and related compounds.[a]

Compd	*T. brucei* IC_{50} (μM)	*T. brucei* IC_{90} (μM)	L6 cells IC_{50} (μM)	SI[b]	P_e (10^{-6} cm s^{-1})[c] (prediction)	*Ee*AChE IC_{50} (μM)
1	3.33 ± 0.18	4.39 ± 0.04	7.08 ± 0.11	2.1	[d]	0.15 ± 0.01[e]
2	2.10 ± 0.07	2.90 ± 0.02	7.99 ± 0.25	3.8	[d]	1.05 ± 0.18
3	1.00 ± 0.03	1.19 ± 0.02	6.78 ± 1.26	6.8	7.4 ± 0.2 (CNS+)	3.67 ± 0.55
26	>30	>30	[d]	[d]	6.8 ± 0.3 (CNS+)	1.19 ± 0.15
27	6.07 ± 0.54	10.5 ± 0.2	38.8 ± 1.7	6.4	14.3 ± 0.1 (CNS+)	1.13 ± 0.17
28	17.3 ± 2.1	28.6 ± 6.7	[d]	[d]	20.0 ± 1.1 (CNS+)	2.20 ± 0.30
29	>30	>30	[d]	[d]	16.2 ± 0.1 (CNS+)	3.27 ± 0.43
30	0.92 ± 0.05	1.57 ± 0.03	2.54 ± 0.92	2.8	7.4 ± 2.6 (CNS+)	0.87 ± 0.08
31	2.44 ± 0.13	3.48 ± 0.05	8.92 ± 0.25	3.7	4.6 ± 0.2 (CNS±)	0.97 ± 0.02
32	2.33 ± 0.12	3.35 ± 0.05	7.02 ± 0.27	3.0	11.6 ± 0.2 (CNS+)	1.20 ± 0.13
33	1.25 ± 0.05	2.12 ± 0.02	3.07 ± 0.66	2.5	4.0 ± 1.0 (CNS±)	0.44 ± 0.04
35	4.16 ± 0.07	5.61 ± 0.05	20.4 ± 0.4	4.9	18.3 ± 0.6 (CNS+)	[d]
37	>30	>30	[d]	[d]	7.0 ± 0.7 (CNS+)	[d]
38	9.61 ± 0.27	13.7 ± 1.0	36.3 ± 8.1	3.8	29.7 ± 3.8 (CNS+)	2.70 ± 0.45
39	1.46 ± 0.02	1.77 ± 0.02	7.00 ± 0.19	4.8	15.5 ± 1.8 (CNS+)	>30[f]
42	21.7 ± 1.2	29.3 ± 0.5	[d]	[d]	3.5 ± 0.4 (CNS±)	16.3 ± 1.5
43	18.0 ± 0.4	27.6 ± 1.1	[d]	[d]	14.4 ± 1.6 (CNS+)	9.39 ± 0.82
44	35.7 ± 1.8	70.6 ± 1.5	[d]	[d]	10.3 ± 1.5 (CNS+)	[d]
45	28.0 ± 0.7	42.9 ± 1.5	[d]	[d]	28.4 ± 1.2 (CNS+)	[d]
47	>30	>30	[d]	[d]	17.9 ± 1.1 (CNS+)	[d]
49	3.56 ± 0.17	4.93 ± 0.17	9.44 ± 0.14	2.7	12.9 ± 0.1 (CNS+)	≈30[g]
50	6.33 ± 0.94	12.6 ± 0.9	14.7 ± 2.3	2.3	20.9 ± 0.5 (CNS+)	[d]

[a] *In vitro* activity against bloodstream form of *T. brucei* (pH 7.4), rat myoblast L6 cells, and *Electrophorus electricus* AChE, expressed at the concentration that inhibited growth or enzyme activity by 50% (IC_{50}) and 90% (IC_{90}, for *T. brucei*). Data are the mean of triplicate experiments ± SEM.

[b] SI: selectivity index is the ratio of cytotoxic to trypanocidal IC_{50} values.

[c] Permeability values from the PAMPA-BBB assay. Values are expressed as the mean ± SD of three independent experiments.

[d] Not determined.

[e] Taken from ref. [40], involving the same experimental conditions.

[f] 45% Inhibition at 30 μM (the IC_{50} could not be determined).

[g] 54% Inhibition at 30 μM (the IC_{50} could not be determined).

All the novel heterofused quinoline derivatives featuring a protonatable aminomethylphenyl group at the B-ring, including the benzo[*h*][1,6]naphthyridines **2**, **3**, **31** and **33**, the pyrrolo[3,2-*c*]quinoline **30**, the azepino[3,2-*c*]quinoline **32**, and the pyrano[3,2-*c*]quinoline **39**, were found to be 1.5–4-fold more potent than hit **1**, with IC_{50} and IC_{90} values in the range 0.92–2.44 μM and 1.19–3.48 μM, respectively (Table 1). In contrast, their nitrile precursors **26**–**29**, **37**, and **38**, as well as the 5-(2-furyl)- and 5-(2-thienyl)-substituted pyrano[3,2-*c*]quinolines **42** and **43**, all of them bearing a neutral group at the B-ring, were clearly less potent. This highlights the relevance for trypanosomal activity of the presence of a protonatable group at the side chain of the substituent at the B-ring of the tricyclic heterofused quinoline derivatives.

Within the most potent tricyclic heterofused quinoline derivatives, the best substitution pattern for activity against *T. brucei* seems to involve i) Bn-N > O > NH at position 1 of the A-ring, with compound **3** being 1.5- and 2.4-fold more potent than **39** and **31**, respectively, ii) a five-membered A-ring, with compound **30** being 2.5-fold more potent than **31** and **32**, bearing a six- and seven-membered A ring, respectively, and iii) the presence of the chlorine atom at position *meta* relative to the quinoline nitrogen atom, with compound **33** being 2-fold more potent than **31**.

As in the tricyclic heterofused quinoline derivatives, the presence of a protonatable nitrogen atom at the side chain of ring-open quinoline analogues seems to be play a role in the activity of these compounds against *T. brucei*, with amines **35**, **49**, and **50** exhibiting IC_{50} values around 5 μM (Table 1), whereas compounds **44**, **45**, and **47**, with neutral hydroxy or cyano groups at the side chain were clearly less potent (IC_{50} > 25 μM).

2.2.2. Brain permeation

Brain penetration is a desirable property for novel drugs against HAT, as it will make them effective against the late-stage disease, when parasites have invaded the CNS. Thus, the brain permeability of the novel compounds was evaluated *in vitro* through the widely used PAMPA-BBB method [49], which is based on the use of a porcine brain

lipid extract as an artificial BBB model. The novel compounds had *in vitro* permeabilities (P_e) clearly above the threshold established for a high BBB permeation, i.e. CNS+ with *Pe* (10^{-6} cm s^{-1}) > 5.25, with the exceptions of compounds **31**, **33**, and **42**, for which an uncertain BBB permeation was predicted (Table 1).

2.2.3. Cytotoxicity and acetylcholinesterase inhibitory activity

To assess potential toxic effects of the novel derivatives, all the compounds with IC_{50} values against *T. brucei* below 10 μM were subjected to cytotoxicity studies using rat myoblast L6 cells. All the tested compounds were selective for *T. brucei* vs mammalian cells, being more selective than the hit **1**, although with rather low selectivity indices, i.e. in the range 2.1–6.8 (Table 1).

Because the hit **1** was developed as an AChE inhibitor with potential application against Alzheimer's disease, this kind of activity might result in unwanted cholinergic side effects if the novel compounds were used as anti-protozoan agents. We therefore evaluated their AChE inhibitory activity using *Electrophorus electricus* AChE (*Ee*AChE), a widely used and affordable enzyme source for screening this activity. All the structural modifications carried out around the structure of the hit **1** led to a decrease in *Ee*AChE inhibitory activity (3–110-fold). However, despite their decreased AChE inhibitory activity relative to hit **1**, most tested compounds were more potent against *Ee*AChE than against *T. brucei*. Only the benzonaphthyridine **3**, the pyranoquinoline **39** and the ring-open quinoline derivative **49** turned out to be more potent against *T. brucei* than against *Ee*AChE (4-, >20- and ~8-fold, respectively).

Of note, hit **1** is 6-fold less potent against human recombinant AChE (hAChE) than against *Ee*AChE (IC_{50} = 0.15 μM compared with IC_{50} = 0.94 μM) [40]. Even though this might also be the case for the novel compounds reported here, future lead optimization should focus on decreasing AChE inhibitory activity and increasing selectivity indices.

2.2.4. In vitro activity against T. cruzi and L. infantum

The occurrence of common metabolic pathways in trypanosomatid parasites makes it potentially feasible to develop anti-protozoan agents endowed with a multi-trypanosomatid profile [14,50]. Thus, after having confirmed the significant activity against *T. brucei* of all the novel target heterofused quinoline derivatives and some of the ring-open analogues and assessed their brain permeation, cytotoxicity and AChE

inhibitory activity, we undertook the evaluation of all the novel compounds against epimastigote forms of *T. cruzi* (strain MHOM/ES/2203/BCN590 (Tcl)) and promastigote forms of *L. infantum* (strain MCAN/ES/92/BCN722), using benznidazole and potassium antimony (III) tartrate hydrate as reference compounds.

Most of the tested compounds exhibited activity against *T. cruzi*, albeit with two-digit micromolar IC_{50} values (Table 2). Interestingly, there was a similar SAR profile as had been found with *T. brucei*. First, isomerization of the chlorine and aminomethyl substituents from compound **2** to **3** results in increased potency against *T. cruzi* (4-fold). Also, higher potencies were observed for those tricyclic heterofused quinoline analogues bearing a protonatable 4-(aminomethyl)phenyl group at the B-ring, relative to those bearing a 4-cyanophenyl, 2-furyl, or 2-thienyl groups. Thus, amines **30**, **31**, **32**, and **39** were 2–6-fold more potent than their nitrile precursors **26**, **27**, **28**, and **38**, respectively, and amine **39** was also 3- and 10-fold more potent than the 5-(2-furyl)- and 5-(2-thienyl)-substituted derivatives **42** and **43**, respectively. The sole exception was amine **33**, which turned out to be 2-fold less potent than its nitrile precursor **29**. Also, within the aminomethylphenyl-substituted analogues, the order of potencies related to the subtitution at position 1 of the A-ring was: Bn-N > O > NH, with the N_1-benzylated benzonapththyridine **3** being 3- and 5-fold more potent than pyranoquinoline **39** and N_1-unsubstituted benzonapththyridine **31**. Regarding the size of the A-ring, again the presence of a five- or a seven-membered ring A led to increased potency relative to the derivatives with a six-membered A-ring, with the pyrroloquinoline **30** and the azepinoquinoline **32** being 1.5-fold more potent than the benzonaphthyridine **31**. For this activity, unlike against *T. brucei*, a higher potency seems to arise from the presence of a chlorine atom at position *para* relative to the quinoline nitrogen atom, with compound **31** being 1.5-fold more potent than **33**. Overall, the most potent analogue of the series against *T. cruzi* was compound **3**, which exhibited an IC_{50} value of 9.47 μM, 4-fold more potent than the reference compound benznidazole. In addition, six other derivatives turned out to be slighly more potent or equipotent to benznidazole, with IC_{50} values around 30 μM.

Table 2

In vitro activity of the novel heterofused quinolines and related compounds against epimastigotes of *Trypanosoma cruzi* and promastigotes of *Leishmania infantum*.[a]

Compd	*T. cruzi* IC_{50} (μM)	*L. infantum* IC_{50} (μM)
1		
2	38.1 ± 9.46	8.11 ± 1.9
3	9.47 ± 2.5	31.08 ± 2.9
26	>150	>200
27	147 ± 19.1	15.3 ± 3.6
28	64.6 ± 12.5	13.7 ± 2.2
29	39.4 ± 0.19	19.0 ± 3.0
30	37.3 ± 11.0	6.55 ± 1.4
31	50.5 ± 14.3	11.6 ± 2.5
32	32.4 ± 0.61	4.85 ± 0.7
33	76.1 ± 3.17	13.0 ± 0.6
35	78.8 ± 1.69	16.2 ± 4.0
37	676 ± 37.0	>200
38	178 ± 92.4	23.5 ± 2.4
39	29.2 ± 3.71	6.14 ± 0.2
42	76.1 ± 7.84	38.4 ± 21.6
43	>250	51.4 ± 2.3
44	29.3 ± 12.0	19.3 ± 11.3
45	51.7 ± 19.4	37.3 ± 2.3
47	51.7 ± 5.07	23.3 ± 5.9
49	35.2 ± 12.6	13.1 ± 5.8
50	77.6 ± 11.2	13.6 ± 1.5
Benznidazole	36.2 ± 5.11	[b]
Sb (III)[c]	[b]	24.3 ± 1.7

[a] *In vitro* activity against epimastigote form of *T. cruzi* and promastigote form of *L. infantum*, expressed at the concentration that inhibited growth by 50% (IC_{50}). Data are the mean ± SD of duplicate experiments performed at least twice.

[b] Not determined.

[c] Potassium antimony (III) tartrate hydrate.

All of the novel compounds turned out to be leishmanicidal agents, with IC_{50} values in the low micromolar range in most cases, being more potent (up to 5-fold) than the reference compound potassium antimony (III) tartrate hydrate (Table 2). Thus, these compounds were more active against *L. infantum* than against *T. cruzi*, with the sole exception of compound **3**, the most potent antichagasic derivative of the series. Some of the SARs of the leishmanicidal activity of the novel tricyclic heterofused quinoline analogues were very similar to those found for anti-trypanosome activities, with the best substitution pattern involving the presence of: i) a protonatable 4-(aminomethyl)phenyl group at the B-ring, with amines **30**, **31**, **32**, **33**, and **39** being 1.5 to >31-fold more potent than their nitrile precursors **26**, **27**, **28**, **29**, and **38**, respectively, and amine **39** being 6- and 8-fold more potent than the 5-(2-furyl)- and 5-(2-thienyl)-substituted derivatives **42** and **43**, respectively; ii) a five- or a seven-membered A-ring, with the pyrroloquinoline **30** and the azepinoquinoline **32** being approximately 2-fold more potent than the benzonaphthyridine **31**, bearing a six-membered ring A; and iii) an aromatic B-ring, with compound **38** being >9-fold more potent than the saturated analogue **37**. For this activity, the presence of an oxygen atom a position 1 of the A-ring led to increased potency relative to an NH group, with compound **39** being 2-fold more potent than **31**. However, a reverse SAR trend relative to those found for the anti-trypanosome activities was observed regarding the presence of a Bn-N group at position 1 of the A-ring and the isomerization of the chlorine and aminomethyl substituents. Thus, the presence of a Bn-N group at position 1 of the A-ring was detrimental for leishmanicidal activity, with compound **3** being 3- and 5-fold less potent than the NH- and O-substituted counterparts **31** and **39**, respectively, whereas the interchange of the chlorine and aminomethyl substituents from compound **2** to **3** resulted in decreased potency against *L. infantum* (4-fold). The position of the chlorine substituent at the C-ring had no influence on the leishmanicidal activity of the novel compounds. Of note, as found when measuring *T. brucei* activities, the three ring-open analogues featuring a protonatable amino group at the side chain, i.e. **35**, **49**, and **50**, exhibited significant leishmanicidal activity, with IC_{50} values around 15 μM (Table 2).

The most potent analogues of the series against *L. infantum* were benzonaphthyridines **2**, **30**, and **32**, and pyranoquinoline **39**, with IC_{50} values in the range 5–8 μM.

3. Conclusion

We have synthesized a series of tricyclic heterofused quinolines, namely benzo[*h*][1,6]naphthyridines, pyrrolo[3,2-*c*]quinolines, azepino[3,2-*c*]quinolines, and pyrano[3,2-*c*]quinolines, through 2–4-step synthetic sequences that involve as the key step an initial Povarov multicomponent reaction between a cyclic enamide or enol ether as an activated olefin and a properly substituted aniline and aromatic aldehyde. The novel compounds have been designed from benzonaphthyridine **1**, a submicromolar inhibitor of AChE previously developed in our group that has been found to display a significant *in vitro* activity against *T. brucei*. Initial structural modifications around hit **1**, including *N*-dealkylation of the side chain at position 9 and isomerization by interchange of the chlorine atom at the *para* position of the 5-phenyl group and the aminomethyl substituent at position 9, have led to benzonaphthyridine **3**, which has turned out to be 3-fold more potent than hit **1** against *T. brucei*. The structure of compound **3** has been further modified by N_1-debenzylation, A-ring contraction and expansion, bioisosteric NH→O replacement at position 1, and substitution of the 5-(4-aminomethyl)phenyl group by 5-(2-furyl) and 5-(2-thienyl). During the synthesis of the target tricyclic compounds, some quinoline derivatives with a side chain at position 3, arising from opening of the A-ring, were obtained. To further expand the SAR studies, the structure of these ring-open derivatives was subsequently modified by introduction of a protonatable amino group or a neutral cyano group at the end of the side chain.

Trypanosomatid parasites responsible for HAT, Chagas disease and visceral leishmaniasis seem to share common metabolic pathways [14,50], thereby being potentially amenable to treatment by common drugs. Consistent with this, we have found some common SAR trends related to the activities of the novel tricyclic heterofused quinoline analogues against *T. brucei*, *T. cruzi* and *L. infantum*, with several of these compounds being moderately potent against two or three of these parasites. Thus, the presence of an oxidized B-ring featuring a protonatable 4-(aminomethyl)phenyl group and the bioisosteric NH→O replacement at position 1 led to higher potencies against the three parasites. Benzonaphthyridines **2**, **30** and **32**, and pyranoquinoline **39** exhibit an interesting multi-trypanosomatid profile, with single digit micromolar IC_{50} values against *T. brucei* and *L. infantum* and IC_{50} around 30 μM against *T. cruzi*, whereas benzonaphthyridine **3** exhibits single digit micromolar IC_{50} values against *T. brucei* and *T. cruzi* and IC_{50} around 30 μM against *L. infantum*. Interestingly, all of these multi-trypanosomatid compounds have been predicted to be

able to cross the BBB, which is of utmost importance for the treatment of late-stage HAT, and have better drug-like properties than hit **1**, both in terms of lower lipophilicity and molecular weight. A significant AChE inhibitory activity in most of these compounds, albeit lower than that of hit **1**, and significant toxicity to rat L6 cells are their main drawbacks, which should be addressed in further lead optimization. To this end, the dual trypanocidal and leishmanicidal pyranoquinoline **39**, which displays the lowest AChE inhibitory activity, and hence, the lowest potential for cholinergic side effects, is likely to be the best starting point.

4. Experimental part

4.1. Chemistry. General methods.

Melting points were determined in open capillary tubes with a MFB 595010M Gallenkamp melting point apparatus. 400 MHz ^{1}H/100.6 MHz ^{13}C NMR spectra were recorded on a Varian Mercury 400 spectrometer. The chemical shifts are reported in ppm (δ scale) relative to solvent signals (CD_3OD at 3.31 and 49.0 ppm in the ^{1}H and ^{13}C NMR spectra, respectively; $CDCl_3$ at 7.26 and 77.00 ppm in the ^{1}H and ^{13}C NMR spectra, respectively), and coupling constants are reported in Hertz (Hz). Assignments given for the NMR spectra of the new compounds have been carried out by comparison with the NMR data of **3**, **9**, **28**, **37**, **42**, **43**, **44**, **45**, **47**, and **50**, which in turn, were assigned on the basis of DEPT, COSY ^{1}H/^{1}H (standard procedures), and COSY ^{1}H/^{13}C (gHSQC or gHMBC sequences) experiments. IR spectra were run on a Perkin-Elmer Spectrum RX I or on a Thermo Nicolet Nexus spectrophotometer. Absorption values are expressed as wavenumbers (cm^{-1}); only significant absorption bands are given. Column chromatography was performed on silica gel 60 AC.C (35–70 mesh, SDS, ref 2000027). Thin-layer chromatography was performed with aluminum-backed sheets with silica gel 60 F_{254} (Merck, ref 1.05554), and spots were visualized with UV light and 1% aqueous solution of $KMnO_4$. NMR spectra of all of the new compounds were performed at the Centres Científics i Tecnològics of the University of Barcelona (CCiTUB), while elemental analyses and high resolution mass spectra were carried out at the Mycroanalysis Service of the IIQAB (CSIC, Barcelona, Spain) with a Carlo Erba model 1106 analyzer, and at the CCiTUB with a LC/MSD TOF Agilent Technologies spectrometer, respectively. The HPLC measurements were performed using a HPLC Waters Alliance HT apparatus comprising a pump (Edwards RV12) with degasser, an autosampler, a diode array detector and a column as specified below. The reverse phase

HPLC determinations were carried out on a YMC-Pack ODS-AQ column (50×4.6 mm, D S. 3 μm, 12 nm). Solvent A: water with 0.1% formic acid; Solvent B: acetonitrile with 0.1% formic acid. Gradient: 5% of B to 100% of B within 3.5 min. Flux: 1.6 mL/min at 50 ºC. The analytical samples of all of the compounds that were subjected to pharmacological evaluation were dried at 65 ºC / 2 Torr for at least 2 days (standard conditions) and possess a purity ≥95% as indicated by their elemental analyses and/or HPLC measurements.

*4.1.1. 1-Benzyl-9-(tert-butoxycarbonylaminomethyl)-5-(4-chlorophenyl)-1,2,3,4-tetrahydro-2-oxobenzo[h][1,6]naphthyridine **8***

To a stirred solution of *p*-chlorobenzaldehyde, **6** (1.16 g, 8.25 mmol) and aniline **5** (1.83 g, 8.23 mmol) in anhydrous CH_3CN (30 mL), 4 Å molecular sieves and $Sc(OTf)_3$ (0.81 g, 1.65 mmol) were added. The mixture was stirred at room temperature under argon atmosphere for 5 min and then treated with a solution of enamine **4** (1.50 g, 8.01 mmol) in anhydrous CH_3CN (16 mL). The resulting suspension was stirred at room temperature under argon atmosphere for 3 days. Then, the resulting mixture was diluted with sat. aq. $NaHCO_3$ (150 mL) and extracted with EtOAc (3 × 200 mL). The combined organic extracts were dried over anhydrous Na_2SO_4 and evaporated under reduced pressure to give a solid residue (4.71 g), mainly consisting of a diastereomeric mixture of octahydrobenzonaphthyridines **7**, which was used in the next step without further purification.

To a solution of crude diastereomeric mixture **7** (4.58 g of a crude of 4.71 g) in anhydrous $CHCl_3$ (150 mL), DDQ (4.85 g, 21.4 mmol) was added. The reaction mixture was stirred at room temperature under argon atmosphere overnight, diluted with CH_2Cl_2 (150 mL) and washed with sat. aq. $NaHCO_3$ (3 × 250 mL). The combined organic extracts were dried over anhydrous Na_2SO_4 and evaporated under reduced pressure to give a solid residue (5.33 g), which was purified through column chromatography (35–70 μm silica gel, hexane/EtOAc mixtures, gradient elution). On elution with hexane/EtOAc 80:20, compound **8** (1.94 g, 47% yield) was isolated as a white solid; R_f 0.83 (hexane/EtOAc 1:1).

A solution of **8** (30 mg, 0.06 mmol) in CH_2Cl_2 (5 mL) was filtered through a 0.2 μm PTFE filter and evaporated at reduced pressure. The solid was washed with pentane (3 × 5 mL) to give, after drying under standard conditions, the analytical sample of **8** (27

mg): mp 90–91 °C; IR (ATR) *v* 3347 (NH st), 1691 (C=O, Ar–C–C and Ar–C–N st) cm^{-1}; ^1H NMR (400 MHz, $CDCl_3$) δ 1.47 [s, 9H, $C(CH_3)_3$], 2.61 (t, *J*=6.8 Hz, 2H, 4-H_2), 2.90 (t, *J*=6.8 Hz, 2H, 3-H_2), 4.36 (d, *J*=6.0 Hz, 2H, 9-C*H*$_2$-NH), 4.96 (br s, 1H, 9-CH_2-N*H*), 5.33 (s, 2H, 1-C*H*$_2$-Ar), 7.12 [dd, *J*=8.0 Hz, *J'*=1.6 Hz, 2H, 1-CH_2-Ar-C2(6)-*H*], 7.20–7.29 [complex signal, 3H, 1-CH_2-Ar-C3(5)-*H*, 1-CH_2-Ar-C4-*H*], 7.46 [dm, *J*=8.8 Hz, 2H, 5-Ar-C3(5)-*H*], 7.53 [dm, *J*=8.8 Hz, 2H, 5-Ar-C2(6)-*H*], 7.61 (dd, *J*=8.8 Hz, *J'*=1.6 Hz, 1H, 8-H), 7.77 (br s, 1H, 10-H), 8.11 (d, *J*=8.8 Hz, 1H, 7-H); ^{13}C NMR (100.6 MHz, $CDCl_3$) δ 23.5 (CH_2, C3), 28.4 [3CH_3, C(*C*H_3)$_3$], 32.7 (CH_2, C4), 44.5 (CH_2, 9-CH_2-NH), 52.2 (CH_2, 1-*C*H_2-Ar), 79.9 [C, *C*$(CH_3)_3$], 119.9 (C, C10a), 120.8 (CH), 127.3 (CH), 127.5 (CH), 128.5 (CH), 128.6 (CH), 130.5 (CH) (Ar-CH), 121.7 (C, C4a), 129.2 (C, C9), 135.1 (C, 1-CH_2-Ar-*C*1), 137.4 (C), 137.5 (C) (5-Ar-*C*1, 5-Ar-*C*4), 146.8 (C, C6a), 147.7 (C, C5), 155.9 (C), 156.6 (C) (C10b, NCOO), 172.8 (C, C2); HRMS (ESI), calcd for [$C_{31}H_{30}{}^{35}ClN_3O_3 + H^+$] 528.2048, found 528.2045.

4.1.2. N-{1-Benzyl-5-(4-chlorophenyl)-1,2,3,4-tetrahydro-2-oxobenzo[h][1,6]naphthyridin-9-yl}methanamine ***9***

Compound **8** (1.94 g, 3.67 mmol) was dissolved in 4M HCl/dioxane solution (24 mL) at 0 ºC. The mixture was stirred at room temperature overnight and concentrated *in vacuo*. The solid residue was diluted in water (20 mL), treated with 1N NaOH (20 mL), and the aqueous phase was extracted with a 10% MeOH/$CHCl_3$ mixture (3 × 50 mL). The combined organic extracts were dried over anhydrous Na_2SO_4 and evaporated at reduced pressure to give a crude product (1.42 g), which was purified through column chromatography (35–70 μm silica gel, EtOAc/MeOH/50% aq. NH_4OH, gradient elution). On elution with EtOAc/MeOH/50% aq. NH_4OH 98.8:1:0.2 to 94.8:5:0.2, amine **9** (690 mg, 44% yield) was isolated as a yellow solid; R_f 0.78 (CH_2Cl_2/MeOH/50% aq. NH_4OH 9:1:0.05).

A solution of **9** (130 mg, 0.30 mmol) in CH_2Cl_2 (5 mL) was filtered through a 0.2 μm PTFE filter and treated with a methanolic solution of HCl (0.53 N, 1.58 mL, 0.84 mmol). The resulting solution was evaporated at reduced pressure and the solid was washed with pentane (3 × 5 mL) to give, after drying under standard conditions, **9**·2HCl (119 mg) as a yellow solid: mp 218–220 ºC; IR (ATR) *v* 3500–2500 (max at 3386, 2919, 2850, 2610, $^+$NH and CH st), 1704 (C=O st), 1609, 1590, 1580, 1520, 1503 (C=O, Ar–C–C and Ar–C–N st) cm^{-1}; ^1H NMR (400 MHz, CD_3OD) δ 2.83 (br t, *J*=6.8 Hz, 2H, 3-H_2), 3.09 (br t, *J*=6.8 Hz, 2H, 4-H_2), 4.28 (s, 2H, 9-C*H*$_2$-NH_2), 4.88 (s, $^+$NH,

$^{+}NH_3$), 5.57 (s, 2H, 1-CH_2-Ar), 7.24–7.36 (complex signal, 5H, 1-CH_2-Ar-*H*), 7.75 [br d, *J*=8.0 Hz, 2H, 5-Ar-C3(5)-H], 7.82 [br d, *J*=8.0 Hz, 2H, 5-Ar-C2(6)-H], 8.19 (br d, *J*=8.8 Hz, 1H, 8-H), 8.29 (d, *J*=8.8 Hz, 1H, 7-H), 8.43 (br s, 1H, 10-H); ^{13}C NMR (100.6 MHz, CD_3OD) δ 23.2 (CH_2, C4), 31.8 (CH_2, C3), 43.9 (CH_2, 9-CH_2-NH_2), 54.7 (CH_2, 1-*C*H_2-Ar), 121.1 (C, C10a), 123.2 (CH, C7), 124.7 (C, C4a), 127.3 (CH, C10), 128.4 [2CH, 1-CH_2-Ar-*C*2(6)], 128.8 (CH, 1-CH_2-Ar-*C*4), 129.9 [2CH, 1-CH_2-Ar-*C*3(5)], 130.7 [2CH, 5-Ar-*C*3(5)], 130.8 (C, 5-Ar-*C*1), 132.5 [2CH, 5-Ar-*C*2(6)], 134.9 (C, C9), 135.6 (CH, C8), 138.6 (C, 1-CH_2-Ar-*C*1), 139.4 (C, 5-Ar-*C*4), 140.7 (C, C6a), 154.3 (C, C5), 156.9 (C, C10b), 173.3 (C, C2); HRMS (ESI), calcd for [$C_{26}H_{22}{}^{35}ClN_3O$ + H^+] 428.1524, found 428.1522.

*4.1.3. N-{1-Benzyl-5-(4-chlorophenyl)-1,2,3,4-tetrahydrobenzo[h][1,6]naphthyridin-9-yl}methanamine **2***

To a suspension of $Zn(OAc)_2$ (49 mg, 0.27 mmol) in anhydrous THF (0.7 mL) $(EtO)_3SiH$ (0.10 mL, 89 mg, 0.54 mmol) was added. The mixture was stirred at room temperature for 30 min and then treated with a solution of amino lactam **9** (117 mg, 0.27 mmol) in anhydrous THF (2.1 mL). The reaction mixture was stirred at 65 ºC for 48 h in a sealed vessel. The resulting mixture was cooled to room temperature, poured onto 1N NaOH (5 mL), stirred for 10 min, and then extracted with EtOAc (3 × 15 mL). The combined organic extracts were dried over anhydrous Na_2SO_4 and concentrated under reduced pressure to give a solid (313 mg), which was purified through column chromatography (35–70 μm silica gel, CH_2Cl_2/MeOH/50% aq. NH_4OH mixtures, gradient elution). On elution with CH_2Cl_2/MeOH/50% aq. NH_4OH 98.5:1.5:0.2, amine **2** (74 mg, 66% yield) was isolated as a white solid; R_f 0.50 (CH_2Cl_2/MeOH/50% aq. NH_4OH 9:1:0.05).

A solution of **2** (54 mg, 0.13 mmol) in CH_2Cl_2 (5 mL) was filtered through a 0.2 μm PTFE filter and treated with a methanolic solution of HCl (0.53 N, 2.25 mL, 1.19 mmol). The resulting solution was evaporated at reduced pressure and the solid was washed with pentane (3 × 5 mL) to give, after drying under standard conditions, **2**·2HCl (54 mg) as a yellowish solid: mp 230–232 ºC; IR (ATR) *v* 3500–2500 (max at 3369, 2918, 2855, 2616, $^{+}$NH and CH st), 1633, 1595, 1578, 1560, 1518 (Ar–C–C and Ar–C–N st) cm^{-1}; ^{1}H NMR (400 MHz, CD_3OD) δ 2.05 (m, 2H, 3-H_2), 2.75 (t, *J*=6.0 Hz, 2H, 4-H_2), 3.64 (t, *J*=4.8 Hz, 2H, 2-H_2), 4.07 (s, 2H, 9-C*H*$_2$-NH_2), 4.85 (s, $^{+}$NH, $^{+}NH_3$), 5.32 (s, 2H, 1-C*H*$_2$-Ar), 7.39–7.53 (complex signal, 5H, 1-CH_2-Ar-*H*), 7.66–7.71 (complex

signal, 4H, 5-Ar-*H*), 7.94–8.01 (complex signal, 2H, 7-H, 8-H), 8.18 (br s, 1H, 10-H); ^{13}C NMR (100.6 MHz, CD_3OD) δ 21.4 (CH_2, C3), 26.5 (CH_2, C4), 44.2 (CH_2, C2), 52.9 (CH_2, 9-CH_2-NH_2), 61.7 (CH_2, 1-*C*H_2-Ar), 115.4 (C, C4a), 118.1 (C, C10a), 121.9 (CH, C7), 128.3 [2CH, 1-CH_2-Ar-*C*2(6)], 128.5 (CH, 1-CH_2-Ar-*C*4), 129.4 (CH, C10), 130.48 [2CH, 1-CH_2-Ar-*C*3(5)], 130.50 [2CH, 5-Ar-*C*3(5)], 131.3 (C, C9), 131.9 [2CH, 5-Ar-*C*2(6)], 132.4 (C, 5-Ar-*C*4), 134.5 (CH, C8), 137.0 (C, 1-CH_2-Ar-*C*1), 138.2 (C, 5-Ar-*C*1), 140.6 (C, C6a), 150.3 (C, C5), 159.7 (C, C10b); HRMS (ESI), calcd for [$C_{26}H_{24}{}^{35}ClN_3$ + H^+] 414.1732, found 414.1732; Elemental analysis, calcd for $C_{26}H_{24}ClN_3 \cdot 2HCl \cdot 2.2H_2O$ C 59.31%, H 5.82%, N 7.98%, found C 59.70%, H 5.71%, N 7.58%. HPLC purity: 97%.

*4.1.4. 4-{1-Benzyl-9-chloro-1,2,3,4-tetrahydro-2-oxobenzo[h][1,6]naphthyridin-5-yl}benzonitrile **13***

It was prepared as described for **8**. From 4-chloroaniline, **10** (794 mg, 6.22 mmol), 4-formylbenzonitrile, **11** (816 mg, 6.22 mmol), $Sc(OTf)_3$ (595 mg, 1.21 mmol), and enamine **4** (1.13 g, 6.04 mmol), a solid residue (2.71 g), mainly consisting of a diastereomeric mixture of octahydrobenzonaphthyridines **12**, was obtained and used in the next step without further purification.

From crude diastereomeric mixture **12** (2.71 g) and DDQ (3.65 g, 16.1 mmol), a solid residue (1.97 g) was obtained and purified through column chromatography (35–70 μm silica gel, hexane/EtOAc mixtures, gradient elution). On elution with hexane/EtOAc 75:25 to 60:40, compound **13** (886 mg, 35% yield) was isolated as a brown solid; R_f 0.46 (hexane/EtOAc 7:3).

A solution of **13** (396 mg, 0.93 mmol) in CH_2Cl_2 (10 mL) was filtered through a 0.2 μm NYL filter and evaporated at reduced pressure. The resulting solid was recrystallized from EtOAc (6 mL) and washed with pentane (3 × 5 mL) to give, after drying under standard conditions, the analytical sample of **13** (228 mg) as a beige solid: mp 252–254 ºC; IR (KBr) ν 2228 (CN st), 1687, 1605, 1559, 1543 (C=O, Ar–C–C and Ar–C–N st) cm^{-1}; ^{1}H NMR (400 MHz, $CDCl_3$) δ 2.64 (t, J = 6.8 Hz, 2H, 4'-H_2), 2.90 (t, J = 6.8 Hz, 2H, 3'-H_2), 5.33 (s, 2H, 1'-CH_2-Ar), 7.13 [dm, J = 8.4 Hz, 2H, 1'-CH_2-Ar-C2(6)-*H*], 7.22–7.31 (complex signal, 3H, 1'-CH_2-Ar-C3(5)-*H*, 1'-CH_2-Ar-C4-*H*), 7.64 (dd, J = 9.2 Hz, J' = 2.4 Hz, 1H, 8'-H), 7.71 (dm, J = 8.4 Hz, 2H) and 7.80 (dm, J = 8.4 Hz, 2H) [C2(6)-H, C3(5)-H], 7.92 (d, J = 2.4 Hz, 1H, 10'- H), 8.06 (d, J = 9.2 Hz, 1H, 7'-H);

^{13}C NMR (100.6 MHz, $CDCl_3$) δ 23.5 (CH_2, C3'), 32.5 (CH_2, C4'), 52.2 (CH_2, 1'-*C*H2-Ar), 112.8 (C, C1), 118.4 (C, CN), 120.9 (C, C10a'), 122.1 (C, C4a'), 122.2 (CH), 127.2 (2 CH), 127.7 (CH), 128.6 (2 CH), 129.9 (2 CH), 130.6 (CH), 132.1 (CH), 132.3 (2 CH) (Ar-*C*H), 132.7 (C, C9'), 137.0 (C, 1'-CH_2-Ar-*C*1), 143.5 (C), 146.4 (C), 146.9 (C) (C4, C6a', C10b'), 156.2 (C, C5'), 172.3 (C, C2'); HRMS (ESI), calcd for [$C_{26}H_{18}{}^{35}ClN_3O$ + H^+] 424.1211, found 424.1213.

*4.1.5. 4-{1-Benzyl-9-chloro-1,2,3,4-tetrahydrobenzo[h][1,6]naphthyridin-5-yl}benzylamine **3***

A solution of compound **13** (120 mg, 0.28 mmol) in anhydrous THF (10 mL) was treated with $LiAlH_4$ (71 mg, 1.87 mmol). The reaction mixture was stirred under reflux overnight, cooled to 0 ºC with an ice bath and treated dropwise with 1N NaOH (5 mL), then diluted with H_2O (5 mL), and extracted with EtOAc (3 × 15 mL). The combined organic extracts were dried over anhydrous Na_2SO_4 and evaporated under reduced pressure to give a brown oily residue (210 mg), which was purified through column chromatography (35–70 μm silica gel, CH_2Cl_2/MeOH/50% aq. NH_4OH mixtures, gradient elution). On elution with CH_2Cl_2/MeOH/50% aq. NH_4OH 99:1:0.2 to 98:2:0.2, amine **3** (26 mg, 22% yield) was isolated as a beige solid; R_f 0.35 (CH_2Cl_2 /MeOH/NH_4OH 9.75:0.25:0.1).

A solution of **3** (26 mg, 0.06 mmol) in CH_2Cl_2 (40 mL) was filtered through a 0.2 μm NYL filter and treated with a methanolic solution of HCl (2.36 N, 0.12 mL, 0.28 mmol). The resulting solution was evaporated at reduced pressure and the solid was washed with pentane (3 × 2 mL) to give, after drying under standard conditions, **3**·2HCl (21 mg) as a beige solid: mp 171–173 ºC; IR (ATR) ν 3500–2500 (max at 3382, 2921, 2850, $^+$NH, NH and CH st), 1633, 1623, 1615, 1575, 1567, 1559, 1539, 1534, 1515 (Ar–C–C and Ar–C–N st) cm^{-1}; ^{1}H NMR (400 MHz, CD_3OD) δ 2.07 (m, 2H, 3'-H_2), 2.76 (t, J = 6.0 Hz, 2H, 4'-H_2), 3.68 (t, J = 5.6 Hz, 2H, 2'-H_2), 4.30 (s, 2H, 1-C*H*$_2$-NH_2), 4.85 (s, $^+$NH, $^+NH_3$) 5.20 (s, 2H, 1'-C*H*$_2$-Ar), overimposed in part 7.44 (m, 1H, 1'-CH_2-Ar-C4-*H*), 7.47 [d, J = 7.2 Hz, 2H, 1'-CH_2-Ar-C2(6)-*H*], 7.54 [t, J = 7.2 Hz, 2H, 1'-CH_2-Ar-C3(5)-*H*], 7.77–7.79 [complex signal, 4H, C2(6)-H, C3(5)-H], 7.82 (dd, J = 9.2 Hz, J' = 2.0 Hz, 1H, 8'-H), 7.90 (d, J = 9.2 Hz, 1H, 7'-H), 8.07 (d, J = 2.0 Hz, 1H, 10'-H); ^{13}C NMR (100.6 MHz, CD_3OD) δ 21.1 (CH_2, C3'), 26.7 (CH_2, C4'), 43.9 (CH_2, 1-CH_2-NH_2), 53.4 (CH_2, C2'), 61.4 (CH_2, 1'-*C*H_2-Ar), 115.4 (C, C4a'), 119.1 (C, C10a'), 122.8 (CH, C7'), 126.1 (CH, C10'), 127.5 [2 CH, 1'-CH_2-Ar-*C*2(6)]), 129.4 (CH, 1'-

CH_2-Ar-*C*4), 130.6 [2 CH, 1'-CH_2-Ar-*C*3(5)], 130.8 (2 CH) and 130.9 (2 CH) [C2(6), C3(5)], 132.1 (C, C9'), 134.5 (C, C4), 134.6 (CH, C8'), 136.7 (C, 1'-CH_2-Ar-*C*1), 137.4 (C, C1), 139.0 (C, C6a'), 150.7 (C, C5'), 159.0 (C, C10b'); HRMS (ESI), calcd for [$C_{26}H_{24}{}^{35}ClN_3$ + H^+] 414.1732, found 414.1743; Elemental analysis, calcd for $C_{26}H_{24}ClN_3 \cdot 2HCl \cdot 0.75H_2O$ C 62.41%, H 5.54%, found C 62.65%, H 5.70%. HPLC purity: 97%.

*4.1.6. 4-{1-(tert-Butoxycarbonyl)-8-chloro-2,3-dihydro-1H-pyrrolo[3,2-c]quinolin-4-yl}benzonitrile **22***

It was prepared as described for **8**. From 4-chloroaniline, **10** (1.33 g, 10.4 mmol), 4-formylbenzonitrile, **11** (1.36 g, 10.4 mmol), $Sc(OTf)_3$ (1.02 g, 2.07 mmol), and enamine **14** (1.80 mL, 1.76 g, 10.4 mmol), a sticky yellow solid residue (5.00 g), mainly consisting of a diastereomeric mixture of pyrroloquinolines **18**, was obtained and used in the next step without further purification.

From crude diastereomeric mixture **18** (5.00 g) and DDQ (4.72 g, 20.8 mmol), a solid residue (4.53 g) was obtained and purified through column chromatography (35–70 μm silica gel, hexane/EtOAc mixtures, gradient elution). On elution with hexane/EtOAc 70:30, compound **22** (2.47 g, 59% yield) was isolated as a grey solid; R_f 0.60 (hexane/EtOAc 1:1).

A solution of **22** (100 mg, 0.25 mmol) in CH_2Cl_2 (5 mL) was filtered through a 0.2 μm PTFE filter and diluted with hexane/EtOAc 2:1 (6 mL). The resulting solid precipitate was washed with pentane (3 × 5 mL) to give, after drying under standard conditions, the analytical sample of **22** (74 mg) as a grey solid: mp 210–211 ºC; IR (ATR) *v* 2229 (CN st), 1700 (C=O st), 1604, 1564, 1540 (Ar–C–C and Ar–C–N st) cm^{-1}; ^1H NMR (400 MHz, $CDCl_3$) δ 1.59 [s, 9H, C(CH_3)$_3$], 3.31 (t, *J*=8.0 Hz, 2H, 3'-H_2), 4.30 (t, *J*=8.0 Hz, 2H, 2'-H_2), 7.61 (dd, *J*=8.8 Hz, *J'*=2.4 Hz, 1H, 7'-H), 7.80 (dm, *J*=8.8 Hz, 2H) and 7.94 (dm, *J*=8.8 Hz, 2H) [C2(6)-H, C3(5)-H], 8.05 (d, *J*=8.8 Hz, 1H, 6'-H), 8.16 (d, *J*=2.4 Hz, 1H, 9'-H); ^{13}C NMR (100.6 MHz, $CDCl_3$) δ 28.2 [3CH_3, C(*C*H_3)$_3$], 28.8 (CH_2, C3'), 51.5 (CH_2, C2'), 82.9 [C, *C*(CH_3)$_3$], 112.5 (C, C1), 118.6 (C, CN), 119.6 (C), 124.4 (C) (C3a', C9a'), 124.9 (CH), 130.3 (CH), 131.4 (CH) (C6', C7', C9'), 129.1 (2CH), 132.3 (2CH) [C2(6), C3(5)], 131.1 (C, C8'), 143.7 (C), 147.7 (C), 148.1 (C) (C4, C5a', C9b'), 153.0 (C), 153.2 (C) (NCOO, C4'); HRMS (ESI), calcd for [$C_{23}H_{20}{}^{35}ClN_3O_2$ + H^+] 406.1317, found 406.1308.

*4.1.7. 4-{1-(tert-Butoxycarbonyl)-9-chloro-1,2,3,4-tetrahydrobenzo[h][1,6]naphthyridin-5-yl}benzonitrile **23***

It was prepared as described for **8**. From 4-chloroaniline, **10** (1.24 g, 9.72 mmol), 4-formylbenzonitrile, **11** (1.27 g, 9.69 mmol), $Sc(OTf)_3$ (0.95 g, 1.93 mmol), and enamine **15** (1.80 mL, 1.78 g, 9.70 mmol), a yellow solid residue (5.31 g), mainly consisting of a diastereomeric mixture of benzonaphthyridines **19**, was obtained and used in the next step without further purification.

From crude diastereomeric mixture **19** (5.31 g) and DDQ (4.40 g, 19.4 mmol), a brown residue (4.74 g) was obtained and purified through column chromatography (35–70 μm silica gel, hexane/EtOAc mixtures, gradient elution). On elution with hexane/EtOAc 90:10, compound **23** (2.79 g, 69% yield) was isolated as a white solid; R_f 0.60 (hexane/EtOAc 1:1).

A solution of **23** (71 mg, 0.17 mmol) in CH_2Cl_2 (8 mL) was filtered through a 0.2 μm PTFE filter and evaporated at reduced pressure. The resulting solid was washed with pentane (3 × 5 mL) to give, after drying under standard conditions, the analytical sample of **23** (70 mg) as a white solid: mp 146–147 ºC; IR (ATR) *v* 2222 (CN st), 1702 (C=O st), 1602, 1578, 1560 (Ar–C–C and Ar–C–N st) cm^{-1}; ^1H NMR (400 MHz, $CDCl_3$) δ 1.40 [s, 9H, $C(CH_3)_3$], 1.99 (br signal, 2H, 3'-H_2), 2.76 (t, *J*=6.8 Hz, 2H, 4'-H_2), 3.20–4.20 (br signal, 2H, 2'-H_2), 7.58 (dd, *J*=9.2 Hz, *J'*=2.4 Hz, 1H, 8'-H), 7.69 (dm, *J*=8.4 Hz, 2H), 7.79 (dm, *J*=8.4 Hz, 2H) [C2(6)-H, C3(5)-H], superimposed 7.80 (m, 1H, 10'-H), 7.98 (d, *J*=9.2 Hz, 1H, 7'-H); ^{13}C NMR (100.6 MHz, $CDCl_3$) δ 23.9 (CH_2, C3'), 25.3 (CH_2, C4'), 27.9 [$3CH_3$, $C(CH_3)_3$)], 44.6 (CH_2, C2'), 82.3 [C, $C(CH_3)_3$], 112.3 (C, C1), 118.6 (C, CN), 123.6 (CH+C), 124.5 (C), 129.8 (3CH), 131.1 (CH), 132.2 (2CH) [C2(6), C3(5), C4a', C7', C8', C10', C10a'), 131.8 (C, C9'), 144.1 (C), 144.4 (C), 145.4 (C) (C4, C6a', C10b'), 153.8 (C, C5'), 157.7 (C, NCOO); HRMS (ESI), calcd for [$C_{24}H_{22}{}^{35}ClN_3O_2 + H^+$] 420.1473, found 420.1475.

*4.1.8. 4-{1-(tert-Butoxycarbonyl)-10-chloro-2,3,4,5-tetrahydro-1H-azepino[3,2-c]quinolin-6-yl}benzonitrile **24***

It was prepared as described for **8**. From 4-chloroaniline, **10** (0.59 g, 4.62 mmol), 4-formylbenzonitrile, **11** (0.61 g, 4.65 mmol), $Sc(OTf)_3$ (0.46 g, 0.93 mmol), and enamine **16** (0.90 mL, 924 mg, 4.69 mmol), a yellow solid residue (2.33 g), mainly consisting of a diastereomeric mixture of benzonaphthyridines **20**, was obtained and used in the next step without further purification.

From crude diastereomeric mixture **20** (2.33 g) and DDQ (2.11 g, 9.30 mmol), a solid residue (1.99 g) was obtained and purified through column chromatography (35–70 μm silica gel, hexane/EtOAc mixtures, gradient elution). On elution with hexane/EtOAc 80:20, compound **24** (1.58 g, 79% yield) was isolated as a white solid; R_f 0.58 (hexane/EtOAc 1:1).

A solution of **24** (200 mg, 0.46 mmol) in CH_2Cl_2 (10 mL) was filtered through a 0.2 μm PTFE filter and diluted with hexane/EtOAc 2:1 (3 mL). The solid precipitate was washed with with pentane (3 × 5 mL) to give, after drying under standard conditions, the analytical sample of **24** (100 mg) as a white solid: mp 177–179 ºC; IR (ATR) *v* 2223 (CN st), 1698 (C=O st), 1602, 1579, 1564, 1550 (Ar–C–C and Ar–C–N st) cm^{-1}; ^1H NMR (400 MHz, $CDCl_3$) δ 1.25 [s, $C(CH_3)_3$], 1.46 (m), 1.84–1.94 (complex signal) 1.98–2.16 (complex signal), 2.70 (tm, *J*=14.0 Hz), 2.82 (tm, *J*=14.0 Hz), 2.92 (ddm, *J*=14.4 Hz, *J'*=5.2 Hz), 4.40 (dm, *J*=14.4 Hz, 2'-H_2 minor rotamer), 4.58 (dt, *J*=14.0 Hz, *J'*=3.2 Hz, 2'-H_2 major rotamer), superimposed in part 7.61 (dd, *J*=9.2 Hz, *J'*=2.4 Hz, 9'-H minor rotamer), 7.63 (dd, *J*=9.2 Hz, *J'*=2.4 Hz, 9'-H major rotamer), superimposed in part 7.65 [dm, *J*=8.4 Hz, C2(6)-H or C3(5)-H minor rotamer], 7.70 (dm, *J*=8.4 Hz), 7.80 dm, (*J*=8.4 Hz) [C2(6)-H, C3(5)-H major rotamer], 7.78 (d, *J*=2.4 Hz, 11'-H minor rotamer), superimposed in part 7.79 [dm, *J*=8.4 Hz, C3(5)-H or C2(6)-H minor rotamer], 7.82 (d, *J*=2.4 Hz, 11'-H major rotamer), 8.01 (d, *J*=9.2 Hz, 8'-H minor rotamer) 8.03 (d, *J*=9.2 Hz, 8'-H major rotamer); ^{13}C NMR (100.6 MHz, $CDCl_3$) δ significant signals of the major rotamer 24.8 (CH_2, C4'), 28.0 [$3CH_3$, $C(CH_3)_3$], 28.6 (CH_2), 29.81 (CH_2) (C3', C5'), 47.3 (CH_2, C2'), 81.2 [C, $C(CH_3)_3$], 112.3 (C, C1), 118.56 (C, CN), 122.2 (C), 125.5 (C) (C5a', C11a'), 144.9 (C), 145.6 (C), 147.7 (C) (C4, C7a', C11b'), 152.8 (C, C5'), 158.9 (C, NCOO); ^{13}C NMR (100.6 MHz, $CDCl_3$) δ significant signals of the minor rotamer 24.9 (CH_2, C4'), 28.3 [$3CH_3$, $C(CH_3)_3$], 29.4 (CH_2), 29.75 (CH_2) (C3', C5'), 48.4 (CH_2, C2'), 81.5 [C, $C(CH_3)_3$], 112.2 (C, C1), 118.59 (C, CN), 122.0 (C), 125.7 (C) (C5a', C11a'), 145.0 (C), 145.8 (C), 147.9 (C) (C4, C7a', C11b'), 153.5 (C, C5'), 159.0 (C, NCOO); HRMS (ESI), calcd for $[C_{25}H_{24}{}^{35}ClN_3O_2 + H^+]$ 434.1630, found 434.1628.

*4.1.9. 4-{1-(tert-Butoxycarbonyl)-8-chloro-1,2,3,4-tetrahydrobenzo[h][1,6]naphthyridin-5-yl}benzonitrile **25***

It was prepared as described for **8**. From 3-chloroaniline, **17** (1.03 mL, 1.25 g, 9.77 mmol), 4-formylbenzonitrile, **11** (1.27 g, 9.69 mmol), $Sc(OTf)_3$ (0.95 g, 1.93 mmol),

and enamine **15** (1.80 mL, 1.78 g, 9.70 mmol), a solid residue (4.90 g), mainly consisting of a diastereomeric mixture of benzonaphthyridines **21**, was obtained and used in the next step without further purification.

From crude diastereomeric mixture **21** (4.90 g) and DDQ (4.40 g, 19.4 mmol), a residue (4.42 g) was obtained and purified through column chromatography (35–70 μm silica gel, hexane/EtOAc mixtures, gradient elution). On elution with hexane/EtOAc 90:10, compound **25** (2.53 g, 62% yield) and 4-{3-[3-(*tert*-butoxycarbonylamino)propyl]-7-chloroquinolin-2-yl}benzonitrile, **34** (705 mg, 17% yield) were successively isolated; $R_{f\,(\mathbf{26})}$ 0.46; $R_{f\,(\mathbf{35})}$ 0.24 (hexane/EtOAc 70:30).

A solution of **25** (2.53 g, 6.04 mmol) in CH_2Cl_2 (25 mL) was filtered through a 0.2 μm PTFE filter and evaporated at reduced pressure. The resulting solid was washed with Et_2O (3 × 10 mL) and pentane (3 × 8 mL) to give, after drying under standard conditions, the analytical sample of **25** (1.09 g) as a white solid: mp 162–164 ºC; IR (ATR) *v* 2223 (CN st), 1698 (C=O st), 1608, 1575, 1561 (Ar–C–C and Ar–C–N st) cm^{-1}; ^1H NMR (400 MHz, $CDCl_3$) δ 1.41 [s, 9H, C(C*H*$_3$)$_3$], 1.99 (br signal, 2H, 3'-H_2), 2.75 (t, *J*=6.8 Hz, 2H, 4'-H_2), 3.4–4.4 (br signal, 2H, 2'-H_2), 7.47 (dd, *J*=8.8 Hz, *J'*=2.0 Hz, 1H, 9'-H), 7.69 (dm, *J*=8.4 Hz, 2H), 7.79 (dm, *J*=8.4 Hz, 2H) [C2(6)-H, C3(5)-H], 7.74 (d, *J*=8.8 Hz, 10'-H), 8.04 (d, *J*= 2.0 Hz, 1H, 7'-H); ^{13}C NMR (100.6 MHz, $CDCl_3$) δ 23.9 (CH_2, C3'), 25.2 (CH_2, C4'), 28.0 [3CH_3, C(*C*H_3)$_3$], 44.8 (CH_2, C2'), 82.1 [C, *C*(CH_3)$_3$], 112.3 (C, C1), 118.6 (C, CN), 122.3 (C), 123.0 (C) (C4a', C10a'), 125.8 (CH), 126.7 (CH), 128.3 (CH) (C7', C9', C10'), 129.7 (2CH), 132.2 (2CH) [C2(6), C3(5)], 134.8 (C, C8'), 144.4 (C), 145.0 (C), 147.4 (C) (C4, C6a', C10b'), 153.9 (C, C5'), 158.5 (C, NCOO); HRMS (ESI), calcd for [$C_{24}H_{22}{}^{35}ClN_3O_2$ + H^+] 420.1473, found 420.1469.

A solution of **34** (30 mg, 0.07 mmol) in CH_2Cl_2 (2 mL) was filtered through a 0.2 μm PTFE filter and evaporated at reduced pressure. The resulting solid was washed with Et_2O (3 × 5 mL) and pentane (3 × 5 mL) to give, after drying under standard conditions, the analytical sample of **34** (19 mg) as a yellow solid: mp 124–126 ºC; IR (ATR) *v* 3358 (NH st), 2229 (CN st), 1680 (C=O st), 1623, 1591, 1519 (Ar–C–C and Ar–C–N st) cm^{-1}; ^1H NMR (400 MHz, $CDCl_3$) δ 1.41 [s, 9H, C(C*H*$_3$)$_3$], 1.71 (tt, *J*=7.6 Hz, *J'*=6.4 Hz, 2H, 2"-H_2), 2.78 (t, *J*=7.6 Hz, 2H, 1"-H_2), 3.06 (dt, *J*=*J'*=6.4 Hz, 2H, 3"-H_2), 4.42 (br s, 2H, NHCOO), 7.52 (dd, *J*=9.2 Hz, *J'*=2.0 Hz, 1H, 6'-H), 7.67 (dm, *J*=8.4 Hz, 2H), 7.80 (dm, *J*=8.4 Hz, 2H) [C2(6)-H, C3(5)-H], 7.76 (d, *J*=9.2 Hz, 1H, 5'-H), 8.08 (br s, 1H,

4'-H), 8.09 (d, *J*=2.0 Hz, 1H, 8'-H); ^{13}C NMR (100.6 MHz, $CDCl_3$) δ 28.4 [3CH_3, C(*C*H_3)$_3$], 29.9 (CH_2), 31.0 (CH_2) (C1", C2"), 39.9 (CH_2, C3"), 79.4 [C, *C*(CH_3)$_3$], 112.4 (C, C1), 118.5 (C, CN), 126.1 (C, C4a'), 128.2 (2CH), 128.3 (CH), 129.6 (2CH), 132.3 (2CH) [C2(6), C3(5), C5', C6', C8'], 132.7 (C), 135.3 (C) (C7', C8a'), 136.2 (CH, C4') 144.8 (C), 146.8 (C) (C4, C3'), 155.8 [C, C2'], 159.2 (C, NHCOO); HRMS (ESI), calcd for [$C_{24}H_{24}{}^{35}ClN_3O_2$ + H^+] 422.1630, found 422.1623.

4.1.10. 4-{8-Chloro-2,3-dihydro-1H-pyrrolo[3,2-c]quinolin-4-yl}benzonitrile ***26***

It was prepared as decribed for **9**. From **22** (877 mg, 2.16 mmol) and 4M HCl/dioxane solution (18 mL), a solid residue (430 mg) was obtained. Recrystallization from EtOAc/hexane 1:1.5) afforded nitrile **26** (307 mg, 46% yield) as a orange solid; R_f 0.30 (hexane/EtOAc 1:1).

A solution of **26** (100 mg, 0.33 mmol) in CH_2Cl_2 (10 mL) was filtered through a 0.2 μm PTFE filter and treated with a methanolic solution of HCl (0.53 N, 1.85 mL, 0.98 mmol). The resulting solution was evaporated at reduced pressure and the solid was washed with pentane (3 × 5 mL) to give, after drying under standard conditions, **26**·HCl (108 mg) as a yellow solid: mp 324–326 ºC; IR (ATR) *v* 3500–2500 (max at 3359, 3183, 3023, 2925, 2749, $^+$NH, NH and CH st), 2228 (CN st), 1633, 1604, 1588, 1556, 1519 (Ar–C–C and Ar–C–N st) cm^{-1}; ^{1}H NMR (400 MHz, CD_3OD) δ 3.42 (t, *J*=9.0 Hz, 2H, 3'-H_2), 4.18 (t, *J*=9.0 Hz, 2H, 2'-H_2), 4.85 (s, $^+$NH, NH), 7.90–7.92 (complex signal, 2H, 6'-H, 7'-H), 7.97 [br d, *J*=8.4 Hz, 2H, C3(5)-H], 8.02 [br d, *J*=8.4 Hz, 2H, C2(6)-H], 8.21 (m, 1H, 9'-H); ^{13}C NMR (100.6 MHz, CD_3OD) δ 27.1 (CH_2, C3'), 49.4 (CH_2, C2'), 114.0 (C, C3a'), 116.0 (C, C1), 118.8 (C, CN), 119.7 (C, C9a'), 122.7 (CH),124.6 (CH) (C6', C9'), 130.7 [2CH, C3(5)], 133.0 (C, C8'), 134.2 [2CH, C2(6)], 136.2 (CH, C7'), 137.5 (C, C5a'), 140.1 (C, C4), 146.0 (C, C4'), 162.6 (C, C9b'); HRMS (ESI), calcd for [$C_{18}H_{12}{}^{35}ClN_3$ + H^+] 306.0793, found 306.0792; Elemental analysis, calcd for $C_{18}H_{12}ClN_3$·HCl·1/2H_2O C 61.55%, H 4.02%, N 11.96%, found C 61.35%, H 4.07%, N 11.73%. HPLC purity: 94%.

4.1.11. 4-{9-Chloro-1,2,3,4-tetrahydrobenzo[h][1,6]naphthyridin-5-yl}benzonitrile ***27***

It was prepared as decribed for **9**. From **23** (1.76 g, 4.20 mmol) and 4M HCl/dioxane solution (29 mL), nitrile **27** (915 mg, 68% yield) was obtained as a yellowish solid; R_f 0.60 (hexane/EtOAc 1:1).

A solution of **27** (154 mg, 0.48 mmol) in CH_2Cl_2 (10 mL) was filtered through a 0.2 μm PTFE filter and treated with a methanolic solution of HCl (0.53 N, 2.73 mL, 1.45 mmol). The resulting solution was evaporated at reduced pressure and the solid was washed with pentane (3 × 5 mL) to give, after drying under standard conditions, **27**·HCl (148 mg) as a beige solid: mp 343–344 ºC; IR (ATR) *v* 3500–2500 (max at 3170, 3077, 2708, $^+$NH, NH and CH st), 2226 (CN st), 1627, 1584, 1566 (Ar–C–C and Ar–C–N st) cm^{-1}; ^{1}H NMR (400 MHz, CD_3OD) δ 1.98 (tt, *J*=6.0 Hz, *J'*=5.6 Hz, 2H, 3'-H_2), 2.71 (t, *J*=6.0 Hz, 2H, 4'-H_2), 3.69 (t, *J*=5.6 Hz, 2H, 2'-H_2), 4.85 (s, $^+$NH, NH), 7.84 (d, *J*=8.8 Hz, 1H, 7'-H), 7.85 [br d, *J*=8.4 Hz, 2H, C3(5)-H], 7.90 (dd, *J*=8.8 Hz, *J'*=2.0 Hz, 1H, 8'-H), 8.02 [br d, *J*=8.4 Hz, 2H, C2(6)-H], 8.41 (d, *J*=2.0 Hz, 1H, 10'-H); ^{13}C NMR (100.6 MHz, CD_3OD) δ 19.9 (CH_2, C3'), 24.9 (CH_2, C4'), 43.0 (CH_2, C2'), 109.8 (C, C4a'), 115.8 (C, C1), 117.8 (C, C10a'), 118.9 (C, CN), 122.8 (CH), 122.9 (CH) (C7', C10'), 131.3 [2CH, C3(5)], 133.6 (C, C9'), 134.0 [2CH, C2(6)], 135.1 (CH, C8'), 137.4 (C, C6a'), 138.0 (C, C4), 150.3 (C, C5'), 154.7 (C, C10b'); HRMS (ESI), calcd for [$C_{19}H_{14}{}^{35}ClN_3$ + H^+] 320.0949, found 320.0948; Elemental analysis, calcd for $C_{19}H_{14}ClN_3$·HCl C 64.06%, H 4.24%, N 11.80%, found C 63.79%, H 4.22%, N 11.79%. HPLC purity > 99%.

*4.1.12. 4-{10-Chloro-2,3,4,5-tetrahydro-1H-azepino[3,2-c]quinolin-6-yl}benzonitrile **28***

It was prepared as decribed for **9**. From **24** (997 mg, 2.30 mmol) and 4M HCl/dioxane solution (16 mL), nitrile **28** (392 mg, 51% yield) was obtained as a beige solid; R_f 0.50 (hexane/EtOAc 1:1).

A solution of **28** (392 mg, 1.17 mmol) in CH_2Cl_2 (8 mL) was filtered through a 0.2 μm PTFE filter and diluted with hexane/EtOAc 2:1 (3 mL). The solid precipitate (aliquot of 111 mg of a total amount of 232 mg) was treated with a methanolic solution of HCl (0.53 N, 1.88 mL, 1.00 mmol). The resulting solution was evaporated at reduced pressure and the solid was washed with pentane (3 × 5 mL) to give, after drying under standard conditions, **28**·HCl (114 mg) as a yellowish solid: mp 338–340 ºC; IR (ATR) *v* 3500–2500 (max at 3167, 3085, 3033, 2930, 2795, 2715, 2635, $^+$NH, NH and CH st), 2222 (CN st), 1627, 1599, 1573, 1560, 1501 (Ar–C–C and Ar–C–N st) cm^{-1}; ^{1}H NMR (400 MHz, CD_3OD) δ 2.04 (m, 2H, 4'-H_2), 2.19 (m, 2H, 3'-H_2), 2.85 (m, 2H, 5'-H_2), 3.96 (m, 2H, 2'-H_2), 4.85 (s, $^+$NH, NH), superimposed in part 7.82 (d, *J*=8.8 Hz, 1H, 8'-H), 7.84 [br d, *J*=8.4 Hz, 2H, C3(5)-H], 7.89 (dd, *J*=8.8 Hz, *J'*=2.4 Hz, 1H, 9'-H), 8.02

[br d, *J*=8.4 Hz, 2H, C2(6)-H], 8.43 (d, *J*=2.4 Hz, 1H, 11'-H); ^{13}C NMR (100.6 MHz, CD_3OD) δ 26.3 (CH_2, C4'), 27.7 (CH_2, C3'), 27.9 (CH_2, C5'), 44.9 (CH_2, C2'), 114.7 (C, C5a'), 115.9 (C, C1), 118.8 (C, CN), 119.3 (C, C11a'), 122.7 (CH, C8'), 123.0 (CH, C11'), 131.4 [2CH, C3(5)], 133.8 (C, C10'), 134.0 [2CH, C2(6)], 135.1 (CH, C9'), 137.3 (C, C7a'), 138.8 (C, C4), 152.6 (C, C6'), 160.0 (C, C11b'); HRMS (ESI), calcd for [$C_{20}H_{16}{}^{35}ClN_3$ + H^+] 334.1105, found 334.1106; Elemental analysis, calcd for $C_{20}H_{16}ClN_3 \cdot HCl \cdot 0.3H_2O$ C 63.94%, H 4.72%, N 11.18%, found C 63.72%, H 4.56%, N 10.85%. HPLC purity > 99%.

*4.1.13. 4-{8-Chloro-1,2,3,4-tetrahydrobenzo[h][1,6]naphthyridin-5-yl}benzonitrile **29***

It was prepared as decribed for **9**. From **25** (2.24 g, 5.34 mmol) and 4M HCl/dioxane solution (37 mL), nitrile **29** (1.60 g, 94% yield) was obtained as a yellow solid; R_f 0.34 (hexane/EtOAc 1:1).

A solution of **29** (275 mg, 0.86 mmol) in CH_2Cl_2 (15 mL) was filtered through a 0.2 μm PTFE filter and treated with a methanolic solution of HCl (0.53 N, 5.16 mL, 2.73 mmol). The resulting solution was evaporated at reduced pressure and the solid was recrystallized from MeOH/hexane 1:3.75 (1.9 mL) and washed with pentane (3 × 8 mL) to give, after drying under standard conditions, **29**·HCl (166 mg) as a brown solid: mp 360–362 ºC; IR (ATR) ν 3500–2500 (max at 3148, 3078, 3035, 2905, 2734, $^+$NH, NH and CH st), 2228 (CN st), 1629, 1583, 1500 (Ar–C–C and Ar–C–N st) cm^{-1}; ^{1}H NMR (400 MHz, CD_3OD) δ 1.98 (tt, *J*=6.0 Hz, *J'*=5.2 Hz, 2H, 3'-H_2), 2.70 (t, *J*=6.0 Hz, 2H, 4'-H_2), 3.69 (t, *J*=5.2 Hz, 2H, 2'-H_2), 4.85 (s, $^+$NH, NH), 7.67 (dd, *J*=8.8 Hz, *J'*= 1.6 Hz, 1H, 9'-H), superimposed in part 7.84 (m, 1H, 7'-H), 7.85 (br d, *J*=7.6 Hz, 2H), 8.02 (br d, *J*=7.6 Hz, 2H) [C2(6)-H, C3(5)-H], 8.29 (d, *J*=8.8 Hz, 1H, 10'-H); ^{13}C NMR (100.6 MHz, CD_3OD) δ 20.0 (CH_2, C3'), 24.9 (CH_2, C4'), 43.1 (CH_2, C2'), 109.7 (C, C4a'), 115.4 (C), 115.9 (C) (C1, C10a'), 118.9 (C, CN), 120.0 (CH), 125.5 (CH), 128.4 (CH) (C7', C9', C10'), 131.3 (2CH), 134.0 (2CH) [C2(6), C3(5)], 138.0 (C), 139.6 (C), 140.8 (C) (C4, C6a', C8'), 150.5 (C, C5'), 155.4 (C, C10b'); HRMS (ESI), calcd for [$C_{19}H_{14}{}^{35}ClN_3$ + H^+] 320.0949, found 320.0946; Elemental analysis, calcd for $C_{19}H_{14}ClN_3 \cdot HCl$ C 64.06%, H 4.24%, N 11.80%, found C 64.02%, H 4.41%, N 11.85%. HPLC purity > 99%.

*4.1.14. 4-{8-Chloro-2,3-dihydro-1H-pyrrolo[3,2-c]quinolin-4-yl}benzylamine **30***

It was prepared as described for **3**. From nitrile **26** (216 mg, 0.71 mmol) and $LiAlH_4$ (0.13 g, 3.43 mmol), a yellow solid residue (210 mg) was obtained and purified by column chromatography (35–70 μm silica gel, CH_2Cl_2/MeOH/50% aq. NH_4OH mixtures, gradient elution). On elution with CH_2Cl_2/MeOH/50% aq. NH_4OH 99:1:0.2 to 98.5:1.5:0.2, the amine **30** (163 mg, 74% yield) was isolated as a beige solid; R_f 0.22 (CH_2Cl_2/MeOH/50% aq. NH_4OH 9:1:0.05).

A solution of **30** (138 mg, 0.45 mmol) in CH_2Cl_2 (10 mL) was filtered through a 0.2 μm PTFE filter and treated with a methanolic solution of HCl (0.53 N, 7.54 mL, 4.00 mmol). The resulting solution was evaporated at reduced pressure and the solid was recrystallized from MeOH/EtOAc 1:3 (4 mL), and then washed with pentane (3 × 5 mL) to give, after drying under standard conditions, **30**·2HCl (108 mg) as a yellow solid: mp 319–320 ºC; IR (ATR) *ν* 3500–2500 (max at 3364, 3111, 3043, 2943, 2614, $^+$NH, NH and CH st), 1638, 1605, 1573, 1529, 1511 (Ar–C–C and Ar–C–N st) cm^{-1}; ^{1}H NMR (400 MHz, CD_3OD) δ 3.42 (t, *J*=8.8 Hz, 2H, 3'-H_2), 4.17 (t, *J*=8.8 Hz, 2H, 2'-H_2), 4.29 (s, 2H, 1-C*H*$_2$-NH_2), 4.85 (s, $^+$NH, $^+NH_3$, NH), 7.78 (br d, *J*=8.4 Hz, 2H), 7.90 (br d, *J*=8.4 Hz, 2H) [C2(6)-H, C3(5)-H], 7.86 (dd, *J*=9.2 Hz, *J'*=2.4 Hz, 1H, 7'-H), 7.95 (d, *J*=9.2 Hz, 1H, 6'-H), 8.19 (m, 1H, 9'-H); ^{13}C NMR (100.6 MHz, CD_3OD) δ 27.4 (CH_2, C3'), 43.8 (CH_2, 1-CH_2-NH_2), 49.2 (CH_2, C2'), 113.9 (C, C3a'), 119.1 (C, C9a'), 122.7 (CH, C6'), 124.6 (CH, C9'), 130.4 (2CH), 131.0 (2CH) [C2(6), C3(5)], 132.7 (C, C4), 133.8 (C, C8'), 135.9 (CH, C7'), 137.7 (C, C1), 140.0 (C, C5a'), 147.2 (C, C4'), 162.4 (C, C9b'); HRMS (ESI), calcd for [$C_{18}H_{16}{}^{35}ClN_3$ + H^+] 310.1106, found 310.1101; Elemental analysis, calcd for $C_{18}H_{16}ClN_3$·2HCl·1.5H_2O C 52.76%, H 5.17%, N 10.26%, found C 52.63%, H 5.21%, N 9.91%. HPLC purity > 99%.

*4.1.15. 4-{9-Chloro-1,2,3,4-tetrahydrobenzo[h][1,6]naphthyridin-5-yl}benzylamine **31***

It was prepared as described for **3**. From nitrile **27** (720 mg, 2.25 mmol) and $LiAlH_4$ (0.43 g, 11.3 mmol), a white solid residue (892 mg) was obtained and purified by column chromatography (35–70 μm silica gel, CH_2Cl_2/MeOH/50% aq. NH_4OH mixtures, gradient elution). On elution with CH_2Cl_2/MeOH/50% aq. NH_4OH 97:3:0.2 to 95:5:0.2, the amine **31** (632 mg, 87% yield) was isolated as a white solid; R_f 0.18 (CH_2Cl_2/MeOH/50% aq. NH_4OH 9:1:0.05).

A solution of **31** (632 mg, 1.95 mmol) in CH_2Cl_2 (10 mL) was filtered through a 0.2 μm PTFE filter and treated with a methanolic solution of HCl (0.53 N, 33 mL, 17.5 mmol).

The resulting solution was evaporated at reduced pressure and the solid was washed with pentane (3 × 10 mL) to give, after drying under standard conditions, **31**·2HCl (640 mg) as a beige solid: mp 346–347 ºC; IR (ATR) *v* 3500–2500 (max at 3028, 2987, 2941, $^{+}$NH, NH and CH st), 1612, 1573, 1511 (Ar–C–C and Ar–C–N st) cm^{-1}; ^{1}H NMR (400 MHz, CD_3OD) δ 1.97 (tt, *J*=6.4 Hz, *J'*=5.2 Hz, 2H, 3'-H_2), 2.74 (t, *J*=6.4 Hz, 2H, 4'-H_2), 3.69 (t, *J*=5.2 Hz, 2H, 2'-H_2), 4.30 (s, 2H, 1-CH_2-NH_2), 4.86 (s, $^{+}$NH, $^{+}NH_3$, NH), 7.75 (br d, *J*=8.4 Hz, 2H), 7.78 (br d, *J*=8.4 Hz, 2H) [C2(6)-H, C3(5)-H], 7.86 (dd, *J*=9.2 Hz, *J'*=2.0 Hz, 1H, 8'-H), 7.89 (d, *J*=9.2 Hz, 1H, 7'-H), 8.41 (d, *J*=2.0 Hz, 1H, 10'-H); ^{13}C NMR (100.6 MHz, CD_3OD) δ 20.0 (CH_2, C3'), 25.1 (CH_2, C4'), 42.9 (CH_2, C2'), 43.9 (CH_2, 1-CH_2-NH_2), 109.7 (C, C4a'), 117.7 (C, C10a'), 122.8 (CH, C7'), 122.9 (CH, C10'), 130.7 (2CH), 130.9 (2CH) [C2(6), C3(5)], 133.4 (C, C9'), 134.3 (C, C4), 134.8 (CH, C8'), 137.4 (2C, C1, C6a'), 151.6 (C, C5'), 154.5 (C, C10b'); HRMS (ESI), calcd for [$C_{19}H_{18}{}^{35}ClN_3$ + H^+] 324.1262, found 324.1263; Elemental analysis, calcd for $C_{19}H_{18}ClN_3$·2HCl·1/2H_2O C 56.24%, H 5.22%, N 10.36%, found C 56.44%, H 5.25%, N 10.14%. HPLC purity > 99%.

*4.1.16. 4-{10-Chloro-2,3,4,5-tetrahydro-1H-azepino[3,2-c]quinolin-6-yl}benzylamine **32***

It was prepared as described for **3**. From nitrile **28** (172 mg, 0.52 mmol) and $LiAlH_4$ (0.10 g, 2.64 mmol), a yellow solid residue (363 mg) was obtained and purified by column chromatography (35–70 μm silica gel, CH_2Cl_2/MeOH/50% aq. NH_4OH mixtures, gradient elution). On elution with CH_2Cl_2/MeOH/50% aq. NH_4OH 99:1:0.2, impure amine **32** (189 mg) was obtained. Recrystallization from hexane/EtOAc 2:1 (3 mL) afforded pure amine **32** (97 mg, 55% yield) as a white solid; R_f 0.20 (CH_2Cl_2/MeOH/50% aq. NH_4OH 9:1:0.05).

A solution of **32** (97 mg, 0.29 mmol) in CH_2Cl_2 (5 mL) was filtered through a 0.2 μm PTFE filter and treated with a methanolic solution of HCl (0.53 N, 4.88 mL, 2.59 mmol). The resulting solution was evaporated at reduced pressure and the solid was washed with pentane (3 × 5 mL) to give, after drying under standard conditions, **32**·2HCl (98 mg) as a yellowish solid: mp 310–311 ºC; IR (ATR) *v* 3500–2500 (max at 3379, 3219, 3028, 2936, $^{+}$NH, NH and CH st), 1627, 1586, 1511 (Ar–C–C and Ar–C–N st) cm^{-1}; ^{1}H NMR (400 MHz, CD_3OD) δ 2.02 (m, 2H, 4'-H_2), 2.18 (m, 2H, 3'-H_2), 2.88 (m, 2H, 5'-H_2), 3.96 (m, 2H, 2'-H_2), 4.30 (s, 2H, 1-CH_2-NH_2), 4.86 (s, $^{+}$NH, $^{+}NH_3$, NH), 7.74 (br d, *J*=8.4 Hz, 2H), 7.78 (br d, *J*=8.4 Hz, 2H) [C2(6)-H, C3(5)-H], 7.84–

7.90 (complex signal, 2H, 8'-H, 9'-H), 8.44 (m, 1H, 11'-H); ^{13}C NMR (100.6 MHz, CD_3OD) δ 26.4 (CH_2, C4'), 27.8 (CH_2, C3'), 28.0 (CH_2, C5'), 43.9 (CH_2, 1-CH_2-NH_2), 44.9 (CH_2, C2'), 114.7 (C, C5a'), 119.2 (C, C11a'), 122.7 (CH, C8'), 123.0 (CH, C11'), 130.8 (2CH), 131.1 (2CH) [C2(6), C3(5)], 133.6 (C, C10'), 134.8 (CH, C9'), 135.1 (C, C4), 137.3 (C) and 137.5 (C) (C1, C7a'), 153.9 (C, C6'), 159.8 (C, C11b'); HRMS (ESI), calcd for [$C_{20}H_{20}{}^{35}ClN_3$ + H^+] 338.1419, found 338.1416; Elemental analysis, calcd for $C_{20}H_{20}ClN_3 \cdot 2HCl \cdot 2.5H_2O$ C 52.70%, H 5.97%, N 9.22%, found C 53.02%, H 5.69%, N 8.72%. HPLC purity > 99%.

*4.1.17. 4-{8-Chloro-1,2,3,4-tetrahydrobenzo[h][1,6]naphthyridin-5-yl}benzylamine **33***

It was prepared as described for **3**. From nitrile **29** (1.17 g, 3.66 mmol) and $LiAlH_4$ (0.69 g, 18.2 mmol), a yellow solid residue (3.07 g) was obtained. An aliquot of this crude product (1.50 g) was purified by column chromatography (35–70 μm silica gel, EtOAc/MeOH/50% aq. NH_4OH mixtures, gradient elution). On elution with EtOAc/MeOH/50% aq. NH_4OH 98:2:0.2, the amine **33** (390 mg, 67% yield) was isolated; R_f 0.29 (EtOAc/MeOH/50% aq. NH_4OH 7:3:0.05).

A solution of **33** (390 mg, 1.20 mmol) in CH_2Cl_2 (20 mL) was filtered through a 0.2 μm PTFE filter and treated with a methanolic solution of HCl (0.53 N, 20.4 mL, 10.8 mmol). The resulting solution was evaporated at reduced pressure and the solid was washed with pentane (3 × 15 mL) to give, after drying under standard conditions, **33**·2HCl (400 mg) as a yellowish solid: mp 305–307 ºC; IR (ATR) ν 3500–2500 (max at 3369, 3212, 2926, 2869, 2614, $^+$NH, NH and CH st), 1625, 1583, 1516 (Ar–C–C and Ar–C–N st) cm^{-1}; ^{1}H NMR (400 MHz, CD_3OD) δ 1.97 (tt, J=6.0 Hz, J'=5.6 Hz, 2H, 3'-H_2), 2.74 (t, J=6.0 Hz, 2H, 4'-H_2), 3.70 (t, J=5.6 Hz, 2H, 2'-H_2), 4.30 (s, 2H, 1-CH_2-NH_2), 4.85 (s, $^+$NH, $^+NH_3$, NH), 7.63 (dd, J=9.2 Hz, J'=2.0 Hz, 1H, 9'-H), 7.75 (br d, J=8.4 Hz, 2H), 7.78 (br d, J=8.4 Hz, 2H) [C2(6)-H, C3(5)-H], 7.90 (d, J=2.0 Hz, 1H, 7'-H), 8.32 (d, J=9.2 Hz, 1H, 10'-H); ^{13}C NMR (100.6 MHz, CD_3OD) δ 20.0 (CH_2, C3'), 25.0 (CH_2, C4'), 43.0 (CH_2, C2'), 43.9 (CH_2, 1-CH_2-NH_2), 109.5 (C, C4a'), 115.3 (C, C10a'), 119.9 (CH), 125.5 (CH), 128.2 (CH) (C7', C9', C10'), 130.8 (2CH), 130.9 (2CH) [C2(6), C3(5)], 134.3 (C), 137.4 (C), 139.5 (C) 140.5 (C) (C1, C4, C6a', C8'), 151.7 (C, C5'), 155.1 (C, C10b'); HRMS (ESI), calcd for [$C_{19}H_{18}{}^{35}ClN_3$ + H^+] 324.1262, found 324.1258; Elemental analysis, calcd for $C_{19}H_{18}ClN_3 \cdot 2HCl \cdot 1.8H_2O$ C 53.17%, H 5.54%, N 9.79%, found C 53.56%, H 5.54%, N 9.34%. HPLC purity: 98%.

*4.1.18. 4-[3-(3-Aminopropyl)-7-chloroquinolin-2-yl]benzonitrile **35***

It was prepared as decribed for **9**. From **34** (705 mg, 1.67 mmol) and 4M HCl/dioxane solution (12 mL), amino nitrile **35** (486 mg, 90% yield) was obtained; R_f 0.17 (EtOAc/MeOH/50% aq. NH_4OH 7:3:0.05).

A solution of **35** (109 mg, 0.34 mmol) in CH_2Cl_2 (8 mL) was filtered through a 0.2 μm PTFE filter and treated with a methanolic solution of HCl (0.80 N, 1.27 mL, 1.02 mmol). The resulting solution was evaporated at reduced pressure and the solid was recrystallized from MeOH/EtOAc 1:4 (3 mL) and washed with pentane (3 × 5 mL) to give, after drying under standard conditions, **35**·2HCl (70 mg) as a red solid: mp 153–154 ºC; IR (ATR) *v* 3500–2500 (max at 3369, 2954, 2609, $^+$NH, NH and CH st), 2226 (CN st), 1698, 1639, 1607, 1591, 1555, 1534, 1500 (Ar–C–C and Ar–C–N st) cm^{-1}; ^{1}H NMR (400 MHz, CD_3OD) δ 1.99 (tt, *J*=8.0 Hz, *J'*=7.6 Hz, 2H, 2''-H_2), superimposed in part 2.93 (t, *J*=7.6 Hz, 2H), 2.97 (t, *J*=8.0 Hz, 2H) (1''-H_2, 3''-H_2), 4.88 (s, $^+NH_3$, $^+$NH), 7.92 (dd, *J*=8.8 Hz, *J'*=2.0 Hz, 1H, 6'-H), 7.96 (br d, *J*=8.0 Hz, 2H), 8.07 (br d, *J*=8.0 Hz, 2H) [C2(6)-H, C3(5)-H], 8.23 (d, *J*=2.0 Hz, 1H, 8'-H), 8.32 (d, *J*=8.8 Hz, 1H, 5'-H), 9.10 (s, 1H, 4'-H); ^{13}C NMR (100.6 MHz, CD_3OD) δ 28.7 (CH_2), 29.8 (CH_2) (C1'', C2''), 40.0 (CH_2, C3''), 116.0 (C, C1), 118.9 (C, CN), 122.4 (CH), 131.46 (CH), 131.8 (CH) (C5', C6', C8'), 128.6 (C, C4a'), 131.51 (2CH), 134.09 (2CH) [C2(6), C3(5)], 135.4 (C), 138.7 (C), 141.0 (C), 141.1 (C) (C4, C3', C7', C8a'), 145.8 (CH, C4'), 157.6 (C, C2'); HRMS (ESI), calcd for [$C_{19}H_{16}{}^{35}ClN_3$ + H^+] 322.1106, found 322.1103; Elemental analysis, calcd for $C_{19}H_{16}ClN_3$·2HCl·1.2H_2O C 54.81%, H 4.94%, N 10.09%, found C 55.02%, H 4.75%, N 9.61%. HPLC purity: 94%.

*4.1.19. 4-{9-Chloro-3,4-dihydro-2H-pyrano[3,2-c]quinolin-5-yl}benzonitrile **38***

It was prepared as described for **8**. From 4-chloroaniline, **10** (1.51 g, 11.8 mmol), 4-formylbenzonitrile, **11** (1.56 g, 11.9 mmol), $Sc(OTf)_3$ (1.18 g, 2.40 mmol), and 3,4-dihydro-2*H*-pyran, **36** (1.08 mL, 994 mg, 11.8 mmol), a solid residue (4.72 g) was obtained and purified by column chromatography (35–70 μm silica gel, hexane/EtOAc mixtures, gradient elution). On elution with hexane/EtOAc 80:20 to 50:50, a 1:1 diastereomeric mixture **37** (3.65 g, 95% yield) was isolated as a white solid. After a second column chromatography separation of 1.00 g of diastereomeric mixture **37** (35–70 μm silica gel, hexane/EtOAc mixtures, gradient elution), pure all-*cis*-diatereoisomer (90 mg) was isolated as a white solid; R_f 0.43 (hexane/EtOAc 7:3).

A solution of all-*cis*-**37** (90 mg, 0.28 mmol) in CH_2Cl_2 (5 mL) was filtered through a 0.2 μm PTFE filter and evaporated at reduced pressure. The resulting solid was washed with pentane (3 × 5 mL) to give, after drying under standard conditions, the analytical sample of all-*cis*-**37** (85 mg) as a white solid: mp 284–285 ºC; IR (ATR) *ν* 3348 (NH st), 2225 (CN st), 1604, 1575 (Ar–C–C and Ar–C–N st) cm^{-1}; ^1H NMR (400 MHz, $CDCl_3$) *δ* 1.16–1.22 (m, 1H, 4'-H_a), 1.42–1.56 (complex signal, 3H, 3'-H_a, 3'-H_b, 4'-H_b), 2.17 (m, 1H, 4a'-H), 3.41 (ddd, *J*=*J'*=11.2 Hz, *J''*=3.2 Hz, 1H, 2'-H_a), 3.62 (dm, *J*=11.2 Hz, 1H, 2'-H_b), 3.86 (br s, 1H, NH), 4.72 (d, *J*=2.4 Hz, 1H, 5'-H), 5.27 (d, *J*=5.6 Hz, 1H, 10b'-H), 6.56 (d, *J*=8.4 Hz, 1H, 7'-H), 7.06 (ddd, *J*=8.4 Hz, *J'*=2.4 Hz, *J''*=0.8 Hz, 1H, 8'-H), 7.40 (dd, *J*=2.4 Hz, *J'*=0.8 Hz, 1H, 10'-H), 7.53 [dm, *J*=8.4 Hz, 2H, C3(5)-H], 7.68 [dm, *J*=8.4 Hz, 2H, C2(6)-H]; ^{13}C NMR (100.6 MHz, $CDCl_3$) *δ* 18.0 (CH_2, C4'), 25.1 (CH_2, C3'), 38.5 (CH, C4a'), 59.2 (CH, C5'), 60.8 (CH_2, C2'), 72.1 (CH, C10b'), 111.6 (C, C1), 116.0 (CH, C7'), 118.6 (C, CN), 121.7 (C, C10a'), 123.9 (C, C9'), 127.3 (CH, C10'), 127.5 [2CH, C3(5)], 128.2 (CH, C8'), 132.3 [2CH, C2(6)], 143.0 (C, C6a'), 146.3 (C, C4); HRMS (ESI), calcd for [$C_{19}H_{17}{}^{35}ClN_2O$ + H^+] 325.1102, found 325.1101; Elemental analysis, calcd for $C_{19}H_{17}ClN_2O$ C 70.26%, H 5.28%, N 8.62%, found C 70.34%, H 5.37%, N 8.80%. HPLC purity > 99%.

From diastereomeric mixture **37** (2.70 g, 8.31 mmol) and DDQ (3.77 g, 16.6 mmol), a solid residue (2.55 g) was obtained and purified through column chromatography (35–70 μm silica gel, hexane/EtOAc mixtures, gradient elution). On elution with hexane/EtOAc 80:20, compound **38** (1.09 g, 41% yield) was isolated as a white solid; R_f 0.57 (hexane/EtOAc 1:1).

A solution of **38** (200 mg, 0.62 mmol) in CH_2Cl_2 (15 mL) was filtered through a 0.2 μm PTFE filter and treated with a methanolic solution of HCl (0.53 N, 3.53 mL, 1.87 mmol). The resulting solution was evaporated at reduced pressure and the solid was washed with pentane (3 × 10 mL) to give, after drying under standard conditions, **38**·HCl (200 mg) as a beige solid: mp 222–224 ºC; IR (ATR) *ν* 3650–2500 (max at 3628, 3342, 3085, 3061, 2921, 2560, $^+$NH and CH st), 2231 (CN st), 1634, 1602, 1576, 1505 (Ar–C–C and Ar–C–N st) cm^{-1}; ^1H NMR (400 MHz, CD_3OD) *δ* 2.20 (tt, *J*=6.0 Hz, *J*=5.2 Hz, 2H, 3'-H_2), 2.84 (t, *J*=6.0 Hz, 2H, 4'-H_2), 4.82 (t, *J*=5.2 Hz, 2H, 2'-H_2), 4.87 (s, $^+$NH), 7.97 (br d, *J*=8.0 Hz, 2H), 8.08 (br d, *J*=8.0 Hz, 2H) [C2(6)-H, C3(5)-H], overimposed in part 8.07 (dm, *J*=8.8 Hz, 1H, 8'-H), 8.15 (d, *J*=8.8 Hz, 1H, 7'-H), 8.42 (d, *J*=2.0 Hz, 1H, 10'-H); ^{13}C NMR (100.6 MHz, CD_3OD) *δ* 21.4 (CH_2, C3'), 23.3

(CH_2, C4'), 71.5 (CH_2, C2'), 115.8 (C, C4a'), 116.6 (C, C1), 118.7 (C, CN), 122.0 (C, C10a'), 123.09 (CH), 123.13 (CH) (C7', C10'), 131.5 (2CH), 134.1 (2CH) [C2(6), C3(5)], 136.0 (C, C9'), 136.2 (CH, C8'), 136.5 (C, C4), 138.0 (C, C6a'), 155.9 (C, C5'), 166.5 (C, C10b'); HRMS (ESI), calcd for [$C_{19}H_{13}{}^{35}ClN_2O$ + H^+] 321.0789, found 321.0786; Elemental analysis, calcd for $C_{19}H_{13}ClN_2O{\cdot}HCl{\cdot}0.4H_2O$ C 62.62%, H 4.09%, N 7.69%, found C 62.79%, H 4.26%, N 7.48%. HPLC purity > 99%.

*4.1.20. 4-{9-Chloro-3,4-dihydro-2H-pyrano[3,2-c]quinolin-5-yl}benzylamine **39***

It was prepared as described for **3**. From nitrile **38** (1.00 g, 3.12 mmol) and $LiAlH_4$ (59 mg, 1.55 mmol), a residue (1.29 g) was obtained and purified by column chromatography (35–70 μm silica gel, EtOAc/MeOH/50% aq. NH_4OH mixtures, gradient elution). On elution with EtOAc/MeOH/50% aq. NH_4OH 95:5:0.2 to 80:20:0.2, the amine **39** (595 mg, 59% yield) was isolated as a yellow solid; R_f 0.14 (EtOAc/MeOH/50% aq. NH_4OH 9:1:0.05).

A solution of **39** (595 mg, 1.84 mmol) in CH_2Cl_2 (25 mL) was filtered through a 0.2 μm PTFE filter and treated with a methanolic solution of HCl (0.53 N, 31 mL, 16.4 mmol). The resulting solution was evaporated at reduced pressure and the solid was recrystallized from MeOH/hexane 1:4 (5 mL) and washed with pentane (3 × 20 mL) to give, after drying under standard conditions, **39**·2HCl (720 mg) as a beige solid: mp 153–155 ºC; IR (ATR) *v* 3500–2500 (max at 3374, 2858, 2706, 2614, $^+$NH and CH st), 1634, 1615, 1604, 1580, 1513 (Ar–C–C and Ar–C–N st) cm^{-1}; ^{1}H NMR (400 MHz, CD_3OD) δ 2.18 (tt, *J*=6.4 Hz, *J'*=5.2 Hz, 2H, 3'-H_2), 2.85 (t, *J*=6.4 Hz, 2H, 4'-H_2), 4.32 (s, 2H, 1-CH_2-NH_2), 4.80 (t, *J*=5.2 Hz, 2H, 2'-H_2), 4.86 (s, $^+$NH, $^+NH_3$), 7.82 (d, *J*=8.4 Hz, 2H), 7.86 (d, *J*=8.4 Hz, 2H) [C2(6)-H, C3(5)-H], 8.04 (dd, *J*=8.8 Hz, *J'*=2.4 Hz, 1H, 8'-H), 8.15 (d, *J*=8.8 Hz, 1H, 7'-H), 8.40 (d, *J*=2.4 Hz, 1H, 10'-H); ^{13}C NMR (100.6 MHz, CD_3OD) δ 21.5 (CH_2, C3'), 23.6 (CH_2, C4'), 43.8 (CH_2, 1-CH_2-NH_2), 71.3 (CH_2, C2'), 115.7 (C, C4a'), 121.9 (C, C10a'), 123.0 (CH), 123.3 (CH) (C7', C10'), 130.8 (2CH), 131.1 (2CH) [C2(6), C3(5)], 133.2 (C, C4), 135.7 (C, C9'), 135.9 (CH, C8'), 138.17 (C), 138.23 (C) (C1, C6a'), 157.4 (C, C5'), 166.0 (C, C10b'); HRMS (ESI), calcd for [$C_{19}H_{17}{}^{35}ClN_2O$ + H^+] 325.1102, found 325.1096; Elemental analysis, calcd for $C_{19}H_{17}ClN_2O{\cdot}2HCl{\cdot}1.1H_2O$ C 54.65%, H 5.12%, N 6.71%, found C 54.96%, H 5.66%, N 6.44%. HPLC purity: 96%.

*4.1.21. 9-Chloro-5-(2-furyl)-3,4-dihydro-2H-pyrano[3,2-c]quinoline **42***

It was prepared as described for **8**. From 4-chloroaniline, **10** (1.52 g, 11.9 mmol), furan-2-carboxaldehyde, **40** (0.98 mL, 1.14 g, 11.8 mmol), $Sc(OTf)_3$ (1.18 g, 2.40 mmol), and 3,4-dihydro-2*H*-pyran, **36** (1.08 mL, 994 mg, 11.8 mmol), and heating the reaction mixture at 50 ºC, a brown oily residue (4.67 g) was obtained and used in the next step without further purification.

From this crude (4.67 g) and DDQ (5.39 g, 23.7 mmol), a brown solid residue (4.22 g) was obtained and purified through column chromatography (35–70 μm silica gel, hexane/EtOAc mixtures, gradient elution). On elution with hexane/EtOAc 80:20, compound **42** (916 mg, 27% yield) was isolated as a yellowish solid. On elution with hexane/EtOAc 50:50, 3-[6-chloro-2-(2-furyl)quinolin-3-yl]-1-propanol, **44** (1.01 g, 30% yield) was isolated as a yellowish solid; $R_{f(\mathbf{43})}$ 0.51; $R_{f(\mathbf{45})}$ 0.35 (hexane/EtOAc 1:1).

Compound **42** (916 mg, 3.21 mmol) was recrystallized from hexane/EtOAc 57:43 (7 mL), taken in CH_2Cl_2 (15 mL), filtered through a 0.2 μm PTFE filter and treated with a methanolic solution of HCl (0.53 N, 11 mL, 5.83 mmol). The resulting solution was evaporated at reduced pressure and the solid was washed with pentane (3 × 15 mL) to give, after drying under standard conditions, **42**·HCl (585 mg) as a yellowish solid: mp 243–245 ºC; IR (ATR) *ν* 3500–2400 (max at 3085, 2435, $^+$NH and CH st), 1629, 1602, 1580, 1514 (Ar–C–C and Ar–C–N st) cm^{-1}; ^{1}H NMR (400 MHz, CD_3OD) δ 2.30 (tt, *J*=6.4 Hz, *J'*=5.6 Hz, 2H, 3-H_2), 3.17 (t, *J*=6.4 Hz, 2H, 4-H_2), 4.79 (t, *J*=5.6 Hz, 2H, 2-H_2), 4.85 (s, $^+$NH), 6.96 (dd, *J*=3.6 Hz, *J'*=1.6 Hz, 1H, 4'-H), 7.72 (d, *J*=3.6 Hz, 1H, 3'-H), 7.99 (dd, *J*=8.8 Hz, *J'*=2.4 Hz, 1H, 8-H), 8.18 (d, *J*=1.6 Hz, 1H, 5'-H), 8.26 (d, *J*=8.8 Hz, 1H, 7-H), 8.29 (d, *J*=2.4 Hz, 1H, 10-H); ^{13}C NMR (100.6 MHz, CD_3OD) δ 21.3 (CH_2, C3), 23.7 (CH_2, C4), 70.8 (CH_2, C2), 113.4 (C, C4a), 115.3 (CH, C4'), 121.2 (C, C10a), 122.7 (CH, C3'), 122.8 (CH, C7), 122.9 (CH, C10), 135.3 (C, C9), 135.9 (CH, C8), 137.7 (C, C6a), 144.8 (C, C5), 145.2 (C, C2'), 149.8 (CH, C5'), 165.6 (C, C10b); HRMS (ESI), calcd for [$C_{16}H_{12}{}^{35}ClNO_2$ + H^+] 286.0629, found 286.0629; Elemental analysis, calcd for $C_{16}H_{12}ClNO_2$·HCl C 59.65%, H 4.07%, N 4.35%, found C 59.72%, H 4.00%, N 4.46%. HPLC purity: 97%.

A solution of **44** (100 mg, 0.35 mmol) in CH_2Cl_2 (7 mL) was filtered through a 0.2 μm PTFE filter and treated with a methanolic solution of HCl (0.53 N, 2.1 mL, 1.11 mmol). The resulting solution was evaporated at reduced pressure and the solid was

recrystallized from MeOH/hexane 1:2 (4.5 mL) and washed with pentane (3 × 5 mL) to give, after drying under standard conditions, **44**·HCl (110 mg) as a brown solid: mp 202–203 ºC; IR (ATR) *ν* 3500–2400 (max at 3384, 3121, 3072, 3053, 2927, 2487, $^{+}$NH, OH, and CH st), 1696, 1633, 1589, 1556, 1524 (Ar–C–C and Ar–C–N st) cm^{-1}; ^{1}H NMR (400 MHz, CD_3OD) *δ* 2.03 (tt, *J*=8.0 Hz, *J'*=6.0 Hz, 2H, 2-H_2), 3.30 (t, *J*=8.0 Hz, 2H, 3-H_2), 3.76 (t, *J*=6.0 Hz, 2H, 1-H_2), 4.88 (s, OH and $^{+}$NH), 6.99 (dd, *J*=3.6 Hz, *J*=1.6 Hz, 1H, 4"-H), 7.93 (d, *J*=3.6 Hz, 1H, 3"-H), 8.05 (dd, *J*=9.2 Hz, *J'*=2.4 Hz, 1H, 7'-H), 8.21 (d, *J*=1.6 Hz, 1H, 5"-H), 8.28 (d, *J*=2.4 Hz, 1H, 5'-H), 8.38 (d, *J*=9.2 Hz, 1H, 8'-H), 8.93 (s, 1H, 4'-H); ^{13}C NMR (100.6 MHz, CD_3OD) *δ* 30.6 (CH_2, C3), 32.8 (CH_2, C2), 61.8 (CH_2, C1), 115.6 (CH, C4"), 123.2 (CH, C3"), 123.3 (CH, C8'),128.3 (CH, C5'), 129.4 (C, C4a'), 136.0 (CH, C7'), 136.2 (C, C6'), 136.4 (C, C8a'), 137.1 (C, C3'), 144.7 (C, C2'), 145.6 (C, C2"), 146.5 (CH, C4'), 150.4 (CH, C5"); HRMS (ESI), calcd for [$C_{16}H_{14}{}^{35}ClNO_2$ + H^+] 288.0786, found 288.0785; Elemental analysis, calcd for $C_{16}H_{14}ClNO_2$·HCl C 59.28%, H 4.66%, N 4.32%, found C 58.92%, H 4.68%, N 4.10%.

4.1.22. 9-Chloro-3,4-dihydro-5-(2-thienyl)-2H-pyrano[3,2-c]quinoline ***43***

It was prepared as described for **8**. From 4-chloroaniline, **10** (1.52 g, 11.9 mmol), thiophene-2-carboxaldehyde, **41** (1.11 mL, 1.33 g, 11.9 mmol), $Sc(OTf)_3$ (1.17 g, 2.38 mmol), and 3,4-dihydro-2*H*-pyran, **36** (1.08 mL, 994 mg, 11.8 mmol), and heating the reaction mixture at 80 ºC, a brown oily residue (3.64 g) was obtained and used in the next step without further purification.

From this crude (3.64 g) and DDQ (5.40 g, 23.8 mmol), a residue (4.07 g) was obtained and purified through column chromatography (35–70 μm silica gel, hexane/EtOAc mixtures, gradient elution). On elution with hexane/EtOAc 90:10, compound **43** (1.43 g, 40% yield) was isolated. On elution with hexane/EtOAc 60:40, 3-[6-chloro-2-(2-thienyl)quinolin-3-yl]-1-propanol, **45** (854 mg, 24% yield) was isolated; $R_{f\,(\mathbf{44})}$ 0.70 (hexane/EtOAc 7:3); $R_{f\,(\mathbf{46})}$ 0.34 (hexane/EtOAc 1:1).

A solution of **43** (500 mg, 1.66 mmol) in CH_2Cl_2 (10 mL) was filtered through a 0.2 μm PTFE filter and treated with a methanolic solution of HCl (0.53 N, 9.4 mL, 4.98 mmol). The resulting solution was evaporated at reduced pressure and the solid was recrystallized from MeOH/EtOAc 1:2 (3 mL) and washed with pentane (3 × 8 mL) to give, after drying under standard conditions, **43**·HCl (469 mg) as a yellowish solid: mp

224–225 ºC; IR (ATR) *ν* 3500–2500 (max at 3245, 3056, 2935, 2603, $^{+}$NH and CH st), 1629, 1602, 1569, 1530 (Ar–C–C and Ar–C–N st) cm^{-1}; ^{1}H NMR (400 MHz, CD_3OD) *δ* 2.22 (tt, *J*=6.0 Hz, *J'*=5.4 Hz, 2H, 3-H_2), 3.08 (t, *J*=6.0 Hz, 2H, 4-H_2), 4.79 (t, *J*=5.4 Hz, 2H, 2-H_2), 4.88 (s, $^{+}$NH), 7.43 (dd, *J*=5.2 Hz, *J'*=4.0 Hz, 1H, 4'-H), 7.88 (dd, *J*=4.0 Hz, *J'*=1.2 Hz, 1H, 3'-H), 8.02 (dd, *J*=8.8 Hz, *J'*=2.4 Hz, 1H, 8-H), 8.08 (dd, *J*=5.2 Hz, *J'*=1.2 Hz, 1H, 5'-H), 8.16 (d, *J*=8.8 Hz, 1H, 7-H), 8.35 (d, *J*=2.4 Hz, 1H, 10-H); ^{13}C NMR (100.6 MHz, CD_3OD) *δ* 21.5 (CH_2, C3), 24.1 (CH_2, C4), 71.1 (CH_2, C2), 115.7 (C, C4a), 121.7 (C, C10a), 123.0 (2CH, C7, C10), 129.5 (CH, C4'), 131.9 (C, C2'), 134.2 (CH, C5'), 134.9 (CH, C3'), 135.5 (C, C9), 136.0 (CH, C8), 138.1 (C, C6a), 151.6 (C, C5), 165.9 (C, C10b); HRMS (ESI), calcd for [$C_{16}H_{12}{}^{35}ClNOS$ + H^{+}] 302.0401, found 302.0399; Elemental analysis, calcd for $C_{16}H_{12}ClNOS{\cdot}HCl$ C 56.81%, H 3.87%, N 4.14%, S 9.48%, found C 56.99%, H 3.85%, N 3.98%, S 9.27%. HPLC purity: 97%.

A solution of **45** (411 mg, 1.35 mmol) in CH_2Cl_2 (4.5 mL) was filtered through a 0.2 μm PTFE filter and treated with a methanolic solution of HCl (0.53 N, 8.1 mL, 4.29 mmol). The resulting solution was evaporated at reduced pressure and the solid was washed with pentane (3 × 5 mL) to give, after drying under standard conditions, **45**·HCl (110 mg) as a yellowish solid: mp 198–199 ºC; IR (ATR) *ν* 3500–2400 (max at 3337, 3076, 3029, 2918, 2886, 2476, $^{+}$NH, OH and CH st), 1633, 1583, 1538, 1514 (Ar–C–C and Ar–C–N st) cm^{-1}; ^{1}H NMR (400 MHz, CD_3OD) *δ* 1.92 (tt, *J*=8.0 Hz, *J'*=6.0 Hz, 2H, 2-H_2), 3.21 (t, *J*=8.0 Hz, 2H, 3-H_2), 3.63 (t, *J*=6.0 Hz, 2H, 1-H_2), 4.92 (s, OH and $^{+}$NH), 7.43 (dd, *J*=5.2 Hz, *J'*=4.0 Hz, 1H, 4"-H), 7.90 (dd, *J*=4.0 Hz, *J'*=1.2 Hz, 1H, 3"-H), 8.07 (dd, *J*=9.2 Hz, *J'*=2.0 Hz, 1H, 7'-H), superimposed in part 8.08 (dd, *J*=5.2 Hz, *J'*=1.2 Hz, 1H, 5"-H), 8.28 (d, *J*=9.2 Hz, 1H, 8'-H), 8.34 (d, *J*=2.0 Hz, 1H, 5'-H), 9.01 (s, 1H, 4'-H); ^{13}C NMR (100.6 MHz, CD_3OD) *δ* 30.4 (CH_2, C3), 33.7 (CH_2, C2), 61.8 (CH_2, C1), 123.6 (CH, C8'), 128.3 (CH, C5'), 129.6 (CH, C4"), 130.2 (C, C4a'), 132.4 (C, C2"), 134.3 (CH, C5"), 135.1 (CH, C3"), 135.9 (CH, C7'), 136.7 (C, C6'), 137.6 (C, C8a'), 138.6 (C, C3'), 146.2 (CH, C4'), 151.9 (C, C2'); HRMS (ESI), calcd for [$C_{16}H_{14}{}^{35}ClNOS$ + H^{+}] 304.0557, found 304.0555; Elemental analysis, calcd for $C_{16}H_{14}ClNOS{\cdot}HCl.1/5H_2O$ C 55.89%, H 4.51%, N 4.07%, found C 55.86%, H 4.73%, N 3.55%.

4.1.23. N-(tert-butyldimethylsilyloxy)-N-[3-(6-chloro-2-(2-thienyl)quinolin-3-yl)propyl]-4-methylbenzenesulfonamide ***46***

To a solution of alcohol **45** (400 mg, 1.32 mmol) in anhydrous toluene (4 mL) and THF (1.2 mL), *N*-(*tert*-butyldimethylsilyloxy)-4-methylbenzenesulfonamide (397 mg, 1.32 mmol) and PPh_3 (691 mg, 2.63 mmol) were added. The mixture was cooled to 0 ºC and treated dropwise with DEAD (40% solution in toluene, 0.86 mL, 1.98 mmol). The reaction mixture was stirred at room temperature for 5 min, concentrated at reduced pressure and purified through column chromatography (35–70 μm silica gel, hexane/EtOAc mixtures, gradient elution). On elution with hexane/EtOAc 90:10, slightly impure **46** (913 mg) was isolated; R_f 0.60 (hexane/EtOAc 1:1); mp 91–92 ºC; IR (ATR) *v* 1594, 1548, 1522 (Ar–C–C and Ar–C–N st), 1359, 1168 (SO_2) cm^{-1}; ^1H NMR (400 MHz, $CDCl_3$) δ 0.09 [s, 6H, $Si(CH_3)_2$], 0.72 [s, 9H, $Si[C(CH_3)_3]$], 1.80 (tt, *J*=*J'*=7.4 Hz, 2H, 2-H_2), 2.25 (s, 3H, tosyl CH_3), 2.81 (t, *J*=7.2 Hz, 2H), 2.90 (t, *J*=7.6 Hz, 2H) (1-H_2 and 3-H_2), 6.97 (dd, *J*=4.8 Hz, *J'*=4.0 Hz, 1H, 4''-H), 7.09–7.18 (complex signal), 7.20–7.24 (complex signal) [4H, 3''-H, 5''-H, and tosyl-C3(5)-H], 7.42 (dd, *J*=9.2 Hz, *J'*=2.0 Hz, 1H, 7'-H), 7.51 [br d, *J*=8.4 Hz, 2H, tosyl-C2(6)-H], 7.57 (d, *J*=2.0 Hz, 1H, 5'-H), 7.74 (s, 1H, 4'-H), 7.85 (d *J*=9.2 Hz, 1H, 8'-H); ^{13}C NMR (100.6 MHz, $CDCl_3$) δ – 4.1 [$2CH_3$, $Si(CH_3)_3$], 18.4 [C, $SiC(CH_3)_3$], 21.8 (CH_3, tosyl CH_3), 26.1 [$3CH_3$, $SiC(CH_3)_3$], 27.3 (CH_2, C2), 30.8 (CH_2, C3), 55.4 (CH_2, C1), significant aromatic signals: 125.7 (CH, C8'), 129.5 [2CH, tosyl-*C*3(5)], 130.0 [2CH, tosyl-*C*2(6)], 132.4 (C), 132.8 (C) (C6', C8a'), 136.0 (CH, C4'), 144.8 (C, C3'), 152.9 (C, C2'); HRMS (ESI), calcd for [$C_{29}H_{35}{}^{35}ClN_2O_3S_2Si + H^+$] 587.1620, found 587.1596.

4.1.24. 3-[6-Chloro-2-(2-thienyl)quinolin-3-yl]propanenitrile ***47***

To a solution of **46** (450 mg of a total amount of 913 mg of slightly impure **46**, obtained from 1.32 mmol of alcohol **45**) in anhydrous CH_3CN (8 mL), CsF (233 mg, 1.53 mmol) was added. The reaction mixture was stirred at 60 ºC for 2.5 h, diluted with saturated aq. NH_4Cl (20 mL), and extracted with EtOAc (2 × 20 mL). The combined organic extracts were washed with brine (50 mL), dried over anhydrous Na_2SO_4 and evaporated at reduced pressure to give a crude (252 mg), which was purified through column chromatography (35–70 μm silica gel, hexane/EtOAc mixtures, gradient elution). On elution with hexane/EtOAc 70:30, nitrile **47** (164 mg, 84% overall yield from alcohol **45**) was isolated as a yellowish solid; R_f 0.57 (hexane/EtOAc 1:1).

A solution of **47** (32 mg, 0.11 mmol) in CH_2Cl_2 (4.5 mL) was filtered through a 0.2 µm PTFE filter and treated with a methanolic solution of HCl (0.53 N, 1.7 mL, 0.90 mmol). The resulting solution was evaporated at reduced pressure and the solid was washed with pentane (3 × 5 mL) to give, after drying under standard conditions, **47**·HCl (34 mg) as a yellowish solid: mp 65–67 ºC; IR (ATR) *ν* 3600–2400 (max at 3371, 3111, 3070, 2925, 2853, 2599, $^{+}$NH and CH st), 2243 (CN st), 1636, 1591, 1540 (ar–C–C and ar–C–N st) cm^{-1}; ^{1}H NMR (400 MHz, CD_3OD) *δ* 2.89 (t, *J*=5.6 Hz, 2H, 2-H_2), 3.46 (m, 2H, 3-H_2), 4.92 (s, $^{+}$NH), 7.42 (m, 1H, 4''-H), 7.86 (br d, *J*=2.8 Hz, 1H, 3''-H), 8.02–8.08 (complex signal, 2H, 7'-H, 5''-H), 8.25 (d, *J*=8.8 Hz, 1H, 8'-H), 8.33 (br s, 1H, 5'-H), 9.01 (s, 1H, 4'-H); ^{13}C NMR (100.6 MHz, CD_3OD) *δ* 17.8 (CH_2, C2), 29.5 (CH_2, C3), 119.8 (C, C1), 125.7 (CH, C8'), 128.2 (CH, C5'), 129.6 (CH, C4''), 129.9 (C, C4a'), 133.3 (CH, C5''), 133.8 (CH, C3''), 134.3 (C, C3'), 134.8 (C, C2''), 135.3 (CH, C7'), 136.2 (C, C6'), 140.2 (C, C8a'), 144.2 (CH, C4'), 152.6 (C, C2'); HRMS (ESI), calcd for [$C_{16}H_{11}{}^{35}ClN_2S$ + H^+] 299.0404, found 299.0402; Elemental analysis, calcd for $C_{16}H_{11}ClN_2S$·HCl.1.3H_2O C 53.58%, H 4.10%, found C 53.80%, H 3.79%; HPLC purity: 96%.

*4.1.25. 3-[6-Chloro-2-(2-thienyl)quinolin-3-yl]propyl methanesulfonate **48***

A solution of alcohol **45** (494 mg, 1.63 mmol) and freshly distilled Et_3N (271 µL, 197 mg, 1.94 mmol) was cooled to 0 ºC and treated dropwise with MsCl (163 µL, 241 mg, 2.11 mmol) over 10 min. The reaction mixture was stirred at 0 ºC for 30 min, poured into a mixture of H_2O (30 mL) and ice (6 mL), and extracted with CH_2Cl_2 (2 × 20 mL). The combined organic extracts were washed with saturated aq. $NaHCO_3$ (20 mL), brine (20 mL), dried over anhydrous Na_2SO_4 and evaporated at reduced pressure to give crude mesylate **48** (633 mg), which was used in the next step without further purification; R_f 0.50 (hexane/EtOAc 1:1); mp 130–132 ºC; IR (ATR) *ν* 1593, 1548, 1522 (ar–C–C and ar–C–N st), 1358, 1339, 1169 (SO_2) cm^{-1}; ^{1}H NMR (400 MHz, $CDCl_3$) *δ* 2.11 (tt, *J*=7.6 Hz, *J'*=6.0 Hz, 2H, 2-H_2), 3.00 (s, 3H, CH_3SO_3), 3.21 (t, *J*=7.6 Hz, 2H, 3-H_2), 4.27 (t, *J*=6.0 Hz, 2H, 1-H_2), 7.20 (dd, *J*=4.8 Hz, *J'*=4.0 Hz, 1H, 4''-H), 7.55 (d, *J*=4.8 Hz, 1H, 5''-H), 7.62 (d, *J*=4.0 Hz, 1H, 3''-H), superimposed in part 7.64 (dd, *J*=9.2 Hz, *J'*=2.0 Hz, 1H, 7'-H), 7.77 (d, *J*=2.0 Hz, 1H, 5'-H), 8.03 (s, 1H, 4'-H), 8.15 (d, *J*=9.2 Hz, 1H, 8'-H); ^{13}C NMR (100.6 MHz, $CDCl_3$) *δ* 29.3 (CH_2), 29.5 (CH_2) (C2, C3), 37.4 (CH_3, CH_3SO_3), 68.6 (CH_2, C1), 125.6 (C+CH, C4a', C8'), 127.7 (C, C2''), 127.9 (CH), 129.0 (CH), 129.1 (CH), 129.6 (CH), 131.2 (CH) (C5', C7', C3'', C4'', C5''), 132.4 (C),

133.0 (C) (C6', C8a'), 137.2 (CH, C4'), 143.7 (C, C3'), 152.2 (C, C2'); HRMS (ESI), calcd for [$C_{17}H_{16}{}^{35}ClNO_3S_2$ + H^+] 382.0333, found 382.0335.

*4.1.26. N-{3-[6-Chloro-2-(2-thienyl)quinolin-3-yl]propyl}pyrrolidine **49***

To a solution of crude mesylate **48** (296 mg of a total amount of 633 mg of crude mesylate **48** obtained from 1.63 mmol of alcohol **45**) in anhydrous DMF (10 mL), pyrrolidine (0.13 mL, 111 mg, 1.56 mmol) and K_2CO_3 (322 mg, 2.33 mmol) were added. The reaction mixture was stirred at 85 ºC overnight, cooled to room temperature, treated with saturated aq. $NaHCO_3$ (20 mL), and extracted with EtOAc (3 × 30 mL). The combined organic extracts were washed with H_2O (3 × 15 mL), dried over anhydrous Na_2SO_4 and evaporated at reduced pressure to give a crude (165 mg), which was purified through column chromatography (35–70 μm silica gel, EtOAc/MeOH/50% aq. NH_4OH mixtures, gradient elution). On elution with EtOAc/MeOH/50% aq. NH_4OH 80:20:0.2, amine **49** (84 mg, 31% overall yield from alcohol **45**) was isolated; R_f 0.10 (hexane/EtOAc 1:1).

A solution of **49** (84 mg, 0.24 mmol) in CH_2Cl_2 (4.5 mL) was filtered through a 0.2 μm PTFE filter and treated with a methanolic solution of HCl (0.53 N, 4.0 mL, 2.12 mmol). The resulting solution was evaporated at reduced pressure and the solid was washed with pentane (3 × 5 mL) to give, after drying under standard conditions, **49**·2HCl (88 mg) as a yellowish solid: mp 136–138 ºC; IR (ATR) ν 3200–2600 (max at 3076, 2941, 2931, 2858, $^+$NH and CH st), 1594, 1548, 1525 (ar–C–C and ar–C–N st) cm^{-1}; ^{1}H NMR (400 MHz, CD_3OD) δ 2.04 (br signal, 2H, 2-H_2), 2.12–2.26 [complex signal, 4H, pyrrolidine 3(4)-H_2], 3.10 (br signal, 2H), 3.24 (br signal, 4H), 3.66 (br signal, 2H) [1-H_2, 3-H_2, pyrrolidine 2(5)-H_2], 7.45 (br s, 1H, 4"-H), 7.93 (br s, 1H, 3"-H), 8.04–8.12 (complex signal, 2H, 7'-H, 5"-H), 8.30 (d, J=8.4 Hz, 1H, 8'-H), 8.39 (br s, 1H, 5'-H), 9.14 (s, 1H, 4'-H); ^{13}C NMR (100.6 MHz, CD_3OD) δ 24.1 [2CH_2, pyrrolidine C3(4)], 27.1 (CH_2, C2), 30.6 (CH_2, C3), 55.19 (CH_2, C1), 55.21 [2CH_2, pyrrolidine C2(5)], 123.8 (CH, C8'), 128.5 (CH, C5'), 129.8 (CH, C4"), 130.2 (C, C4a'), 132.2 (C, C2"), 134.4 (CH, C5"), 135.4 (CH, C3"), 136.1 (CH, C7'), 136.66 (C), 136.73 (C) (C6', C8a'), 137.9 (C, C3'), 146.3 (CH, C4'), 152.0 (C, C2'); HRMS (ESI), calcd for [$C_{20}H_{21}{}^{35}ClN_2S$ + H^+] 357.1187, found 357.1187; Elemental analysis, calcd for $C_{20}H_{21}ClN_2S$·2HCl.3H_2O C 49.64%, H 6.04%, N 5.79%, found C 49.98%, H 5.72%, N 5.29%; HPLC purity: 96%.

*4.1.27. N-{3-[6-Chloro-2-(2-thienyl)quinolin-3-yl]propyl}-N,N-diethylamine **50***

It was prepared as described for **49**. From crude mesylate **48** (293 mg of a total amount of 585 mg of crude mesylate **48** obtained from 0.82 mmol of alcohol **45**) and freshly distilled Et_2NH (320 μL, 226 mg, 3.09 mmol), a crude product (157 mg) was obtained and purified by column chromatography (35–70 μm silica gel, EtOAc/MeOH/50% aq. NH_4OH mixtures, gradient elution). On elution with EtOAc/MeOH/50% aq. NH_4OH 80:20:0.2, the amine **50** (24 mg, 16% overall yield from alcohol **45**) was isolated; R_f 0.10 (hexane/EtOAc 1:1).

A solution of **50** (24 mg, 66.9 μmol) in CH_2Cl_2 (4.5 mL) was filtered through a 0.2 μm PTFE filter and treated with a methanolic solution of HCl (0.53 N, 1.2 mL, 0.64 mmol). The resulting solution was evaporated at reduced pressure and the solid was washed with pentane (3 × 5 mL) to give, after drying under standard conditions, **50**·2HCl (24 mg) as a yellowish solid: mp 98–100 ºC; IR (ATR) *v* 3500–2500 (max at 3422, 3117, 3071, 2933, 2863, 2648, $^+$NH and CH st), 1637, 1592, 1540 (ar–C–C and ar–C–N st) cm^{-1}; ^{1}H NMR (400 MHz, CD_3OD) δ 1.32 [m, 6H, $N(CH_2CH_3)_2$], 2.16 (br signal, 2H, 2-H_2), 3.16–3.28 [complex signal, 8H, 1-H_2, 3-H_2, $N(CH_2CH_3)_2$], 4.89 (s, $^+$NH), 7.43 (br s, 1H, 4”-H), 7.90 (br s, 1H, 3”-H), 8.04–8.09 (complex signal, 2H, 7’-H, 5”-H), 8.25 (d, *J*=8.8 Hz, 1H, 8’-H), 8.36 (br s, 1H, 5’-H), 9.08 (s, 1H, 4’-H); ^{13}C NMR (100.6 MHz, CD_3OD) δ 9.24 [CH_3, $N(CH_2CH_3)_2$], 25.2 (CH_2, C2), 30.7 (CH_2, C3), 48.6 [CH_2, $N(CH_2CH_3)_2$], 52.2 (CH_2, C1), 124.3 (CH, C8’), 128.4 (CH, C5’), 129.7 (CH, C4”), 130.2 (C, C4a’), 133.1 (C, C2”), 134.0 (CH, C5”), 134.9 (CH, C3”), 135.8 (CH, C7’), 136.5 (C), 136.6 (C) (C6’, C8a’), 138.5 (C, C3’), 145.6 (CH, C4’), 152.2 (C, C2’); HRMS (ESI), calcd for [$C_{20}H_{23}{}^{35}ClN_2S$ + H^+] 359.1343, found 359.1347; Elemental analysis, calcd for $C_{20}H_{23}ClN_2S$·2HCl.2.5H_2O C 50.37%, H 6.34%, N 5.87%, found C 50.55%, H 6.07%, N 5.38%; HPLC purity: > 99%.

4.2. Biological assays

4.2.1. T. brucei culturing and evaluation of trypanocidal activity

Bloodstream form *T. brucei* (strain 221) was cultured at 37 ºC in modified Iscove's medium [51]. Trypanocidal activity was assessed by growing parasites in the presence of various concentrations of the novel compounds and determining the levels which inhibited growth by 50% (IC_{50}) and 90% (IC_{90}). *T. brucei* in the logarithmic phase of growth were diluted back to 2.5×10^4 mL^{-1} and aliquoted into 96-well plates. The compounds were then added at a range of concentrations and the plates incubated at 37 °C. Each drug concentration was tested in triplicate. Resazurin was added after 48 h and the plates incubated for a further 16 h and the plates then read in a Spectramax plate reader. Results were analysed using GraphPad Prism.

4.2.2. T. cruzi and L. infantum culturing and evaluation of trypanocidal and leishmanicidal activity

Stock solutions of the novel compounds in DMSO were prepared at concentrations of 20 mg mL^{-1}, with the final DMSO concentration being lower than 2% for all experiments. Trypanocidal leishmanicidal activity was assessed by growing parasites in the presence of various concentrations of the novel compounds and determining the levels which inhibited growth by 50% (IC_{50}). The IC_{50} was determined from a least-squares linear regression of growth rate versus log drug concentrations.

T. cruzi strain MHOM/ES/2203/BCN590 (Tcl) was used. Epimastigote forms were cultured in liver infusion tryptose broth (LIT) with 10% fetal bovine serum and 1% penicillin (100 U mL^{-1}) – streptomycin (100 µg mL^{-1}) solution (Sigma P-4333) at 28 ºC.

For evaluation of *T. cruzi* activity serial dilutions of the novel compounds in LIT culture medium were aliquoted in 96-well microtiter plates (Costar 3596). Then 4×10^6 mL^{-1} epimastigotes culture medium in the logarithmic growth phase were added to each well, incubating at 28 ºC for 72 h. Benznidazole was used as the reference drug at concentrations from 2.50 mM to 2.42 µM. Parasite inhibition for each drug concentration was determined using an automated cell counter (TC20 BIO-RAD). All assays were performed in duplicate at least twice.

L. infantum strain MCAN/ES/92/BCN722, isolated from a dog with visceral leishmaniosis, was used. Promastigote forms were cultured in Schneider's insect

medium (Sigma S-8995), pH 7, with 20% heat-inactivated fetal calf serum, 25 μg mL^{-1} gentamycin solution (Sigma G-1397), and 1% penicillin (100 U mL^{-1}) – streptomycin (100 μg mL^{-1}) solution (Sigma P-4333) at 26 ºC. Serial dilutions of the novel compounds in Schneider culture medium were performed in 96-well microtiter plates (Costar 3596). Then 10^6 mL^{-1} promastigotes in their logarithmic growth phase was added to each well (100 μL/well), incubating at 26 ºC for 48 h. Potassium antimony (III) tartrate hydrate was used as the reference drug at concentrations from 815 to 0.80 μM. Growth was measured through the acid phosphatase activity [52]. All assays were performed in duplicate at least twice.

4.2.3. Cytotoxic activity against rat skeletal myoblast L6 cells

Cytotoxicity against mammalian cells was assessed using microtitre plates following a described procedure [53]. Briefly, rat skeletal muscle L6 cells were seeded at 1×10^4 mL^{-1} in 200 μL of growth medium containing different compound concentrations. The plates were incubated for 6 days at 37 ºC and 20 μL resazurin was then added to each well. After a further 8 h incubation, the fluorescence was determined using a Spectramax plate reader.

4.2.4. Acetylcholinesterase inhibitory activity

The inhibitory activity against *Electrophorus electricus* (Ee) AChE (Sigma-Aldrich) was evaluated spectrophotometrically by the method of Ellman *et al.* [54]. The reactions took place in a final volume of 300 μL of 0.1 M phosphate-buffered solution pH 8.0, containing EeAChE (0.03 u/mL) and 333 μM 5,5'-dithiobis(2-nitrobenzoic) acid (DTNB; Sigma-Aldrich) solution used to produce the yellow anion of 5-thio-2-nitrobenzoic acid. Inhibition curves were performed in duplicates using at least 10 increasing concentrations of inhibitors and preincubated for 20 min at 37 ºC before adding the substrate. One duplicate sample without inhibitor was always present to yield 100% of AChE activity. Then substrate, acetylthiocholine iodide (450 μM; Sigma-Aldrich), was added and the reaction was developed for 5 min at 37 ºC. The colour production was measured at 414 nm using a labsystems Multiskan spectrophotometer.

Data from concentration–inhibition experiments of the inhibitors were calculated by non-linear regression analysis, using the GraphPad Prism program package (GraphPad Software; San Diego, USA), which gave estimates of the IC_{50} (concentration of drug

producing 50% of enzyme activity inhibition). Results are expressed as mean ± S.E.M. of at least 4 experiments performed in duplicate.

4.2.5. Determination of brain permeability: PAMPA-BBB assay

The *in vitro* permeability (P_e) of the novel compounds and fourteen commercial drugs through lipid extract of porcine brain membrane was determined by using a parallel artificial membrane permeation assay [49]. Commercial drugs and the target compounds were tested using a mixture of PBS:EtOH 70:30. Assay validation was made by comparing experimental and described permeability values of the commercial drugs, which showed a good correlation: P_e (exp) = 1.583 P_e (lit) – 1.079 (R^2 = 0.9305). From this equation and the limits established by Di *et al.* for BBB permeation, three ranges of permeability were established: compounds of high BBB permeation (CNS+): P_e (10^{-6} cm s^{-1}) > 5.25; compounds of low BBB permeation (CNS–): P_e (10^{-6} cm s^{-1}) < 2.09; and compounds of uncertain BBB permeation (CNS±): 5.25 > P_e (10^{-6} cm s^{-1}) > 2.09.

Acknowledgments

This work was supported by Ministerio de Ciencia e Innovación (MICINN) (CTQ2011-22433, CTQ2012-30930) and Generalitat de Catalunya (GC) (2014SGR52, 2014SGR137, 2014SGR1241). JMK acknowledges funding support from the Wellcome Trust (Grant number WT084175). Fellowships from GC to O.D.P. and E.V. are gratefully acknowledged.

Appendix A. Supplementary material

Supplementary data related to this article can be found at http://dx.doi.org/. These data include calculated molecular properties of the novel compounds, additional results from the PAMPA-BBB assay, as well as copies of the ^{1}H and ^{13}C NMR spectra of the tested compounds.

References

[1] Centers for Disease Control and Prevention, Neglected Tropical Diseases, http://www.cdc.gov/globalhealth/ntd/. Accessed July 7th 2015.

[2] P.J. Hotez, M. Alvarado, M.-G. Basáñez, I. Bolliger, R. Bourne, M. Boussinesq, S.J. Brooker, A. Shah Brown, G. Buckle, C.M. Budke, H. Carabin, L.E. Coffeng, E.M. Fèvre, T. Fürst, Y.A. Halasa, R. Jasrasaria, N.E. Johns, J. Keiser, C.H. King, R. Lozano, M.E. Murdoch, S. O'Hanlon, S.D.S. Pion, R.L. Pullan, K.D. Ramaiah, T. Roberts, D.S. Shepard, J.L. Smith, W.A. Stolk, E.A. Undurraga, J. Utzinger, M. Wang, C.J.L. Murray, M. Naghavi, The Global Burden of Disease Study 2010: Interpretation and implications for the neglected tropical diseases, PLoS Neglected Trop. Dis. 8 (2014) e2865.

[3] P.J. Hotez, A. Fenwick, L. Savioli, D.H. Molyneux, Rescuing the bottom billion through control of neglected tropical diseases, Lancet 373 (2009) 1570–1575.

[4] K. Chibale, New developments in antiinfectives research for tropical infectious diseases, Bioorg. Med. Chem. (2015) in press, DOI: 10.1016/j.bmc.2015.04.077.

[5] M. Zucca, S. Scutera, D. Savoia, New chemotherapeutic strategies against malaria, leishmaniasis and trypanosomiases, Curr. Med. Chem. 20 (2013) 502–526.

[6] L.S. Goupil, J.H. McKerrow, Introduction: Drug discovery and development for neglected diseases, Chem. Rev. 114 (2014) 11131–11137.

[7] A. Rassi Jr., A. Rassi, J.A. Marin-Neto, Chagas disease, Lancet 375 (2010) 1388–1402; G.A. Schmunis, Z.E. Yadon, Chagas disease: a Latin American health problem becoming a world health problem, Acta Trop. 115 (2010) 14–21.

[8] A.S. Nagle, S. Khare, A. Babu Kumar, F. Supek, A. Buchynskyy, C.J.N. Mathison, N. Kumar Chennamaneni, N. Pendem, F.S. Buckner, M.H. Gelb, V. Molteni, Recent developments in drug discovery for leishmaniasis and human African trypanosomiasis, Chem. Rev. 114 (2014) 11305–11347.

[9] S. Alsford, S. Eckert, N. Baker, L. Glover, A. Sanchez-Flores, K.F. Leung, D.J. Turner, M.C. Field, M. Berriman, D. Horn, High-throughput decoding of antitrypanosomal drug efficacy and resistance, Nature 482 (2012) 232–236.

[10] I.M. Vincent, D. Creek, D.G. Watson, M.A. Kamleh, D.J. Woods, P.E. Wong, R.J. Burchmore, M.P. Barrett, A molecular mechanism for eflornithine resistance in African trypanosomes, PLoS Pathog. 6 (2010) e1001204.

[11] A.R. Renslo, J.H. McKerrow, Drug discovery and development for neglected parasitic diseases, Nat. Chem. Biol. 2 (2006) 701–710.

[12] S.L. Croft, M.P. Barrett, J.A. Urbina, Chemotherapy of trypanosomiases and leishmaniasis, Trends Parasitol. 21 (2005) 508–512.

[13] M. Ouellette, J. Drummelsmith, B. Papadopoulou, Leishmaniasis: drugs in the clinic, resistance and new developments, Drug Resist. Updat. 7 (2004) 257–266.

[14] M.P. Barrett, S.L. Croft, Management of trypanosomiasis and leishmaniasis, Br. Med. Bull. 104 (2012) 175–196.

[15] M. Njoroge, N.M. Njuguna, P. Mutai, D.S.B. Ongarora, P.W. Smith, K. Chibale, Recent approaches to chemical discovery and development against malaria and the neglected tropical diseases human African trypanosomiasis and schistosomiasis, Chem. Rev. 114 (2014) 11138–11163.

[16] P.-Y. Shi, P.W. Smith, T.T. Diagana, Therapeutics for neglected infectious diseases: progress and challenge, ACS Infect. Dis. 1 (2015) 76–78.

[17] A.K. Carrillo, W.A. Guiguemde, R.K. Guy, Evaluation of histone deacetylase inhibitors (HDACi) as therapeutic leads for human African trypanosomiasis, Bioorg. Med. Chem. (2015), in press, DOI: 10.1016/j.bmc.2014.12.066.

[18] R. Urich, R. Grimaldi, T. Luksch, J.A. Frearson, R. Brenk, P.G. Wyatt, The design and synthesis of potent and selective inhibitors of Trypanosoma brucei glycogen synthase kinase 3 for the treatment of human African trypanosomiasis, J. Med. Chem. 57 (2014) 7536–7549.

[19] I.V. Ogungbe, J.D. Ng, W.N. Setzer, Interactions of antiparasitic alkaloids with *Leishmania* protein targets: a molecular docking analysis, Fut. Med. Chem. 5 (2013) 1777–1799.

[20] G. Colotti, P. Baiocco, A. Fiorillo, A. Boffi, E. Poser, F. Di Chiaro, A. Ilari, Structural insights into the enzymes of the trypanothione pathway: targets for antileishmaniasis drugs, Fut. Med. Chem. 5 (2013) 1861–1875.

[21] N. Singh, M. Kumar, R.K. Singh, Leishmaniasis: current status of available drugs and new potential drug targets, Asian Pac. J. Trop. Med. 5 (2012) 485–497.

[22] A.H. Fairlamb, Infectious disease: Genomics decodes drug action, Nature 482 (2012) 167–169.

[23] F. Prati, E. Uliassi, M.L. Bolognesi, Two diseases, one approach: multitarget drug discovery in Alzheimer's and neglected tropical diseases, Med. Chem. Commun. 5 (2014) 853–861.

[24] J.N. Burrows, R.L. Elliott, T. Kaneko, C.E. Mowbray, D. Waterson, The role of modern drug discovery in the fight against neglected and tropical diseases, Med. Chem. Commun. 5 (2014) 688–700.

[25] F. Annang, G. Pérez-Moreno, R. García-Hernández, C. Cordon-Obras, J. Martín, J.R. Tormo, L. Rodríguez, N. de Pedro, V. Gómez-Pérez, M. Valente, F. Reyes, O. Genilloud, F. Vicente, S. Castanys, L.M. Ruiz-Pérez, M. Navarro, F. Gamarro, D. González-Pacanowska, High-throughput screening platform for natural product-based drug discovery against 3 neglected tropical diseases: Human African trypanosomiasis, Leishmaniasis, and Chagas disease, J. Biomol. Screening 20 (2015) 82–91.

[26] A. Manos-Turvey, E.E. Watson, M.L. Sykes, A.J. Jones, J.B. Baell, M. Kaiser, V.M. Avery, R.J. Payne, Synthesis and evaluation of phenoxymethylbenzamide analogues as anti-trypanosomal agents, Med. Chem. Commun. 6 (2015) 403–406.

[27] W. Seebacher, V. Wolkinger, J. Faist, M. Kaiser, R. Brun, R. Saf, F. Bucar, B. Gröblacher, A. Brantner, V. Merino, Y. Kalia, L. Scapozza, R. Perozzo, R. Weis, Synthesis of 3-azabicyclo[3.2.2]nonanes and their antiprotozoal activities, Bioorg. Med. Chem. Lett. 25 (2015), 1390–1393.

[28] L. Ferrins, R. Rahmani, J.B. Baell, Drug discovery and human African trypanosomiasis: a disease less neglected? Fut. Med. Chem. 5 (2013) 1801–1841.

[29] K. Chibale, Economic drug discovery and rational medicinal chemistry for tropical diseases, Pure Appl. Chem. 77 (2005), 1957–1964.

[30] S. Manda, S.I. Khan, S.K. Jain, S. Mohammed, B.L. Tekwani, I.A. Khan, R.A. Vishwakarma, S.B. Bharate, Synthesis, antileishmanial and antitrypanosomal activities of N-substituted tetrahydro-β-carbolines, Bioorg. Med. Chem. Lett. 24 (2014) 3247–3250.

[31] M.M. Salem, K.A. Werbovetz, Natural products from plants as drug candidates and lead compounds against leishmaniasis and trypanosomiasis, Curr. Med. Chem. 13 (2006) 2571–2598.

[32] R.S. Upadhayaya, S.S. Dixit, A. Földesi, J. Chattopadhyaya, New antiprotozoal agents: their synthesis and biological evaluations, Bioorg. Med. Chem. Lett. 23 (2013) 2750–2758.

[33] C.C. Musonda, V. Yardley, R.C. Carvalho de Souza,, K. Ncokazi, T.J. Egan, K. Chibale, Antiplasmodial, β-haematin inhibition, antitrypanosomal and cytotoxic activity *in vitro* of novel 4-aminoquinoline 2-imidazolines, Org. Biomol. Chem. 6 (2008), 4446–4451.

[34] C.C. Musonda, J. Gut, P.J. Rosenthal, V. Yardley, R.C. Carvalho de Souza, K. Chibale, Application of multicomponent reactions to antimalarial drug discovery. Part 2: New antiplasmodial and antitrypanosomal 4-aminoquinoline γ- and δ-lactams via a "catch and release" protocol, Bioorg. Med. Chem. 14 (2006) 5605–5615.

[35] I. Sola, S. Castellà, E. Viayna, C. Galdeano, M.C. Taylor, S.Y. Gbedema, B. Pérez, M.V. Clos, D.C. Jones, A.H. Fairlamb, C.W. Wright, J.M. Kelly, D. Muñoz-Torrero, Synthesis, biological profiling and mechanistic studies of 4-aminoquinoline-based heterodimeric compounds with dual trypanocidal–antiplasmodial activity, Bioorg. Med. Chem. (2015) in press, DOI: 10.1016/j.bmc.2015.01.031.

[36] For an appraisal, see: J. Zhu, Q. Wang, M.-X. Wang, Multicomponent Reaactions in Organic Synthesis, Wiley-VCH, Weinheim, 2015.

[37] T. Zarganes-Tzitzikas, A. Doemling, Modern multicomponent reactions for better drug syntheses, Org. Chem. Front. 1 (2014) 1834–1837.

[38] C. Hulme, Applications of multicomponent reactions in drug discovery - lead generation to process development, in: J. Zhu, H. Bienaymé (Eds.), Multicomponent Reactions, Wiley-VCH, Weinheim, 2005, pp 311–341.

[39] I. Akritopoulou-Zanze, S.W. Djuric, Applications of MCR-derived Heterocycles in Drug Discovery, in: R.V.A. Orru, E. Ruijter (Eds.), Synthesis of Heterocycles via Multicomponent Reactions II, Springer, 2010, Heidelberg, pp 231–287.

[40] O. Di Pietro, E.Viayna, E. Vicente-García, M. Bartolini, R. Ramón, J. Juárez-Jiménez, M.V. Clos, B. Pérez, V. Andrisano, F.J. Luque, R. Lavilla, D. Muñoz-Torrero, 1,2,3,4-Tetrahydrobenzo[*h*][1,6]naphthyridines as a new family of potent peripheral-to-midgorge-site inhibitors of acetylcholinesterase: Synthesis, pharmacological evaluation and mechanistic studies, Eur. J. Med. Chem. 73 (2014) 141–152.

[41] V.V. Kouznetsov, Recent synthetic developments in a powerful imino Diels-Alder reaction (Povarov reaction): application to the synthesis of *N*-polyheterocycles and related alkaloids, Tetrahedron 65 (2009) 2721–2750.

[42] D. Bello, R. Ramon, R. Lavilla, Mechanistic variations of the Povarov multicomponent reaction and related processes, Curr. Org. Chem. 14 (2010) 332–356.

[43] Calculated using Molinspiration: http//www.molinspiration.com.

[44] C.A. Lipinski, F. Lombardo, B.W. Dominy, P.J. Feeney, Experimental and computational approaches to estimate solubility and permeability in drug discovery and development settings, Adv. Drug. Delivery Rev. 46 (2001) 3–26.

[45] E. Vicente-García, F. Catti, R. Ramón, R. Lavilla, Unsaturated lactams: new inputs for Povarov-type multicomponent reactions, Org. Lett. 12 (2010) 860–863.

[46] D.A. Powell, R.A. Batey, Total synthesis of the alkaloids martinelline and martinellic acid via a hetero Diels−Alder multicomponent coupling reaction, Org. Lett. 4 (2002) 2913–2916.

[47] O. Jiménez, G. de la Rosa, R. Lavilla, Straightforward access to a structurally diverse set of oxacyclic scaffolds through a four-component reaction, Angew. Chem., Int. Ed. 44 (2005) 6521–6525.

[48] S. Das, D. Addis, S. Zhou, K. Junge, M. Beller, Zinc-catalyzed reduction of amides: unprecedented selectivity and functional group tolerance, J. Am. Chem. Soc. 132 (2010) 1770–1771.

[49] L. Di, E.H. Kerns, K. Fan, O.J. McConnell, G.T. Carter, High throughput artificial membrane permeability assay for blood-brain barrier, Eur. J. Med. Chem. 38 (2003) 223–232.

[50] M.A. Alves, A.C. de Queiroz, M.S. Alexandre-Moreira, J. Varela, H. Cerecetto, M. González, A.C. Doriguetto, I.M. Landre, E.J. Barreiro, L.M. Lima, Design, synthesis, and *in vitro* trypanocidal and leishmanicidal activities of novel semicarbazone derivatives, Eur. J. Med. Chem. 100 (2015) 24–33.

[51] S.R. Wilkinson, S.R. Prathalingam, M.C. Taylor, A. Ahmed, D. Horn, J.M. Kelly, Functional characterisation of the iron superoxide dismutase gene repertoire in *Trypanosoma brucei*, Free Radical Biol. Med. 40 (2006), 198–209.

[52] J. Carrió, M. de Colmenares, C. Riera, M. Gállego, M. Arboix, M. Portús, *Leishmania infantum*: Stage-specific activity of pentavalent antimony related with the assay conditions, Exp. Parasitol. 95 (2000) 209–214.

[53] C. Bot, B.S. Hall, N. Bashir, M.C. Taylor, N.A. Helsby, S.R. Wilkinson, Trypanocidal activity of aziridinyl nitrobenzamide prodrugs, Antimicrob. Agents Chemother. 54 (2010) 4246–4252.

[54] G.L. Ellman, K.D. Courtney, V. Andres Jr., R.M. Featherstone, A new and rapid colorimetric determination of acetylcholinesterase activity, Biochem. Pharmacol. 7 (1961) 88–95.

Supplementary Material

Multicomponent reaction-based synthesis and biological evaluation of tricyclic heterofused quinolines with multi-trypanosomatid activity

Ornella Di Pietro[a], Esther Vicente-García[b], Martin C. Taylor[c], Diana Berenguer[d], Elisabet Viayna[a], Anna Lanzoni[a], Irene Sola[a], Helena Sayago[b], Cristina Riera[d], Roser Fisa[d], M. Victòria Clos[e], Belén Pérez[e], John M. Kelly[c], Rodolfo Lavilla[b,f], Diego Muñoz-Torrero[a,*]

[a] *Laboratori de Química Farmacèutica (Unitat Associada al CSIC), Facultat de Farmàcia, and Institut de Biomedicina (IBUB), Universitat de Barcelona, Av. Joan XXIII, 27-31, E-08028, Barcelona, Spain*

[b] *Barcelona Science Park, Baldiri Reixac 10-12, E-08028, Barcelona, Spain*

[c] *Department of Pathogen Molecular Biology, London School of Hygiene and Tropical Medicine, Keppel Street, London WC1E 7HT, United Kingdom*

[d] *Laboratori de Parasitologia, Departament de Microbiologia i Parasitologia Sanitàries, Facultat de Farmàcia, Universitat de Barcelona, Av. Joan XXIII, 27-31, E-08028, Barcelona, Spain*

[e] *Departament de Farmacologia, de Terapèutica i de Toxicologia, Institut de Neurociències, Universitat Autònoma de Barcelona, E-08193, Bellaterra, Barcelona, Spain*

[f] *Laboratori de Química Orgànica, Facultat de Farmàcia, Universitat de Barcelona, Av. Joan XXIII, 27-31, E-08028, Barcelona, Spain*

* Corresponding author. Tel.: +34 934024533; fax: +34 934035941.

E-mail address: dmunoztorrero@ub.edu (D. Muñoz-Torrero).

Table S1

Calculated molecular properties of the novel heterofused quinolines and related compounds.[a]

Compd	miLogP	TPSA	MW	nON	nOHNH	nrotb	volume	nviolations
1	6.64	28.16	442.01	3	1	6	411.95	1
2	5.89	42.15	413.95	3	2	4	377.47	1
3	5.89	42.15	413.95	3	2	4	377.47	1
26	4.30	48.71	305.77	3	1	1	260.85	0
27	4.82	48.71	319.80	3	1	1	277.65	0
28	5.09	48.71	333.82	3	1	1	294.45	1
29	4.82	48.71	319.80	3	1	1	277.65	0
30	3.73	50.94	309.80	3	3	2	272.08	0
31	4.25	50.94	323.83	3	3	2	288.88	0
32	4.52	50.94	337.85	3	3	2	305.68	0
33	4.25	50.94	323.83	3	3	2	288.88	0
35	3.67	62.71	321.81	3	2	4	287.38	0
37	4.31	45.05	324.81	3	1	1	286.44	0
38	5.02	45.92	320.78	3	0	1	274.23	1
39	4.45	48.15	324.81	3	2	2	285.46	0
42	4.40	35.27	285.73	3	0	1	238.94	0
43	5.04	22.13	301.80	2	0	1	248.08	1
44	3.62	46.26	287.75	3	1	4	248.81	0
45	4.26	33.12	303.81	2	1	4	257.96	0
47	4.08	36.68	298.80	2	0	3	250.00	0
49	5.33	16.13	356.92	2	0	5	319.09	1
50	5.68	16.13	358.94	2	0	7	329.45	1

[a] Molecular properties (Log P, topological polar surface area (TPSA), molecular weight (MW), number of hydrogen bond acceptors (nON), number of hydrogen bond donors (nOHNH), number of rotatable bonds (nrotb), molecular volume, and number of violations of Lipinski's rules (nviolations)) calculated using Molinspiration (http://molinspiration.com).

Table S2

Reported and experimental permeability values (P_e 10^{-6} cm s^{-1}) of the 14 commercial drugs used for the PAMPA-BBB assay validation.

Compound	Literature value[a]	Experimental value[b]
Cimetidine	0.0	0.70 ± 0.03
Lomefloxacin	1.1	0.70 ± 0.04
Norfloxacin	0.1	0.90 ± 0.02
Ofloxacin	0.8	0.98 ± 0.04
Hydrocortisone	1.9	1.40 ± 0.05
Piroxicam	2.5	1.80 ± 0.02
Clonidine	5.3	6.50 ± 0.05
Corticosterone	5.1	6.70 ± 0.10
Imipramine	13	12.3 ± 0.10
Promazine	8.8	13.8 ± 0.30
Progesterone	9.3	16.8 ± 0.30
Desipramine	12	17.8 ± 0.10
Testosterone	17	23.1 ± 0.20
Verapamil	16	25.8 ± 0.30

[a] Taken from ref. [1].

[b] Values are expressed as the mean ± SD of three independent experiments.

References

[1] L. Di, E.H. Kerns, K. Fan, O.J. McConnell, G.T. Carter, High throughput artificial membrane permeability assay for blood-brain barrier, Eur. J. Med. Chem. 38 (2003) 223–232.

N-{1-Benzyl-5-(4-chlorophenyl)-1,2,3,4-tetrahydrobenzo[h][1,6]naphthyridin-9-yl}methanamine ***2***

^{1}H NMR (400 MHz , CD_3OD)

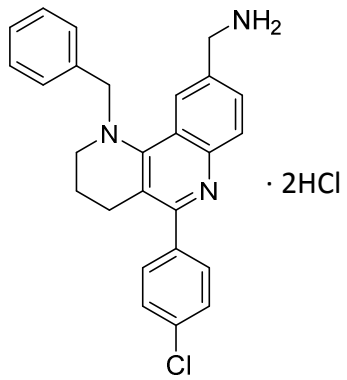

· 2HCl

N-{1-Benzyl-5-(4-chlorophenyl)-1,2,3,4-tetrahydrobenzo[h][1,6]naphthyridin-9-yl}methanamine ***2***

^{13}C NMR (100.6 MHz, CD_3OD)

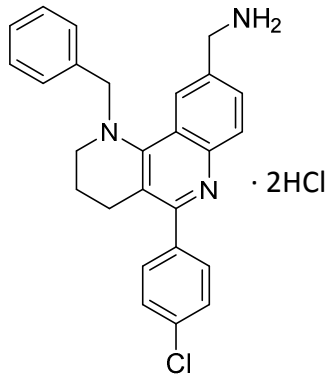

4-{1-Benzyl-9-chloro-1,2,3,4-tetrahydrobenzo[h][1,6]naphthyridin-5-yl}benzylamine ***3***

^{1}H NMR (400 MHz , CD_3OD)

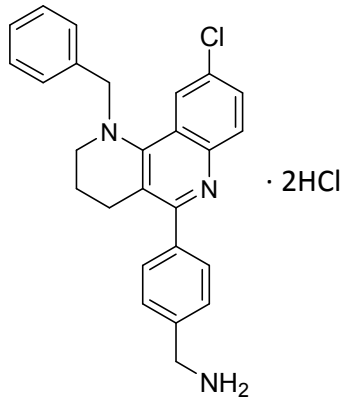

· 2HCl

4-{1-Benzyl-9-chloro-1,2,3,4-tetrahydrobenzo[h][1,6]naphthyridin-5-yl}benzylamine ***3***

^{13}C NMR (100.6 MHz, CD_3OD)

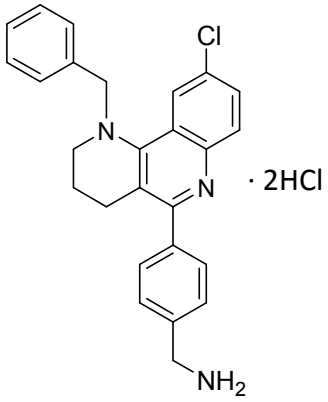

4-{8-Chloro-2,3-dihydro-1H-pyrrolo[3,2-c]quinolin-4-yl}benzonitrile ***26***

^{1}H NMR (400 MHz , CD_3OD)

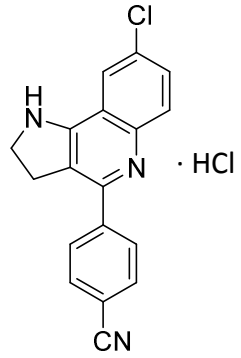

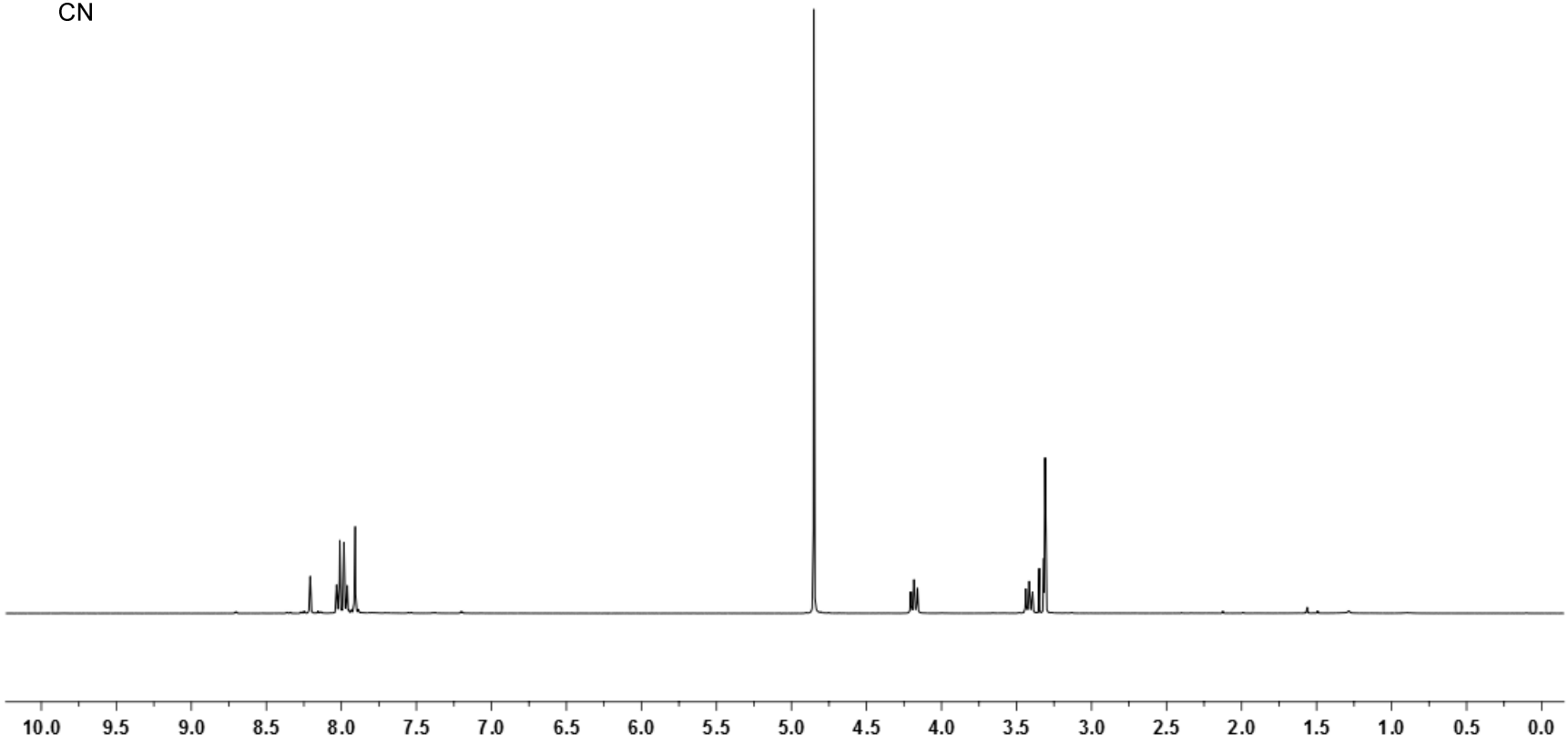

4-{8-Chloro-2,3-dihydro-1H-pyrrolo[3,2-c]quinolin-4-yl}benzonitrile ***26***

^{13}C NMR (100.6 MHz, CD_3OD)

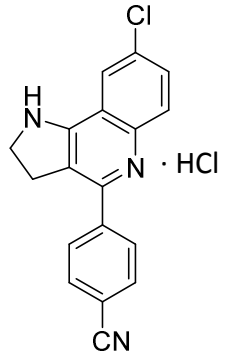

4-{9-Chloro-1,2,3,4-tetrahydrobenzo[h][1,6]naphthyridin-5-yl}benzonitrile ***27***

^{1}H NMR (400 MHz , CD_3OD)

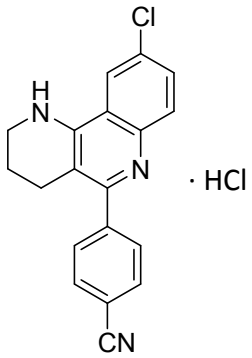

· HCl

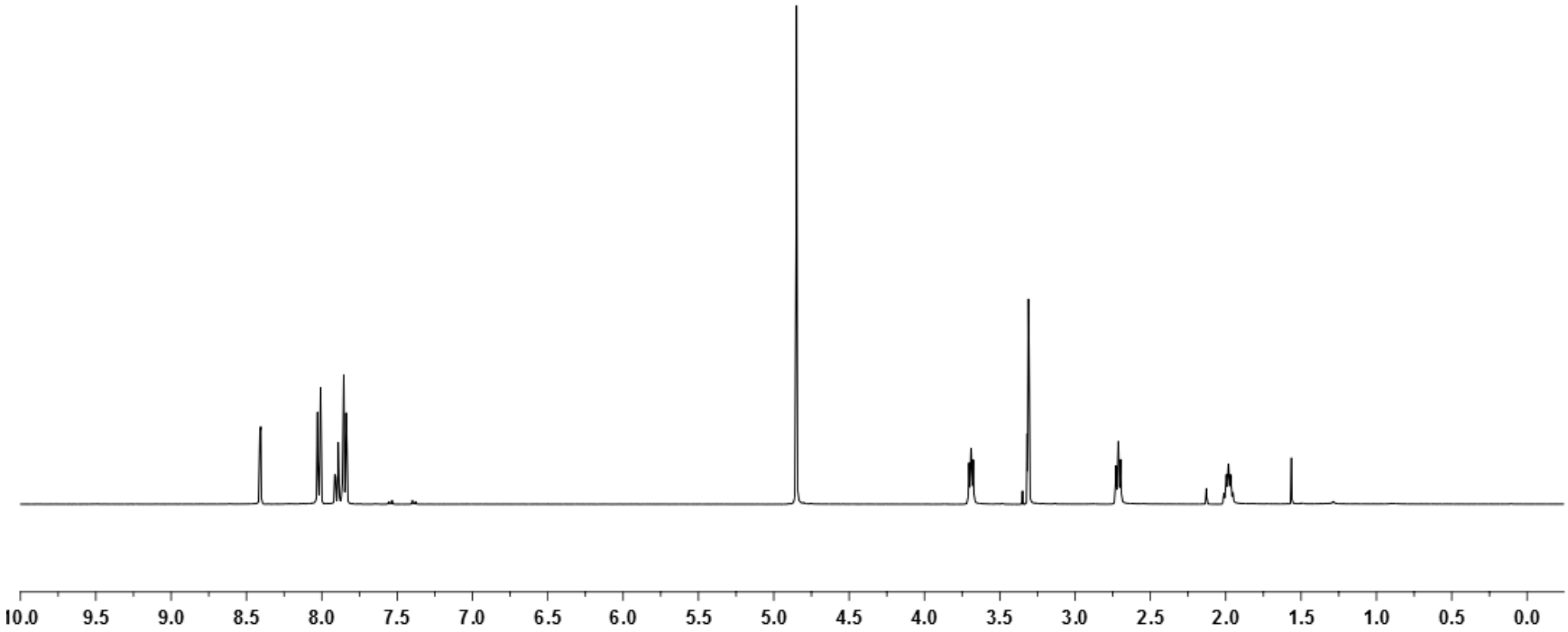

4-{9-Chloro-1,2,3,4-tetrahydrobenzo[h][1,6]naphthyridin-5-yl}benzonitrile ***27***

^{13}C NMR (100.6 MHz, CD_3OD)

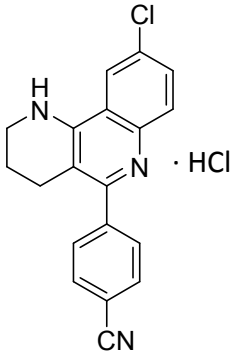

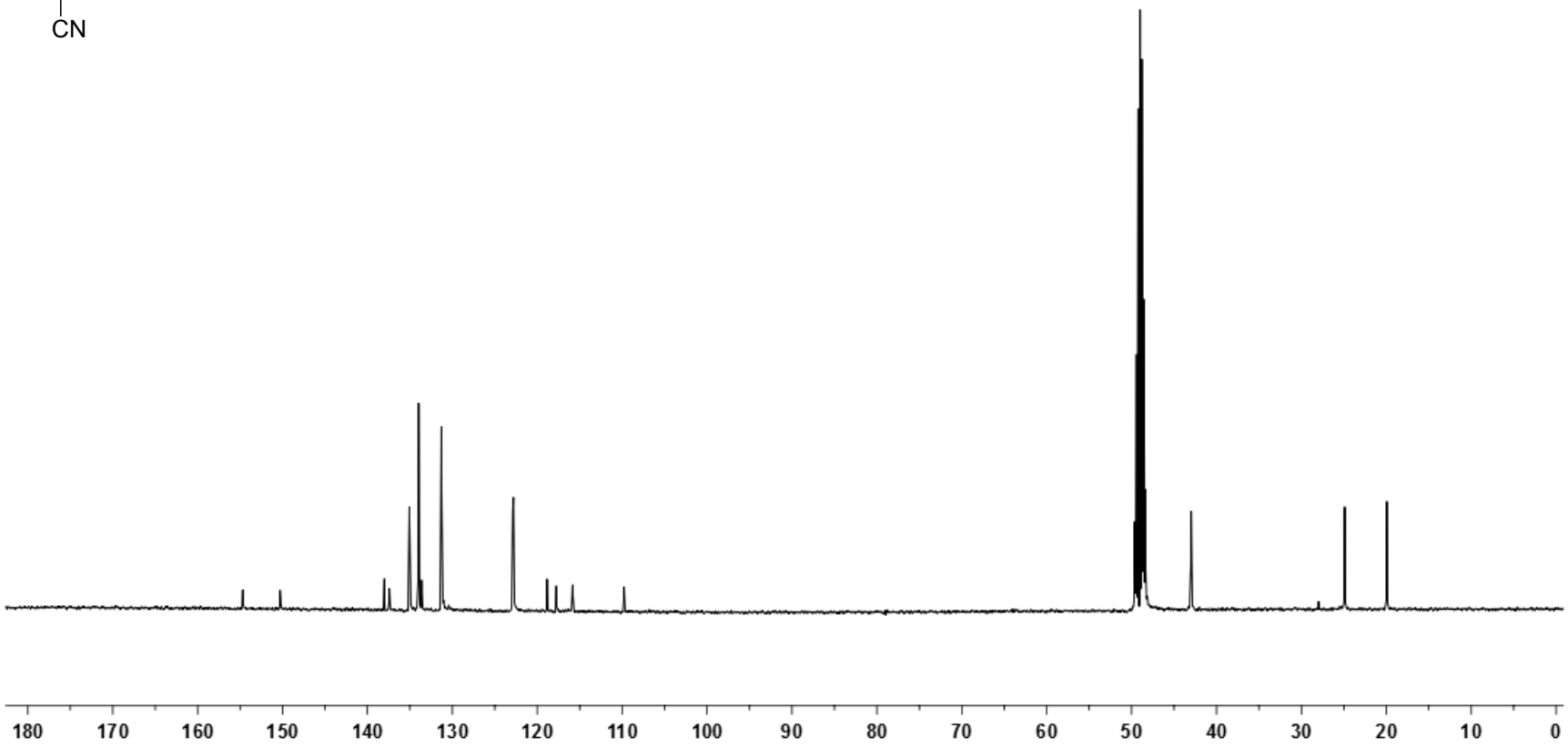

4-{10-Chloro-2,3,4,5-tetrahydro-1H-azepino[3,2-c]quinolin-6-yl}benzonitrile ***28***

^{1}H NMR (400 MHz , CD_3OD)

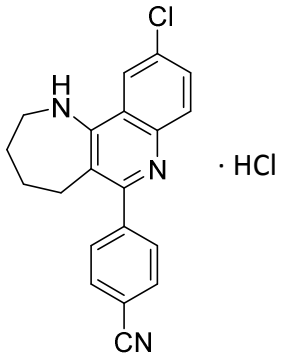

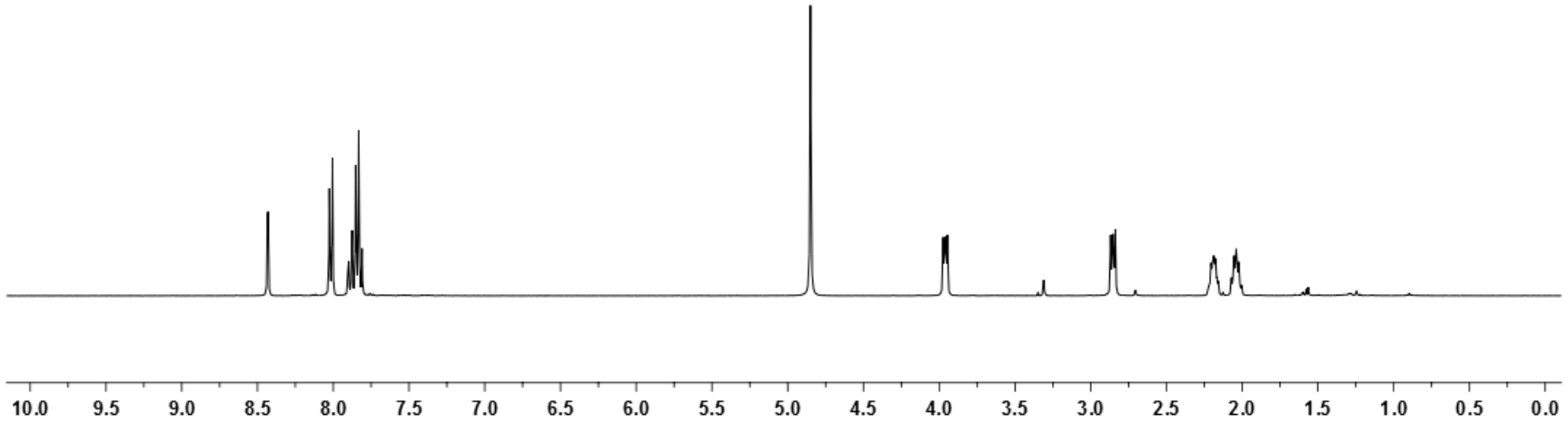

4-{10-Chloro-2,3,4,5-tetrahydro-1H-azepino[3,2-c]quinolin-6-yl}benzonitrile ***28***

^{13}C NMR (100.6 MHz, CD_3OD)

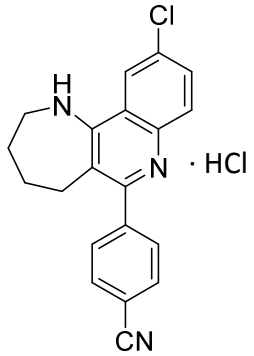

4-{8-Chloro-1,2,3,4-tetrahydrobenzo[h][1,6]naphthyridin-5-yl}benzonitrile ***29***

^{1}H NMR (400 MHz , CD_3OD)

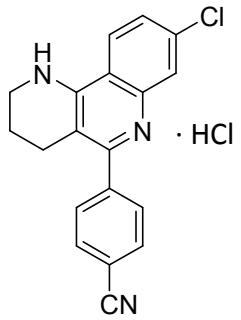

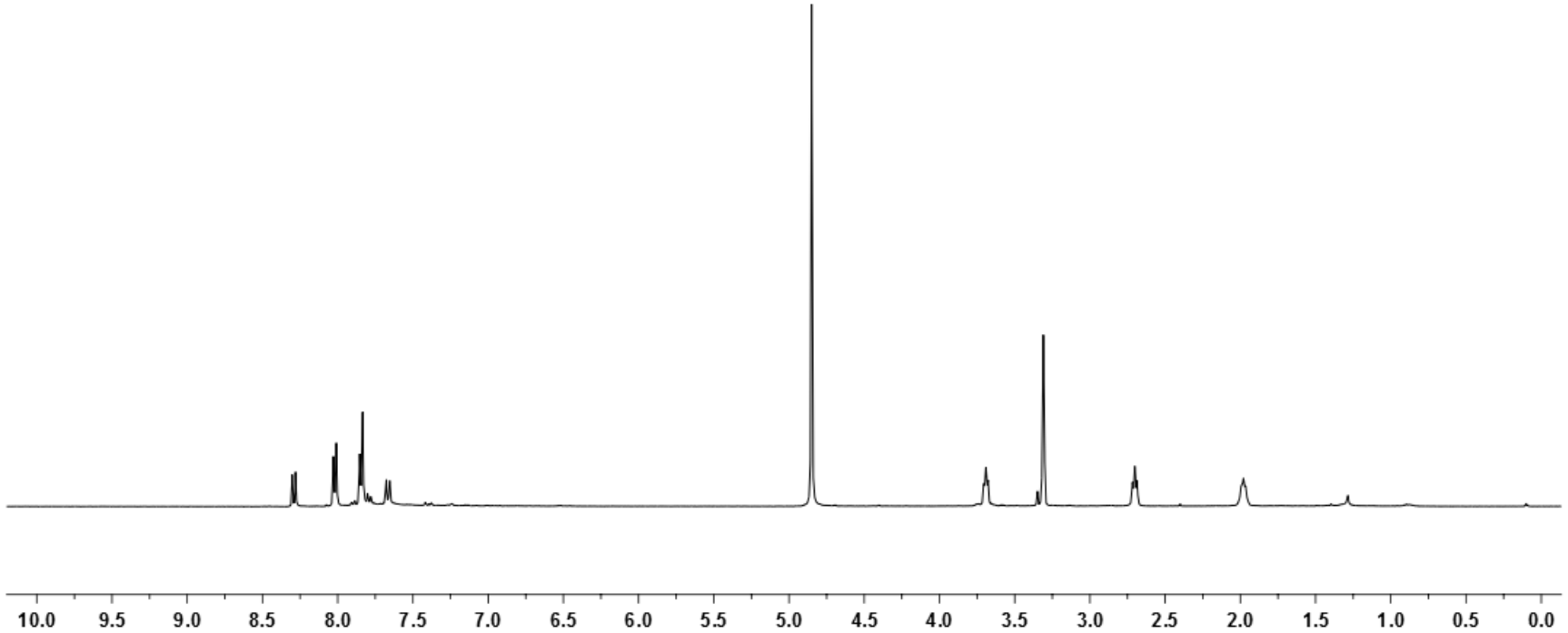

4-{8-Chloro-1,2,3,4-tetrahydrobenzo[h][1,6]naphthyridin-5-yl}benzonitrile ***29***

^{13}C NMR (100.6 MHz, CD_3OD)

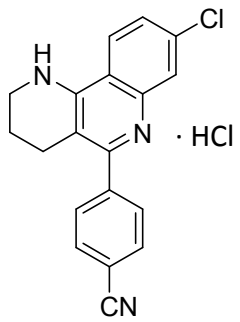

4-{8-Chloro-2,3-dihydro-1H-pyrrolo[3,2-c]quinolin-4-yl}benzylamine ***30***

^{1}H NMR (400 MHz , CD_3OD)

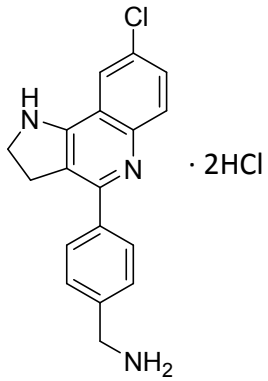

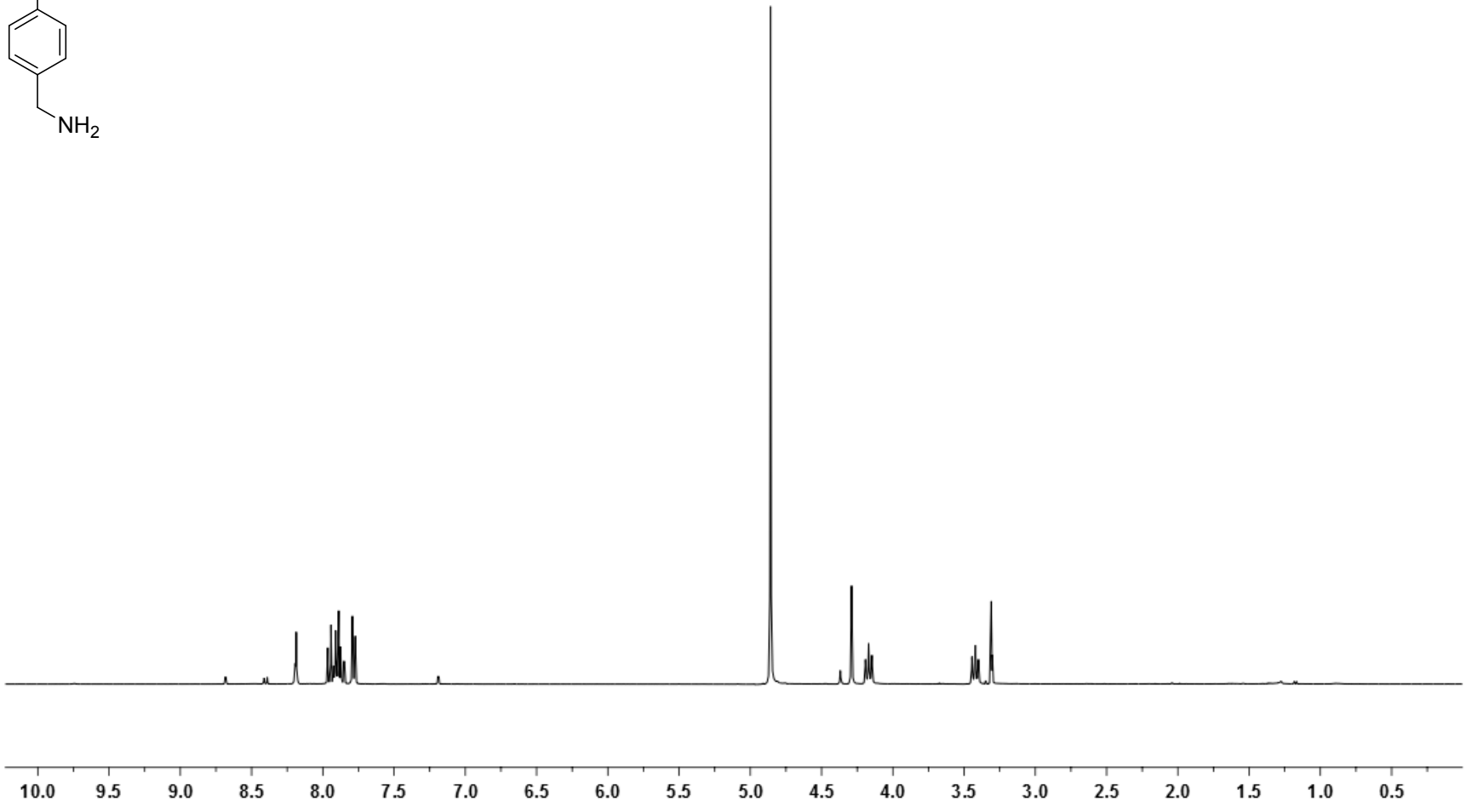

4-{8-Chloro-2,3-dihydro-1H-pyrrolo[3,2-c]quinolin-4-yl}benzylamine ***30***

^{13}C NMR (100.6 MHz, CD_3OD)

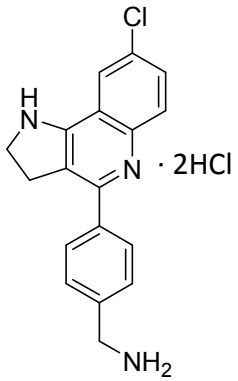

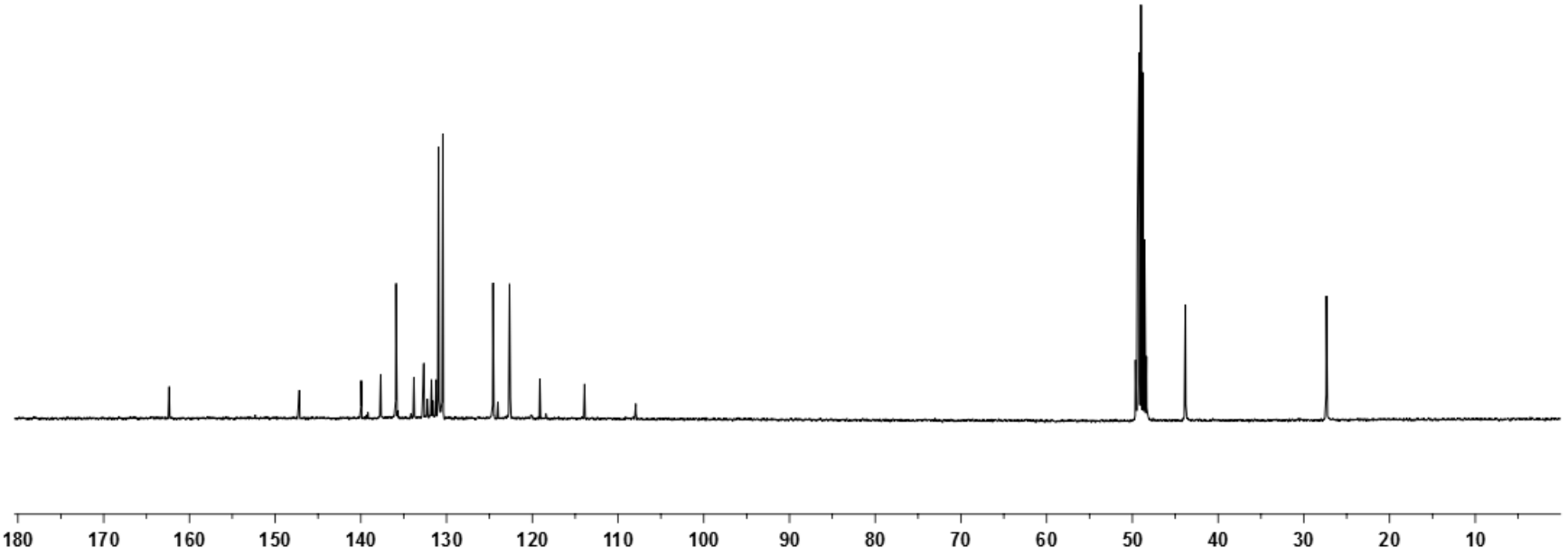

4-{9-Chloro-1,2,3,4-tetrahydrobenzo[h][1,6]naphthyridin-5-yl}benzylamine ***31***

^{1}H NMR (400 MHz , CD_3OD)

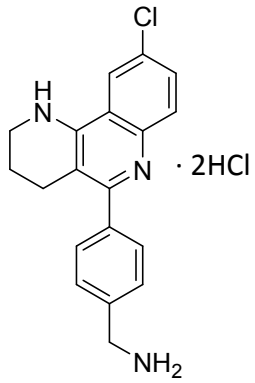

4-{9-Chloro-1,2,3,4-tetrahydrobenzo[h][1,6]naphthyridin-5-yl}benzylamine ***31***

^{13}C NMR (100.6 MHz, CD_3OD)

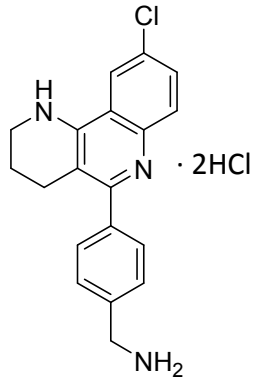

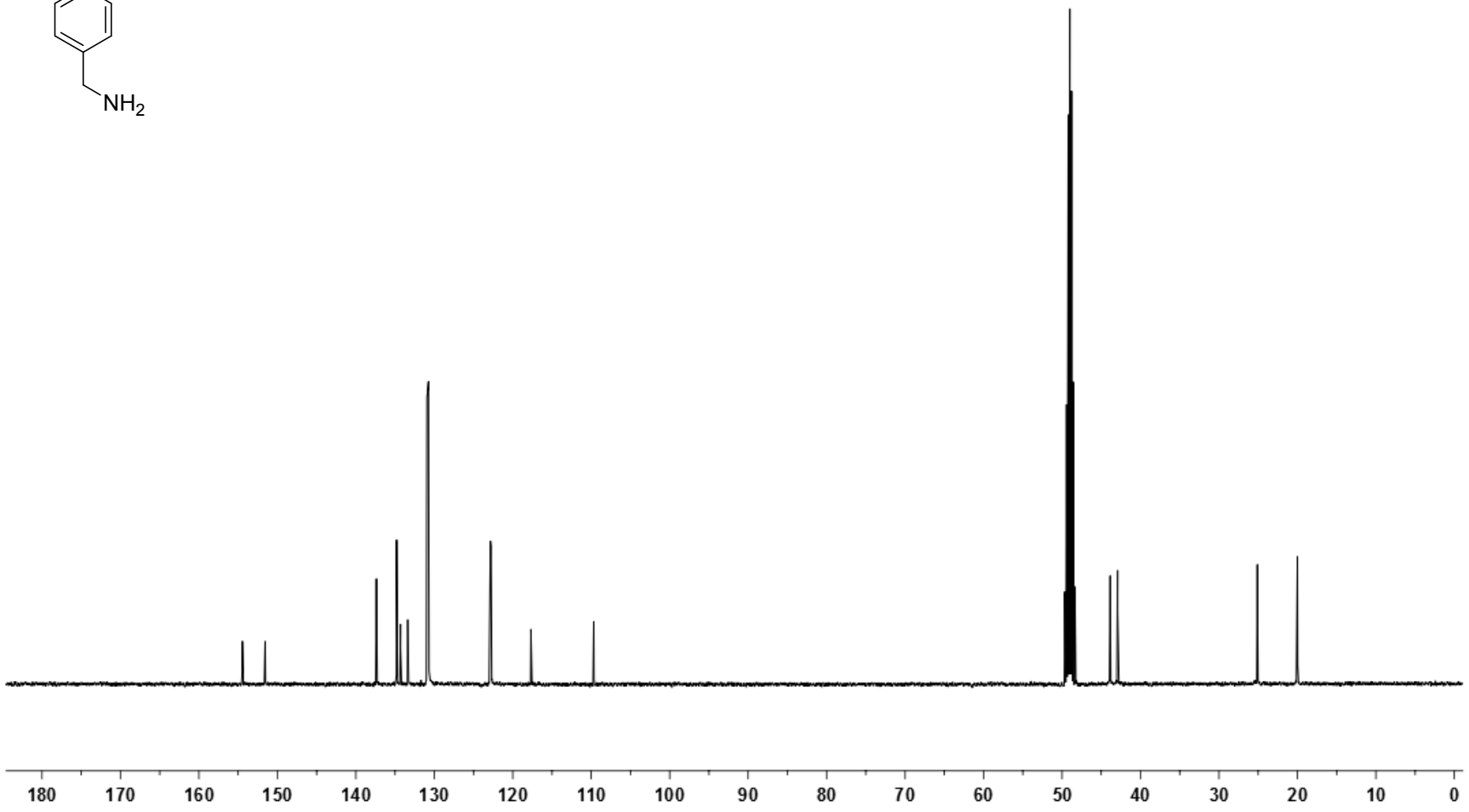

4-{10-Chloro-2,3,4,5-tetrahydro-1H-azepino[3,2-c]quinolin-6-yl}benzylamine ***32***

^{1}H NMR (400 MHz , CD_3OD)

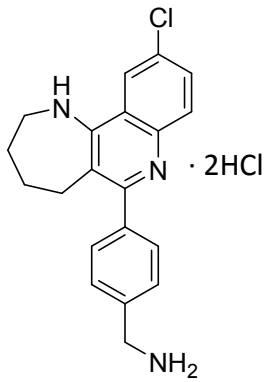

4-{10-Chloro-2,3,4,5-tetrahydro-1H-azepino[3,2-c]quinolin-6-yl}benzylamine ***32***

^{13}C NMR (100.6 MHz, CD_3OD)

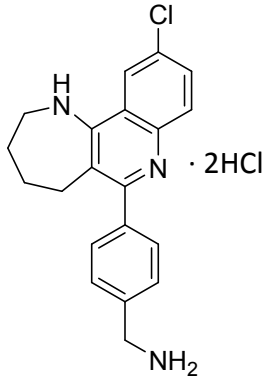

4-{8-Chloro-1,2,3,4-tetrahydrobenzo[h][1,6]naphthyridin-5-yl}benzylamine ***33***

^{1}H NMR (400 MHz , CD_3OD)

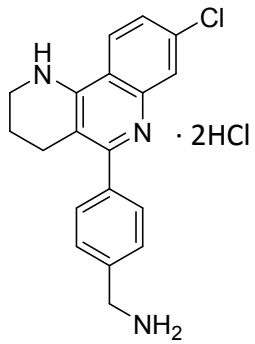

4-{8-Chloro-1,2,3,4-tetrahydrobenzo[h][1,6]naphthyridin-5-yl}benzylamine ***33***

^{13}C NMR (100.6 MHz, CD_3OD)

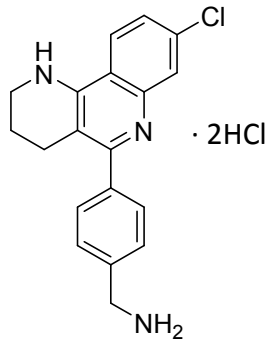

4-[3-(3-Aminopropyl)-7-chloroquinolin-2-yl]benzonitrile ***35***

^{1}H NMR (400 MHz , CD_3OD)

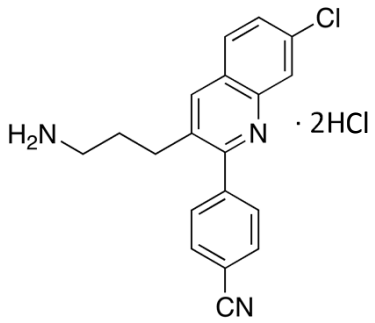

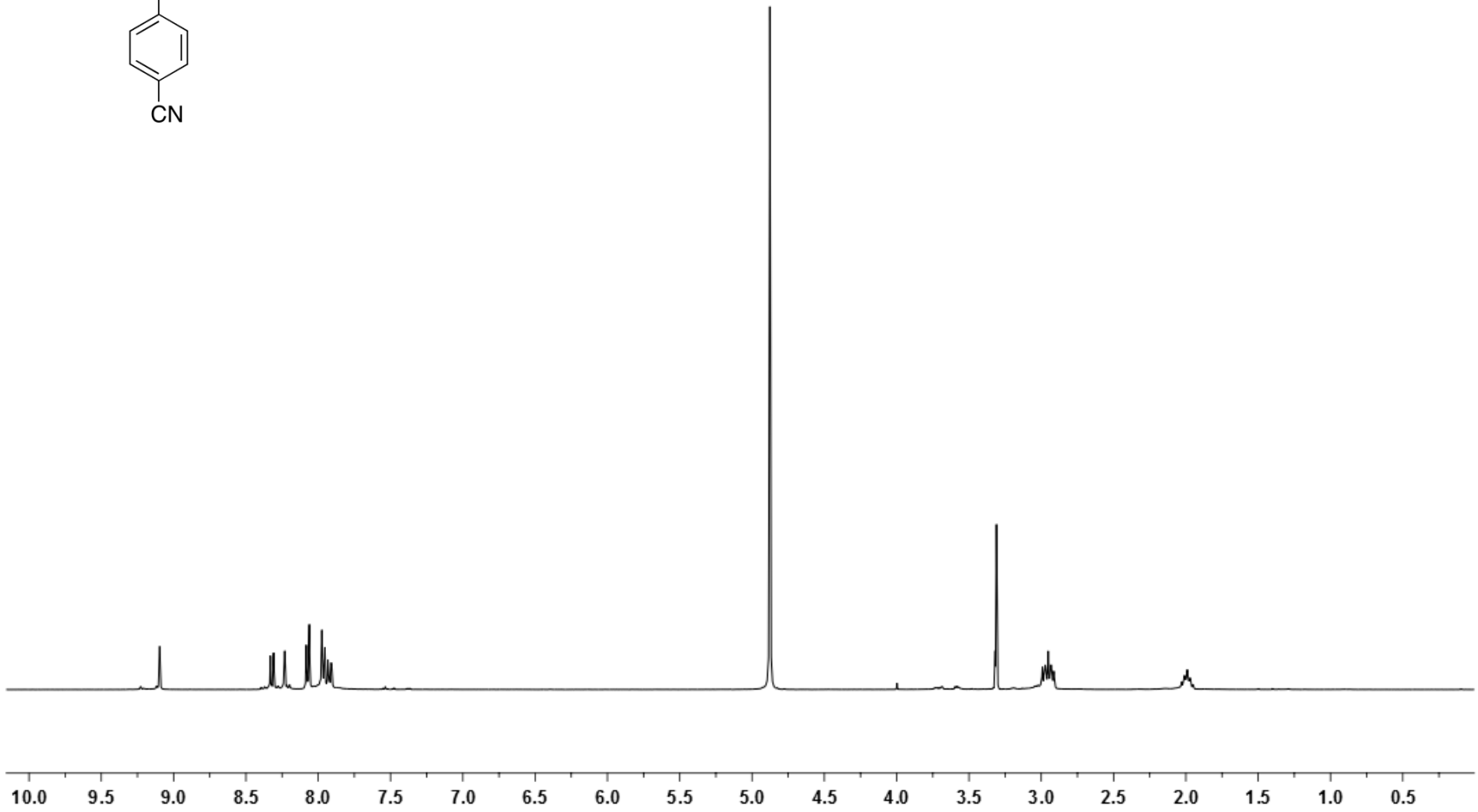

4-[3-(3-Aminopropyl)-7-chloroquinolin-2-yl]benzonitrile ***35***

^{13}C NMR (100.6 MHz, CD_3OD)

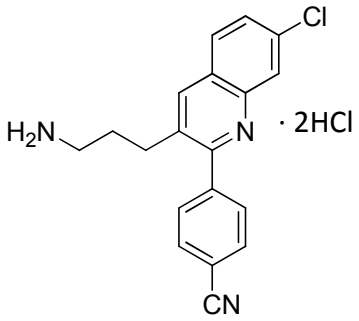

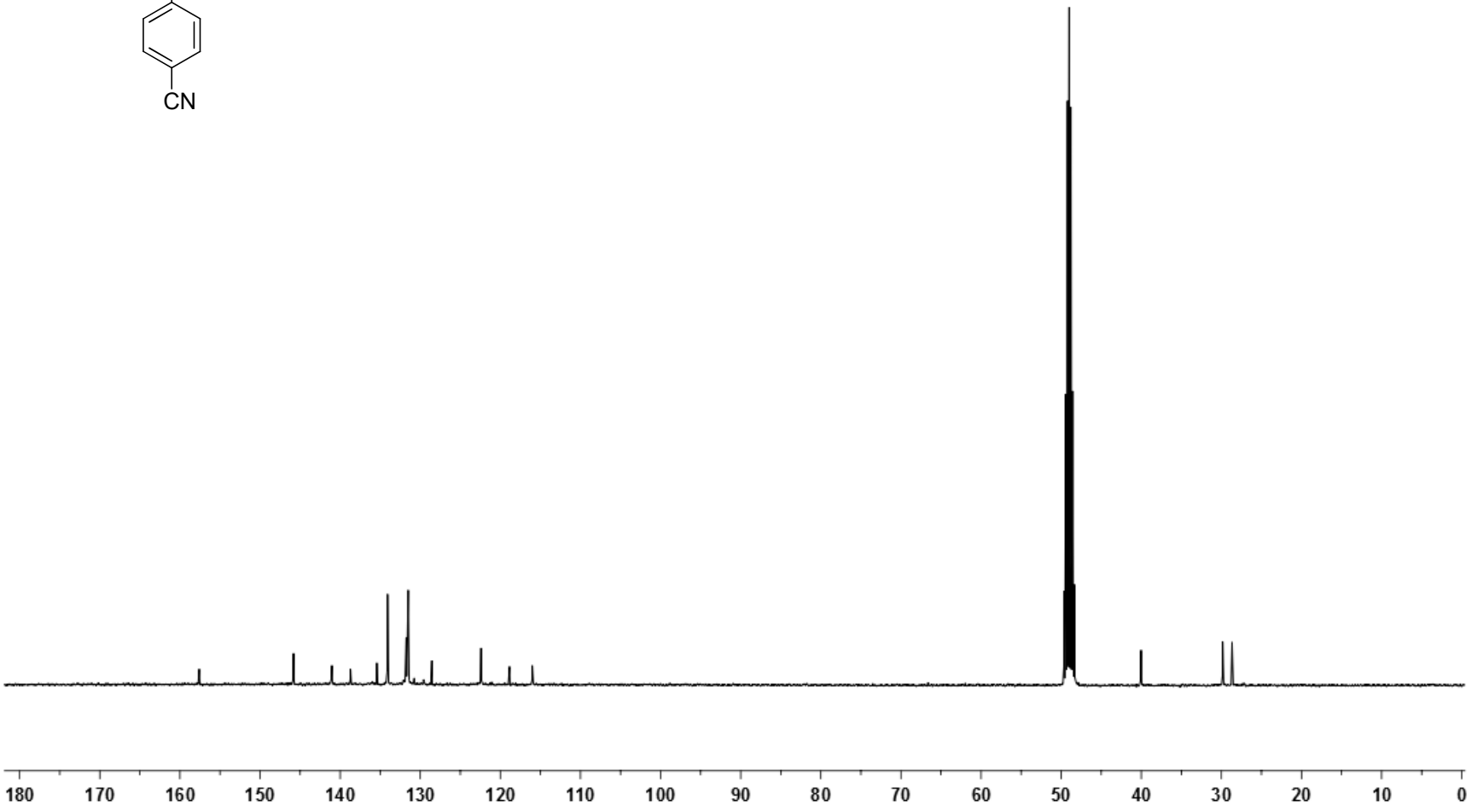

4-{9-Chloro-3,4,4a,5,6,10b-hexahydro-2H-pyrano[3,2-c]quinolin-5-yl}benzonitrile ***37***

^{1}H NMR (400 MHz , $CDCl_3$)

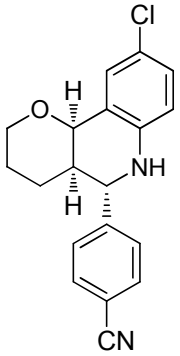

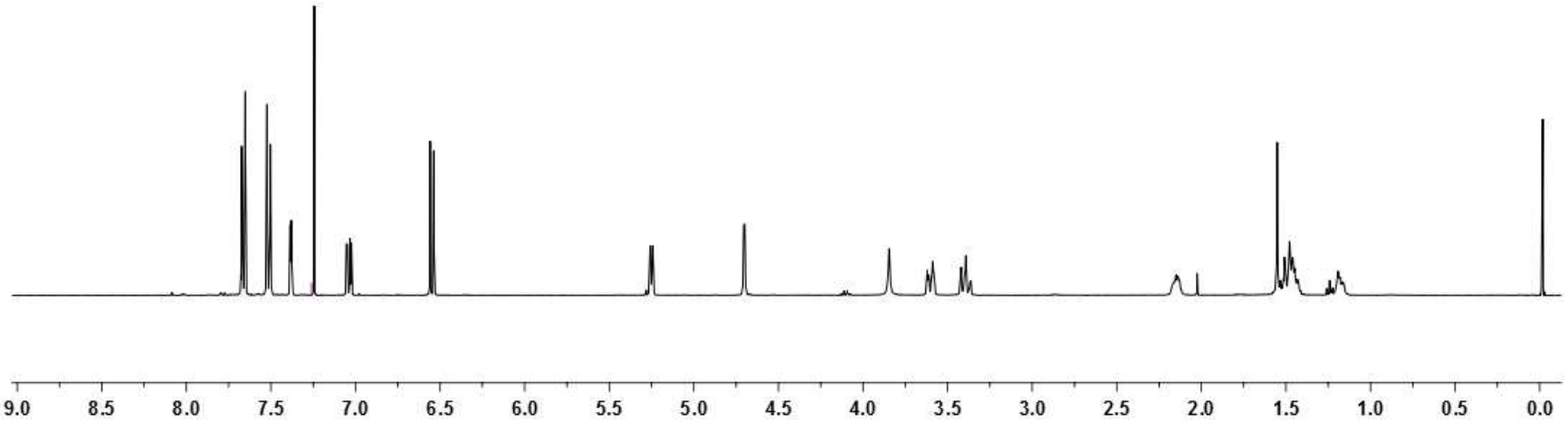

4-{9-Chloro-3,4,4a,5,6,10b -hexahydro-2H-pyrano[3,2-c]quinolin-5-yl}benzonitrile ***37***

^{13}C NMR (100.6 MHz, $CDCl_3$)

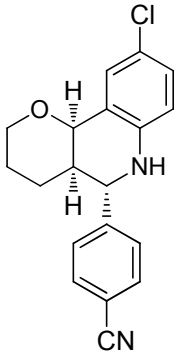

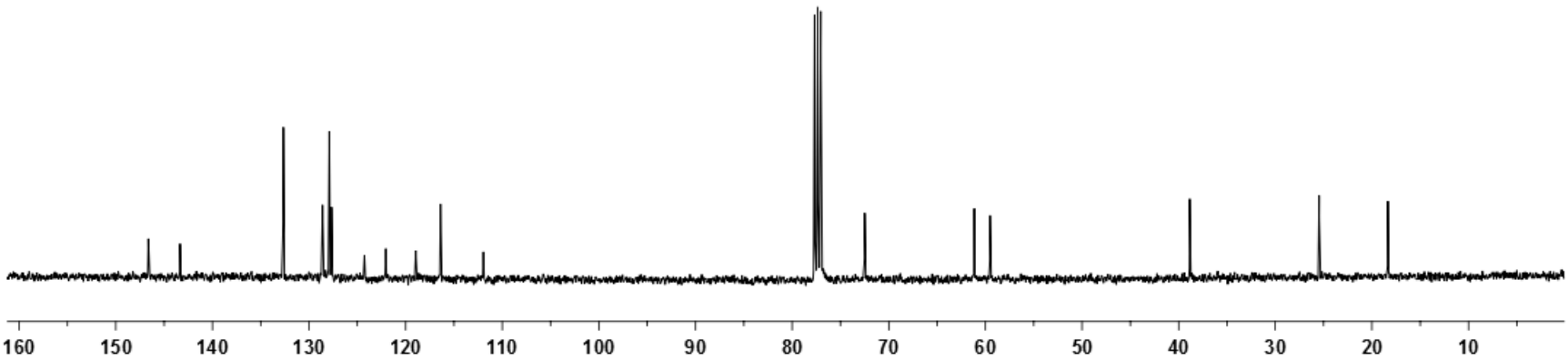

4-{9-Chloro-3,4-dihydro-2H-pyrano[3,2-c]quinolin-5-yl}benzonitrile ***38***

^{1}H NMR (400 MHz , CD_3OD)

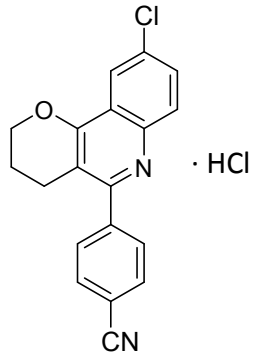

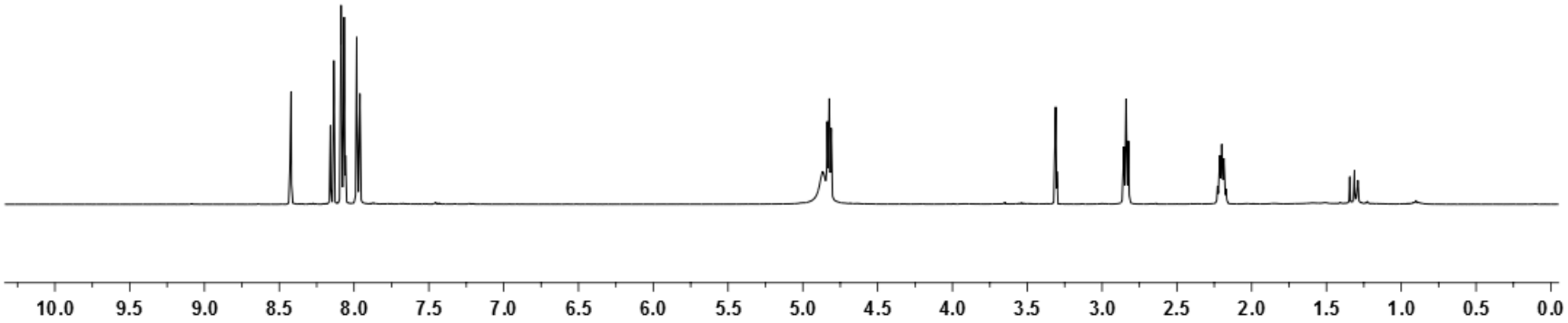

4-{9-Chloro-3,4-dihydro-2H-pyrano[3,2-c]quinolin-5-yl}benzonitrile ***38***

^{13}C NMR (100.6 MHz, CD_3OD)

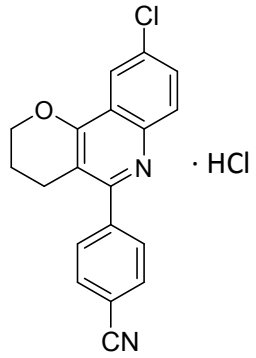

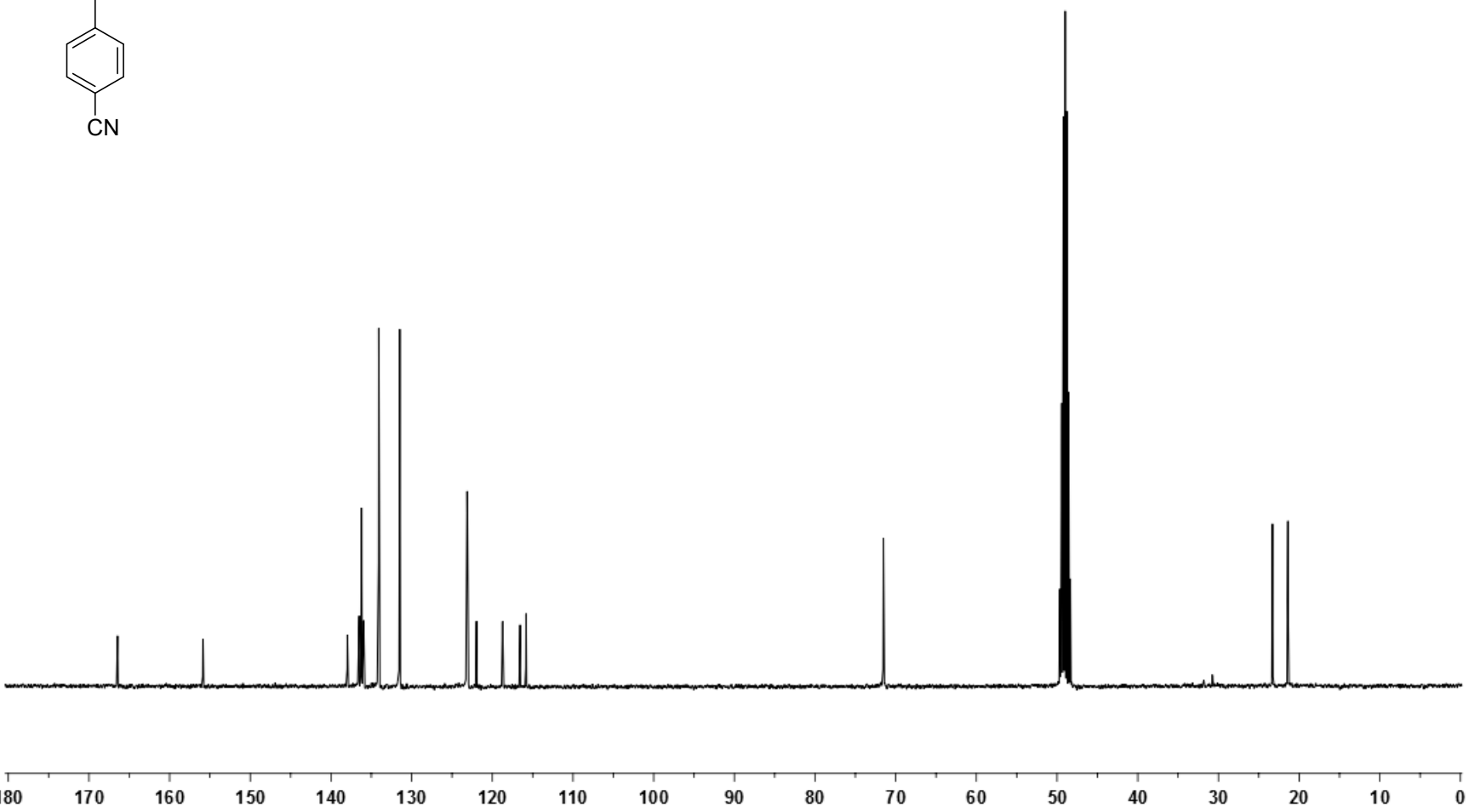

4-{9-Chloro-3,4-dihydro-2H-pyrano[3,2-c]quinolin-5-yl}benzylamine ***39***

^{1}H NMR (400 MHz , CD_3OD)

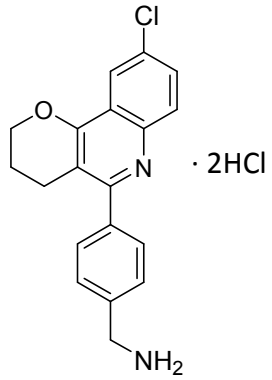

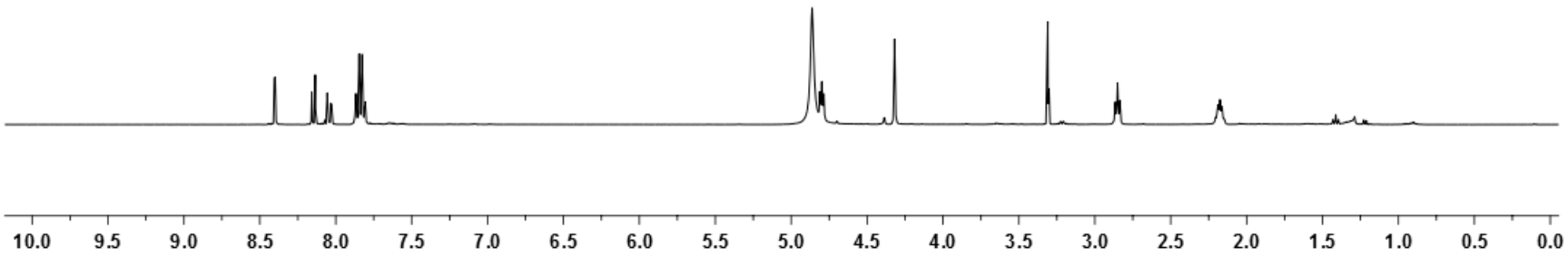

4-{9-Chloro-3,4-dihydro-2H-pyrano[3,2-c]quinolin-5-yl}benzylamine ***39***

^{13}C NMR (100.6 MHz, CD_3OD)

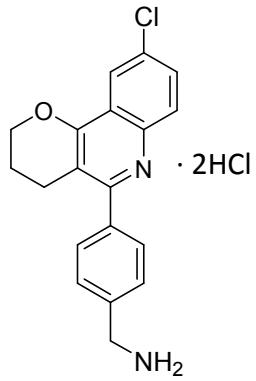

9-Chloro-5-(2-furyl)-3,4-dihydro-2H-pyrano[3,2-c]quinoline ***42***

^{1}H NMR (400 MHz , CD_3OD)

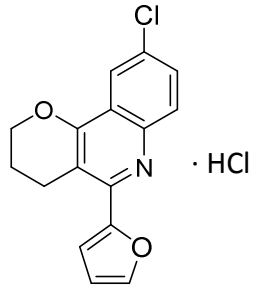

· HCl

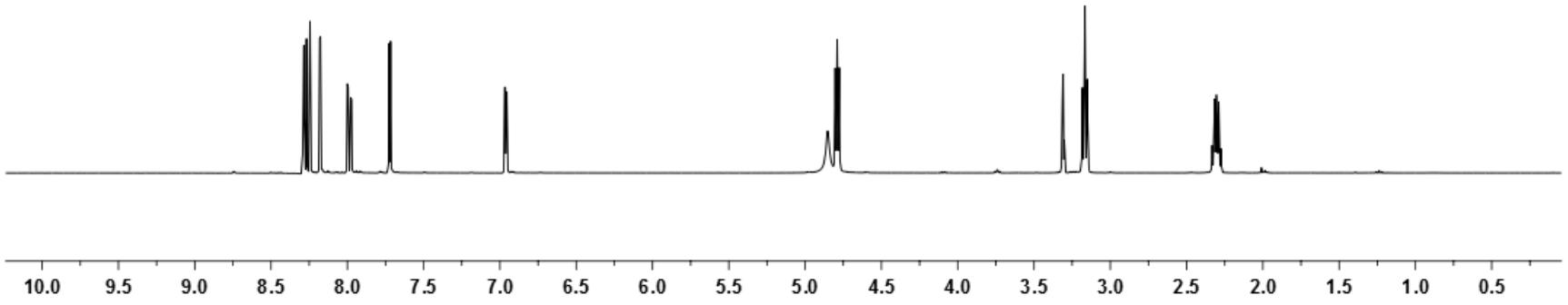

9-Chloro-5-(2-furyl)-3,4-dihydro-2H-pyrano[3,2-c]quinoline ***42***

^{13}C NMR (100.6 MHz, CD_3OD)

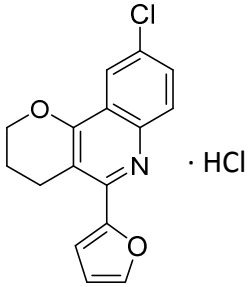

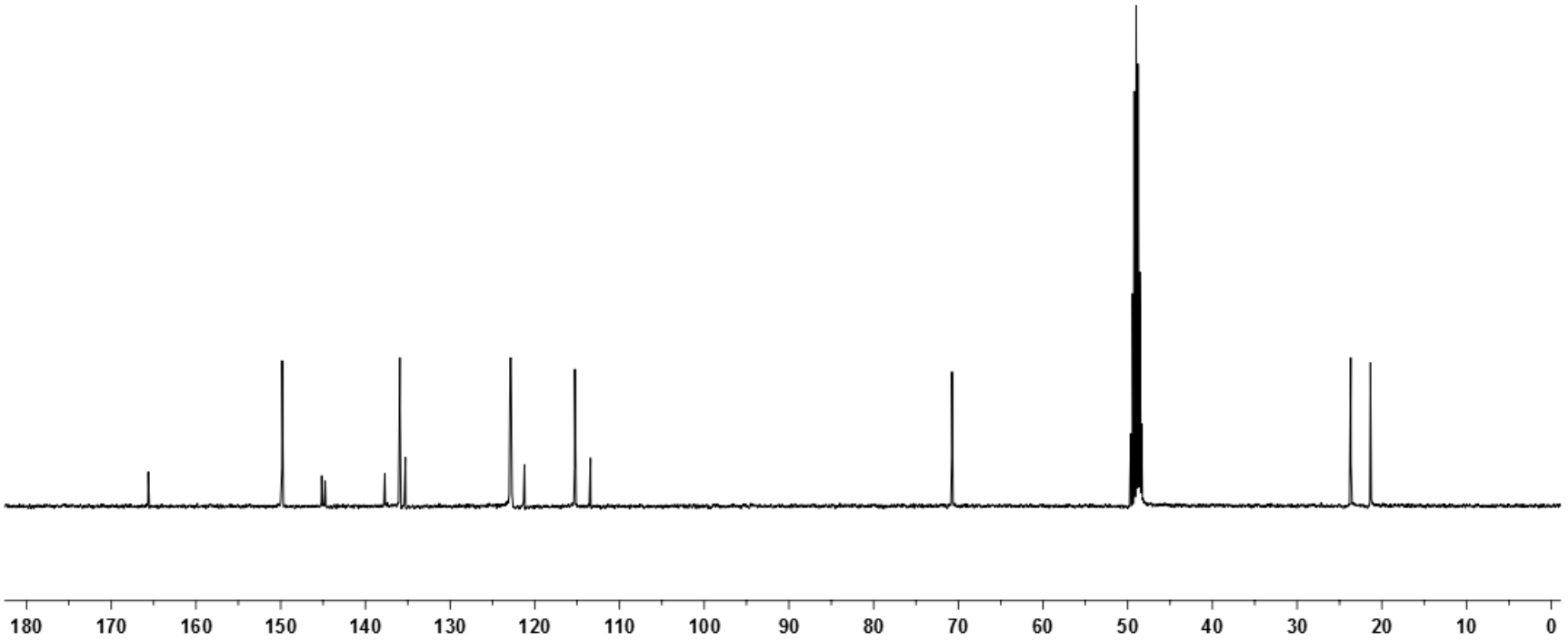

9-Chloro-3,4-dihydro-5-(2-thienyl)-2H-pyrano[3,2-c]quinoline ***43***

^{1}H NMR (400 MHz , CD_3OD)

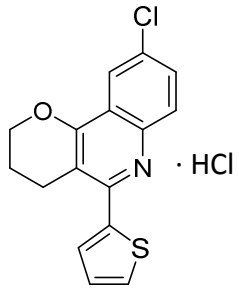

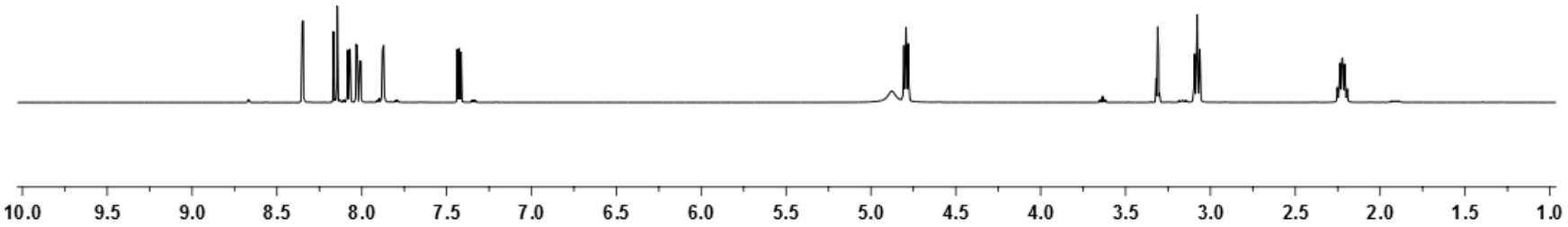

9-Chloro-3,4-dihydro-5-(2-thienyl)-2H-pyrano[3,2-c]quinoline ***43***

^{13}C NMR (100.6 MHz, CD_3OD)

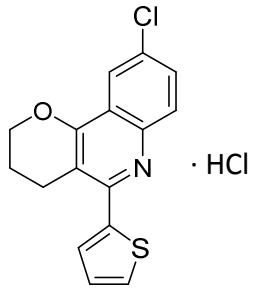

· HCl

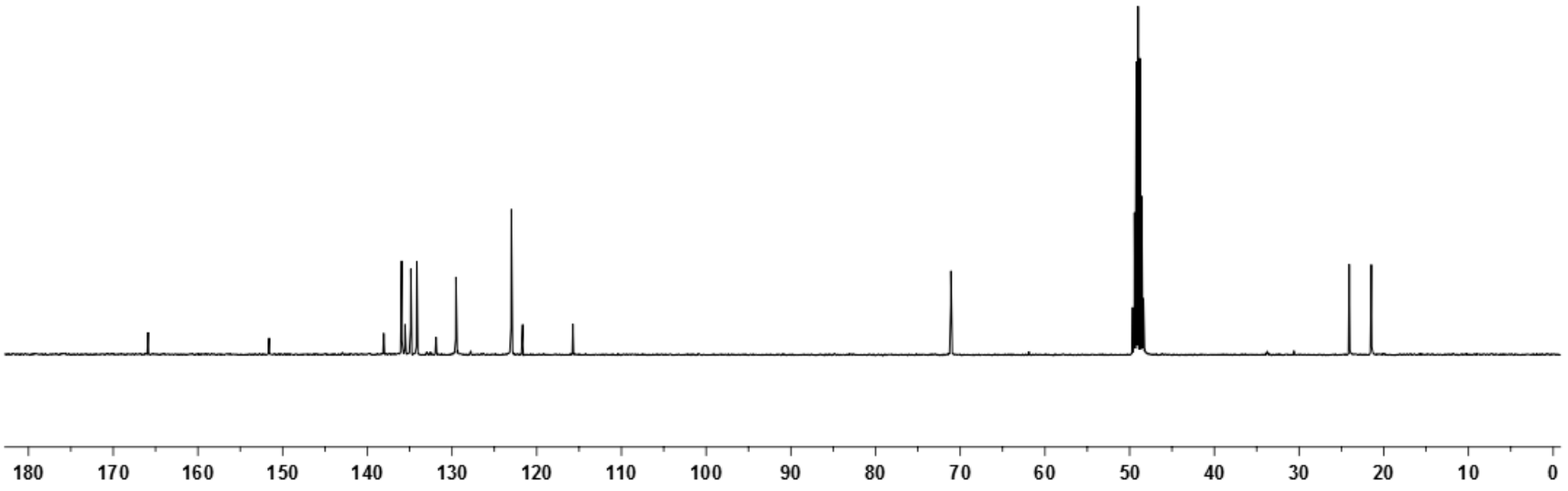

3-[6-Chloro-2-(2-furyl)quinolin-3-yl]-1-propanol **44**

^{1}H NMR (400 MHz , CD_3OD)

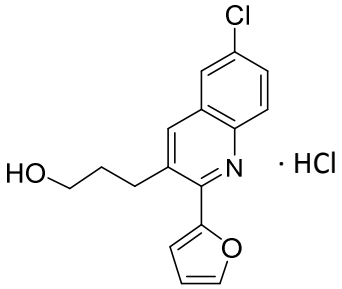

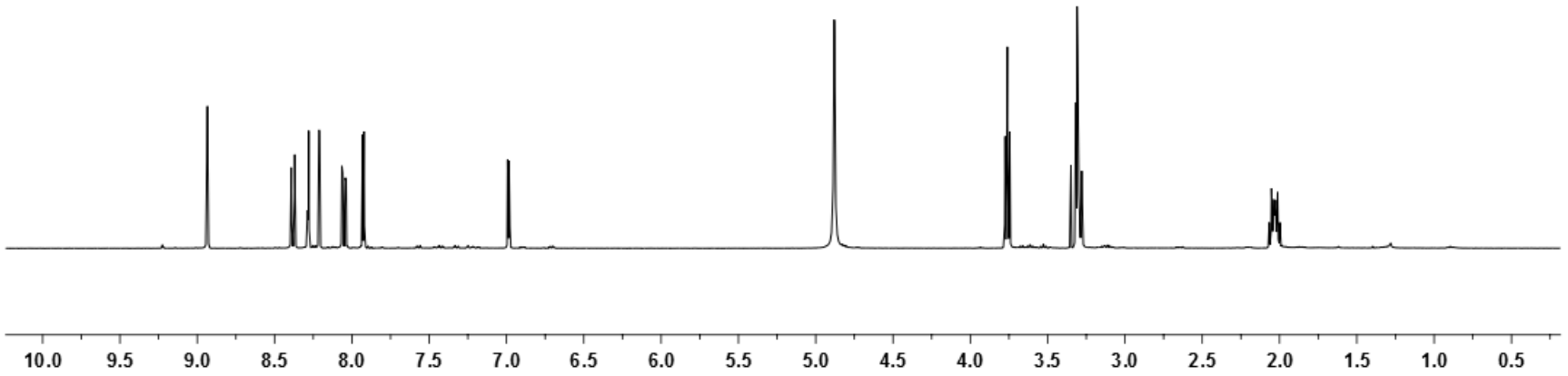

3-[6-Chloro-2-(2-furyl)quinolin-3-yl]-1-propanol **44**

^{13}C NMR (100.6 MHz, CD_3OD)

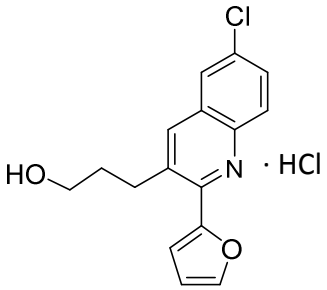

3-[6-Chloro-2-(2-thienyl)quinolin-3-yl]-1-propanol **45**

^{1}H NMR (400 MHz , CD_3OD)

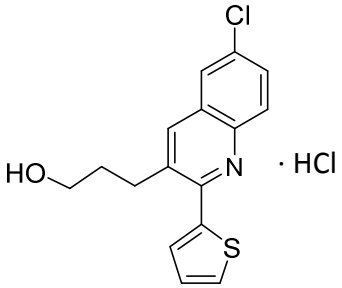

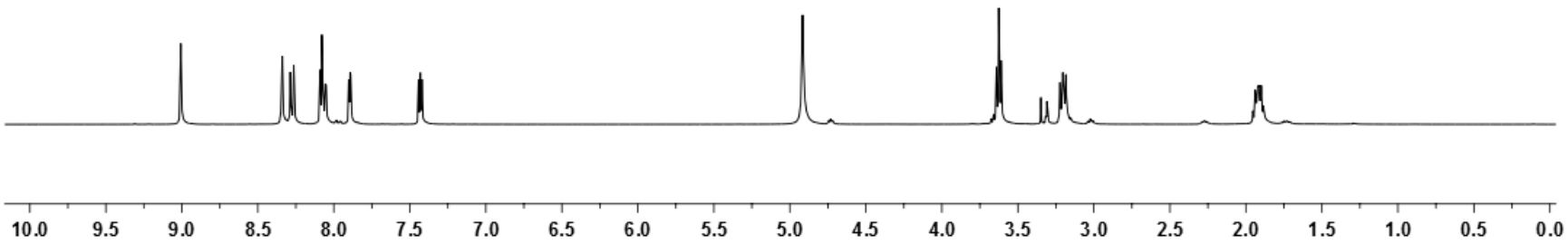

3-[6-Chloro-2-(2-thienyl)quinolin-3-yl]-1-propanol **45**

^{13}C NMR (100.6 MHz, CD_3OD)

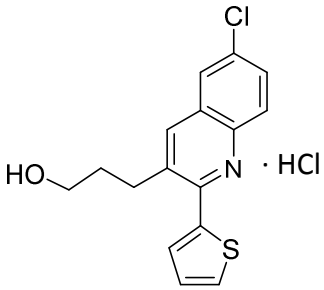

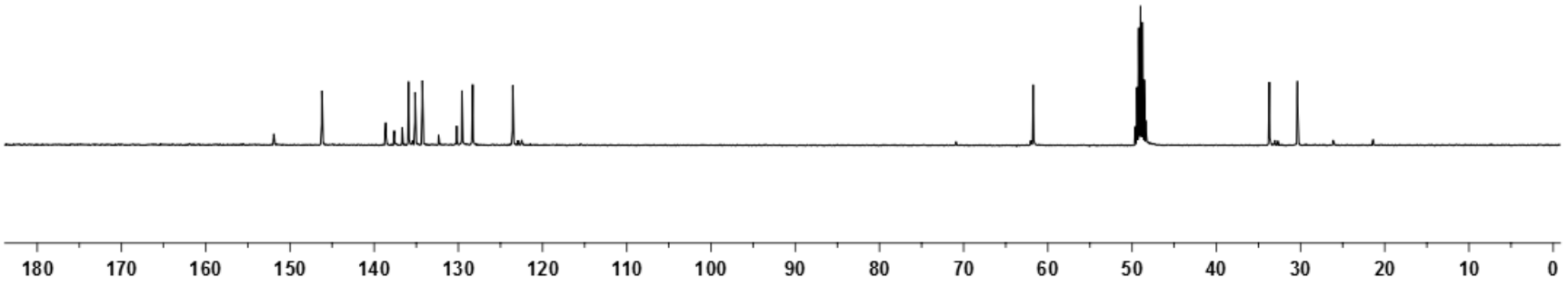

3-[6-Chloro-2-(2-thienyl)quinolin-3-yl]propanenitrile ***47***

^{1}H NMR (400 MHz , CD_3OD)

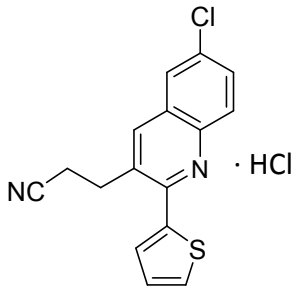

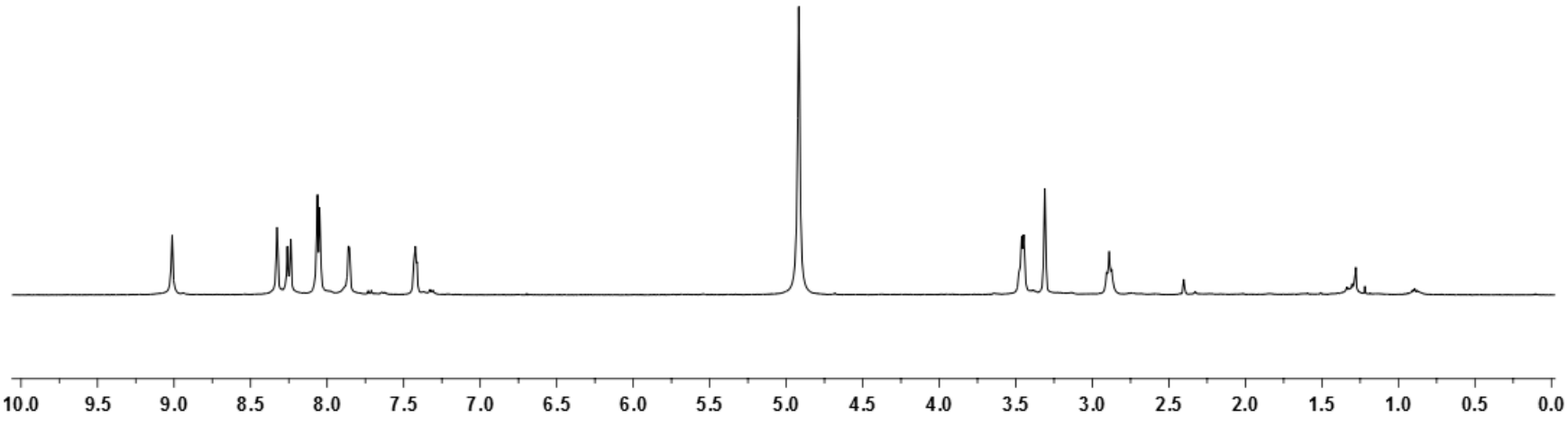

3-[6-Chloro-2-(2-thienyl)quinolin-3-yl]propanenitrile ***47***

^{13}C NMR (100.6 MHz, CD_3OD)

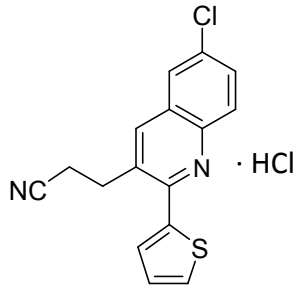

N-{3-[6-Chloro-2-(2-thienyl)quinolin-3-yl]propyl}pyrrolidine ***49***

^{1}H NMR (400 MHz , CD_3OD)

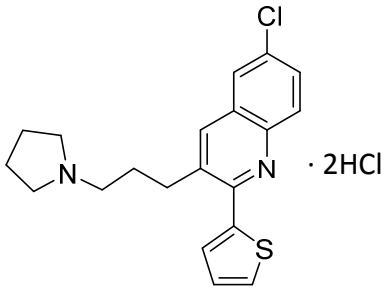

N-{3-[6-Chloro-2-(2-thienyl)quinolin-3-yl]propyl}pyrrolidine ***49***

^{13}C NMR (100.6 MHz, CD_3OD)

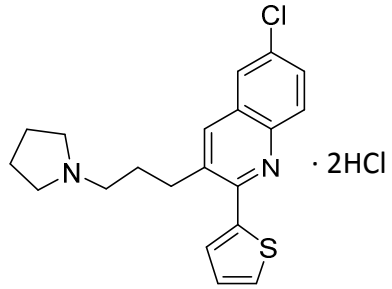

N-{3-[6-Chloro-2-(2-thienyl)quinolin-3-yl]propyl}-N,N-diethylamine ***50***

^{1}H NMR (400 MHz , CD_3OD)

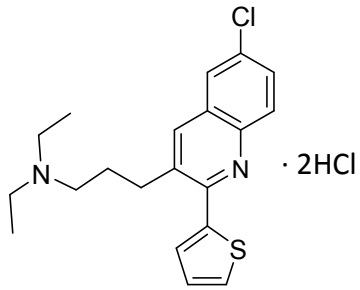

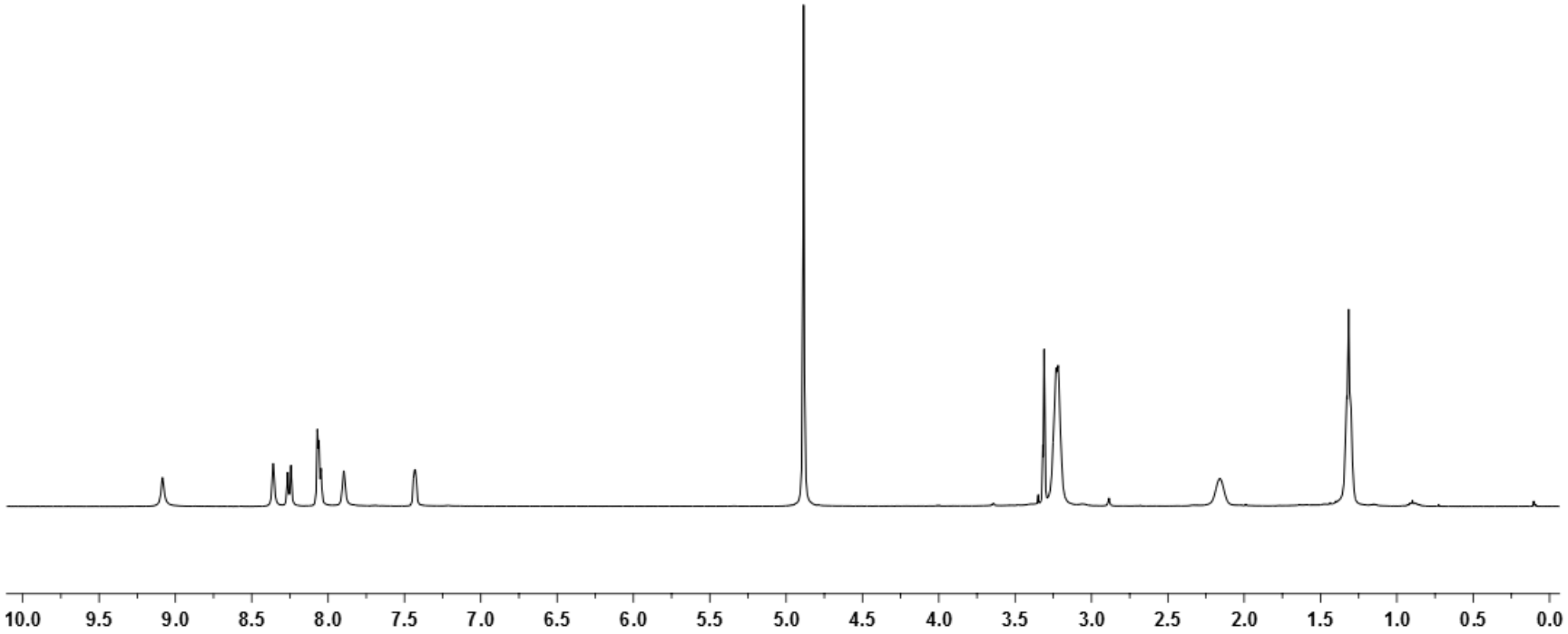

N-{3-[6-Chloro-2-(2-thienyl)quinolin-3-yl]propyl}-N,N-diethylamine ***50***

^{13}C NMR (100.6 MHz, CD_3OD)

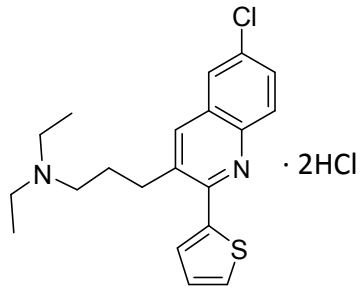

· 2HCl

9 Conclusions

Chapter

- The first objective of this PhD thesis regarded the design, synthesis and molecular modelling studies of an optimized family of propidium-related PAS-binding AChEIs featuring a tetrahydrobenzo[*h*][3,2-*c*]naphthyridine unit. The *Povarov*-type MCR of an activated alkene, an aniline and two alternative aromatic aldehydes, followed by DDQ oxidation of the corresponding diastereomeric mixture, successfully provided the desired set of compounds differently substituted at position 5 of the naphthyridine ring. Further derivatization of the ethyl esther group at position 9, through basic hydrolysis followed by amidation with ethylamine hydrochloride and final $LiAlH_4$-reduction to the corresponding amine, allowed us to explore the effect on the biological activity induced by additional structural modifications in the core structure. Naphthyridines **62**, **63**, **68** and **69** were fully characterized and pharmacologically evaluated against *ee*AChE, *h*AChE and *h*BChE, and their membrane permeability assessed through the PAMPA-BBB assay. Overall, the *hit-to-lead* optimization process from **45** to **68**, involving a double O → NH bioisosteric replacement at position 1 and in the side chain at position 9, gave rise to a dramatic increase in both the *ee*AChE (> 217-fold) and *h*AChE (> 154-fold) inhibitory activities. The kinetic studies and propidium-displacement assays confirmed the ability of this class of compounds to bind the PAS. Molecular modelling studies suggested that the nanomolar potency of **68** might arise from hydrogen bond interactions of its amide side chain at position 9 with midgorge residues of *h*AChE. Overall, the high inhibitory potency of **68** together with the ability of 9 to penetrate along the gorge projecting towards the CAS, made it an interesting candidate for hybridization with CAS inhibitors leading to novel dual-binding site AChEIs.

- The MD-driven optimization of the molecular hybridization of compound **68** with 6-chlorotacrine,led to 1,2,3,4-tetrahydrobenzo[*h*][1,6]naphthyridine–6-chlorotacrine hybrid **81a**, which turned out to be one of the most potent non-covalent *h*AChEIs ever described, with an IC_{50} value in the low picomolar range. This outstanding anticholinesterase activity is likely ascribable to the network of interactions established by the amide group in the three-methylene linker with midgorge residues. Tetra-, penta-, and octamethylene-linked homologues **81b**-**d** were also prepared following a similar synthetic route, consisting of the initial aromatic nucleophilic substitution of the 6,9-dichloroacridine intermediate with the appropriate α,ω-alkanediamines, and further HOBt/EDC amidation-coupling reaction with the tetrahydrobenzo[*h*][1,6]naphthyridine **66**·HCl. These homologues, **81b**-**d**, were potent *h*AChEIs, exhibiting IC_{50} values in the low nanomolar range and remarkable selectivity for

*h*AChE *vs.* *h*BChE inhibition. All the hybrids were moderate dual inhibitors of $A\beta_{42}$ and tau aggregation in intact *E. coli* cells, with IC_{50} values in the low micromolar range. Although better balanced potencies against the different targets would have been desirable, the multi-target profile of these novel 6–chlorotacrine-based hybrids and their predicted ability to cross the BBB make them *lead* compounds of considerable interest in the scenario of a polypharmacological approach for the treatment of AD.

- A *Cu*-catalyzed version of the click-chemistry synthetic approach, followed by a sequence of conventional organic chemistry transformations, was employed for the synthesis of new 1,4-disubstituted 1,2,3-triazoles, bearing a propargylamine group, as potential inhibitors of MAO-B enzyme. Different azides and alkynes were conveniently coupled to expand the chemical diversity of these compounds. The novel triazole derivatives, differing for the substitution patterns at positions 1, 4 and 5 of the core structure, were obtained, apart from some exceptions, in excellent yields and with no need of chromatography purification. The whole series was evaluated *in vitro* against both MAO-A and MAO-B, and their ability to cross the BBB predicted through the well-established PAMPA-BBB assay. Triazole **95** was additionally subjected to reversibility and kinetic studies, overall providing strong evidence of an irreversible, slow time-dependent MAO-B inhibition. Two promising hit candidates, namely **121**, displaying the best potency against MAO-B (IC_{50} 0.607 μM), and **95**, exhibiting the best *selectivity index* MAO-B/MAO-A (SI 0.036), have been chosen as starting points for further *lead* optimization, currently in progress in our laboratory, aimed at incorporating both high MAO-B inhibitory potency and MAO-B/MAO-A selectivity in one single chemical entity. Moreover, the evaluation of metal-chelation, a property already reported in the literature with respect to other structurally similar 1,2,3-triazoles, has been proposed. This additional feature, if confirmed, would open the way for the development of a structurally innovative family of drug-like compounds endowed with multipotent biological profile.

- The high BACE-1 inhibitory potency (IC_{50} 80 nM) displayed by the *in-house* multipotent rhein-huprine hybrid **15** together with the results from previous computational studies on the much less potent homologue **143** (IC_{50} 2020 nM) and a notable example in literature of other low micromolar structurally related chromene-tacrine hybrids developed by Rodríguez-Franco *et al.* (general structure **VII**), supported the hypothesis that the rhein moiety of **15** could reasonably fill a transient secondary pocket in BACE-1 never described so far. An extensive

computation of the BACE-1 *apo* conformational ensemble combined with Principal Component Analysis (PCA) was carried out, allowing an exhaustive study of the intrinsic high flexibility of the loops defining the walls of a novel secondary pocket and found to affect the orientation of a crucial residue for the ligand binding (Arg307), as also attested by the available X-ray structures. Clustering of the protein conformations allowed to select several representative structures and the druggability features of the cavity were characterized. The hypothesized binding mode of both the rhein-huprine and chromene-tacrine hybrids **15** and **144**, respectively, was confirmed by preliminary MD simulations, which provided quite stable trajectories throughout the simulated time. Finally, a virtual screening of a library of 500.000 commercially available fragments has been carried out and three suitable candidates selected for further hybridization with racemic huprine Y. In this PhD thesis the synthetic routes to achieve the target novel hybrids have been already designed and are currently in progress in our laboratory.

- Finally, the structure of benzonaphthyridine **57**, previously developed in our research group as PAS-binding AChEI and later found to also display a low micromolar *in vitro* activity against *T. brucei*, has provided a suitable template for the exploration of novel quinoline-based anti-trypanosomatid agents. The initial *N*-dealkylation of the side chain at position 9 and positional isomerization of the chlorine atom and the aminomethyl group of compound **57** provided benzonaphthyridine **161**, a 3-fold more potent agent against *T. brucei*. Further modifications of compound **161**, including N_1-debenzylation, ring contraction and expansion, bioisosteric NH → O replacement at position 1, and substitution of the phenyl group at position 5 by other heterocycles, were easily afforded performing as the key step of the synthetic sequences a *Povarov* MCR between different sets of commercially available or easy-to-prepare activated olefins, properly substituted anilines, and aromatic aldehydes. Moreover, the formation of several byproducts deriving from collateral ring-opening reactions allowed the study of other quinoline derivatives. Since the trypanosomatid parasites causing HAT, Chagas disease and visceral leishmaniasis likely share common metabolic pathways, these compounds were subjected to a phenotypic *whole-cell* screening against *T. brucei*, *T. cruzi* and *L. infantum*. Several compounds turned out to be moderately potent against two or even three of these parasites. Indeed, benzonaphthyridines **167**, **184** and **186**, and pyranoquinoline **193** exhibited single digit micromolar IC_{50} values against *T. brucei* and *L. infantum* and IC_{50} around 30 µM against *T. cruzi*, whereas benzonaphthyridine **161** displayed single digit micromolar IC_{50} values against *T. brucei* and *T. cruzi* and IC_{50} around 30 µM against *L. infantum*. Additionally, all

the screened compounds were predicted to efficaciously cross the BBB, thus being potentially effective also for the treatment of late-stage HAT. However, AChE constitutes a relevant off-target for most of the evaluated compounds, with the sole exception of the dual trypanocidal and leishmanicidal pyranoquinoline **193**, thereby emerging as the best starting point for a future *lead* optimization.

Bibliography

1. *Alzheimer's Disease International*. *World Alzheimer Report: The global prevalence of dementia* **2009**.
2. Muñoz-Torrero, D. *Curr. Med. Chem.* **2008**, *15*, 2433.
3. *Alzheimer's Disease International*. *World Alzheimer Report*: *The benefits of early diagnosis and intervention* **2011**.
4. Walsh, D.M.; Selkoe, D.J. *Neuron* **2004**, *44*, 181.
5. Gray, L. *Cell* **2012**, *18*, 6.
6. Cummings, J.L.; Askin-Edgar, S. *CNS Drugs* **2000**, *13*, 385.
7. Leonard, B.E. *Hum. Psycopharmacol.* **1998**, *13*, 83.
8. Lahiri, D.K.; Farlow, M.R.; Sambamurti, K.; Greig, N.H.; Giacobini, E.; Schneider, L.S. *Curr. Drug. Targets* **2003**, *4*, 97.
9. Goate, A.; Chartier-Harling, N.C.; Mullan, M.; Brown, J.; Crawford, F.; Fidani, L.; Giuffra, L.; Haynes, A.; Irving, N.; James, L.; Mant, R.; Newton, P.; Rooke, K.; Roques, P.; Talbot, C.; Pericak-Vance, M.; Roses, A.; Williamson, R.; Rossor, M.; Owen, M.; Hardy, J. *Nature* **1991**, *349*, 704.
10. Sherringtone, R.; Rogaev, E.I.; Liang, Y.; Rogaeva, E.A.; Levesque, G.; Ikeda, M.; Chi, H.; Lin, C.; Li, G.; Holman, K.; Tsuda, T.; Mar, L.; Foncin, J.-F.; Bruni, A.C.; Montesi, M.P.; Sorbi, S.; Rainero, I.; Pinessi, L.; Nee, L.; Chumakov, I.; Pollen, D.; Brookes, A.; Sanseau, P.; Polinsky, R.J.; Wasco, W.; Da Silva, H.A.R.; Haines, J.L.; Perikac-Vance, M.A.; Tanzi, R.E.; Roses, A.D.; Fraser, P.E.; Rommens, J.M.; St. George-Hyslop, P.H. *Nature* **1995**, *375*, 754.
11. Levy-Lehad, E.; Wijsman, E.M.; Nemens, E.; Anderson, A.L.; Goddard, K.A.B.; Wiltfang, J. *Brain* **2006**, *129*, 743.
12. Klafki, H.-W.; Staufenbiel, M.; Kornhuber, J.; Wiltfang, J. *Brain* **2006**, *129*, 2840.
13. Schönheit, B.; Zarski, R.; Ohm, T.G. *Neurobiol. Aging* **2004**, *25*, 743.
14. Castellani, R.J.; Zhu, X.; Lee, H.-G.; Moreira, P.I.; Perry, G.; Smith, M.A. *Expert Rev. Neurother.* **2007**, *7*, 473.
15. Hamley, I.W. *Chem. Rev.* **2012**, *112*, 5147.
16. Goedert, M.; Spillantini, M.G. *Science* **2006**, *314*, 777.
17. Hardy, J.; Allsop, D. *Trends Pharm. Sci.* **1991**, *12*, 383.
18. Hardy, J. *Curr. Alzheimer Res.* **2006**, *3*, 71.
19. Coughlan, C.M.; Breen, K.C. *Pharmacol. Ther.* **2000**, *86*, 111.
20. Bartolini, M.; Andrisano, V. *ChemBioChem* **2010**, *11*, 1018.
21. Citron, M. *Nat. Rev. Drug Discovery* **2010**, *9*, 387.
22. Bodles, A.M.; Gurthrie, D.J.S.; Greer, B.; Irvine, G.B. *J. Neurochem.* **2001**, *78*, 384.

23. Inestrosa, N.C. *Las incomunicaciones del Alzheimer, Atenea Impresores Ltda.* **2007**.
24. Goedert, M. *Trends Neurosci.* **1993**, *16*, 460.
25. Camps, P.; Muñoz-Torrero, D. *Mini-Rev. Med. Chem.* **2002**, *2*, 11.
26. Sussman, J.L.; Harel, M.; Frolow, F.; Oefner, C.; Goldman, A.; Toker, L.; Silman, I. *Science* **1991**, *253*, 872.
27. Fernández-Bachiller, M.I.; Pérez, C.; Monjas, L.; Rademann, J.; Rodríguez-Franco, M.I. *J. Med. Chem.* **2012**, *55*, 1303.
28. Perry, R.H.; Blessed, G.; Tomlinson, B.E. *Neuropathol. Appl. Neurobiol.* **1978**, *4*, 273.
29. Lane, R.M.; Potkin, S.G.; Enz, A. *Int. J. Neuropsychopharmacol.* **2006**, *9*, 101.
30. Greig, N.; Utsuki, T.; Ingram, D.; Wang, Y.; Pepeu, G.; Scali, C.; Yu, Q.; Mamczarz, J.; Holloway, H.; Giordano, T.; Chen, D.; Furukawa, K.; Sambamurti, K.; Brossi, A.; Lahiri, D. *Proc. Natl. Acad. Sci. U.S.A.* **2005**, *102*, 17213.
31. Venneri, A.; McGeown, W.J.; Shanks, M.F. *Neuroreport* **2005**, *16*, 107.
32. Venneri, A.; Shanks, M.F.; Staff, R.T.; Pestell, S.J.; Forbes, K.E.; Gemmell, H.G.; Murray, A.D. *Neuroreport* **2002**, *13*, 83.
33. Venneri, A.; Lane, R. *Neuroreport* **2009**, *20*, 285.
34. Shanks, M.; Kivipelto, M.; Bullok, R.; Lane, R. *Curr. Med. Res. Opin.* **2009**, *25*, 2439.
35. Lipton, S.A. *Nature* **2004**, *428*, 473.
36. Gualtieri, F.; Due, S.; Manetti, D.; Romanelli, M.N. *Farmaco* **1995**, *50*, 489.
37. Davis, K.L.; Thal, L.J.; Gamzu, E.R.; Davis, C.S.; Woolson, R.F.; Gracon, S.I.; Drachman, D.A.; Schneider, L.S.; Whitehouse, P.J.; Hoover, T.M. *New Engl. J. Med.* **1992**, *327*, 1253.
38. Marx, J. *Science* **1996**, *273*, 50.
39. Sugimoto, H.; Iimura, Y.; Yamanishi, Y.; Yamatsu, K. *J. Med. Chem.* **1995**, *38*, 4821.
40. Polinsky, R.J. *Clin. Therap.* **1998**, *20*, 634.
41. Sramek, J.J.; Frackiewicz, E.J.; Ctler, N.R. *Expert Opin. Invest. Drugs* **2000**, *9*, 2393.
42. Giacobini, E. *Neurochem. Res.* **2000**, *25*, 1185.
43. Francis, P.T.; Nordberg, A.; Arnold, S.E. *Trends Pharmacol. Sci.* **2005**, *26*, 104.
44. Riepe, M.W. *Eur. J. Neurol.* **2005**, *12*, 3.
45. Geerts, H. *Brain Res. Bull.* **2005**, *64*, 519.
46. Muñoz-Torrero, D. *Neuroprotección en la enfermedad de Alzheimer*, Edicomplet **2007**, Madrid.
47. Wang, X.-D.; Chen, X.-Q.; Yang, H.-H.; Hu, G.;-Y. *Neurosci. Lett.* **1999**, *272*, 21.
48. Takada-Takatori, Y.; Kume, T.; Sugimoto, M.; Katsui, H.; Sugimoto, H.; Akaike, A. *Neuropharmacology* **2006**, *51*, 474.

49. Kihara, T.; Sawada, H.; Nakamizo, T.; Kanki, R.; Yamashita, H.; Maelicke, A.; Shimoama, S. *Biochem. Biophys. Res. Commun.* **2004**, *325*, 976.
50. Meunier, J.; Ieni, J.; Maurice, T. *Br. J. Pharmacol.* **2006**, *149*, 998.
51. Meunier, J.; Ieni, J.; Maurice, T. *J. Pharmacol. Exp. Ther.* **2006**, *306*, 53.
52. Inestrosa, N.C.; Alvarez, A.; Pérez, C.A.; Moreno, R.D.; Vicente, M.; Linker, C.; Casanueva, O.I.; Soto, C.; Garrido, C. *Neuron* **1996**, *16*, 81.
53. Alvarez, A.; Alarcón, R.; Opazo, C.; Campos, E.O.; Muñoz, F.J.; Calderón, F.H.; Dajas, F.; Gentry, M.K.; Doctor, B.P.; De Mello, F.G.; Inestrosa, N.C. *J. Neurosci.* **1998**, *18*, 3213.
54. Muñoz, F.; Inestrosa, N.C. *FEBS Lett.* **1999**, *450*, 205.
55. Reyes, A.E.; Chacón, M.A.; Dinamarca, M.C.; Cepa, W.; Morgan, C.; Inestrosa, N.C. *Am. J. Pathol.* **2004**, *164*, 2163.
56. Rees, T.; Hammond, P.I.; Soreq, H.; Younkin, S.; Brimijoin, S. *Neurobiol. Aging* **2003**, *24*, 777.
57. Rees, T.M.; Brimijoin, S. *Drugs Today* **2005**, *39*, 75.
58. De Ferrari, G.V.; Canales, M.A.; Shin, I.; Inestrosa, N.C. *Biochemistry* **2001**, *40*, 10447.
59. Castro, A.; Martínez, A. *Curr. Pharm. Design* **2006**, *12*, 4377.
60. Pang, Y.-P.; Quiram, P.; Jelacic, T.; Hong, F.; Brimijoin, S. *J. Biol. Chem.* **1996**, *271*, 23646.
61. Carlier, P.R.; Han, Y.F.; Chow, E.S.-H.; Li, C.P.-L.; Wang, H.; Lieu, T.X.; Wong, H.S.; Pang, Y.-P. *Bioorg. Med. Chem.* **1999**, *7*, 351.
62. Bolognesi, M.L.; Cavalli, A.; Valgimigli, L.; Bartolini, M.; Rosini, M.; Andrisano, V.; Recanatini, M.; Melchiorre, C. *J. Med. Chem.* **2007**, *50*, 6446.
63. Piazzi, L.; Rampa, A.; Bisi, A.; Gobbi, S.; Belluti, F.; Cavalli, A.; Bartolini, M.; Andrisano, V.; Valenti, P.; Recanatini, M. *J. Med. Chem.* **2003**, *46*, 2279.
64. Muñoz-Ruiz, P.; Rubio, L.; García-Palomero, E.; Dorronsoro, I.; del Monte-Millán, M.; Valenzuela, R.; Usán, P.; de Austria, C.; Bartolini, M.; Andrisano, V.; Bidon-Chanal, A.; Orozco, M.; Luque, F.J.; Medina, M.; Martínez, A. *J. Med. Chem.* **2005**, *48*, 7223.
65. Cavalli, A.; Bolognesi, M.L.; Capsoni, S.; Andrisano, V.; Bartolini, M.; Margotti, E.; Cattaneo, A.; Recanatini, M.; Melchiorre, C. *Angew. Chem. Int. Ed.* **2007**, *46*, 3689.
66. Camps, P.; El Achab, R.; Görbig, D.M.; Morral, J.; Muñoz-Torrero, D.; Badia, A.; Baños, J.E.; Vivas, N.M.; Barril, X.; Orozco, M.; Luque, F.J. *J. Med. Chem.* **1999**, *42*, 3227.
67. Camps, P., Formosa, X.; Galdeano, C.; Gómez, T.; Muñoz-Torrero, D.; Ramírez, L.; Gómez, E.; Isambert, N.; Lavilla, R.; Badia, A.; Clos, M.V.; Bartolini, M.; Mancini, F.; Andrisano, V.; Arce, M.P.; Rodríguez-Franco, M.I.; Huertas, O.; Dafni, T.; Luque, F.J. *J. Med. Chem.* **2009**, *52*, 5365.
68. Melnikova, I. *Nat. Rev. Drug Discovery* **2007**, *6*, 341.

69. Skovronsky, D.M.; Lee, V.M.-Y.; Trojanowski, J.Q. *Annu. Rev. Pathol. Mech. Dis.* **2006**, *1*, 151.
70. Chiang, K.; Koo, E.H. *Annu. Rev. Pharmacol. Toxicol.* **2014**, *54*, 381.
71. Vassar, R. *Alzheimers Res. Ther.* **2014**, *6*, 89.
72. De Strooper, B.; Vassar, R.; Golde, T. *Nat. Rev. Neurol.* **2010**, *6*, 99.
73. Kacker, P.; Bottegoni, G, Cavalli, A. *Curr. Med. Chem.* **2012**, *19*, 6095.
74. Willem, M., Garratt, A.N.; Novak, B.; Citron, M., Kaufmann, S.; Rittger, A.; De Strooper, B.; Saftig, P.; Birchmeier, C.; Haass, C. *Science* **2006**, *314*, 664.
75. McConlogue, L.; Buttini, M.; Anderson, J.P.; Brigham, E.F.; Chen, K.S.; Freedman, S.B.; Games, D. Johnson-Wood, K.; Lee, M.; Zeller, M.; Liu, W.; Motter, R.; Sinha, S. *J. Biol. Chem.* **2007**, *282*, 26326.
76. Hong, L.; Koelsch, G.; Lin, X.; Wu, S.; Terzyan, S.; Ghosh, A.K.; Zhang, X.C.; Tang, J. *Science* **2000**, *290*, 150.
77. Martínez, A.; Castro, A.; Dorronsoro, I.; Alonso, M. *Med. Res. Rev.* **2002**, *22*, 373.
78. Dringenberg, H.C. *Behav. Brain Res.* **2000**, *115*, 235.
79. Garcia-Alloza, M.; Gil-Bea, F.J.; Diez-Ariza, M.; Chen, C.P.L.H.; Francis, P.T.; Lasheras, B.; Ramirez, M.J. *Neuropsychologia* **2005**, *43*, 442.
80. Binda, C.; Newton-Vinson, P.; Hubálek, F.; Edmondson, D.E.; Mattevi, A. *Nat. Struct. Biol.* **2002**, *9*, 22.
81. Youdim, M.B.H.; Weinstock, M. *Neurotoxicology* **2004**, *25*, 243.
82. Carreiras, M.C.; Marco, J.L. *Curr. Pharm. Des.* **2004**, *10*, 3167.
83. Good, P.F.; Werner, P.; Hsu, A.; Olanow, C.W.; Perl, D.P. *Am. J. Pathol.* **1996**, *149*, 21.
84. Ebadi, M.; Sharma, S.; Shavadi, S. El Refakey, K. *J. Neurosci. Res.* **2002**, *67*, 285.
85. Hopkins, A.L. *Nat. Chem. Biol.* **2008**, *4*, 682.
86. Hopkins, A.L. *Nat. Biotechnol.* **2007**, *25*, 1110.
87. Janga, S.C.; Tzakos, A. *Mol. BioSyst.* **2009**, *5*, 1536.
88. Bianchi, M.T. *Medical Hypotheses* **2010**, *74*, 297.
89. Viayna, E.; Sola, I., Di Pietro, O. Muñoz-Torrero, D. *Curr. Med. Chem.* **2013**, *20*, 1623.
90. Morphy, R.; Rankovic, Z. *J. Med. Chem.* **2005**, *48*, 6523.
91. Viayna, E.; Sola, I.; Bartolini, M.; De Simone, A., Tapia-Rojas, C.; Serrano, F.; Sabaté, R.; Juárez-Jiménez, J.; Pérez, B.; Luque, F.J.; Andrisano, V.; Clos, M.V.; Inestrosa, N.C.; Muñoz-Torrero, D. *J. Med. Chem.* **2014**, *57*, 2549.
92. Sterlig, J.; Herzig, Y.; Goren, T.; Finkelstein, N.; Lerner, D.; Goldenberg, W.; Miskolczi, I.; Molnar, S.; Rantal, F.; Tamas, T.; Toth, G.; Zagyva, A.; Zekany, A.; Finberg, J.; Lavian, G.;

Gross, A.; Friedman, R.; Razin, M.; Huang, W.; Krais, B.; Chorev, M.; Youdim, M.B.; Weinstock, M. *J. Med. Chem.* **2002**, *45*, 5260.

93. Farina, R.; Pisani, L.; Catto, M.; Nicolotti, O.; Gadaleta, D.; Denora, N.; Soto-Otero, R.; Mendez-Alvarez, E.; Passos, C.S.; Muncipinto, G.; Altomare, C.D.; Nurisso, A.; Carrupt, P.-A.; Carotti, A. *J. Med. Chem.* **2015**, *58*, 5561.
94. Centre for Disease Control and Prevention, Neglected Tropical Diseases, http://www.cdc.gov/globalhealth/ntd/, accessed 4th April 2015.
95. World Health Organization, Neglected Tropical Diseases, http://www.who.int/neglected_diseases/diseases/en/, accessed 4th April 2015.
96. McMichael, A.J. *Philos. Trans. R. Soc. Lond. B Biol. Sci.* **2004**, *359*, 1049.
97. De Silva, N.R.; Brooker, S.; Hotez, P.J.; Montresor, A.; Engels, D.; Savioli, L. *Trends Parasitol.* **2003**, *19*, 547.
98. Mackey, T.K.; Liang, B.A.; Cuomo, R.; Hafen, R.; Brouwer, K.C.; Lee, D.E. *Clinic. Microb. Rev.* **2014**, *27*, 949.
99. WHO. **2013**. Sustaining the drive to overcome the global impact of neglected tropical diseases. World Health Organization, Geneva, Switzerland, http://www.who.int/en/.
100. Hotez, P.J., Pecoul, B. 2010. *PLoS Negl. Trop. Dis.* **2010**, *4*, 718.
101. Trouiller, P.; Olliaro, P.; Torreele, E.; Orbinski, J.; Laing, R.; Ford, N. *Lancet* **2002**, *359*, 2188.
102. Pedrique, B.; Sturb-Wourgaft, N.; Some, C.; Olliaro, P.; Trouiller, P.; Ford, Pécoul, B.; Bradol, J.-H. *Lancet Global Health* **2013**, *1*, 371.
103. Njoroge, M.; Njuguna, N.M.; Mutai, P.; Ongarora, D.S.B.; Smith, P.W.; Chibale, K. *Chem. Rev.* **2014**, *114*, 11138.
104. Simarro, P.P.; Diarra, A.; Ruiz Postigo, J.A.; Franco, J.R.; Jannin, J.G. *PLoS Negl. Trop. Dis.* **2011**, *5*, 1007.
105. Jones, A.J.; Avery, V.M. *Expert Opin. Drug Discov.* **2013**, *8*, 495.
106. Pepi, J.; Meda, H.A. *Adv. Parasitol.* **2001**, *49*, 71.
107. Vickerman, K. *Br. Med. Bull.* **1985**, *41*, 105.
108. Apted, F.I.C.; Mulligan, H.W. George Allen and Unwin LTD, London, **1970**, 661.
109. Atouguia, J.L.M.; Kennedy, P.G.E.; Davis, L.E. Butterworth-Heinemann, Oxford, **2000**, 321.
110. Gelfan, M. *Trans. R. Soc. Trop. Med. Hyg.* **1947**, *41*, 255.
111. Lundkvist, G.B.; Kristensson, K.; Bentivoglio, M. *Physiology* **2004**, *19*, 198.
112. Bentovoglio, M.; Grassi-Zucconi, G.; Olsson, T.; Kristensson, K. *Trends Neurosci*. **1994**, *17*, 325.

113. Apted, F.I.C.; Mullerhorvath, R. George Allen and Unwin Ltd, London, **1970**, 684.
114. Burri, C.; Stich, A.; Brun, R. CABI Publishing, Trowbridge, **2004**, 403.
115. WHO. Control and surveillance of African trypanosomisis. World Health Organization, Geneve, **1998**.
116. Pepin, J.; Milord, F. *Adv. Parasitol.* **1994**, *33*, 1.
117. Bacchi, C.J.; Nathan, H.C.; Hutner, S.H. *Science* **1980**, *210*, 332.
118. Priotto,G.; Kasparian, S.; Ngouama, D. *et al. Lancet* **2009**, *374*, 56.
119. Priotto, G.; Kasparian, S.; Ngouama, D. *et al. Clin. Infect. Dis.* **2007**, *45*, 1435.
120. Rossi, A.; Marin-Neto, J.A. *Lancet* **2010**, *375*, 1388.
121. Nunes, M.C.P.; Dones, W.; Morillo, C.A.; Encina, J.J.; Ribeiro, A.L. *J. Am. College Cardiol.* **2013**, *62*, 767.
122. Conteh, L.; Engels, T.; Molyneux, D.H. *Lancet* **2010**, *375*, 239.
123. Manning-Cela, R.; Jaishankar, S.; Swindle, J. *Arch. Med. Res.* **2006**, *37*, 593.
124. Bern, C.; Kjos, S.; Yabsley, M.J.; Mongtomery, S.P. *Clin. Microbiol. Rev.* **2011**, *24*, 655.
125. Lattes, R.; Lasala, M.B. *Clin. Microbiol. Infect.* **2014**, *20*, 300.
126. Hashimoto, K.; Yioshoka, K. *Adv. Parasitol.* **2012**, *79*, 375.
127. Hotez, P.J.; Molyneux, D.H.; Fenwick, A.; Kumaresan, J.; Sachs, S.E.; Sachs, J.D.; Savioli, L. *N. Engl. J. Med.* **2007**, *357*, 1018.
128. World Health Organization, Global Health Observatory Map Gallery, http://gamapserver.who.int/mapLibrary/, accessed 23th April 2015.
129. World Health Organization, Leishmaniasis, The disease and its epidemiology, http://www.who.int/leishmaniasis/disease_epidemiology/en/index.html, accessed 25th April 2015.
130. Burrows, J.N.; Elliot, R.L.; Kaneko, T.; Mowbray, C.E.; Waterson, D. *Med. Chem. Commun.* **2014**, *5*, 688.
131. Leifso, K.; Cohen-Freue, G.; Dogra, N.; Murray, A.; McMaster, W.R. *Mol. Biochem. Parasitol.* **2007**, *152*, 35.
132. Wellcome Trust, Neglected tropical diseases, the London declaration, http://wellcometrust.wordpress.com/2012/01/31/neglected-tropical-diseases-the-london-declaration/, accessed 4th April 2015.
133. London Declaration on Neglected Tropical Diseases, http://www.unitingtocombatntds.org/downloads/press/london_declaration_on_ntds.pdf, accesses 22th March 2015.
134. Swinney, D.C.; Anthony, J. *Nat. Rev. Drug Discovery* **2011**, *10*, 507.
135. Denny, P.W.; Steel, P.G. *J. Biomol. Screening* **2015**, *20*, 56.

136. Butera, J.A. *J. Med. Chem.* **2013**, *56*, 7715.
137. Kotz, J. *Sci. Exch.* **2012**, *5*, 1.
138. Wells, T.N.C. *Science* **2010**, *329*, 1153.
139. Sykes, M.L.; Baell, J.B.; Kaiser, M.; Chatelain, E.; Moawad, S.R.; Ganame, D.; Ioset, J.-R., Avery, V.M. *PLoS Neglected Trop. Dis.* **2012**, *6*, 1896.
140. Ferrins, L.; Rahmani, R.; Sykes, M.L.; Jones, A.J.; Avery, V.M.; Teston, E.; Almohaywi, B.; Yin, J.; Smith, J.; Hyland, C.; White, K.L.; Ryan, E.; Campbell, M.; Charman, S.A.; Kaiser, M.; Baell, J.B. *Eur. J. Med. Chem.* **2013**, *66*, 450.
141. Nare, B.; Wring, S.; Bacchi, C.; Beaudet, B.; Bowling, T.; Brun, R.; Chen, D.; Ding, C.; Freund, Y.; Gaukel, E.; Hussain, A.; Jarnagin, K.; Jenks, M.; Kaiser, M.; Mercer, L.; Mejia, E.; Noe, A.; Orr, M.; Parham, R.; Plattner, J.; Randolph, R.; Rattendi, D.; Rewerts, C.; Sligar, J.; Yarlett, N.; Don, R.; Jacobs, R. *Antimicrob. Agents Chemoter.* **2010**, *54*, 4379.
142. Ding, D.; Zhao, Y.; Meng, Q.; Xie, D.; Nare, B.; Chen, D.; Bacchi, C.J.; Yarlett, N.; Zhang, Y.-K.; Hernandez, V.; Xia, Y.; Freund, Y.; Abdulla, M.; Ang, K.-H.; Rstman, J.; McKerrow, J.H.; Jacobs, R.T.; Zhou, H.; Plattner, J.J. *ACS Med. Chem. Lett.* **2010**, *1*, 165.
143. Jacobs, R.T.; Nare, B.; Wring, S.A.; Orr, M.D.; Chen, D.; Sligar, J.M.; Jenks, M.X.; Noe, R.A.; Bowling, T.S.; Mercer, L.T.; Rewerts, C.; Gaukel, E.; Owens, J.; Parham, R.; Randolph, R.; Beaudet, B.; Bacchi, C.J.; Yarlett, N.; Plattner, J.J.; Freund, Y.; Ding, C.; Akama, T.; Zhang, Y.-K.; Brun, R.; Kaiser, M.; Scandale, I.; Don, R.; *PLoS Neglected Trop. Dis.* **2011**, *5*, 1151.
144. Munos, B. *Nat. Rev. Drug Discov.* **2009**, *8*, 959.
145. Paul, S.M.; Mytelka, D.S.; Dunwiddie, C.T.; Persinger, C.C.; Munos, B.H.; Lindborg, S.R.; Schacht, A.L. *Nat. Rev. Drug Discov.* **2010**, *9*, 203.
146. Bleicher, K.H.; Böhm H.J.; Müller, K.; Alanine, A.L. *Nat. Rev. Drug Discov.* **2003**, *2*, 369.
147. Fattori, D. *Drug Discov. Today* **2004**, *9*, 229.
148. Evans, B.E.; Rittle, K.E.; Bock, M.G.; Di Pardo, R.M.; Freidinger, R.M.; Whitter, W.L.; Lundell, G.F.; Veber, D.F.; Anderson, P.S.; Chang, R.S. *J. Med. Chem.* **1988**, *31*, 2235.
149. Bongarzone, S.; Bolognesi, M.L. *Expert Opin. Drug Discov.* **2011**, *6*, 251.
150. Welsch, M.E.; Snyder, S.A.; Stockwell, B.R. *Curr. Opin. Chem. Biol.* **2010**, *14*, 347.
151. O'Neil, P.M.; Ward, S.A.; Berry, N.G.; Jeyadevan, J.P.; Biagini, G.A.; Asadollaly, E.; Park, B.K.; Bray, P.G. *Curr. Top. Med. Chem.* **2006**, *6*, 479.
152. Musiol, R.; Serda, M.; Hensel-Bielowka, S.; Polanski, J. *Curr. Med. Chem.* **2010**, *17*, 1960.
153. Tekwani, B.L.; Walker, L.A. *Curr. Opin. Infect. Dis.* **2006**, *19*, 623.
154. Warshakoon, N.C.; Sheville, J.; Bhatt, R.T.; Ji, W.; Mendez-Andino, J.L.; Meyers, K.M.; Kim, N.; Wos, J.A.; Mitchel, C.; Paris, J.L.; Pinney, B.B.; Reizes, O.; Hu, X.E. *Bioorg. Med. Chem. Lett.* **2006**, *16*, 5207.

155. DeRuiter, J.; Brubaker, A.N.; Whitmer, W.L.; Stein, J.L. Jr. *J. Med. Chem.* **1986**, *29*, 2024.
156. Knight, S.D.; Adams, N.D.; Burgess, J.L.; Chaudhari, A.M.; Darcy, M.G.; Donatelli, C.A.; Luengo, J.I.; Newlander, K.A.; Parrish, C.A.; Ridgers, L.H.; Sarpong, M.A.; Schimdt, S.J.; Van Aller, G.S.; Carson, J.D.; Diamond, M.A.; Elkins, P.A.; Gardiner, C.M.; Garver, E., Gilbert, S.A.; Gontarek, R.R.; Jackson, J.R.; Kershner, K.L.; Luo, L.; Raha, K.; Sherk, C.S.; Sung, C.-M.; Sutton, D.; Tummino, P.J.; Wegrzyn, R.J.; Auger, K.R.; Dhanak, D. *ACS Med. Chem. Lett.* **2010**, *1*, 39.
157. Dorn, A.; Vippagunta, S.R.; Matilde, H.; Jaquet, C.; Vennerstrom, J.L.; Ridley, R.G. *Biochem. Pharmacol.* **1998**, *55*, 727.
158. Kaur, K.; Jain, M.; Reddy, R.P.; Jain, R. *Eur. J. Med. Chem.* **2010**, *45*, 3245.
159. Kouznetsov, V.V.; Gomez-Barrio, A. *Eur. J. Med. Chem.* **2009**, *44*, 3091.
160. Muregi, F.W.; Ishih, A. *Drug Dev. Res.* **2010**, *71*, 20.
161. Davis, T.M.; Hung, T.Y.; Sim, I.K.; Hung, T.Y. *Drugs* **2005**, *65*, 75.
162. Palit, P.; Paira, P.; Hazra, A., Banerjee, S.; Das Gupta, A.; Dastidar, S.G.; Mondal, N.B. *Eur. J. Med. Chem.* **2009**, *44*, 845.
163. Defaux, J.; Sala, M.; Formosa, X.; Galdeano, C.; Taylor, M.C.; Alobaid, W.A.A.; Kelly, J.M.; Wright, C.W.; Camps, P.; Muñoz-Torrero, D. *Bioorg. Med. Chem.* **2011**, *19*, 1702.
164. Sola, I.; Castellà, S.; Viayna, E.; Galdeano, C.; Taylor, M.C.; Gbedema, S.Y.; Pérez, B.; Clos, M.V.; Jones, D.C.; Fairlamb, A.H.; Wright, C.W.; Kelly, J.M.; Muñoz-Torrero, D. *Bioorg. Med. Chem.* **2015**, *23*, 5156.
165. Ugi, I.; Dömling, A.; Hörl, W. *Endeavour* **1994**, *18*, 115.
166. Zhu, J.; Bienaymé, H. Wiley-VCH, Weinheim, **2005**.
167. Dömling, A. *Chem. Rev.* **2006**, *106*, 17.
168. Bienaymé, H.; Hulme, C.; Oddon, G.; Schmitt, P. *Chem-Eur. J.* **2000**, *6*, 3321.
169. Brauch, S.; van Berkel, S.S.; Westermann, B. *Chem. Soc. Rev.* **2013**, *42*, 4948.
170. Kouznetsov, V.V. *Tetrahedron* **2009**, *65*, 2721.
171. Lavilla, R.; Bernabeu, M.C.; Carranco, I.; Díaz, J.L. *Org. Lett.* **2003**, *5*, 717.
172. Kumar, A. *Chem. Rev.* **2001**, *101*, 1.
173. Nicolaou, K.C.; Snyder, S.A.; Montagnon, T.; Vassilikogiannakis, G. *Angew. Chem. Int. Ed.* **2002**, *41*, 1669.
174. Povarov, L.S. *Russ. Chem. Rev.* **1967**, *36*, 656.
175. Zhu, J.; Bilnaymé, H.; Eds.; Wiley-VCH: Weinheim, **2005**.
176. Orru, R.V.A.; de Greef, M. *Synthesis* **2003**, 1471.
177. Taber, D.F. Springer: Berlin, **1984**.
178. Bear, B.R.; Sparks, S.M.; Shea, K.J. *Angew. Chem. Int. Ed.* **2001**, *40*, 820.

179. Kobayashi, S.; Ishitani, H.; Nagayama, S. *Synthesis* **1995**, 1195.
180. Buonora, P.; Olsen, J.-C.; Oh, T. *Tetrahedron* **2001**, *57*, 6099.
181. Alves, M.J.; Azoia, N.G.; Fortes, A.G. *Tetrahedron* **2007**, *63*, 727.
182. Di Pietro, O.; Viayna, E.; Vicente-García, E.; Bartolini, M.; Ramón, R.; Juárez-Jiménez, J.; Clos, M.V.; Pérez, B.; Andrisano, V.; Luque, F.J.; Lavilla, R.; Muñoz-Torrero, D. *Eur. J. Med. Chem.* **2014**, *73*, 141.
183. Di Pietro, O.; Vicente-García, E.; Taylor, M.C.; Berenguer, D., Viayna, E.; Lanzoni, A.; Sola, I.; Sayago, H.; Riera, C.; Fisa, R.; Clos, M.V.; Pérez, B.; Kelly, J.M.; Lavilla, R.; Muñoz-Torrero, D. *Eur. J. Med. Chem.* **2015** (accepted with minor revision).
184. Galdeano, C. PhD thesis. *Unitat de Química Farmacèutica, Departament de Farmacologia i Química Terapèutica, Universitat de Barcelona*, **2012**.
185. Viayna, E. PhD thesis. *Unitat de Química Farmacèutica, Departament de Farmacologia i Química Terapèutica, Universitat de Barcelona*, **2013**.
186. Fernández-Bachiller, M.I.; Pérez, C.; Monjas, L.; Rademann, J.; Rodríguez-Franco, M.I. *J. Med. Chem.* **2012**, *55*, 1303.
187. Soreq, H.; Seidman, S. *Nat. Rev. Neurosci.* **2001**, *2*, 294.
188. Cavalli, A.; Bottegoni, G., Raco, C.; De Vivo, M.; Recanatini, M.A. *J. Med. Chem.* **2004**, *47*, 3991.
189. Vicente-García, E. PhD thesis. *Unitat de Química Farmacèutica, Departament de Farmacologia i Química Terapèutica, Universitat de Barcelona*, **2013**.
190. Ellman, G.L.; Courtney, K.D.; Andres, B. Jr.; Featherstone, R.M.; *Biochem. Pharmacol*. **1961**, *7*, 88.
191. Bolognesi, M.L.; Andrisano, V.; Bartolini, M.; Banzi, R.; Melchiorre, C. *J. Med. Chem.* **2005**, *48*, 24.
192. Bolognesi, M.L. *Curr. Med. Chem.* **2013**, *20*, 1639.
193. Pau, A.; Catto, M.; Pinna, G.; Frau, S.; Murineddu, G.; Asproni, B.; Curzu, M.M.; Pisani, L.; Leonetti, F.; Loza, M.I.; Brea, J.; Pinna, G.A.; Carotti, A. ChemMedChem **2015**, *10*, 1054.
194. Carlier, P.R.; Chow, E.S.-H.; Han, Y.; Liu, J.; El Yazal, J.; Pang, Y.-P. *J. Med. Chem.* **1999**, *42*, 4225.
195. Galdeano, C. Experimental Master. *Unitat de Química Farmacèutica, Departament de Farmacologia i Química Terapèutica, Universitat de Barcelona*, **2006**.
196. Ramírez, L. Experimental Master. *Unitat de Química Farmacèutica, Departament de Farmacologia i Química Terapèutica, Universitat de Barcelona*, **2008**.
197. Chan, L.C.; Cox, B.G. *J.Org. Chem.* **2007**, *72*, 8863.
198. Valeur, E.; Bradley, M. *Chem. Soc. Rev.* **2009**, *38*, 606.

199. Muñoz-Ruiz, P.; Rubio, L.; García-Palomero, E.; Dorronsoro, I.; del Monte-Millán, M.; Valenzuela, R.; Usan, P.; de Austria, C.; Bartolini, M.; Andrisano, V.; Bidon-Chanal, A.; Orozco, M.; Luque, F.J.; Medina, M.; Martínez, A. *J. Med. Chem.* **2005**, *48*, 7223.
200. Xie, S.S.; Wang, X.; Jiang, N.; Yu, W.; Wang, K.D.G.; Lan, J.S. *Eur. J. Med. Chem.***2015**, *95*, 153.
201. Novaroli, L.; Reist, M.; Favre, E.; Carotti, A.; Catto, M.; Carrupt, P.-A. *Bioorg. Med. Chem.* **2005**, *13*, 6212.
202. Bolea, I.; Gella, A.; Unzeta, M. *J Neural Transm.* **2013**, *120*, 893.
203. Szewczuk, L.M.; Culhane, C., Yang, M.; Majumdar, A.; Yu, H.; Cole, P.A. *Biochemistry* **2007**, *46*, 6892.
204. Yang, M.; Culhane, J.C.; Szewczuk, L.M.; Gocke, C.B.; Brautingam, C.A.; Tomchick, D.R.; Machius, M.; Cole, P.A.; Yu, H. *Nat. Struct. Mol. Biol.* **2007**, *14*, 535.
205. Song, M.S.; Matveychuk, D.; MacKenzie, E.M.; Duchcherer, M.; Mousseau, D.D.; Baker, G.B. *Neuropsychopharmacol. Biol. Psychiatry* **2013**, *44*, 118.
206. Riederer, P.; Danielczyk, W.; Grunblatt, E. *Neurotoxicology* **2004**, *25*, 271.
207. Tatton, W.; Chalmers-Redman, R.; Tatton, N. *J. Neural Transm.* **2003**, *110*, 509.
208. Weinreb, O.; Amit, T.; Bar-Am, O.; Sagi, Y.; Mandel, S.; Youdim, M.B. *J. Neural Transm. Suppl.* **2006**, *70*, 457.
209. Youdim, M.B.H.; Weinstock, M. *Cell. Mol. Neurobiol.* **2001**, *21*, 555.
210. Mindt, T.L.; Struthers, H.; Brans, L.; Anguelov, T.; Schweinsberg, C.; Maes, V.; Tourwé, D.; Schibli, R. *J. Am. Chem. Soc.* **2005**, *127*, 10824.
211. Schulze, B.; Schubert, U.S. *Chem. Soc. Rev.* **2014**, *43*, 2522.
212. Kolb, H.C.; Finn, M.G.; Sharpless, K.B. *Angew.Chem. Int. Ed.* **2001**, *40*, 2004.
213. Huisgen, P.; Padwa, A. *Ed. Wiley*: New York **1984**, *1*.
214. Rostovtsev, V.V.; Green, L.G.; Fokin, V.V. Sharpless, K.B. *Angew. Chem. Int. Ed.* **2002**, *41*, 2596.
215. Tornoe, C.W.; Christensen, C.; Meldal, M. *J. Org. Chem.* **2002**, *67*, 3057.
216. Himo, F.; Lovell, T.; Hilgraf, R.; Rostovtsev, V.V.; Noodleman, L.; Sharpless, K.B.; Fokin, V.V. *J. Am. Chem. Soc.* **2005**, *127*, 210.
217. Manetsch, R.; Krasinski, A.; Radic, Z.; Raushel, J.; Taylor, P.; Sharpless, K.B.; Kolb, H.C. *J. Am. Chem. Soc.* **2004**, *126*, 12809.
218. Struthers, H.; Mindt, T.; Schibli, R. *Dalton Trans.* **2010**, *39*, 675.
219. Crowley, J.D.; Bandeen, P.H. *Dalton Trans.* **2010**, *39*, 612.
220. Shi, Z.-J.; Yu, D.-G. *Comprehensive Org. Chem.* **2013**, *II 6*, 47.

221. Orsini, A.; Vitérisi, A.; Bodlenner, A.; Weibel, J.-M.; Pale, P. *Tetrahedron Lett.* **2005**, *46*, 2259.
222. Guido, R.V.C.; Oliva, G.; Andricopulo, A.D. *Curr. Med. Chem.* **2008**, *15*, 37.
223. Jorgensen, W.L. *Science* **2004**, *303*, 1813.
224. Hardy, L.W.; Malikayil, A. *Curr. Med. Chem.* **2003**, *3*, 15.
225. Maryanoff, B.E. *J. Med. Chem.* **2004**, *47*, 769.
226. Schmidtke, P.; Barril, X. *J.Med. Chem.* **2010**, *53*, 5858.
227. Shoicket, B.K.; McGovern, S.L.; Wei, B.; Irwin, J.J. *Curr. Opin. Chem. Biol.* **2002**, *6*, 439.
228. Blake, J.F.; Laird, E.R. *Annu. Rep. Med. Chem.* **2003**, *38*, 305.
229. Taylor, R.D.; Jewsbury, P.J.; Essex, J.W. *J. Comput. Aided Mol. Des.* **2002**, *16*, 151.
230. Zhao, H.; Huang, D.; Caflisch, A. *ChemMedChem* **2012**, *7*, 1983.
231. Cuchillo, R.; Pinto-Gil, K.; Michel, J. *J. Chem. Theory Comput.* **2015**, *11*, 1292.
232. Cole, S.L.; Vassar, R. *Curr. Genomics* **2007**, *8*, 509.
233. Vassar, R. *J. Mol. Neurosci.* **2001**, *17*, 157.
234. McGaughey, G.B.; Holloway, M.K. *Expert Opin. Drug Discov.* **2007**, *2*, 1129.
235. Patel, S.; Vuillard, L.; Cleasby, A.; Murray, C.W.; Yon, J. *J. Mol. Biol.* **2004**, *343*, 407.
236. Gorfe, A.A.; Caflisch, A. *Structure* **2005**, *13*, 1487.
237. Andreeva, N.S.; Rumsh, L.D. *Protein Sci.* **2001**, *10*, 2439.
238. Andreeva, N.; Dill, J.; Gilliland, G.L. *Biochem. Biophys. Res. Commun.* **1992**, *184*, 1074.
239. Tang, J.; Koelsch, G. *Peptide Lett.* **1995**, *2*, 257.
240. Bahar, I.; Lezon, T.R.; Bakan, A.; Shrivastava, I.H. *Chem. Rev.* **2010**, *110*, 1463.
241. Morley, S.D.; Afshar, M. *J. Comput. Aided Mol. Des.* **2004**, *187*, 10-22.
242. Friesner, R.; Murphy, R.B.; Repasky, M.P.; Frye, L.L.; Greenwood, J.R.; Halgren, T.A.; Sanschagrin, P.C.; Mainz, D.T. *J. Med. Chem.* **2006**, *49*, 6177.
243. Md. Mushtaque, S. *Eur. J. Med. Chem.* **2015**, *90*, 280.
244. Vicente-García, E.; Ramón, R.; Preciado, S.; Lavilla, R. *Beilstein J. Org. Chem.* **2011**, *7*, 980.
245. Das, S.; Addis, D.; Zhou, S.; Junge, K.; Beller, M. *J. Am. Chem. Soc.* **2010**, *132*, 1770.
246. Fletcher, S. *Org. Chem. Font.* **2015**, *2*, 739.
247. Kitahara, K.; Toma, T.; Shimokawa, J.; Fukuyama, T. *Org. Lett.* **2008**, *10*, 2259.

1 Other publications

Annex

and presentations in scientific meetings

Journal publications

- Sola, I.; Aso, E.; Frattini, D.; López-González, I.; Espargaró, A.; Sabaté, R.; **Di Pietro, O.**; Luque, F.J.; Clos, M.V.; Ferrer, I.; Muñoz-Torrero, D. Novel levetiracetam derivatives that are effective against the Alzheimer-like phenotype in mice: synthesis, in vitro, ex vivo, and in vivo efficacy studies, *J. Med. Chem.* **2015**, *58*, 6018-6032.

- Pérez-Areales, F.J.; **Di Pietro, O.**; Espargaró, A.; Vallverdú-Queralt, A.; Galdeano, C.; Ragusa, M.I.; Viayna, E.; Guillou, C.; Clos, M.V.; Pérez, B.; Sabaté, R.; Lamuela-Raventós, R.M.; Luque, F.J.; Muñoz-Torrero, D. Shogaol–huprine hybrids: dual anticholinesterase and antioxidant agents with β-amyloid and tau anti-aggregating properties**,** *Bioorg. Med. Chem.* **2014**, *22*, 5298-5307.

- Viayna, E.; Sola, I.; **Di Pietro, O.**; Muñoz-Torrero, D. Human disease and drug pharmacology, complex as real life. *Curr. Med. Chem.*, **2013**, *20*, 1623-1634.

Presentations in scientific meetings

- Poster entitled "*Synthesis, molecular modeling and evaluation of pyrido[3,2-c]quinolines as peripheral site inhibitors of acetylcholinesterase*" (Viayna, E., Vicente-García, E., **Di Pietro, O.**, Ramón, R.; Clos, M.V.; Pérez, B.; Badia, A., Bartolini, M., Andrisano, V.; Luque, F.J.; Lavilla, R.; Muñoz-Torrero, D.) presented at the 9th Spanish-Italian Symposium on Organic Chemistry (SISOC-IX). Tenerife (SPAIN).

- Poster entitled "*Benzo[h][1,6]naphthyridines as a novel family of achetylcholinesterase inhibitors*" (E. Viayna, E. Vicente-García, **O. Di Pietro**, R. Ramon, M. V. Clos, B. Pérez, M. Bartolini, V. Andrisano, F. J. Luque, R. Lavilla, D. Muñoz-Torrero) presented at the XVII National Meeting of the SEQT. Madrid (SPAIN)**,** 2013.

- Poster entitled "*Synthesis and screening of a small library of quinolones and tricyclic heterofused quinolones against Trypanosoma brucei*" (**O. Di Pietro**, E. Vicente-García,

E. Viayna, A. Lanzoni, M. C. Taylor, B. Pérez, J. M. Kelly, R. Lavilla, D. Muñoz-Torrero) presented at the XVII National Meeting of the SEQT. Madrid (SPAIN), 2013.

- Poster entitled "*Hit-to-Lead optimization from an inactive to a picomolar inhibitor of Acetylcholinesterase*" (**O. Di Pietro**, F. Javier Pérez-Areales, Elisabet Viayna, Esther Vicente-García, Alba Espargaró, Jordi Juárez-Jiménez, Rosario Ramón, M. Victoria Clos, Belén Pérez, Manuela Bartolini, Vincenza Andrisano, Raimon Sabaté, F. Javier Luque, Rodolfo Lavilla, Diego Muñoz-Torrero) presented at the I Simposio de Jóvenes Investigadores de la SEQT. Madrid (SPAIN), 2014.

- Poster entitled "*Shogaol–huprine hybrids: dual anticholinesterase and antioxidant agents with β-amyloid and tau anti-aggregating properties*" (F. J. Pérez-Areales, **O.Di Pietro**, A. Espargaró, A. Vallverdú-Queralt, C. Galdeano, M. I. Ragusa, E. Viayna, C. Guillou, M. V. Clos, B. Pérez, R. Sabaté, R. M. Lamuela-Raventós, F. J. Luque, D. Muñoz-Torrero) presented at the I Simposio de Jóvenes Investigadores de la SEQT. Madrid (SPAIN), 2014.

- Poster entitled "*Tetrahydrobenzo[h][1,6]naphthyridine-6-chlorotacrine hybrids as a new family of anticholinesterasic agents with dual β-amyloid and tau anti-aggregating properties*" (**O. Di Pietro**, F. Javier Pérez-Areales, Elisabet Viayna, Esther Vicente-García, Alba Espargaró, Jordi Juárez-Jiménez, Rosario Ramón, M. Victoria Clos, Belén Pérez, Manuela Bartolini, Vincenza Andrisano, Raimon Sabaté, F. Javier Luque, Rodolfo Lavilla, Diego Muñoz-Torrero) presented at the Barcelona BioMed Conference. Barcelona (SPAIN), 2014.

- Poster entitled "*Searching for novel transient druggable pockets in BACE-1. Conformational analysis and definition of new pharmacophores*" (**O. Di Pietro**, J. Juárez-Jiménez, D. Muñoz-Torrero, C. Laughton, F.J. Luque) presented at the Spanish Italian Medicinal Chemistry Congress (SIMCC2015). Barcelona (SPAIN), 2015.

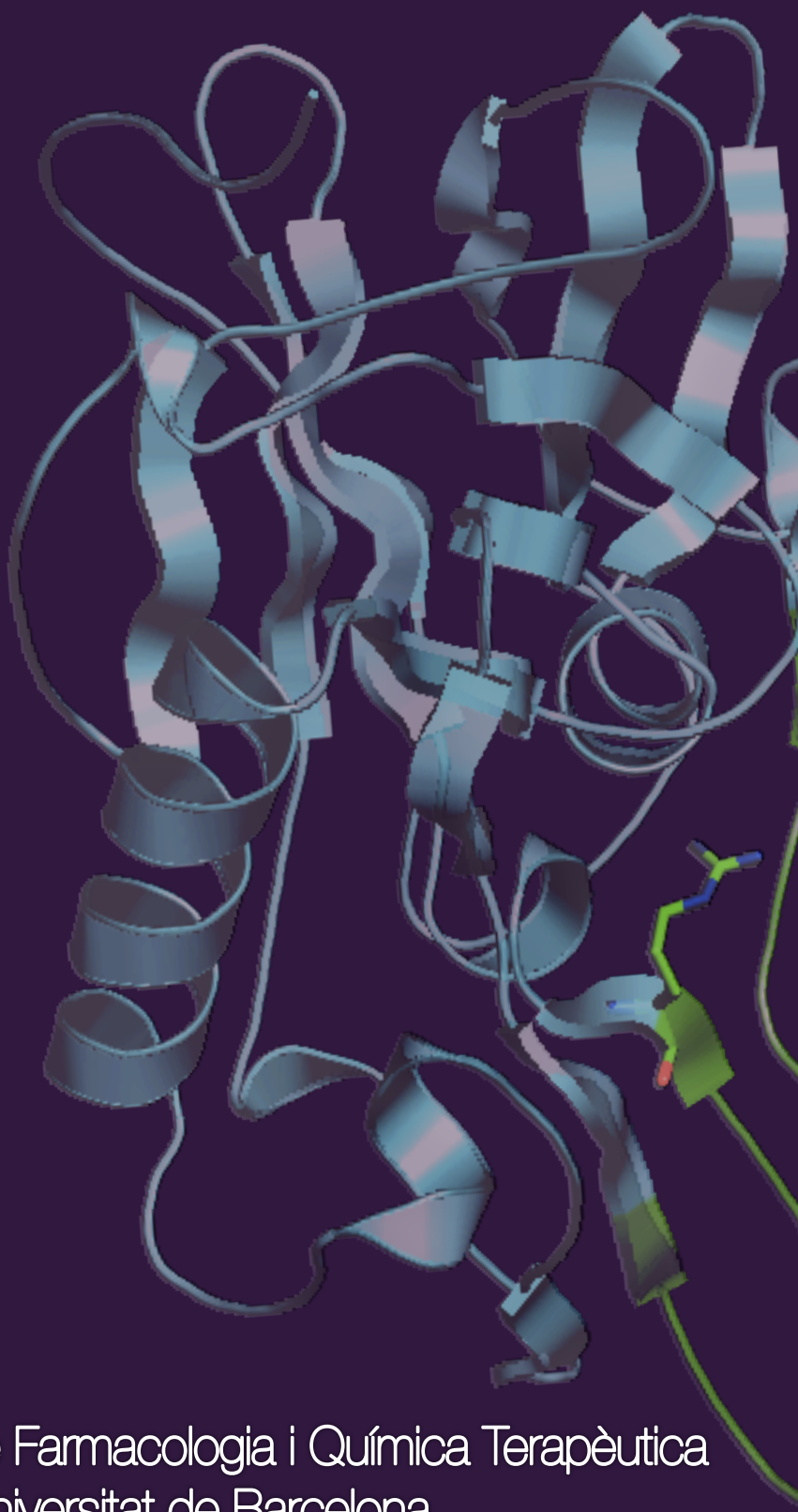

Departament de Farmacologia i Química Terapèutica
Universitat de Barcelona